Phosphorus and Nitrogen Cycling in the Mediterranean Sea:

Circulation, biogeochemistry and anthropogenic forcing

by

Helen Rebecca Powley

A thesis
presented to the University of Waterloo
in fulfillment of the
thesis requirement for the degree of
Doctor of Philosophy
in
Earth Sciences

Waterloo, Ontario, Canada, 2017

©Helen Rebecca Powley 2017

Examination Committee Membership

The following served on the Examining Committee for this thesis. The decision of the Examining Committee is by majority vote.

External Examiner	Dr. Kathleen Ruttenberg Professor Department of Oceanography University of Hawaii
Supervisor	Dr. Philippe Van Cappellen Canada Excellence Research Chair Department of Earth and Environmental Sciences University of Waterloo
Internal Member	Dr. Hans Dürr Research Assistant Professor, Department of Earth and Environmental Sciences University of Waterloo
Internal-External Member	Dr. Ralph Smith Professor Department of Biology University of Waterloo
Other Member	Dr. Michael Krom Professor, Charney School of Marine Sciences University of Haifa University of Leeds (Professor Emeritus) University of Waterloo (Adjunct Professor)

Author's Declaration

This thesis consists of material all of which I authored or co-authored: see Statement of Contributions included in the thesis. This is a true copy of the thesis, including any required final revisions, as accepted by my examiners.

I understand that my thesis may be made electronically available to the public.

Statement of Contributions

This thesis consists of a series of co-authored papers. As first author of each paper, I was primarily responsible of the study design and its execution. The following summarizes the contributions of the co-authors of each chapter. The co-authors participated in discussions on research design and data analysis and helped review and edit the paper.

Chapter 2

Philippe Van Cappellen (PVC), Michael Krom (MK) and Kay Emeis (KE) develop the initial conceptual model of nutrient cycling in the EMS (Appendix A). I created the model forcing functions with input from PVC. I wrote the paper, with help from PVC and MK.

Chapter 3

I designed the study with input from PVC, Ana Lima (AL), Hans Dürr (HD), and MK. I performed the research and analyzed the results. AL and HD helped with the data analysis: AL provided the speciation data for phosphorus in different wastewater treatment types; HD helped assemble validation data. I wrote the paper with help of PVC.

Chapter 4

PVC, MK and I co-developed the conceptual model. I implemented the mathematical model and performed the simulations and analyzed the results with help from PVC. I wrote the paper with help of PVC.

Chapter 5

PVC, MK and I co-developed the conceptual model. I implemented the mathematical model and performed the simulations and analyzed the results with help from MK and PVC. I wrote the paper with help of MK and PVC.

Chapter 6

PVC and I designed the research. I performed the research and analyzed data with help from PVC and MK. I wrote the paper.

Abstract

The Mediterranean Sea (MS) is an oligotrophic marine basin despite being semi-enclosed with unusually low inorganic phosphorus (P) and nitrogen (N) concentrations, and high nitrate (NO_3):phosphate (PO_4) ratios comparative to the global ocean. In addition distinct biogeochemical differences occur between the Western Mediterranean Sea (WMS) and Eastern Mediterranean Sea (EMS). Episodic deposition of organic rich sediments in the EMS indicate that fast changes in biogeochemical cycling within the MS may have occurred in the recent geological past with the development of eutrophic conditions and anoxic deep waters. Currently, close to 430 million people live within the drainage basin of the MS. The pace of population growth, coastal urbanization, land use changes and climate change are increasingly modifying hydrological and biogeochemical cycling within the MS with potential for major ecological consequences. In this thesis, a coupled P and N mass balance model is created with the goal of: (1) understanding the unique biogeochemistry of the MS and (2) delineating how anthropogenic activities and circulation affect P and N cycling and primary productivity within the MS.

Anthropogenic inputs to the aquatic systems have dramatically increased since 1950. In Chapter 2, anthropogenic inputs of reactive P and N into the EMS between 1950 and 2000 were reconstructed and applied to a steady state mass balance model for P and N cycling in the EMS. The WMS provided the main source of P and N to the EMS over 1950 to 2000. Reactive P and N inputs increased by a maximum of 24% and 65% respectively over 1950 to 2000 yet primary productivity only increased by 16%. The excess P provided to the EMS after 1950 was largely exported out of the EMS through the Strait of Sicily to the WMS or stored within the deep water, maintaining the oligotrophy of the sea.

Direct discharges of domestic wastewater are typically not included in mass balance nutrient models of the MS and were not included in the P and N inputs in Chapter 2. Chapter 3 used an empirical model to determine that P and N inputs from direct domestic wastewater discharges into the MS were on the same order of magnitude as inputs from rivers for the year 2003 and therefore should be included in nutrient budgets for the MS. Population growth, dietary changes and expanded connectivity to sewers were expected to further increase direct wastewater nutrient inputs to the MS in the future, especially in southern and eastern regions of the Mediterranean basin. Regionally targeted upgrades to tertiary wastewater treatment, combined with enhanced wastewater recycling and banning phosphates from laundry and dishwasher detergents, may be the most cost-effective way to prevent the expansion of coastal eutrophication.

The Mediterranean region is one of the most sensitive globally to climate change but impact on the thermohaline circulation is uncertain. In Chapter 4, the sensitivity of dissolved oxygen (O_2) concentrations to climate change was assessed using a mass balance model of O_2 cycling in the MS. To achieve this, a circulation model for the WMS was created and coupled to the pre-existing EMS circulation model. Results show that the MS is unlikely to go hypoxic within the foreseeable future despite large potential changes in the thermohaline circulation. The change in the provision of labile dissolved organic carbon with deep water formation may result in a negative feedback, reducing the effects of climate driven changes in circulation on oxygen consumption.

The coupled WMS-EMS circulation model created in Chapter 4 is used to create a mass balance model for P and N cycling in the MS for 1950 (Chapter 5). Direct wastewater and submarine groundwater discharges are included for the first time in a nutrient budget for the MS. The nutrient budgets for both the WMS and EMS are dominated by marine derived inputs. In addition, up to 5 times more marine derived reactive P and N entered the WMS than EMS per unit surface area and this is primary the cause of the west to east differences in biogeochemical properties observed across the MS: land derived inputs are approximately similar per unit surface area between the basins. The high NO_3:PO_4 deep water ratio of the MS is caused by the high N:P ratio of inputs, in particular atmospheric inputs, together with low denitrification rates. The low NO_3:PO_4 ratio of the inflow through Gibraltar helps drive the lower N:P ratio in the WMS than EMS.

The magnitude and strength of year on year deep water formation within the MS is highly variable and the response of P and N concentrations to inter-annual changes in intermediate water and deep water formation versus that from anthropogenic enrichment is unknown. In Chapter 6, anthropogenic reactive P and N inputs into the MS between 1950 and 2030 were reconstructed and applied to the coupled WMS-EMS steady state P and N model created in Chapter 5. The anthropogenic nutrient signature of the MS is diluted by the dominance of the Atlantic surface water and exchanges across the Straits of Sicily in providing P and N to the WMS and EMS. In addition, the anti-estuarine circulation removes approximately 50% of the anthropogenic nutrients input into the MS by 2030. Consequently, anthropogenic nutrient enrichment cannot be observed in water column dissolved reactive P concentrations over the noise created by inter-annual variability in circulation. Anthropogenic enrichment of dissolved reactive N concentrations may be observed after 1970 for DON and 1990 for NO_3.

Overall, nutrient inputs into the MS are dominated by laterally sourced marine derived inputs. Thus the MS behaves more like a subtropical gyre than an enclosed marine basin. The important contribution of organic matter in nutrient cycling is highlighted in this thesis with anthropogenic reactive N inputs

predicted to accumulate in the DON reservoir. The MS acts as a bioreactor for organic matter cycling, converting organic nutrients to inorganic ones at depth which are then exported out of the basin by the anti-estuarine circulation. Future work should concentrate on understanding the lability of organic matter from input sources to the MS and within the water column of the MS.

Acknowledgements

I would firstly like to thank my supervisor, Philippe Van Cappellen, who has guided me to become the researcher I am today. His ability to always suggest ideas to research problems, quickly switch subjects, and shear breadth of knowledge never ceases to amaze me. I would also like to thank Michael Krom for his encouragement, support and advice throughout my degree. In addition, I would like to thank my advisory committee members Hans Dürr and Sherry Schiff for committing their time and advice to help me with this research. I wish to also thank Ralph Smith and Kathleen Ruttenberg for agreeing to be part of my examination committee. I am indebted to Sannan Mansoor, who transferred all my code to MATLAB and guided me down the path of "real" coding. I would also like to acknowledge Scott Smith and Avi Shaviv for guiding me to datasets used in this thesis, Pere Masque for providing me with sediment core samples and Paul Myers for discussing ideas on modeling the Mediterranean circulation. In addition I wish to thank Chris Parsons and Kassandra Ma for taking the time to teach and guide me through the laboratory work undertaken as part of this thesis.

I would like to thank Kristen Mitchell for being like a mentor to me when I first started within the Ecohydrology Research Group. The Ecohydrology Research Group has been my family while undertaking this thesis. They have helped me through various mishaps and in particular I wish to thank Nienke, Feriedoun, Saliy, Hans, Brad, Kristen, Taylor, Ana, and Radmila for their support. Finally, I would have never have made it through this thesis without the support of my friends. I particularly wish to thank Taylor and Erin for all their climbing belays over the years as well as their support, encouragement and exciting scientific discussions, Zahra for being an awesome office mate, Maddy for all the coffee breaks and events you have hosted over the years and Krista for the listening ear. Finally I wish to thank the Canada Excellence Research Chair program for funding my research.

Table of Contents

List of Figures

List of Tables

List of Acronyms

In alphabetical order

ADW	Adriatic deep water
ASW	Atlantic surface water
BiOS	bimodal oscillation system
C	carbon
DIN	dissolved inorganic nitrogen (nitrate plus ammonium)
DIP	dissolved inorganic phosphorus
DOC	dissolved organic carbon
DON	dissolved organic nitrogen
DOP	dissolved organic phosphorus
DW	deep water
E	evaporation
EMC	East Mediterranean Countries
EMDW	Eastern Mediterranean Deep Water
EMIW	Eastern Mediterranean Intermediate Water
EMS	Eastern Mediterranean Sea
EMSW	Eastern Mediterranean surface water
EMT	Eastern Mediterranean Transient
IW	intermediate water
K_z	vertical turbulent mixing diffusivity coefficient
LIW	Levantine Intermediate Water
MS	Mediterranean Sea
N	nitrogen
NH_3	ammonia
NH_4	dissolved ammonium
NO	nitrous oxide
NO_3	dissolved nitrate plus nitrite
NMC	North Mediterranean Countries
NWM	north-west Mediterranean
P	phosphorus
PIP	particulate inorganic phosphorus
PO_4	dissolved inorganic phosphorus
POC	particulate organic carbon
PON	particulate organic nitrogen
POP	particulate organic phosphorus
O_2	dissolved oxygen gas
R	riverine discharge
SGD	submarine groundwater discharge
SMC	South Mediterranean Countries
Sv	Sverdrop (10^6 m^3 s^{-1})
SW	surface water
TDW	Tyrrhenian Deep Water
THC	thermohaline circulation
TN	total nitrogen
TP	total phosphorus
WMS	Western Mediterranean Sea
WMDW	Western Mediterranean Deep Water
WMIW	Western Mediterranean Intermediate Water

WMSW	Western Mediterranean Surface Water
WMT	Western Mediterranean Transition
WWTP	Wastewater Treatment Plant

Chapter 1.

Introduction

1.1 Mediterranean Basin

The Mediterranean Sea (MS) has a surface area of $2508x10^3$ km^2 (Ludwig et al., 2009) and a coastline of 46,000 km, of which 41% are associated with islands (Plan-Bleu, 2005). The MS is separated from the North Atlantic Ocean by the Strait of Gibraltar, a narrow sill between Spain and Morocco with an average depth of 600 m (minimum depth of 297 m) and minimum width of 13 km. Two main basins compose the MS: the Western Mediterranean Sea (WMS) and the Eastern Mediterranean Sea (EMS). The EMS is the largest of the two basins with a surface area of 1669 x 10^3 km^2; the WMS covers 840 x 10^3 km^2. The WMS and EMS are separated by the Strait of Sicily, a wider and shallower sill than the Strait of Gibraltar with a maximum depth of 316 m and a width of 145 km. In addition, various sub-basins and regional seas make up the MS; those referred to in this thesis are shown in Figure 1.1. Note that in Chapters 2, 4 and 5 the term EMS excludes the Adriatic and Aegean Seas, while in Chapter 3 the EMS includes the Adriatic and Aegean Seas.

Twenty-three countries from three different continents surround the MS with per capita GDP ranging from US$ 2,700 to US$ 145,000 in 2010 (excluding Gaza and Syria; World Bank, 2016). The Mediterranean countries exhibit very disparate levels of economic development, demographic trends and capacities for adaptation to global change and technological innovation. Overall, the population in the Mediterranean basin is increasing rapidly. Between 1970 and 2000 the population of Mediterranean coastal regions increased by 71%, from 95 million to 143 million; it is expected to reach 174 million in 2025 (Plan-Bleu, 2005). In addition, coastal areas experience high seasonal influxes of both national and international tourists. Between 1990 and 2000, tourism around the MS increased by 67%, reaching 176 million people by the turn of the century (Plan-Bleu, 2005). Thus, the annual number of tourists visiting the Mediterranean coastal areas exceeds the permanent population. (Note: the effects of recent conflicts and accelerating migration towards EU countries are not included in population estimates cited.)

Because of the large coastal populations, along with tourism and the long coastline of the MS, anthropogenic activities significantly impact marine ecosystems, in particular in nearshore settings (Micheli et al., 2013). Anthropogenic impacts include ocean acidification, sea surface temperature changes, and anomalies in UV light; together they account for 60-75% of the cumulative anthropogenic impact on the entire MS (Micheli et al., 2013). By 2001, ocean acidification had already decreased pH of water masses in the MS by 0.05-0.14 pH units compared to the pre-industrial era (Touratier and Goyet, 2011), while measurable increases in sea surface temperatures are altering population abundance and survival rates of marine biota (Lejeusne et al., 2010; Marbà et al., 2015). Shipping, overfishing, habitat

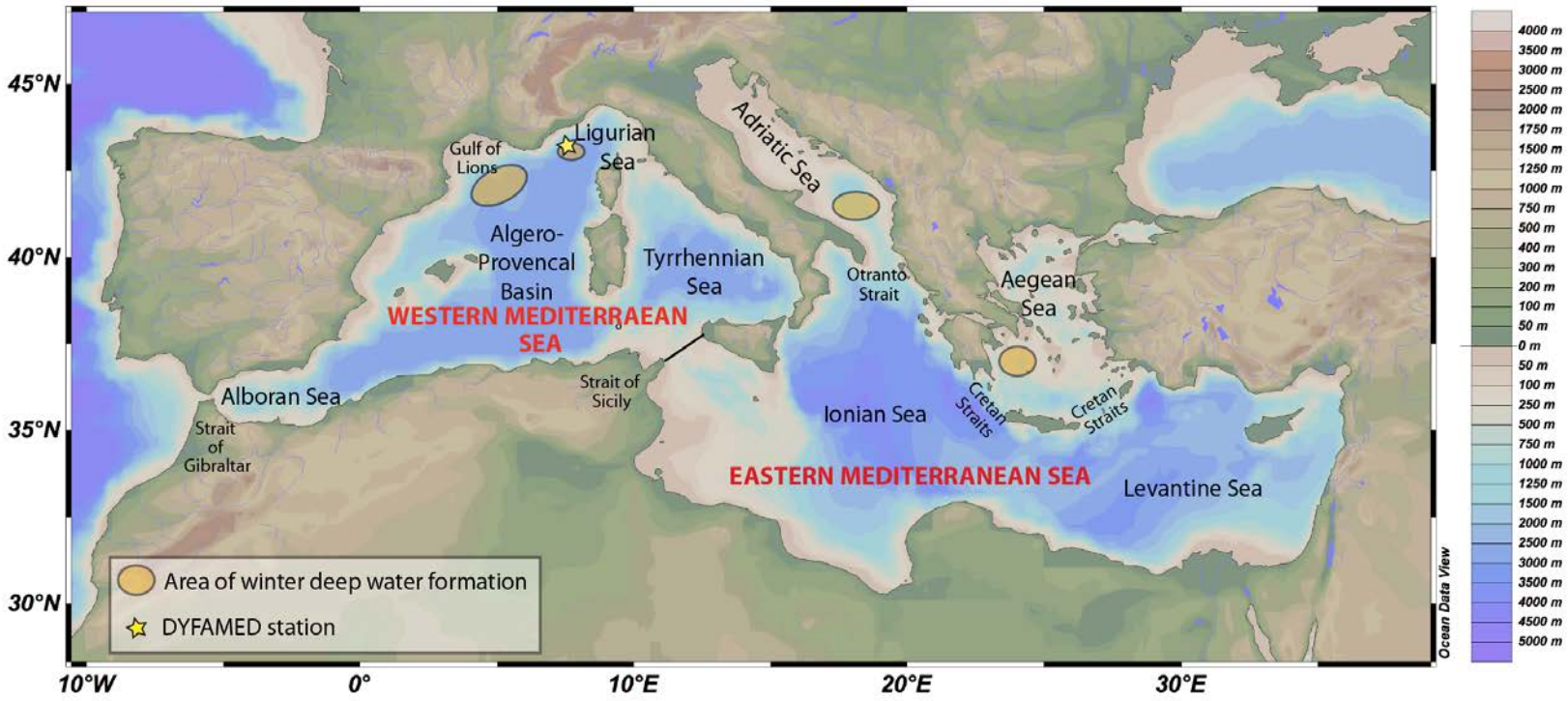

Figure 1.1: Bathymetry of Mediterranean Sea, areas of deep-water formation (de Madron et al., 2011), and location of sub-basins mentioned in this thesis.

destruction and pollution are some of the other activities having a large impact on the MS ecosystems (Lejeusne et al., 2010). The opening of the Suez Canal, shipping, and aquaculture have led to the introduction of around 1000 invasive species into the MS, of which more than half are established and spreading (Katsanevakis et al., 2014). An example of a major socio-economic impact caused by anthropogenic activities is the collapse of Egyptian fisheries after the construction of the Aswan Dam (Nixon, 2003).

1.2 Thermohaline circulation

The MS exhibits an anti-estuarine circulation (Figure 1.2). Atlantic surface water (ASW) enters the MS through the Strait of Gibraltar and travels from west to east across the WMS eventually entering the EMS through the Strait of Sicily. High evaporation rates cause the salinity and density of surface water (SW) to increase eastward across MS. Within the EMS, the SW eventually sinks to form Levantine Intermediate Water (LIW) primarily in the Rhodes gyre. The LIW moves out of the EMS through the Strait of Sicily and into the WMS whereby it circulates across the basin in an anticlockwise direction.

The MS is one of the only areas in the oceans outside the polar regions where deep water (DW) formation occurs. Eastern Mediterranean Deep Water (EMDW) is formed mainly in the Adriatic Sea with a smaller amount of EMDW produced in the Aegean Sea. Upwelling moves EMDW into LIW, which in turn is exported out of the EMS through the Strait of Sicily or into the Adriatic and Aegean Seas (Figures 1.2 and 4.1). Deep water in the WMS forms in the northwestern Mediterranean (NWM), near to the Gulf of Lions, and in the Ligurian Sea (Figure 1.1). During winter months, high salinity LIW from the EMS is mixed with overlying SW, leading to intermediate and deep water formation in the NWM (Rhein, 1995). Both Western Mediterranean intermediate water (WMIW) and Western Mediterranean deep water (WMDW) exit the WMS through the Strait of Gibraltar. Quantitative estimates of water fluxes in the WMS and EMS are found in Chapter 4.

In recent years changes have been observed in location and strength of DW formation processes within the MS. Between 1987 and 2001, the main source of DW formation in the EMS switched from the Adriatic Sea to the Aegean Sea. This switch is known as the Eastern Mediterranean Transient (EMT; Roether and Schlitzer, 1991). The accompanying changes in DW formation are reviewed in Chapters 2 and 4. The main pulse of the EMT occurred between 1992 and 1995 (Roether et al., 2007) and resulted in very dense water exiting the Aegean Sea through the eastern Cretan Strait. The water subsequently travelled westward following the bottom topography and swiftly covered most of the EMS' seafloor. The young Aegean DW replaced approximately 20% of EMDW below 1500 m depth (Klein et al., 2003).

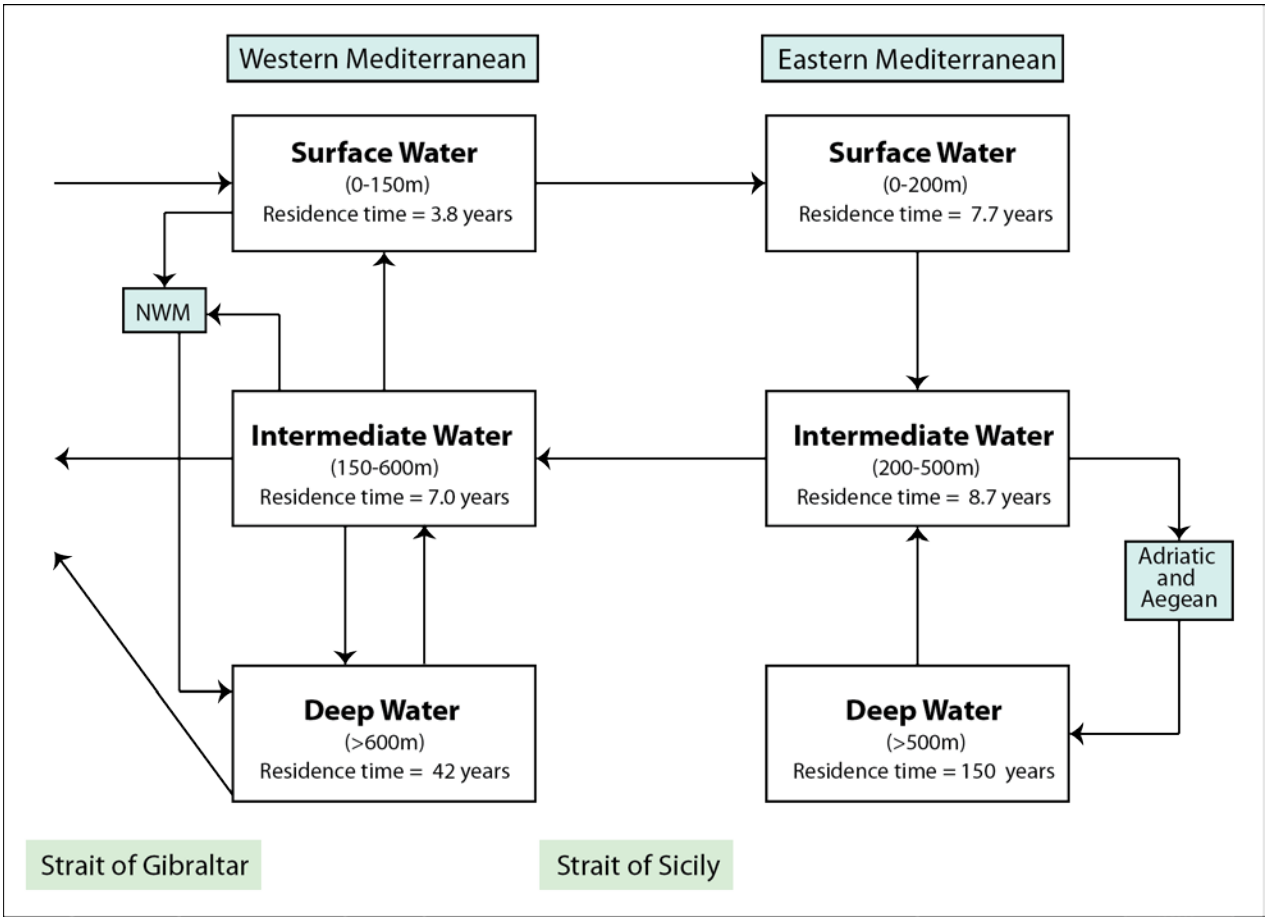

Figure 1.2: Circulation of Mediterranean Sea. See Figure 4.1 and Chapter 4 for quantification of water fluxes. NWM = north-west Mediterranean.

After 1995, incoming waters from the Aegean Sea only reached depths of 800-1000 m (Kress et al., 2003), sandwiching a layer of old Adriatic deep water between two younger water masses. The effects of the EMT were also observed in the WMS. The EMT caused increased salinity of the LIW entering the WMS through the Strait of Sicily and contributed up to approximately half of the increase in density that caused extensive WMDW formation during the cold winters of 2004/2005 and 2005/2006 (Schroeder et al., 2006; Schroeder et al., 2010b). This series of events is termed the Western Mediterranean Transition (WMT; CIESM, 2009).

Enhanced salinity and cooling of SW within the Aegean Sea, relative to previous years, is the likely driver of the EMT (Pinardi et al., 2015). Beuvier et al. (2010) highlight seven potential preconditioning factors for the EMT: 1) lower freshwater input from the Black Sea; 2) blocking anti-cyclones south of Crete altering the circulation of LIW, and thus directing it towards the Aegean Sea; 3) different Eastern Mediterranean surface water circulation altering the salinity of water received by the Aegean Sea; 4) formation of dense north Aegean water; 5) cold winters in 1991 and 1992 inducing high heat losses from the Aegean Sea; and 6) slow creation of dense Aegean DW throughout the 1970s and 1980s. The change in SW salinity of the Aegean Sea is hypothesized to be linked to the bimodal oscillation (BiOS) of the northern Ionian gyre, switching from anticyclonic to cyclonic with a frequency of approximately 10 years (Gačić et al., 2010; Pinardi et al., 2015) (see section 1.4.2 for details). Modeling studies also suggest that the EMT may not be a one off event. Similar DW formation events in the Aegean Sea may be a recurrent phenomenon (Beuvier et al., 2010; Vervatis et al., 2013; Georgiou et al., 2015; Incarbona et al., 2016), but observations are not available to corroborate this.

The Mediterranean region is one of the most sensitive globally to climate change (Giorgi, 2006). The MS has been warming at approximately three times the global average (Marbà et al., 2015) with clear temperature and salinity increases of the DW observed since at least the 1960's (Béthoux et al., 1990; Béthoux and Gentili, 1999; Vargas-Yanez et al., 2010; Borghini et al., 2014). Climate change predictions also indicate a trend toward warmer and dryer climate in the Mediterranean region during the 21st century (Kristensen et al., 2004; Collins et al., 2013). Although a large number of studies has investigated the impact of climate change on SW temperatures, salinity, heat fluxes, evaporative fluxes and sea level changes of the MS (Gualdi et al., 2013 and references therein), a much more limited number has addressed the resulting effects on the thermohaline circulation (THC) of the MS. Temperature and salinity increases have opposing effects on the density of water which represents a challenge for modeling the response of the THC to climate change. Existing model predictions predict both enhanced (Adloff et al., 2015) and weakened (Thorpe and Bigg, 2000; Somot et al., 2006; Herrmann et al., 2009; Adloff et al., 2015) THC in the coming decades. With the exception of Adloff et al. (2015) all other referenced studies

only used one climate scenario and did not explore the sensitivity of projections to boundary conditions such as river runoff, and the properties of inflowing ASW to the MS. The potential changes in the THC due to ongoing climate warming and the consequences for DW oxygenation are the topic of in Chapter 4.

1.3 Phosphorus and Nitrogen Cycling

1.3.1 Marine sources of P and N

Humans have dramatically modified the cycles of P and N, especially since the mid 20th century (Cordell et al., 2011; Mackenzie et al., 2011; Galloway, 2014; Ruttenberg, 2014). The ultimate natural source of reactive P is weathering of rocks, but humans have accelerated this process through mining (Figure 1.3). Phosphorus enters the aquatic system as a result of fertilizer application, wastewater discharges and industrial aerosols, while deforestation and crop cultivation further enhance the transfer of P to aquatic systems (Ruttenberg, 2014). The transfer of P to marine basins occurs from riverine inputs, submarine groundwater discharge (SGD), and direct discharges or runoff from land into the coastal zone. In the Mediterranean region, Saharan dust is an important source of P, which can become bioavailable upon deposition at the sea surface. Saharan dust is enriched in P compared to average crustal material (0.2% P abundance in Saharan dust compared to 0.1% P in normal soil derived dust; Bergametti et al., 1992). Acid processing in the atmosphere may further enhance the bioavailability of P in dust (Nenes et al., 2011).

The majority of N on Earth exists as N_2 gas, which makes up 71% of the atmosphere. Inert N_2 gas is naturally converted into reactive N by lightning and biological nitrogen fixation in terrestrial and aquatic ecosystems. Humans dramatically perturbed the N cycle following the invention of the Haber-Bosch process in 1913 whereby ammonia (NH_3) is produced from N_2 and hydrogen gas (H_2) under high pressure (Figure 1.4). The NH_3 was initially used for the fabrication of ammunitions during the first World War, but is now mainly used in the production of fertilizers, although NH_3 is present in many other industrial products such as household cleaners. Anthropogenic NH_3 enters the aquatic system through runoff, groundwater discharge and wastewater inputs. Fossil fuel combustion is another source of reactive N, both through the conversion of N_2 in engines and the release of N in the fossil fuel itself.

The importance and origin of organic forms of P and N delivered by atmospheric deposition and rivers to receiving water bodies is a topic of relatively recent research. Dissolved organic phosphorus (DOP) and dissolved organic nitrogen (DON) account for 6-91% and 9-42% of dissolved P and N in rivers, respectively (Ludwig et al., 2009; Berner and Berner, 2012), while DON contributes 20-35% of total atmospheric N deposition to aquatic systems globally (Cornell et al., 2003; Cape et al., 2011a; Kanakidou et al., 2012; Jickells et al., 2013; Kanakidou et al., 2016). The positive correlation observed between total

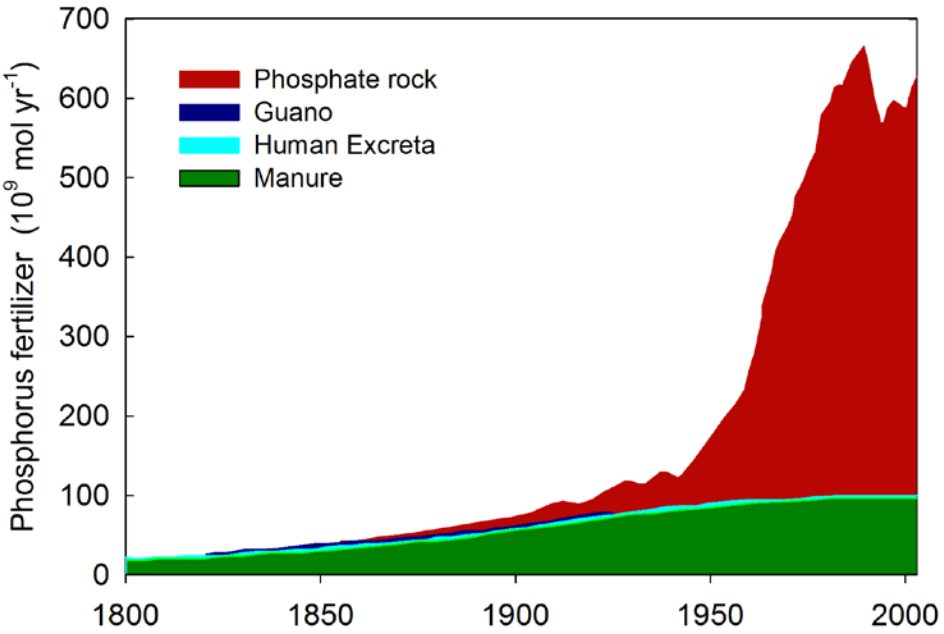

Figure 1.3: Historical global sources of phosphorus fertilizers from 1800 to 2000. Adapted from Cordell et al. (2011).

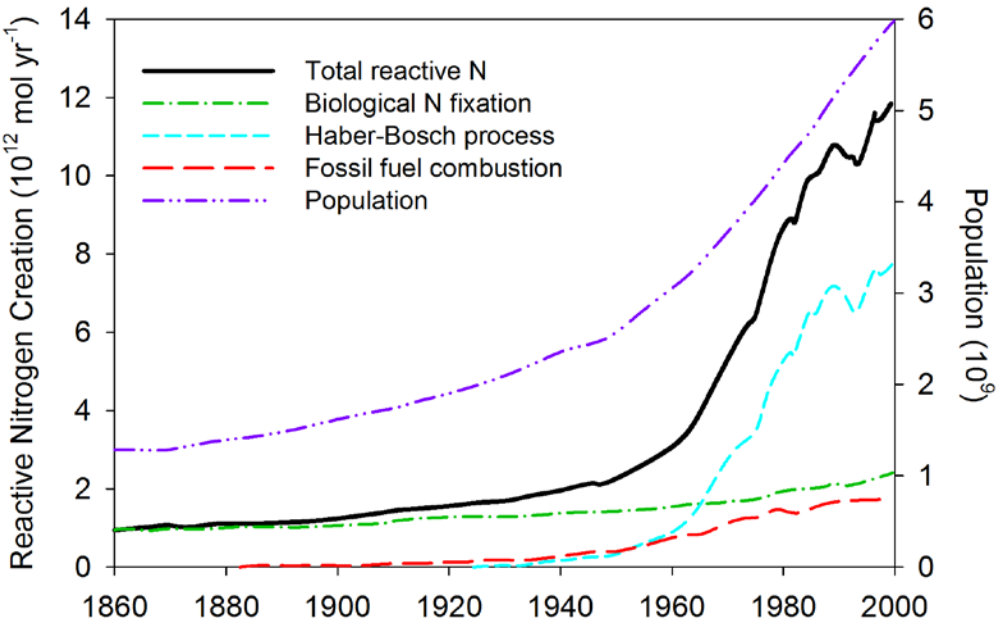

Figure 1.4: Global population (right axis) and reactive N production (left axis) between 1860 and 2000. Total reactive N production is broken down in the contributions of the Haber-Bosch process (fertilizer and non-fertilizer products), biological N fixation of cultivated plants, and fossil fuel combustion. Adapted from Galloway (2014)

dissolved N and DON in atmospheric deposition suggests that a significant fraction of the DON is of anthropogenic origin (Jickells et al., 2013). Fewer studies exist on the atmospheric deposition of DOP. Kanakidou et al. (2012) suggest that 20-83% (median ~ 35%) of total dissolved P deposited globally is in the form of DOP, although only 10% of organic P in the atmosphere is from anthropogenic sources. Dust samples collected over the MS were found to be dominated by organic P in 93% of the cases, while detailed near-edge X-ray fluorescence spectroscopy (P-NEXFS) showed that much of the organic P is contained within bacterial material (Longo et al., 2014).

1.3.2 Assimilation and mineralization

Phosphorus and N are essential nutrients required for phytoplankton growth. In the oceans, phytoplankton assimilate P and N into organic matter within the photic zone, while mineralization processes throughout the water column regenerate inorganic P and N. These processes are often represented by the following chemical stoichiometry:

$$106CO_2 + 16HNO_3 + H_3PO_4 \; + \; 122H_2O \leftrightarrow \; (CH_2O)_{106}(NH_3)_{16}(H_3PO_4) + \; 138O_2 \quad (1.1)$$

where the forward and backward reactions correspond to photosynthesis and (aerobic) respiration, respectively. Although it is usually assumed that phytoplankton assimilate inorganic nutrients according to the Redfield C:N:P ratio of 106:16:1 (Redfield et al., 1963; Equation 1.1), assimilation of organic species of carbon (C), P and N is also known to occur (Zehr and Ward, 2002; Karl and Björkman, 2015; Sipler and Bronk, 2015). The backward reaction in Equation 1.1 regroups a variety of processes involving bacteria, viruses and micro/macro-zooplankton (Figure 1.5). According to Equation 1.1, the remineralization of autochthonous organic matter consumes on average 138 moles of O_2 per 106 moles of organic C oxidized to CO_2, although slightly different global stoichiometric relationships have been proposed, for example O_2:C = 172:122 (Takahashi et al., 1985). Further note that in Equation 1:1, organic N is mineralized into nitrate. In fact, ammonification first converts organic N into ammonium, which is then oxidized to nitrate via nitrification.

Assimilation of P in the photic zone and mineralization of P and N throughout the water column are key processes controlling the biogeochemical cycle of P in the oligotrophic, P starved MS (Appendix A). Other processes influence the fate of reactive P in marine environments, for example, the sorption of P on ferric iron (hydr)oxides and its subsequent release under anoxic conditions, or the production and re-dissolution of biogenic apatite (Ruttenberg, 2014). These processes, however, are assumed to play minor roles in the transformations between different forms of reactive P in the water column, and are therefore ignored in the modeling work presented in this thesis. Similarly, processes other than assimilation and

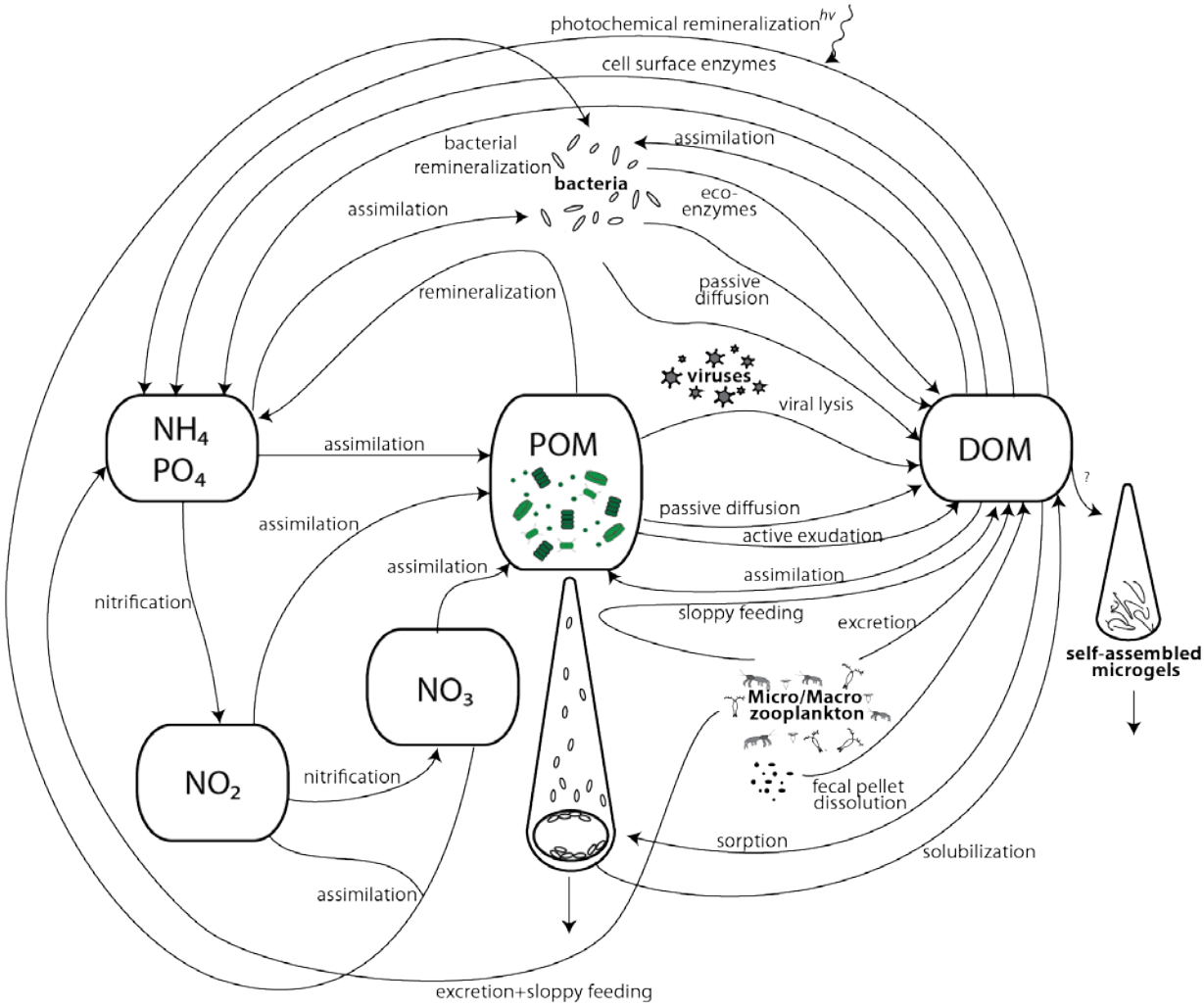

Figure 1.5: Internal nutrient cycling in the photic zone of a marine system explicitly showing the microbial loop. Adapted from: Zehr and Ward (2002); Carlson and Hansell (2015); Sipler and Bronk (2015)

mineralization (including ammonification and nitrification) are not considered in the water column cycling of N.

1.3.3 Sinks of P and N

The ultimate sink of P in the oceans is burial in sediments. Globally, the main sedimentary sink of reactive P is in the form of particulate organic P, which contributes 61% of total reactive P burial (Berner and Berner, 2012). Dispersed authigenic carbonate fluorapatite formation, primarily along the continental margins contributes about 17% of total reactive P burial, while phosphate sorbed to hydrous ferric oxides makes up an additional 19% (Berner and Berner, 2012). Here, only burial of particulate organic P (POP) is considered as a reactive P sink, because under the severe P limitation of the MS biota likely optimize the assimilation of all inorganic reactive P into biomass.

Burial of particulate organic N (PON) is the primary mechanism of N burial, with no appreciable N buried with minerals. In addition to burial, denitrification also removes N from marine systems when dissolved O_2 concentrations are low, converting nitrate (NO_3) to N_2 gas, and to a much lesser extent nitrous oxide. Most denitrification in marine environments is coupled to the oxidation of organic carbon. Denitrification accounts for 96% of N removal in the global oceanic N budget with only 4% attributed to organic N burial (Berner and Berner, 2012). The contribution of denitrification in the MS, however, is much smaller, because of low organic matter fluxes and the fully oxygenated conditions of the deep waters.

Reactive P and N are also removed from the WMS and EMS via outflows driven by the anti-estuarine circulation. Thus, dissolved P and N are exported from the EMS with outflow of intermediate water via the Strait of Sicily, while for the WMS, export of dissolved P and N is due to surface water outflow to the EMS through the Strait of Sicily, and outflow of intermediate and deep water to the Atlantic Ocean through the Strait of Gibraltar (Figure 1.2).

1.4 Nutrient cycling in the Mediterranean Sea

1.4.1 Characteristic features of the Mediterranean Sea

The MS is oligotrophic despite being almost entirely surrounded by land, with primary productivity decreasing from approximately 160 g C m^{-2} yr^{-1} in the WMS to 90 g C m^{-2} yr^{-1} in the EMS (excluding the Adriatic and Aegean Seas) (Antoine et al., 1995). The oligotrophy of the MS is attributed to its anti-estuarine circulation (section 1.2). Usually, authors focus on the fate of the dissolved inorganic forms of P and N (essentially, dissolved phosphate and nitrate): ASW flowing into the MS via the Strait of Gibraltar brings relatively low concentrations of dissolved inorganic P (DIP) and dissolved inorganic N (DIN),

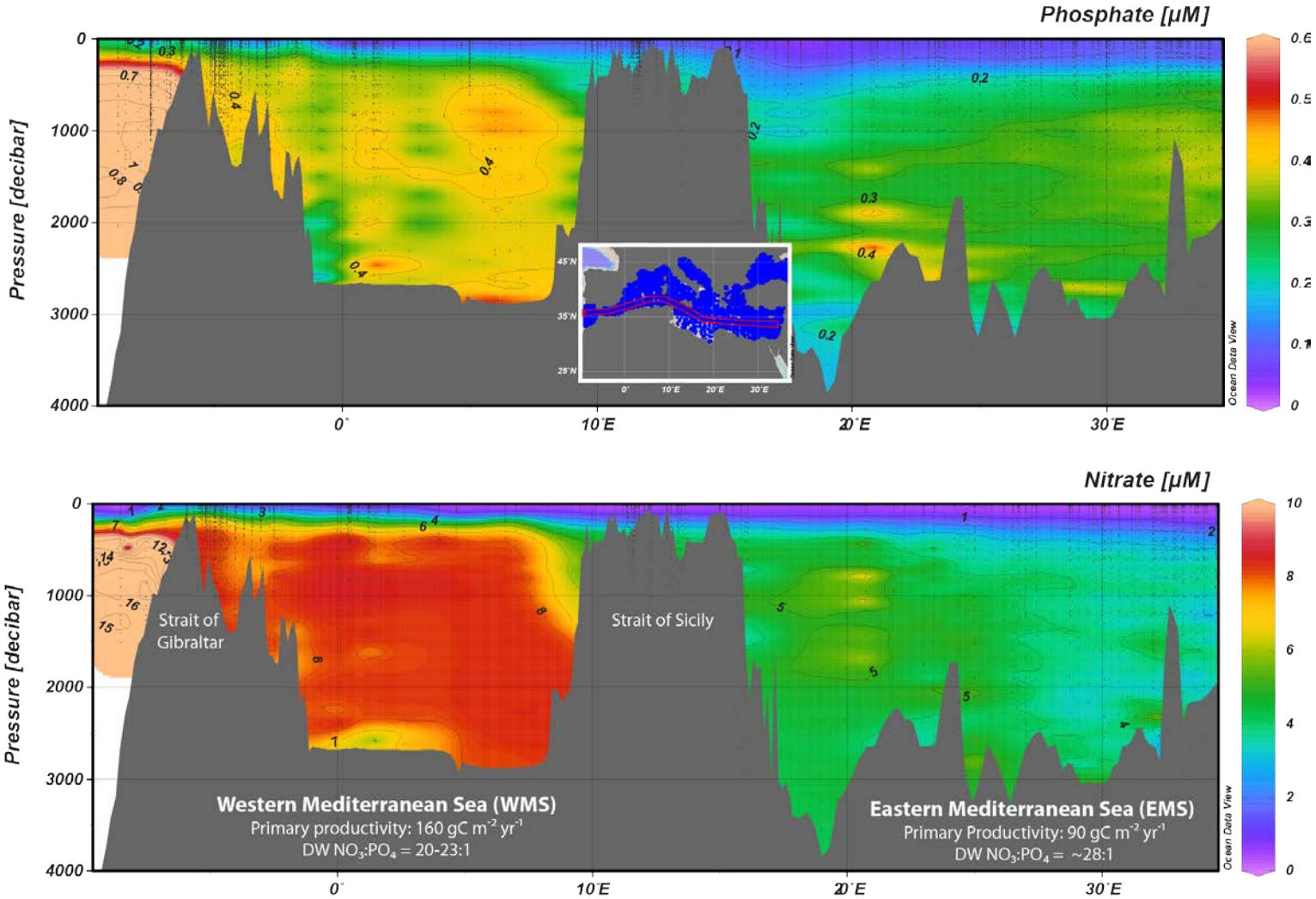

Figure 1.6: West to east cross-section across the Mediterranean Sea of phosphate and nitrate concentrations (µM) from 1909 to 1999 (MEDAR Group, 2002). Note difference in concentration scales between the two cross-sections.

while WMIW and WMDW flowing out into the North Atlantic Ocean export higher DIP and DIN. The increasing oligotrophy from west to east across the MS is reflected in the differences in the average DW DIP and DIN concentrations, decreasing from 1.8 μM DIP and 20 μM DIN in Atlantic deep water, via 0.35 μM DIP and 8 μM DIN in WMDW, to 0.25 μM DIP and 4.5 μM DIN in EMDW (Figure 1.6; Krom et al., 2003).

The EMS is also the largest known marine basin to be unequivocally P limited (Krom et al., 1991) given that most marine systems are considered to be N limited (Ryther and Dunstan, 1971; Howarth and Marino, 2006). During the winter phytoplankton bloom in the EMS, nitrate (NO_3) is still available within the SW while there is no detectable dissolved phosphate (PO_4) (Krom et al., 1992). However, in summer P and N co-limitation may occur (Thingstad et al., 2005a; Tanaka et al., 2011). The situation in the WMS is not so clear. The spring phytoplankton bloom has been reported to be N limited (Marty et al., 2002), N and P co-limited (Pasqueron de Fommervault et al., 2015) or P limited (in particular in the Gulf of Lions; (Diaz et al., 2001). In the stratification period P limitation generally occurs for both phytoplankton and heterotrophic bacteria (Thingstad and Rassoulzadegan, 1995; Thingstad et al., 1998; Marty et al., 2002; Van Wambeke et al., 2002; Pinhassi et al., 2006; Pasqueron de Fommervault et al., 2015).

Further evidence for P limitation is the higher than Redfield molar C:N:P ratios across the entire MS for both inorganic and organic nutrients (except sometimes in the SW). The dissolved organic molar C:N:P ratios (DOC:DON:DOP) in the photic zone (top 200m) of 920-1560:50-220:1 (Santinelli, 2015) are much greater than those observed in the surface waters of the global ocean, 374±59:27±6:1 ((Hopkinson and Vallino, 2005). In contrast, the DW DOC:DON:DOP ratios in the MS of (993-5000):(67-400):1 (Santinelli, 2015) are similar to those of the global ocean DW, (3511±1314):(202±113):1 (Hopkinson and Vallino, 2005). The most commonly reported ratio, however, is the molar NO_3:PO_4 within the DW masses of the MS. This ratio increases from west to east from 20-23:1 in the WMS (Béthoux et al., 1998; Ribera d'Alcalà et al., 2003) to 28:1 in the EMS (Kress and Herut, 2001; Ribera d'Alcalà et al., 2003; Krom et al., 2005), compared to the Redfield ratio of 16:1 normally observed in the global ocean (Redfield et al., 1963). The latter is explained by the balance between denitrification and N_2 fixation (Tyrrell, 1999).

In the pelagic MS, little denitrification is expected because the dissolved O_2 concentrations remain above 70% saturation throughout the water column (>180 μM; Figure D.1). Hence, significant denitrification should be restricted to coastal zones along shallow shelves, for example in the North Adriatic Sea (Degobbis et al., 2000; Karydis and Kitsiou, 2012). In addition, there have never been any reports of high rates of N_2 fixation in the MS (Ibello et al., 2010b; Bonnet et al., 2011). The severe P limitation of the

MS further argues against significant rates of N_2 fixation (Sañudo-Wilhelmy et al., 2001; Krom et al., 2004; Mills et al., 2004). Interestingly, Rahav et al. (2016) recently proposed that heterotrophic N_2 fixation within the EMS is DOC limited. Nevertheless, N_2 fixation has been suggested to be one of the main drivers of the high NO_3:PO_4 ratios observed in the MS (Béthoux et al., 1992). As supporting evidence, the observed ^{15}N depletion of NO_3 in the MS has been invoked (Béthoux et al., 2002b; Pantoja et al., 2002; Ribera d'Alcalà et al., 2003). However, for the EMS Emeis et al. (2010) attribute the ^{15}N depleted isotopic composition of NO_3 to extensive recycling of N together with low $\delta^{15}N$ values of anthropogenic NO_3, in particular in atmospheric deposition. The alternative explanation for the high NO_3:PO_4 ratios of the MS, which is also explored in Chapters 2 and 5, is that they reflect the high NO_3:PO_4 ratio in atmospheric deposition combined with low denitrification rates (Krom et al., 2010).

1.4.2 Impact of circulation changes: EMT and WMT

As a result of the EMT, fresh Aegean water entered the EMDW. This water was relatively depleted in inorganic nutrients and enriched in O_2 relative to the older Adriatic water. The inflow of Aegean DW also caused the uplift of the older Adriatic deep water bringing the inorganic nutrients closer to the photic zone (Klein et al., 1999). However, no significant changes in primary production of the EMS were observed as a consequence of the EMT (D'Ortenzio, 2003; Kress et al., 2012).

Surprisingly, the additional O_2 from Aegean DW was consumed within 4 years of entering the EMDW. In fact, by 1999 lower O_2 concentrations than prior to the EMT were recorded in some localities. Apparently, relatively labile DOC in the Aegean DW was the cause of the rapid O_2 depletion: the estimated O_2 consumption rates within the newly formed DW were more than double those in EMDW prior to the EMT (Roether and Well, 2001; Klein et al., 2003; Kress et al., 2003). In addition, O_2 consumption was predicted to be highest at the end of the peak inflow of Aegean DW in the EMS in 1995, and decreasing afterwards (Kress et al., 2003). Unfortunately, DOC measurements are not available for the same time period. Generally speaking, measurements of dissolved organic matter are not routinely made within the MS. Hence, reconstructing the temporal changes in DOC, DON and DOP is difficult given the limited observations across the MS.

Relatively little work has been done describing the impacts of the WMT on P and N distributions and O_2 consumption in the WMS. Schroeder et al. (2010a) report distinctive O_2, PO_4 and NO_3 concentrations in young and old DW masses during the WMT, with NO_3 concentrations ranging from 7 µM near the DW formation site in the NWM to 9 µM in the older DW, while at the same time PO_4 ranges from 0.40 µM in older water to 0.38 µM in younger water. Reduced O_2 concentrations in the Algero-Provencal basin in

2011 relative to 1991 and 1995 suggest that the WMT also increased O_2 consumption due to the enhanced input of organic matter to the WMDW reservoir (Schneider et al., 2014).

The BiOS system also produces distinct physical and biological signatures in the Adriatic Sea (Civitarese et al., 2010) and potentially the rest of the EMS (Ozer et al., 2016). Low salinity SW in the southern Adriatic Sea is observed when an anticyclonic gyre is present. Surface water entering the EMS through the Strait of Sicily is directed towards the Adriatic Sea leading to elevated inorganic nutrient concentrations and high primary productivity within the south Adriatic Sea. In contrast, high salinity within the South Adriatic Sea is associated with low primary productivity and low inorganic nutrient concentrations, and occurs when a cyclonic gyre is present. This further affects the properties of SW flowing into the Levantine basin. An anticyclonic North Ionian Gyre results in less water entering the Levantine basin with, as a result, higher salinity and inorganic nutrient contents for the SW and newly formed LIW (Ozer et al., 2016). Thus, Ozer and co-authors hypothesize that circulation controls the P and N concentrations in the LIW. Note, however, that this hypothesis is in contrast to Moon et al. (2016) who propose that observed temporal changes in PO_4 and NO_3 concentrations in WMIW and EMIW are due to the inputs of anthropogenic P and N.

1.4.3 Sapropels

The presence of organic rich sapropels in the sedimentary record indicates that the MS has not always been oligotrophic. The most recent sapropel was deposited only 6.4-10.2 kyrs ago (Grimm et al., 2015), with sapropels found to occur periodically until at least 13.5 million years ago (Rohling et al., 2015). Sapropels generally contain 1-10% organic C although extremes of up to 30% have been recorded (Rohling et al., 2015). They are largely confined to the EMS although organic rich layers are observed in the WMS. Sapropels are usually laminated and lack benthic foraminifera, thus suggesting that they were deposited during times of bottom water anoxia (Rohling et al., 2015).

Sapropels are hypothesized to have formed under climatic conditions that were cooler and wetter than today, initiated by Milankovitch cycles (Picotti et al., 2014). African monsoonal rains caused high freshwater discharges to the MS, especially via the Nile River. High freshwater influxes from the Black Sea and the northern MS coastline possibly also occurred. Melting of ice sheets during deglaciation induced sea level rise and a freshening of the SW. Nonetheless, the exact mechanisms responsible for the formation of sapropels are still debated, in particular with regard of the THC of the MS and the balance between primary productivity and preservation during sapropel deposition. Hypotheses to explain sapropel S1, that is, the most recent sapropel, include increased primary productivity due to high nutrient

delivery by rivers, and changes in THC ranging from stagnation to a switch from anti-estuarine to estuarine circulation (Sarmiento et al., 1988; Stratford et al., 2000).

Grimm et al. (2015) used a coupled hydrodynamic-biogeochemical model to run scenarios investigating the formation of S1. They show that an increase in primary production alone would not push the system to anoxia: DW O_2 concentrations would remain elevated even for a factor of three increase in the input of inorganic nutrients to the MS. Their results suggest that S1 deposition was primarily driven by deglaciation, which caused stagnation of the MS water column. They also found that a preconditioning period of at least 5500 years was required before stagnation ultimately resulted in anoxic bottom waters. In the scenarios investigated, increased nutrient inputs to the MS were not required to produce the particulate organic C (POC) burial fluxes during S1 deposition, although higher POC deposition fluxes at the seafloor are not excluded. These results of Grimm and co-workers imply that estuarine circulation or increased external nutrient inputs are not essential conditions for sapropels to form.

A number of climate change projections for the coming decades indicate that the THC of the MS may become increasingly stagnant (section 1.2). This creates a concern that the deep waters of the MS may become anoxic at some point in the future. This topic is addressed in Chapter 4 of this thesis.

1.5 Phosphorus and nitrogen models of the Mediterranean Sea

Models investigating nutrient cycles in marine systems vary in complexity. The simplest approach involves building a mass balance budget where all inputs to and outputs from the system are quantified, often integrated over a relatively long time period. This approach has been used for the MS (Béthoux et al., 1992; Ribera d'Alcalà et al., 2003; Krom et al., 2004; Huertas et al., 2012). Nutrient budgets for the MS typically contain inputs of inorganic P and N from atmospheric deposition, riverine input and water exchanges through the Straits of Sicily and Gibraltar (i.e. Krom et al., 2004; Huertas et al., 2012). However, they often neglect the contributions of DOP and DON to the nutrient budgets. In addition, despite the MS being almost entirely landlocked with many cities close to the shoreline, direct wastewater discharges to the sea have so far been neglected in P and N budgets (see Chapter 3). Inputs of DIP and DIN via SGD into the MS has only been quantified in recent years (Rodellas et al., 2015). Rodellas et al. (2015) claim that SGD is an important contributor to nutrient budgets of the MS, although they calculate inputs through re-circulated seawater rather than from the much smaller inflow of freshwater. Finally, losses of P and N associated with sediment burial and denitrification are sometimes ignored in mass balance budgets (i.e., Béthoux et al., 1992; Ribera d'Alcalà et al., 2003).

The majority of dynamic nutrient models for the MS focus on ecosystem processes, mainly those occurring in the euphotic layer on monthly to seasonal timescales. These models have been applied to specific locations (i.e. DYFAMED site; Levy et al., 1998; north west Mediterranean; Auger et al., 2014; south east Mediterranean; Suari and Brenner, 2015) or to the entire MS. Models investigating the entire MS vary from more simple one-dimensional (1D) coupled hydrodynamic-ecology models simulating steady state conditions (Crispi et al., 2001; Allen et al., 2002) to 3D hydrodynamic-biogeochemical models that incorporate up to 9 planktonic groups and five elements (P, N, silicon, C and O_2) (Crispi et al., 2002; Lazzari et al., 2012; Mattia et al., 2013; Macias et al., 2014; Guyennon et al., 2015).

Simpler models may sometimes provide deeper insights into the overall functioning of a biogeochemical system than more complex models that include a large number of processes and forcings. Crispi et al. (2001), for example, use a simple box modeling approach to conclude that the anti-estuarine circulation alone does not entirely explain the oligotrophic nature of the MS. They find that the downward fluxes of organic matter, and thus the biological pump, are key in maintaining oligotrophy. In addition, they show that trophic gradients from east to west across the MS arise from unbalanced loads between the seas and are maintained by the biological pump. Using a 1D model, Allen et al. (2002) illustrate the importance of mixing processes in the MS in explaining primary production. Their model results indicate that bacterial production is nutrient limited in the EMS and grazer controlled in the WMS, with higher levels of heterotrophic activity in the WMS than EMS.

Only two published modeling studies attempt to investigate the long-term (decadal timescales) biogeochemical changes across the entire MS (Béthoux et al., 1992; Macias et al., 2014). Bethoux et al. (1992) used measured PO_4 concentrations in the DWs of the WMS and EMS to derive changes in atmospheric deposition and terrestrial inputs of PO_4 and NO_3 over the 1960-2000 time period. They then use the inputs to model the evolution of PO_4 concentrations in the WMDW and EMDW reservoirs. Macias et al. (2014) use a coupled hydrodynamical-biogeochemical model to investigate relative changes in primary productivity and zooplankton density in the MS between 1960 and 2010. They validate their results with data on fishery catches in the MS. However, their modeling study only accounts for the temporal changes in inputs of NO_3 and PO_4 from rivers.

Very few modeling studies address the impacts of climate change on the biogeochemistry across the whole MS. Lazzari et al. (2014) use a 3D hydrodynamic-biogeochemical model and consider one potential circulation scenario. They compare their model results for the period 2090-2100 to the baseline results for the period 1990-2000. Only the riverine inputs of PO_4 and NO_3 to the sea are varied over time. Their results highlight the effect of increasing water temperatures on reaction kinetics and thus

metabolism with both gross primary production and respiration rates increasing. Macias et al. (2015) use a dynamic approach and four atmospheric forcing scenarios to investigate the impact of climate change on primary production in the MS. However, in their scenarios, P and N inputs are assumed to remain constant. Finally, the only other modeling study that examines the potential impacts of climate change on marine biogeochemistry is by Herrmann et al. (2014), who simulate the effect of climate change in the north-west Mediterranean by imposing the circulation scenario developed by Somot et al. (2006).

A review of current biogeochemical models for the MS indicates that some models ignore external inputs of nutrients by rivers arguing that these inputs do not reach the pelagic domain. Inputs from atmospheric deposition are also often ignored, although existing nutrient budgets indicate they can be a significant source of P and N to the WMS and EMS. A recent 1D model for the EMS indicates that including atmospheric deposition increases predicted primary production by 5 to 35% (Christodoulaki et al., 2013). In addition, atmospheric deposition may be important in controlling the unusually large NO_3:PO_4 ratios of the DW of the MS (Krom et al., 2010; Christodoulaki et al., 2013; Christodoulaki et al., 2016). However, few existing modeling studies attempt to explain the unusual N:P ratios found in the MS or assess the long-term (10-100 years) effects of changes in the inputs of reactive P and N on nutrient distributions and primary production. This thesis intends to help remediate some of these shortcomings.

1.6 Thesis

The overall objective of this thesis is to carry out a comprehensive and quantitative analysis of P and N cycling in the MS, specifically to understand the processes responsible for the unique features of these cycles. In addition, a key task is to account for the changes in P and N inputs into the MS driven by human activity. The results of this thesis therefore contribute to a better delineation of how anthropogenic forcings are altering the biogeochemical functioning of this marine basin. The modeling approach used in this thesis is based on relatively simple mass balance, or box models. These models require relatively little data and have low temporal and spatial resolution, yet they can yield some profound insights into the large scale dynamics of a biogeochemical system such as the MS. The basic mass balance equations in box models is:

$$\frac{dM_i}{dt} = inputs_i - outputs_i \qquad (1.2)$$

where $\frac{dM_i}{dt}$ is the change with time of the mass of a given chemical compound in the *i*-th reservoir, while $inputs_i$ ($outputs_i$) correspond to the sum of all inputs (outputs) of the compound to (from) the reservoir.

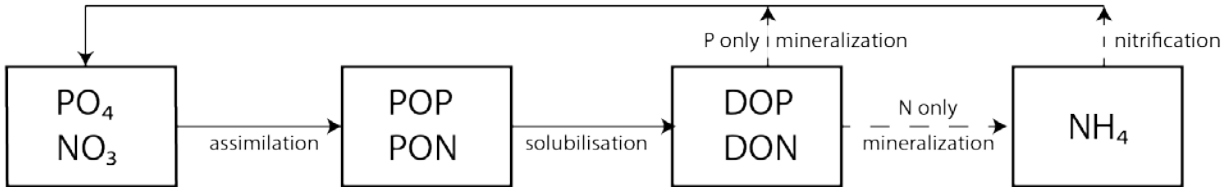

Figure 1.7: Simplified nutrient cycling included in the P and N mass balance model used in this thesis. Note that assimilation of PO_4 and NO_3 only occurs in surface water, while the other processes also take place in the intermediate and deep water masses.

A large part of this thesis focuses on the effects of anthropogenic forcings on P and N cycling in the MS in the period 1950-2030 and beyond. The 1950-2030 period is chosen because anthropogenic inputs of P and N, to aquatic systems in general (Figures 1.3, 1.4) and the MS in particular, substantially increased after 1950. In addition, the relatively short residence times of Mediterranean deep waters of 20-150 years (Roether and Schlitzer, 1991; Stratford et al., 1998; Roether and Well, 2001) means that the effect of anthropogenic nutrient enrichment may in principle be observable in the DW masses over this time period. The mass balance P and N models presented in this thesis are initialized for the year 1950 (see Appendix A for details on initialization) assuming that anthropogenic inputs had little impact on biogeochemical cycling in the MS prior to this time period. It is further assumed that in 1950 the circulation and the P and N cycles within the MS were at steady state.

1.6.1 Research Questions

This thesis addresses the following research questions:

1. What causes the west to east differences in phosphate (PO_4) and nitrate (NO_3) concentrations, primary productivity and NO_3:PO_4 DW ratios in the MS?
2. Why does the MS have a high DW NO_3:PO_4 ratio in comparison to the rest of the world's oceans?
3. Are direct discharges of domestic wastewater into the MS an important component of the MS nutrient budget?
4. How have humans modified nutrient cycling in the MS since 1950? Why is the MS oligotrophic despite being surrounded by land?
5. Can anthropogenic reactive P and N inputs be detected within water column nutrient measurements in the MS?
6. How will climate change impact biogeochemical cycling in the MS?

1.6.2 1950 steady state EMS model (Van Cappellen et al., 2014; Appendix A)

The building block of this thesis is a steady state biogeochemical model of P and N cycling in the EMS for 1950 created by Van Cappellen et al. (2014) and presented in Appendix A. This section briefly describes the model created by Van Cappellen et al. and explains terminology used throughout this thesis specifically related to P and N cycling in the MS. The water column of the EMS is split into three layers: surface water, intermediate water and deep water (Figures 1.2 and A.1). The Adriatic and Aegean Seas are excluded from the model domain. Water is transferred between the Adriatic and Aegean Seas and the

EMS through the Otranto Strait and Cretan Strait, respectively, and between the WMS and EMS through the Strait of Sicily.

The term nutrient includes both the dissolved inorganic and dissolved organic forms P and N. The reactive P species considered in the model are: dissolved inorganic P or soluble reactive P, referred to as phosphate or PO_4 in this thesis; particulate organic phosphorus (POP) and dissolved organic phosphorus (DOP). The reactive N species considered in this thesis are: nitrate (including nitrite) (NO_3), ammonium (NH_4), particulate organic nitrogen (PON) and dissolved organic nitrogen (DON). Intermediate species such as nitrite (NO_2), nitrous oxide (N_2O) and nitric oxide (NO) created during processes such as ammonification (termed mineralization in this thesis), nitrification and denitrification are not explicitly included as they are only present in extremely low concentrations in marine systems.

Figure 1.7 shows the schematic of the P and N cycles used within each water layer for this thesis. The transformation of POP and PON to DOP and DON respectively within the model is termed solubilization. Processes involving the microbial loop are all lumped together in this pathway and include hydrolysis, passive diffusion or active exudation from phytoplankton, viral and bacterial induced cell lysis, sloppy feeding by zooplankton and bacteriavory. Mineralization is the transformation of DOP and DON back into inorganic P and N and is primarily undertaken through enzymatic hydrolysis. Finally nitrification occurs converting NH_4 to NO_3. Note we do not include NH_4 assimilation in the model as isotopic analysis suggest that recycling of NH_4 into NO_3 is an important process (Emeis et al., 2010) and the winter phytoplankton bloom in the EMS and spring phytoplankton bloom in the WMS are fed by NO_3 mixed into the photic zone. Primary production within the model is assumed to be P limited so the assimilation of NO_3 is 16 times that of PO_4 assimilation, following the Redfield ratio for uptake (Equation 1.1).

1.6.3 Organization

This thesis is arranged as a series of five research papers (Chapters 2-6). Each chapter builds upon the previous, adding an additional feature or complexity to the model. Chapter 2, published in *Journal of Marine Systems* (Powley et al., 2014), uses the steady model of P and N cycling in the EMS (Appendix A), to investigate how humans have altered the biogeochemical cycling of P and N in the EMS between 1950 and 2000. In addition the role of changing circulation due to the EMT in altering primary productivity and nutrient reservoirs of the EMS is also investigated. Direct wastewater discharges were not included in the EMS model in Chapter 2 and Appendix A for a lack of quantification of these discharges to the MS within the literature, despite the MS having a long coastline and high coastal populations. Thus Chapter 3 quantifies the direct domestic wastewater discharges into the MS using an

empirical modeling approach and a published database of wastewater resources in coastal cities of the MS, and is published in *Environmental Science &Technology* (Powley et al., 2016a).

A key conclusion of Chapter 2 and Appendix A is the important role of exchanges of water and nutrients across the Strait of Sicily in controlling the P and N cycles in the EMS. Therefore, in Chapter 4 a water cycle model for the WMS is created and coupled to the pre-existing EMS circulation model. In addition, an O_2 model is created to investigate how climate change may alter O_2 concentrations in the MS both in the near future and on long-term timescales. This chapter is published in the *Journal of Geophysical Research: Oceans* (Powley et al., 2016b). In Chapter 5 the water cycle for the entire MS created in Chapter 4 is used to create a model for the coupled biogeochemical cycling of P and N in 1950 for the WMS and coupled to the pre-existing EMS model (Appendix A and Chapter 2). Direct discharges of wastewater inputs into the MS are included for the first time in P and N budgets for the MS using data from Chapter 3. This model is used to explain the unique biogeochemistry of the MS such as the differences in PO_4 and NO_3 concentrations, primary productivity and N:P ratios from west to east across the basin. Chapter 5 is currently under review in *Global Biogeochemical Cycles*. Finally, Chapter 6 uses the model created in Chapter 5 to elucidate the role of anthropogenic P and N inputs to the MS between 1950 and 2030 versus the role of inter-annual variability in IW and DW formation on controlling the temporal changes in key biogeochemical parameters in the MS.

Chapter 2.

A biogeochemical model of phosphorus and nitrogen cycling in the Eastern Mediterranean Sea.

Part 2.

Response of nutrient cycles and primary production to anthropogenic forcing: 1950-2000

Modified from: **Helen R. Powley**, Michael D. Krom, Kay-Christian Emeis, and Philippe Van Cappellen. (2014) A biogeochemical model for phosphorus and nitrogen cycling in the Eastern Mediterranean Sea. Part 2. Response of nutrient cycles and primary production to anthropogenic forcing: 1950-2000. *Journal of Marine Systems,***139**, 420-432, doi: 10.1016/j.jmarsys.2014.08.017.

2.1 Summary

Anthropogenic inputs of nutrient phosphorus (P) and nitrogen (N) to the Eastern Mediterranean Sea (EMS) increased significantly after 1950. Nonetheless, the EMS remained ultra-oligotrophic, with eutrophication only affecting a restricted number of nearshore areas. To better understand this apparent contradiction, we reconstructed the external inputs of reactive P and N to the EMS for the period 1950 to 2000. Although the inputs associated with atmospheric deposition and river discharge more than doubled, the inflow of surface water from the Western Mediterranean Sea (WMS) remained the dominant source of nutrient P and N to the EMS during the second half of the 20th century. The combined external input of reactive P rose by 24% from 1950 to 1985, followed by a slight decline. In contrast, the external reactive N input increased continuously from 1950 to 2000, with a 62% higher input in 2000 compared to 1950. When imposing the reconstructed inputs to the dynamic model of P and N cycling in the EMS developed in Appendix A, a maximum increase of primary production of only 16% is predicted. According to the model, integrated over the period 1950-2000, outflow of Eastern Mediterranean Intermediate Water to the WMS exported the equivalent of about one third of the P supplied in excess of the 1950 input, while another one third was translocated to the Eastern Mediterranean Deep Water. Together, both mechanisms efficiently counteracted enhanced P input to the EMS, by drawing nutrient P away from primary producers in the surface waters. Furthermore, between 1950 and 2000, inorganic and organic dissolved N:P ratios increased in all water masses. Thus, the EMS became even more P limited because of anthropogenic nutrient inputs. A model simulation incorporating the circulation changes accompanying the Eastern Mediterranean Transient between 1987 and 2000 yielded a 4% increase of EMS primary productivity relative to the baseline scenario.

2.2 Introduction

The Eastern Mediterranean Sea (EMS) is nearly completely surrounded by land. In addition, the watershed of the EMS is experiencing rapid demographic growth and economic development, much of which is concentrated in the coastal areas. Relative to 1970, the number of people living in the countries bordering the EMS had increased by 50% by the year 2000 – in 2025 it will have doubled (UNEP/MAP, 2012). The resulting anthropogenic pressures on the EMS raise concerns about the environmental and ecological consequences, including the impacts of habitat loss, eutrophication, overfishing, invasive species, pathogens and climate change (UNEP-MAP-RAC/SPA, 2010).

A dominant anthropogenic driver of ecological change of marine environments is the increased supply of macronutrients, in particular phosphorus (P) and nitrogen (N). Worldwide, anthropogenic P and N loadings have risen dramatically since the 1950s (Mackenzie et al., 2002; Galloway et al., 2004; Seitzinger et al., 2005). This is also the case for the EMS (this chapter). However, while in other semi-enclosed marine basins, such as the Baltic Sea, increased supplies of P and N have caused widespread eutrophication in both coastal and open water areas (Larsson et al., 1985; Gray et al., 2002; Helcom, 2010), in the EMS eutrophication appears to be limited to a few specific coastal areas (Karydis and Kitsiou, 2012). The existing evidence does not support significant increases in primary production or inorganic nutrient concentrations at the scale of the entire EMS (Krom et al., 2010; Appendix A).

In the companion paper, we developed a dynamic mass balance model for the coupled P and N cycles in the EMS (Appendix A). The model is based on a simple representation of the water cycle of the EMS. However, in contrast to most previous mass balance studies of the EMS (e.g., Béthoux et al., 1998; Ribera d'Alcalà et al., 2003; Krom et al., 2004), the model explicitly accounts for the organic reservoirs of P and N. The model was initialized for the year 1950, assuming relatively limited prior anthropogenic disturbance of the nutrient cycles (Béthoux et al., 1998). The model explains the ultra-oligotrophic nature of the EMS and the systematically higher-than-Redfield N:P ratios observed in the water column. Results of sensitivity analyses underline the key roles of circulation within the EMS, water exchanges with adjacent basins, most importantly with the Western Mediterranean Sea (WMS), and the nature and extent of organic P and N recycling processes.

In the present paper, we reconstruct the P and N loadings to the EMS for the period 1950-2000. The latter time interval is chosen because (1) the available information sources provide a reasonable coverage for this time period, and (2) the EMS experienced the largest inputs of anthropogenic P and N during the second half of the 20th century. The time-dependent P and N loadings from 1950 to 2000 are then imposed as input to the coupled P and N cycling model, which is run forward in time starting from the

initial 1950 conditions. The goal of the simulations is to predict the basin-wide changes in P and N cycling and primary production driven by the inputs of anthropogenic nutrients, on a decadal timescale. Particular attention is given to the fate of the excess anthropogenic nutrients added to the EMS, the partitioning of the nutrient elements between their inorganic and organic pools, the changes in water column N:P ratios, and the implications for nutrient data acquisition. Where possible, the predictions are compared to existing data, including data that were not used in developing and initializing the coupled P and N cycling model.

2.3 Phosphorus and nitrogen inputs: 1950-2000

2.3.1 Anthropogenic forcing functions

In the model, the water column is divided in three layers: Eastern Mediterranean surface water (EMSW; 0-200m), Eastern Mediterranean Intermediate Water (EMIW, 200-500m; commonly termed Levantine Intermediate Water (LIW) within the literature) and Eastern Mediterranean Deep Water (EMDW, >1500m). External inputs of reactive P and N are supplied to EMSW via rivers, inflow from the WMS plus atmospheric deposition, and to EMDW via deep water formation in the Adriatic and Aegean Seas. The model differentiates between the following reactive P pools: dissolved inorganic phosphorus (PO_4), dissolved organic P (DOP) and particulate organic P (POP). For N, the reactive pools are dissolved nitrate plus nitrite (NO_3), dissolved ammonium (NH_4), dissolved organic nitrogen (DON), and particulate organic nitrogen (PON).

Post-1950 changes of the inputs are considered to be mainly due to anthropogenic factors. The anthropogenic forcing function describing the input of a given P or N species *i* from an external source *j* is then defined as:

$$f_{ij} = \frac{\text{input flux}(t)}{\text{input flux}(1950)} \qquad (2.1)$$

where time *t* corresponds to the year of interest. Values for the 1950 input fluxes are those given in Appendix A. The 1950 inputs of reactive P and N to the EMS are used as starting point for the model simulations.

Because the earliest research cruises in the EMS date back to the late 1950s, little data are available to assess the state of the EMS at earlier times. Our work further leans heavily on the systematic reconstruction of riverine P and N fluxes into the Mediterranean Sea by Ludwig et al. (2009). These authors carried out their analysis up to 1998. The model simulations therefore are limited to the second

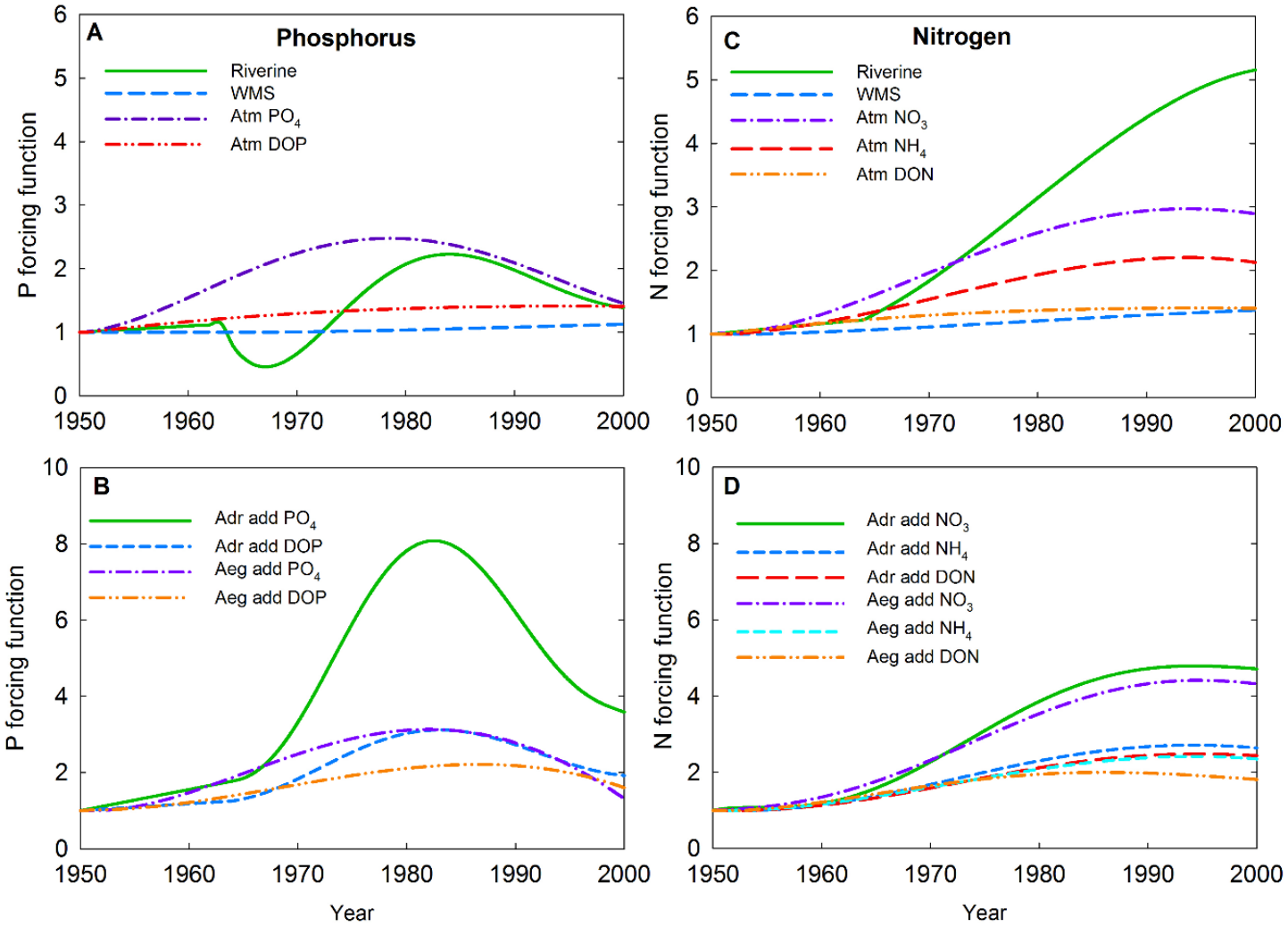

Figure 2.1: Anthropogenic forcing functions of P and N imposed in the model simulations. For each external source, the forcing function indicates, at any given time, the change in input relative to the corresponding 1950 input (Equation 2.1 in text). Symbols: atm = atmospheric deposition; Adr = Adriatic deep water formation; Aeg = Aegean deep water formation; add = additional nutrient acquired by EMIW during Adriatic or Aegean deep water formation (see text for details).

half of the 20th century, which is also the time interval when anthropogenic inputs of the limiting nutrient P to the EMS peaked (this chapter). During the latter part of the 20th century, circulation in the EMS further underwent a major perturbation known as the Eastern Mediterranean Transient or EMT. As the latter is well characterized (Roether et al., 1996; Roether et al., 2007), we are able to account for the circulation changes accompanying the EMT in the model simulations. Thus, the time period 1950-2000 offers the opportunity to investigate the response of the P and N cycles in the EMS to changes in the inputs of the nutrient elements, while minimizing the effects of unknowns or potential confounding factors.

2.3.2 Rivers

Riverine inputs of P and N to the Ionian and Levantine Basins are obtained from Ludwig et al. (2009). These authors provide nutrient fluxes at river mouths for every 5 years between 1963 and 1998. (Note: between 1950 and 1963, we assume a linear forcing function for the riverine inputs, using the 1950 input fluxes estimated in Appendix A. Ludwig and coworkers further estimate that, on average, 48% of the total riverine P flux is delivered as PO_4, 8% as DOP and the rest as particulate P. Because of the P-starved nature of the EMS, Appendix A assumes that 75% of the particulate riverine P flux is eventually solubilized to PO_4. For N, Ludwig and coworkers estimate that, on average, 75% of total N from rivers occurs as NO_3, 20% as DON and 5% as NH_4. In the absence of more definitive constraints, we impose the same, constant proportions of riverine P and N species during the period 1950 to 2000.

Closure of the Aswan High Dam in 1965 caused a major perturbation of the riverine supply of P to the EMS. According to Nixon (2003), before the dam was completed more than half of the reactive P delivered by the Nile River to the EMS was derived from the desorption of PO_4 from suspended particulate matter. After 1965, sediment was trapped in Lake Nasser, hence drastically reducing the P flux from the Nile River. As reactive N in rivers primarily occurs in the dissolved load, a similar drop of the Nile River N flux to the EMS did not occur. Rasmussen et al. (2009) further propose that by the end of the century, the P flux from the Nile delta to the EMS had recovered to pre-dam values, because of increasing sewage discharges into coastal lagoons and subsequent leakage into the EMS.

The reconstructed forcing functions for the surface flow inputs of P and N to the EMS are shown in Figure 2.1 (see Appendix B for numerical values). Note that, in addition to the nutrient fluxes delivered by rivers to the EMS, the forcing functions account for dissolved P and N supplied via the surface inflows from the Adriatic Sea and Aegean Sea. As the latter represent very small contributions to the total external inputs of reactive P and N to the EMS (<1%), they are kept constant during the simulations. The decrease in the forcing function for P during the late 1960s reflects the closure of the Aswan High Dam:

by 1967 the riverine P influx to the EMS is estimated to have dropped to half of its 1950 value. After the 1967 minimum, the anthropogenic forcing function rises again due to the increasing use of P fertilizers and detergents, as well as expanding sewerage around the basin. It reaches a peak value of 2.2 in the early 1980s, followed by a decreasing trend because of the ban on P detergents and upgrades of wastewater treatment plants (Ludwig et al., 2009). Hence, by the year 2000, the riverine PO_4 and DOP inputs to the EMS are estimated to be comparable to those in the mid 1970s. Unlike P, the resulting forcing function for riverine inputs of N increases steadily from 1950 to 2000, to a maximum of 5.2 in 2000, due principally to the continued rise in diffuse agricultural and sewage inputs.

2.3.3 Inflow from the Western Mediterranean Sea (WMS)

According to our previous estimations, the inflow of Western Mediterranean Surface Water (WMSW; commonly termed Modified Atlantic Water in the literature) through the Strait of Sicily represents the major external input of dissolved P and N to the EMS in 1950 (Appendix A). In addition, DOP and DON dominate the inputs associated with the inflow of WMSW. Relative changes in WMSW PO_4 input from 1950 to 2000 are assumed to parallel the changes in water column PO_4 concentrations of the Western Mediterranean Sea (WMS) reported by Béthoux et al. (1992) for the period 1960-1990, augmented with more recent PO_4 concentrations obtained by Moutin and Raimbault (2002). The resulting time series of PO_4 concentrations show a slow but continuous increasing trend during the second half of the 20^{th} century (Figure 2.1A and Appendix B). The corresponding modeled influx of PO_4 from the WMS for the year 2000 is 1.80×10^9 mol P yr^{-1}. For a water inflow rate through the Strait of Sicily of 1.14 Sv (Appendix A), this corresponds to a PO_4 concentration of 50 nM. The latter value matches depth-integrated PO_4 concentrations measured across the upper 200 m of the WMS in recent decades (Moutin and Raimbault, 2002; Pujo-Pay et al., 2011), although it is somewhat lower than the concentration of 80 nM reported by Karafistan et al. (2002) for the top 50 m of water in the Strait of Sicily.

A major source of uncertainty in reconstructing nutrient supply from the WMS is the very limited data on DOP and DON concentrations in waters flowing from the WMS into the EMS. Hence, unless stated otherwise, the molar PO_4:DOP ratio is kept fixed at the baseline value of 0.48, which agrees with the data of Banoub and Williams (1972) and Moutin and Raimbault (2002). These authors report DOP concentrations in surface waters of the WMS approximately twice those of PO_4, although they performed their measurements 30 years apart. The effect of changes in P speciation of inflowing WMSW was further tested by allowing the PO_4:DOP ratio to randomly vary from year to year in the range 0.36-0.60. These variations, and similar year-to-year random variations of the PO_4 concentration of WMS inflow by ±10%, have negligible impacts on the model outcomes (results not shown).

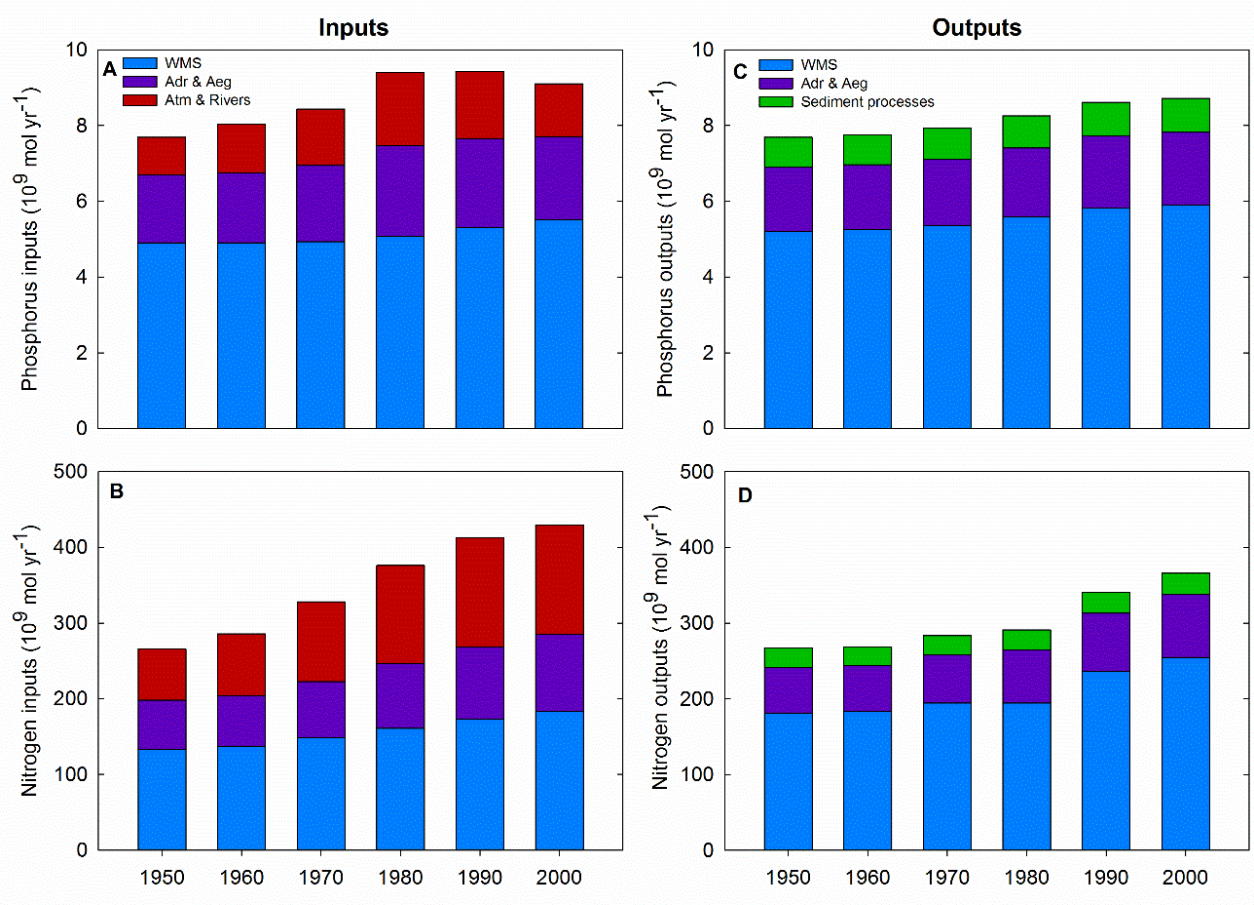

Figure 2.2: Fluxes of reactive P and N from external sources into the EMS (Inputs), and export fluxes of reactive P and N from the EMS (Outputs), over the time period 1950-2000. Note the difference in scales for the P and N fluxes. Symbols: WMS = inflow from (Inputs) and outflow to (Outputs) the Western Mediterranean Sea; Adr & Aeg = deep water inflow from (Inputs) and outflow of EMIW to (Outputs) the Adriatic and Aegean Seas; Atm & Rivers = atmospheric deposition, river discharge and surface inflow from the Adriatic and Aegean Seas; Sediment processes = sedimentary burial (for P and N) plus denitrification (for N only).

Riverine N inputs to the WMS rose faster than those of P during the second half of the 20th century (Ludwig et al., 2009). It is thus reasonable to assume that the dissolved N inputs associated with inflow of WMSW from 1950 to 2000 systematically outpace the rise in P inputs. Due to scarcity of time series data on WMSW nutrient concentrations, the N forcing function is adjusted until the modeled nitrate input through the Strait of Sicily in 2000 matches reported water inflow from the WMS and WMS surface water NO_3 concentrations around the turn of the century. The resulting modeled NO_3 input flux from the WMS in 2000 is 44×10^9 mol N yr^{-1}, which, for an imposed water flow of 1.14 Sv, corresponds to a WMS surface water concentration of 1.2 µM, which agrees with observed values (1.2-1.6 µM; Moutin and Raimbault, 2002; Pujo-Pay et al., 2011). As for P, the same forcing function is applied to all the dissolved N species (Figure 2.1C and Appendix B). Measurements in the 1970s and early 2000s yield molar NO_3:DON ratios between 0.26 and 0.35 (Banoub and Williams, 1972; Moutin and Raimbault, 2002; Pujo-Pay et al., 2011), that is, values consistent with the NO_3:DON ratio of 0.32 imposed in the model simulations. (Note: similar to P, random year-to-year variations in the NO_3 concentration of the WMS inflow to the EMS by ±10% have a negligible effect on the predicted nutrient distributions.) According to the forcing functions, in 2000 the dissolved P and N inputs from the WMS are, respectively, 13 and 38% higher than in 1950. Furthermore, during the entire second half of the 20th century, inflow of WMSW from the WMS remains the major external supply of P and N to the EMS (Figure 2.2).

2.3.4 Atmospheric deposition

Saharan dust is the principal source of soil-derived mineral P to the EMS (Krom et al., 2004). However, the fraction of soluble PO_4 that is released to seawater from deposited dust depends on the extent of acid processing of the mineral aerosols in the atmosphere, when Saharan dust mixes with polluted air masses emanating from Europe, and in recent decades increasingly from the Middle East (Nenes et al., 2011). As the acids reacting with the mineral aerosols are predominantly H_2SO_4 and HNO_3, we assume that the anthropogenic forcing on the atmospheric input of PO_4 to the EMS is controlled by the emissions of SO_2 and NO_x from Europe, Africa, and the Middle East. An atmospheric PO_4 forcing function is then constructed by combining estimates of regional and global SO_2 and NO_x emissions (Lamarque et al., 2010; Smith et al., 2011). The resulting PO_4 forcing function increases more than 2-fold from 1950 to 1979, and decreases thereafter mainly because of the decline in SO_2 and NO_x emissions from Europe (Figure 2.1A and Appendix B).

The forcing functions for atmospheric deposition of inorganic N are assumed to parallel the nitrate and ammonium depositional fluxes obtained from alpine ice cores by Preunkert et al. (2003) and Fagerli et al. (2007), respectively. This yields nitrate deposition fluxes that increase three-fold from 1950 to the 1990s, followed by a slow decline thereafter (Figure 2.1B and Appendix B). The initial large increase reflects

increased atmospheric pollution over Western and Central Europe due to industrial processes and vehicle use, while the introduction of catalytic converters and cleaner methods of burning fuel explains why NO_x emissions level off after 1990 (Preunkert et al., 2003). The forcing function for ammonium deposition follows a comparable trend (Figure 2.1C and Appendix B), although its main source are emissions of ammonia associated with agricultural activities (van Aardenne et al., 2001). Furthermore, the rate of ammonium aerosol formation from ammonia plays a key role in regulating NH_4 deposition fluxes (Fagerli et al., 2007). Because atmospheric NH_4 aerosol formation is limited by the availability of H_2SO_4 and HNO_3 in the atmosphere, the decline of SO_2 and NO_x since the mid-1980s explains the decrease in the forcing function for NH_4 deposition after 1990 (Fagerli et al., 2007).

Deposition fluxes of inorganic P and N derived from the forcing functions are consistent with available data on wet and dry deposition for the EMS. Herut et al. (1999) report an average PO_4 deposition flux (wet plus dry leachable) of 580 μmol P m^{-2} yr^{-1} for the period 1992 to 1998. Extrapolated over the entire surface area of the EMS ($1336x10^3$ km^2) this gives a deposition flux of $0.77x10^9$ mol P yr^{-1}, which agrees well with the range $0.60\text{-}0.75x10^9$ mol P yr^{-1} predicted from the forcing function for the same time interval. Using measurements obtained in 2001 and 2002 at 7 stations across the EMS, Markaki et al. (2010) estimate PO_4 depositional fluxes between $0.32x10^9$ and $0.64x10^9$ mol P yr^{-1}, which bracket the predicted deposition flux of PO_4 for the year 2000 ($0.55x10^9$ mol P yr^{-1}). Based on the same data set, Markaki et al. (2010) obtain deposition fluxes of soluble inorganic N between 24 and $104x10^9$ mol N yr^{-1}, compared to the predicted depositional flux in 2000 of $86x10^9$ mol yr^{-1} ($57x10^9$ mol NO_3 yr^{-1} + $29x10^9$ mol NH_4 yr^{-1}).

The limited available data indicate that organic P and N typically represent between 5 and 40% of the total water-soluble P and N in atmospheric deposition (Cornell et al., 2003; Chen et al., 2007; Cape et al., 2011b; Jickells et al., 2013). Recent measurements by Markaki et al. (2010) and Violaki et al. (2010) for the EMS fall toward the higher end of this range: based on their measurements, we assume that in 2000 DOP and DON represent 38 and 32% of total deposited water-soluble P and N, respectively. The deposition fluxes of DOP and DON for the year 2000 are then calculated using these fractions and the previously estimated inorganic P and N deposition fluxes of inorganic P and N for 2000. In contrast to their inorganic counterparts, however, very little is known about the historical trends in DOP and DON deposition (Cape et al., 2011b). Here, we assume that the atmospheric deposition fluxes of DOP and DON in the EMS correlate with changes in biomass burning in the northern hemisphere. A forcing function for DOP and DON is then derived from the work of Ito and Penner (2005), who provide regional estimates of organic carbon emissions from biomass burning between 1870 and 2000. The resulting forcing function represents a rough, preliminary guess, given the multiple sources and transfer pathways

of atmospheric DOP and DON (Cornell et al., 2003). According to the forcing function, DOP and DON deposition fluxes increase from 1950 till the mid 1990s, and subsequently remain nearly constant at levels ~40% higher than in 1950 (Figure 2.1A, 1C and Appendix B).

2.3.5 Deep water formation

In the model, the fluxes of dissolved P and N associated with deep water inflow from the Adriatic and Aegean Seas into the EMDW reservoir change over time due to variations in (1) the concentrations of dissolved P and N in EMIW that upwells into the Adriatic Sea and Aegean Sea, and (2) the inputs of land-derived P and N loadings to the Adriatic Sea and Aegean Sea (for details, see Appendix A). Time variable EMIW concentrations of dissolved P and N are accounted for automatically in the model simulations, as concentrations of the various P reservoirs in the EMS are updated at each time step. Therefore, we only derive forcing functions that account for the additional P and N supplied to the Adriatic Sea and Aegean Sea by rivers and atmospheric deposition.

Relative changes in riverine inputs are calculated as in section 2.3.2 from the river P and N fluxes to the Adriatic and Aegean seas given by Ludwig et al. (2009). For the Aegean Sea, the Black Sea represents a further source of dissolved N (Krom et al., 2004). From samples collected between 1986 and 1992, a net flux of DON through the Bosphorus of 9.1×10^9 mol N yr^{-1} is estimated (Polat and Tugrul, 1995). The variability of this DON inflow over the period 1950-2000 is assumed to correlate with the relative changes in the reactive N river fluxes to the Black Sea provided by Ludwig et al. (2009). Based on the existing data, the Black Sea is assumed to be a negligible source of dissolved P and dissolved inorganic N to the Aegean Sea (Krom et al., 2004). For the atmospheric deposition fluxes in the Adriatic Sea and Aegean Sea, the same historical trends as those for the EMS are imposed (section 2.3.4). By combining the riverine and atmospheric inputs, forcing functions for the individual P and N species are then created (Figure 2.1B, 2-1D and Appendix B).

The reconstructed inputs of additional PO_4 and DOP to the EMDW via Adriatic and Aegean deep water formation increase from 1950 to the early 1980s by factors of 2 to 3, except for additional Adriatic deep water PO_4 which increases by a factor of 8 (Figure 2.1B and Appendix B). After the mid-1980s, the forcing functions decline again, although by 2000 additional Adriatic deep water PO_4 is still more than three times higher than in 1950. As for additional P, the forcing functions for additional N exhibit initially upward trends (Figure 2.1D and Appendix B). However, they reach their peak values later than for P, generally in the mid-1990s, and experience less pronounced declines afterwards. [Note: The forcing function for additional DON in Aegean deep water reaches its maximum in 1986 due to the input from the Black Sea.] The largest relative increases are seen for additional NO_3, with peak values 4.8 and 4.4 higher

than in 1950 for the Adriatic Sea and Aegean Sea, respectively. By 2000, the additional NO_3 inputs via deep water formation are still over 4 times higher than in 1950. The relatively large increases in the forcing functions for additional P and N reflect the elevated anthropogenic nutrient inputs to the Adriatic and Aegean seas that accompanied rapid post-1950 economic development in the respective catchment areas. In particular for the northern Adriatic Sea these inputs have been linked to severe coastal eutrophication (Justic, 1987; Justic et al., 1987; Degobbis et al., 2000).

Adriatic deep water formation is a major source of P and N to the EMS (Figure 2.2). Integrated over the period 1950-2000, inflow from the Adriatic Sea into the EMDW accounts for approximately 20% of the total external inputs of dissolved P and N to the EMS. For comparison, the Aegean Sea contributes less than 3%. However, it is important to note that the majority of the dissolved P and N in both the Adriatic and Aegean deep water originate from the upwelled EMIW. Even during the 1980s and 1990s, additional P and N only account for at most 25 and 20% of the total dissolved P and N inputs via Adriatic deep water inflow, respectively.

2.3.6 Eastern Mediterranean Transient (EMT)

In the baseline simulation, the water fluxes remain unchanged from 1950 to 2000. The majority of deep formation occurs in the Adriatic Sea (0.36 Sv) with only a small amount (0.04 Sv) produced in the Aegean Sea (Appendix A). In the Eastern Mediterranean Transient (EMT) scenario, the same baseline water fluxes apply to the period 1950 to 1987. From 1987 on, the Aegean deep water inflow is modified based on the estimations summarized by Roether et al. (2007). It increases to 0.06 Sv between 1987 and the middle of 1992, followed by a strong pulse of deep water formation of 2.7 Sv from mid-1992 till the end of 1994. Afterwards, Aegean deep water inflow drops and stays constant at 0.25 Sv until the end of the century. The Adriatic deep water inflow to the EMS is assumed to remain unchanged from 1950 to 2000. Note that, relative to the baseline scenario, the imposed EMT water fluxes imply a higher net inflow into EMDW between 1987 and 2000 and, thus, a higher water upflow from EMDW to EMIW during the same time period.

2.4 Results and discussion

2.4.1 Phosphorus concentrations

The model-predicted relative changes of P concentrations in the three EMS reservoirs for the baseline scenario over the period 1950 to 2000 are shown in Figure 2.3A. Corresponding numerical values for the concentrations are listed in Table 2.1, while Table 2.2 summarizes available measured data to which the

model values can be compared. Appendix B further illustrates how the modeled P concentrations respond to changes in the input of reactive P and N from the WMS (Figure B.1 and Table B.2).

For all three water masses, the model yields PO_4 concentrations in 2000 that exceed those in 1950. The largest relative change (15%) is predicted to occur in the SW reservoir, where the PO_4 concentration rises from 25 to 29 nM. Most of the increase takes place during the 1970-1980 period (~6% increase per decade), with little further change after 1990. However, it is not possible to verify the predicted 4 nM increase in SW PO_4 concentration given the significant spatial and seasonal variability of measured PO_4 concentrations within the upper 200 m of the EMS. Furthermore, many surface water measurements fall below the analytical limit of detection of 20 nM for samples preserved frozen prior to subsequent analysis in the laboratory. The 20 nM detection limit was determined by Krom et al. (2005) who compared results of shipboard analyses of dissolved inorganic P performed immediately after sample collection, with those of analyses carried out in a land-based laboratory on frozen samples.

In EMIW, the modeled PO_4 concentration increases by 12% between 1950 and 2000, following a trend similar to that of EMSW. The EMDW exhibits a far smaller relative increase in the PO_4 concentration from 1950 to 2000 (4%). The modeled EMIW and EMDW PO_4 concentrations for the year 2000 (121 and 183 nM) fall within the ranges of concentrations measured around the turn of the century (Table 2.2). The model results also agree with measurements performed between 1980 and 2010, which do not exhibit any detectable change in EMDW PO_4 concentrations over time (Lavezza et al., 2011). The relative changes in modeled DOP concentrations are comparable to those of PO_4. Between 1950 and 2000, the EMSW, EMIW and EMDW DOP concentrations increase by 15, 15 and 6%, respectively. The resulting model-predicted DOP concentration of EMDW in 2000 (45 nM) is consistent with values measured at water depths exceeding 1000 m (Table 2.2).

While the relative changes in concentration of the dissolved P species from 1950 to 2000 are markedly lower for EMDW, compared to EMSW and EMIW, this is not the case for POP. Relative to 1950, the POP concentrations increase by 15% in all three water reservoirs (Figure 2.3A). The different behavior of dissolved and particulate P reflects their transport properties. According to the model, as the concentrations of PO_4 and DOP increase in EMIW, the corresponding export fluxes to the Western Mediterranean Sea (WMS) increase, hence counteracting the accumulation of dissolved P in EMDW. In contrast, when the POP concentration of EMIW increases it enhances the settling flux to the EMDW reservoir, where POP accumulates. Note that the model predicted POP concentration within EMDW of 3.9 nM in 2000 is of the same order of magnitude as measured deep-water values reported in Krom et al. (2005) and Pujo-Pay et al. (2011) (1 to 8 nM, Table 2.2).

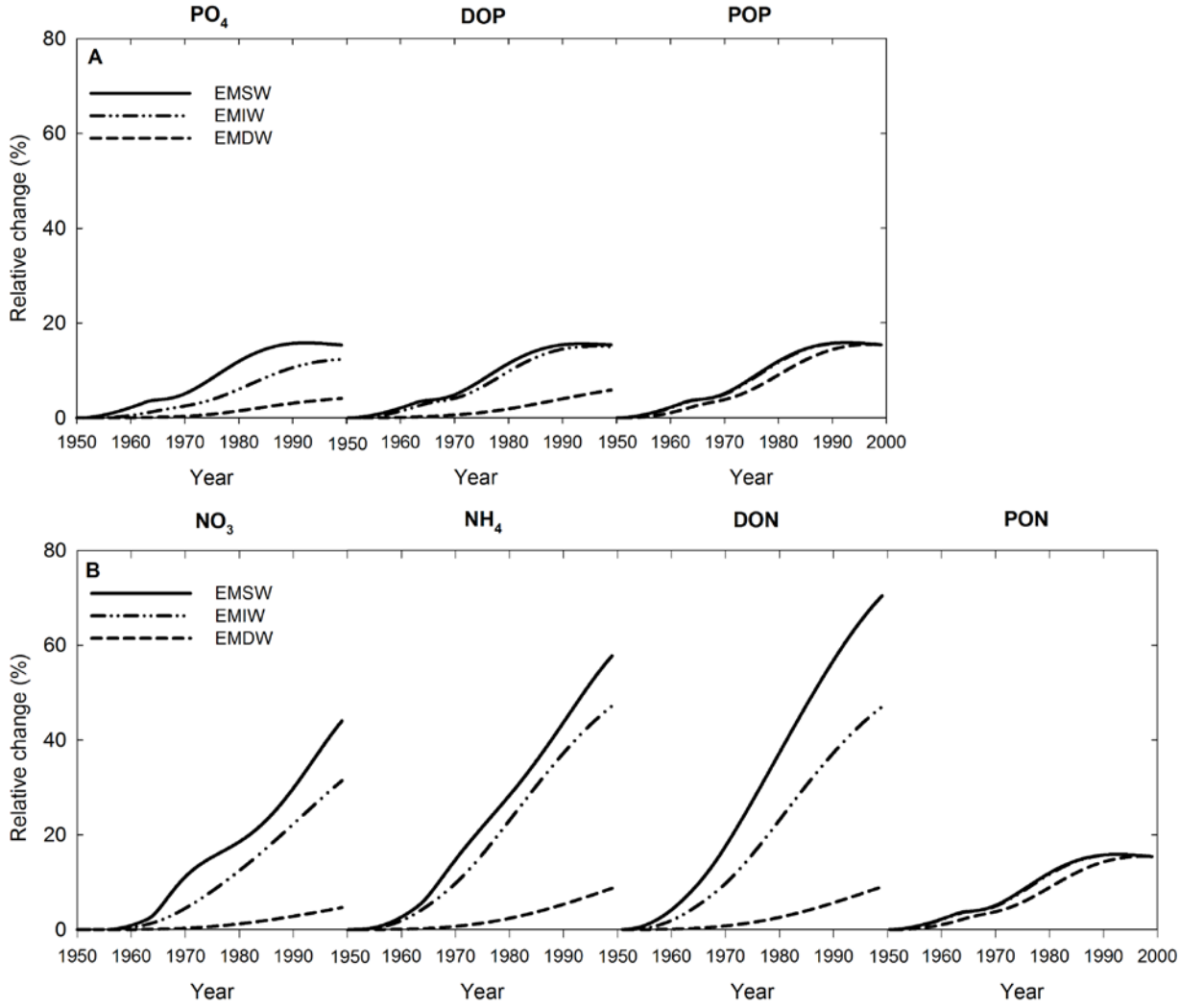

Figure 2.3: Relative concentration changes of the reactive P (PO_4, DOP and DOP) and N (NO_3, NH_4, DON and PON) reservoirs considered in the model, over the period 1950-2000, in EMSW (solid line), EMIW (dotted line) and EMDW (dashed line).

	Water Mass	1950	1960	1970	1980	1990	2000	EMT
PO_4 (nM)	EMSW	25	25	26	28	29	29	30
	EMIW	108	108	110	114	119	121	131
	EMDW	176	176	177	179	181	183	177
DOP (nM)	EMSW	50	51	53	56	58	58	60
	EMIW	43	43	44	47	49	49	50
	EMDW	42	42	42	43	44	45	45
POP (nM)	EMSW	7.1	7.2	7.4	7.9	8.2	8.1	8.4
	EMIW	5.3	5.4	5.6	5.9	6.1	6.1	6.3
	EMDW	3.4	3.4	3.5	3.7	3.9	3.9	4.0
NO_3 (μM)	EMSW	0.5	0.5	0.6	0.6	0.7	0.8	0.7
	EMIW	2.6	2.6	2.7	2.9	3.1	3.4	3.5
	EMDW	4.8	4.8	4.9	4.9	5.0	5.1	4.9
NH_4 (μM)	EMSW	0.08	0.08	0.09	0.11	0.12	0.13	0.13
	EMIW	0.05	0.05	0.05	0.06	0.07	0.07	0.07
	EMDW	0.05	0.05	0.05	0.05	0.05	0.06	0.06
DON (μM)	EMSW	2.6	2.7	3.1	3.6	4.1	4.5	4.5
	EMIW	2.6	2.7	2.9	3.3	3.6	3.9	3.9
	EMDW	2.5	2.5	2.6	2.6	2.7	2.8	2.9
PON (μM)	EMSW	0.28	0.29	0.30	0.32	0.33	0.33	0.34
	EMIW	0.16	0.17	0.17	0.18	0.19	0.19	0.20
	EMDW	0.11	0.11	0.11	0.12	0.12	0.13	0.13
NO_3:PO_4	EMSW	21	21	22	22	24	27	24
	EMIW	24	24	24	25	26	28	27
	EMDW	28	28	28	27	27	28	28
DON:DOP	EMSW	52	53	59	64	71	78	76
	EMIW	62	62	65	69	74	80	77
	EMDW	60	60	61	61	61	62	64
PON:POP	EMSW	40	40	40	40	40	40	40
	EMIW	31	31	31	31	31	31	31
	EMDW	32	32	32	32	32	32	32

Table 2.1: Model predicted P and N concentrations plus N:P ratios in the Eastern Mediterranean Surface Water (EMSW), Eastern Mediterranean Intermediate Water (EMIW) and Eastern Mediterranean Deep Water (EMDW) reservoirs at 10 year intervals between 1950 and 2000. The last column lists the model predicted values for year 2000 in the Eastern Mediterranean Transient (EMT) scenario (see text for details).

Overall, the model-predicted changes in PO_4, DOP and POP concentrations in the EMS are relatively small (≤16%). Even if complete time-series data were available, distinguishing long-term temporal changes in concentration from the small-scale heterogeneity of P distributions due to mesoscale and submesoscale processes within the EMS would be challenging. For example, deep-water PO_4 concentrations measured around the turn of the century range from 140 to 230 nM (Krom et al., 2005; Pujo-Pay et al., 2011). This variability significantly exceeds the model-predicted difference in PO_4 concentration of the EMDW between 1950 and 2000 of 7 nM (= 183 nM – 176 nM).

2.4.2 Nitrogen concentrations

The relative changes of the N concentrations for the baseline simulation are shown in Figure 2.3B, while the corresponding concentration values are given in Table 2.1. The sensitivity of the modeled N distribution to changes in reactive P and N input via the Strait of Sicily is illustrated in Figure B.2 and Table B.2 of Appendix B; as for P, the imposed changes in input from the WMS do not fundamentally change the temporal trends of the N concentrations.

In the EMSW, the relative changes in dissolved N concentrations are much larger than those of dissolved P: between 1950 and 2000, the concentrations of NO_3, NH_4, and DON are predicted to increase by 45, 59 and 72%, respectively. The accumulation of EMSW dissolved N reflects the higher-than-Redfield N:P ratios of external nutrient inputs to the EMSW, combined with P-limited primary productivity. In addition, the dissolved N concentrations grow continuously over the 1950 to 2000 time interval, while the dissolved P concentrations are predicted to remain approximately constant after the mid-1980s. The different EMSW trends for P and N reflect the time-dependent anthropogenic nutrient inputs to the EMS, which decrease for P during the last decade of the 20th century, while continuing to increase for N (Figure 2.2).

In contrast to the dissolved species, the predicted relative increase of the EMSW PON concentration (15%) between 1950 and 2000 is the same as that of POP. This reflects the tight coupling of the production rates of both species through the Redfield ratio, which remains constant in the model simulations. The predicted EMSW PON concentration in 2000 (0.3 μM) falls within the range of measured values (0.1-0.7 μM; Krom et al., 2005; Pujo-Pay et al., 2011).

It is worth emphasizing that all model-calculated concentrations represent annual averaged values. That is, the model does not account for seasonal variations in concentrations. This is particularly important for EMSW NO_3, which, unlike PO_4, exhibits marked seasonal variations. During and immediately after deep winter mixing, when the winter phytoplankton bloom takes place, PO_4 is entirely consumed while excess

Location		Model	CYCLOPS, (SE Levantine basin)	South Levantine Basin	BOUM cruise across Ionian + Levantine Basin
Year		2000	2003	1989-1995	2008
Reference		This study	(Krom et al., 2005)	(Kress and Herut, 2001)	(Pujo-Pay et al., 2011)
PO_4	**EMSW**	29	0-30 (5)	10-30 (20)	0-100 (30)
(nM)	**EMIW**	121	0-230 (140)	30-210 (130)	50-200 (150)
	EMDW	183	140-230 (180)	140-240 (210)	140-200 (180)
DOP	**EMSW**	58	30-100 (50)		10-80 (30)
(nM)	**EMIW**	49	30-90 (40)		0-70 (10)[1]
	EMDW	45	20-90 (40)		0-70 (20)[2]
POP	**EMSW**	8.1	7.6-9.1 (8.1)[3]		4-30 (14)[3]
(nM)	**EMIW**	6.1			1-13 (6)[1]
	EMDW	3.9	3.8[4]		1-8 (5)[2]
NO_3	**EMSW**	0.8	0-1.0 (0.2)	0-1.9 (0.8)	0-3.5 (0.6)
(µM)	**EMIW**	3.4	0.25-5.8 (2.5)	0.8-5.7 (3.3)	3.0-5.5(5)
	EMDW	5.1	4.7-5.8 (5.0)	4.7-6.5(5.8)	5.0-6.0(5.5)
NH_4	**EMSW**	0.13	0.04-0.08(0.06)		0-0.03 (0.01)
(µM)	**EMIW**	0.07	0.05-0.13 (0.06)		0-0.023 (0.002)
	EMDW	0.06	0.06-0.13 (0.06)		nd
DON	**EMSW**	4.5	0.9-12 (5.4)		3.3-6.0 (4.5)
(µM)	**EMIW**	3.9	0-5.8 (4.0)		3.0-4.5 (4.0)
	EMDW	2.8	0-4.7 (3.3)		3.0-4.5 (3.0)
PON	**EMSW**		0.29-0.39		0.08-0.66 (0.30)[3]
(µM)		0.33	(0.32)[3]		
	EMIW	0.19			0.01-0.21 (0.08)[1]
	EMDW	0.13	0.11[4]		0.01-0.13 (0.07)[2]

Table 2.2: Model predicted P and N concentrations for the year 2000 versus reported concentrations for samples collected during the late 20th and early 21st centuries. The depth intervals for the measured concentrations match those used to represent the three vertical water masses in the model (EMSW: 0-200 m; EMIW: 200-500 m; EMDW: >500 m). Observed concentration ranges are given with average values indicated between brackets. (nd = not detected.) Depth intervals: [1]150-1250m, [2]1000-3000m, [3]0-250m and [4]350-1600m.

NO_3 remains (Krom et al., 1991). As a result, relatively high residual EMSW NO_3 concentrations of up to 1-2 μM are observed after the bloom (e.g. Kress and Herut, 2001). During spring (March to May) the NO_3 is progressively used up by phytoplankton, ultimately leading to a complete depletion of NO_3 in the uppermost water layers (Thingstad et al., 2005b). As expected, the model therefore predicts EMSW NO_3 concentrations (0.5 and 0.8 μM in 1950 and 2000, respectively) that are lower than the observed winter peak values.

The modeled EMSW concentrations of NH_4 and DON follow similar trends, as both dissolved N species are produced by grazing and decomposition of PON. The relative change in DON is larger than that of NH_4, however, because EMSW NH_4 is nitrified or taken up by phytoplankton, while DON is not (Krom et al., 2005). The modeled EMSW NH_4 concentration increases from 0.08 μM to 0.13 μM between 1950 and 2000. While these values are in general agreement with the measurements reported by Krom et al. (2005), they are about 10 times higher than those obtained by Pujo-Pay et al. (2011) during the BOUM cruise (Table 2.2). The discrepancy could be due to analytical difficulties associated with the determination of very low levels of ammonium. Alternatively, it may reflect the temporal variability of EMSW NH_4 concentrations. The BOUM data were obtained in midsummer (June and July), when a lower phytoplankton biomass presumably results in less NH_4 production through grazing and decomposition.

The modeled EMIW and EMDW NH_4 concentrations remain essentially unchanged at 0.05-0.07 μM from 1950 to 2000. During the same period, the EMIW NO_3 concentration grows by 32%, from 2.6 to 3.4 μM. Consequently, the model predicts a much larger relative increase in NO_3 export to the WMS compared to PO_4, 32% versus 12% (section 2.4.1). For EMDW, the model yields only a small increase in NO_3 concentration of 5%. The corresponding concentration range (4.8-5.1 μM) is comparable to measured EMDW NO_3 concentrations (Table 2.2). In addition, time series measurements suggest a gradual rise in EMDW NO_3 concentrations on the order of 8% between 1980 and 2010 (Lavezza et al., 2011). This upward trend is of comparable magnitude as the predicted one and, according to the model, can be attributed to the accumulation of anthropogenic N in the EMS.

The largest EMSW N reservoir is DON, which also shows the largest relative change between 1950 and 2000. The initial 1950 DON depth profile is approximately constant, with concentrations estimated to range from 2.5 to 2.6 μM in all three water reservoirs. Similar to NO_3 and NH_4, the modeled EMSW DON concentration starts to increase rapidly during the 1960s. This trend continues throughout the rest of the model run. By 2000, the anthropogenic N inputs to the EMS have caused significant concentration differences between the water layers. In the EMSW, the modeled DON concentration increases from 2.6 to 4.5 μM (72%) between 1950 and 2000, in the EMIW it increases from 2.6 to 3.9 μM (48%). The DON

concentration in the EMDW is predicted to only increase by 0.3 μM, however. The resulting EMDW DON concentration of 2.8 μM in 2000 is consistent with measured values obtained around the end of the 20th century (Table 2.2).

The results of the model simulations imply that the temporal trends in the EMSW and EMIW concentrations of DON may be sensitive diagnostic indicators of anthropogenically driven changes in the nutrient budgets of the EMS (see also Figure B.1; Appendix B). The magnitudes of the predicted changes are, in principle, sufficiently large to be detectable with current analytical capabilities. To our knowledge, however, no suitable time-series data sets are available to verify the predicted changes in DON concentration. Based on the model results, we therefore strongly recommend that DON measurements be included in future biogeochemical monitoring of the EMS.

2.4.3 N:P ratios

Higher-than-Redfield NO_3:PO_4 ratios are a characteristic feature of the EMS water column. Anthropogenic nutrient inputs should, according to the model, have caused marked increases in the EMSW and EMIW molar NO_3:PO_4 ratios over the period 1950 to 2000, from values of 21 and 24 to 27 and 28, respectively (Table 2.1). For EMSW, near-detection PO_4 levels and seasonal variations in the NO_3 concentration (sections 2.4.1 and 2.4.2) prevent the verification of the predicted trend of the EMSW NO_3:PO_4 ratio. The modeled EMIW NO_3:PO_4 ratio for the year 2000 (28:1) is lower than the average value of 31 reported by Kress and Herut (2001) for samples collected in 1999, but well within the range of the values measured by the same authors (18-54). Furthermore, EMIW field measurements depend on the depth chosen as the base of the EMIW, because the latter generally falls within the nutricline, the depth of which also varies from location to location as a result of mesoscale activity.

The EMDW has the highest initial NO_3:PO_4 ratio (Appendix A). As the model only produces a very small increase of the EMDW NO_3:PO_4 ratio from 1950 to 2000, the differences in NO_3:PO_4 ratio between the vertical water masses decrease with time, however. The small increase in EMDW NO_3:PO_4 ratio is due to the relatively long residence time of EMDW (150 years, Appendix A). If nutrient inputs beyond 2000 would remain at the 2000 levels, the model predicts that the EMDW NO_3:PO_4 would eventually reach a value of 39. Thus, anthropogenic inputs of nutrients could have a significant long-term effect on EMDW nutrient concentrations and ratios, with the EMS becoming even more P limited over time.

From 1950 to 2000, the modeled EMSW DON:DOP ratio increases by 49%, from 52 to 78. The increase for EMIW is markedly smaller, 29% (from 62 to 80), while the modeled DON:DOP ratio of the EMDW hardly changes. The EMDW DON:DOP ratio in the model (60-62) falls within the range of measured values (Moutin and Raimbault, 2002; Krom et al., 2005). The faster build-up of DON, relative to DOP, in

EMSW and, to a lesser extent, in EMIW reflects differences in recycling of the two dissolved organic pools. Between 1950 and 2000, the recycling efficiency of DOP back to PO_4 remains approximately constant in both EMSW (97%) and EMIW (76%). During the same time period, the recycling efficiency of DON drops from 91 to 82% in EMSW, and from 50 to 47% in EMIW. While both DON and DOP are produced by grazing and decomposition of phytoplankton biomass, the breakdown of DOP to PO_4 appears to be promoted by the relatively high concentrations of alkaline phosphatase observed in the upper water column of the EMS (Zohary and Robarts, 1998; Van Wambeke et al., 2002; Thingstad and Mantoura, 2005). An enhanced release of alkaline phosphatase by the EMSW microbial community may represent an adaptation to the P limited nature of the EMS.

Because of the preferential accumulation of DON, the DON:DOP ratios in the EMS are considerably higher than in the rest of the oceans. Average oceanic DON:DOP ratios in surface and deep waters are on the order of 22 and 25, respectively (Benner, 2002). The model further implies that anthropogenic nutrient inputs to the EMS may have significantly increased the DON:DOP ratios in the upper part of the water column. The higher model-predicted DON:DOP ratios for EMSW compared to EMDW after 1980 agree with the DOP and DON concentrations reported by Krom et al. (2005).

2.4.4 Primary Production

Gross primary production is obtained by multiplying the modeled photosynthetic PO_4 assimilation flux with the standard Redfield carbon to phosphorus ratio (C:P = 106:1; Redfield et al., 1963). The calculated primary production in the EMS increases by 16%, from 59.8 gC m^{-2} yr^{-1} in 1950 to 69.2 gC m^{-2} yr^{-1} in 1992, followed by a slight decline after 1992 (Figure 2.4). By 2000, primary production equals 68.9 gC m^{-2} yr^{-1}, that is, a value 15% higher than the 1950 value. The model-predicted primary productivities fall within the observed range of 10-185 gC m^{-2} yr^{-1} (average: 64 gC m^{-2} yr^{-1}) reported by Berman-Frank and Rahav (2012) for the period 1980-1997. The latter authors found no significant temporal trend in primary production over this time period, which is consistent with the very small change in the modeled primary production between 1980 and 1997 (4%).

The model-predicted trend in primary production of the EMS can further be compared to that of reconstructed ocean surface chlorophyll concentrations derived by Wernand et al. (2013) from Forel-Ule (FU) values recorded since the late 1800s. Based on data for the entire Mediterranean Sea, Wernand and coworkers estimate that chlorophyll concentrations, and hence primary production, increased by 41% from 1950 to 1990. In contrast, the model yields only a 16% increase in the EMS for the same time interval. The difference, however, may be explained by the inclusion of the Western Mediterranean Sea (WMS) in the analysis of Wernand et al. (2013). The WMS experienced higher nutrient inputs than the

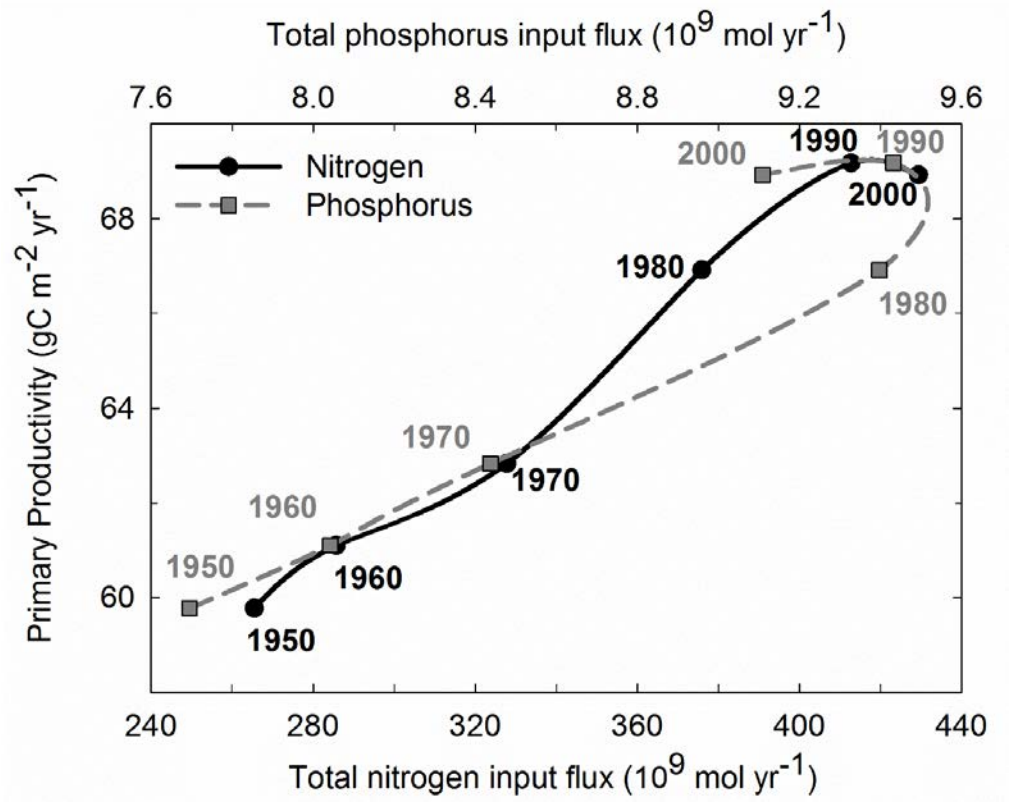

Figure 2.4: Model predicted gross primary production in the EMS plotted against the external input fluxes of reactive P and reactive N. Note that, according to the reconstructed anthropogenic forcing functions, the external input of reactive P reaches its maximum in 1985, while the N input continues to increase over the entire modeled 1950-2000 time period.

EMS during the second half of the 20th century, being surrounded by the more highly industrialized countries France, Italy and Spain (Ludwig et al., 2009). The inferred increase in primary production of 41% may thus be more representative of the WMS than the EMS.

At first, the relatively limited increase in primary production between 1950 and 1992 predicted by the model (16%) seems at odds with the near doubling of reactive P input to the EMS via atmospheric deposition and rivers during the same time period. The main external supply of P (and N) to the EMS, however, is through inflow from the WMS (Figure 2.2). When the latter is included, the total external input of P peaks in 1985 at a value 24% higher than in 1950. When imposing higher or lower forcing functions to the WMS P input, the modeled primary production increases or decreases proportionally (Figure B.4, Appendix B). The dominant role of dissolved P input from the WMS is consistent with the factorial design analysis presented in Appendix A, which show that the modeled primary production is most sensitive to the inflow of DOP and PO_4 via the Strait of Sicily. Unfortunately, changes in dissolved P inputs from the WMS over time are poorly constrained. In addition to being a major source of nutrient P and N for the EMS, the WMS is also the main recipient of P and N exported from the EMS. Increased efforts to systematically monitor nutrient exchanges between the eastern and western basins of the Mediterranean Sea for periods of one or more decades are therefore strongly recommended. This could be achieved, for instance, by installing additional sensors on existing, long-term moorings deployed in the Strait of Sicily (Schroeder et al., 2013).

A comparison of the inputs and outputs of P and N shows, as expected, a delayed response of the outputs (Figure 2.2). While the total input of reactive P to the EMS decreases after the 1990s, the total output increases steadily from 1950 to 2000. When the computations are extended beyond 2000, while keeping the P and N inputs constant at their 2000 values, primary production continues to slowly increase, ultimately reaching 71 gC m^{-2} yr^{-1} (compared to 68.9 gC m^{-2} yr^{-1} in 2000). When the inputs are reset instantaneously back to their 1950 values, primary production beyond 2000 drops rapidly in a matter of a few years. These model responses reflect the very efficient removal of PO_4 from the EMIW reservoir to the WMS and the EMDW reservoir, which limits PO_4 return to the EMSW of the EMS.

2.4.5 Where do the nutrients go?

The net loss of dissolved P to the WMS via outflow of EMIW through the Strait of Sicily is generally invoked to explain the ultra-oligotrophic nature of the EMS (e.g. Sarmiento et al., 1988; Krom et al., 2003). Béthoux et al. (1998) further propose that the excess anthropogenic P and N that are not exported from the Mediterranean Sea accumulate as deep water PO_4 and NO_3. Below, we revise both hypotheses based on the results of the coupled P and N cycling model for the EMS.

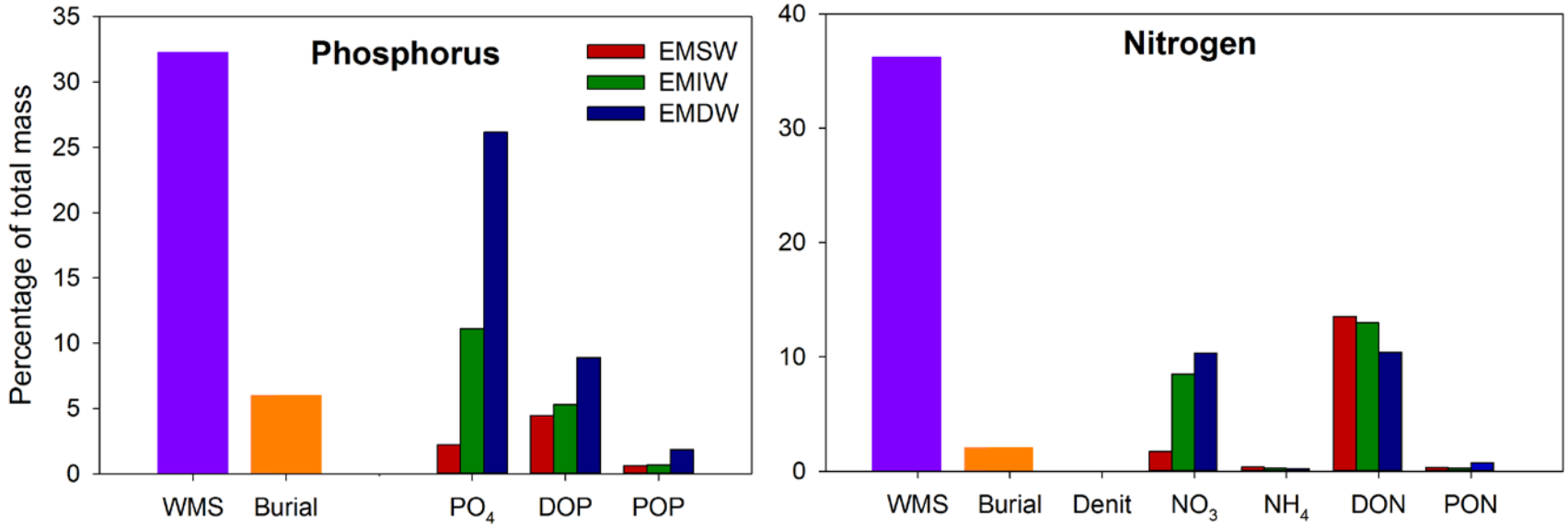

Figure 2.5: Fate of anthropogenic P and N. Export to the Western Mediterranean Sea (WMS), sediment burial and accumulation in the water masses are expressed as percentages of the external P and N supplied in excess of the 1950 inputs, integrated over the period 1950-2000. Because P and N exported with EMIW into the Adriatic and Aegean Seas are assumed to return to the EMDW via deep water formation, only the additional dissolved P and N acquired in the Adriatic and Aegean basins are included in the calculation of excess P and N inputs to the EMS. Note that the export to the WMS and sediment burial are expressed as percentages total reactive P or N, while accumulation in the water column differentiates between the different chemical forms of the nutrient elements.

The model predicts that the net export of dissolved P (PO_4 + DOP) from the EMS to the WMS is actually fairly small. Subtracting the WMS surface inflow from the outflow of EMIW to the WMS yields a net export of dissolved P of only 0.31×10^9 mol P yr^{-1} in 1950, and a maximum of 0.54×10^9 mol P yr^{-1} during the 1980s. As emphasized in our companion paper, it is the difference in chemical speciation of dissolved P between the inflow from and outflow to the WMS that is the key to explaining the ultra-oligotrophy of the EMS, rather than the net export of dissolved P. While DOP dominates the input from the WMS, PO_4 dominates the output to the WMS (Appendix A). The latter limits the build-up of PO_4 in EMIW and hence the upward mixing of PO_4 to the photic zone. (Note: a similar switch in organic-inorganic speciation between inflow from the WMS and outflow of EMIW is also predicted for N.)

According to the model calculations, integrated over the period 1950-2000, respectively 32 and 36% of P and N supplied in excess to the 1950 baseline inputs are exported through the Strait of Sicily to the WMS (Figure 2.5). The equivalent of about one-third of reactive P supplied in excess to the 1950 input accumulates in the EMDW, primarily as PO_4 (26%), and to a lesser extent as DOP (9%) and POP (2%). For N, only 20% of the excess supply ends up in the EMDW, distributed evenly over NO_3 (10%) and DON (10%). The largest accumulation of excess N within the EMS (27%) is under the form of DON in EMSW and EMIW.

The results imply that the accumulation of anthropogenic P in the EMS diverges substantially from that of anthropogenic N, not only in terms of where the nutrient elements accumulate but also under which chemical forms. The predictions of the model should therefore be helpful in guiding future data acquisition in the EMS. Particularly useful would be long-term ($\geq$ 10 years) measurements of nutrient concentrations in EMIW and EMDW, as these are less prone to short-term ($\leq$ 1 year) variability than their EMSW counterparts.

2.4.6 Eastern Mediterranean Transient (EMT)

According to factorial design analysis, primary production and P and N dynamics in the EMS are sensitive to changes in circulation (Appendix A). The EMT provides the possibility to investigate the effects of a well-constrained modification of deep water formation on the biogeochemistry of the EMS. During the EMT, Aegean deep water formation increased (Roether et al., 2007). As this new Aegean water was denser than the older Adriatic deep water (ADW) it produced a recognizable water mass along the bottom of the EMS and pushed relatively nutrient rich ADW into the EMIW, which, in turn, would have enhanced the upward mixing of P and N into the euphotic zone (Kress et al., 2012). The EMT has therefore been hypothesized to cause an increase in primary productivity of the EMS (Klein et al., 1999).

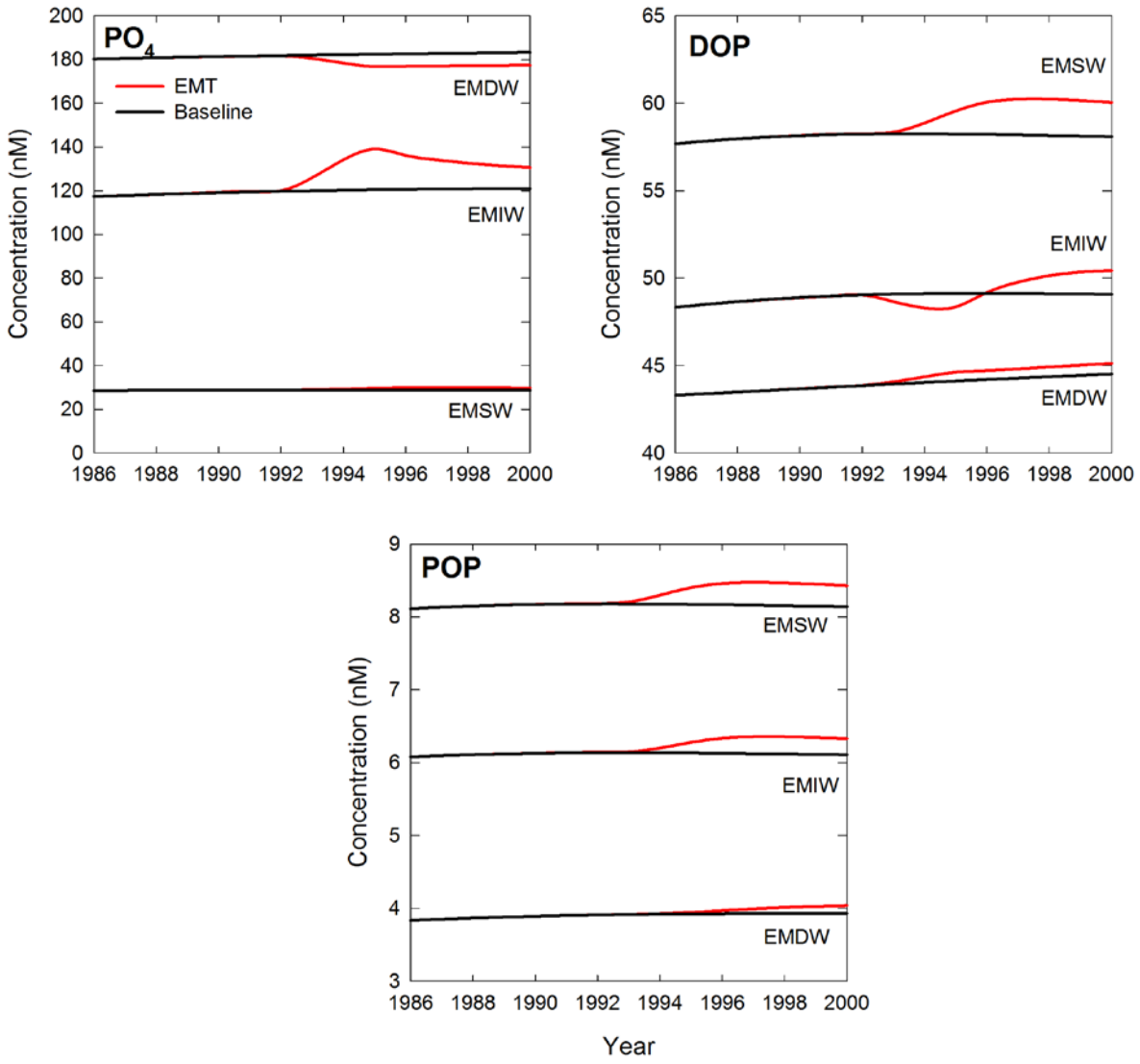

Figure 2.6: Comparison of reactive P (PO_4, DOP and POP) concentrations in the baseline model (dark line) with those in the EMT scenario (red line) for the period 1986 to 2000. Results are shown for Eastern Mediterranean Surface Waters (EMSW), Eastern Mediterranean Intermediate Water (EMIW) and Eastern Mediterranean Deep Water (EMDW). (Note: the EMT started in 1987.)

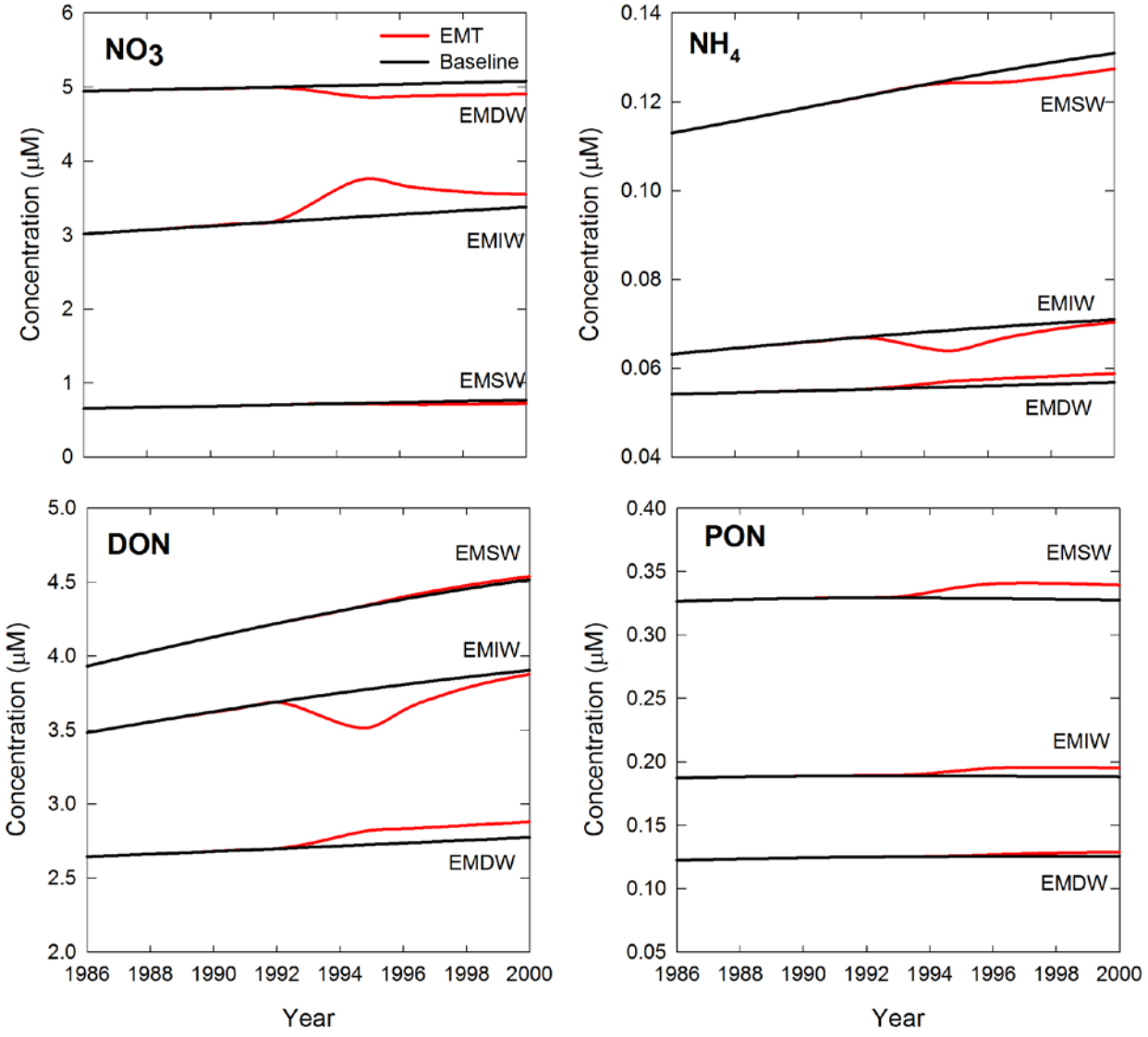

Figure 2.7: Comparison of reactive N (NO_3, NH_4, DON and PON) concentrations in the baseline model (dark line) with those in the EMT scenario (red line) for the period 1986 to 2000. Results are shown for Eastern Mediterranean Surface Waters (EMSW), Eastern Mediterranean Intermediate Water (EMIW) and Eastern Mediterranean Deep Water (EMDW). (Note: the EMT started in 1987.)

When implemented in the model, the EMT scenario produces significant differences in EMIW concentrations: the PO_4 and NO_3 concentrations reach maximum values that are 15% higher than in the baseline scenario (Figures 2.6 and 2.7). Primary production, however, only increases by at most 4%, because large proportions of the additional dissolved P and N transferred from the EMDW to the EMIW are removed to the WMS through the anti-estuarine circulation of the EMS and, therefore, do not contribute to enhanced primary production in the EMSW. Note that the predicted lack of a notable change in primary production is consistent with the satellite chlorophyll data presented by D'Ortenzio et al. (2003). The latter authors conclude that the data do not yield discernible differences in the biological dynamics of the surface EMS between the early 1980s and late 1990s.

Kress et al. (2012) further suggest that the EMT may have modified the EMDW NO_3:PO_4 ratio, because Aegean deep water NO_3:PO_4 ratios are higher than those of Adriatic deep waters. Field data indeed show slightly higher NO_3:PO_4 ratios in the very deepest part of the EMDW, which may be traceable to the younger inflowing Aegean deep water displacing older Adriatic deep water (Kress et al., 2012). The model, however, represents the EMDW as a single, homogeneous reservoir model and, therefore, is unable to resolve the observed spatial differences. The model yields no significant change in the EMDW NO_3:PO_4 ratio during the EMT (Table 2.1).

The EMT represents a short-term modification of the circulation of the EMS. In addition, it does not alter the anti-estuarine circulation of the EMS, which is a primary mechanism maintaining the EMS in its ultra-oligotrophic state. More profound changes in EMS circulation have occurred in the recent geological past, for example during periods of sapropel formation (Stratford et al., 2000 and references therein). Ongoing climate change in the Mediterranean region may potentially lead to a significant restructuring of basin-wide circulation within the present and next century (Thorpe and Bigg, 2000; Somot et al., 2006). Future work will be required to fully explore how the productivity and biogeochemistry of the EMS will respond to major, long-term changes in circulation.

2.5 Conclusions

The reconstructed anthropogenic forcing functions imply large increases of P and N inputs by atmospheric deposition, river discharge and deep water formation during the decades following 1950. Nonetheless, the inflow from the WMS remains the largest supplier of P and N to the EMS from 1950 to 2000. The combined external input of the limiting nutrient P increases from 1950 to 1985 by 24% to a maximum of 9.5×10^9 mol yr^{-1}. Thereafter, the external P supply slowly decreases; by 2000 it totals 9.1×10^9 mol yr^{-1}, that is, 18% higher than in 1950. In contrast, the external input of reactive N

continuously increases over the entire time period simulated, reaching 429×10^9 mol yr^{-1} in 2000, or 62% higher than in 1950.

The modeled gross primary production increases to a maximum value of 69.2 gC m^{-2} yr^{-1} in 1992, that is, 16% higher than in 1950. It decreases thereafter following the decline of P inputs to the EMS. A key outcome of the model is that water exchanges with the WMS exert a major control on the biological productivity in the EMS. Not only does inflow of DOP and DON from the WMS dominate the external inputs of the two nutrient elements, the outflow of PO_4 to the WMS is the key mechanism maintaining ultra-oligotrophic conditions in the EMS. Integrated over the period 1950-2000, the model predicts that the equivalent of about one-third of the external P and N added to the EMS in excess to the 1950 inputs is removed again from the EMS with the outflow of EMIW to the WMS.

Post-1950 inputs of anthropogenic nutrients also lead to a build-up of P and N in the water column of the EMS. The accumulation patterns differ significantly between the two elements, however. For P, most accumulation occurs as PO_4 in the EMDW, while N mainly accumulates under the form of DON in EMSW and EMIW. Because of the higher-than-Redfield N:P ratios of the nutrient inputs to the EMS, together with the absence of denitrification, the dissolved N:P ratios increase in all the water masses between 1950 and 2000 (with the exception of the EMDW NO_3:PO_4 ratio). The model predicts that the DON:DOP ratio of the EMSW reservoir experiences the largest change of all the N:P ratios. Overall, anthropogenic nutrient inputs should have driven the EMS to become even more P-limited over time.

The coupled P and N model offers an admittedly simplified representation of nutrient cycling in the EMS. In particular, it does not account for mesoscale and submesoscale processes and, hence, does not resolve seasonal and lateral variations in the nutrient distributions within the basin. Nevertheless, the model predicts concentrations of P and N species in year 2000 that are in general agreement with independent field data (i.e., data not used when building and initializing the model). The consistency with existing data supports the usefulness of the model to analyze the responses of nutrient cycling in the EMS to anthropogenic pressures, on time scales of decades and more. The model can help identify priority areas for future biogeochemical research and monitoring in the EMS. For example, the model results highlight the importance of acquiring time-series data on the P and N fluxes across the Strait of Sicily, and they point to the need to include dissolved organic P and N concentrations when assessing nutrient distributions and their temporal evolution in the EMS.

Chapter 3.

Direct discharges of domestic wastewater are an important source of phosphorus and nitrogen to the Mediterranean Sea

Modified from: **Helen R. Powley**, Hans H. Dürr, Ana T. Lima, Michael D. Krom, Philippe Van Cappellen. (2016) Direct discharges of domestic wastewater are a major source of phosphorus and nitrogen to the Mediterranean Sea, *Environmental Science and Technology*. **50**, 8722-8730. doi:10.1021/acs.est.6b01742.

3.1 Summary

Direct discharges of treated and untreated wastewater are important sources of nutrients to coastal marine ecosystems and contribute to their eutrophication. Here, we estimate the spatially distributed annual inputs of phosphorus (P) and nitrogen (N) associated with direct domestic wastewater discharges from coastal cities to the Mediterranean Sea (MS). According to our best estimates, in 2003 these inputs amounted to 0.9×10^9 mol P yr^{-1} and 15×10^9 mol N yr^{-1}, that is, values on the same order of magnitude as riverine inputs of P and N to the MS. By 2050, in the absence of any mitigation, population growth plus higher per capita protein intake and increased connectivity to the sewer system are projected to increase P inputs to the MS via direct wastewater discharges by 254, 163 and 32% for South, East and North Mediterranean countries, respectively. Complete conversion to tertiary wastewater treatment would reduce the 2050 inputs to below their 2003 levels, but at an estimated additional cost of over €2 billion yr^{-1}. Management of coastal eutrophication may be best achieved by targeting tertiary treatment upgrades to the most affected near-shore areas, while simultaneously implementing legislation limiting P in detergents and increasing wastewater reuse across the entire basin.

3.2 Introduction

Wastewater discharges can be an important source of nutrients, contaminants and pathogens and, hence, may have a range of, often undesirable, impacts on the receiving water bodies, including harmful algal blooms and hypoxia (Toze, 1999; Gray et al., 2002; Van Drecht et al., 2009; Schwarzenbach et al., 2010). Both treated and untreated wastewater from coastal cities are discharged directly into the Mediterranean Sea (MS), either at the surface or via submarine pipes (UNEP/MAP/MED-POL/WHO, 2004). Hereafter, these inputs are referred to as direct wastewater discharges. Phosphorus (P) and nitrogen (N) inputs associated with direct wastewater discharges have been invoked as possible drivers of eutrophication and hypoxia in coastal areas of the MS, for example the Nile delta region (Diaz et al., 2011). However, direct wastewater inputs have so far been neglected in existing P and N budgets of the MS (Béthoux et al., 1992; Béthoux et al., 1998; Ribera d'Alcalà et al., 2003; Krom et al., 2004; Krom et al., 2010; Chapter 2).

The MS is a semi-enclosed basin, with a coastline of more than 45,000 km (Table 3.1). The coastal urban population of the MS is rapidly growing, with a projected increase of over 30% from 2000 to 2025 (Plan-Bleu, 2005). In addition to the permanent population of about 143 million, 176 million tourists visited the Mediterranean coast in 2000; this number is expected to almost double to 312 million per year by 2025 (Plan-Bleu, 2005). Rising domestic wastewater loads accompanying population growth can drive increases in P and N delivery to the MS. For instance, according to Ludwig et al. (2010), by 2050 total riverine P discharge to the MS could be 18 to 42% greater than in year 2000. Changes in P and N emissions, however, are expected to vary significantly because of the large economic and demographic differences among the countries surrounding the MS. In particular, population and water stress are increasing faster in the southern Mediterranean countries, where there are generally less resources available to install treatment infrastructure to help mitigate the effects of the rising production of wastewater. Extensive wastewater re-use is currently limited to a few countries, including Cyprus, Israel and Tunisia, although the importance of ‘grey’ water for use in agriculture is likely to increase in Mediterranean countries in the decades to come (Angelakis et al., 1999; Angelakis and Durham, 2008).

The climate in much of the Mediterranean basin is arid to semi-arid, leading to relatively low river flows. With climate change, river flows and runoff are projected to decrease even further in the future (Arnell, 2004; Ludwig et al., 2010; García-Ruiz et al., 2011; McDonald et al., 2011; Haddeland et al., 2014; Schewe et al., 2014). Thus, compared to riverine inputs and the previously overlooked source of submarine groundwater discharge (Rodellas et al., 2015), direct discharges of treated and untreated wastewater could be a significant pathway delivering P and N to the MS, and become increasingly so in the future. Based on answers provided by local authorities to a United Nations survey questionnaire, the

aggregated direct discharges of domestic plus industrial wastewater from Mediterranean coastal cities of over 100,000 inhabitants delivered $2.4x10^9$ mol P yr^{-1} and $18.5x10^9$ mol N yr^{-1} to the MS around the turn of the century (UNEP/WHO, 1999). For P, the estimated loading from direct wastewater discharges is on the same order of magnitude as the P input delivered by rivers (Ludwig et al., 2009).

Other than the data collected by UNEP/WHO (1999), estimates of P and N inputs associated with wastewater effluents are only available for selected regions and local areas of the MS (e.g., Degobbis and Gilmartin, 1990; de Madron et al., 2003b; de Madron et al., 2010; Mercado et al., 2012; Table E.4). Furthermore, the variable reliability of data sources, and the lack of consistent estimation methods, complicates the assessment of uncertainties associated with reported wastewater inputs of P and N to the MS. Here, we use a systematic approach to quantify the spatially distributed fluxes of P and N associated with direct discharges of domestic wastewater to the MS. The method not only yields internally consistent estimates, but also enables projections of how the direct domestic wastewater P and N discharges may respond to scenarios of changing anthropogenic pressures or improved wastewater management practices.

3.3 Methods

3.3.1 Modeling approach

For any given coastal city, fluxes of total P (TP) and total N (TN) associated with direct discharges to the MS of both treated and untreated domestic wastewater effluents were estimated according to the flowchart in Figure 3.1, using the empirical formula proposed by Kristensen et al. (2004):

$$D_{P,N} = P,N_{capita} \bullet pop \bullet f_c \bullet (1 - f_R) \qquad (3.1)$$

where $D_{P,N}$ is expressed in units of mol yr^{-1}, P,N_{capita} is the annual P or N domestic wastewater load per inhabitant (mol $capita^{-1}$ yr^{-1}), *pop* is the population of the city, f_c is the fraction of the city's population connected to the sewer system, and f_R is the fraction of P or N removed from the wastewater stream in the city's wastewater treatment plants (WWTPs), which is dependent on the type of treatment – primary, secondary or tertiary.

Per capita domestic P and N inputs to WWTPs were obtained following the approach of Morée et al. (2013). The total dietary P or N consumption rates were calculated as:

$$P,N_{diet} = (protein\ supplied - retail\ losses\ ) * P,N_{protein} * \ (1 - f_H) \qquad (3.2)$$

where *protein supplied* is the yearly per capita protein supply quantity for a given country as compiled by Faostat (2013), *retail losses* are the average regional P or N losses by retail businesses and households

(Morée et al., 2013), P,$N_{protein}$ represents the average P or N content of dietary protein (Morée et al., 2013), and f_H represents the fraction of the dietary P or N consumed that does not end up in the wastewater stream (Morée et al., 2013). For N_{capita}, we assumed that $N_{capita} = N_{diet}$; for P_{capita}, we also accounted for P inputs resulting from the use of laundry (P_L) and dishwasher detergents (P_D) (Van Drecht et al., 2009):

$$P_{capita} = P_{diet} + P_D + P_L \qquad (3.3)$$

The values of N_{capita}, P_{capita}, P_D and P_L for each of the countries around the MS are compiled in Table C.7.

Data on population, sewerage, WWTPs and wastewater recycling of Mediterranean coastal cities were gathered from two surveys, one for cities of more than 10,000 inhabitants, the other for cities with 2000 to 10,000 inhabitants (UNEP/MAP/MED-POL/WHO, 2004; 2008), supplemented with data for Gaza (WHO, 2005) and Lake Manzella (or Manzala) along the coast of Egypt (Taha et al., 2004; Rasmussen et al., 2009). For the survey of coastal cities with more than 10,000 inhabitants (UNEP/MAP/MED-POL/WHO, 2004), city-specific parameter values were used in Equation 3.1. Because of data limitations, for coastal cities of 2000-10,000 inhabitants (UNEP/MAP/MED-POL/WHO, 2008) average parameter values for the corresponding countries were entered in Equation 3.1 (Table C.12).

The fraction of domestic wastewater collected by the sewage system, f_c, is divided into the fraction of wastewater that is treated (f_t) and the fraction that is untreated (f_u), or

$$f_c = f_t + f_u \qquad (3.4)$$

Together with the fraction of the population that is not connected to the sewage network (f_n), we then have

$$f_t + f_u + f_n = 1 \qquad (3.5)$$

Equation (3.1) assumes that the fraction f_n of the coastal urban population does not contribute to direct wastewater discharges entering the MS (see also Van Drecht et al. (2009)). Some of the P and N associated with unconnected wastewater, however, may ultimately reach the MS through other delivery pathways, such as riverine discharge and submarine groundwater outflow.

Details on how the values on the right hand side of Equation 3.1 were assigned are given in Appendix C. Values representative for the early years of the 21st century were used to calculate baseline P and N input fluxes associated with direct wastewater outflow into the MS for the nominal year 2003. Note that, when

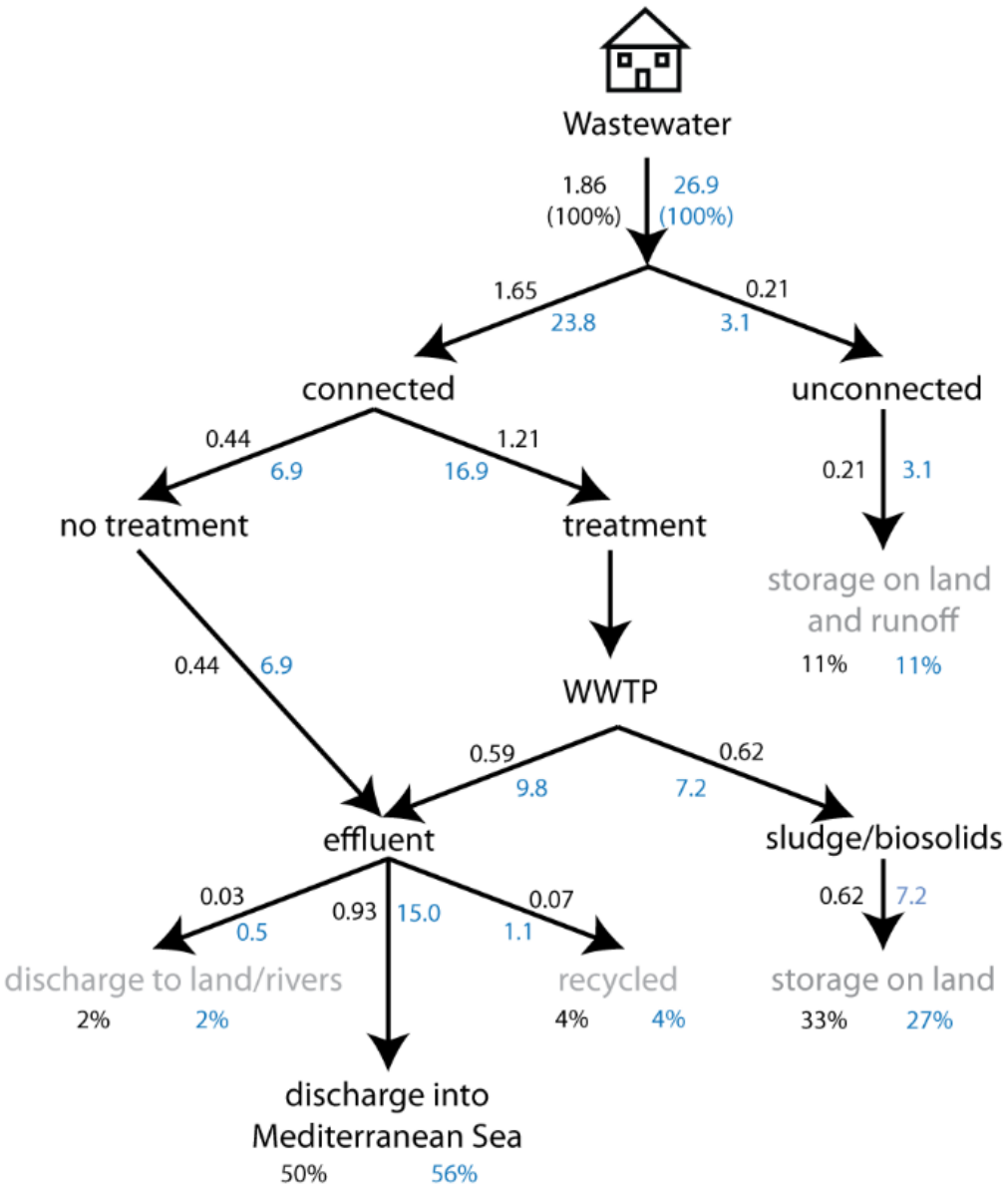

Figure 3.1: Flowchart for the calculation of direct domestic wastewater discharges of total P (TP) and total N (TN) into the Mediterranean Sea. The numerical values correspond to year 2003 (baseline values) fluxes of P (black) and N (blue) in units of 10^9 mol yr^{-1}, unless given as percentages of the corresponding total raw wastewater inputs.

information on treatment for a given WWTP could not be obtained, we assumed secondary treatment, as it is the most common treatment type in the countries around the MS. If a WWTP was under construction or out of order in 2003, we assumed that no wastewater treatment occurred. In addition, if f_c for a given city was unavailable, the average f_c of the host country for the year closest to 2003 was imposed (Table C.8). Wastewater treatment costs were estimated taking into account the capital, operational and maintenance costs (COM_i in € per m^3) for each treatment type i (primary, secondary or tertiary; Table C.14). The total wastewater treatment costs for a given coastal city were then computed as:

$$Cost = \sum(V_i * COM_i) \qquad (6)$$

where V_i ($m^3\,yr^{-1}$) is the annual volume of wastewater undergoing treatment type i.

The UNEP-MAP surveys provide the most comprehensive dataset on the distribution of WWTPs along the Mediterranean coastline in the early 21st Century (UNEP/MAP/MED-POL/WHO, 2004; 2008). Nonetheless, there are significant gaps in the data set, for example, lack of information on the connectivity to the sewage system or wastewater treatment type. In addition, the data quality varies from country to country. For instance, in the UNEP-MAP survey of cities with more than 10,000 inhabitants (UNEP/MAP/MED-POL/WHO, 2004), data for Spain do not include information on the level of connectivity of the population to the sewage network (f_c), whilst for Italy no treatment type is reported for about 50% of WWTPs (Table C.1a). In order to account for the uncertainties associated with the data, as well as with the assumptions made in our estimates, we calculated high and low values for the TP and TN discharges from individual WWTPs (see Table C.10 and C.11 for the imposed uncertainty ranges in the calculations). The uncertainties on the per capita P and N inputs to the sewerage system were assessed by assigning an uncertainty to each parameter in Equations 3.2 and 3.3 (Table C.11) and applying the average uncertainties on P,N_{capita} to Equation 3.1 across all Mediterranean countries.

A full validation of the empirical method used to estimate the direct domestic wastewater TP and TN discharges into the MS is currently impractical, primarily because of the lack of open reporting of direct monitoring data for surface and submarine outfalls. Nonetheless, measured outflows of P and N from a number of WWTPs in Spain and Italy (EEA, 2012) are in general agreement with values predicted based on Equation 3.1 (Nash Sutcliffe efficiencies, E, of 0.328 and 0.862 for P and N, respectively, Figure C.1). Differences in observed versus modelled discharge values mainly reflect uncertainties in treatment type and retention efficiencies. (For instance, for 50% of the WWTPs of Italian coastal cities with a population greater than 10,000 no treatment type is reported.)

Region	Acronym	Countries[1.]	Coastline (10^3 km)	Population (10^6 people)	P (10^9 mol yr^{-1})		N (10^9 mol yr^{-1})	
					Wastewater input	% treated	Wastewater input	% treated
North Mediterranean Countries	NMCs	2003 EU countries (France, Greece, Italy and Spain) plus Albania, Croatia, Cyprus, Malta, Montenegro, Slovenia	34.2[1]	37.2	0.48 (0.15-1.07)	79	7.5 (4.2-14.9)	80
East Mediterranean Countries	EMCs	Turkey, Syria, Lebanon, Israel, Gaza	5.8[1]	19.3	0.22 (0.13-0.32)	16	3.7 (2.2-4.8)	22
South Mediterranean Countries	SMCs	Egypt, Libya, Tunisia, Algeria, Morocco	5.7[1]	19.5	0.23 (0.15-0.35)	36	3.9 (2.8-5.2)	38
Total			45.8	76.0	0.93 (0.44-1.74)	53	15.0 (9.2-24.8)	55

Table 3.1: Mediterranean regions. Numerical values correspond to year 2003 (baseline values): coastal urban populations, model-derived direct wastewater discharges of TP and TN (values in brackets are minimum and maximum estimates), percentages of TP and TN discharges associated with treated wastewater.[1.]Plan-Bleu (2005).

3.3.2 Projections (Year 2050)

Projections of direct domestic wastewater P discharges to the MS in year 2050 were carried out taking into account the potential effects of population growth, changes in dietary habits, regulatory measures and upgrades in sewerage and water treatment infrastructure. The projections focus on P, because primary production in the MS tends to be P rather than N limited (Krom et al., 2010). The 2050 populations of coastal cities were estimated by extrapolating for each country the reported coastal urban population growth rate between 2000 and 2025 (Plan-Bleu, 2005) to 2050. In addition, we assigned a constant value of 115 g capita^{-1} day^{-1} to the 2050 protein intake in all the Mediterranean countries, that is, the combined average value of France, Greece, Italy and Spain in 2003 [30]. Thus protein intake decreased slightly in France, Greece and Israel in 2050 relative to 2003. We further imposed a minimum of 75% connectivity to all the coastal cities, which is the current EU average. Note that in all 2050 projections we assumed that cities maintain enough wastewater treatment capacity to accommodate the growth in wastewater inflow. Projections for the 2050 direct P and N discharge fluxes carry the same uncertainties as those in 2003.

The scenarios considered for the 2050 projections are summarized in Table 3.2 and their implementation described in detail in Appendix A. Scenarios B to I were designed to assess the potential effectiveness of various mitigation strategies in reducing the increases in direct domestic wastewater TP discharges relative to the no-mitigation scenario A (Figure 3.3). Mitigation measures included upgrading WWTPs using the average P retentions in Table C.9, extending EU legislation limiting the use of P in detergents to all Mediterranean countries (Regulation (EU) 2012), which would reduce P laundry detergent inputs by 92% and dishwasher detergents by 85% (BIO by Deloitte, 2014), and imposing a minimum of 50% re-use of treated wastewater – a reasonable future average recycling rate for the Mediterranean basin (FAO, 2014). We assumed that re-used wastewater does not contribute to the direct wastewater discharges of P and N to the MS.

3.4 Results

3.4.1 Direct domestic wastewater P and N inputs: Baseline (year 2003)

For 2003, our best estimates of the aggregated inputs of domestic TP and TN discharged directly into the entire MS, by 534 cities with population ≥10,000 plus 950 cities with 2000-10,000 inhabitants, are 0.93x10^{9} mol P yr^{-1} and 15x10^{9} mol N yr^{-1} (lower and higher bounds are 0.44-1.74x10^{9} mol P yr^{-1} and 9.2-24.8x10^{9} mol N yr^{-1}, see Tables C.1, C.10 and C.11 for details). For P, our best direct wastewater input estimate is comparable to the riverine input to the MS, while for N it is distinctly lower (Figure 3.2). According to Ludwig et al. (2009), in 1998 riverine input fluxes to the entire MS were 1.6x10^{9} mol P yr^{-1} and 77x10^{9} mol N yr^{-1}. A more detailed comparison shows that Ludwig, et al.'s 1998 riverine TP input is

Scenario	Acronym	Description
A	NMIT	**No mitigation:** projected change in direct TP inputs associated with domestic wastewater discharge due to (a) population growth, (b) per capita dietary P of 115 g capita^{-1} day^{-1}, plus (c) connecting at least 75% of the population to the sewage network in all coastal cities
B	REC50	At least **50% of treated wastewater is recycled** in all countries bordering the Mediterranean Sea and, hence not discharged to the MS.
C	ETER	All cities in **eutrophic areas** identified in Figure 3.4 **have minimum of tertiary treatment.**
D	LEG	**EU legislation** to reduce P in laundry (92% reduction) and dishwasher **detergent** (82% reduction) is applied to all countries (BIO by Deloitte, 2014).
E	ETER+LEG	Scenarios D and C combined
F	MSEC	All discharged wastewater has a **minimum of secondary treatment;** all current and projected WWTPs are assumed to be operational.
G	MSEC+LEG	Scenarios D and F combined.
H	MSEC+REC50	Scenarios B and F combined.
I	MTER	All wastewater discharged to the MS has a **minimum of tertiary treatment**; all current and projected WWTPs are assumed to be operational.

Table 3.2: Scenarios used in the year 2050 projections. In scenarios B-I all conditions are identical to those in scenario A, except for the imposed mitigation strategy.

1.6 times greater than our best estimate of direct domestic wastewater TP input to the Western Mediterranean (WMS), and 1.8 times greater for the Eastern Mediterranean Sea (EMS). Direct domestic wastewater TP inputs, however, exceed riverine inputs in the Alboran, Central, and North Levantine basins. For TN, riverine inputs are systematically higher than our best estimates of direct domestic wastewater inputs in every sub-basin of the MS, except in the Alboran Sea. (Note: see Figure 3.4 for the definitions of the Mediterranean sub-basins).

Among the three regions of the MS defined in Table 3.1. , North Mediterranean Countries (NMCs) contribute the highest direct domestic TP and TN wastewater discharges: 0.48×10^9 mol P yr^{-1} and 7.5×10^9 mol N yr^{-1}. Mainly, this reflects the higher coastal population of NMCs (37.2 million) compared to East Mediterranean Countries (EMCs, 19.3 million) and South Mediterranean Countries (SMCs, 19.5 million). Per person, NMCs discharge more P than EMCs and SMCs: 12.9, 11.5 and 11.8 mol P per year, respectively, while the N input per capita in NMCs is similar to SMCs and higher than EMCs (Table C.2). Incomplete data for Spain and Italy, however, represent a major source of uncertainty on the direct domestic wastewater inputs of NMCs (Table C.1a). As a consequence, the lower bound estimates for NMCs (0.15×10^9 mol P yr^{-1} and 4.2×10^9 mol N yr^{-1}) fall within the ranges calculated for EMCs and SMCs.

Treated wastewater contributes most to the direct domestic wastewater P and N inputs from NMCs (79% and 80% of the TP and TN total inputs, respectively); for EMCs and SMCs untreated wastewater is the main source, with only 16 and 36% contributions from treated wastewater, respectively (Table 3.1). Lebanon, Libya and Syria, in particular, lack adequate wastewater treatment facilities: 95-100% of all P and N in effluent outfalls into the MS comes from untreated wastewater. Of all the sub-basins of the EMS, the North Levantine basin yields the highest per capita TP and TN inputs from direct domestic wastewater discharges (Table C.2).

3.4.2 Direct domestic wastewater P inputs: Projections (year 2050)

Population growth is generally the main driver of the projected increases in TP inputs. The total population of Mediterranean coastal cities is predicted to increase from 76 million in 2003 to 130 million in 2050 (Table C.5). For the entire MS basin, population growth alone would result in a 72% higher direct domestic wastewater TP input in 2050, relative to 2003. For EMCs and SMCs, the corresponding increases are 103% and 159%, respectively, but only 15% for NMCs (see scenario A in Figure 3.3, and Table C.5).

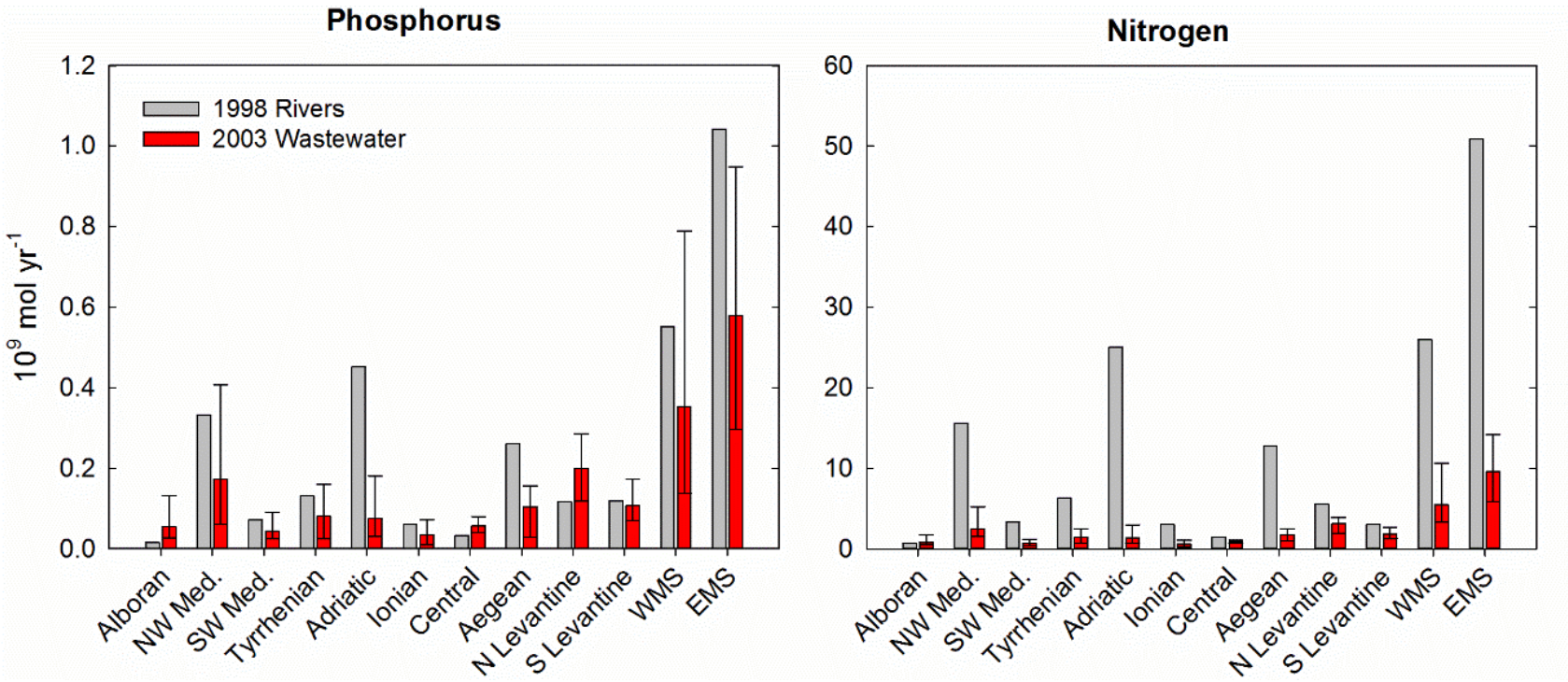

Figure 3.2: Inputs of TP and TN to the Mediterranean Sea: direct domestic wastewater versus riverine discharges. Wastewater inputs are those calculated in this study for year 2003 (baseline), riverine inputs are those reported in Ludwig et al. (2009) for year 1998. Error bars represent estimated flux ranges (see Tables C.10 and C.11 for details). WMS = Western Mediterranean Sea, EMS = Eastern Mediterranean Sea. For the definition of the sub-basins: see Figure 3.4.

The results of scenarios B-I illustrate the large differences among the three Mediterranean regions (Figure 3.3). For NMCs, all mitigation scenarios bring the 2050 direct domestic TP inputs below that in 2003, except for scenarios C and F. The wastewater treatment upgrades imposed in scenarios C and F are not highly effective for NMCs, because most direct urban wastewater discharge already undergoes secondary or tertiary treatment. This is not the case for EMCs and SMCs and, in these regions, scenario F in particular results in large relative decreases of the direct P discharges. Re-cycling of treated wastewater alone has a greater relative impact for SMCs than EMCs (scenario B), because much wastewater goes untreated in EMCs and over 50% of treated wastewater in most EMCs was already being recycled in 2003 (FAO, 2014; Table C.15). However, when recycling of treated wastewater is combined with a minimum secondary treatment (scenario H), the predicted 2050 direct wastewater TP discharges decrease significantly relative to the no-mitigation scenario A. In EMCs, scenario H even yields 2050 TP inputs below the 2030 value. Introducing EU legislation limiting P in detergents to all Mediterranean countries strongly reduces direct domestic TP inputs in EMCs (scenarios D and G), because of the current high laundry and dishwasher detergent use in Israel (Table C.7). For the three regions, major relative reductions in TP inputs, to at least 74% below 2003 values, would be achieved by switching to 100% tertiary wastewater treatment (scenario I).

3.5 Discussion

The calculated TP and TN inputs show that direct discharges of treated and untreated domestic wastewater is an important, so far mostly ignored, pathway for transporting nutrients to the MS (Figure 3.2). This is more pronounced for P than N. The estimated 2003 direct domestic wastewater TP input to the entire MS (0.93×10^9 mol P yr^{-1}) is comparable to atmospheric deposition of total dissolved P, 1.0-2.5×10^9 mol yr^{-1} (Markaki et al., 2010), and an order of magnitude greater than estimates of the freshwater dissolved inorganic P (DIP) delivered by submarine groundwater discharge, 0.02×10^9 mol yr^{-1} (Rodellas et al., 2015). The direct domestic wastewater input of TN to the MS (15×10^9 mol yr^{-1}) is relatively less important, but still significant compared to total dissolved N deposited from the atmosphere, 67-176×10^9 mol yr^{-1} (Markaki et al., 2010), or dissolved inorganic N (DIN) delivered via fresh submarine groundwater discharge, 30×10^9 mol yr^{-1} (Rodellas et al., 2015). Thus, direct wastewater discharges into the MS need to be accounted for in the N and P biogeochemical budgets of the MS.

The inputs summarized in Table 3.1 are low-end estimates, for the following reasons. (i) They are derived from the permanent coastal population sizes (when the data are available), rather than population equivalents, hence neglecting the increase in summer population due to tourism. (ii) They apply high-end estimates for P and N retention by WWTPs (Table C.9). (iii) They assume that P and N associated with wastewater not collected by sewers remain on land (Van Drecht et al., 2009). (iv) They do not include the

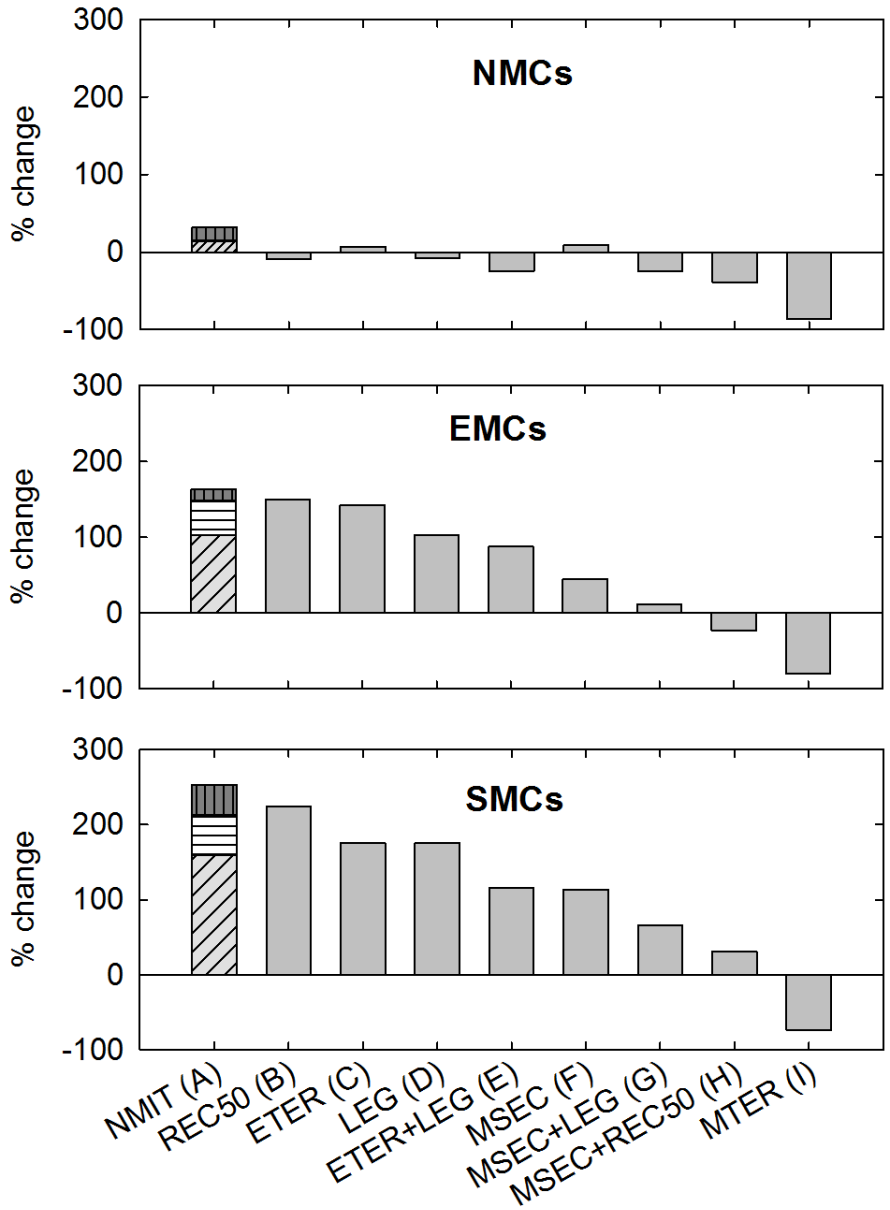

Figure 3.3: Changes in direct domestic wastewater TP inputs to the Mediterranean Sea in 2050, expressed as percentages relative to the corresponding 2003 inputs, for the scenarios defined in Table 3.2. For the non-mitigation scenario A (NMIT), the diagonal, horizontal and vertical lines identify the relative contributions of population growth, changes in diet, and connecting at least 75% of all inhabitants of coastal cities to the sewage network. See text for further details.

contributions of direct industrial wastewater discharges. Thus, the total inputs of P and N associated with direct disposal of wastewaters into the MS could be considerably larger than the estimates presented here.

According to Morée et al. (2013), industrial P and N discharges globally amount to about 15% of the corresponding domestic sources. For the Baltic Sea, industrial sources of P and N make up 14-16% of the total – municipal plus industrial – wastewater inputs (Larsson et al., 1985), while industrial inputs may represent up to 50% of the direct wastewater P releases to the Laurentian Great Lakes (Dolan and Chapra, 2012). Data reported by UNEP/WHO (1999) also imply that industrial effluents are a large source of nutrients in direct wastewater discharges to the MS. The available data, however, are insufficient to produce spatially explicit estimations of industrial P and N inputs to the MS, similar to those of the domestic inputs in Figure 3.4. More complete estimations will require countries sharing the MS to more consistently and openly report discharges from WWTPs and industrial sources.

In particular for coastal areas where riverine inputs are minimal, for example offshore Lebanon and the Athens metropolitan area, direct wastewater discharges are a probable driver of observed eutrophication (Figure 3.4). However, the ecological impacts of P and N delivery to aquatic environments not only depend on the total input fluxes, but also on the speciation of the nutrient elements (Chapter 2; Appendix A). Based on average effluent compositions for the three wastewater treatment types (Table C.13), we estimate that domestic wastewater discharges supply TP to the MS in approximately the following proportions: 43% dissolved inorganic P, 22% particulate inorganic P, 25% particulate organic P, and 10% dissolved organic P (Table C.3). A similar calculation yields 65% of discharged TN in the form of dissolved NH_4, which tends to be preferentially assimilated by phytoplankton compared to other N species (Zehr and Ward, 2002).

The large economic contrasts between Mediterranean regions are reflected in the differences in domestic wastewater nutrient inputs discharged into the sea. The higher TP input per capita in NMCs, compared to EMCs and SMCs, largely reflects higher contributions from laundry and dishwashers detergents (Tables C.2a and C.7). A surprisingly large number of European countries bordering the MS still consumed P-containing laundry detergents in 2003, with only Italy, Monaco and Slovenia reporting 100% P-free detergents (Table C.7). Legislative measures, intended to be implemented by 2017, should reduce P inputs from laundry and dishwasher detergents in EU countries by 92% and 85%, respectively (Regulation (EU) 2012; BIO by Deloitte, 2014, EU regulation 259/2012). These regulatory changes alone would reduce the 2003 direct P input from NMCs by 33% (Figure C.3) and, if implemented by 2050, would result in no additional P entering the MS from NMCs via direct wastewater discharges relative to 2003 (scenario D). Enforcement of the same regulations by all countries would achieve an overall

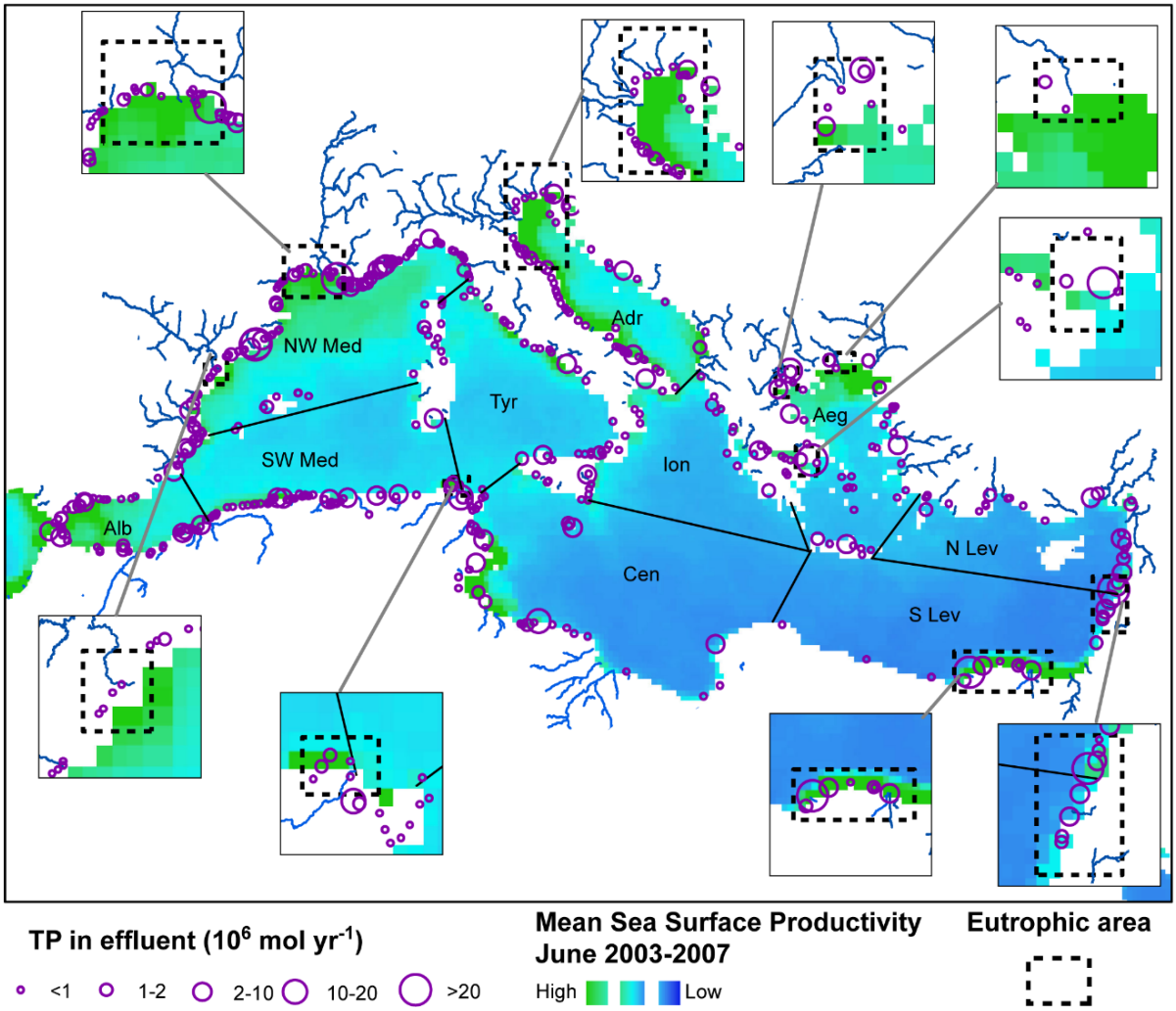

Figure 3.4: Direct domestic wastewater discharges of TP into the Mediterranean Sea from cities with more than 10,000 inhabitants (purple circles) in year 2003 (baseline). Also shown are the spatial distribution of the mean primary productivity across Mediterranean surface waters (Kershaw, 2008), and coastal areas with 2 or more classified eutrophic sites between 1960 and 2010 (dashed boxes; Diaz et al., 2011). Alb = Alboran Sea; NW Med = North-West Mediterranean; SW Med = South West Mediterranean; Tyr = Tyrrhenian Sea; Cen = Central Mediterranean; Ion = Ionian Sea; Adr = Adriatic Sea; Aeg = Aegean Sea; N Lev = North Levantine; S Lev = South Levantine.

lowering of wastewater discharges of P by 30% for the entire MS (Figure C.3). Phosphorus-limiting legislation is thus an attractive strategy to help reduce direct wastewater P inputs (Figure 1.1, scenario D), also given that phosphate-free detergents do not increase manufacturing costs substantially, while a reduction in phosphorus loading to WWTPs lowers their operational costs (BIO by Deloitte, 2014).

Re-use of treated wastewater can also effectively curb P inputs from direct wastewater discharges (scenarios B and H; Figure 3.3). In the early 2000s, significant re-use of treated wastewater was already occurring in many Mediterranean countries, including Syria (100% re-use), Libya (100%), Lebanon (50%), Cyprus (95%), Israel (88%), Egypt (28%), Tunisia (23%), Spain (13%) and France (11%) (Table C.15; Angelakis et al., 1999; UNEP/MAP/MED-POL/WHO, 2004; FAO, 2014). With growing populations and increasingly arid conditions in the future, water re-use is bound to become more important in North Africa and the Middle East (Angelakis et al., 1999; Hamoda, 2004; García-Ruiz et al., 2011). Additional incentives are (i) the cost, which is approximately half that of creating usable water by desalination plants (Hamoda, 2004), and (ii) the recovery of P and N, under the form of biosolids, sludge and wastewater itself, which can be used as fertilizer for agricultural production. The latter also represents a mitigation measure to deal with the projected depletion of P mining reserves within the next 50-400 years (Van Vuuren et al., 2010; Cordell et al., 2011; Desmidt et al., 2015). Increasing the re-use of treated wastewater in SMCs and EMCs, however, will require further investment in WWTPs coupled to stringent regulations and monitoring (Brissaud, 2008).

Of all mitigation measures considered, only the complete upgrade of all WWTPs to tertiary treatment results in 2050 P wastewater discharges from SMCs that are below the corresponding 2003 values (scenarios I, Figure 3.3). However, the added costs associated with the complete conversion to tertiary treatment may be prohibitive: relative to the 2050 no-mitigation scenario, the additional costs are estimated to be on the order of €930 million yr^{-1} for SMCs alone, and €2.2 billion yr^{-1} for the entire MS basin (Table 3.3). These estimations are based on the differences in average costs for primary, secondary and tertiary treatment (Table C.14). Therefore, a more achievable course of action to manage coastal eutrophication caused by direct wastewater discharges may be to limit upgrades to tertiary treatment to recognized eutrophic areas, while accelerating the transition to phosphate-free detergents, and promoting the re-use of treated wastewater throughout the Mediterranean region.

A unique aspect of the Mediterranean basin is that it includes countries of widely different levels of economic development. Hence, trends observed for the MS may provide lessons for other parts of the world. In coastal areas with rapidly growing populations a first public health response is typically to expand the sewerage system. If this is not matched by increased wastewater treatment or other mitigation

measures, discharges of nutrients and other contaminants to the coastal zone may actually increase. Results for EMCs and SMCs indicate that for less developed countries curbing coastal wastewater nutrient inputs may represent a major financial challenge (Table 3.3). Direct discharges of wastewater are thus likely to continue to threaten many coastal areas around the world.

	2003	2050: scenario A	2050: scenario C	2050: scenario F	2050: scenario I
NMC	682	861	984	1052	1452
EMC	96	244	339	715	960
SMC	110	362	658	920	1296

Table 3.3: Annual costs of wastewater treatment (in 10^6 € yr^{-1}) for the 2003 baseline and 2050 projections. Scenario A: no mitigation; scenario C: minimum tertiary treatment in eutrophic areas; scenario F: minimum secondary treatment of all wastewater; scenario I: minimum tertiary treatment of all wastewater. See Table 3.2 for complete definitions of scenarios.

Chapter 4.

Circulation and oxygen cycling in the Mediterranean Sea:

Sensitivity to future climate change

Modified from: **Helen R. Powley**, Michael D. Krom, Philippe Van Cappellen. (2016) Circulation and oxygen cycling in the Mediterranean Sea: Sensitivity to future climate change. *Journal of Geophysical Research:Oceans,* **121,** 8230-8247, doi*:* 10.1002/2016JC012224.

4.1 Summary

Climate change is expected to increase temperatures and decrease precipitation in the Mediterranean Sea (MS) basin, causing substantial changes in the thermohaline circulation (THC) of both the Western Mediterranean Sea (WMS) and Eastern Mediterranean Sea (EMS). The exact nature of future circulation changes remains highly uncertain, however, with forecasts varying from a weakening to a strengthening of the THC. Here, we assess the sensitivity of dissolved oxygen (O_2) distributions in the WMS and EMS to THC changes using a mass balance model, which represents the exchanges of O_2 between surface, intermediate and deep water reservoirs, and through the Straits of Sicily and Gibraltar. Perturbations spanning the ranges in O_2 solubility, aerobic respiration kinetics and THC changes projected for the year 2100 are imposed to the O_2 model. In all scenarios tested, the entire MS remains fully oxygenated after 100 years; depending on the THC regime, average deep-water O_2 concentrations fall in the ranges 151-205 and 160-219 μM in the WMS and EMS, respectively. On longer timescales (>1000 years), the scenario with the largest (> 74%) decline in deep-water formation rate leads to deep-water hypoxia in the EMS but, even then, the WMS deep-water remains oxygenated. In addition, a weakening of THC may result in a negative feedback on O_2 consumption as supply of labile dissolved organic carbon to deep-water decreases. Thus, it appears unlikely that climate-driven changes in THC will cause severe O_2 depletion of the deep-water masses of the MS in the foreseeable future.

4.2 Introduction

The Mediterranean Sea (MS) basin is considered one of the world's regions most responsive to global climate change (Giorgi, 2006). Major changes in circulation and environmental status as a result of natural climate change have punctuated the MS's recent geological past (Rohling et al., 2015 and references therein). Over the coming decades, the MS is predicted to become warmer and drier (Collins et al., 2013; Kirtman et al., 2013), thus increasing water column temperature and salinity (Gualdi et al., 2013, and references therein). Temperature and salinity have opposing effects on the density of water and therefore on the Mediterranean thermohaline circulation (THC). Modeling results generally predict that the THC will weaken in response to projected future climate change, with lower water flows into and out of the deep water layers (Thorpe and Bigg, 2000; Somot et al., 2006; Herrmann et al., 2008a; Planton et al., 2012). Adloff et al. (2015), however, show that Mediterranean THC model responses to climate change are very sensitive to the imposed boundary conditions: depending on how the latter are formulated, predictions range from a weakening to a strengthening of the THC.

The MS has been described as a laboratory for studying environmental change in ocean systems (Bergamasco and Malanotte-Rizzoli, 2010). Deep water (DW) temperature and salinity of the Western Mediterranean Sea (WMS) have been increasing since at least the 1960s (e.g. Béthoux et al., 1990; Rixen et al., 2005; Marty and Chiaverini, 2010; Borghini et al., 2014), reflecting a strong coupling of water column properties to atmospheric forcing. In recent decades, a major change was detected in the circulation of the Eastern Mediterranean (EMS), with DW formation strengthening and switching location temporarily from the Adriatic Sea to the Aegean Sea, a phenomenon referred to as the Eastern Mediterranean Transient (EMT; Roether et al., 1996). The EMT altered the salinity and heat signatures of intermediate water (IW) flowing through the Strait of Sicily (Gasparini et al., 2005; Roether and Lupton, 2011), in turn triggering enhanced DW formation in the WMS between 2004 and 2006 (Schroeder et al., 2006; Schroeder et al., 2008b), known as the Western Mediterranean Transition (WMT). The EMT left distinct biogeochemical signatures on the water masses of the MS, including changes in the distributions of oxygen (O_2), phosphorus and nitrogen (Klein et al., 1999; Klein et al., 2003; Kress et al., 2003; Kress et al., 2012; Kress et al., 2014; Schneider et al., 2014; Chapter 2).

Dissolved O_2 is a biogeochemical master variable in marine and freshwater ecosystems. The biogeochemical cycles of carbon and nutrients are closely coupled to that of O_2 through primary production and organic matter respiration. Oxygen consumption rates in the DW of the MS are relatively high when compared to DW of the Atlantic and Pacific Oceans (Christensen et al., 1989; Roether and Well, 2001). In the MS, DW O_2 consumption is partly coupled to the respiration of dissolved organic

carbon (DOC) supplied from areas of DW formation, which supplements aerobic degradation of sinking particulate organic carbon (POC) (Christensen et al., 1989; Lefèvre et al., 1996; Santinelli et al., 2010). At the present time, relatively high rates of DW formation and low primary productivity keep the MS well ventilated with DW O_2 saturation levels above 70%.

In this paper, we use an O_2 mass balance model coupled to a simple representation of the water cycle in the WMS and EMS to analyze the potential effects of predicted future changes in THC driven by climate change on the O_2 levels of the IW and DW masses of the MS. Specifically we impose perturbations to the O_2 and water cycles that span the published range of changes in temperature, salinity and circulation projected for the year 2100. The relative effects of O_2 solubility, respiration kinetics and circulation are assessed, with particular attention given to the differences in O_2 dynamics in the WMS versus the EMS.

4.3 Coupled water-oxygen cycling model

4.3.1 Baseline water cycle

The water cycle model of the MS builds on that previously developed for the EMS (Appendix A). The water columns of both WMS and EMS are split into 3 depth intervals (Figure 4.1): surface water (WMSW and EMSW), intermediate water (WMIW and EMIW) and deep water (WMDW and EMDW). The water reservoirs defined in Figure 4.1 approximate water masses referred to by different names in the literature: WMSW and EMSW correspond roughly to Atlantic Water (AW), while Levantine Intermediate Water (LIW) is used to refer to WMIW and EMIW. Note, however, that Western Intermediate Water and Tyrrhenian Deep Water are also included in WMIW and WMDW, respectively. A detailed justification of the fluxes associated with the EMS water cycle can be found in Appendix A.

The MS is an evaporative basin. Long-term evaporation (E) minus precipitation (P) in the WMS is 490±7 mm yr^{-1}, based on data from 1948 to 2009 (Criado-Aldeanueva et al., 2012). Average riverine input (R) of freshwater into the WMS between 1960 and 2000 is estimated at 123±10 km^3 yr^{-1} (Ludwig et al., 2009). Fresh submarine groundwater discharge (SGD) for the entire MS is estimated at 68 km^3 yr^{-1} by Zekster et al. (2007). The latter authors also provide region-by-region SGD values for the MS, from which we derive a fresh SGD input to the WMS of 27±2 km^3 yr^{-1}. Net evaporation (E-P-R-SGD) for the WMS is therefore 249±18 km^3 yr^{-1}, or 0.008±0.0004 Sv (Figure 4.1). In the EMS, net evaporation is estimated at 0.055 Sv (see Appendix A for details).

Quantifying the flow of water through the Strait of Gibraltar is key to the water balance of the MS. Estimates of the outflow to the Atlantic Ocean range from 0.68 Sv, using direct flow measurements over the course of one year (Bryden et al., 1994), to 1.6 Sv based on salt and heat balance calculations

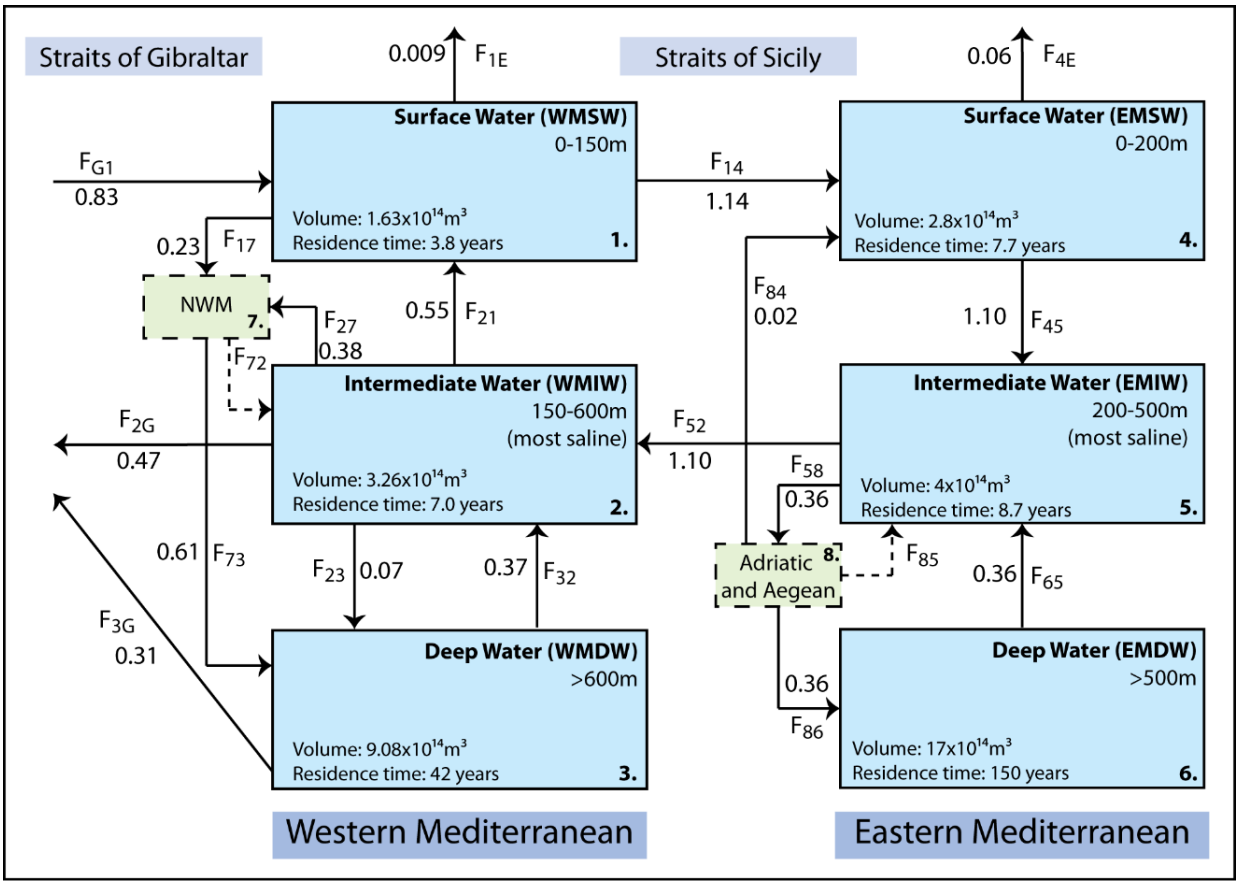

Figure 4.1: Water cycle model. Reservoir volumes assume WMS and EMS surface areas of 815 x 10^3 km^2 and 1336 x 10^3 km^2, respectively. Fluxes are given in Sv (10^6 m^3 s^{-1}). The North-West Mediterranean (NWM) represents the area where DW formation occurs. Dashed arrows represent fluxes that are only included in the climate change scenarios, dashed boxes fall outside the model domain. See text for complete discussion.

(Béthoux and Gentili, 1999). Recent continuous deployments of Acoustic Doppler current profilers from 2004 to 2007 yield an outflow flux of 0.78±0.05 Sv (Sánchez-Román et al., 2009; Soto-Navarro et al., 2010), which is the value used in our model. The net inflow of water through the Strait of Gibraltar calculated from a global freshwater balance for the MS is 0.038±0.007 Sv (Soto-Navarro et al., 2010). Hence, the steady state inflow from the Atlantic Ocean must be close to 0.82±0.06 Sv. The final model value is adjusted to 0.83 Sv to maintain a steady state water balance for the WMSW. The water exiting the WMS through the Strait of Gibraltar is a mixture of intermediate and deep water (Millot, 2009; 2014). Based on a recent statistical analysis of continuous pH measurements at the Espartel Sill from 2012 to 2015, Flecha et al. (2015) estimate that 40% of the outflow is comprised of WMDW and 60% of WMIW, in agreement with previous estimates by García Lafuente et al. (2007). Imposing the same fractions in our water cycle then gives the water fluxes through the Strait of Gibraltar in Figure 4.1.

After entering the WMS through the Strait of Gibraltar, WMSW travels along the African coast and, in part, flows into the EMS via the Strait of Sicily, while the other part flows into the Tyrrhenian Sea (Schroeder et al., 2008c). Upon flowing into the EMS, surface water (SW) continues traveling eastwards while evaporation increases salinity. Ultimately, EMSW sinks to form EMIW that, in turn, exits the EMS through the Strait of Sicily to the WMS, and through the Strait of Otranto and the Cretan Straits to the Adriatic and Aegean Seas, respectively. Deep-water formation in the Adriatic and Aegean Seas returns modified EMIW to the EMDW reservoir at a combined rate of 0.36 Sv (Appendix A). Note that the Adriatic and Aegean Seas fall outside the model domain, hence allowing us to impose DW formation as an external forcing to the THC of the EMS. To maintain the water balance of the MS, EMDW formation is offset by upwelling of EMDW into EMIW.

Deep-water in the WMS forms primarily in the northwestern Mediterranean Sea (NWM). Similar to the EMS, we exclude the area of DW formation in the NWM from the model domain. The corresponding area is estimated to cover about 25000km^2 (L'Hévéder et al., 2013). Two mechanisms contribute to DW formation in the NWM: open ocean convection and cascading of shelf water from the Gulf of Lions. Annual WMDW formation from open ocean convection in the NWM for the period 1959-2001 ranges between 0 and 3.2 Sv (L'Hévéder et al., 2013; Table D.1), depending on the severity of the preceding winter. From the 1959-2001 record, we estimate a long-term annual average rate of DW formation by open ocean convection of 0.60 Sv.

Dense water cascading downslope from the Gulf of Lions also occasionally contributes to DW formation. Over a 28 day period in 1999, 0.18 Sv of water flowed down from the Gulf of Lions shelf into the WMDW reservoir (Béthoux et al., 2002a). Assuming this was the only event occurring that year, an

equivalent annual average rate of WMDW formation of 0.01 Sv is obtained, which is the value used in the water cycle model. Note, however, that WMDW formation through this mechanism may be as high as 0.07 Sv (or 6% of the open ocean convection DW flux), as occurred during the extreme winters of 2005 and 2012 (de Madron et al., 2005; Ulses et al., 2008; de Madron et al., 2013). Using the lower value of 0.01 Sv is reasonable given that cascading of deep water only occurred in four years during the 1971-2000 period (Béthoux et al., 2002a). In the baseline simulations, the total WMDW formation rate originating from the NWM area is thus 0.61 Sv, nearly twice the DW formation rate in the EMS (Figure 4.1). Deep water convection arises from preconditioning of WMSW by cyclonic circulation and Mistral wind activity, plus admixing of high salinity WMIW which further increases water density (Medoc Group, 1970). Rhein (1995) estimates that 38% of WMDW formation originates from WMSW and 62% from WMIW, based on chlorofluoromethane distributions. Here, we assign the same proportions to the WMDW formation flux, yielding 0.23 Sv of WMDW produced from WMSW and 0.38 Sv from WMIW.

In addition to DW formation in the NWM, Tyrrhenian Deep Water (TDW) is formed in the Tyrrhenian Sea through cascading and mixing of EMIW after it enters the WMS through the Strait of Sicily (Gasparini et al., 2005). As the inflowing EMIW water is much denser than surface and intermediate waters of the Tyrrhenian Sea it cascades down to depths of up to 2000 m. The formation of TDW is represented in the water cycle model as a conversion of WMIW into WMDW. Based on the flows of WMDW entering and exiting the Tyrrhenian Sea reported by Schroeder et al. (2008c), we estimate that TDW contributes 0.07 Sv to the DW reservoir of the WMS.

The upwelling fluxes from WMDW to WMIW and from WMIW to WMSW are derived assuming a steady state water cycle for the WMS. The net upwelling from WMIW to WMSW is the result of the lower water fluxes through the Strait of Gibraltar compared to the Strait of Sicily. Nonetheless, downwelling from WMSW to WMIW occasionally occurs (Millot, 1999; Fuda et al., 2000; Vargas-Yáñez et al., 2012). Because of the lack of quantitative information on the downwelling flux, it is not included explicitly in the water cycle model.

The water cycle illustrated in Figure 4.1 yields a WMDW residence time of 42 years, three times shorter than for the EMDW (150 years). The large difference in DW residence time between the two basins of the MS is due to more intense DW formation in the WMS plus the smaller WMDW reservoir size. The residence times for SW and IW are similarly smaller for the WMS than EMS. The WMDW residence time in the water cycle model is at the upper end of the 20-40 year range reported in older studies (Rhein, 1995; Stratford et al., 1998; Béthoux and Gentili, 1999), and somewhat lower than the recently proposed

50-70 year range of Schneider et al. (2014), who derived mean water ages in the WMS from CFC-12 distributions.

4.3.2 Oxygen cycle

The O_2 mass balance model explicitly computes O_2 reservoir sizes of the IW and DW layers. Oxygen in SW is assumed to remain near saturation with the atmosphere so is not explicitly modeled. The model is initialized by assigning average O_2 concentrations to the SW, IW and DW layers obtained from the MEDATLAS database for the period 1906-1987 (MEDAR Group, 2002) (Figure 4.2; Figure D.1;Table D.2). For comparison, O_2 concentrations reported for individual cruises are compiled in Table D.2. With the exception of the turbulent mixing exchanges, O_2 fluxes between reservoirs are computed by multiplying the corresponding water flow with the O_2 concentration of the source reservoir. For the water supplied to the WMDW reservoir from the NWM DW formation area, the O_2 concentration is assumed to be that of the WMSW, because of the intense mixing that occurs during deep convection (Medoc Group, 1970). For DW formation in the EMS, we impose average winter O_2 concentrations measured in the deeper (>800m) waters of the Adriatic and Aegean Seas because these water masses are the source areas of the newly formed DW entering the EMDW through the Strait of Otranto and Cretan Straits, respectively (Table D.2).

Appendix A modeled the turbulent mixing fluxes of P and N between EMSW and EMIW assuming a linear dependence on the concentration differences between the two water masses, with an effective diffusion coefficient K_z of 2.3 x 10^{-4} m^2 s^{-1}. Because turbulent mixing is somewhat weaker in the WMS (Moutin and Raimbault, 2002), a comparable, but smaller K_z value (1.2 x 10^{-4} m^2 s^{-1}) is used to calculate mixing fluxes of O_2 between WMSW and WMIW. Cuypers et al. (2012) further showed that very little mixing occurs between IW and DW water layers. Therefore, we impose a low K_z value of 10^{-7} m^2 s^{-1} for turbulent diffusion of O_2 between WMIW and WMDW, and between EMIW and EMDW. This value falls at the lower end of the reported range of measured K_z values in the MS (10^{-7} to 7 x 10^{-4} m^2 s^{-1}; Bianchi et al., 1999; Copin-Montégut, 2000; Moutin and Raimbault, 2002; Cuypers et al., 2012; Forryan et al., 2012).

Once the O_2 fluxes between reservoirs are known, the pre-EMT O_2 consumption rates are obtained assuming a steady state O_2 cycle (Figure 4.2). In order to model transient changes in O_2 cycling, two formulations for the O_2 consumption rate are considered. In the first formulation, a simple saturation kinetics expression is used:

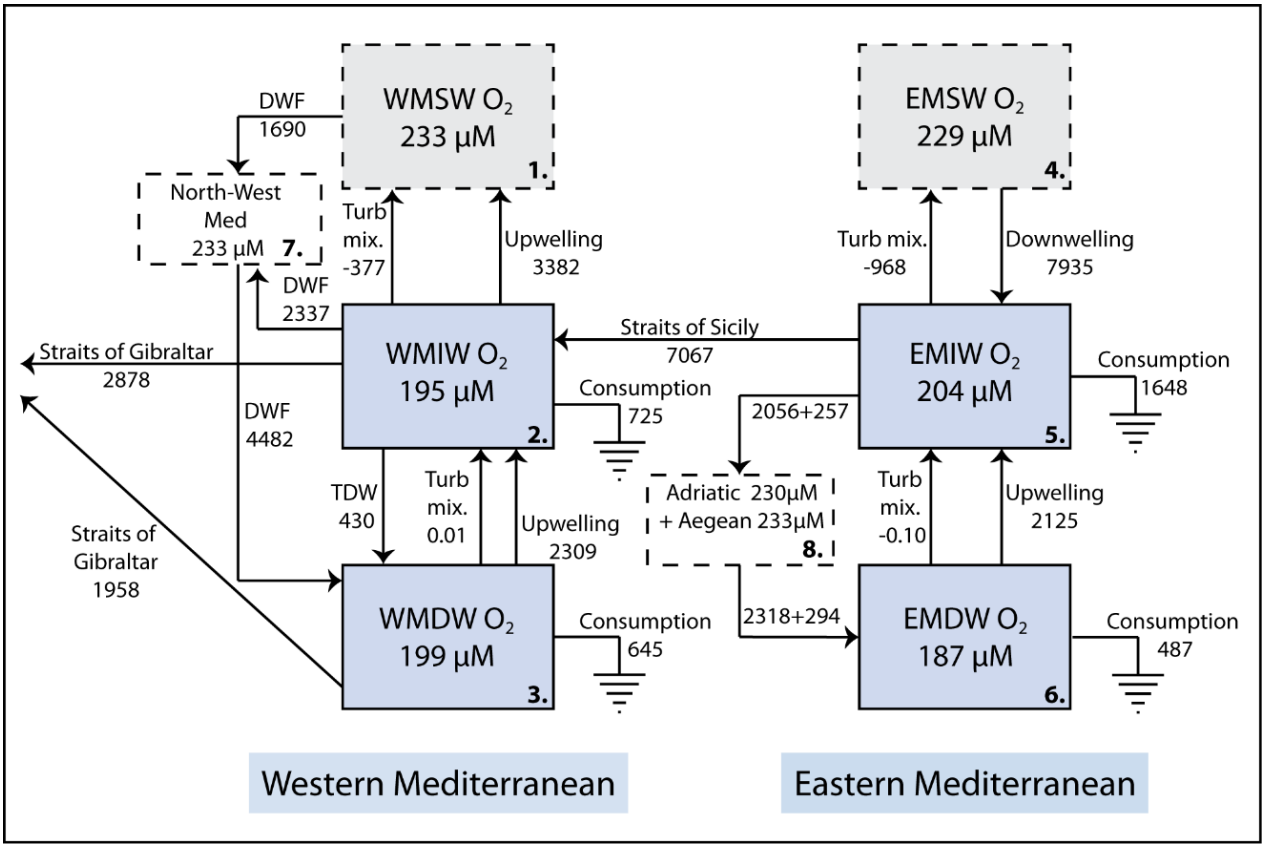

Figure 4.2: Baseline (pre-EMT) steady state oxygen cycle. Dashed boxes represent reservoirs outside the model domain. Fluxes are given in 10^9 mol yr^{-1}. DWF= deep water formation; TDW = Tyrrhenian deep water formation. See text for complete discussion.

$$F_{O_2,i} = F_{max,i} \cdot \frac{[O_2]_i}{[O_2]_i + K_s} \quad i = \text{WMIW, WMDW, EMIW, EMDW} \qquad (4.1)$$

where F_{O_2} is the annual O_2 consumption rate in a given water layer (in mol yr^{-1}), F_{max} is the maximum (or potential) O_2 consumption rate in the same water layer, when O_2 is non-limiting, $[O_2]$ is the O_2 concentration of the water layer (μM), and K_s is the O_2 half-saturation concentration, which is assigned the value of 6.25 μM proposed by Testa et al. (2014). For each of the IW plus DW reservoirs the value of F_{max} is calculated from the corresponding pre-EMT steady state O_2 concentration and consumption rate (Table D.3).

Equation (4.1) is based on the classical Michaelis-Menten saturation formulation for the biological utilization of a substrate. When the O_2 concentration significantly exceeds the half saturation value K_s, the O_2 consumption rate is independent of $[O_2]$ and approaches its maximum value F_{max}. This is the case for the present-day open MS for which $[O_2] >> K_s$ at all depths. The use of Equation (4.1) assumes that the reducing power available for O_2 respiration in a given water layer does not change over time. The main source of reducing power is the supply of degradable organic matter, either as POC associated with sinking particulate matter or DOC present in inflowing water.

Marked increases in DW O_2 consumption during the EMT and WMT have been attributed to the enhanced supply of (relatively) labile DOC originating from the areas of DW formation (Klein et al., 2003; Schneider et al., 2014). The second formulation for the oxygen consumption rate in the DW reservoirs therefore expands Equation (4.1) in order to account for both the relatively fast respiration of labile DOC, supplied from the Adriatic Sea, Aegean Sea and NWM, and the slower degradation of sinking POC:

$$F_{O_2,i} = \left(F^{DOC}_{max,i} \cdot \frac{[DOC]_i}{[DOC]_i + K_{DOC}} + F^{POC}_{max,i} \right) \cdot \frac{[O_2]_i}{[O_2]_i + K_s} \quad i = \text{WMDW, EMDW} \qquad (4.2)$$

where F^{DOC}_{max} and F^{POC}_{max} are the maximum DW O_2 consumption rates associated with DOC and POC respiration, respectively, $[DOC]$ is the DOC concentration in the DW reservoir, and K_{DOC} is the DOC half-saturation concentration, which is assigned the value of 4.16 μM proposed by Testa et al. (2014). As written, Equation (4.2) requires the explicit calculation of the changes in DW DOC concentrations. To circumvent this requirement, we replace $[DOC]$ in Equation (4.2) by the (virtual) DOC-associated O_2 concentration, that is, the portion of the total O_2 concentration in the DW reservoir that can react with DOC. To use the modified Equation (4.2), values must be assigned to F^{POC}_{max} and F^{DOC}_{max}, as well as to the initial DOC-associated O_2 concentration of the DW reservoir. The DOC half-saturation concentration

K_{DOC} is converted into an O_2 half saturation concentration using a molar O_2:C ratio of 172:122 (Takahashi et al., 1985).

For the EMS, F_{max}^{POC} is estimated based on the EMDW O_2 consumption rates before and during the EMT. The pre-EMT O_2 consumption rate is that derived for the steady state O_2 cycle (487 x 10^9 mol yr^{-1} or 0.29 µM yr^{-1}, Figure 4.2). For the EMT, the rate is approximated by considering the observed O_2 consumption in Aegean DW (2.2 µmol kg^{-1} yr^{-1}; Klein et al., 2003) and the total volume of Aegean DW that entered the EMDW reservoir during the EMT, that is, between 1987 and 1995 (2.3 x 10^{14} m^3; Roether et al., 2007). Assigning the pre-EMT O_2 consumption rate (0.29 µM yr^{-1}) to the volume of EMDW not replaced by inflowing Aegean DW over the same period of time then yields an average annual O_2 consumption rate for the entire EMDW during the EMT of 965 x 10^9 mol yr^{-1} (or 0.57 µM yr^{-1}). If we further assume a linear dependence of the rate of EMDW O_2 consumption on the rate of DW formation (Figure D.2), a value of F_{max}^{POC} of 295 x 10^9 mol yr^{-1} is derived from the y-intercept of the linear relationship. We are now left with two unknowns, F_{max}^{DOC} and the DOC-associated O_2 concentration. These two variables are coupled to one another via Equation (4.2) under the steady state, pre-EMT conditions. Next, the initial DOC-associated O_2 concentration is varied until the predicted temporal trend of the EMDW O_2 concentration satisfactorily reproduces the observed O_2 variations during the EMT (see section 4.4.1).

For the WMS, Christensen et al. (1989) estimate that, before the WMT, 22% of O_2 respiration in the WMDW was associated with the flux of sinking POC and 78% with the mineralization of inflowing DOC. If for the WMS we assume the same maximum DOC associated O_2 consumption rate per unit volume of water as for the EMS, then the initial DOC-associated O_2 concentration in WMDW can be calculated directly from the pre-WMT steady state O_2 consumption rate. With all parameter values in Equation (4.2) known, the fractions of DOC-associated O_2 in water flows supplied to the WMDW and EMDW can be calculated from the condition of steady state. Maximum (potential) O_2 consumption rates used in Equation (4.2) for the WMS and EMS are summarized in Table D.4.

4.3.3 Numerical solution and factorial design analysis

The ordinary differential equations describing the O_2 mass balances of the two IW and two DW reservoirs are solved in MATLAB using ODE solver 15s. A 2^{25-15} fractional factorial design analysis (Box et al., 1978; Appendix A) of the model with Equation (4.1) is used to assess the sensitivity of O_2 concentrations in the IW and DW reservoirs to model parameters. A factorial design analysis measures the sensitivity of a given model response (here the IW and DW O_2 concentrations) to each individual model parameter, as well as to interactions between model parameters. Here, we only consider first (one parameter) and second order (two parameter) interactions as the fairly simple model dynamics are largely insensitive to

higher order parameter interactions (Appendix A.) Parameters included in the analysis are the SW O_2 concentration of the EMS and WMS, the O_2 concentration of inflowing DW from the Adriatic and Aegean Seas, the values of F_{max}, K_s and K_z, plus all water fluxes in the water cycle. All model parameters are varied by ±10%, and the effects on the model responses are calculated using Yate's algorithm (Box et al., 1978). The results of the factorial design analysis are plotted on a probability versus effect graph for each of the four model responses (the O_2 concentrations of WMIW, WMDW, EMIW and EMDW; Figure D.3): parameters that yield responses along the vertical line centered on the origin are considered insensitive, the further a response deviates from the vertical line, the more sensitive the corresponding parameter.

4.4 Scenarios

4.4.1 Recent changes: EMT and WMT

The EMT and WMT are simulated using the changes in water fluxes summarized in Table 4.1. For the EMS, these changes are the same as those imposed in Chapter 2 which assessed the EMT impacts on the cycling of P and N in the EMS. The main EMT pulse occurred between 1992 and 1994 during which Aegean DW formation increased by almost 2 orders of magnitude relative to that prior to the EMT (Roether et al., 2007). After 2002, circulation in the EMS is assumed to return to pre-EMT conditions.

The WMDW formation rate during the 2004-2006 WMT is estimated at 2.4 Sv, that is, four times the pre-WMT average. The upwelling fluxes in the WMS (F_{21} and F_{32} in Figure 4.1) are adjusted to balance the higher DW formation rate during the WMT. This is consistent with observations: by October 2006, less than 2 years after the WMT started, the newly formed WMDW had spread across most of the WMS, with the exception of the Tyrrhenian Sea and the western part of the Alboran Sea (Schroeder et al., 2008b). Variations in the WMDW formation rate also affect the mix of WMDW and WMIW exiting the WMS through the Strait of Gibraltar (García Lafuente et al., 2007). On an annual basis, about 10% of the total outflow through the Strait of Gibraltar is generated by seasonal DW formation, while 30% is uncoupled from the seasonal signal (García Lafuente et al., 2007). Presumably, the latter 30% correspond to WMDW outflow driven by Bernoulli suction resulting from the fast current speeds through the Strait. Assuming that the yearly outflow of WMDW by Bernoulli suction remains fixed at 30%, increased WMDW formation during the WMT raised the contribution of WMDW from 40% to 66% while, simultaneously, the contribution of WMIW dropped from 60% to 34%.

The changes in O_2 concentrations accompanying the EMT and WMT are assessed using either Equation (4.1) for all four IW and DW reservoirs, or Equation (4.1) for the IW reservoirs and Equation (4.2) for the DW reservoirs. In the first case, potential O_2 consumption rates of each reservoir remain unchanged (i.e.,

	Pre-EMT	EMT			WMT	Climate Change Scenarios		
		1987 -1992	1992-1994	1994 -2002	2004-2006	WC1 Weaker THC	WC2 Weaker in WMS, stronger in EMS	WC3 Stronger THC
WMS								
Net evaporation (F_{1E})	**0.01**	0.01	0.01	0.01	0.01	0.01	0.01	0.01
Atlantic SW (F_{G1})	**0.83**	0.83	0.83	0.83	0.83	0.83	0.84	0.83
IW-Atl (F_{2G})	**0.47**	0.47	0.47	0.47	0.27	0.51	0.47	0.40
DW-Atl (F_{3G})	**0.31**	0.31	0.31	0.31	0.52	0.24	0.29	0.36
IW-SW (F_{21})	**0.55**	0.55	0.55	0.55	1.22	0.04	0.73	0.84
SW-NWM (F_{17})	**0.23**	0.23	0.23	0.23	0.90	0.18	0.19	0.40
IW-NWM (F_{27})	**0.38**	0.38	0.38	0.38	1.50	0.30	0.31	0.66
NWM-IW (F_{72})	**0**	0	0	0	0	0.33	0	0
NWM-DW (F_{73})	**0.61**	0.61	0.61	0.61	2.40	0.16	0.50	1.06
IW-DW (F_{23})	**0.07**	0.07	0.07	0.07	0.07	0.09	0.06	0.12
DW-IW (F_{32})	**0.37**	0.37	0.37	0.37	1.95	0	0.27	0.82
Strait of Sicily								
WMS-EMS SW (F_{14})	**1.14**	1.14	1.14	1.14	1.14	0.67	1.37	1.26
EMS-WMS IW (F_{52})	**1.10**	1.10	1.10	1.10	1.10	0.61	1.30	1.20
EMS								
Net evaporation (F_{4E})	**0.06**	0.06	0.06	0.06	0.06	0.07	0.08	0.07
Adr+Aeg to SW (F_{84})	**0.02**	0.02	0.02	0.02	0.02	0	0.01	0.01
SW-IW (F_{45})	**1.10**	1.10	1.10	1.10	1.10	0.61	1.30	1.20
IW to Adri+Aeg (F_{58})	**0.36**	0.38	3.02	0.57	0.36	0.47	2.35	2.30
Adr+Aeg to IW (F_{85})	**0**	0	0	0	0	0.42	0	0
Adri+Aeg to DW (F_{86})	**0.36**	0.38	3.02	0.57	0.36	0.05	2.35	2.30
DW-IW (F_{65})	**0.36**	0.38	3.02	0.57	0.36	0.05	2.35	2.30

Table 4.1: Water fluxes assigned to pre-EMT (before 1987), EMT, WMT and the three climate change scenarios (WC1-WC3). Numbering of fluxes is that of Figure 4.1. Atl = Atlantic, NWM = North-West Mediterranean, Adri = Adriatic, Aeg = Aegean. Net evaporation = evaporation – river discharge - submarine groundwater discharge. Units: Sv (10^6 m^3 s^{-1}).

F_{max} is constant). In the second case, the potential O_2 consumption rate coupled to the oxidation of sinking POC remains constant (i.e., F_{max}^{POC} is constant). For the DW reservoirs, however, the O_2 consumption rate associated with the oxidation of labile DOC responds to changes in DW formation, because of the corresponding variations in the DOC input to the DW reservoir.

4.4.2 Future changes: Climate change perturbations

Adloff et al. (2015) estimate that by 2100 climate change will raise temperatures and salinities in the top 150 m of the MS between 1.29 and 2.30°C and between 0.58 and 0.74, respectively, altering O_2 solubility of SW (Scenario Sol). Increased water temperatures may also increase the rate of organic matter degradation and thus oxygen consumption (Brewer and Peltzer, 2016). The temperature effect on the O_2 consumption kinetics (Scenario Kin) are simulated using Equation (4.1) and assuming a Q_{10} value of 2 (Vichi et al., 2015), together with predicted 2100 temperature increases for IW (1.26-2.0°C) and DW (0.68-1.38ºC) (Adloff et al., 2015). Details on the implementation of the scenarios are given in Table 4.2. Note that spatial differences in temperature and salinity changes between the EMS and WMS are ignored. As shown below, this does not affect the main conclusions.

Three different scenarios (WC1, WC2 and WC3) cover the range of projected changes in Mediterranean THC by the year 2100. The first scenario (WC1) is based on the work of Somot et al. (2006), who predict a weakening of THC in both the WMS and EMS. Scenarios WC2 and WC3 are based on the results of the A2-ARF and B1-ARF scenarios of Adloff et al. (2015), respectively. In WC2 THC becomes weaker in the WMS, but strengthens in the EMS, while in WC3 THC is more vigorous in both the WMS and EMS. The corresponding changes in the water fluxes are summarized in Table 4.1. For each scenario, a step-wise change to the pre-EMT water cycle is imposed and the O_2 mass balance model is run until a new steady state is reached. For the DW reservoirs, either Equation (4.1) or Equation (4.2) is used to calculate O_2 consumption (see Table 4.2). Each circulation scenario is combined with the maximum and minimum changes in SW O_2 solubility and O_2 consumption kinetics.

In WC1, WMDW formation decreases by 74% and that of EMDW by 85%, relative to the baseline values. These changes are attributed to temperature-driven density changes and a decrease in wind stress at the DW formation sites *(Somot et al., 2006)*, both important factors in the preconditioning of water prior to DW formation. The volume of water flowing over the Otranto shelf out of the Adriatic Sea, however, increases by 37% compared to pre-EMT circulation. This water, however, does not cascade deeper than 1000 m (Somot et al., 2006). In WC1, excess water exiting the Adriatic and Aegean Seas that does not become EMDW is therefore redirected into the EMIW reservoir, which requires adding an additional water flow in the water cycle (F_{85} on Figure 4.1). Similarly, for the WMS the additional flow

Scenario	Description
Sol	**Solubility:** Decrease SW solubility by 2.8 and 6.3%, use **Equation (4.1)**
Kin	**Kinetics**: Increase F_{max} by 7.8 and 14.9% in IW, and 4.8 and 10.0% in DW, use **Equation (4.1)**
WC1.1	**Water Circulation** scenario **1** with **Equation (4.1)** for deep water oxygen consumption plus scenarios **Sol** and **Kin.** *THC:* 75% decrease in WMDW production, 85% decrease in EMDW production, 45% decrease in EMIW to WMIW based on Somot et al. (2006)
WC1.2	**Water Circulation** scenario **1** with **Equation (4.2)** (see section 4.4.2 for details) plus scenarios **Sol** and **Kin**
WC2.1	**Water Circulation** scenario **2** with **Equation (4.1)** plus scenarios **Sol** and **Kin.** *THC:* 18% decrease in WMDW production, 553% increase in EMDW production, 18% increase in EMIW to WMIW, based on A2-ARF: Adloff et al. (2015)
WC2.2	**Water Circulation** scenario **2** with **Equation (4.2)** plus scenarios **Sol** and **Kin**
WC3.1	**Water Circulation** scenario **3** with **Equation (4.1)** plus scenarios **Sol** and **Kin:** *THC:* 73% increase in WMDW production, 539% increase in EMDW formation, 9% increase in EMIW to WMIW, based on B1-ARF: Adloff et al. (2015)
WC3.2	**Water Circulation** scenario **3** with **Equation (4.2)** plus scenarios **Sol** and **Kin**

Table 4.2: Climate change scenarios.

F_{72} accounts for the shallower penetration of DW formation originating in the NWM as a result of climate warming, as also proposed by Herrmann et al. (2008a).

Somot et al. (2006) further predict a 45% decrease in the westward flow of EMIW between the Ionian and Levantine basins. In WC1, we assume that this decrease in flow propagates to the Strait of Sicily, that is, we impose a 45% drop in the EMIW outflow to the WMS. To maintain water balance, the model then requires a 45% decrease in EMIW formation. In addition, cessation of surface flow from the Adriatic and Aegean Seas into the EMS occurs because, under the projected climate conditions, both basins transition from net dilution (E-R-P<0) to net concentration (E-P-R>0) (Somot et al., 2006). The projected circulation changes of Somot et al. (2006) also predict a small, 4% decline in the outflow from the WMS to the Atlantic Ocean, while the decreased WMDW formation implies a smaller contribution of WMDW to the outflow across the Strait of Gibraltar: 33% in WC1, compared to 40% in the baseline water cycle. In WC2, an EMT-like circulation regime is simulated, based on the A2–ARF scenario of Adloff et al. (2015). The imposed 18% decrease in WMDW formation assumes that the relative change in DW formation is proportional to the change in mixed layer depth of the NWM in the A2-ARF scenario. The 2.2 Sv DW formation from the Aegean Sea is derived from the EMT index, which compares the maximum zonal overturning function in the deep Ionian Basin to the minimum value in the Levantine Basin (Adloff et al., 2015). Adriatic DW formation is estimated at 0.15 Sv based on the meridonal overturning function at the Strait of Otranto. The flux of water through the Strait of Sicily is estimated to increase by 0.2 Sv (Figure 5 in Adloff et al., 2015), while evaporation over the entire MS increases by 52%.

In WC3, SW density increases throughout the MS, leading to a strengthening of the THC in both EMS and WMS. The same method as in WC2 is applied to derive fluxes from the results of the B2-ARF scenario reported by Adloff et al. (2015). A 73% increase in DW formation over the Gulf of Lions is estimated, while the contribution of Aegean DW formation is slightly weaker at 2.0 Sv, with the Adriatic contributing 0.3 Sv. The water balance then requires a 0.1 Sv increase in the flux of water through the Strait of Sicily.

4.5 Results and discussion

The expansion of bottom water hypoxia in marine environments as a result of global warming is a growing concern (Rabalais et al., 2010; Doney et al., 2012; Altieri and Gedan, 2015). The potential for O_2 depletion is particularly high in shallow coastal environments, and in marginal or semi-enclosed marine basins such as the Bohai, Baltic and Mediterranean Seas (Zhai et al., 2012; Carstensen et al., 2014; Friedrich et al., 2014). The Mediterranean sedimentary record further shows that, during the recent

geological past, the EMS experienced repeated periods of basin-wide hypoxia characterized by the deposition of sapropels (Rohling et al., 2015 and references therein). Thus, with the MS region expected to undergo some of the world's fastest warming in the coming decades (Giorgi, 2006), the sensitivity of deep-water oxygenation to climate change deserves particular attention. Our approach is based on simple mass balance calculations of the water and dissolved O_2 cycles in the MS. The approach does not resolve the spatial and intra annual variability in circulation and oxygen consumption across the MS basin. Rather the approach is designed to interrogate the key dynamic couplings between circulation and the biogeochemical functioning of the MS system on a yearly-averaged, basin-wide scale (Béthoux et al., 1992; Chapter 2; Appendix A).

4.5.1 Baseline O_2 cycling (pre-EMT)

The factorial design analysis indicates that O_2 concentrations in WMIW and EMIW are highly sensitive to the imposed SW O_2 concentrations (Figure D.1and D.3B). Interestingly, the WMIW O_2 concentration is more sensitive to the SW O_2 concentration of the EMS than that of the WMS (Figure D.3A). This is a direct consequence of the water cycle model in which the majority of WMIW is produced by inflow of EMIW, thus highlighting the closely intertwined O_2 dynamics of the two Mediterranean basins. Not surprisingly, deep-water O_2 concentrations in both the WMS and EMS are sensitive to the water flows in and out of the DW reservoirs, as well as the O_2 concentrations in the water reservoirs where DW formation originates (Figure D.3C and Figure D.3D). In addition, the O_2 concentrations in all IW and DW reservoirs are sensitive to the maximum potential rates of O_2 consumption.

Per unit volume, the baseline O_2 consumption rates are greater in WMDW than in EMDW, but lower in WMIW than EMIW despite the higher primary productivity in the WMS compared with the EMS (Antoine et al., 1995). A higher influx of labile and semi-labile DOC into the WMDW (Santinelli, 2015), which enhances heterotrophic respiration in the DWs of the WMS (Luna et al., 2012), helps explain the 2.5 times larger O_2 consumption rate in WMDW (0.71 $\mu M\ yr^{-1}$; Table D.5) compared to EMDW (0.29 $\mu M\ yr^{-1}$; Table D.5). The two-fold difference in O_2 consumption rate between EMIW (4.12 $\mu M\ yr^{-1}$) and WMIW (2.23 $\mu M\ yr^{-1}$) is similarly attributed to differences in the input of degradable DOC. Downwelling in the eastern part of the EMS supplies relatively labile DOC from the euphotic zone to the EMIW. However, by the time the EMIW exits the EMS through the Strait of Sicily, the remaining DOC supplied to the WMIW is more refractory than that in the EMIW. Upwelling of WMDW into WMIW likely also delivers relatively refractory DOC. Thus, the lower O_2 respiration rates in WMIW compared to EMIW are primarily the result of differences in the supply of DOC, rather than that of POC, which is actually 1.8 times greater per unit surface area in the WMS than EMS (Moutin and Raimbault, 2002).

The predicted baseline O_2 consumption rates generally agree with literature estimates for the period prior to the EMT (1987) for the EMS, and prior to the WMT (2004) for the WMS. For example, electron transport system (ETS) activity measurements by Christensen et al. (1989) in the WMS yield an equivalent O_2 respiration rate for the 500-3500 m depth range on the order of 0.6 µM O_2 yr^{-1}, which is close to the value of 0.71 µM O_2 yr^{-1} we derive for the WMDW. Similarly, our modeled WMIW rate of 2.2 µM O_2 yr^{-1} falls in the range for the 110-1000 m depth interval (1.4-5.5 µM O_2 yr^{-1}) inferred from ETS activity measurements (Savenkoff et al., 1993; Lefèvre et al., 1996; Tanaka and Rassoulzadegan, 2004). Using a mass balance approach, Roether and Well (2001) derived an O_2 consumption rate of 0.55 µM O_2 yr^{-1} for the EMS below 1000 m, compared to our EMDW value of 0.29 µM O_2 yr^{-1}. We are not aware of independent O_2 consumption rate determinations for the EMIW prior to the onset of the EMT.

The O_2 consumption rates in WMDW and EMDW are higher than the average respiration rate of 0.13±0.03 µM O_2 yr^{-1} reported by Williams (2014) for the bathypelagic depth range (1000-4000 m) of the global ocean. In contrast, O_2 consumption rates in WMIW and EMIW are lower than the global average mesopelagic (150-1000 m) value of 4.18±0.68 µM O_2 yr^{-1} (Williams, 2014). Our analysis suggests that the anomalous depth distribution of O_2 consumption rates of the MS reflects the important contribution to DW respiration of labile and semi-labile DOC supplied from the SW source areas of deep-water formation. However, the relatively high DW temperatures of the MS may also in part explain why the DW O_2 consumption rates exceed the world ocean average value (Roether and Well, 2001).

4.5.2 EMT-WMT

The responses of the DW and IW O_2 concentrations to the well-documented, large-scale changes in THC known as EMT and WMT provide an opportunity to test the coupled water-O_2 cycle model. Overall, modeled O_2 concentrations of EMIW and EMDW are quite sensitive to the EMT (Figure 4.3A). Use of both Equations (4.1) and (4.2) captures the approximately 5 µM increase in EMDW O_2 concentration measured immediately following the main EMT pulse (Klein et al., 2003; Kress et al., 2003). However, with Equation (4.1), the model predicts a further increase in EMDW O_2 concentration until at least the turn of the century, contrary to the reported decrease after 1995 (Klein et al., 2003). In contrast, Equation (4.2) predicts a decrease of post-1995 EMDW O_2 concentrations. The trend in EMDW O_2 consumption predicted using Equation (4.2) reflects the decomposition of the relatively labile DOC accompanying the pulse of enhanced Aegean DW formation during the EMT.

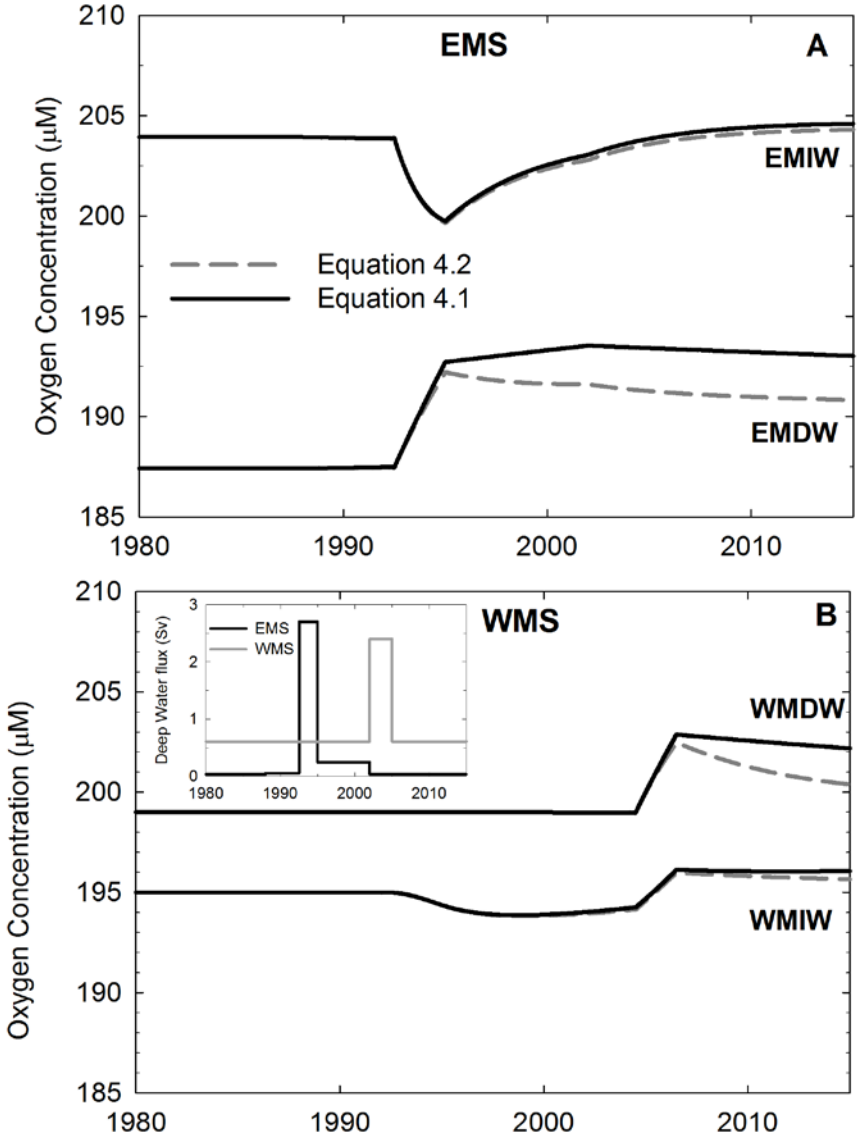

Figure 4.3: Response of O_2 concentrations (μM) to the EMT and WMT in A) the EMS and B) the WMS between 1980 and 2015 using Equation (4.1) (black solid lines) and Equation (4.2) (grey dashed lines) for DW O_2 consumption. Inset figure shows the time dependent changes in water influx (Sv) from the Aegean Sea (EMS: black line) and from the NWM (WMS; grey line).

The modeled EMIW O_2 concentration shows an opposite trend to that of EMDW, with a decrease between 1987 and 1995 followed by a recovery to pre-EMT values (Figure 4.3A). Equations (4.1) and (4.2) yield nearly identical temporal trends for the EMIW O_2 concentration. The initial model-derived drop of about 4 µM is lower than some observed reductions in EMIW O_2 concentration caused by the EMT. For instance, within the Levantine Basin the IW O_2 concentration dropped by as much as 40 µM between 1987 and 1999 (Kress et al., 2003). During that period, however, a blocking anticyclone stopped the eastward flow of SW into the Levantine Basin (Kress et al., 2003), hence regionally increasing the IW residence time and allowing for a more extensive drawdown of O_2. Similarly, in the Ionian basin, the EMT brought older, more O_2 depleted, Adriatic DW into the EMIW, causing the O_2 concentration to decrease by 15 µM (Kress et al., 2003). Our model, however, does not resolve these intra-basin mesoscale circulation features, but rather averages them out over the entire EMS. The model-predicted average EMIW O_2 consumption rate of 4.1 µM yr^{-1} between 1999 and 2008 is of the same order of magnitude as the values of 6-8 µM O_2 yr^{-1} derived from DOC mineralization fluxes estimated by Santinelli et al. (2010; 2012b) for the same time period.

According to the model, between 1987 and 1999 the EMT caused a slight decrease of the WMIW O_2 concentration of about 1 µM, but it had no effect on the WMDW O_2 concentration (Figure 4.3B). The WMT, however, increased O_2 concentrations in both WMIW and WMDW reservoirs. This agrees with the high O_2 content reported for newly formed WMDW associated with the WMT (Schroeder et al., 2008a). With Equation (4.1) the model predicts that, following the WMT, the WMDW O_2 concentration would remain elevated until at least 2015. Applying Equation (4.2), however, results in a distinct drop in the WMDW O_2 concentration after 2007, which is consistent with observed WMDW O_2 concentrations in 2011 that are even lower than pre-WMT values in some localities (Schneider et al., 2014). For WMIW, both Equations (4.1) and (4.2) yield little change in the post-2007 O_2 concentration, in line with the lack of a systematic temporal change in measured WMIW O_2 concentrations between 2007 and 2011 (Schneider et al., 2014). Overall, Equation (4.2), which implicitly accounts for the combined transport of SW-derived O_2 and DOC during DW formation, results in the better match to the observed, basin-scale changes in DW and IW O_2 concentrations caused by the EMT and WMT.

4.5.3 Sensitivity to climate change

Climate warming is expected to strongly impact the Mediterranean region (Giorgi, 2006; Collins et al., 2013; Kirtman et al., 2013). The climate change perturbations implemented in the water-O_2 mass balance model are designed to test the sensitivity of DW and IW O_2 concentrations in the MS to potential variations in biogeochemical factors (O_2 solubility, mineralization kinetics) and THC regimes driven by

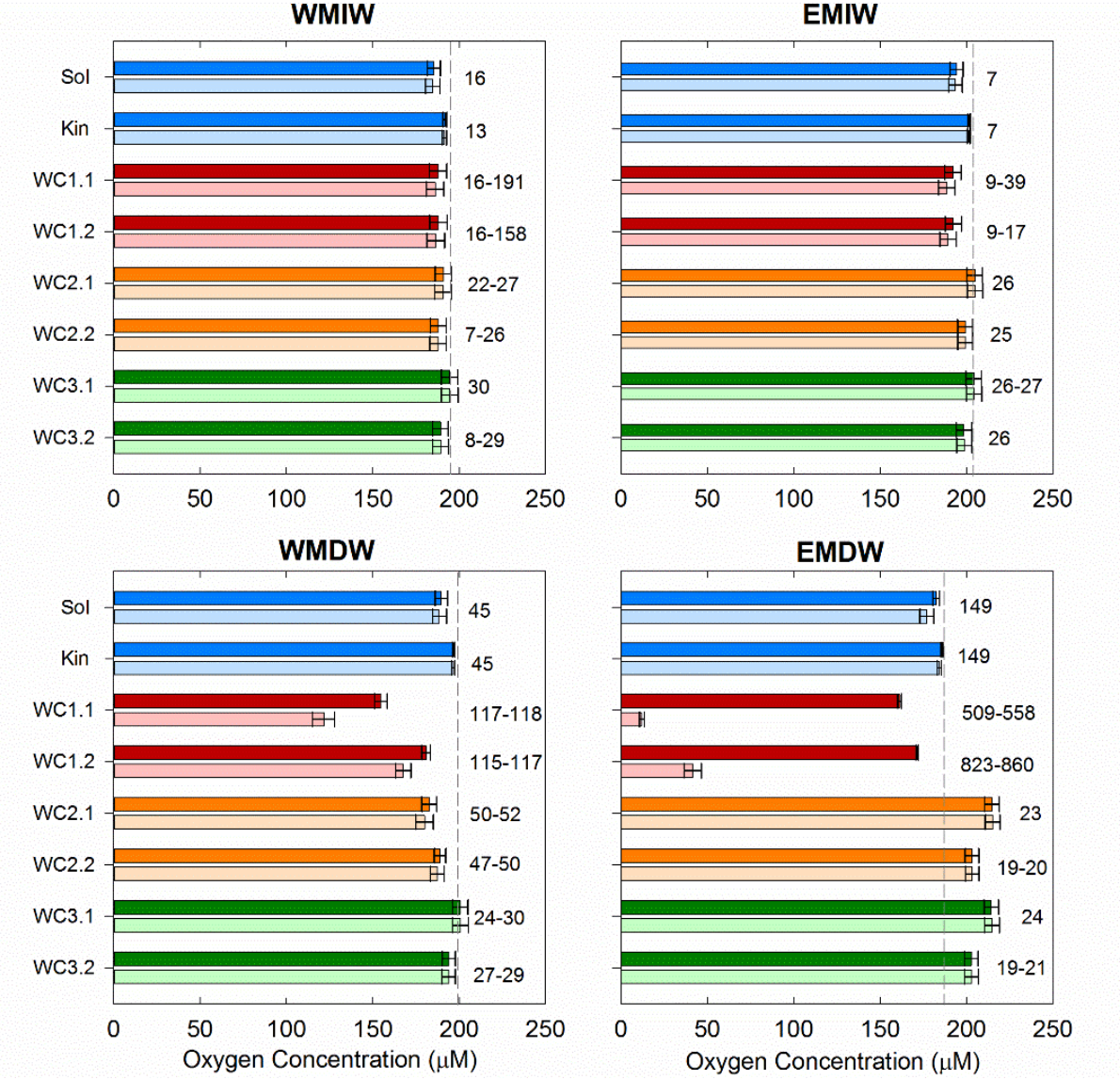

Figure 4.4: Intermediate and deep water O_2 concentrations of the WMS and EMS for the climate scenarios, relative to the baseline values (dashed vertical line), after 100 years (dark bars) and upon reaching steady state (light bars). Results for WC1.1, WC2.1 and WC3.1 are those obtained using Equation (4.1) for IW and DW; results for WC1.2, WC2.2 and WC3.2 are those using Equation (4.1) for IW and Equation (4.2) for DW. Error bars reflect the uncertainties associated with the projected increases in water column temperatures and salinities by the year 2100. Numbers adjacent to the horizontal bars are the response times (e-folding times) to the imposed perturbations (years).

the climatic conditions that are anticipated to prevail toward the end of the 21st Century. Figure 4.4 shows the resulting changes in O_2 concentrations in each of the five climate change scenarios (Sol, Kin, WC1, WC2, WC3).

4.5.3.1 Short term responses (≤ 100 years)

Luna et al. (2012) hypothesize that climate warming will accelerate microbial degradation of organic matter in the MS, resulting in lower water column O_2 concentrations. Scenario Kin, however, only yields very small decreases in O_2 concentrations (2-5 μM or 1-2%) for the IW and DW reservoirs in both basins of the MS (Figure 4.4). Decreased SW O_2 solubility due to increased temperatures and salinity (Scenario Sol) produces somewhat larger effects on IW and DW O_2 concentrations, in line with the results of the factorial design analysis (Figure D.3). After 100 years of lower SW O_2 solubilities, IW and DW O_2 concentrations in the WMS and EMS drop by 2-7% (3-13 μM), while the combined changes in solubility and kinetics produces decreases between 2 and 9% in IW and DW O_2 concentrations.

Changes in THC have the largest impacts on the O_2 concentrations of the WMDW and EMDW (Figure 4.4). In scenario WC1.1 the weakening of the THC causes the WMDW O_2 concentration to decrease to 151-158 μM (i.e., a 21-24% drop relative to the initial value) after 100 years, and those in the EMDW to 160-162 μM (or a drop of 13-15%). Consequently, on a 100-year timescale WMDW appears to be more sensitive to a weakening of THC than EMDW. Climate change, however, may not necessarily result in a generalized decrease in THC across the MS. In WC2.1, where a weakening of the THC occurs in the WMS and a strengthening in the EMS, the EMDW O_2 concentration after 100 years is 23-32 μM (12-17%) higher than in the baseline simulation. Over the same time period, the WMDW O_2 concentration decreases by 12-21 μM (6-10%). As a result, the WMDW O_2 concentration drops below that of the WMIW, in contrast to the baseline simulation where the WMIW exhibits a lower O_2 concentration than both the WMSW and WMDW.

Strengthening of the THC in both WMS and EMS in scenario WC3.1 increases the O_2 DW concentration of the EMS. For the WMDW, the decrease in O_2 SW solubility and faster degradation kinetics offset the effect of increased ventilation. Hence, despite the 74% increase in WMDW formation, the WMDW O_2 concentration only changes by approximately 3% relative to the baseline results. Overall, the changes in SW O_2 solubility and aerobic degradation kinetics due to climate warming buffer the potential increases in DW O_2 concentrations associated with enhanced DW formation in WC2.1 and WC3.1, while they enhance the decline in O_2 concentrations due to slower DW formation in WC1.1.

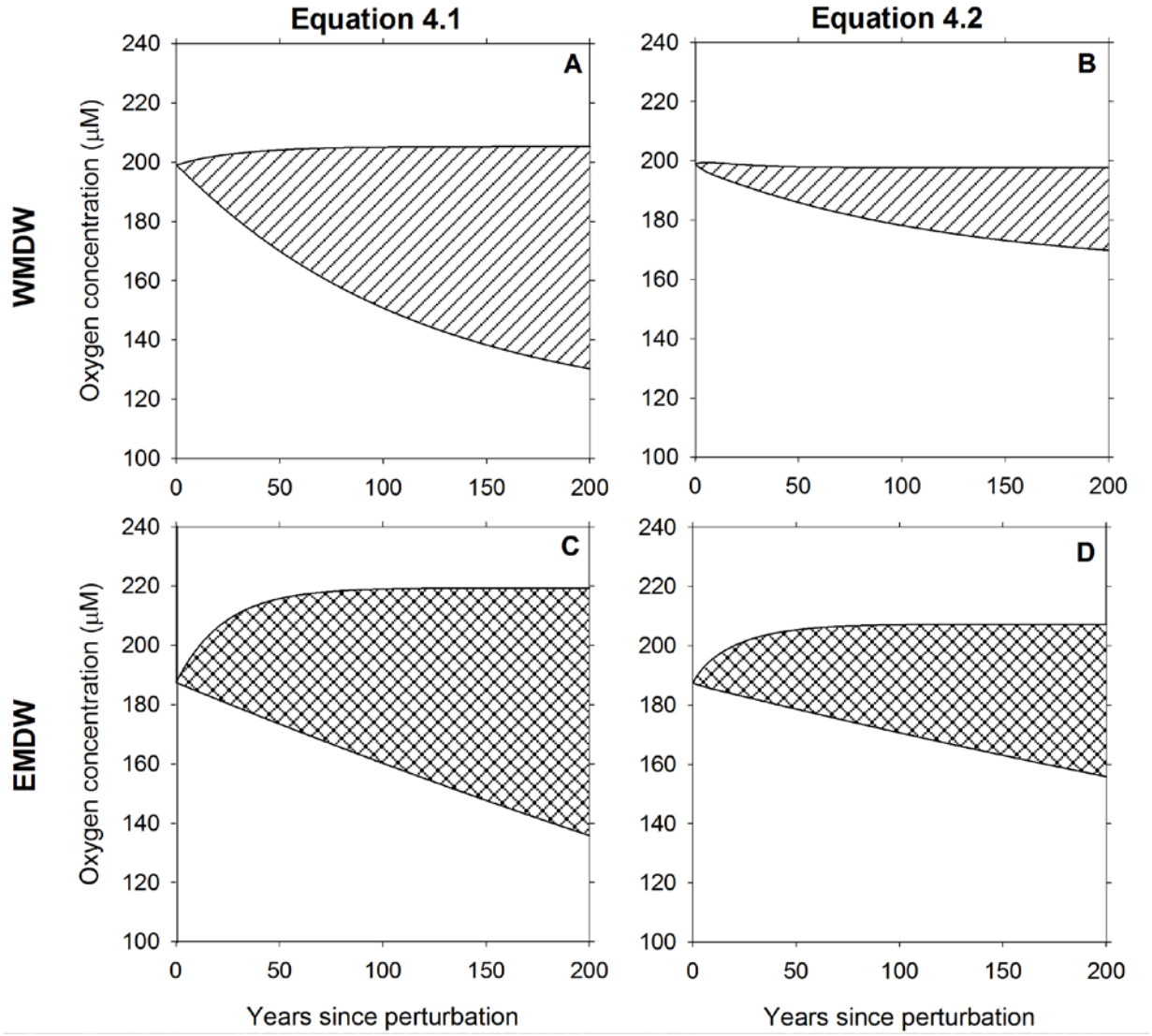

Figure 4.5: Ranges in simulated O_2 concentrations in WMDW (A and B) and EMDW (C and D) for 200 years after imposing the perturbations using Equation (4.1) (A and C) and Equation (4.2) (B and D) for the DW O_2 consumption rate. The ranges enclose the results of all the scenarios described in Table 4.2.

The results discussed so far are based on applying Equation (4.1) to both IW and DW. That is, they assume that O_2 consumption rates only respond to changes in O_2 concentration. The EMT and WMT simulations, however, imply that changes in THC also affect the supply of degradable DOC to the DW reservoirs (section 4.5.2). Therefore, the MS may exhibit a DOC-based negative feedback mechanism on DW oxygenation. As shown in Figure 4.5, using Equation (4.2) in the circulation scenarios (i.e., scenarios WC1.2, WC2.2 and WC3.2) substantially reduces the predicted ranges of the responses of DW O_2 concentrations to the imposed changes in THC. This is particularly the case in WC1.2 where after 100 years the WMDW and EMDW O_2 concentrations decrease to 178-183 μM and 171-172 μM, respectively, compared to 151-158 μM and 160-162 μM using Equation (4.1) (Figure 4.4). Likewise, in WC3.2 enhanced THC across the entire MS supplies more degradable DOC to the DW, leading to an increase in O_2 consumption and, hence, lower DW O_2 concentrations than those predicted in WC3.1.

Factors other than those considered here will undoubtedly affect the future trends of water column O_2 levels in the MS. In particular, future increases in anthropogenic nutrients inputs into the MS (Ludwig et al., 2010; Lazzari et al., 2014; Christodoulaki et al., 2016; Chapter 3) may promote higher primary productivity in the SWs, which in turn would enhance O_2 consumption in the IW and DW reservoirs. Furthermore, our model results only pertain to basin-wide O_2 trends in the offshore IW and DW masses of the MS. Increased local nutrient supply, together with lower O_2 solubility and faster respiration rates, have the potential to enhance hypoxia in a limited number of nearshore areas around the MS basin.

4.5.3.2 Long term responses (>100 years)

The time scales over which DW O_2 concentrations respond to the imposed circulation changes in WC2 and WC3 are ≤50 years (Figure 4.4). In contrast, the response times in WC1 exceed 115 years for WMDW and 500 years for EMDW. Thus, we expect relatively slow adjustments of the DW O_2 concentrations to a generalized drop in DW formation, especially in the EMS. For EMDW O_2 concentrations to drop within 1 μM of the steady state values requires more than 1300 years in scenario WC1.1, and 3400 years in scenario WC1.2. Furthermore, although the EMDW O_2 concentrations in WC1.1 and WC1.2 decrease to steady state values of 11-47 μM, the WMDW retains O_2 concentrations well above 100 μM (Figure 4.4). On long time scales, EMDW is thus more sensitive to O_2 depletion caused by a weakening of the THC than WMDW, in contrast to the behavior observed at shorter time scales (section 4.5.3.1).

The weakened and shallower THC in scenario WC1 is not unlike the circulation regime inferred for sapropel formation in the EMS, despite the probably very different - cooler and wetter - climate conditions (Rohling et al., 2015). Grimm et al. (2015) propose that the formation of sapropel S1 was

preceded by thousands of years of preconditioning of the water masses following DW stagnation, that is, similar to the time scales required by EMDW to approach hypoxic conditions in the WC1 simulations. Other authors have proposed that only a massive, long-term change in THC, such as a reversal of the anti-estuarine circulation, could have produced anoxia in the EMS (Sarmiento et al., 1988; Stratford et al., 2000). In line with the WC1 results, the available evidence indicates that DW O_2 concentrations in the WMS remained relatively high at the same time that sapropels were being deposited under the O_2-depleted DW of the EMS. Rohling et al. (2015) hypothesize that WMDW remained oxygenated because of the efficient removal of old WMDW by Bernoulli suction through the Strait of Gibraltar, while this mechanism was absent at the Strait of Sicily.

The sensitivity of WMDW and EMDW oxygenation to the rates of DW formation is summarized in Figure 4.6. Steady state O_2 concentrations of WMDW and EMDW are plotted as a function of the relative rates of DW formation in the WMS and EMS. The figure shows that, all other conditions equal, (1) only the EMDW can develop hypoxia, but not the WMDW, (2) the inclusion of the DOC-based negative feedback dampens the response of the O_2 concentrations to changes in DW formation, and (3) the rate of EMDW formation must drop to at least 24% of its pre-EMT value in order to develop basin-wide DW hypoxic conditions in the EMS. The figure also implies that changes in the long-term rates of WMDW and EMDW formation by factors of ±2 should have relatively limited impact on the average DW O_2 concentrations ($\leq$25% change). In other words, DW oxygenation of the MS appears to be fairly resilient to potential changes in circulation that may occur in the foreseeable future.

4.6 Conclusions

A mass balance modeling approach is used to assess the sensitivity of IW and DW O_2 distributions in the MS to climate-driven changes in O_2 solubility, organic matter degradation kinetics and THC. The present-day O_2 distributions are based on a simplified representation of the water cycle that incorporates the most recent flow estimates through the Strait of Gibraltar. The model yields O_2 consumption rates in the various reservoirs of the WMS and EMS that fall within the ranges of reported values. Prior to the EMT, EMIW exhibits approximately two times faster O_2 consumption than WMIW, while the O_2 consumption rate is 2.5 times greater in WMDW than EMDW. In order to reproduce the general trends in O_2 concentrations and consumption observed during and after the EMT and WMT, the model must account for the variations in labile DOC influxes to the WMDW and EMDW associated with changes in DW formation. The coupling between the delivery of O_2 and DOC to the DW reservoirs creates a negative feedback that dampens the magnitude of the changes in DW O_2 concentrations that accompany changes in THC.

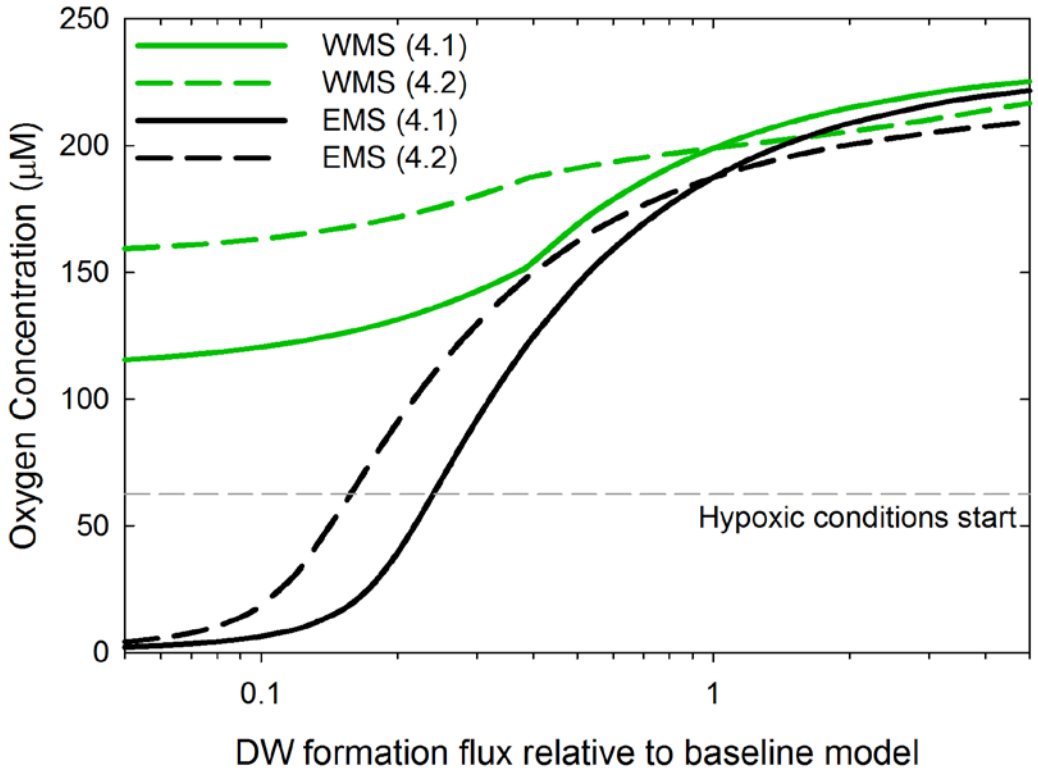

Figure 4.6: Steady state DW O_2 concentrations as a function of the DW formation rates in the EMS (from the Adriatic and Aegean Seas) and WMS (from the NWM and Tyrrhenian Sea), relative to the baseline (pre-EMT) rates. Numbers in brackets correspond to the equation used for DW O_2 consumption rates: Equation (4.1) or Equation (4.2). The calculations assume that the contribution of Bernoulli suction of WMDW to total outflow at the Strait of Gibraltar remains constant at 30%, while upwelling fluxes from DW to IW (F_{65} and F_{32} in Figure 4.1) are adjusted to maintain steady state. In the WMS, the F_{32} flux switches from upwelling to downwelling when the DW formation flux drops below 37% of its pre-EMT value. Note a reduction in the DW formation flux to 0.15 and 0.26 relative to the baseline model in the EMS and WMS, respectively, correspond to the reduction imposed in WC1.

In the climate change scenarios, the predicted variations in O_2 concentrations of WMDW and EMDW are most strongly affected by changes in water circulation: the imposed perturbations to the THC change DW O_2 concentrations by up to 25% within 100 years, compared to the maximum changes of 7 and 2% for the imposed decreases in O_2 solubility and aerobic respiration kinetics, respectively. Even after 100 years of strongly reduced DW formation, the WMS and EMS are predicted to stay fully oxygenated. On timescales of several thousands of years, a sustained decrease in THC of 75% or more relative to today would result in hypoxic bottom waters in the EMS. The average WMDW O_2 concentration, however, would still remain above 110 µM, because Bernoulli suction through the Strait of Gibraltar keeps the WMDW reservoir well ventilated. Overall, while the model results imply that climate warming in the Mediterranean region will significantly impact water column O_2 cycling, it is unlikely to cause basin-wide bottom water hypoxia within the 21st Century. Note, however, that the predicted changes in O_2 distributions do not account for additional factors that may affect O_2 consumption rates, in particular, rising inputs of anthropogenic nutrients to the MS.

A key limitation of our ability to forecast the effects of climate-driven changes in THC on the biogeochemical functioning of the MS are the large uncertainties surrounding not only the magnitude of the potential circulation changes, but also their direction. As the recent study of Adloff et al. (2015) illustrates, even the question whether future climate warming will strengthen or weaken THC in the MS has yet to be satisfactorily answered. As emphasized by our mass balance results, monitoring the changes in the water column O_2 distributions can yield powerful insights into the coupling between the geophysical and ecological dynamics of the MS and their response to climate forcing.

Chapter 5.

Understanding the unique biogeochemistry of the Mediterranean Sea:

Insights from a coupled phosphorus and nitrogen model

Modified from: **Helen R. Powley**, Michael D. Krom, Philippe Van Cappellen. (in review). Understanding the unique biogeochemistry of the Mediterranean Sea: Insights from a coupled phosphorus and nitrogen model. *Global Biogeochemical Cycles.*

5.1 Summary

The Mediterranean Sea (MS) is a highly oligotrophic, almost entirely landlocked, marine basin exhibiting low dissolved inorganic phosphorus (P) and nitrogen (N) concentrations, unusually high nitrate (NO_3) to phosphate (PO_4) ratios, and distinct biogeochemical differences between the Western Mediterranean Sea (WMS) and Eastern Mediterranean Sea (EMS). To better understand the unique biogeochemical features of the MS, a new mass balance model of the P and N cycles in the WMS is coupled to a pre-existing model for the EMS. Steady state fluxes representative of the mid-20th century reveal that land-derived inputs of reactive P and N to the WMS and EMS are similar per unit surface area, but that marine-derived inputs are approximately four times greater for the WMS than EMS. The higher lateral inflows of dissolved reactive P and N into the WMS through the Strait of Gibraltar, relative to those entering the EMS via the Strait of Sicily, explain the approximately 3 times higher primary productivity of the WMS compared to the EMS. Inflow of Atlantic surface water (ASW) is responsible for 39% of new production in the WMS; inflow of Western Mediterranean surface water (WMSW) accounts for 37% of new production in the EMS. The large role of the lateral supply of marine-derived P, particularly in the form of dissolved organic P (DOP), in supporting new production is not unlike that observed for open ocean gyres. Overall, the MS is net heterotrophic: DOP and dissolved organic N (DON) entering the WMS and EMS, mainly via the straits of Gibraltar and Sicily, are mineralized to PO_4 and NO_3 and subsequently exported by the prevailing anti-estuarine circulation. The deep water (DW) molar NO_3:PO_4 ratios in excess of the Redfield value (16:1) are caused by the high reactive N:P ratio of the external inputs to the WMS and EMS, combined with low denitrification rates. The lower DW NO_3:PO_4 ratio of the WMS compared to the EMS is ascribed to a lower reactive N:P ratio of inputs to the WMS, in particular due to the low N:P ratio of ASW flowing into the WMS. Simulations show that the DW NO_3:PO_4 in both WMS and EMS would approach 16:1 in the absence of atmospheric deposition of reactive P and N, or if denitrification would increase by a factor of 2.2 and 8 in the WMS and EMS, respectively. In the latter case, the corresponding denitrification rates (0.05 mol m^{-2} yr^{-1} in the WMS and 0.01 mol m^{-2} yr^{-1} in the EMS) would fall within the range typically observed in other marine basins.

5.2 Introduction

The Mediterranean Sea (MS) is a major inland basin connected to the North Atlantic via the Strait of Gibraltar. It is oligotrophic, despite relatively high inputs of the essential nutrients phosphorus (P) and nitrogen (N) (Béthoux et al., 2005; Ludwig et al., 2009; Chapter 2; Chapter 3). This apparent contradiction is ascribed to the unusual anti-estuarine circulation (Krom et al., 2010) driven by excess evaporation within the basin (Béthoux, 1980). Atlantic surface water (ASW) with relatively low inorganic P and N concentrations enters the Western Mediterranean Sea (WMS) through the Strait of Gibraltar, while deeper waters enriched in the inorganic nutrients are returned to the Atlantic Ocean. A similar exchange occurs between the WMS and the Eastern Mediterranean Sea (EMS) via the Strait of Sicily, a narrow passageway between Europe and Africa with a water depth of 360-430 m.

The two major basins that make up the MS, the WMS and EMS, have distinct biogeochemical properties. Deep water (DW) phosphate (PO_4) and nitrate (NO_3) concentrations are approximately twice as high in the WMS compared to the EMS (Moutin and Raimbault, 2002; Pujo-Pay et al., 2011), while primary productivity is 2.5-3.3 times greater in the WMS than the EMS (Turley et al., 2000; Berman-Frank and Rahav, 2012). The differences in inorganic P and N concentrations and trophic conditions between the WMS and EMS appear to originate with the differences in nutrient loading to the two basins and are subsequently maintained by the biological pump (Crispi et al., 2001).

The EMS is the largest body of water that is unequivocally P limited (Krom et al., 1991). The winter phytoplankton bloom consumes all the dissolved phosphate within the surface water (SW), while measurable nitrate persists (Krom et al., 1992). In addition to the phytoplankton, bacteria in the EMS have also been shown to be strongly P limited (Zohary and Robarts, 1998). Under summer conditions, bacteria and micrograzers in the EMS are P limited, while autotrophs tend to be P and N co-limited (Thingstad et al., 2005a). The situation in the WMS is not as clear-cut. The spring phytoplankton bloom has been proposed to be N limited (Marty et al., 2002) or N and P co-limited (Pasqueron de Fommervault et al., 2015), while P limitation has been reported for the Gulf of Lions (Diaz et al., 2001). Pasqueron de Fommervault et al. (2015) argue that the low dissolved inorganic N:P ratio of SW (<20:1) implies that there are periods of N limitation and periods of P limitation during the phytoplankton bloom, rather than only N limitation (Marty et al., 2002). During the summer stratification period in the WMS, P limitation generally occurs for both phytoplankton and heterotrophic bacteria (Thingstad and Rassoulzadegan, 1995; Thingstad et al., 1998; Marty et al., 2002; Van Wambeke et al., 2002; Pinhassi et al., 2006; Pasqueron de Fommervault et al., 2015). Model results further indicate that, overall, P is the limiting nutrient for phytoplankton growth throughout the MS in all seasons (Lazzari et al., 2016).

There is a general consensus that the global ocean as a whole is autotrophic: it is responsible for about half the net productivity of the biosphere (Falkowski et al., 2000), which in turn supports annual fish catches of 96 million tons (Duarte et al., 2009). Marine productivity, however, is not evenly distributed, with coastal areas and upwelling areas exhibiting particularly high productivity. In addition, it has been suggested that oligotrophic areas of the ocean are net heterotrophic (Duarte et al., 2013) though this conclusion has been challenged (Williams et al., 2013). The MS offers an unusual situation. As an inland sea, it receives large external inputs of non-marine P and N, which would favour autotrophy. Formation of intermediate and deep waters in the MS, and their ultimate export to the Atlantic Ocean, however, maintain ultra-oligotrophic conditions. At present, whether the MS is net autotrophic or heterotrophic remains an open question.

The molar NO_3:PO_4 DW ratios of the MS are especially high compared to the global ocean, increasing from 20-24:1 on average in the WMS to 26-30:1 within the EMS (Krom et al., 1991; Béthoux et al., 1998; Kress and Herut, 2001; Moutin and Raimbault, 2002; Ribera d'Alcalà et al., 2003; Schroeder et al., 2010a; Pujo-Pay et al., 2011). Recent analyses suggest that, for the EMS, the high N:P ratio of the external inputs, together with very limited denitrification (Krom et al., 2010; Appendix A), explain the very high NO_3:PO_4 DW ratios, while for the WMS N_2 fixation has also been invoked to explain the unusual high DW NO_3:PO_4 ratio (Béthoux et al., 1992; Béthoux et al., 2002b).

Existing biogeochemical models of the MS (e.g. Crispi et al., 2001; Allen et al., 2002; Lazzari et al., 2012; Macias et al., 2014; Lazzari et al., 2016) focus on biological processes in the upper water column and the resulting ecosystem responses on seasonal timescales. Few models address the longer-term changes (i.e., $\geq$ 1 year) of the coupled P and N cycles across the entire MS, including the DW reservoirs. A biogeochemical mass balance model of P and N cycling in the EMS (excluding the Adriatic and Aegean Seas) was recently developed and applied to the second half of the 20th Century (1950-2000) (Chapter 2; Appendix A). The model incorporates the most up-to-date conceptual understanding of the key biogeochemical processes controlling the fate of P and N in the EMS, coupled to a simplified representation of the water cycle across the basin. The EMS model accounts for both inorganic and organic forms of P and N, as well as the temporal trajectories of P and N inputs and outputs.

Here, we build on our previous work by developing a mass balance model for the P and N cycles in the WMS and then coupling it to the existing EMS model. The resulting WMS-EMS model is used to interpret the unusual biogeochemical features of the MS and, in particular, the differences in productivity and P and N distributions between the WMS and EMS. We also analyze whether the MS is net autotrophic or net heterotrophic. The conclusions presented in this paper rely on the reconstructed P and

N cycles for the year 1950, that is, before the large increases in anthropogenic P and N inputs to the MS that took place during the second half of the 20th century (Chapter 2). The effects of post-1950 changes in P and N inputs on primary productivity and water column nutrient concentrations of the MS are addressed in Chapter 6.

5.3 Mass balance model

5.3.1 Circulation

Basin-scale circulation is represented using the water cycle model of Chapter 4. Briefly, the WMS and EMS are both divided into three horizontal layers: surface water (WMSW and EMSW), intermediate water (WMIW and EMIW) and deep water (WMDW and EMDW) (Figure 5.1). The water cycle model accounts for the bidirectional flows across the Straits of Gibraltar and Sicily, as well as DW formation and upwelling in both the WMS and EMS. In the EMS, DW formation occurs in the Adriatic and Aegean Seas, which are separated from the Levantine and Ionian Basins by the Otranto and Cretan Straits, respectively. The Adriatic and Aegean Seas are excluded from the EMS model domain, that is, DW formation is modeled by imposing the water flux entering the EMDW. In the WMS, open-ocean DW formation originates near the Gulf of Lions in the northwestern part of the WMS. The corresponding area of about 25,000 km^2 falls outside the model domain; throughout this paper we will refer to this area as NWM. The water cycle is assumed to be at steady state: annual flows in and out of each of the water reservoirs balance each other. A complete description of the water cycle can be found in Chapter 4. Note that the estimated water residence time of 44 years for WMDW is approximately three times lower than that of 150 years for EMDW (Figure 5.1).

5.3.2 Phosphorus and nitrogen cycling in the WMS

The WMS P and N concentrations and fluxes are assigned following the same approach used for the EMS as in Appendix A. Key model assumptions are:

1. Annual average primary production in the WMS is P limited; NO_3 assimilation is coupled to PO_4 uptake through the Redfield ratio (N:P = 16:1; Redfield et al., 1963).
2. Prior to 1950, anthropogenic pressures on P and N cycling within the WMS were limited and relatively stable, hence, the P and N cycles in 1950 are assumed to be at steady state.

Phosphorus limitation of primary production is clearly established for the EMS, less so for the WMS. In fact, the Alboran Sea is probably N limited (Ramirez et al., 2005; Lazzari et al., 2016). However, at the scale of the entire WMS basin, annual primary production is still mostly P, rather than N, limited. The phytoplankton bloom in the WMS is typically initiated by mixing of the water column, which brings

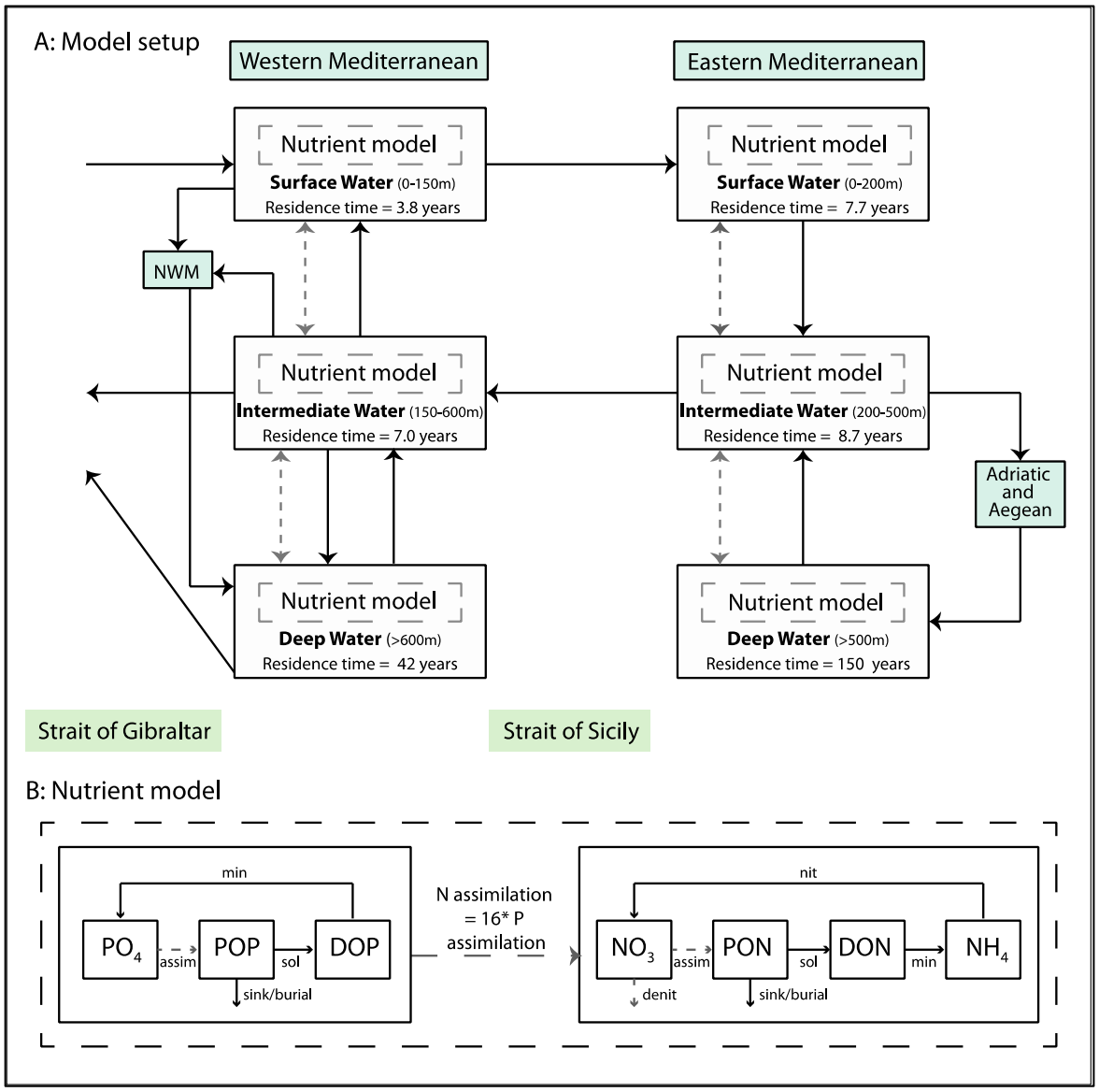

Figure 5.1: Conceptual model framework. A) Water reservoirs and circulation: black arrows represent advective water fluxes, grey-dashed arrows represent turbulent mixing fluxes, water residence times are given for all reservoirs. B) Nutrient model: note that assimilation of P and N only occurs in the surface water (SW) reservoirs, denitrification and burial only in the deep-water (DW) reservoirs (grey-dashed arrows). Assim = assimilation; sol = solubilization; min = mineralization; nit = nitrification.

NO_3-enriched water (i.e., with NO_3:PO_4>16) into the photic zone (Severin et al., 2014), suggesting that P is the ultimate limiting nutrient. Lazzari et al. (2016) further conclude that on an annual basis the WMS is P limited based on their model simulations in which a variable intracellular N:P quota controls nutrient uptake by phytoplankton.

In most of the open ocean, the average, whole-phytoplankton community NO_3:PO_4 uptake ratio closely follows the Redfield value of N:P = 16 (Klausmeier et al., 2004; Arrigo, 2005), although instantaneous ratios within and among different phytoplankton species may vary substantially (between 6:1 and 45:1; Geider and La Roche, 2002; Klausmeier et al., 2004) Particularly in P limited systems, such as the MS, the uptake ratio may exceed the Redfield value. For instance, for the EMS, Krom et al. (2014) report values of 16-25:1. In the absence of more definitive data, we impose the standard 16:1 Redfield value to calculate N assimilation in both WMSW and EMSW. To assess the sensitivity of the model predictions to the selected NO_3:PO_4 uptake ratio, we also performed a set of simulations with a NO_3:PO_4 uptake ratio of 23:1, a value that may be more representative of a P limited marine ecosystem (Klausmeier et al., 2004). The results are discussed in section 5.3.8.

The P reservoirs represented in the model are: dissolved inorganic P (PO_4), particulate organic P (POP) and dissolved organic P (DOP). The N reservoirs are: dissolved nitrate plus nitrite (NO_3), dissolved ammonium (NH_4), particulate organic N (PON), and dissolved organic N (DON). All of the P and N reservoirs are included in each of the water layers, resulting in a total of 9 P and 12 N reservoirs in the WMS model, or 18 P and 24 N reservoirs for the combined WMS-EMS model.

Throughout this paper total P (TP) encompasses both dissolved and particulate pools of P, that is, TP is the sum of PO_4, POP, DOP and particulate inorganic P (PIP). Reactive P is defined as the sum of PO_4, POP, DOP, and for non-marine inputs to the MS, also the fraction of PIP that is released to solution in seawater. Dissolved reactive P encompasses PO_4 and DOP. Likewise reactive N is the sum of NO_3, PON, DON and NH_4, while dissolved reactive N only includes NO_3, DON and NH_4. Assuming that particulate inorganic N is negligible, total N (TN) equals reactive N. Dissolved inorganic N (DIN) is the sum of NO_3 and NH_4.

The P and N concentrations in the water reservoirs and the corresponding ranges obtained from the literature are given in Table 5.1. Note that the concentration values are those obtained after spinning the model up to steady state. The WMS and EMS nutrient models are coupled via the fluxes of the various forms of dissolved P and N through the Strait of Sicily. The following sources of P and N to the WMS are

	PO_4	POP	DOP	NO_3	PON	DON	NH_4
	nM			μM			
WMS							
SW	48	17	72	0.8	0.4	2.8	0.03
	(0-350)	(1-100)	(0-400)	(0-7.3)	(0.1-2.2)	(2.0-7.5)	(0-0.06)
IW	269	8	44	6.6	0.1	2.7	0.01
	(0-420)	(0-55)	(0-140)	(3.3-9.9)	(0.01-0.3)	(0.1-4.6)	(0-0.007)
DW	369	3	27	7.7	0.05	2.5	0.01
	(140-480)	(0-15)	(0-140)	(1.6-9.5)	(0.00-0.4)	(1.4-6.7)	(nd)
EMS							
SW	23	7	47	0.6	0.3	2.7	0.09
	(0-100)	(4-20)	(10-100)	(0.01-3)	(0.1-0.5)	(2-11)	(0.04-0.08)
IW	102	5	40	2.6	0.2	2.7	0.05
	(30-200)	(3-10)	(30-80)	(0.5-6)	(0.1-0.3)	(2-5)	(0.05-0.06)
DW	169	3	38	4.8	0.1	2.6	0.05
	(130-230)	(2.5-8)	(0-70)	(3-6)	(0.05-0.15)	(0-5)	(<0.1)

Table 5.1: Reactive P and N concentrations after model spin up and ranges (in brackets) from the literature. Literature ranges for the WMS are from Chapter 6 and for the EMS from Appendix A. nd = no data

considered: inflow of ASW via the Strait of Gibraltar, atmospheric deposition, river inflow, submarine groundwater discharge (SGD) and direct domestic wastewater discharges. In addition, and in contrast to the EMS, N_2 fixation represents a non-negligible input of reactive N to the WMS (Garcia et al., 2006; Sandroni et al., 2007; Ibello et al., 2010b; Bonnet et al., 2011) and is therefore explicitly included. The estimated P and N input fluxes from direct wastewater discharges (Chapter 3) and SGD (Rodellas et al., 2015) are based on recent studies. Because they were not considered in the original EMS model, the latter is updated as described below. The outputs of P and N considered in the model are sedimentary burial, denitrification and outflows to adjacent basins.

5.3.3 External inputs of P and N

The incoming NO_3 flux from the Atlantic Ocean is calculated using reported NO_3 concentrations in the Strait of Gibraltar (Huertas et al., 2012), corrected for the effect of solute mixing within the Strait (Macias et al., 2007; see Appendix F for details). The corresponding PO_4 flux is calculated using a NO_3:PO_4 ratio of 10:1 (Coste et al., 1984; Gómez et al., 2000; Dafner et al., 2003; Huertas et al., 2012). Concentrations of DON (4.5 μM) and DOP (0.14 μM) in the incoming Atlantic Surface Water (ASW) are derived from data from Station 7, west of the Strait of Gibraltar, measured during the MEDRIPOD IV cruise (La Corre et al., 1984). Nutrient concentrations are multiplied by the ASW inflow of 0.83 Sv to yield the input fluxes listed in Table 5.2. In a similar fashion, the inputs of the various P and N species from the EMS are computed by multiplying the EMIW concentrations by the inflow via the Strait of Sicily.

The 1950 riverine inputs of TP and TN to the WMS are assigned the values estimated by Ludwig et al. (2009) for 1963, assuming little change occurred between 1950 and 1963. Riverine TP is further assumed to consist of 48% PO_4, 8% DOP and 44% PIP, while riverine TN is 75% NO_3, 20% DON and 5% NH_4 (Ludwig et al., 2009). It is assumed that 75% of PIP solubilizes to PO_4 upon addition to seawater (Appendix A). The 1950 riverine fluxes of dissolved reactive P and dissolved reactive N to the WMS are then equal to 0.16×10^9 mol P yr^{-1} and 3.9×10^9 mol N yr^{-1} (Table 5.2).

Atmospheric deposition in the WMS has two main sources: Saharan dust and anthropogenic emissions from Europe, mainly from industry and transportation (Bergametti et al., 1992). The estimated average total deposition fluxes of leachable inorganic P and inorganic N measured over the period 1984-2005 are 0.37×10^9 mol P yr^{-1} and 36.7×10^9 mol N yr^{-1}, respectively (Appendix E, section E.1.1.2; Table E.1). We further estimate that 38% of leachable P and 32% of leachable N in atmospheric deposition are in the form of DOP and DON, respectively (Markaki et al., 2010; Appendix A). The resulting atmospheric fluxes of reactive P and N are representative of the 1990s and are therefore back-projected to 1950 values using the forcing functions presented in Chapter 2. These functions are derived from: 1) ice core records

for NO_3 and NH_4 deposition, 2) sulphur and NO_x emissions for PO_4 deposition as they cause acid processing of atmospheric dust thereby increasing P solubility (Nenes et al., 2011; Stockdale et al., 2016), and 3) biomass burning trends to account for changes in atmospheric deposition of DOP and DON. The resulting 1950 values, imposed in the model are listed in Table 5.2.

Nitrogen fixation has been suggested to account for 38-53% of the total external N input to the MS (or 50-90x10^9 mol N yr^{-1}) in order to balance the N budget (Béthoux et al., 1992). However, direct measurements of N_2 fixation within the MS have only recently been undertaken, yielding estimates between 0.97x10^9 and 29x10^9 mol N yr^{-1} for the whole WMS (Garcia et al., 2006; Sandroni et al., 2007; Ibello et al., 2010b; Bonnet et al., 2011). Here, a flux of 12.1x10^9 mol N yr^{-1} is assigned to N_2 fixation based on data obtained during the BOUM cruise along an east to west transect across the WMS (Bonnet et al., 2011).

Recent estimates of the direct domestic wastewater discharges of TP and TN into the WMS in the year 2003 are 0.35x10^9 mol P yr^{-1} and 5.4x10^9 mol N yr^{-1} (Chapter 3). Wastewater TP is assumed to comprise 43% PO_4, 25% POP, 10% DOP and 22% PIP, while wastewater TN consists of 16% NO_3; 7% PON, 12% DON and 65% NH_4 (Chapter 3). The 1950 reactive N input fluxes are obtained from the corresponding 2003 values by assuming that direct domestic wastewater N discharges scale proportionally to the coastal population. For reactive P, direct domestic wastewater is assumed to follow riverine N:P trends, hence accounting for changes in laundry and dishwasher detergent use between 1950 and 2003 (Chapter 6). The resulting 1950 input fluxes are given in Table 5.2.

Submarine groundwater discharges of PO_4 and DIN are calculated by multiplying the flow of fresh SGD into the WMS (Chapter 4) and the average PO4 and DIN concentrations in Mediterranean coastal aquifers (Rodellas et al., 2015). Imposing a NO3:DIN ratio of 0.99 (Table E.2), and assuming DOP and DON contribute one third of dissolved reactive P and N in SGD, respectively (Table E.3), yields SGD fluxes of 0.015x10^9 mol P yr^{-1} and 14.4x10^9 mol N yr^{-1} for the year 2000. The reactive N flux from SGD (Table 5.2) in 1950 is then derived from fertilizer and manure application trends (Erisman et al., 2011; FAOSTAT, 2015a; b) and assuming a 30 year time lag between SGD recharge and discharge (Table E.4). We further assume that anthropogenic inputs of reactive P are retained in the aquifer due to the low dissolved reactive P concentration in SGD reported for the year 2000 (Rodellas et al., 2015). Thus the 1950 dissolved reactive P flux from 1950 is the same as that for 2000.

	Sea	PO_4	DOP	POP	NO_3	DON	NH_4	PON
Input								
Riverine	EMS	0.23	0.06		2.4	0.6	0.2	
	WMS	0.14	0.01		2.9	0.8	0.2	
Atmospheric	EMS	0.38	0.33		19.8	30.8	13.8	
	WMS	0.16	0.15		8.1	12.3	5.8	
N_2 fixation	EMS							0
	WMS							12.1
SGD*	EMS	0.004	0.002		0.4	1.8	0.01	
	WMS	0.008	0.004		1.1	3.3	0.01	
Wastewater	EMS	0.13	0.02	0.05	0.2	0.4	2.0	0.2
	WMS	0.17	0.03	0.08	0.7	0.4	2.1	0.2
Output								
Burial	EMS			0.71				20.7
	WMS			0.55				10.6
Denitrification	EMS				2.4			
	WMS				18.0			
Inflow/outflow from adjacent basins								
Atl-WMSW (Conc)		4.05	3.66		41.8	117.5	2.6	
		(0.155)	(0.14)		(1.6)	(4.5)	(0.1)	
WMSW - EMSW		1.72	2.60		29.4	100.0	1.1	
EMIW-WMIW		3.52	1.39		90.5	93.2	1.6	
WMIW-Atl		3.97	0.65		97.3	40.4	0.1	
WMDW-Atl		3.63	0.27		76.2	24.4	0.1	
Adr-EMDW		1.08	0.42		28.5	29.9	0.5	
EMIW-Adr		1.02	0.40		26.3	27.1	0.5	
Aeg-EMDW		0.14	0.05		3.7	3.6	0.1	
EMDW-Aeg		0.13	0.05		3.3	3.4	0.1	
NWM-WMDW		3.57	1.05		85.2	53.1	0.3	
(WMSW+WMIW)-NWM		3.57	1.05		84.9	53.0	0.3	

Table 5.2: Input and output fluxes of P (PO_4, POP, DOP) and N (NO_3, DON, NH_4, PON) for the WMS and EMS (in units of 10^9 mol yr^{-1}). *SGD = freshwater derived submarine groundwater discharge.

5.3.4 Outputs of P and N

Fluxes of dissolved reactive P and N exiting the WMS through the Strait of Gibraltar are calculated by multiplying the corresponding water fluxes with the concentrations of the various P and N species in WMIW and WMDW (Table 5.1; Table 5.2). Similarly, the outputs of dissolved reactive P and N to the EMS are obtained by multiplying the concentrations in WMSW with the flow of water from the WMS to the EMS via the Strait of Sicily.

To the authors' knowledge, no published estimates exist for POP burial in the WMS. We therefore obtained samples from 8 sediment cores from the Alboran Sea and Catalan Shelf, courtesy of Dr. Pere Masqué (T6, Alb 1, Alb 2, Alb E, Alb D, T3, EB2, CN36; Sanchez-Cabeza et al., 1999; Masqué et al., 2003) and measured POP concentrations following the SEDEX protocol (Ruttenberg et al., 2009). Briefly, TP was determined by ashing the sample for 2 hours at 500^{o}C, followed by 16 hours of 1M HCl digestion; PIP was measured after 16 hours of 1M HCl digestion. The POP concentration was calculated as the difference between the two experimental values (see Appendix E for details on the core locations and experimental methods and results).

The POP concentration of sediment samples varies by only a factor of two (3.1-7.1 μmol g^{-1} dry weight; Table E.7), in contrast to reported sediment accumulation rates which vary by an order of magnitude (0.063-0.51 g cm^2 yr^{-1}; Table E.6; Sanchez-Cabeza et al., 1999; Masqué et al., 2003). The open WMS POP burial flux is estimated using the average POP sediment concentration measured in the cores retrieved at water depths exceeding 1000 m (5.6 μmol g^{-1} dry weight), multiplied by sediment accumulation rates from the Algero-Balearic basin (41 g m^{-2} yr^{-1}; Zúñiga et al., 2007a) and DYFAMED site (168 g m^{-2} yr^{-1}; Heimbürger et al., 2012) (Table E.5). Burial of POP in the Alboran Sea is estimated using the average POP burial rate from the 6 cores located in the Alboran Sea. Finally, the sediment POP concentration for the Catalan shelf (core CN 36) together with reported sediment accumulation rates are used to approximate POP burial in the Gulf of Lions (Van Den Broeck and Moutin, 2002; Table E.8). The resulting range for the POP burial flux in the WMS is then 0.56-1.1x10^9 mol P yr^{-1} (Table E.5). We use the low-end estimate as representative of the 1950 POP burial flux. The final burial flux after model spin up is reported in Table 5.2.

Sediment PON burial is estimated separately for the Alboran Sea, Gulf of Lions and the remainder of the WMS, using reported burial rates of PON (Masqué et al., 2003; Heimbürger et al., 2012) and POC (de Madron et al., 2003a; Zúñiga et al., 2007a). To convert from POC to PON burial rates, molar POC:PON ratios of 9.4 and 5.5 are assigned to the Gulf of Lions (Denis and Grenz, 2003) and the open WMS (Zúñiga et al., 2007b), respectively. The resulting total PON burial flux for the WMS is on the order of 11x10^9 mol yr^{-1} (see Appendix E; Table E.5). The denitrification flux for the

WMS ($20x10^9$ mol yr^{-1}, see Appendix E; Table E.9) is derived from denitrification rates measured over the course of one year at the DYFAMED site (Gehlen et al., 1997), plus sediment core incubation results for the Gulf of Lions (Denis and Grenz, 2003). Slight adjustments after model spin-up yield the N removal fluxes given in Table 5.2.

5.3.5 Primary production

Annual primary productivity in the WMS is assigned to be 2.5 times of that in the EMS based on the primary production measurements in the WMS and EMS between 1970 and 2010 compiled by Berman-Frank and Rahav (2012). The resulting 1950 primary productivity in the WMS after model spin up is then 148 g C m^{-2} yr^{-1}, compared to 56 g C m^{-2} yr^{-1} in the EMS. Primary productivity is converted to P and N assimilation fluxes using the Redfield C:N:P ratio of 106:16:1 (Redfield et al., 1963). At steady state, export production equals new production (Eppley and Peterson, 1979). The export production in the WMS is 28-35 g C m^{-2} yr^{-1} according to Béthoux (1989) and Zúñiga et al. (2008). Using molar POC:PON and POC:POP ratios of sinking organic matter of 7.7 and 169, respectively (Marty et al., 2009) we obtain export fluxes of 11.4-14.1$x10^9$ mol yr^{-1} for POP and 259-318$x10^9$ mol yr^{-1} for PON. The lower values of these two ranges are assigned to the 1950 fluxes of POP and PON from WMSW to WMIW, in order to account for the increased productivity since 1950 because of higher inputs of anthropogenic nutrients to the MS (Chapter 6). The final sinking fluxes upon model spin-up are given in Table E.10

5.3.6 Deep-water formation

Incoming WMDW through DW formation in the NWM contains the dissolved reactive P and N originally present in the WMSW and WMIW exported to the NWM. A small correction for additional external inputs to the NWM from N_2 fixation and atmospheric deposition is applied to the deep water P and N fluxes into the WMDW similar to the approach used in Appendix A for the EMS. Total reactive dissolved fluxes of $4.6x10^9$ mol P yr^{-1} and $139x10^9$ mol N yr^{-1} are then estimated to enter the WMDW through DW formation in 1950, of which $0.009x10^9$ mol P yr^{-1} and $0.43x10^9$ mol N yr^{-1} are attributed to the additional external inputs into the NWM (Table 5.2; see Appendix E for further details).

5.3.7 Modifications to existing EMS model

The original EMS model of Appendix A is modified by adding SGD and direct domestic wastewater discharges as sources of P and N, following the same procedures as for the WMS (section 5.3.3). The EMS wastewater reactive P and N inputs for the year 2003 from Chapter 3 are reduced taking into account the changes in the coastal populations and riverine N:P ratios (Chapter 6), to yield 1950 wastewater fluxes into the EMS of $0.2x10^9$ and $2.7x10^9$ mol yr^{-1} for reactive P and N, respectively. The

1950 dissolved reactive P and N fluxes associated with SGD are computed using a fresh SGD water flux to the EMS of 15.1 km^3 yr^{-1} derived from regional estimates by Zekster et al. (2007), PO_4 and DIN concentrations of 0.28 and 370 μM, respectively (Rodellas et al., 2015), and assuming that DOP and DON contribute one-third of the reactive P and N inputs (section 5.3.3). The additional P and N inputs cause slight changes to the EMS model; the largest ones involve adjustments of the first-order rate constants (*k*) for P solubilization and mineralization in EMDW, N mineralization in EMIW and EMDW, and EMDW nitrification. These changes, however, are within 9% of the original *k* values. All other *k* values remain unchanged.

5.3.8 Numerical solution and sensitivity analyses

The model consists of 42 differential equations that are solved simultaneously in MATLAB with solver ODE15s. The numerical approach followed is the same as described in Appendix A for the EMS model. The fluxes in the model are described by simple first-order rate expressions with respect to the source reservoir mass. Exceptions are the turbulent diffusion fluxes, which depend linearly on the concentration differences between source and sink reservoir. Vertical eddy diffusion coefficients are the same as in Chapter 4. Slightly modified rate expressions are also used to represent DON mineralization and nitrification in the WMSW and EMSW (see Appendix A). Upwelling and downwelling fluxes, along with the bidirectional fluxes between the EMS and WMS through the Strait of Sicily, are computed from the nutrient concentrations in the source reservoir and the corresponding water flow to the receiving water body (Chapter 4). Final model values for the internal nutrient fluxes (Table E.10) and corresponding rate parameters (*k*) are obtained by spinning the model up to steady state.

A global model sensitivity analysis is carried out with a fractional factorial design analysis (Box et al., 1978; Appendix A) of the coupled WMS-EMS model. Four model responses are tested (WMS and EMS primary productivity, and WMS and EMS NO_3:PO_4 DW ratio) using three sets of parameters: water cycle (2^{14-4} fractional factorial design), internal fluxes (2^{44-34} fractional factorial design) and external fluxes. For the latter, a 2^{28-18} factorial design analysis is used to assess the sensitivity of primary productivity, while, due to the high number of variables, the responses of NO_3:PO_4 DW ratios were investigated separately for the WMS and EMS variables. Model parameters within each set are varied by ± 10%. Thus, for example, when internal parameters are varied, external and water cycle parameters remain constant. Results are plotted on effect versus probability graphs. Because higher order effects only have negligible effects on the model dynamics (Appendix A), only first and second order interactions are plotted. Results that deviate from the vertical axis through the origin imply that the model response is sensitive to the corresponding parameter.

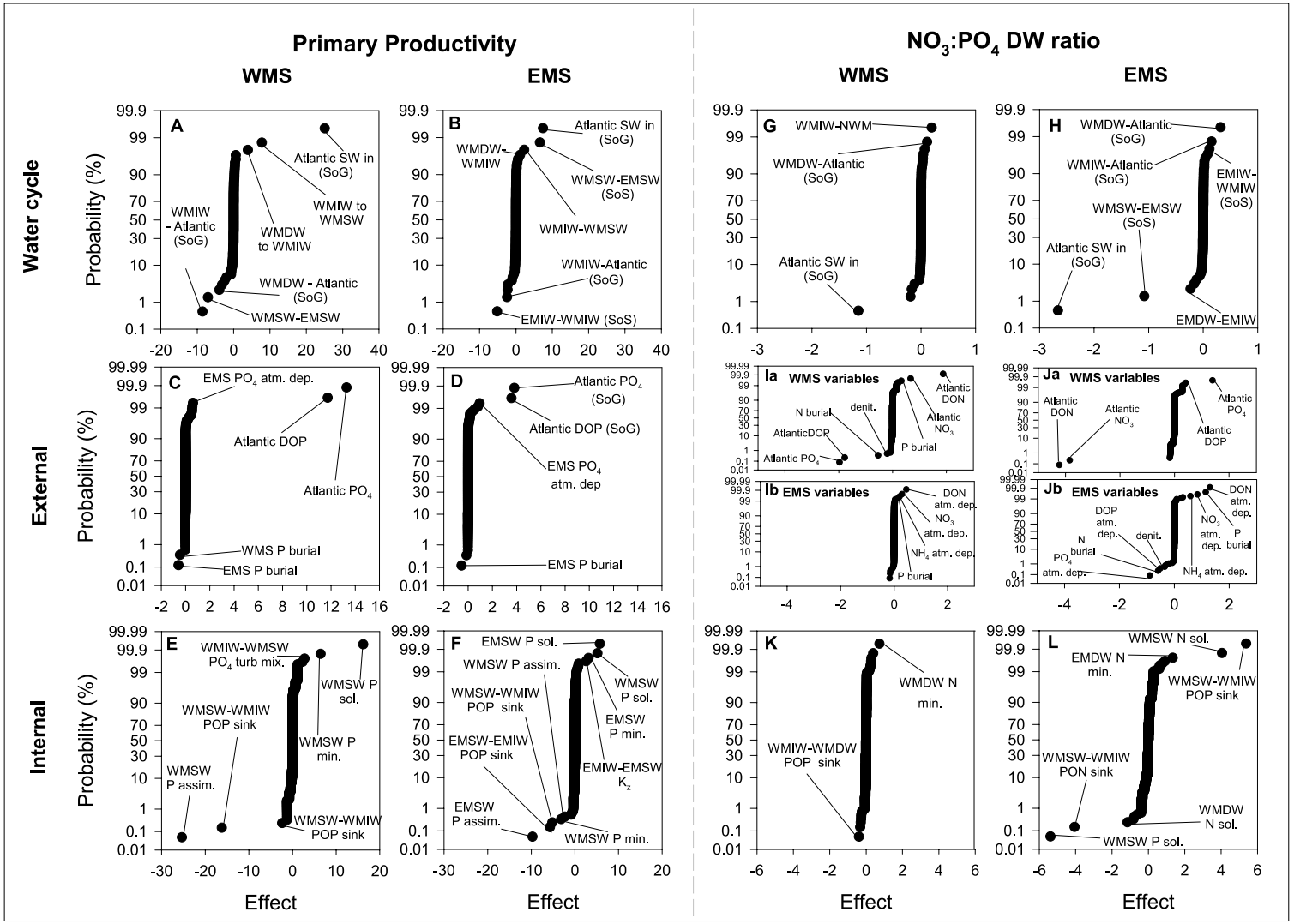

Figure 5.2: Factorial design analysis: panels show the sensitivity of two model outcomes, primary productivity (panels A-F) and the DW NO_3:PO_4 ratio (panels G-L), in the WMS and EMS to various sets of model variables associated with the MS water cycle (upper row panels), external P and N sources (middle row panels) and processes occurring within the MS (lower row panels). See text for details.

The sensitivity analyses indicate that primary productivity in both the WMS and EMS is particularly sensitive to inflow of PO_4 and DOP from the Atlantic Ocean, plus atmospheric deposition of PO_4 in the respective basins (Figure 5.2 A-D). Primary productivity in both WMS and EMS is also sensitive to the solubilization of POP and subsequent mineralization of DOP within the SW, highlighting the role of heterotrophic processes in recycling P, as well as to other internal cycling processes such as P assimilation, sinking of POP out of the SW, and, in the EMS, turbulent mixing (Figure 5.2 E). Interestingly, primary productivity in the EMS is sensitive to processes in the WMSW that are involved in the recycling of P and the fluxes of P into and out of WMSW (Figure 5.2 F).

The WMDW NO_3:PO_4 ratio is most sensitive to the inflow of PO_4 and DON from the Atlantic Ocean, together with atmospheric DON deposition in the EMS (Figure 5.2 G, I and K). For EMDW, the NO_3:PO_4 ratio is more sensitive to processes that alter the N:P of the water entering the DW rather than processes taking place in the EMDW reservoir itself (Figure 5.2 H, J and L). Furthermore, the EMDW NO_3:PO_4 ratio is more sensitive to processes taking place in the WMS, such as sinking of POP out of WMSW, solubilization of POP and PON in the WMSW, or dissolved P and N entering the WMS through the Strait of Gibraltar, than to any process occurring in the EMS. For example, increasing the WMSW solubilization flux of PON by 10% results in a 7% increase in the EMDW NO_3:PO_4 ratio (Table E.12). In comparison, a 10% change in the EMSW or EMDW PON solubilization flux only changes the EMDW NO_3:PO_4 ratio by 0.1 and 1.5%, respectively. Overall, the sensitivity analyses also suggest that the EMDW NO_3:PO_4 ratio is more sensitive to change than the WMDW NO_3:PO_4 ratio.

When the model is run with a NO_3:PO_4 uptake ratio of 23:1 during SW assimilation (see section 5.3.2), it is possible to reproduce the same water column distributions of P and N concentrations in the WMS and EMS than with the 16:1 uptake ratio, if the rate constants (k) describing the recycling of PON in the SW (i.e., solubilization, mineralization and nitrification) are increased by about 40%. In other words, variations in the photosynthetic NO_3:PO_4 uptake ratio can be compensated by adjusting the recycling efficiency of PON in the SW reservoirs accordingly. However, the trends in DW NO_3:PO_4 ratios and the conclusions regarding the recycling of P and N within the two basins remain unchanged, and are thus robust model results.

5.4 Results and discussion

The mass balance model we have developed integrates the state of knowledge about the biogeochemical cycling of P and N in the MS. The coupled WMS-EMS model represents the nutrient elements' external sources, biogeochemical transformations, physical redistribution within and between the two basins, and ultimate sinks. Here, we analyze the features of the modeled P and N cycles before the large increases in

anthropogenic nutrient inputs that took place during the second half of the 20th century. The steady state P and N model fluxes in 1950 thus provide the quantitative basis for interpreting some of the characteristic and unusual biogeochemical properties of the MS prior to their large-scale perturbation by human activity. The changes in the P and N cycles that occurred since 1950 are the topic of Chapter 6. It is important to recognize the limitations of the model. In particular, the simple physical and biogeochemical structure of the model does not account for lateral variations in nutrient distributions and process rates in the WMS and EMS, nor does it resolve sub-annual features of the P and N cycles. Instead, the model aims to reproduce the basin-wide, yearly averaged fluxes and transformations of the nutrients.

5.4.1 External phosphorus and nitrogen inputs to the MS

Because it is nearly entirely surrounded by land, one might expect terrestrial sources to dominate the inputs of reactive P and N to the MS. However, according to our estimations, the main source of P and N to the MS is inflow of ASW through the Strait of Gibraltar, which provides 79% of reactive P and 56% of reactive N inputs to the entire MS (Figure 5.3; Table 5.2). The aggregated supplies of non-marine reactive P and N, that is, the combined inputs from atmospheric deposition, rivers, SGD, direct wastewater discharges, N_2 fixation, and additional reactive P and N from the NWM and the Adriatic and Aegean Seas, are similar for the WMS and EMS when normalized per unit surface area: approximately 0.001 mol P m^{-2} yr^{-1} and 0.06 mol N m^{-2} yr^{-1}. By contrast, the inputs of marine sourced reactive P and N are four to five times greater for the WMS than the EMS. The combined inputs of ASW and EMIW entering the WMS through the Straits of Gibraltar and Sicily amount to 0.015 mol P m^{-2} yr^{-1} and 0.4 mol N m^{-2} yr^{-1}, while only 0.003 mol P m^{-2} yr^{-1} and 0.1 mol N m^{-2} yr^{-1} enter the EMS with inflow of WMSW through the Strait of Sicily (Figure 5.3).

The estimated external nutrient inputs therefore reveal a key difference between the WMS and EMS. For the WMS, non-marine reactive P and N fluxes are added to a relatively enriched background of reactive P and N that originate from the North Atlantic and EMIW. In contrast, for the EMS, the comparable non-marine reactive P and reactive N inputs are added to inflow of WMSW through the Strait of Sicily that is severely depleted in reactive P and reactive N as observed by Ribera d'Alcala et al. (2009), Karafistan et al. (2002)and Denis-Karafistan et al. (1998).

5.4.2 Primary production and new production

The significantly higher marine-derived reactive P input to the WMS, compared to the EMS, largely explains the difference in primary productivity between the two basins. (Note: here we focus on reactive P inputs, as the model assumes that the yearly averaged primary productivity of the WMS and EMS is P limited.) The total reactive P input to the WMS is 3.9 times greater per m^2 than for the EMS (Table 5.2),

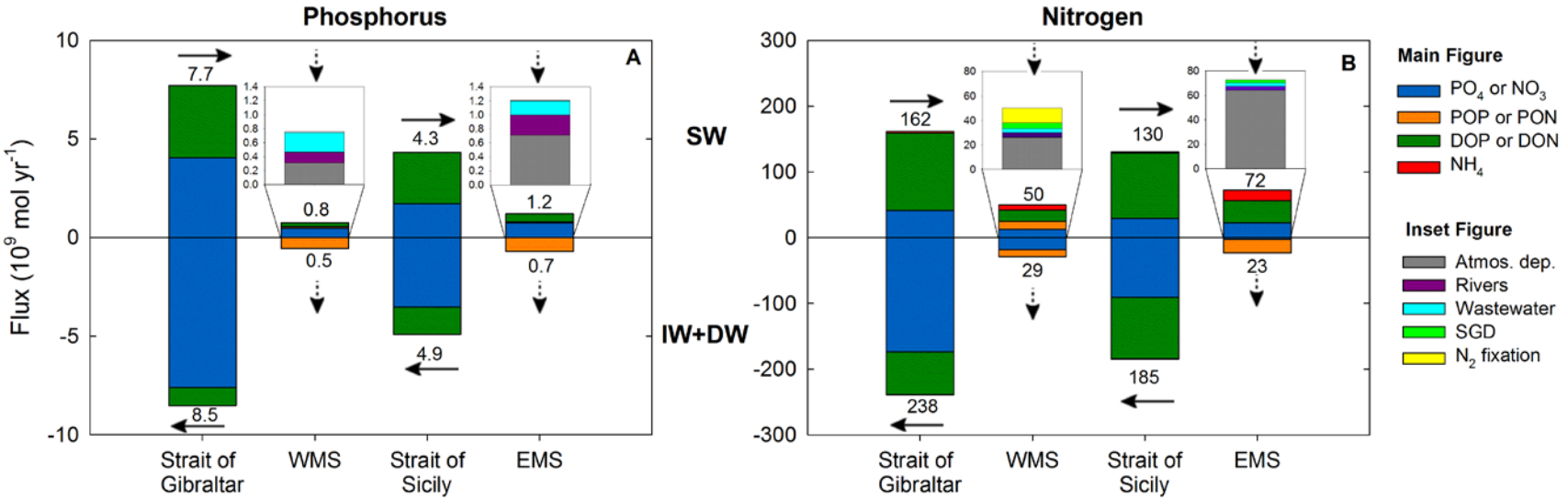

Figure 5.3: Speciation of A) phosphorus and B) nitrogen in the inputs to and outputs from the MS in the year 1950. Numbers at top and bottom of the columns represent total fluxes in 10^9 mol yr^{-1}. Horizontal arrows indicate direction of flow of water through the Strait of Gibraltar and the Strait of Sicily; vertical arrows indicate input (positive numbers) and output (negative numbers) of P and N for the WMS and EMS (excluding the exchanges through the straits). The removal of POP or PON in the WMS and EMS is due to burial in sediments; removal of NO_3 corresponds to denitrification. Inset figures represent the contributions of different external inputs to the WMS and EMS (excluding flows through the straits). See Table 5.2 for numerical values.

while primary production is 2.6 times greater in the WMS (148 versus 56 g C m^{-2} yr^{-1} in the WMS and EMS, respectively). If only external inputs to SW are considered (i.e., excluding internal inputs associated with upwelling and turbulent mixing), WMSW receives 2.5 times more reactive P per m^2 than EMSW (0.01 vs 0.004 mol P m^{-2} yr^{-1}).

In addition to the large difference in external reactive P inputs, the two basins diverge in their thermohaline circulation (Figure 5.1). In the WMS upwelling (from WMIW to WMSW) brings additional dissolved reactive P (and N) into the photic zone. In contrast, the thermohaline circulation of the EMS is dominated by downwelling (from EMSW to EMIW), which removes dissolved nutrients from the surface waters. The dissolved reactive P (and N) accumulating in EMIW is largely exported through the Strait of Sicily to the WMS. In the EMS, turbulent mixing is the only internal transport process providing additional reactive P to the photic zone. As a result, the WMS and EMS not only differ in their primary production, but also in their new production.

Here, new production is defined as the portion of yearly primary production that is supported by sources of dissolved reactive P supplied from outside the SW reservoir. We assume that all recycled production from the solubilization of POP in SW is regenerated, and that the difference between DOP mineralization and POP solubilization is the new production supported by DOP (see Figure 5.1 for model schematic). Overall, 39% of new production in the WMS is sustained by dissolved reactive P delivered with the inflow of ASW and 45% by upwelling of WMIW (Figure 5.4). In comparison, in the EMS 37% of new production is supported by inflow of WMSW and 48% by turbulent mixing (Figure 5.4). Thus, in both basins large fractions of new production are due to the lateral transfer of (marine) nutrients via surface flow through the Straits of Gibraltar and Sicily. The new production estimates further suggest that 26% and 37% of DOP supplied to WMSW and EMSW, respectively, are remineralized and potentially used for autotrophic assimilation. This is a significant finding, given that the dissolved organic pools of the P and N are usually not considered to be important sources of new production in marine systems.

The MS is therefore unusual not only because of the important role lateral flows play in supplying P (and N) to the photic zone, but also because of the large fractions of new production that are supported by DOP (and DON). Appendix A previously proposed that DOP constitutes a major fraction (about 60%) of reactive P entering the EMS from the WMS, and that it contributes a substantial portion of new production in the EMS. Similarly, inflow of ASW through the Strait of Gibraltar comprises a large fraction of reactive P in the form of DOP (47%) (Figure 5.3 A; Table 5.2). However, not all DOP entering the WMSW and EMSW is used for new production, but instead gets removed by downwelling and lateral outflow. In fact, our calculations imply that 74 and 63% of DOP entering the WMSW and EMSW,

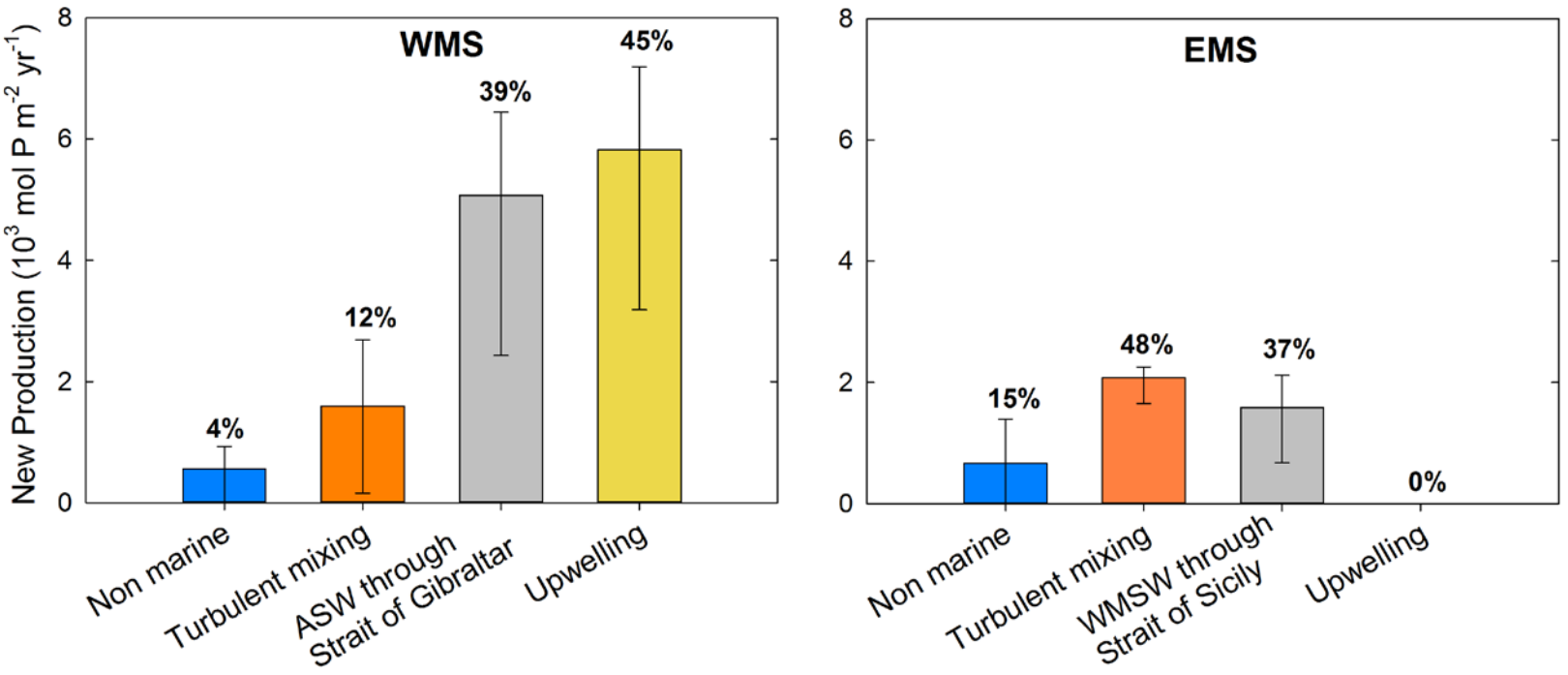

Figure 5.4: Source attribution of new production in the WMS and EMS. Error bars represent the uncertainty of individual source contributions for a total new production of 10.6×10^9 mol P yr^{-1} in the WMS and 5.8×10^9 mol P yr^{-1} in the EMS.

respectively, leave the SW reservoirs without contributing to export production. It is likely that the latter DOP is mainly refractory, given that both the WMS and especially the EMS exhibit high levels of alkaline phosphatase activity (Zaccone et al., 2012; see also section 5.4.4).

The importance of the lateral supply of nutrients in the MS, particularly as DOP and DON, bears a strong resemblance to the recent hypothesis developed by Letscher et al. (2016). These authors propose that lateral advection is a major source of nutrients supporting new production in subtropical oceanic gyres, in addition to vertical mixing. They estimate that lateral supplies of P and N support 44-67% and 24-36% of new production in subtropical gyres, respectively, with the lateral supply of DOP and DON contributing 22-46% and 12-19% of export production, respectively. That the MS behaves similarly to the open ocean gyres with respect to lateral nutrient supply may at first seem surprising given that it is an almost entirely landlocked marine basin. The reason stems from the anti-estuarine circulation, which drives the large lateral inflow of ASW, and its associated nutrient load, into the MS.

The model-derived new production equals 10.6×10^9 mol P yr^{-1} in the WMS and 5.8×10^9 mol P yr^{-1} in the EMS. In comparison, total primary production, expressed as P assimilation in the SW, equals 95×10^9 mol P yr^{-1} in the WMS and 59×10^9 mol yr^{-1} in the EMS. Thus, recycled production through organic matter breakdown by far exceeds new production in both WMSW and EMSW, accounting for 89-90% of primary production. The resulting *f* ratio, that is, the ratio of new production to primary production (Eppley and Peterson, 1979), is slightly lower in the EMS (0.10) than WMS (0.11). The low *f* ratios for both WMS and EMS are typical of oligotrophic marine water bodies; they are similar to other values reported for the MS (Béthoux, 1989; Béthoux et al., 1998; Diaz and Raimbault, 2000; Kouvarakis et al., 2001; L'Helguen et al., 2002), the Sargasso Sea (Mongin et al., 2003), and the Equatorial Pacific (McCarthy et al., 1996).

5.4.3 Why is the MS oligotrophic?

The dominance of ASW as a source of reactive P and N to the MS may seem at odds with the commonly held view that the oligotrophy of the MS is due to the anti-estuarine circulation, which brings in nutrient depleted surface water into the WMS (EMS) through the Strait of Gibraltar (Strait of Sicily) and returns nutrient enriched water from deeper reservoirs. This view, however, only focuses on the inorganic forms of dissolved P and N. In fact, according to our estimates, the dissolved reactive P flux associated with outflow of WMIW and WMDW through the Strait of Gibraltar is only 10% larger than the dissolved reactive P flux entering the WMS with ASW (Figure 5.3 A; Table 5.2). The key difference, however, is the chemical speciation of the dissolved P: 47% of the ASW P inflow is under the form of DOP compared

to only 11% in the outflow (Figure 5.3 A; Table 5.2). Thus, 88% more PO_4 exits the MS through the Strait of Gibraltar than enters at the surface. A similar speciation switch happens at the Strait of Sicily. While the dissolved reactive P flux leaving the EMS is only 14% greater than the dissolved reactive P flux entering the EMS, PO_4 represents 72% of the EMIW outflow compared to 40% in the WMSW inflow (Figure 5.3 A; Table 5.2). In other words, for both the WMS and EMS the anti-estuarine circulation exports more readily bioavailable P (i.e., PO_4) than it imports.

In comparison, significantly more dissolved reactive N leaves the MS through the Strait of Gibraltar than enters from the Atlantic (Figure 5.3 B; Table 5.2), reflecting a higher influence of land-derived inputs for reactive N than for P. The flux of dissolved reactive N leaving the MS through the Strait of Gibraltar is 47% larger than the flux entering as ASW, and contains more than four times greater NO_3 mass. Similarly, at the Strait of Sicily 42% more N exits the EMS as IW than enters as SW, with three times more NO_3 leaving the EMS than flowing in.

5.4.4 The MS as a net heterotrophic system

Heterotrophy of the MS is a consequence of the anti-estuarine circulation combined with the recycling of organic matter supplied externally from marine and non-marine sources. Fluxes of dissolved and particulate organic P and N entering the MS exceed those leaving the MS by outflow through the Strait of Gibraltar and sediment burial: 4.4×10^9 mol organic P yr^{-1} and 183×10^9 mol organic N yr^{-1} enter the MS from marine and non-marine sources in comparison to 2.2×10^9 mol organic P yr^{-1} and 96×10^9 mol organic N yr^{-1} leaving the MS. Based on the differences between DOP and DON inputs and outputs, net heterotrophy in the WMS (0.002 mol P m^{-2} yr^{-1} and 0.8 mol N m^{-2} yr^{-1}) exceeds that of the EMS (0.001 mol P m^{-2} yr^{-1} and 0.03 mol m^{-2} N yr^{-1}). The net heterotrophy of the MS inferred from the model fluxes agree with the suggestion of Luna et al. (2012) that the deeper waters of the MS act as "bioreactors" converting organic P and N into dissolved inorganic nutrients, hence explaining why bacterial enzymatic activities are up to an order of magnitude greater in the MS than in the global ocean.

Duarte et al. (2013) speculate that the excess organic matter supplied to the MS to fuel heterotrophy originates from terrestrial sources, primarily delivered via rivers. Our analysis, however, suggests that most of the DOP and DON supplied to the WMS and EMS is from inflow through the Straits of Gibraltar and Sicily, with atmospheric deposition representing a secondary source (Table 5.2). In comparison, riverine inputs of DOP and DON are fairly minor.

The concentrations of DOP and DON of IW and DW are similar for the WMS and EMS, or even higher in the EMS, despite the higher reactive P and N inputs and higher PO_4 and NO_3 concentrations of the WMS (Moutin and Raimbault, 2002; Pujo-Pay et al., 2011). Integrated across the entire water column

	POM recycling efficiency (%)			Residence time (years)			% inorganic portion of inputs		% inorganic
	SW	IW	DW	SW	IW	DW	Total	To SW	In water Column
Phosphorus									
WMS	89	65	85	1.4	5.1	40	60	54	88
EMS	90	77	48	2.5	5.4	117	45	45	76
Nitrogen									
WMS	82	68	88	1.5	5.3	38	40	37	71
EMS	83	74	50	3.7	6.0	119	34	34	59

Table 5.3: Key model outputs: recycling efficiencies, residence times, inorganic fractions of total reactive P and N inputs, integrated inorganic P and N contents across the entire water column. POM = POP or PON.

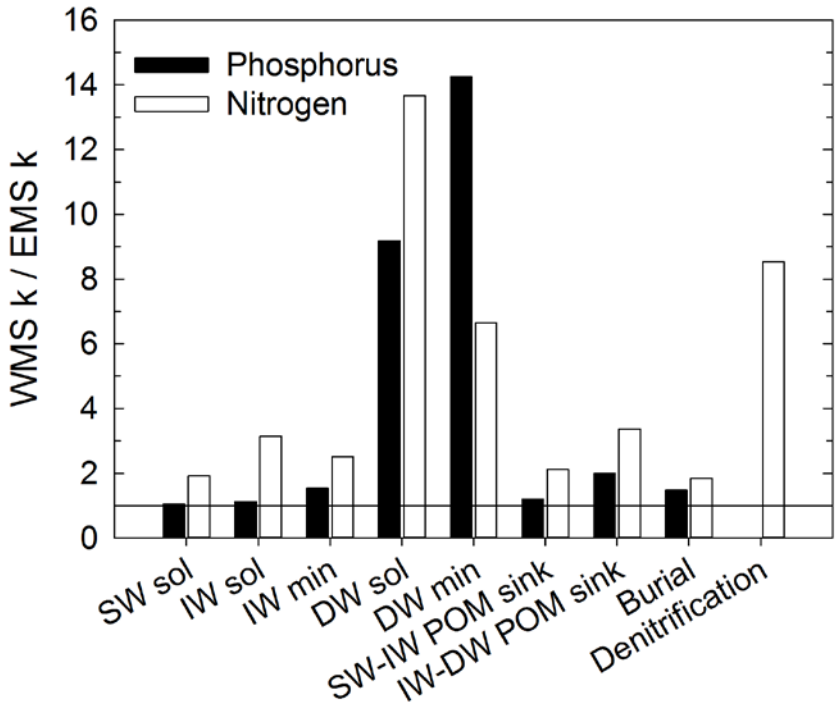

Figure 5.5: Comparison of first order rate constants (*k* values in the model) in WMS and EMS. For any given process, a value greater than 1 correspond to a *k* value in the WMS exceeding that in the EMS, and vice versa. Black bars represent *k* values for P fluxes; white bars for N fluxes. See Figure 5.1 for the definitions of the processes. POM = POP or PON.

PO_4 and NO_3 account for 76% and 59% of dissolved reactive P and N in the EMS, respectively (Appendix A), compared to 88% and 71% in the WMS (Table 5.3). The differences in nutrient distributions between the two basins can be explained by a faster recycling of DOP and DON to PO_4 and NO_3 in the DW of the WMS compared to the EMS, with the higher reactive P and N inputs into the WMS supporting greater bacterial activity in the WMS than the EMS (Luna et al., 2012). In the model, the first order rate coefficients (*k*) describing DW P solubilization and mineralization are 9 and 14 times greater in the WMS than EMS, respectively (Figure 5.5).

The model *k*-values further suggest that the particulate and dissolved organic P and N in the EMS are less labile than their counterparts in the WMS, especially in the DW reservoirs. This is consistent with the higher cell specific alkaline phosphatase activities measured in EMDW compared to WMDW (Zaccone et al., 2012), which imply greater efforts by the EMS microbial community to access the less available POP and DOP. The longer residence time of EMDW (Figure 5.1) likely results in the accumulation of refractory organic matter within the EMDW. In contrast, Bernoulli suction forces WMDW out into the Atlantic Ocean through the Strait of Gibraltar, hence actively removing accumulating refractory DOP and DON, whereas a similar mechanism does not operate in the EMS (Rohling et al., 2015). To exit the EMDW reservoir, refractory DOP and DON must first be transferred to the EMIW via upwelling before it can be transported out of the EMS via the Strait of Sicily.

5.4.5 N:P ratios: WMS versus EMS

Unusually high N:P ratios in all water column reservoirs are a defining feature of the EMS (Krom et al., 2005) and, although somewhat less pronounced, also of the WMS (Pujo-Pay et al., 2011). While all reservoirs exhibit molar N:P ratios in excess of the Redfield ratio of 16:1, it is the NO_3:PO_4 ratios of the DW reservoirs that have received most attention. Measured NO_3:PO_4 ratios increase from around 20-23:1 in WMDW to 28:1 in EMDW (Krom et al., 1991; Béthoux et al., 1998; Kress and Herut, 2001; Moutin and Raimbault, 2002; Ribera d'Alcalà et al., 2003; Schroeder et al., 2010a; Pujo-Pay et al., 2011). The very high EMDW NO_3:PO_4 ratio has previously been explained by the high N:P ratios of the combined external inputs to the EMS, along with negligible denitrification (Krom et al., 2010; Appendix A).

The molar N:P ratios of all 1950 model reservoirs and fluxes are summarized in Figure 5.6 and Figure 5.7. Note that even before the large increases in anthropogenic P and N inputs that took place after 1950, the reactive N:P ratios of external inputs to the MS exceeded the Redfield ratio. In particular, the soluble reactive N:P ratios of atmospheric deposition and SGD are very high: 85-91:1 and 346-381:1, respectively (Figure 5.6). The ratio of the total reactive inputs into the WMS (30:1) is distinctly lower than for the EMS (37:1) (Figure 5.6), which helps explain the lower NO_3:PO_4 ratio of WMDW (21:1)

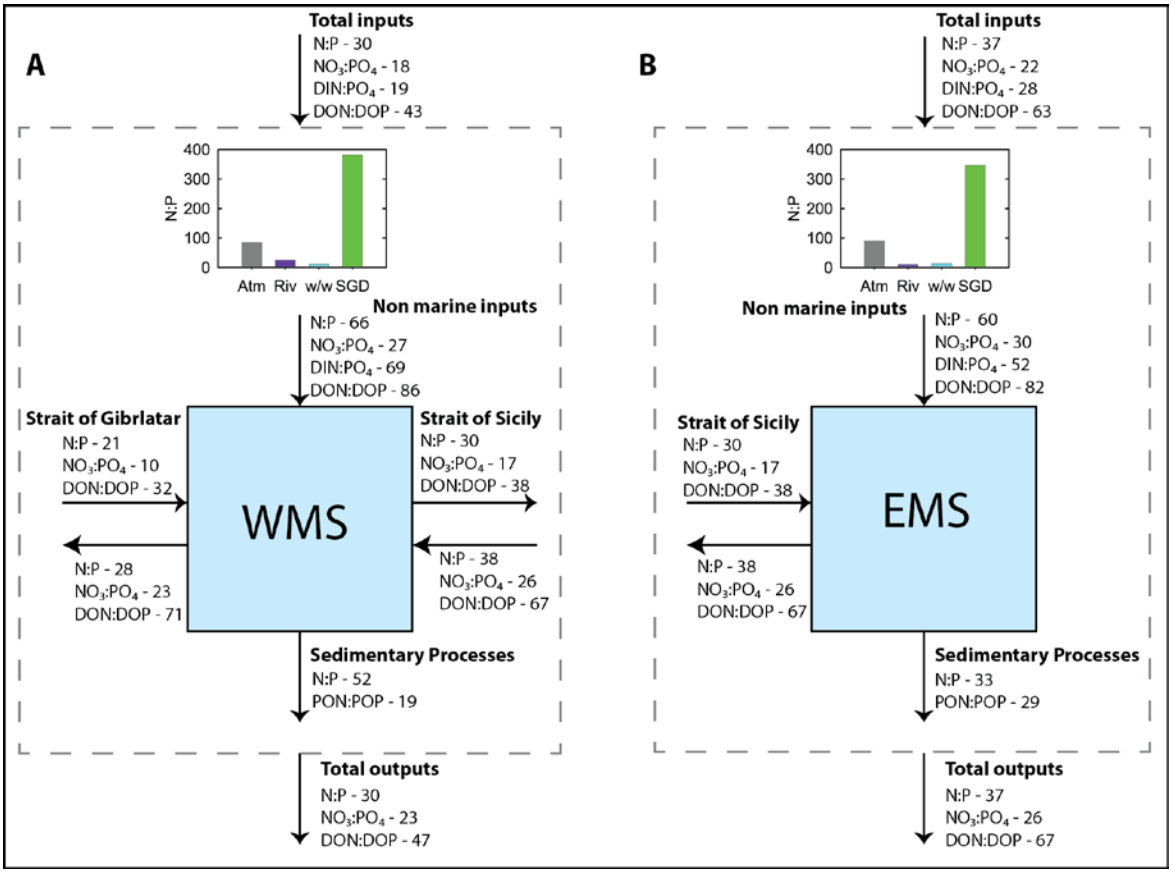

Figure 5.6: Reactive N:P ratios of input and output fluxes to A) the WMS and B) the EMS. $DIN:PO_4$ ratio of fluxes is within 1 unit of $NO_3:PO_4$ ratios unless otherwise stated. Inset figures show the reactive N:P ratios of non marine sources to the MS. Atm = atmospheric deposition; Riv = riverine input; w/w = direct domestic wastewater discharges; SGD = submarine groundwater discharge.

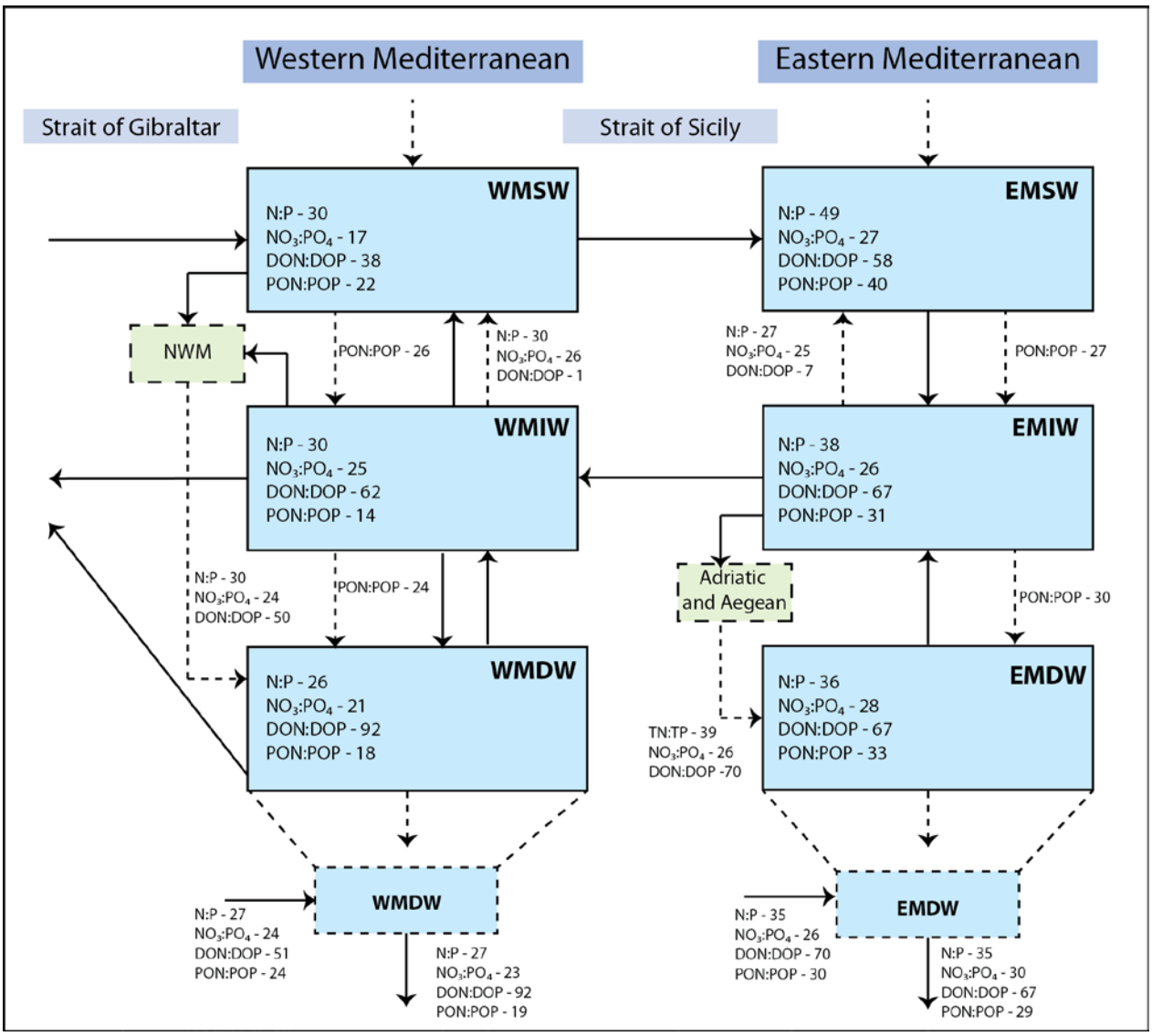

Figure 5.7: N:P ratios of reservoirs and internal fluxes in the model. Solid arrows represent water flows and the associated N:P ratios are those of the corresponding source reservoirs. Dashed arrows represent all other process fluxes with their associated N:P ratios. Dissolved reactive N:P ratios are given (N:P), together with the ratios of individual species. N:P ratios of fluxes entering and exiting WMDW and EMDW (bottom of figure) correspond to external sources and sinks to the DW.

compared to EMDW (28:1) (Figure 5.7). According to the DW NO_3:PO_4 sensitivity analyses (Figure 5.2 G and I), the lower reactive N:P input ratio of the WMS is largely due to the low N:P ratio of the incoming ASW, which represents the main source of reactive P and N to the MS (see also Lazzari et al. (2016).

The ASW flowing into the WMS is depleted in nitrate, with an estimated NO_3:PO_4 ratio of only 10:1. Its dissolved reactive N:P ratio, however, is 21:1, because of the relatively high DON concentration (Figure 5.3 and Figure 5.6). The high N:P of other external inputs to the WMS, causes WMSW entering the EMS through the Strait of Sicily to be more P depleted, relative to N, than ASW entering through the Strait of Gibraltar. Our estimates yield a dissolved reactive N:P ratio of 30:1 for the SW flowing into the EMS from the WMS (Figure 5.6). Thus, the exchanges between the two basins of the MS are a key reason for the more extensive P limitation of the EMS, compared to the WMS. In addition, the greater recycling of DOP relative to DON in WMDW contributes to the lower NO_3:PO_4 ratio in the WMDW than EMDW (Figure 5.6 and 5.7).

Overall, the results summarized in Figure 5.6 align with the conclusions of Krom et al. (2010) and Appendix A which proposed that the NO_3:PO_4 ratio in EMDW is a consequence of a very low denitrification rate in the EMS (0.002 mol N m^{-2} yr^{-1} or 2.4 x 10^9 mol N yr^{-1}), which preserves the signature of the high N:P ratios of the external nutrient sources and the preferential recycling of P compared to N. In the EMS, field measurements further reveal an insignificant role of N_2 fixation in controlling water column NO_3:PO_4 ratios (Ibello et al., 2010b; Bonnet et al., 2011; Rahav et al., 2013). Nitrogen fixation is therefore not considered in the EMS nutrient model.

Measurable N_2 fixation rates have been reported for the WMS, however (Garcia et al., 2006; Sandroni et al., 2007; Ibello et al., 2010b; Bonnet et al., 2011). While N_2 fixation could potentially help explain the relatively high NO_3:PO_4 ratio of WMDW, as previously proposed, our results suggest this is not the case, because the estimated N_2 fixation ($12.1x10^9$ mol N yr^{-1}; Table 5.2, Figure 5.3) is more than offset by the higher denitrification rate of the WMS ($18x10^9$ mol N yr^{-1} or 0.02 mol N m^{-2} yr^{-1}). The potential role of N_2 fixation and denitrification in controlling the WMDW NO_3:PO_4 ratio is also assessed by running the 1950 WMS-EMS model with no N_2 fixation and denitrification. Resulting DW NO_3:PO_4 ratios of 23.2 and 29.2 in the WMDW and EMDW, respectively, indicate that denitrification and N_2 fixation have minimal impacts on the unusual NO_3:PO_4 ratios within the MS, which is also in line with the sensitivity analyses (section 5.3.8 and Figure 5.5). We therefore conclude that, similarly to the EMS, the high NO_3:PO_4 ratio of the WMDW is also due to the high N:P ratio of the external non-marine nutrient sources and low denitrification rates in line with the trends presented by Huertas et al. (2012).

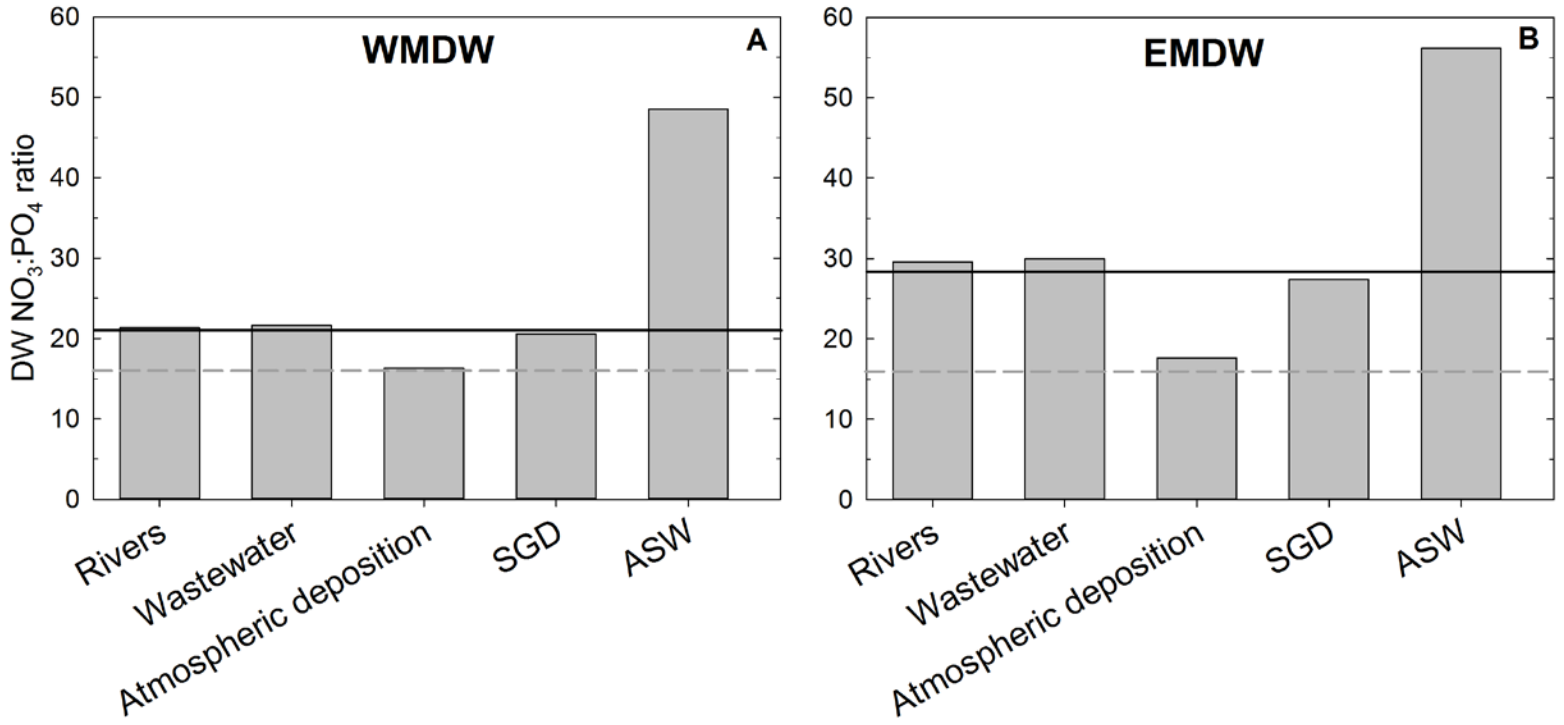

Figure 5.8: Response of the NO_3:PO_4 ratio in A) WMDW and B) EMDW after removing the stated individual input from the 1950 baseline simulation and running the model to its new steady state. Solid line represents the 1950 DW NO_3:PO_4 ratio, dashed line represents the Redfield ratio of 16:1. SGD = submarine ground water discharge; ASW = Atlantic Surface Water input through the Strait of Gibraltar.

The relative impacts of the various external inputs on the NO_3:PO_4 ratios of WMDW and EMDW are illustrated in Figure 5.8, which shows the model-predicted ratios upon removing one nutrient source at the time. A key observation is that when atmospheric deposition is excluded, the new steady state NO_3:PO_4 ratios of the WMS (16:1) and EMS (18:1) drop down to values close to the Redfield value. For the EMS, this is in agreement with Christodoulaki et al. (2013) who predict that if there were no atmospheric inputs to the EMS, the NO_3:PO_4 ratio of EMDW would approach the Redfield ratio. The relative supplies of P and N by atmospheric deposition are thus a major driver of the unusually high NO_3:PO_4 ratios that characterize the MS. The results in Figure 5.8 further indicate that riverine inputs, direct wastewater discharges and SGD have little impact on the DW NO_3:PO_4 ratios. However, in the absence of ASW inflow through the Strait of Gibraltar the NO_3:PO_4 ratios increase to 48 in the WMDW and 56 in the EMDW, confirming the important role of ASW inflow in buffering against even higher than observed DW NO_3:PO_4 ratios. Interestingly, the impact of ASW inflow through the Strait of Gibraltar on the DW NO_3:PO_4 ratios is greater for the EMS than the WMS.

Finally, the model results also demonstrate the importance of the low rates of denitrification in the MS compared to the global ocean (Tyrrell, 1999). To bring the DW NO_3:PO_4 ratios down to the Redfield value of 16:1, the denitrification flux in the WMS would need to increase to 0.05 mol N m^{-2} yr^{-1} (i.e., 2.2 times greater than the 1950 flux) and in the EMS to 0.01 mol N m^{-2} yr^{-1} (i.e., 8 times greater than the 1950 flux). These values are comparable to rates in denitrification found in the global ocean (0.04-0.10 mol N m^{-2} yr^{-1}; Codispoti, 2007; DeVries et al., 2012). In other words, if the MS supported rates of denitrification similar to those generally observed in marine systems its NO_3:PO_4 ratios would fall on the global oceanic trend of 16:1.

5.5 Conclusions

The distinctive biogeochemical signatures of the MS are interpreted with the help of a mass balance model of the cycles of P and N. The model provides estimates of all the inputs of P and N to the MS in the mid-20th century, including those associated with the inflow of ASW through the Strait of Gibraltar and, for the first time, SGD and direct domestic wastewater discharges from coastal cities. It further accounts for the transformations among the different pools of P and N, vertical exchanges, including deep-water formation, upwelling and turbulent mixing, and lateral exchanges through the Straits of Gibraltar and Sicily.

The estimated model fluxes highlight the major role of the bidirectional flows through the Straits of Gibraltar and Sicily, which transport both dissolved inorganic and organic P and N in and out of the WMS and EMS. They further emphasize the importance of the cycling of organic P and organic N in the

biogeochemical functioning of the MS. Inflow of ASW represents the main source of reactive P and N to the WMS, providing up to 60% of the total inputs, of which around half or more are in the form of DOP and DON. Similarly, inflow of SW from the WMS through the Strait of Sicily is the major source of reactive P and N to the EMS, providing up to 75% of the nutrient inputs. Primary productivity in the WMS is higher than in the EMS because the total inputs of marine-derived reactive P and N per unit surface area are three to four times higher for the WMS than the EMS. The surface-normalized non-marine (or land-derived) inputs of reactive P and N to the WMS and EMS, however, are of comparable magnitudes.

Inflow of ASW through the Strait of Gibraltar plus upwelling from WMIW to WMSW support approximately 84% of new production in the WMS, consistent with the sensitivity analyses that indicate that primary productivity in the WMS is most sensitive to the inflow of ASW. In the EMS, the thermohaline circulation is dominated by downwelling resulting in 48% of new production supported by turbulent mixing from EMIW with an additional 37% sustained by the inflow of WMSW through the Strait of Sicily. The supply of DOP is an important source of new production, with 26% and 37% of the DOP supplied to WMSW and EMSW, respectively, remineralized and potentially used for new production. The sensitivity analyses highlight the strong coupling of primary production in the EMS to processes occurring in the WMSW. In particular, uptake of PO_4 in the WMSW greatly reduces the proportion of PO_4 in the flux of dissolved reactive P supplied by the WMS to the EMS via the Strait of Sicily. Overall, the larger input of reactive P to the WMS explains the higher primary productivity in the WMS, which in turn supports greater bacterial activity and nutrient recycling in the WMS compared to the EMS. As a consequence, PO_4 and NO_3 concentrations are higher in the WMS than EMS, while DOP and DON concentrations are similar.

The MS acts as a bioreactor of organic nutrient cycling. In addition to the net delivery of DOP and DON from external sources, PO_4 and NO_3 are converted into organic matter in the SW. Downwelling transfers DOP and DON to the deeper layers, where mineralization turn DOP, and to a lesser extent DON, into PO_4 and NO_3. The latter accumulate in the IW and DW and are exported through the Strait of Sicily and, ultimately, through the Strait of Gibraltar to the Atlantic Ocean. The anti-estuarine circulation thus not only maintains the MS in an oligotrophic state, but also explains its net heterotrophy.

Lateral fluxes through the Straits of Gibraltar and Sicily and recycling of organic nutrients play important roles in determining the NO_3:PO_4 ratios of the WMDW and EMDW. Our results imply that the lower NO_3:PO_4 ratio of WMDW than EMDW is caused by the lower reactive N:P ratio of inputs into the WMS than EMS. The latter reflects the low NO_3:PO_4 ratio of ASW entering the WMS, together with faster

recycling of DOP than DON within the WMDW. The high NO_3:PO_4 ratio of the entire MS is largely due to the high reactive N:P ratio of atmospheric deposition: without this input the WMDW and EMDW NO_3:PO_4 ratios would approach the Redfield value. Processes that regulate the NO_3:PO_4 ratio in the global ocean, in particular the balance between N_2 fixation and denitrification, are relatively unimportant in the MS. Finally, our analysis shows that the EMDW NO_3:PO_4 ratio is more sensitive than that of the WMDW ratio to changes of the internal and external models parameters. Thus, changes in the EMDW NO_3:PO_4 ratio could be a more sensitive indicator of changes in anthropogenic nutrient inputs than the changes in the WMDW ratio.

The coupled WMS-EMS model offers a simplified representation of the biogeochemical cycles of P and N, ignoring mesoscale variability and seasonality. However, it helps identify the basin-scale biogeochemical and oceanographic processes that control P and N cycling in the MS on annual to decadal timescales. It also allows us to develop specific hypotheses that can guide the design of further studies on the MS. Based on the work presented here, we suggest that future research should concentrate on improving the quantification of the inputs, distributions, lability and recycling of organic P and N across the MS. We strongly recommend the acquisition of internally comparable, multi-nutrient data in both the WMS and EMS. Particular attention should be given to the lateral fluxes of organic and inorganic P and N through the Straits of Gibraltar and Sicily, and the role of atmospheric deposition in the P and N cycles of the MS.

Chapter 6.

Phosphorus and nitrogen trajectories in the Mediterranean Sea (1950-2030):

Diagnosing basin-wide anthropogenic nutrient enrichment

6.1 Summary

Human activities have significantly modified the inputs of land-derived phosphorus (P) and nitrogen (N) to the Mediterranean Sea (MS). Here, we reconstruct the external inputs of reactive P and N to the Western Mediterranean Sea (WMS) and Eastern Mediterranean Sea (EMS) over the period 1950-2030. We estimate that during this period the anthropogenic land derived P and N loads have increased by a factor of 3 and 2 to the WMS and EMS respectively with reactive P inputs peaking in the 1980s, while reactive N inputs continuously increase from 1950 to 2030. The temporal variations in reactive P and N inputs are imposed to a coupled P and N mass balance model of the MS to simulate the accompanying changes in water column nutrient distributions with time. The key question we address is whether these changes are large enough to be distinguishable from variations caused by confounding factors, specifically the relatively large inter-annual variability in thermohaline circulation (THC) of the MS. Our analysis indicates that the magnitudes of changes in reactive P concentrations due to changes in anthropogenic inputs are relatively small and likely difficult to be detected because of the noise created by the natural circulation variability. Anthropogenic N enrichment should be more readily detectable in time series concentration data for dissolved organic N (DON) after the 1970s, and for nitrate (NO_3) after the 1990s. The concentrations of DON in the EMS are predicted to exhibit the largest anthropogenic enrichment signature. Temporal variations in annual primary production in the period 1950-2050 are dominated by variations in deep-water formation, followed by changes in riverine P inputs for the WMS, and atmospheric P deposition for the EMS. The detection of anthropogenic nutrient concentration trends in the MS is difficult due to the unique nature of the MS. The Atlantic Ocean is the largest nutrient source to the MS, diluting the anthropogenic nutrient signature. In addition the anti-estuarine circulation removes at least 45% of the anthropogenic nutrients inputs to each sea by 2030 while variations in intermediate and deep water formation rates complicate the interpretation of temporal changes in reactive P and N water column concentrations.

6.2 Introduction

Anthropogenic emissions of phosphorus (P) and nitrogen (N) have rapidly increased worldwide since the industrial revolution (Cordell et al., 2011; Mackenzie et al., 2011; Galloway, 2014), causing widespread changes in the structure, functioning and health of aquatic ecosystems. Anthropogenic inputs of reactive N to the environment risen roughly nine-fold since 1860, with a large exponential increase since 1950 (Galloway, 2014). The resulting N load to the oceans has approximately doubled (Galloway, 2014), while P fluxes to the global ocean are 1.5 to three times higher than estimates for pre-anthropogenic times (Follmi, 1996; Paytan and McLaughlin, 2007; Ruttenberg, 2014). Impacts are particularly severe in semi-enclosed seas such as the Baltic and Black Seas where primary production increased by factors of four to six in recent decades (Gustafsson et al., 2012; Mikaelyan et al., 2013).

Given its large, and growing, coastal population, and the ongoing agricultural and industrial intensification (UNEP/MAP, 2012; Micheli et al., 2013), one may expect widespread evidence of nutrient enrichment in the semi-enclosed Mediterranean Sea (MS). For comparison, land-derived inputs of N and P to the Eastern Mediterranean Sea (EMS) per unit surface area are similar to those entering the Baltic Sea (Appendix A). However, despite the high anthropogenic inputs, the MS shows little evidence of increased eutrophication, with the exception of nearshore areas such as the northern Adriatic Sea, the Gulf of Lions, and the Nile delta region (Karydis and Kitsiou, 2012). The anti-estuarine circulation of the MS and the resulting lateral export of nutrient P and N, ultimately to the North Atlantic Ocean, are usually invoked to explain why the MS remains in its oligotrophic state (Crispi et al., 2001; Krom et al., 2010).

The intermediate (IW) and deep (DW) waters of the Western Mediterranean Sea (WMS) and EMS have relatively short residence times (7-150 years; Roether and Schlitzer, 1991; Béthoux and Gentili, 1996; Stratford et al., 1998; Roether and Well, 2001; Chapter 4). Hence, the dissolved P and N concentrations of these reservoirs could potentially record anthropogenic nutrient enrichment on a decadal time scale. However, although DW temperature and salinity data for the WMS have been systematically increasing since the early 20th century (0.3-5x10^{-3} ^{o}C yr^{-1} and 0.6-2.2 x10^{-3} PSU yr^{-1}; Marty and Chiaverini, 2010 and references therein), the temporal trends of dissolved nutrient concentrations in the IW and DW of the MS are associated with far more uncertainty (Béthoux et al., 1998; Denis-Karafistan et al., 1998; Karafistan et al., 2002). For example, Pasqueron de Fommervault et al. (2015) recently reported evidence for increasing dissolved nitrate (NO_3) concentrations at the DYFAMED site, a permanent mooring station located in the Ligurian Sea, between 1990 and 2010, but at the same time they found that the dissolved phosphate (PO_4) concentrations were decreasing.

One major difficulty in interpreting temporal trends in water column P and N concentrations is the natural variability of the thermohaline circulation (THC). A well-known example is the Eastern Mediterranean Transient (EMT), when deep water (DW) supply from the Aegean Sea rose markedly above background values for a period of about ten years (Roether et al., 2007). The changes in properties of intermediate water (IW) entering the Western Mediterranean Sea (WMS) from the EMS through the Strait of Sicily subsequently led to changes in DW formation within the WMS, termed the Western Mediterranean Transition, or WMT (Schroeder et al., 2006). The average DW formation rate in the WMS during the WMT was several times higher than in pre-WMT times (Chapter 4).

In recent years, a bimodal oscillation system (BiOS) has been observed in the northern Ionian Sea and the southern Adriatic Sea whereby the North Ionian Gyre switches from anticyclonic to cyclonic on a decadal time scale (Gačić et al., 2010). The BiOS profoundly changes the physical and chemical properties of water masses in the southern Adriatic Sea, as well as those of surface water (SW) that just entered the EMS through the Strait of Sicily and intermediate water (IW) entering the Levantine Sea from the Ionian Sea (Civitarese et al., 2010; Gačić et al., 2010). The BiOS has also been hypothesized to be one of the triggers of the EMT (Malanotte-Rizzoli et al., 1999; Pinardi et al., 2015). In addition to these relatively long-term variations in circulation regime, the THC of the MS also demonstrates significant inter-annual variability (L'Hévéder et al., 2013; Vervatis et al., 2013; Sevault et al., 2014; Pinardi et al., 2015).

Variations in THC affect the spatial distributions of P and N and can, thus, be a source of variability in time series concentrations measured at given locations in the MS. As an example, changes in PO_4 and NO_3 concentrations in Levantine Intermediate Water (LIW) collected off the coast of Israel appear to coincide with changes in circulation due to BiOS (Ozer et al., 2016). Ozer et al. (2016) therefore propose that the observed changes in the dissolved nutrient concentrations can be explained by variations in circulation driven by BIOS. In contrast, Moon et al. (2016) argue that the temporal trends exhibited by the concentrations of PO_4 and NO_3 in intermediate waters (IW) across the whole MS are driven by changes in anthropogenic inputs of P and N, mainly from rivers for P and atmospheric deposition for N. These opposing views raise the question whether time series P and N concentration data in offshore (or pelagic) waters of the MS can yield records of anthropogenic nutrient enrichment, or not.

The purpose of this study is to evaluate to what extent the trends in dissolved P and N concentrations due to changes in the delivery of anthropogenic nutrients to the MS may be masked by the natural variability in THC. To that end, we first estimate the external reactive P and N inputs to the WMS and EMS between 1950 and 2030. Next, we feed these inputs to an existing coupled P and N mass balance model for the MS (Chapter 5), while at the same time imposing a time-dependent water circulation regime. For the latter,

we consider IW and DW formation rates that either change randomly from year to year, or follow historical trajectories reconstructed from literature data. The results are used to assess how sensitive temporal trends in dissolved P and N concentrations, N:P ratios and annual primary production in the WMS and EMS are to human-driven changes in land-derived nutrient inputs.

6.3 Methods

This paper builds on our previous modeling work on the coupled P and N cycling, first in the EMS (Chapter 2; Appendix A), and subsequently extended to include the WMS (Chapter 4, Chapter 5). The reader is referred to these earlier publications for in-depth presentations of methods, approaches and data sources.

6.3.1 Baseline Model

The conceptual model framework used in this study (Figure 6.1) is the same as in Chapter 5. The water column of the WMS and EMS is divided into three horizontal layers: surface water (WMSW, EMSW), intermediate water (WMIW, EMIW) and deep water (WMDW, EMDW). The WMS and EMS models are coupled by the bidirectional water exchanges through the Strait of Sicily. The WMS receives surface water inflow from the Atlantic Ocean, while WMIW and WMDW flow back to the Atlantic Ocean. Note that the areas of DW formation in the WMS and EMS are excluded from the model domain. For the WMS, this area is located in the northwest Mediterranean (NWM); for the EMS DW formation originates from the Adriatic and Aegean Seas. The surface areas of the WMS and EMS model domains (i.e., excluding the DW formation areas) are then 815×10^3 and 1336×10^3 km^2, respectively.

The model considers three reactive P and four reactive N pools in each horizontal water layer: dissolved inorganic phosphate (PO_4), particulate organic phosphorus (POP), dissolved organic phosphorus (DOP), dissolved nitrate plus nitrite (NO_3), particular organic nitrogen (PON), dissolved organic nitrogen (DON), and dissolved ammonium (NH_4). Annual primary production in both WMS and EMS is assumed to be P limited (Chapter 5); the P and N cycles are coupled by the Redfield ratio, that is, P and N are assimilated in a 1:16 ratio (Redfield et al., 1963). The total reactive P input to the model domain equals the sum of PO_4, POP and DOP inputs, plus the fraction of inorganic particulate phosphorus (PIP) input that becomes soluble after entering the MS (Appendix A). The total reactive N input is the sum of NO_3, PON, DON and NH_4 inputs.

Fluxes of the various reactive P and N species between water reservoirs are calculated by multiplying the corresponding water flows with the species concentrations in the source reservoirs. The turbulent mixing fluxes are the exception. These fluxes are computed by multiplying the difference in concentration

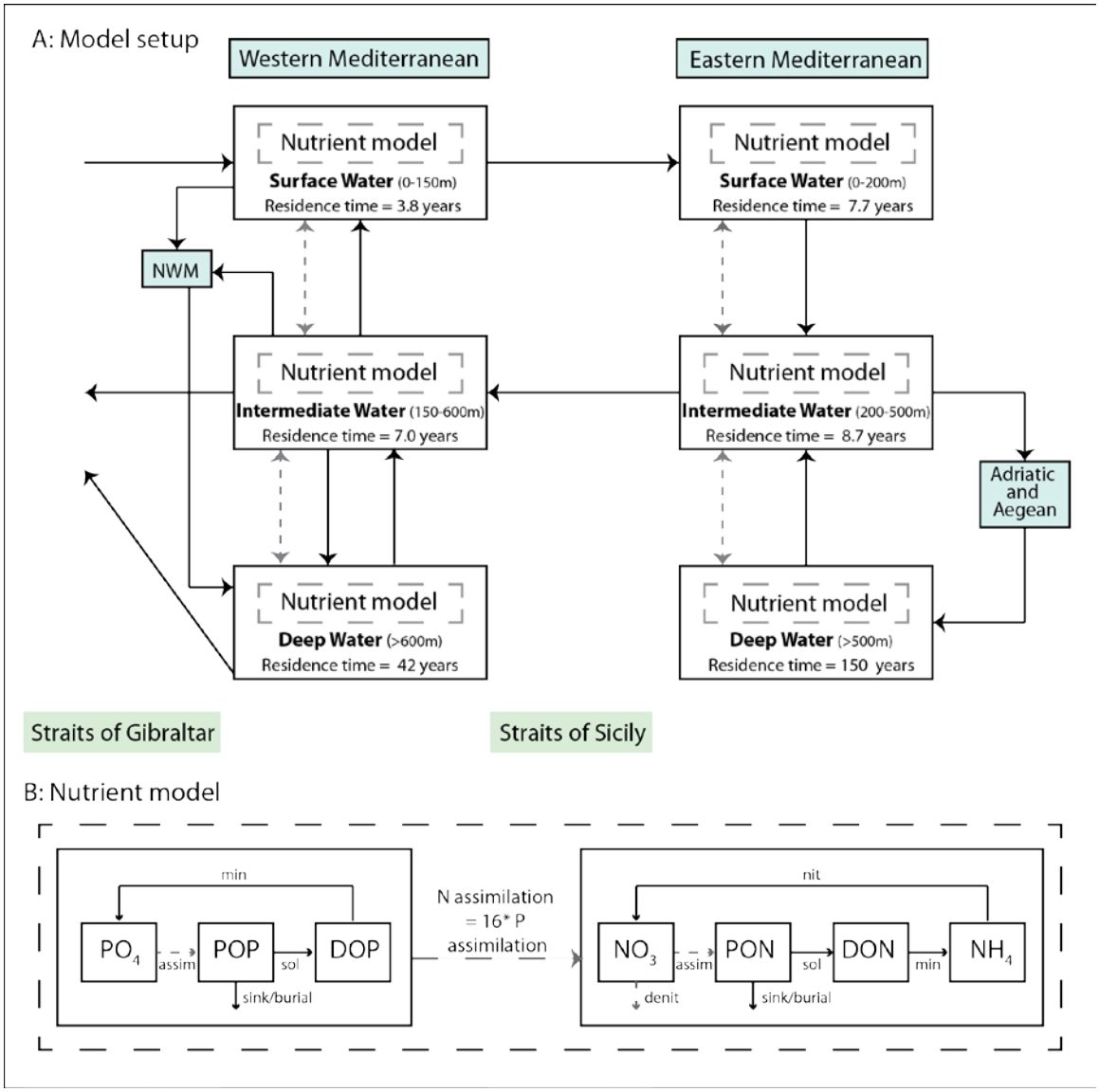

Figure 6.1: Conceptual model framework. A) Circulation structure and general model setup: Black arrows in main model represent water fluxes; grey dashed arrows turbulent mixing fluxes. Residence time represents the water residence time for each box. B) Nutrient model: assimilation of P and N only occur in the SW module and denitrification in the deep water module (grey dashed arrows).

between receiving and source reservoirs with an exchange coefficient, where the latter is related to the turbulent diffusion coefficient (Appendix A). During the simulations, the concentrations of the various P and N species in the water reservoirs change from year to year. The nutrient fluxes within the MS domain may therefore change over time because of changes in concentrations, changes in the water cycle, or both.

6.3.2 Reactive phosphorus and nitrogen inputs: 1950 to 2030

The model considers the following sources of reactive P and N to the WMS and EMS: inflows from adjacent marine basins, atmospheric deposition, N_2 fixation, riverine inputs, submarine groundwater discharge (SGD), and direct domestic wastewater discharges. Chapter 5 estimated the magnitudes of these inputs in 1950, that is, before the large increases in anthropogenic N and P emissions that occurred in subsequent decades. These estimates indicate that the inflow of Atlantic Surface Water (ASW) via the Strait of Gibraltar represents the largest input of reactive P and N to the MS. Because our focus is on the detection of anthropogenic signatures in temporal trends of P and N concentrations within the MS, the supply fluxes of reactive P and N associated with ASW inflow are assumed to remain constant over the period 1950-2030. Thus, all the variations in reactive P and N inputs to the MS since 1950 imposed in the model calculations are assumed to be of anthropogenic origin.

Anthropogenic forcing functions for the individual reactive N and P inputs to the WMS and EMS from 1950 to 2030 are derived following Chapter 2. The values of the reactive P and N inputs in 1950 of Chapter 5 are used as baseline values. For each input, the forcing function then provides for any given year during the 1950-2030 period the change in input flux relative to that in 1950. Thus, a forcing function value of 1.2 in 1994 means the corresponding annual input in 1994 is 20% larger than in 1950. Chapter 2 provides a detailed account on the forcing functions for anthropogenic P and N inputs to the EMS for the period 1950-2000. Table 6.1 summarizes how forcing functions for both WMS and EMS and for the entire 1950-2030 period were derived; full details are given in Appendix F. Because direct measurements that constrain the temporal evolution of reactive P and N inputs to the MS are rather limited, relatively large uncertainties are associated with the estimated forcing functions. This is particularly true for the 2000-2030 period, where the forcing functions depend on projections of ongoing trends of anthropogenic drivers into the future, for example, the growth of coastal populations and upgrades to wastewater treatment plants (WWTPs) in the various countries surrounding the MS. Therefore, for 2000 to 2030, mean values of the forcing functions are given, as well as ranges based on estimated upper and lower limits of the associated anthropogenic drivers.

Table 6.1: Summary of methods in calculating 1950 to 2030 anthropogenic forcing functions applied to the model.

Forcing function	Species	Method and data sources
Atmospheric deposition	PO_4	Deposition of leachable PO_4 in the WMS and EMS is assumed proportional to changes in acid within atmosphere (Nenes et al., 2011), estimated through emissions of NO_x and SO_4 to the atmosphere in Europe, Africa and the Middle East. For 1950-2000 the forcing function is justified in Chapter 2 and references therein. For 2000-2030 data is taken from Lamarque et al. (2013)*.
	DOP and DON	Deposition of organic matter in both WMS and EMS is assumed proportional to the relative change in 1) organic carbon emissions from biomass burning in the northern hemisphere over 1950 to 2000 (Chapter 2 and references therein) and 2) anthropogenic global organic carbon emissions in 2000 and 2030 (IPCC, 2013)*.
	NO_3 and NH_4	Deposition estimates in both the WMS and EMS are calculated from the relative change in 1) NO_x and NH_4 deposition in French alpine ice core records from 1950 to 2000 (Chapter 2 and references therein) and 2) model predicted dry and wet deposition rates for NO_x and NH_4 from Africa, Europe, and former USSR and Middle East in 2000 and 2030 (Lamarque et al., 2013)*.
Rivers	P and N	Ludwig et al. (2009) calculate riverine inputs of P and N to the WMS and EMS for every 5 years between 1963 and 1998 and it is assumed that little change occurs in riverine P and N inputs over 1950 to 1963. The relative change in riverine inputs over 2000 to 2030 are calculated from predictions made using the Millennium Ecosystem Assessment Scenarios (Ludwig et al., 2010)*. The speciation of P and N is assumed to stay constant with time.
Direct wastewater discharges	N	Wastewater discharges are assumed proportional to relative change in population of each Mediterranean country (FAOSTAT, 2016), weighted towards each countries individual wastewater total N input to the MS (Chapter 3). A 5% error is assigned on 2030 population values to represent maximum and minimum values.
	P	Population, laundry and dishwasher detergent use all influence the wastewater P input with time. It is thus assumed that the N:P ratio of direct discharges of wastewater follows the same trend as that of riverine inputs to the MS. For the EMS riverine inputs into the Levantine Basin over 1950 to 2000 (Ludwig et al., 2009) are ignored due to the different in responses of P and N to the closure of the Aswan Dam (Ludwig et al., 2009).
SGD	NO_3 and NH_4	The change in inorganic N in SGD is assumed to follow that inorganic N fertilizer inputs on land with a 30 year lag time (Chapter 5). The forcing function is created using the relative change in total N fertilizer consumption rates Europe for the WMS and rest of the world for the EMS between 1920 to 1960 (Erisman et al., 2011) while nitrogenous fertilizer consumption rates per country (FAOSTAT, 2015a), weighted to regional GW discharges (Zekster et al., 2007), are used for the period 1960 to 2000.
	DON	The change in DON in SGD is assumed to follow the application of manure on land with a 30 year time lag (Chapter 5). Manure application rates are taken from Europe for the WMS and worldwide for the EMS for 1920 to 1960 (Erisman et al., 2011) and for each individual country (FAOSTAT, 2015b) weighted to regional GW discharges (Zekster et al., 2007) for 1960 to 2000.
	P	Assumed constant with time as the 2000 P concentration in SGD is very small suggesting that P from fertilizer input is adsorbed within aquifer
N_2 fixation	N	Assumed constant with time due to lack of evidence on correlation between N_2 fixation and nutrient availability (Sandroni et al., 2007; Berman-Frank and Rahav, 2012).

*The mean of model predicted deposition rates are taken for 2030 with maximum and minimum estimates representing range in values predicted.

A linear relationship is assumed in deposition over 2000 to 2030.

The change in the fluxes of P and N provided by DW formation to the DW of the WMS and EMS are from changes in the P and N carried in the IW and SW that mix to form the DW and the additional nutrients added to the SW at each formation site from rivers and atmospheric deposition. Here we derive forcing functions only for the additional P and N added to each formation site. P and N provided to the DW by the mixing or upwelling of SW and IW are automatically accounted for within model simulations at each time step. Riverine fluxes into the Adriatic Sea and Aegean Sea over 1950-2030 are taken from Ludwig et al. (2009; 2010). In addition the change in the flux of DON flux through the Bosphorus Strait to the Aegean Sea is assumed to change with reactive N riverine inputs to the Black Sea (Ludwig et al., 2009; 2010) while it is assumed that the Bosphorus Strait is a negligible source of inorganic N and P to the Aegean Sea (Krom et al., 2004). The change in riverine flux is not included in the NWM anthropogenic forcing function, as the model area where DW formation is set to occur does not include the coastline. Atmospheric deposition of P and N into the Adriatic Sea, Aegean Sea and NWM is assumed to follow the same historical trend of that input into the EMS and WMS. Combining the inputs from rivers, atmospheric deposition, and Bosphorus Straits for the Aegean Sea then creates the forcing function for each individual species into each sea.

6.3.3 Thermohaline circulation (THC)

This study focuses on the inter-annual variability in the basin wide THC, more specifically, the year-to-year changes in the rates of IW and DW formation originating from the four main source zones in the MS: the NWM for the WMS, and the Rhodes Gyre, Adriatic Sea and Aegean Sea for the EMS. Four different scenarios are considered to illustrate the sensitivity of the P and N distributions to circulation (Table 6.2): 1) time-invariant circulation, 2) random fluctuating IW/DW formation rates, 3) reconstructed (historical) IW/DW formation rates, and 4) attenuated historical IW/DW formation rates. Each circulation scenario is run separately from, and together with, the 1950-2030 reactive P and N inputs (Table 6.2) to separate the contributions of circulation versus anthropogenic nutrient enrichment to changes in reactive P and N concentrations, primary productivity and N:P ratios. Once the prescribed IW/DW formation flows are imposed, the other water fluxes are adjusted to maintain the annual water balance of each reservoir included in the model. The total inflow and outflow water fluxes through the Strait of Gibraltar are kept constant in all model runs, although the proportions of WMIW and WMDW in the outflow to the Atlantic Ocean are allowed to vary over time. Water fluxes between WMSW and WMIW, and WMIW and WMDW, also change direction during some of the model simulations.

Table 6.2: Summary of model simulations consisting of a circulation scenario and reactive P and N input scenario.

Simulation	1	2	3	4	5	6	7
Randomized perturbations in circulation (constant mean): 1950-2030	✓	✓					
Constant circulation: 1950-2030			✓				
Predicted historical circulation (Year on year): 1960-2000				✓	✓		
Predicted historical circulation (5 year moving average):1960-2000						✓	✓
1950 P and N inputs	✓			✓		✓	
1950-2030 P and N inputs		✓	✓		✓		✓

Table 6.3: Deep/intermediate water formation parameters used to initiate random circulation scenarios. See text for details.

Area	Mean formation rate (all years)*	Mean formation events**	Standard deviation formation events	% of years IW/DW formation occurs	Probability distribution function	Range	Reference
NWM	0.61	1.20	0.68	53	Lognormal	$0<x<3.3$***	L'Hévéder et al. (2013)
Levantine	1.10	1.10	0.83	100	Normal	$x-\sigma<x<\sigma+x$	Vervatis et al. (2013)
Adriatic	0.32	0.455	0.25	80	Lognormal	$0<x<0.8$***	Pinardi et al. (2015)
Aegean	0.04	0.069	0.08	62.5	Lognormal	$0<x<0.38$***	Vervatis et al. (2013)

*From Chapter 4; ** corrected so mean of all years using the probability distribution functions equals mean of formation rate; *** Highest model predicted value from reference.

6.3.3.1 Random circulation 1950-2030 (Simulations 1 and 2)

A random normal or lognormal probability distribution function (PDF) is used to generate yearly IW/DW formation rates from each source region between 1950 and 2030 (Table 6.3). The PDF are based on observed frequencies of IW/DW formation in the four regions (Table 6.3): DW formation in the NWM has been reported to occur in 53% of years over the period 1959-2001 (L'Hévéder et al., 2013), 63% of years in the Aegean Sea over the period 1961-2000 (Vervatis et al., 2013), 80% of years in the Adriatic Sea over the period 1987-2007 (Pinardi et al., 2015), while EMIW formation (termed LIW in the literature) occurs every year (Vervatis et al., 2013). Mean values and standard deviations of IW/DW formation fluxes are assigned using long term model estimates from literature, normalized so that the long term mean value of any given IW/DW formation rate equals the steady state values used for the 1950 water cycle presented in Chapter 4. The corresponding THC parameter values are given in Table 6.3. The ranges of variability in P and N concentrations due to random fluctuations in THC are assessed by carrying out 500 model runs with randomly selected values of the IW/DW formation rates. Mean, 10th and 90th percentile concentrations are reported (see below).

6.3.3.2 Historical circulation 1960-2000 (Simulations 4 and 5)

Estimates for historical IW/DW formation rates between 1960 and 2000 are taken from yearly modeled estimates for the formation of LIW, Aegean DW (Vervatis et al., 2013) and NWM (L'Hévéder et al., 2013), normalized as in section 2.3.1 so that the long term mean value of any given IW/DW formation rate equals the steady state values used for the 1950 water cycle presented in Chapter 4. Due to the lack of long term predictions within the literature for DW formation in the Adriatic before 1980, we assume that DW formation in the Adriatic follows that of the BiOS matching the DW formation rate with the cycle of observed salinity(Civitarese et al., 2010). The changes in salinity in the Adriatic Sea due to BiOS, alter the density of the Adriatic water and therefore deep water formation properties. To model the deep water formation as a result of the BiOS we impose a sin wave on the Adriatic water flux (y):

$$y(t) = (Asin(\omega t + \varphi) + 1)\,.\,1950_{water}^{Adr} \qquad (6.1)$$

where A = amplitude, ωt= period, φ = phase shift of the sin wave and 1950_{water}^{Adr} is the 1950 Adriatic water flux (0.32 Sv). A is assigned as 0.98 to represent a total flux of Adriatic deep water into the EMS of 0.006-0.63 Sv, similar to the range in model predicted Adriatic DW formation rates (Sevault et al., 2014; Pinardi et al., 2015). ω is assigned $\pi/8$ to represent a period of 16 years, matching that of observed salinity in the south Adriatic Sea while φ of 0.7 is applied so that the greatest (smallest) deep water formation rate occurs at the highest (lowest) observed salinity (Civitarese et al., 2010). The resulting sin wave applied to the Adriatic DW formation rate is shown in Figure F.2.

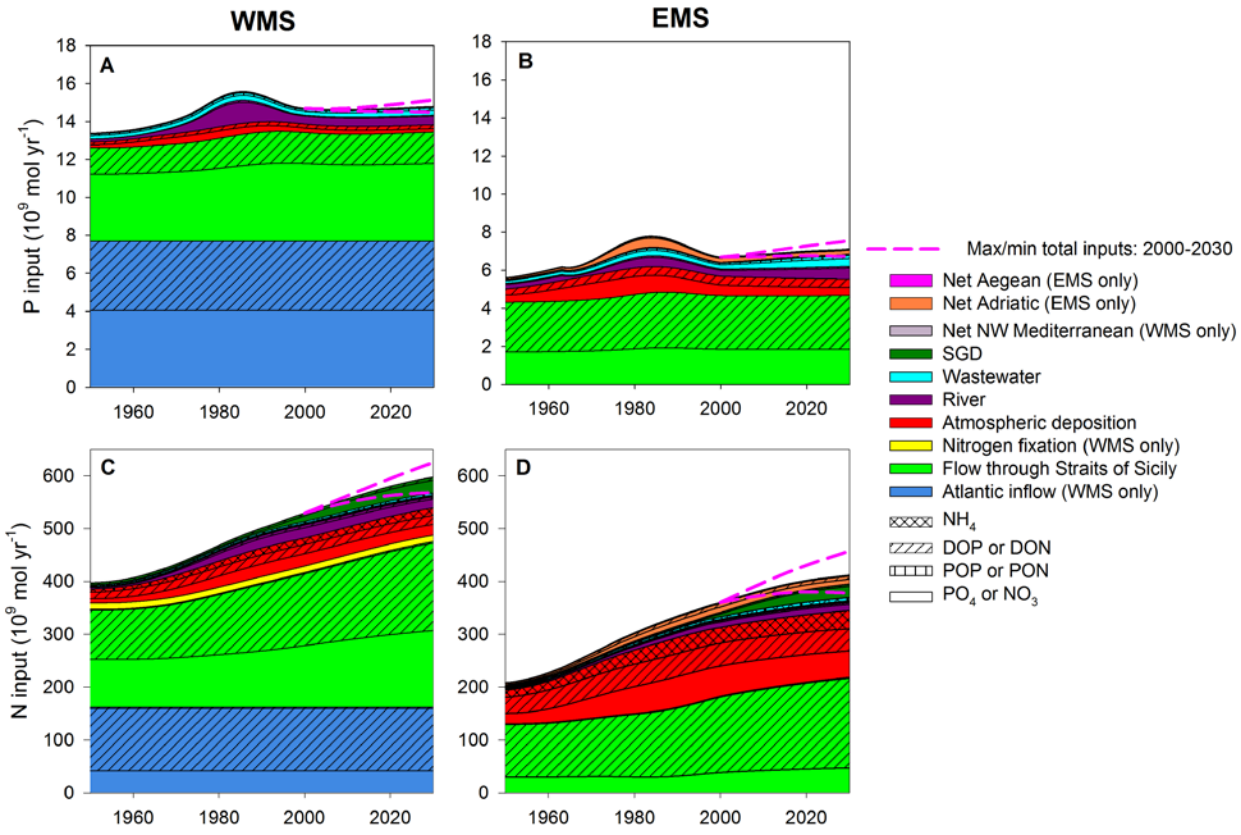

Figure 6.2: Sources and speciation of reactive phosphorus (A+B) and reactive nitrogen (C+D) inputs into the WMS (A+C) and EMS (B+C) between 1950 and 2030. The changes with time (except through the Strait of Sicily) are calculated from forcing functions described in Table 6.1, Table F.1 and Figure F.1. Exchanges of dissolved reactive P and N through the Strait of Sicily are taken from model results of Simulation 3 (constant circulation). Colours indicate sources of external P and N input to each sea, hatchings indicate the chemical speciation of P and N. Pink dashed lines reflect maximum and minimum estimates of predicted total inputs between 2000 and 2030 (see text for details).

6.3.3.3 Attenuated historical IW/DW formation rates (Simulations 6 and 7)

Applying immediate changes in the water fluxes across the entire Mediterranean Sea is an admittedly unrealistic scenario and is a limitation of the box model set-up that is used in this study. To account for attenuation and propagation of water fluxes, a running average of the previous 5 year IW/DW formation rates at each formation site across the MS is calculated and applied to the model. Similar to the previous circulation scenarios, resulting changes in the water fluxes throughout the rest of the model are instantaneously changed to keep a constant water balance.

6.4 Results

6.4.1 Reactive phosphorus and nitrogen inputs: 1950-2030

In the WMS, reactive P inputs from land derived sources increased by a factor of 3 relative to the 1950 input reaching a peak in the 1980s (Figure F.3). However, the dominance of marine derived inputs in the nutrient budgets of the MS, resulted in total reactive P inputs into the WMS increasing by only a maximum of 16% between 1950 and 2030. Reactive P inputs increased from 13.4 x 10^9 mol P yr^{-1} in 1950 to a maximum of 15.6 x 10^9 mol P yr^{-1} in 1985, largely driven by an increase in riverine PO_4 inputs (Figure 6.2A). A subsequent decline in reactive P inputs occurred until the year 2008 after which they slowly increased again to 14.8 x 10^9 mol yr^{-1} in 2030 because of the increasing inputs from riverine and wastewater sources from population growth. The relative change in total reactive P inputs over the course of 1950-2030 is greater in the EMS than WMS despite a smaller relative increase in land derived anthropogenic inputs into the EMS (Figure F.3). A maximum increase of 39% in reactive P inputs within the EMS occurred between 1950 and 2030 from 5.6 x 10^9 mol yr^{-1} in 1950 to 7.8 x 10^9 mol yr^{-1} in 1984, mainly as a result of atmospheric deposition, riverine inputs and input into the EMDW from the Adriatic Sea (Figure 6.2B). Similar to the WMS, reactive P inputs then decreased until 2000 before increasing by 0.4 x 10^9 mol yr^{-1} between 2000 and 2030. The general increase in reactive P inputs between 2000 and 2030 is fairly certain with the minimum input estimate between 2000 and 2030 still increasing relative to 2000 in both seas. Throughout 1950 to 2030 the dominant source of reactive P to the WMS and EMS are from marine-derived sources entering each sea through the Straits of Gibraltar and Sicily, accounting for between 85-94% of reactive P inputs into the WMS and 62-77% of reactive P inputs in the EMS. Hence the EMS has a larger portion of its inputs from non-marine sources than the WMS leading to the greater predicted change in reactive P inputs between 1950 and 2030 in the EMS than for the WMS.

In contrast to P, reactive N inputs continually increased between 1950 and 2030 in both the WMS and EMS (Figure 6.2 C and D) with land-derived reactive N inputs increasing by a factor of 3 and 2.5 relative to the 1950 inputs to the WMS and EMS, respectively. However, the total reactive N input to the WMS,

only increased by 51% from 398 x 10^9 mol yr^{-1} in 1950 to 599 x 10^9 mol yr^{-1} in 2030. Similar to P, the increase is greater in the EMS with reactive N inputs increasing by 85% between 1950 and 2030 from 208 x 10^9 mol yr^{-1} to 412 x 10^9 mol yr^{-1}. The changes in both seas are mainly driven by atmospheric deposition and increases in dissolved reactive N transferring between WMS and EMS through the Strait of Sicily. Marine inputs of dissolved reactive N entering the WMS and EMS through the Straits of Gibraltar and Sicily provide between 79-87% of reactive N inputs into the WMS over 1950 to 2030 and 48-63% of reactive N inputs to the EMS. N_2 fixation, a flux that has been hypothesized to have a significant impact of the N:P ratio of the whole MS (Béthoux et al., 1992; Béthoux et al., 2002b), only accounts for up to 3% of total inputs between 1950 and 2030 in the WMS. SGD of dissolved reactive N, included for the first time in dynamic nutrient budgets, becomes increasingly important in both seas over 1950 to 2030 contributing up to 6% of reactive N inputs in 2030 compared to only 1% in 1950. The range between the maximum and minimum reactive N inputs between 2000 and 2030 are greater than for reactive P inputs. The minimum estimate indicates that reactive N inputs may stabilize in the WMS over 2000 to 2030 or even decrease after 2015 in the EMS, while the upper estimate suggest that reactive N inputs will carry on increasing at an approximate linear rate.

6.4.2 Changes in dissolved reactive phosphorus and nitrogen concentrations

6.4.2.1 Noise from inter-annual variability in circulation (Simulations 1 and 2)

The red shaded areas in Figures 6.3, 6.4 and F.3 illustrate the potential variation in dissolved reactive P and N concentrations within the water column to changes in inter-annual variability of the THC (Simulation 1). Here, PO_4 and NO_3 IW concentrations in both seas generally show the highest absolute sensitivity out of all the dissolved reactive P and N reservoirs to variability in circulation. The mean range between 10^{th} and 90^{th} percentiles of PO_4 concentrations in the WMIW and EMIW is 34 nM (± 6% of mean 1950-2030 value) and 10 nM (± 5% of mean 1950-2030 value), respectively, while NO_3 concentrations vary by 0.7μM (± 5% of mean 1950-2030 value) in the WMIW and 0.3 μM (± 6% of mean 1950-2030 value) in the EMIW. Inorganic P and N concentrations in the WMDW are more sensitive to changes in circulation than the EMDW. A variation of 27 nM (± 4% of mean value) in PO_4 and 0.6 μM (± 4% of mean 1950-2030 value) in NO_3 concentrations in the WMDW compared to only a 3 nM (±1% of mean 1950-2030 value) and 0.1μM (±1% of mean 1950-2030 value) variation in PO_4 and NO_3 concentrations in the EMDW. In contrast to PO_4 and NO_3, the highest absolute sensitivity of DOP and DON concentrations to changing circulation is predicted in the SW, varying by 16 nM (± 11% of mean 1950-2030 value) and 0.9 μM (± 16% of mean 1950-2030 value) for DOP and DON, respectively, in the WMSW and 6 nM (± 6% of mean 1950-2030 value) and 0.2 μM (± 4% of mean 1950-2030 value) in the

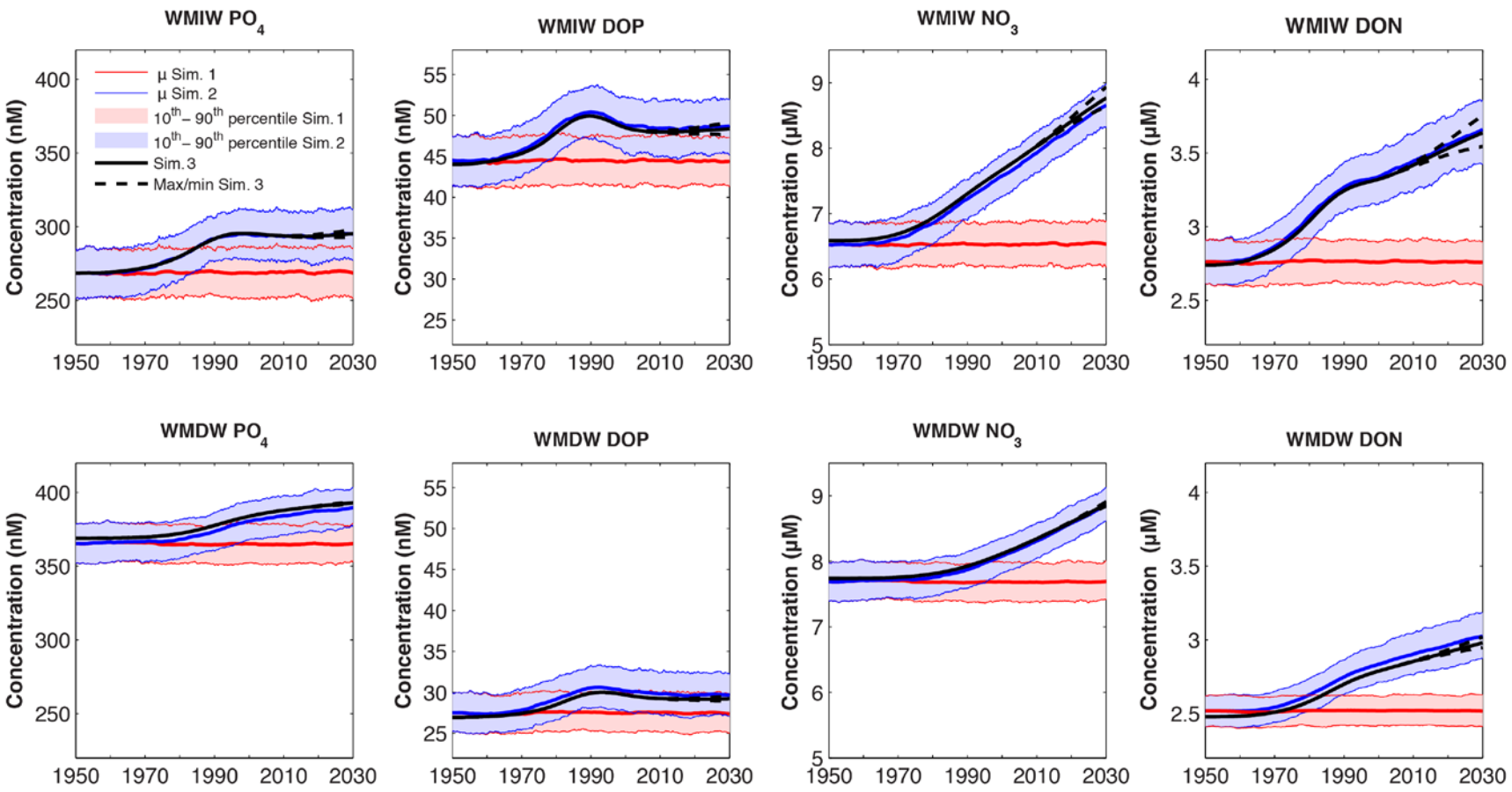

Figure 6.3: Comparison of potential changes in intermediate and deep water P and N concentrations in the WMS due to inter-annual variability in the thermohaline circulation (Simulation 1; red shading and red lines) against those from anthropogenic nutrient enrichment and inter-annual variability in circulation (Simulation 2; blue shading and blue lines), and anthropogenic nutrient enrichment alone (Simulation 3; black line). The model was run 500 times randomly changing the circulation. Mean, 10^{th} and 90^{th} percentiles are shown. Dashed line between 2000 and 2030 represents the range in dissolved P and N concentrations from maximum and minimum estimates of reactive P and N inputs for this time period. Note changes in scale of y axis for each species. See text and Table 6.2 for details of model simulations. Discrepancies between the mean of Simulation 2 and Simulation 3 arise from the switching in direction of WMIW to WMSW flux when the flow through the Strait of Sicily is lower than 0.53 Sv.

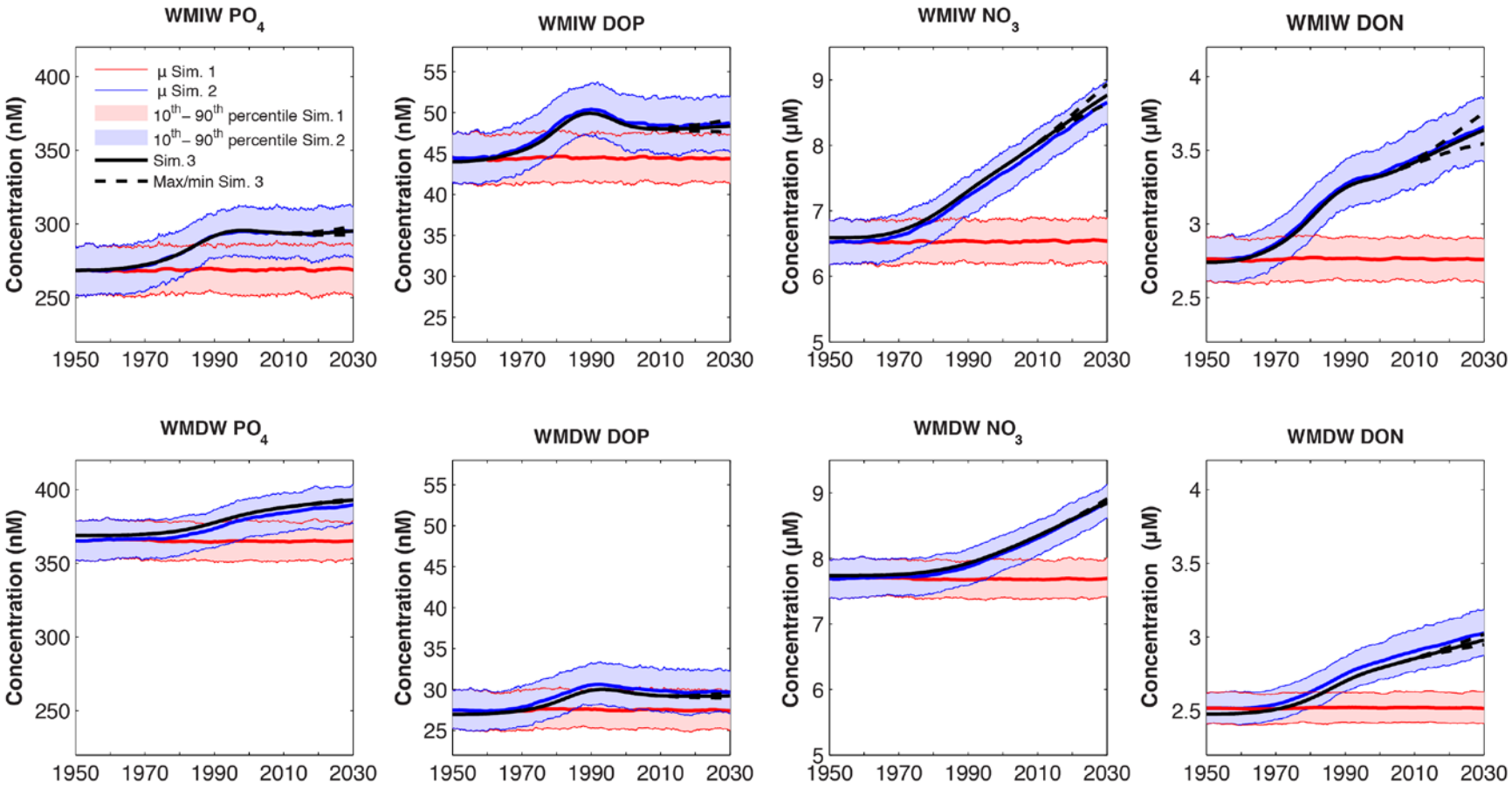

Figure 6.4: Same as Figure 6.3 but for the EMS.

EMSW (Figure 6.4). For Simulation 2, the variability in concentrations due to the inter-annual variability in THC (blue shaded area; Figures 6.2 and 6.3) are the same order of magnitude as in Simulation 1.

6.4.2.2 Anthropogenic nutrient enrichment (Simulations 2 and 3)

The trends in all SW dissolved reactive P and N reservoirs with time in Simulation 3 reflect that of the P and N inputs to the WMS and EMS (Figures 6.2, F.3 and F.4). Surface water P concentrations increased by a maximum of 12% in the WMS and 22% in the EMS in the late 1980s compared to increases in reactive P inputs of 16% and 39% in the WMS and EMS respectively (Figure F.5). Thus SW concentrations in the WMS respond more proportionally to reactive P inputs than those in the EMS. The maximum relative increase in IW reactive P concentrations are generally lower than for SW: from 10-13% in the WMIW and 17-21% in the EMIW (Figures 6.3, 6.4 and F.4). Within the DW, dissolved reactive P concentrations in both WMS and EMS continue to increase throughout 1950-2030 with the exception of WMDW DOP concentrations, which reach a maximum in 1993 (11.3% change since 1950).

In contrast to P, dissolved reactive N concentrations in both seas increase throughout the simulation reaching a maximum in 2030 (Figures 6.3, 6.4, F.3 and F.4). In particular the SW DON reservoir is predicted to strongly increase by a maximum of 70% in the WMS and 123% in the EMS by 2030 relative to 1950 concentrations (Figure F.5). NO_3 concentrations in both seas tend to increase strongly after the 1980s with both IW and DW NO_3 concentrations over 2000-2030 increasing at almost a linear rate of 0.02-0.04 μM yr^{-1} in the WMS and 0.01-0.03 μM yr^{-1} in the EMS (Figures 6.3 and 6.4). By 2030, NO_3 concentrations within WMIW similar are to those in the WMDW. For Simulation 2, the mean dissolved reactive P and N concentrations from anthropogenic enrichment mirror that of Simulation 3.

6.4.2.3 Historical circulation changes (Simulations 4 to 7)

PO_4 concentrations from historical changes in circulation alone (Simulation 4) over 1950 to 2000 vary by a maximum of 75 nM and 29 nM in the WMIW and EMIW respectively (Figure 6.5), while concentrations within the WMDW and EMDW vary by 33 nM and 4 nM (Figure F.6). For NO_3 concentrations, the variation induced by historical circulation is 1.6 μM and 0.6 μM in the EMIW and WMIW respectively (Figure 6.5) and 0.7 μM and 0.1 μM in the WMDW and EMDW (Figure F.6). Including attenuation in the system by implementing a 5-year running average on IW/DW historical formation rates (Simulation 6) results in substantially lower variability in the range in PO_4 and NO_3 concentrations in the WMS compared to the EMS (results not shown). The same trend is observed to a lesser extent for both PO_4 and NO_3 concentrations within the WMDW. The results of Simulations 5 and 7 are shifted upwards from those of Simulation 4 and 6 respectively, due to the inclusion of anthropogenic nutrient inputs in these runs (Figure 6.5 and F.5).

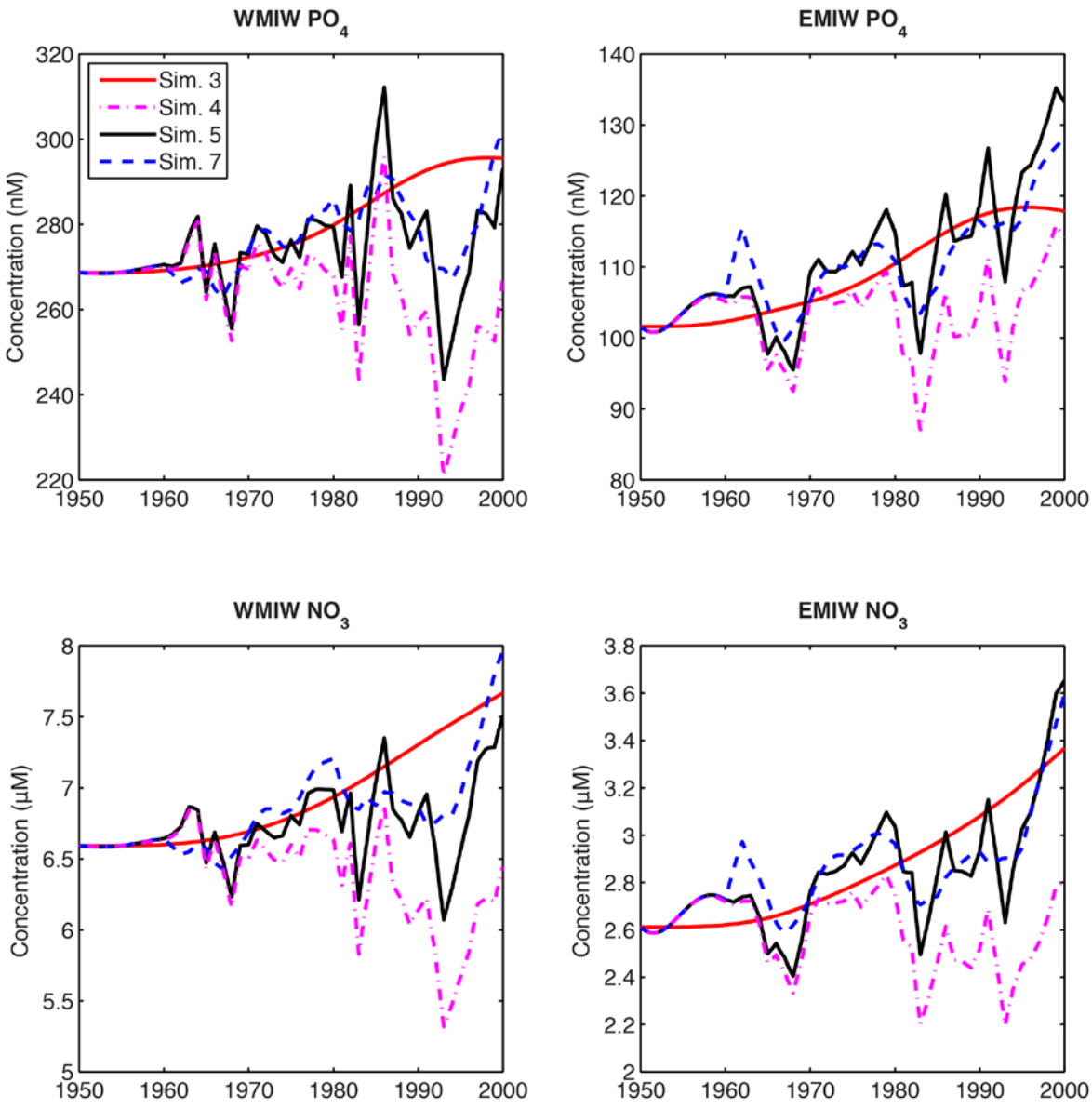

Figure 6.5: Changes in intermediate water PO_4 and NO_3 concentrations from historical inter-annual variability in the thermohaline circulation between 1960 and 2000 with: constant reactive P and reactive N inputs (Simulation 4); 1950-2000 reactive P and reactive N inputs (Simulation 5); and using a 5 year running average with 1950-2000 reactive P and reactive N inputs (Simulation 7), compared to 1950-2000 reactive P and N inputs with constant circulation (Simulation 3; red line). See text for details of how the historical circulation predictions were made.

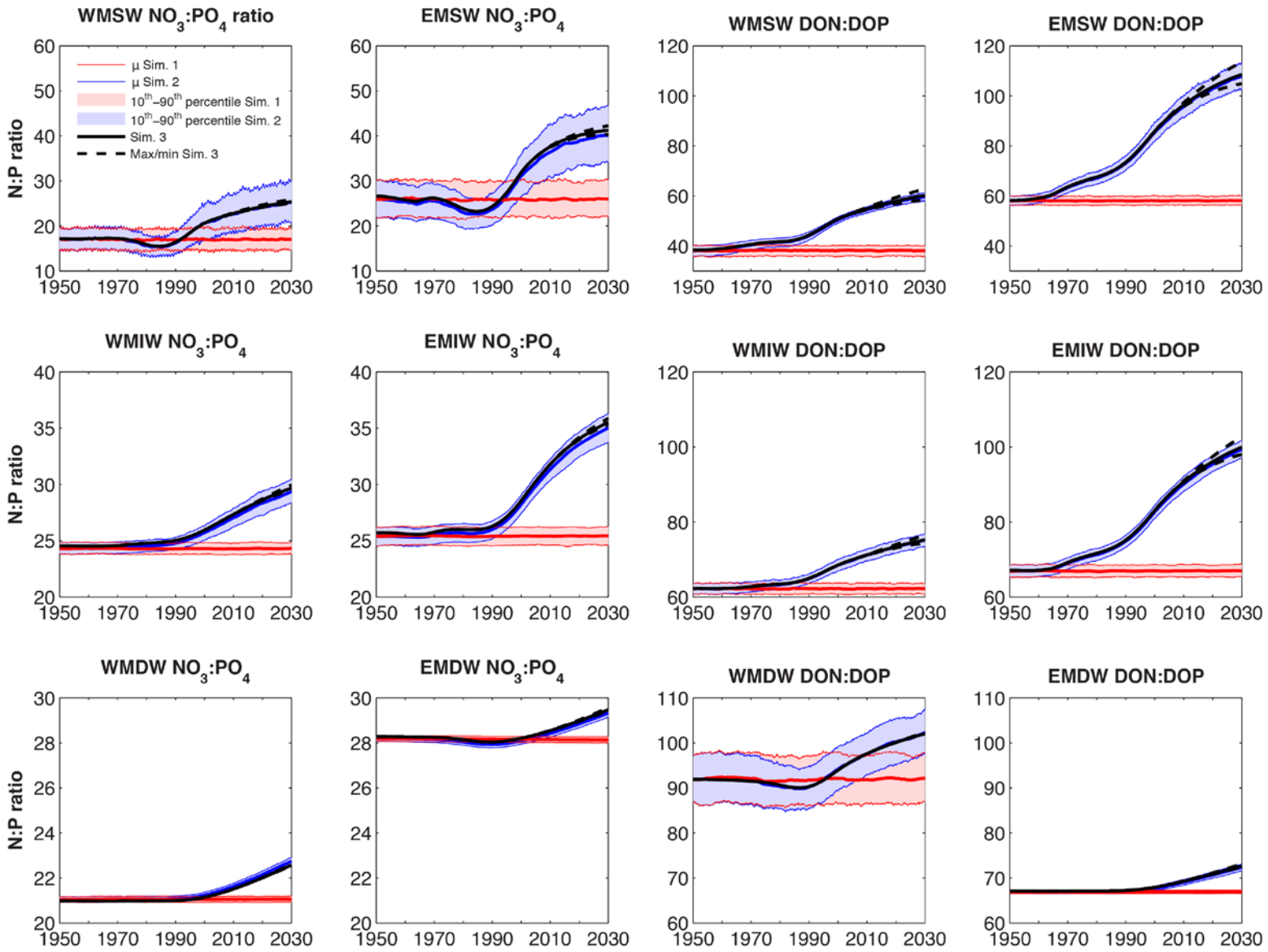

Figure 6.6: Same as Figure 6.3 but for the N:P ratio in the WMS and EMS.

6.4.3 N:P ratio changes

The greatest change in N:P ratios over the course of 1950-2030 occurs in the DON:DOP ratios within the EMS (Table F.2; Figure 6.6). However, it is the NO_3:PO_4 DW ratio which is most commonly measured and reported although it shows the smallest change between 1950 and 2030 of all reactive N:P ratios. In the WMS, the NO_3:PO_4 DW ratio remains approximately constant until 1990 at 21.0 before increasing at an approximate linear rate to a maximum of 22.6 in 2030 (Figure 6.6; Figure F.7). In the EMDW, the NO_3:PO_4 ratio initially decreases from 28.3 in 1950 to a minimum of 28.0 in 1989 and thereafter increasing to a maximum of 29.5 by 2030. The range in N:P ratios caused by inter-annual variability in the THC (Simulation 1) is also smallest for the NO_3:PO_4 DW ratio varying by 0.3 in the WMS and EMS. Historical circulation alone (Simulation 4) results in a variation of 0.4 in the WMDW NO_3:PO_4 ratio with the inclusion of anthropogenic enrichment having a negligible impact on the ratio over 1950 to 2000 (Simulation 5; Figure F.8). In comparison the NO_3:PO_4 DW ratio in in the EMS varies by 0.1 in Simulation 4, while in Simulation 5, anthropogenic enrichment results in a decline in the NO_3:PO_4 ratio relative to Simulation 4 (Figure F.7).

6.4.4 Primary productivity changes

External inputs of anthropogenic reactive P and N (Simulation 3) increase primary productivity in the WMS by a maximum of 12% over 1950-2030 from 147 g C m^{-2} yr^{-1} in 1950 to 166 g C m^{-2} yr^{-1} in 1987 before decreasing to 159 g C m^{-2} yr^{-1} in 2011 (Figure 6.7A). Thereafter primary productivity increases again reaching 160 g C m^{-2} yr^{-1} in 2030. The model predicts a larger maximum relative increase in primary productivity over 1950 to 2030 in the EMS than WMS as a result of anthropogenic reactive P inputs: primary productivity in the EMS increases by a maximum of 22% from 56 g C m^{-2} yr^{-1} in 1950 to 69 g C m^{-2} yr^{-1} in 1989 and a final value of 68 g C m^{-2} yr^{-1} in 2030 (Figure 6.7B). The change in primary productivity in the WMS due to natural circulation variability is greater than the change from anthropogenic enrichment alone, varying by 35 g C m^{-2} yr^{-1} (± 12% of mean value) in comparison to a maximum change of 19 g C m^{-2} yr^{-1} in Simulation 3 (Figure 6.7A). In the EMS, the impact of noise in primary production from inter-annual THC variability is smaller than that in the WMS. Primary production changes by 7 g C m^{-2} yr^{-1} (± 6%) (Figure 6.7B) as a result of variability in THC (Simulation 1) compared to a maximum change from anthropogenic nutrient enrichment of 13 g C m^{-2} yr^{-1} (Simulation 3). Primary productivity as a result of historical circulation has a greater variability in the WMS than in the EMS (Simulations 4-7) with a range in primary productivity of 100 g C m^{-2} yr^{-1} in the WMS in Simulation 4 compared to 22 g C m^{-2} yr^{-1} in the EMS (Figure F.9). Adding anthropogenic enrichment to the historical circulation scenarios (Simulation 5) results in primary productivity greater

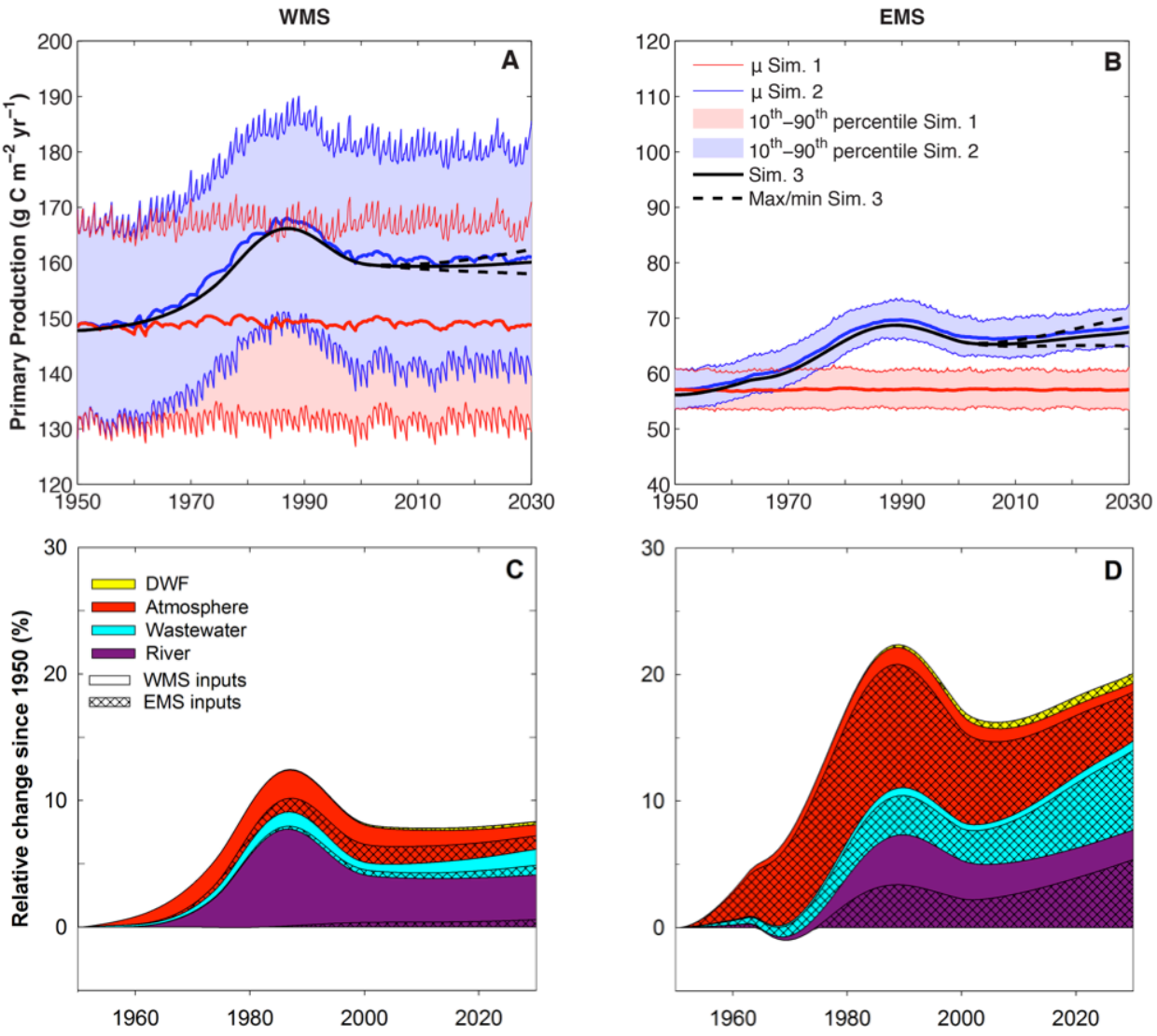

Figure 6.7: A-B: Same as Figure 6.3 except for primary productivity. C-D: Relative change in model predicted primary productivity in the WMS (C) and EMS (D) since 1950 from changes in anthropogenic inputs alone (Simulation 3) and contribution of individual sources of reactive P to primary production supplied to the WMS (clear) and EMS (hatching) between 1950 and 2030.

than 1950 throughout 1950 to 2000 in the EMS whereas in the WMS primary productivity in some years is below 1950 rates.

6.5 Discussion

The MS appears at first glance to be an ideal basin for studying anthropogenic nutrient enrichment within a marine system. It is landlocked, with high population growth and tourism along its coastline (Plan-Bleu, 2005) and has significant land derived nutrient inputs which have substantially changed since 1950 (Guerzoni et al., 1999; Ludwig et al., 2009; Chapter 2; Chapter 3; this study). The residence time of the deep water is less than 150 years indicating that changes in properties of the deep water should be observed on human timescales. Indeed, changes in temperature and salinity of the MS DW are clearly noticeable within long term measurements since 1950 (Béthoux et al., 1990; Béthoux and Gentili, 1999; Vargas-Yanez et al., 2010; Borghini et al., 2014). Long-term trends in biogeochemical parameters such as reactive P and N concentrations are however less easy to observe (Béthoux et al., 1998; Denis-Karafistan et al., 1998; Karafistan et al., 2002). Here, we reconstruct inputs of both inorganic and organic forms of P and N between 1950 and the present day together with predictions up to the year 2030 with the aim of diagnosing basin wide anthropogenic nutrient enrichment within the MS.

The nutrient budgets of the WMS and EMS over 1950 to 2030 are dominated by marine derived inputs from the inflow of ASW and exchanges across the Strait of Sicily (Figure 6.2; Chapter 5). Thus the anthropogenic nutrients deposited into the MS since 1950 are diluted by the background signal of the ASW input which is assumed to stay constant with time. In total, land derived inputs only contribute less than 38% of reactive P inputs and less than 52% of reactive N inputs into the WMS and EMS over 1950 to 2030. This is despite increases in land derived inputs of reactive P and N by a factor of 3 in the WMS and 2.5 in the EMS over the same time period. The anti-estuarine circulation provides an additional dilution factor in the detection of anthropogenic nutrient enrichment exporting dissolved P and N accumulating with the intermediate and deep layers of the WMS and EMS (Figure F.10; Chapter 2). Approximately 60% of anthropogenic nutrients input into the WMS are removed from the water column by 2030 while in the EMS 45% of anthropogenic nutrients are removed, predominantly through the Straits of Gibraltar and Sicily (Figure F.10). Thus the anti-estuarine circulation thus helps protect the MS from the consequences of anthropogenic nutrient enrichment.

In addition to the above factors, significant inter-annual variability in IW/DW formation occurs within the MS (L'Hévéder et al., 2013; Vervatis et al., 2013; Sevault et al., 2014; Pinardi et al., 2015). This creates noise within biogeochemical parameters such as nutrient distributions, N:P ratios and primary productivity further masking the impact of anthropogenic reactive P and N inputs to the MS. In this

paper, we particularly focus on the impact that inter-annual variability in IW/DW formation, and thus the THC of the entire MS, has in determining nutrient enrichment within the MS. Our modeling approach allows the effects of each individual mechanism to be observed. The model does not, however, include any mesoscale variability or seasonality. It represents long term, decadal changes in P and N concentrations integrated over the entire WMS and EMS.

6.5.1 Signals of anthropogenic nutrient enrichment in the Mediterranean Sea

Within the WMS, the anthropogenic enrichment of dissolved reactive P concentrations are masked by the noise created by inter-annual variability of the THC (Figure 6.3). Anthropogenic enrichment of dissolved reactive P concentrations are more likely to be observed in the EMS than WMS (Figures 6.3 and 6.4) but the maximum difference in all reservoirs between the 10^{th} percentile of Simulation 2 and 90^{th} percentile of Simulation 1 is only 10 nM with an analytical precision on frozen samples of 3-5 nM (Krom et al., 2005; Pujo-Pay et al., 2011). Given the sporadic temporal and spatial historical measurements in the MS together with the analytical capabilities in measuring PO_4 and DOP concentrations, we conclude that the magnitude of changes in dissolved reactive P concentrations from anthropogenic enrichment are too small to be observed in time-series data over those changes induced by inter-annual variability in THC.

Anthropogenic enrichment of reactive N concentrations however should be detectable within time series data. Distinct increases in NO_3 concentration, above the background signal from variability in THC, occur in the IW and DW of both WMS and EMS after 1990 (Figures 6.3 and 6.4). However, the largest anthropogenic enrichment signature is predicted to occur within DON concentrations , especially within the EMSW, with the mean increase of 3.4 μM from anthropogenic enrichment over 1950 to 2030 much greater than the 0.19 μM variation in DON concentrations induced by inter-annual THC variability (Figure F.4). Likewise, DON concentrations within the EMIW and EMDW rise above the background signal from IW/DW formation variability after 1970 and 1980 respectively (Figure F.4). In the WMS, anthropogenic enrichment of DON concentrations in time series data are most likely detected within the WMIW after 1980. Anthropogenic enrichment may also be observed in DON concentrations in the WMSW and WMDW after around 1990 (Figures 6.3 and F.3).

The most sensitive indicator of anthropogenic enrichment over 1950-2030 however appears to be reactive molar N:P ratios (Figure 6.6) which change in response to different temporal trends in reactive P inputs and reactive N inputs. The largest anthropogenic increase occurs within DON:DOP ratios with only a small change in the ratios from circulation variability. However, measurements of the DON:DOP ratio within the MS are very heterogeneous ranging between 50-84 and 60-220 in the photic zone of the WMS and EMS, respectively, and 67-400 and 25-260 within the WMDW and EMDW (Santinelli, 2015). The

heterogeneity is likely a result of difficulty in measuring DOP concentrations which tend to be very low and require careful blank correction. Thus systematic decadal changes in the DON:DOP ratio may not be detectable in time series data.

High DW NO_3:PO_4 ratios are a characteristic feature of the MS and the NO_3:PO_4 DW ratio is frequently reported. Although the predicted increase in the DW NO_3:PO_4 ratio from anthropogenic reactive P and N inputs is smaller than the other reservoirs, measured NO_3:PO_4 DW ratios are more consistent than the DON:DOP ratio at 20-23:1 in the WMDW and ~28:1 in the EMDW (Krom et al., 1991; Béthoux et al., 1998; Kress and Herut, 2001; Moutin and Raimbault, 2002; Ribera d'Alcalà et al., 2003; Schroeder et al., 2010a; Pujo-Pay et al., 2011). We predict that the increase in the NO_3:PO_4 DW ratio induced by anthropogenic enrichment of P and N should be detectable in time series data after 2000 in the WMDW and 2010 in the EMDW (Figure 6.6). The mean NO_3:PO_4 DW ratio increases in the WMS and EMS by approximately 1.5-1.6 between 1990 and 2030 in Simulation 3 compared to the variability in the ratio from changes in the THC of 0.3. The stability in our predicted NO_3:PO_4 DW ratio in the WMS prior to 1990 is in agreement with the observations of Béthoux et al. (1998); (2002b). Pasqueron de Fommervault et al. (2015) observe an increase in the NO_3:PO_4 DW ratio at the DYFAMED within the WMS between 1990 and 2010, matching our predictions, although their predicted increase of 4.2 is greater than that predicted here over the same time period.

The response of primary productivity to inter-annual variability in THC is modeled to substantially differ between the WMS and EMS. In the WMS, inter-annual variability in the THC is predicted to dominate the response of primary productivity rather than changes in anthropogenic reactive P inputs (Figure 6.7A). However, in the EMS anthropogenic reactive P inputs are more important in controlling primary productivity than IW/DW formation processes (Figure 6.7B). In the north-west Mediterranean, the important role of circulation in controlling primary productivity was highlighted during two open ocean convection events in spring 2011 which provided the same quantity of PO_4 to the SW as that provided by rivers and atmospheric deposition (Severin et al., 2014). In the model presented here, DW formation within the WMS initiates strong mixing throughout the water column of the WMS with a higher upwelling flux from WMIW to WMSW occurring with greater DW formation. In the EMS model however, the same mechanism is not present, with no upwelling occurring between EMIW and EMSW (Figure 6.1). Hence the impact of inter-annual variability in IW/DW formation is much lower in the EMS than WMS.

Despite the strong influence of inter-annual variation in the THC, the model can still be used to determine the main anthropogenic reactive P input in driving primary productivity. Macias et al. (2014), using a

coupled 3D hydro-dynamical biogeochemical model, hypothesize that rivers, particularly NO_3 in rivers, are statistically responsible for a key portion of primary production within the MS. In the model used in this study however, reactive N inputs cannot influence primary productivity due to the assumed P limitation where the N assimilation flux is controlled by P uptake. We predict that rivers are the main anthropogenic reactive P input driving the change in primary productivity in the WMS over 1950-2030, but in the EMS changes in atmospheric deposition are the most important anthropogenic reactive P input between 1950-2000 (Figure 6.7C and D). By 2030 however, atmospheric deposition, direct wastewater discharges and riverine inputs contribute almost equally to the change in primary productivity since 1950. Interestingly riverine inputs to the WMS are as important in controlling primary productivity in the EMS as changes in riverine inputs directly to the EMS.

The response of the THC to climate change will add further variability to nutrient distributions within the MS although the magnitude and direction of THC changes as a result of climate change are uncertain (Adloff et al., 2015; Chapter 4). Applying the extreme climate change scenario for an enhanced THC in the MS to Simulation 1 for 2000-2030 (Chapter 4; see Appendix F for details on implementation of circulation scenarios) results in an increase in SW and IW dissolved reactive P and N concentrations, and primary productivity in both the WMS and EMS (Scenario S2; Table F.5; Figure F.12). The increase in both nutrient concentrations and primary productivity is a result of the additional supply of dissolved reactive P and N into both the WMS and EMS by exchanges through the Strait of Sicily. In the DW of both the WMS and EMS, PO_4 and NO_3 concentrations decrease while DOP and DON concentrations increase. The opposite pattern in dissolved reactive P and N concentrations throughout the water column and primary productivity generally occurs for a weakened THC (Scenario S1; Table F.5; Figure F.12). However, by 2030 the change in dissolved reactive P and N concentrations, and primary productivity for both an enhanced and weakened THC are minimal comparative to the variation caused by inter-annual variability in the THC (Figure F.12). Hence although changes in circulation from climate change will promote changes in dissolved reactive P and N concentrations, the noise in P and N concentrations from inter-annual changes in circulation are likely to mask the changes, at least for the near future. This is consistent with the conclusions of Macias et al. (2015) whom found no significant difference in primary productivity within the MS at the beginning and end of the 21st century from changes in atmospheric forcing alone. Although increases in gross primary production were predicted in other modeling studies for the MS over the course of the 21st century, this was attributed to increasing water temperatures rather than changes in circulation (Herrmann et al., 2014; Lazzari et al., 2014).

6.5.2 Historical reconstructions of nutrient distributions and primary production

The historical circulation scenarios allow the comparison of model predicted variables with observed data. Substantial noise in nutrient distributions and primary productivity are created by inter-annual variability in the THC between 1960 and 2000. Primary productivity in Simulation 5 (anthropogenic enrichment and historical circulation) varied between 125 g C m^{-2} yr^{-1} and 234 g C m^{-2} yr^{-1} in the WMS over 1950- 2000 and 56-86 g C m^{-2} yr^{-1} in the EMS (Figure F.9). These results are within observed ranges compiled by Berman-Frank and Rahav (2012) between 1970-2009, of 37-475 g C m^{-2} yr^{-1} in the WMS and 10-143 g C m^{-2} yr^{-1} in the EMS. In addition, Berman-Frank and Rahav (2012) found no significant temporal trends in primary productivity in both the WMS and EMS between 1970 and 2009 which is consistent with our results. The variability in primary productivity within the model due to IW/DW formation masks anthropogenic enrichment trends over the same time period (1970 to 2009; Figure 6.7 A-B; Figure F.9).

No clear temporal trend in nutrient enrichment is also observed within the dissolved reactive P and N concentrations in the WMIW in Simulation 5 over 1950 to 2000, while in the EMIW, a slight increasing trend may be inferred (Figure 6.5). Substantial variations in nutrient concentrations do however occur over the course of 1950 to 2000 as a result of historical circulation, and these are much greater than those predicted from nutrient enrichment alone (Simulation 3; Figure 6.5). The high variability in reactive P and N concentrations throughout the water column is demonstrated in observational records with model results of Simulations 1 to 7 falling within the range of reported values in reactive P and N concentrations in both the WMS (Tables F.3 and F.4) and EMS (Chapter 2).

The large response of IW PO_4 and NO_3 concentrations to the combined historical changes in circulation and anthropogenic enrichment scenario (Simulation 5) comparative to those from anthropogenic enrichment alone (Simulation 3) (Figure 6.5) are in contrast to the hypothesis that riverine fluxes of PO_4 and atmospheric deposition of NO_3 are responsible for the large observed increases in PO_4 and NO_3 concentrations within IW (Moon et al., 2016). Moon et al. observe an increase in PO_4 concentrations of 70 nM per decade and NO_3 concentrations of 1.98 μM per decade in the WMIW between 1990 and 2005 and a 50 nM and 0.78 μM increase per decade in EMIW PO_4 and NO_3 concentrations, respectively, between 1985 and 2000. In particular for PO_4, the observations of Moon et al. do not match our model predictions of anthropogenic enrichment. In fact the maximum increase in PO_4 concentrations over the period 1950-2030 in Simulation 3 within the WMIW and EMIW of 15 nM and 17 nM, respectively, is less than the observed decadal increase.

However if historical circulation is included in the analysis, the model predicted trends do match observations. In Simulation 5, a maximum increase in PO_4 concentrations of 49 nM and 27 nM occurs in the WMIW over 1990-2000 and in the EMIW over 1985-2000, respectively, while a maximum increase of 1.4 μM and 1.0 μM occurs in NO_3 concentrations in the WMIW and EMIW over the same time periods (Figure 6.5). Simulating instantaneous changes in circulation fluxes throughout the MS is an admittedly unrealistic scenario (i.e. Simulations 4 and 5). Including attenuation within the water fluxes, by operating a 5 year running average on historical IW/DW formation rates (Simulation 7), still results in a much greater change in PO_4 and NO_3 concentrations than in Simulation 3 (anthropogenic nutrient enrichment alone) indicating our results are robust (Figure 6.5). In addition the evolution of PO_4 and NO_3 concentrations in Moon et al.'s analysis mirror each other extremely well further indicating a strong influence of circulation in driving the changes observed. We therefore conclude that the inter-annual variability in circulation is the cause of the observed increase in PO_4 concentrations within IW in the MS while a combination of anthropogenic nutrient inputs and circulation changes contribute to the observed changes in NO_3 concentrations. These conclusions complement those of Ozer et al. (2016) whom suggest that circulation alone is driving temporal differences in IW NO_3 and PO_4 concentrations within the EMS.

6.6 Conclusions

In this study we have reconstructed plausible changes in reactive P and N inputs to the MS over 1950 to 2030. Although the MS may appear to be an ideal basin for studying anthropogenic nutrient enrichment, land derived inputs only a form a minor component of the nutrient budgets of the WMS and EMS over the period 1950 to 2030 with ASW and exchanges across the Strait of Sicily the dominant source of P and N to the WMS and EMS. Thus anthropogenic nutrient inputs over 1950-2030 are a relatively small component of the whole nutrient budget. In addition the anti-estuarine circulation removes up to 60% of the anthropogenic P and N supplied to the WMS and EMS from the water column by 2030 further diluting the anthropogenic nutrient signature within the water column of the MS. Finally inter-annual variability in IW and DW formation produces noise in reactive P and N concentrations making it even more difficult to detect anthropogenic nutrient enrichment within the MS and increases the possibility of false detection of anthropogenic nutrient enrichment.

Our analysis focuses on the impact of inter-annual variability in the THC of the MS on the ability to detect anthropogenic nutrient enrichment within the MS. Between 1950 and 2030 external reactive P and N inputs increased by a maximum of 16% and 40%, respectively, in the WMS and 39% and 85% in the EMS. The resulting changes in dissolved reactive P concentrations throughout 1950 to 2030 are unlikely to be observed over noise created by inter-annual variability in the THC. The anthropogenic N enrichment signature is expected to be greatest within time series of DON concentrations, especially within the EMS.

Within the IW and DW, anthropogenic nutrient enrichment of DON concentrations should be detectable in time series data in the WMS after around 1980 and EMS after around 1970 over background noise from inter-annual variability in the THC if suitable high accuracy analytical methods are used.

Consequently, the molar DON:DOP ratio is a sensitive indicator to anthropogenic nutrient enrichment. The DON:DOP ratio within the EMSW increases by 50 between 1950 and 2030 compared to a noise of 4 produced by inter-annual circulation variability. However, high spatial heterogeneity of the ratio occurs within observations due to the difficulty in measuring both DON and DOP. The variation in NO_3:PO_4 DW ratios are much more consistent within observations. We predict that increases in the NO_3:PO_4 DW ratio from external reactive P and N inputs should be observed after 2000 in the WMS and 2010 in the EMS.

Our work emphasizes the substantial difference in the biogeochemical functioning of the WMS and EMS. Inter-annual variability in primary production in the WMS is dominated by changes in year-on year DW formation rather than anthropogenic enrichment. In the EMS however, anthropogenic enrichment is more important than inter-annual variability in circulation in predicted primary productivity changes. These differences between the WMS and EMS are further reflected in the high range of dissolved reactive P and N concentrations produced by inter-annual variability in the THC in the WMS compared to the EMS. Thus we conclude that the detection of anthropogenic nutrient enrichment within time series data is likely greater in the EMS than WMS.

The model used in this study is an admittedly simplified representation of biogeochemical cycling in the MS, simplifying circulation features and ignoring seasonality and spatial variability in both external reactive P and N inputs into MS and nutrient distributions within the MS. Results are integrated across an entire water mass so average changes across the entire WMS and EMS are predicted. Nevertheless, the model can be used to identify priority areas for monitoring. The most sensitive indicators to anthropogenic enrichment are DON concentrations and the DON:DOP ratio and thus sampling regimes should prioritize the systematic sampling of both DON and DOP. To observe anthropogenic enrichment in dissolved reactive P concentrations high temporal resolution, decadal sampling regimes, similar to that of the DYFAMED site, are likely required at numerous fixed observatories across the MS using high precision sampling techniques.

Chapter 7.

Conclusions

7.1 Summary

In this thesis, a comprehensive mass balance model of phosphorus (P) and nitrogen (N) cycling within the Western Mediterranean Sea (WMS) and Eastern Mediterranean Sea (EMS) has been created, describing how inputs of anthropogenic P and N have changed with time. For the first time direct wastewater discharges (quantified in Chapter 3), particulate organic P burial in the WMS (Chapter 5) and submarine groundwater discharge (SGD) have been included in a complete P and N budget for the MS for the time period 1950-2030 (Chapters 5 and 6). An updated water budget for the entire MS is created using recent measurements for the water fluxes through the Strait of Gibraltar and portion of intermediate water (IW) and deep water (DW) in the outflow to the Atlantic Sea (Chapter 4) resulting in a change in the net direction of vertical water flows within the WMS from older box model budgets. In addition a dissolved oxygen (O_2) model is used to investigate whether climate warming may impact O_2 distributions within the Mediterranean Sea (MS).

7.1.1 Research questions

The following are summaries of answers to the research questions formulated in the introduction and discussed throughout this thesis.

1. What causes the west to east differences in phosphate (PO_4) and nitrate (NO_3) concentrations, primary productivity and NO_3:PO_4 DW ratios in the MS?

The difference in magnitude of marine derived sources of P and N to the WMS and EMS is the primary driver of the west to east gradients in phosphate (PO_4) and nitrate (NO_3) concentrations, primary productivity, and N:P ratios (Chapter 5). Inputs of land derived P and N are similar between the WMS and EMS per unit surface area yet reactive P inputs are 3.9 times and reactive N inputs 2.6 times greater into the WMS than EMS per unit surface area. In the WMS, reactive P and N inputs from land are added to a background of reactive P and N that originated from the Atlantic and the deep layers of the EMS whereas those in the EMS are added to the inflow of Western Mediterranean Surface Water (WMSW) through the Strait of Sicily that is severely depleted in P and N. In addition, greater recycling of organic P and N to dissolved inorganic forms occurs in the Western Mediterranean Deep Water (EMDW) than Eastern Mediterranean Deep Water (EMDW) likely due to the greater P and N supply supporting greater bacterial activity in the WMS and EMS. Thus dissolved inorganic P and N concentrations are greater in the WMS than EMS yet dissolved organic concentrations remain similar. In addition to the greater inputs of reactive P and N to the WMS than EMS, primary productivity is also supported by upwelling of nutrients into the photic zone in the WMS whereas this mechanism is not present in the EMS. The inflow of Atlantic Surface Water (ASW) into the Mediterranean through the Strait of Gibraltar with a

NO_3:PO_4 ratio of 10:1 is one of the main drivers of the lower NO_3:PO_4 ratio in the WMDW than EMDW and results in a lower reactive N:P ratio of inputs entering the WMS than EMS.

2. Why does the MS have a high DW NO_3:PO_4 ratio in comparison to the rest of the world's oceans?

All dissolved N:P ratios within the Mediterranean Sea (MS) are above the Redfield N:P ratio of 16:1. The unusually high deep water (DW) NO_3:PO_4 ratio observed within the MS is from a combination of little denitrification and high reactive N:P ratio of inputs (Chapter 6). High N_2 fixation is not the cause of the high N:P ratios. The reactive N:P ratio of inputs to the WMS is 30:1 and 37:1 to the EMS. O_2 concentrations above 70% saturation within the DW result in little denitrification. Denitrification rates need to increase by 2.2 and 8 times 1950 values in the WMS and EMS, respectively, to reduce the DW NO_3:PO_4 ratio to 16:1 in both seas. This corresponds to a denitrification rate in the WMS and EMS of 0.05 and 0.01 mol m^{-2} yr^{-1}, respectively, comparable to global oceanic denitrification rates. The high N:P of inputs is largely from atmospheric deposition. In the absence of atmospheric deposition the NO_3:PO_4 DW ratio would approach 16:1

3. Are direct discharges of domestic wastewater into the sea an important component of the MS nutrient budget?

Direct discharges of domestic wastewater are an important component of nutrient budgets in the MS. Wastewater P discharges are similar to riverine inputs into the MS, while N wastewater inputs are on the same order of magnitude as riverine inputs (Chapter 3). In addition direct wastewater discharges are likely to become increasingly important in the future especially from along the north African coastline due to high population growth.

4. How have humans modified nutrient cycling in the MS since 1950? Why is the Mediterranean oligotrophic despite being surrounded by land?

Reactive P inputs into the WMS and EMS over 1950 to 2030 increased by 16 and 39%, respectively, while reactive N inputs increased by 40% and 85% (Chapter 6). Resulting primary productivity from inputs alone is predicted to have increased by 12% and 22% in the WMS and EMS respectively. In the WMS riverine P inputs are the most important anthropogenic input in controlling the change in primary production between 1950 and 2030 while atmospheric P deposition is more important in the EMS.

Intermediate/deep water formation and sinking of PON and POP removes P and N from the SW where it is efficiently converted to dissolved inorganic P and N at depth (Chapters 2 and 5). The anti-estuarine circulation thereby removes the PO_4 and NO_3 within IW and DW which otherwise would accumulate at depth and become increasingly available to enter the photic zone through turbulent mixing (WMS and

EMS) and upwelling (WMS only). The anti-estuarine circulation results in the net export of PO_4 and NO_3 through the Straits of Gibraltar and Sicily despite the net flux of dissolved reactive P across the Straits close to zero. Approximately one third of anthropogenic P and N added to the EMS over 1950 to 2000 exited the EMS through the Strait of Sicily with another third stored in the deep water of the EMS (Chapter 2).

5. Can anthropogenic reactive P and N inputs be detected within water column measurements nutrient in the MS?

The dominance of the marine derived inputs in the nutrient budgets of the WMS and EMS dilutes the signals of anthropogenic nutrients deposited into the MS, in addition to the efficient removal of the anthropogenic nutrient inputs by the anti-estuarine circulation. Inter-annual variability in the thermohaline circulation (THC) further adds noise to the background signal of dissolved reactive P and N concentrations. We predict that these factors result in the anthropogenic enrichment of dissolved reactive P concentrations to be too small to be detected within time series measurements. Anthropogenic N enrichment may be observed after 1970 in DON concentrations and 1990 in NO_3 concentrations. Anthropogenic enrichment of both P and N is more likely to be observed in the EMS than WMS. Finally the change in N:P ratios may be a good indicator of anthropogenic enrichment.

6. How will climate change impact biogeochemical cycling in the MS?

Climate induced warming will decrease the solubility of O_2 within the water column and also increase rates of reaction and thus degradation of organic matter. In addition it will likely either enhance or weaken the THC of the MS. Changes in the THC dominate the response of O_2 to climate warming (Chapter 4). On a 100 year timescale, the predicted extremes in changes in THC are unlikely to result in the deep waters of the MS becoming hypoxic with WMDW and EMDW concentrations changing by up to 25% to 151-205 µM, and 160-219 µM, respectively. On longer timescales if a severe decline in IW/DW formation within the MS occurs the EMDW may become hypoxic but the WMDW remains oxic as the Bernoulli suction at the Strait of Gibraltar forces the WMDW to become replenished.

An enhanced THC of the MS from climatic warming increases primary production as the increased supply of dissolved reactive P through the Strait of Sicily to both EMS and WMS has a larger influence on primary production than the increased loss of P (Chapter 6). The opposite occurs for a decline in the THC. However over the period 2000 to 2030, the changes in primary production from changes in circulation due to climate warming are still small in comparison to the variations induced by inter-annual variability in IW/DW formation.

7.1.2 The MS behaves like subtropical oceanic gyres

A key conclusion of this thesis is that the MS behaves similarly to subtropical oceanic gyres which have little inputs from land derived sources. This is the opposite of what one might expect given the semi-enclosed nature of the MS together with high population densities along large parts of its coastline. The anti-estuarine circulation of the MS is similar to that observed in the subtropical oceanic gyres with lateral flow of water to the center of gyre, which then downwells and then flows to the edge of the gyre as deeper water. The nutrient budgets of these gyres are dominated by the lateral supply of P and N, with the lateral supply of DOP and DON contributing significantly to new production estimates of the gyres (Letscher et al., 2016). Similarly, the nutrient budget of the MS is also dominated by lateral supply of marine derived sources of P and N with up to 37% of DOP inputs also contributing towards new production (Chapter 5). The dominance of marine derived P and N inputs in the nutrient budget also minimizes the detection of anthropogenic enrichment within the MS (Chapter 6).

7.1.3 Important role of organic matter in nutrient cycling

A key theme throughout this thesis has been the importance of organic matter in nutrient dynamics within the MS. Typically DOP and DON have been excluded from contributions of reactive P and reactive N inputs into the MS. Chapter 2 highlights that organic matter input from the WMS through the Strait of Sicily into the EMS exerts a major control on the primary productivity of the EMS. This is further confirmed in Chapter 5 with at least half of the dissolved reactive P and N entering the WMS and EMS as SW through the Straits of Gibraltar and Sicily, respectively, in the form of DOP and DON. The MS acts as a bioreactor of nutrient cycling. Organic matter in SW is efficiently transferred to the deeper layers whereby mineralization turns DOP and DON to PO_4 and NO_3. The anti-estuarine circulation transports the accumulating PO_4 and NO_3 out of the MS to the Atlantic Sea. The change in speciation of P and N through the Strait of Sicily and Gibraltar (Chapter 5) further highlights the bioreactor role of the MS with 52% and 26% of inflow of Atlantic SW entering the MS as dissolved PO_4 and NO_3 respectively, while these consisted of 88 and 73% of the outflow (Chapter 5). It is further predicted that DON may build up within the EMSW and EMIW in response to the anthropogenic input of reactive N (Chapters 2 and 6). Thus time series measurements of DON concentrations may indicate anthropogenic nutrient enrichment with projected increases in DON concentrations predicted to be much greater than the noise in concentrations created by inter-annual variability in circulation.

In addition, the role of organic matter is important in O_2 dynamics within the MS (Chapter 4). Oxygen concentrations before, immediately after and a few years after the EMT clearly demonstrates the role of DW formation in providing organic matter to the deep layers of EMS and consequently stimulating O_2

consumption. A coupling between O_2 concentrations and dissolved organic carbon (DOC) creates a negative feedback that dampens the response of O_2 concentrations to changes in the THC in response to climate warming compared to if organic matter was not present. Thus it is imperative that organic matter is included in both nutrient models and coupled to oxygen consumption in order to make future predictions.

7.1.4 Sensitivity of EMS versus WMS to anthropogenic induced changes in thermohaline circulation and nutrient inputs.

The EMS is historically much more sensitive to environmental changes than the WMS as indicated by the presence of sapropels in the EMS while they are mainly absent in the WMS. Thus, differences in sensitivity of the WMS and EMS to model parameters was explored throughout this thesis:

- On a short term timescale (<100 year) O_2 concentrations in the Western Mediterranean Deep Water (WMDW) are more sensitive to THC circulation changes than those in the Eastern Mediterranean Deep Water (EMDW), likely due to the shorter residence time of the WMDW. However, on a long term timescale (>1000 years) the response of O_2 concentrations is much greater in the EMDW than WMDW (Chapter 4).
- Sensitivity analyses suggest that primary productivity in the WMS is more sensitive to internal cycling processes and external inputs than that in the EMS.
- In contrast the NO_3:PO_4 ratio in the EMDW is more sensitive to changes than in the WMDW. It is more sensitive to inputs from the Atlantic Sea than that in the WMS and is much more sensitive to internal dynamics.
- Anthropogenic nutrient enrichment is more likely to be observed over circulation signals in the EMS than the WMS, partly due to the greater mixing of the water column by IW/DW formation in the WMS than EMS, which creates higher noise in background dissolved reactive P and N concentrations.

7.2 Perspective

This thesis uses a box model mass balance approach which is admittedly an inherent simplification of biogeochemical cycling in the MS. Spatial and seasonal variability is ignored and microbial recycling processes are lumped together in one flux described using first order rate kinetics. Recycling of organic matter within the MS is a complex process involving prokaryotic heterotrophs and higher order members of the food chain (Figure 1.5) as indicated by the unexpected results during the CYCLOPS experiment (Krom et al., 2005). The mass balance approach used in this thesis still yields powerful insights into the coupling between geophysical and ecological dynamics of the MS and their response to P and N inputs

and climate forcing. The simplicity of the model structure allows multiple historical and future scenarios to be tested.

7.2.1 Future Work

The model can act as a building block for further running additional scenarios and adding further complexity. The following are possible actions that can be done to/with the model:

- Improvement of input fluxes of P and N: despite the direct discharges of domestic wastewater was quantified in this thesis, **quantification of direct industrial discharges of P and N still need to be identified** and added to the model. The limited data available suggest that these are potentially a large contribution of P and N to the MS (UNEP/WHO, 1999). For example, phosphogypsum discharges on the coast of Tunisia (i.e. Drira et al., 2016) is one potentially important additional input not included.
- Creation of a **fully coupled P, N, C, O model** investigating how future climate change and anthropogenic P and N inputs will impact the biogeochemistry of the MS. A key challenge to this however is estimating the remineralization ratios of P, N, C and O. Different dynamics at depth are clearly occurring in the MS compared to the global ocean so the ratio of remineralization may also be different.
- **Split the organic matter pools into labile, semi-labile and refractory**. To do this however, information on the lability of organic matter in each individual input will need to be acquired and on the organic matter already existing within the MS.
- **Addition of nitrogen isotopes** to the same model framework for at least the EMS and preferably the entire MS. Coupling to isotopes will constrain some of the internal recycling dynamics within the model.
- **Addition of coastal processes on nutrient dynamics** to model framework. The model currently assumes all P and N reach the pelagic oceans. Coastal processes are not considered. An additional series of sub-models should incorporate burial and recycling terms within the coastal zone with coupling between coastal and pelagic models.
- Use the current model to investigate what the **NO_3:PO_4 DW ratio of the Mediterranean prior to the main onset of anthropogenic inputs** i.e. 1850s.

However, only a limited amount of further information can be obtained from such a model before a more complex representation of mesoscale circulation features and seasonality of the system are required. For example the transfer from P limitation to N and P co-limitation will never be understood using the model

in this thesis. Complex 3D biogeochemical models, describing seasonality and circulation features together with biogeochemistry do exist. The inputs of P and N into these models however are poorly defined, often only including inorganic nutrients and ignoring sources such as atmospheric deposition. A balance needs to be obtained between complexity of hydrodynamics, microbial loop processes and biogeochemical inputs and outputs, and ability to obtain useful long term predictions from models.

7.2.2 Recommendations for the Mediterranean scientific community

The models created in this thesis highlight priority areas for future biogeochemical monitoring and research. In particular the following recommendations are identified:

- Inclusion of the measurement of dissolved organic P, N and C concentrations in routine biogeochemical analyses in programs such as Med-SHIP (Mediterranean Sea Ship based hydrographic investigations programme; Schroeder et al., 2015). Med-SHIP undertakes repeat cross sectional cruises across the Mediterranean but only routinely measures inorganic nutrients.
- Long term time series of inorganic and organic nutrients across the Straits of Gibraltar and Sicily should be acquired.
- Simultaneous cross basin measurement of microbial processes throughout the water column through measurements such as total prokaryotic heterotrophic abundance, prokaryotic heterotrophic production rates and enzymatic activities. Most studies only look at SW and do not combine IW/DW results for both the WMS and EMS.
- Increased understanding on sources, lability and functioning of organic matter within the MS.
- Improved knowledge on how climate change will alter the THC of the MS.
- Observed changes in P and N concentrations, and primary productivity must be put into context with temporal variability of IW/DW formation.

References

Adloff, F., S. Somot, F. Sevault, G. Jordà, R. Aznar, M. Déqué, M. Herrmann, M. Marcos, C. Dubois, E. Padorno, E. Alvarez-Fanjul, and D. Gomis (2015), Mediterranean Sea response to climate change in an ensemble of twenty first century scenarios, *Clim Dynam*, 1-28, doi: 10.1007/s00382-015-2507-3

Allen, J. I., P. J. Somerfield, and J. Siddorn (2002), Primary and bacterial production in the Mediterranean Sea: a modelling study, *J Mar Syst*, *33*, 473-495, doi: 10.1016/s0924-7963(02)00072-6

Altieri, A. H., and K. B. Gedan (2015), Climate change and dead zones, *Glob Change Biol*, *21*(4), 1395-1406, doi: 10.1111/gcb.12754

Aminot, A., and R. Kérouel (2004), Dissolved organic carbon, nitrogen and phosphorus in the N-E Atlantic and the N-W Mediterranean with particular reference to non-refractory fractions and degradation, *Deep Sea Res Part I Oceanogr Res Pap*, *51*(12), 1975-1999, doi: 10.1016/j.dsr.2004.07.016

Angelakis, A. N., M. Do Monte, L. Bontoux, and T. Asano (1999), The status of wastewater reuse practice in the Mediterranean basin: Need for guidelines, *Water Res*, *33*(10), 2201-2217, doi: 10.1016/s0043-1354(98)00465-5

Angelakis, A. N., and B. Durham (2008), Water recycling and reuse in EUREAU countries: Trends and challenges, *Desalination*, *218*(1-3), 3-12, doi: 10.1016/j.desal.2006.07.015

Antoine, D., A. Morel, and J.-M. André (1995), Algal pigment distribution and primary production in the eastern Mediterranean as derived from coastal zone color scanner observations, *Journal of Geophysical Research*, *100*(C8), 16193, doi: 10.1029/95jc00466

Arnell, N. W. (2004), Climate change and global water resources: SRES emissions and socio-economic scenarios, *Glob Environ Change*, *14*(1), 31-52, doi: 10.1016/j.gloenvcha.2003.10.006

Arrigo, K. R. (2005), Marine microorganisms and global nutrient cycles, *Nature*, *437*(7057), 349-355, doi: 10.1038/nature04158

Artioli, Y., J. Friedrich, A. J. Gilbert, A. McQuatters-Gollop, L. D. Mee, J. E. Vermaat, F. Wulff, C. Humborg, L. Palmeri, and F. Pollehne (2008), Nutrient budgets for European seas: A measure of the effectiveness of nutrient reduction policies, *Mar Pollut Bull*, *56*(9), 1609-1617, doi: 10.1016/j.marpolbul.2008.05.027

Asai, K., J. Zhang, K. Asai, K. Mogi, W. Y. Fantong, and A. K. Mandal (2013), Development of an in situ sampler of submarine springs for the analysis of CFCs and SF6, *Geochem J*, *47*(6), 693-696, doi: 10.2343/geochemj.2.0253

Aspila, K. I., H. Agemian, and A. S. Y. Chau (1976), Semi-automated method for determination of inorgainc, organic and total phosphate in sediments, *Analyst*, *101*(1200), 187-197, doi: 10.1039/an9760100187

Astraldi, M., S. Balopoulos, J. Candela, J. Font, M. Gacic, G. P. Gasparini, B. Manca, A. Theocharis, and J. Tintoré (1999), The role of straits and channels in understanding the characteristics of Mediterranean circulation, *Prog Oceanogr*, *44*(1-3), 65-108

Auger, P. A., C. Ulses, C. Estournel, L. Stemmann, S. Somot, and F. Diaz (2014), Interannual control of plankton communities by deep winter mixing and prey/predator interactions in the NW Mediterranean: Results from a 30-year 3D modeling study, *Prog Oceanogr*, *124*, 12-27, doi: 10.1016/j.pocean.2014.04.004

Banoub, M. W., and P. J. Williams (1972), Measuremnets of microbial activity and organic material in the Western Mediterranean Sea, *Deep-Sea Res*, *19*(6), 433-&, doi: 10.1016/0011-7471(72)90053-8

Bayari, C. S., N. N. Ozyurt, M. Oztan, Y. Bastanlar, G. Varinlioglu, H. Koyuncu, H. Ulkenli, and S. Hamarat (2011), Submarine and coastal karstic groundwater discharges along the southwestern Mediterranean coast of Turkey, *Hydrogeology Journal*, *19*(2), 399-414, doi: 10.1007/s10040-010-0677-y

Benner, R. (2002), Chemical Composition and Reactivity, in *Biogeochemistry of Dissolved Organic Matter* edited by D. A. Hansell and C. A. Carlson, pp. 59-90, Academic Press, San Diego, USA.

Bergamasco, A., and P. Malanotte-Rizzoli (2010), The circulation of the Mediterranean Sea: a historical review of experimental investigations, *Advances in Oceanography and Limnology*, *1*(1), 11-28, doi: 10.1080/19475721.2010.491656

Bergametti, G., E. Remoudaki, R. Losno, E. Steiner, B. Chatenet, and P. Buatmenard (1992), Source, transport and deposition of atmospheric phosphorus over the northwestern Mediterranean, *Journal of Atmospheric Chemistry*, *14*(1-4), 501-513, doi: 10.1007/bf00115254

Berman-Frank, I., and E. Rahav (2012), Dinitrogen fixation as a souce for new production inthe Mediterranean Sea: A review, in *Life in the Mediterranean Sea: A look at habitat changes.*, edited by N. Stambler, pp. 199-226, Nova Science Publisheres, New York.

Berner, E., and R. Berner (2012), *Global Environment: Water, Air, and Geochemical Cycles*, 2nd ed., 488 pp., Princeton University Press.

Béthoux, J. P. (1980), Mean water fluxes across sections in the Mediterranean Sea, evaluated on the basis of water and salt budgets and of observed salinities, *Oceanol Acta*, *3*(1), 79-88

Béthoux, J. P. (1981), Phosphorus and nitrogen in the mediterranean sea, budgets and potential fertility, *Mar Chem*, *10*(2), 141-158

Béthoux, J. P. (1989), Oxygen consumption, new production, vertical advection and environmental evolution in the Mediterranean Sea., *Deep-Sea Res Pt A*, *36*(5), 769-781, doi: 10.1016/0198-0149(89)90150-7

Béthoux, J. P., B. Gentili, J. Raunet, and D. Tailliez (1990), Warming trend in the Western Mediterranean Deep-Water, *Nature*, *347*(6294), 660-662, doi: 10.1038/347660a0

Béthoux, J. P., P. Morin, C. Madec, and B. Gentili (1992), Phosphorus and nitrogen behavior in the Mediterranean Sea, *Deep-Sea Res Pt A*, *39*(9A), 1641-1654

Béthoux, J. P., and B. Gentili (1996), The Mediterranean Sea, coastal and deep-sea signatures of climatic and environmental changes, *J Mar Syst*, *7*(2-4), 383-394, doi: 10.1016/0924-7963(95)00008-9

Béthoux, J. P., P. Morin, C. Chaumery, O. Connan, B. Gentili, and D. Ruiz-Pino (1998), Nutrients in the Mediterranean Sea, mass balance and statistical analysis of concentrations with respect to environmental change, *Mar Chem*, *63*(1-2), 155-169

Béthoux, J. P., and B. Gentili (1999), Functioning of the Mediterranean Sea: past and present changes related to freshwater input and climate changes, *J Mar Syst*, *20*(1-4), 33-47, doi: 10.1016/s0924-7963(98)00069-4

Béthoux, J. P., X. D. de Madron, F. Nyffeler, and D. Tailliez (2002a), Deep water in the western Mediterranean: peculiar 1999 and 2000 characteristics, shelf formation hypothesis, variability since 1970 and geochemical inferences, *J Mar Syst*, *33*, 117-131, doi: 10.1016/s0924-7963(02)00055-6

Béthoux, J. P., P. Morin, and D. P. Ruiz-Pino (2002b), Temporal trends in nutrient ratios: chemical evidence of Mediterranean ecosystem changes driven by human activity, *Deep-Sea Res Pt II*, *49*(11), 2007-2016, doi: 10.1016/s0967-0645(02)00024-3

Béthoux, J. P., M. S. El Boukhary, D. Ruiz-Pino, P. Morin, and C. Copin-Montégut (2005), Nutrient, Oxygen and Carbon Ratios, CO2 Sequestrationand Anthropogenic Forcing in the Mediterranean Sea, *5K*, 67-86, doi: 10.1007/b107144

Beuvier, J., F. Sevault, M. Herrmann, H. Kontoyiannis, W. Ludwig, M. Rixen, E. Stanev, K. Beranger, and S. Somot (2010), Modeling the Mediterranean Sea interannual variability during 1961-2000: Focus on the Eastern Mediterranean Transient, *J Geophys Res Oceans*, *115*, 27, doi: C08017 10.1029/2009jc005950

Bianchi, M., C. Fosset, and P. Conan (1999), Nitrification rates in the NW Mediterranean Sea, *Aquat Microb Ecol*, *17*(3), 267-278, doi: 10.3354/ame017267

BIO by Deloitte (2014), Evaluation of the use of phosphates in Consumer Automatic Dishwasher Detergents (CADD)*Rep. Report prepared for European Commission - DG Enterprise and Industry*, 78 pp.

Bonnet, S., O. Grosso, and T. Moutin (2011), Planktonic dinitrogen fixation along a longitudinal gradient across the Mediterranean Sea during the stratified period (BOUM cruise), *Biogeosciences*, *8*(8), 2257-2267, doi: 10.5194/bg-8-2257-2011

Borghini, M., H. Bryden, K. Schroeder, S. Sparnocchia, and A. Vetrano (2014), The Mediterranean is becoming saltier, *Ocean Sci*, *10*(4), 693-700, doi: 10.5194/os-10-693-2014

Box, G. E. P., W. G. Hunter, and J. S. Hunter (1978), *Statistics for experimenters. An introduction to design, data analysis and model building*, 653 pp., John Wiley and Sons, New York.

Brewer, P. G., and E. T. Peltzer (2016), Ocean chemistry, ocean warming, and emerging hypoxia: Commentary, *Journal of Geophysical Research: Oceans*, *121*(5), 3659-3667, doi: 10.1002/2016jc011651

Brissaud, F. (2008), Criteria for water recycling and reuse in the Mediterranean countries, *Desalination*, *218*(1-3), 24-33, doi: 10.1016/j.desal.2006.07.016

Bryden, H. L., J. Candela, and T. H. Kinder (1994), Exchange through the Strait of Gibraltar, *Prog Oceanogr*, *33*(3), 201-248, doi: 10.1016/0079-6611(94)90028-0

Burnett, W. C., P. K. Aggarwal, A. Aureli, H. Bokuniewicz, J. E. Cable, M. A. Charette, E. Kontar, S. Krupa, K. M. Kulkarni, A. Loveless, W. S. Moore, J. A. Oberdorfer, J. Oliveira, N. Ozyurt, P. Povinec, A. M. G. Privitera, R. Rajar, R. T. Ramassur, J. Scholten, T. Stieglitz, M. Taniguchi, and J. V. Turner (2006), Quantifying submarine groundwater discharge in the coastal zone via multiple methods, *Sci Total Environ*, *367*(2-3), 498-543, doi: 10.1016/j.scitotenv.2006.05.009

Burnett, W. C., G. Wattayakorn, M. Taniguchi, H. Dulaiova, P. Sojisuporn, S. Rungsupa, and T. Ishitobi (2007), Groundwater-derived nutrient inputs to the Upper Gulf of Thailand, *Cont Shelf Res*, *27*(2), 176-190, doi: 10.1016/j.csr.2006.09.006

Cape, J. N., S. E. Cornell, T. D. Jickells, and E. Nemitz (2011a), Organic nitrogen in the atmosphere — Where does it come from? A review of sources and methods, *Atmospheric Research*, *102*(1-2), 30-48, doi: 10.1016/j.atmosres.2011.07.009

Cape, J. N., S. E. Cornell, T. D. Jickells, and E. Nemitz (2011b), Organic nitrogen in the atmosphere - Where does it come from? A review of sources and methods, *Atmospheric Research*, *102*(1-2), 30-48, doi: 10.1016/j.atmosres.2011.07.009

Carlson, C. A., and D. A. Hansell (2015), DOM Sources, Sinks, Reactivity and Budgets, in *Biogeochemistry of Marine Dissolved Organic Matter*, edited by D. A. Hansell and C. A. Carlson, pp. 65-126, Elsevier, London.

Carr, M.-E., M. A. M. Friedrichs, M. Schmeltz, M. N. Aita, D. Antoine, K. R. Arrigo, I. Asanuma, O. Aumont, R. Barber, M. Behrenfeld, R. Bidigare, E. T. Buitenhuis, J. Campbell, A. Ciotti, H. Dierssen, M. Dowell, J. Dunne, W. Esaias, B. Gentili, W. Gregg, S. Groom, N. Hoepffner, J. Ishizaka, T. Kameda, C. Le Quéré, S. Lohrenz, J. Marra, F. Mélin, K. Moore, A. Morel, T. E. Reddy, J. Ryan, M. Scardi, T. Smyth, K. Turpie, G. Tilstone, K. Waters, and Y. Yamanaka (2006), A comparison of global estimates of marine primary production from ocean color, *Deep-Sea Res Pt II*, *53*(5-7), 741-770, doi: 10.1016/j.dsr2.2006.01.028

Carstensen, J., J. H. Andersen, B. G. Gustafsson, and D. J. Conley (2014), Deoxygenation of the Baltic Sea during the last century, *Proc Natl Acad Sci U S A*, *111*(15), 5628-5633, doi: 10.1073/pnas.1323156111

Castellari, S., N. Pinardi, and K. Leaman (2000), Simulation of water mass formation processes in the Mediterranean Sea: Influence of the time frequency of the atmospheric forcing, *J Geophys Res Oceans*, *105*(C10), 24157-24181, doi: 10.1029/2000jc900055

Charideh, A., and A. Rahman (2007), Environmental isotopic and hydrochemical study of water in the karst aquifer and submarine springs of the Syrian coast, *Hydrogeology Journal*, *15*(2), 351-364, doi: 10.1007/s10040-006-0072-x

Chen, Y., S. Mills, J. Street, D. Golan, A. Post, M. Jacobson, and A. Paytan (2007), Estimates of atmospheric dry deposition and associated input of nutrients to Gulf of Aqaba seawater, *J Geophys Res-Atmos*, *112*(D4), doi: 10.1029/2006jd007858

Christensen, J. P., T. T. Packard, F. Q. Dortch, H. J. Minas, J. C. Gascard, C. Richez, and P. C. Garfield (1989), Carbon oxidation in the deep Mediterranean Sea: Evidence for dissolved organic carbon source, *Global Biogeochem Cycles*, *3*(4), doi: 10.1029/GB003i004p00315

Christodoulaki, S., G. Petihakis, M. Kanakidou, N. Mihalopoulos, K. Tsiaras, and G. Triantafyllou (2013), Atmospheric deposition in the Eastern Mediterranean. A driving force for ecosystem dynamics, *J Mar Syst*, *109*, 78-93, doi: 10.1016/j.jmarsys.2012.07.007

Christodoulaki, S., G. Petihakis, N. Mihalopoulos, K. Tsiaras, G. Triantafyllou, and M. Kanakidou (2016), Human-Driven Atmospheric Deposition of N and P Controls on the East Mediterranean Marine Ecosystem, *Journal of the Atmospheric Sciences*, *73*(4), 1611-1619, doi: 10.1175/jas-d-15-0241.1

CIESM (2009), Dynamics of Mediterranean deep waters.*Rep.*, 132 pp, Monaco.

Cita, M. B., C. Vergnaudgrazzini, C. Robert, H. Chamley, N. Ciaranfi, and S. Donofrio (1977), Paleoclimatic record of a long deep-sea core from Eastern Mediterranean, *Quat Res*, *8*(2), 205-235, doi: 10.1016/0033-5894(77)90046-1

Civitarese, G., M. Gacic, A. Vetrano, A. Boldrin, D. Bregant, S. Rabitti, and E. Souvermezoglou (1998), Biogeochemical fluxes through the Strait of Otranto (eastern Mediterranean), *Cont Shelf Res*, *18*(7), 773-789, doi: 10.1016/s0278-4343(98)00016-8

Civitarese, G., M. Gačić, M. Lipizer, and G. L. Eusebi Borzelli (2010), On the impact of the Bimodal Oscillating System (BiOS) on the biogeochemistry and biology of the Adriatic and Ionian Seas (Eastern Mediterranean), *Biogeosciences*, *7*(12), 3987-3997, doi: 10.5194/bg-7-3987-2010

Clark, L. L., E. D. Ingall, and R. Benner (1998), Marine phosphorus is selectively remineralized, *Nature*, *393*(6684), 426-426, doi: 10.1038/30881

Codispoti, L. A. (2007), An oceanic fixed nitrogen sink exceeding 400 Tg Na-1 vs the concept of homeostasis in the fixed-nitrogen inventory, *Biogeosciences*, *4*(2), 233-253

Collins, M., R. Knutti, J. Arblaster, J.-L. Dufresne, T. Fichefet, P. Friedlingstein, X. Gao, W.J. Gutowski, T. Johns, G. Krinner, M. Shongwe, C. Tebaldi, A. J. Weaver, and M. Wehner (2013), Long-term Climate Change: Projections, Commitments and Irreversibility, in *Climate Change 2013: The Physical Science Basis. Contribution of Working Group I to the Fifth Assessment Report of the Intergovernmental Panel on Climate Change*, edited by T. F. Stocker, D. Qin, G.-K. Plattner, M. Tignor, S.K. Allen, J. Boschung, A. Nauels, Y. Xia, V. Bex and P. M. Midgley, Cambridge University Press, Cambridge, United Kingdom and New York, NY, USA.

Copin-Montegut, C., and G. Copin-Montegut (1983), Stoichiometry of carbon, nitrogen, and phosphorus in marine particulate matter, *Deep Sea Research Part A. Oceanographic Research Papers*, *30*(1), 31-46, doi: http://dx.doi.org/10.1016/0198-0149(83)90031-6

Copin-Montégut, C. (2000), Consumption and production on scales of a few days of inorganic carbon, nitrate and oxygen by the planktonic community: results of continuous measurements at the Dyfamed Station in the northwestern Mediterranean Sea (May 1995), *Deep Sea Res Part I Oceanogr Res Pap*, *47*(3), 447-477, doi: 10.1016/s0967-0637(99)00098-9

Cordell, D., A. Rosemarin, J. J. Schroder, and A. L. Smit (2011), Towards global phosphorus security: A systems framework for phosphorus recovery and reuse options, *Chemosphere*, *84*(6), 747-758, doi: 10.1016/j.chemosphere.2011.02.032

Cornell, S. E., T. D. Jickells, J. N. Cape, A. P. Rowland, and R. A. Duce (2003), Organic nitrogen deposition on land and coastal environments: a review of methods and data, *Atmos Environ*, *37*(16), 2173-2191, doi: 10.1016/s1352-2310(03)00133-x

Coste, B., H. J. Minas, and M.-C. Bonin (1984), Propriétés hydrologiques et chmiques des eaux du bassin occidental de la Méditerranée. Camagne Medripod IV - 15 Octobre - 17 Novembre 1981*Rep.*, Centre national pour l'exploitation des océans, Brest CEDEX, France.

Coste, B., P. Lecorre, and H. J. Minas (1988), Reevaluation of the nutrient exchanges in the Strait of Gibralter *Deep-Sea Res Pt A*, *35*(5), 767-775, doi: 10.1016/0198-0149(88)90029-5

Criado-Aldeanueva, F., F. J. Soto-Navarro, and J. García-Lafuente (2012), Seasonal and interannual variability of surface heat and freshwater fluxes in the Mediterranean Sea: budgets and exchange through the Strait of Gibraltar, *Int J Climatol*, *32*(2), 286-302, doi: 10.1002/joc.2268

Crispi, G., R. Mosetti, C. Solidoro, and A. Crise (2001), Nutrients cycling in Mediterranean basins: the role of the biological pump in the trophic regime, *Ecol Modell*, *138*(1-3), 101-114, doi: 10.1016/s0304-3800(00)00396-3

Crispi, G., A. Crise, and C. Solidoro (2002), Coupled Mediterranean ecomodel of the phosphorus and nitrogen cycles, *J Mar Syst*, *33*, 497-521, doi: 10.1016/s0924-7963(02)00073-8

Cuypers, Y., P. Bouruet-Aubertot, C. Marec, and J. L. Fuda (2012), Characterization of turbulence from a fine-scale parameterization and microstructure measurements in the Mediterranean Sea during the BOUM experiment, *Biogeosciences*, *9*(8), 3131-3149, doi: 10.5194/bg-9-3131-2012

D'Ortenzio, F. (2003), Did biological activity in the Ionian Sea change after the Eastern Mediterranean Transient? Results from the analysis of remote sensing observations, *Journal of Geophysical Research*, *108*(C9), doi: 10.1029/2002jc001556

D'Ortenzio, F., M. Ragni, S. Marullo, and M. R. d'Alcala (2003), Did biological activity in the Ionian Sea change after the Eastern Mediterranean Transient? Results from the analysis of remote sensing observations, *J Geophys Res Oceans*, *108*, doi: 10.1029/2002jc001556

Dafner, E., R. Boscolo, and H. L. Bryden (2003), The N : Si : P molar ratio in the strait of Gibraltar, *Geophys Res Lett*, *30*(10), doi: 10.1029/2002gl016274

Dale, A. W., P. Regnier, and P. Van Cappellen (2006), Bioenergetic controls on anaerobic oxidation of methane (AOM) in coastal marine sediments: A theoretical analysis, *Am J Sci*, *306*(4), 246-294, doi: 10.2475/ajs.306.4.246

De Lange, G. J., J. Thomson, A. Reitz, C. P. Slomp, M. S. Principato, E. Erba, and C. Corselli (2008), Synchronous basin-wide formation and redox-controlled preservation of a Mediterranean sapropel, *Nat Geosci*, *1*(9), 606-610, doi: 10.1038/ngeo283

de Madron, X. D., L. Denis, F. Diaz, N. Garcia, C. Guieu, C. Grenz, M.-D. Loÿe-Pilot, W. Ludwig, T. Moutin, P. Raimbault, and C. Ridame (2003a), Nutrients and carbon budgets for the Gulf of Lion during the Moogli cruises, *Oceanol Acta*, *26*(4), 421-433, doi: 10.1016/s0399-1784(03)00024-0

de Madron, X. D., L. Denis, F. Diaz, N. Garcia, C. Guieu, C. Grenz, M. D. Loye-Pilot, W. Ludwig, T. Moutin, P. Raimbault, and C. Ridame (2003b), Nutrients and carbon budgets for the Gulf of Lion during the Moogli cruises, *Oceanol Acta*, *26*(4), 421-433, doi: 10.1016/s0399-1784(03)00024-0

de Madron, X. D., V. Zervakis, A. Theocharis, and D. Georgopoulos (2005), Comments on "Cascades of dense water around the world ocean", *Prog Oceanogr*, *64*(1), 83-90, doi: 10.1016/j.pocean.2004.08.004

de Madron, X. D., W. Ludwig, G. Civitarese, M. Gacic, M. Ribera d'Alcala, P. Raimbault, E. Kraskapoulou, and C. Goyet (2010), Marginal Seas: The Mediterranean Sea: The shelf slope systems, in *Carbon and nutrient fluxes in continental margins: a global synthesis*, edited by K.-K. Liu, pp. 364-383, Springer, Berlin.

de Madron, X. D., C. Guieu, R. Sempéré, P. Conan, D. Cossa, F. D'Ortenzio, C. Estournel, F. Gazeau, C. Rabouille, L. Stemmann, S. Bonnet, F. Diaz, P. Koubbi, O. Radakovitch, P. M. Babin, M. Baklouti, C. Bancon-Montigny, S. Belviso, N. Bensoussan, B. Bonsang, I. Bouloubassi, C. Brunet, J. F. Cadiou, F. Carlotti, M. Chami, S. Charmasson, B. Charrière, J. Dachs, D. Doxaran, J. C. Dutay, F. Elbaz-Poulichet, M. Eléaume, F. Eyrolles, C. Fernandez, S. Fowler, P. Francour, J. C. Gaertner, R. Galzin, S. Gasparini, J. F. Ghiglione, J. L. Gonzalez, C. Goyet, L. Guidi, K. Guizien, L. E. Heimbuerger, S. H. M. Jacquet, W. H. Jeffrey, F. Joux, P. Le Hir, K. Leblanc, D. Lefèvre, C. Lejeusne, R. Lemé, M. D. Loÿe-Pilot, M. Mallet, L. Méjanelle, F. Mélin, C. Mellon, B. Mérigot, P. L. Merle, C. Migon, W. L. Miller, L. Mortier, B. Mostajir, L. Mousseau, T. Moutin, J. Para, T. Pérez, A. Petrenko, J. C. Poggiale, L. Prieur, M. Pujo-Pay, V. Pulido, P. Raimbault, A. P. Rees, C. Ridame, J. F. Rontani, D. R. Pino, M. A. Sicre, V. Taillandier, C. Tamburini, T. Tanaka, I. Taupier-Letage, M. Tedetti, P. Testor, H. Thébault, B. Thouvenin, F. Touratier, J. Tronczynski, C. Ulses, F. Van Wambeke, V. Vantrepotte, S. Vaz, and R. Verney

(2011), Marine ecosystems' responses to climatic and anthropogenic forcings in the Mediterranean, *Prog Oceanogr*, *91*(2), 97-166, doi: 10.1016/j.pocean.2011.02.003

de Madron, X. D., L. Houpert, P. Puig, A. Sanchez-Vidal, P. Testor, A. Bosse, C. Estournel, S. Somot, F. Bourrin, M. N. Bouin, M. Beauverger, L. Beguery, A. Calafat, M. Canals, C. Cassou, L. Coppola, D. Dausse, F. D'Ortenzio, J. Font, S. Heussner, S. Kunesch, D. Lefevre, H. Le Goff, J. Martin, L. Mortier, A. Palanques, and P. Raimbault (2013), Interaction of dense shelf water cascading and open-sea convection in the northwestern Mediterranean during winter 2012, *Geophys Res Lett*, *40*(7), doi: 10.1002/grl.50331

Degobbis, D., and M. Gilmartin (1990), Nitrogen, phosphorus and biogenic silicon budgets for the northwestern Adriatic sea, *Oceanol Acta*, *13*(1), 31-45

Degobbis, D., R. Precali, I. Ivancic, N. Smodlaka, D. Fuks, and S. Kveder (2000), Long-term changes in the northern Adriatic ecosystem related to anthropogenic eutrophication, *International Journal of Environment and Pollution*, *13*(1-6), 495-533, doi: 10.1504/ijep.2000.002332

Dell'Anno, A., M. L. Mei, A. Pusceddu, and R. Danovaro (2002), Assessing the trophic state and eutrophication of coastal marine systems: a new approach based on the biochemical composition of sediment organic matter, *Mar Pollut Bull*, *44*(7), 611-622, doi: Pii s0025-326x(01)00302-2 10.1016/s0025-326x(01)00302-2

Denis, L., and C. Grenz (2003), Spatial variability in oxygen and nutrient fluxes at the sediment-water interface on the continental shelf in the Gulf of Lions (NW Mediterranean), *Oceanol Acta*, *26*(4), 373-389, doi: 10.1016/s0399-1784(03)00017-3

Denis-Karafistan, A., J. M. Martin, H. Minas, P. Brasseur, J. Nihoul, and C. Denis (1998), Space and seasonal distributions of nitrates in the Mediterranean Sea derived from a variational inverse model, *Deep Sea Res Part I Oceanogr Res Pap*, *45*(2-3), 387-408, doi: 10.1016/s0967-0637(97)00089-7

Desmidt, E., K. Ghyselbrecht, Y. Zhang, L. Pinoy, B. Van der Bruggen, W. Verstraete, K. Rabaey, and B. Meesschaert (2015), Global Phosphorus Scarcity and Full-Scale P-Recovery Techniques: A Review, *Crit Rev Environ Sci Technol*, *45*(4), 336-384, doi: 10.1080/10643389.2013.866531

DeVries, T., C. Deutsch, F. Primeau, B. Chang, and A. Devol (2012), Global rates of water-column denitrification derived from nitrogen gas measurements, *Nat Geosci*, *5*(8), 547-550, doi: 10.1038/ngeo1515

Diaz, F., and P. Raimbault (2000), Nitrogen regeneration and dissolved organic nitrogen release during spring in a NW Mediterranean coastal zone (Gulf of Lions): implications for the estimation of new production, *Mar Ecol Prog Ser*, *197*, 51-65, doi: 10.3354/meps197051

Diaz, F., P. Raimbault, B. Boudjellal, N. Garcia, and T. Moutin (2001), Early spring phosphorus limitation of primary productivity in a NW Mediterranean coastal zone (Gulf of Lions), *Mar Ecol Prog Ser*, *211*, 51-62, doi: 10.3354/meps211051

Diaz, R., M. Selman, and C. Chique (2011), Global Eutrophic and Hypoxic Coastal Systems. World Resources Institute. Eutrophication and Hypoxia: Nutrient Pollution in Coastal Waters., <wri.org/media/maps/eutrophication/fullscreen.html >, [Accessed 31/10/2014].

Dolan, D. M., and S. C. Chapra (2012), Great Lakes total phosphorus revisited: 1. Loading analysis and update (1994–2008), *J Great Lakes Res*, *38*(4), 730-740, doi: 10.1016/j.jglr.2012.10.001

Doney, S. C., M. Ruckelshaus, J. E. Duffy, J. P. Barry, F. Chan, C. A. English, H. M. Galindo, J. M. Grebmeier, A. B. Hollowed, N. Knowlton, J. Polovina, N. N. Rabalais, W. J. Sydeman, and L. D. Talley (2012), Climate Change Impacts on Marine Ecosystems, in *Annual Review of Marine Science, Vol 4*, edited by C. A. Carlson and S. J. Giovannoni, pp. 11-37.

Doval, M. D., F. F. Perez, and E. Berdalet (1999), Dissolved and particulate organic carbon and nitrogen in the Northwestern Mediterranean, *Deep Sea Res Part I Oceanogr Res Pap*, *46*(3), 511-527, doi: 10.1016/s0967-0637(98)00072-7

Doval, M. D., X. A. Alvarez-Salgado, and F. F. Perez (2001), Organic matter distributions in the Eastern North Atlantic-Azores Front region, *J Mar Syst*, *30*(1-2), 33-49, doi: 10.1016/s0924-7963(01)00036-7

Dowling, C. B., R. J. Poreda, and A. R. Basu (2003), The groundwater geochemistry of the Bengal Basin: Weathering, chemsorption, and trace metal flux to the oceans, *Geochim Cosmochim Acta*, *67*(12), 2117-2136, doi: 10.1016/s0016-7037(02)01306-6

Drira, Z., S. Kmiha-Megdiche, H. Sahnoun, A. Hammami, N. Allouche, M. Tedetti, and H. Ayadi (2016), Assessment of anthropogenic inputs in the surface waters of the southern coastal area of Sfax during spring (Tunisia, Southern Mediterranean Sea), *Mar Pollut Bull*, *104*(1-2), 355-363, doi: 10.1016/j.marpolbul.2016.01.035

Duarte, C. M., M. Holmer, Y. Olsen, D. Soto, N. Marbà, J. Guiu, K. Black, and I. Karakassis (2009), Will the Oceans Help Feed Humanity?, *Bioscience*, *59*(11), 967-976, doi: 10.1525/bio.2009.59.11.8

Duarte, C. M., A. Regaudie-de-Gioux, J. M. Arrieta, A. Delgado-Huertas, and S. Agusti (2013), The Oligotrophic Ocean Is Heterotrophic, in *Annual Review of Marine Science, Vol 5*, edited by C. A. Carlson and S. J. Giovannoni, pp. 551-569.

Dugdale, R. C., and J. J. Goering (1967), Uptake of new and regenerated forms of nitrogen in primary productivity, *Limnol Oceanogr*, *12*(2), 196-&

EEA (2012), Waterbase - UWWTD version 4: Urban Wastewater Treatment directive. , <eea.europa.eu/data-and-maps/data/waterbase-uwwtd-urban-waste-water-treatment-directive-3 >, [Accessed 23/11/2013].

EEA (2013), Changes in wastewater treatment in regions of Europe between 1990 and 2009, <http://www.eea.europa.eu/data-and-maps/figures/changes-in-wastewater-treatment-in-regions-of-europe-between-1990-and-2 >, [Accessed 04/12/13].

El-Gamal, A. A., R. N. Peterson, and W. C. Burnett (2012), Detecting Freshwater Inputs via Groundwater Discharge to Marina Lagoon, Mediterranean Coast, Egypt, *Estuar Coasts*, *35*(6), 1486-1499, doi: 10.1007/s12237-012-9539-2

Emeis, K. C., P. Mara, T. Schlarbaum, J. Möbius, K. Dähnke, U. Struck, N. Mihalopoulos, and M. D. Krom (2010), External N inputs and internal N cycling traced by isotope ratios of nitrate, dissolved reduced nitrogen, and particulate nitrogen in the eastern Mediterranean Sea, *Journal of Geophysical Research-Biogeosciences*, *115*, doi: 10.1029/2009jg001214

Eppley, R. W., and B. J. Peterson (1979), Particulate organic-matter flux and planktonic new production in the deep ocean, *Nature*, *282*(5740), 677-680, doi: 10.1038/282677a0

Erisman, J. W., H. van Grinsven, B. Grizzetti, F. Bouraoui, D. Powlson, M. A. Sutton, A. Bleeker, and S. Reis (2011), The European nitrogen problem in a global perspective, in *The European Nitrogen Assessment*, edited by M. A. Sutton, C. M. Howard, J. W. Erisman, G. Billen, A. Bleeker, P. Grennfelt, H. van Grinsven and B. Grizzetti, Cambridge University Press, Cambridge.

Eurostat (2014), Population connected to wastewater collection and treatment systems, <http://epp.eurostat.ec.europa.eu/tgm/table.do?tab=table&init=1&plugin=1&language=en&pcode=ten00021 >, [Accessed 16/01/14].

Fagerli, H., M. Legrand, S. Preunkert, V. Vestreng, D. Simpson, and M. Cerqueira (2007), Modeling historical long-term trends of sulfate, ammonium, and elemental carbon over Europe: A comparison with ice core records in the Alps, *J Geophys Res-Atmos*, *112*(D23), doi: D23s13 10.1029/2006jd008044

Falkowski, P., R. J. Scholes, E. Boyle, J. Canadell, D. Canfield, J. Elser, N. Gruber, K. Hibbard, P. Hogberg, S. Linder, F. T. Mackenzie, B. Moore, T. Pedersen, Y. Rosenthal, S. Seitzinger, V. Smetacek, and W. Steffen (2000), The global carbon cycle: A test of our knowledge of earth as a system, *Science*, *290*(5490), 291-296, doi: 10.1126/science.290.5490.291

FAO (2003), CLIMAGRImed project: About Mediterranean Region, <http://www.fao.org/sd/climagrimed/c_2_02.html >, [Accessed May, 2013].

FAO (2014), AQUASTAT database - Food and Agriculture Organization of the United Nations (FAO)*Rep.*

Faostat (2013), Food Supply: Livestock and fish primary equivalent <faostat.fao.org/site/610/default.aspx#ancor >, [Accessed 1/12/13].

FAOSTAT (2015a), Fertilizer Consumption: Nitrogenous and Phosphate fertilizers, <http://faostat3.fao.org/download/R/RA/E >, [Accessed 7/05/2016].

FAOSTAT (2015b), Emissions Agriculture: Manure Management: Manure N content, <http://faostat3.fao.org/download/G1/GM/E >, [Accessed 12/05/16].

FAOSTAT (2016), Annual Population, <http://faostat3.fao.org/download/O/OA/E >, [Accessed 13/05/2016].

Federico, G. (2005), *Feeding the World: An Economic History of Agriculture, 1800-2000*, Princeton University Press, Princeton, N.J.

Flecha, S., F. F. Perez, J. Garcia-Lafuente, S. Sammartino, A. F. Rios, and I. Emma Huertas (2015), Trends of pH decrease in the Mediterranean Sea through high frequency observational data: indication of ocean acidification in the basin, *Scientific Reports*, *5*, doi: 10.1038/srep16770

Follmi, K. B. (1996), The phosphorus cycle, phosphogenesis and marine phosphate-rich deposits, *Earth-Sci Rev*, *40*(1-2), 55-124, doi: 10.1016/0012-8252(95)00049-6

Forryan, A., J. T. Allen, E. Edhouse, B. Silburn, K. Reeve, and E. Tesi (2012), Turbulent mixing in the eddy transport of Western Mediterranean Intermediate Water to the Alboran Sea, *Journal of Geophysical Research: Oceans*, *117*(C9), n/a-n/a, doi: 10.1029/2012jc008284

Friedrich, J., F. Janssen, D. Aleynik, H. W. Bange, N. Boltacheva, M. N. Cagatay, A. W. Dale, G. Etiope, Z. Erdem, M. Geraga, A. Gilli, M. T. Gomoiu, P. O. J. Hall, D. Hansson, Y. He, M. Holtappels, M. K. Kirf, M. Kononets, S. Konovalov, A. Lichtschlag, D. M. Livingstone, G. Marinaro, S. Mazlumyan, S. Naeher, R. P. North, G. Papatheodorou, O. Pfannkuche, R. Prien, G. Rehder, C. J. Schubert, T. Soltwedel, S. Sommer, H. Stahl, E. V. Stanev, A. Teaca, A. Tengberg, C. Waldmann, B. Wehrli, and F. Wenzhofer (2014), Investigating hypoxia in aquatic environments: diverse approaches to addressing a complex phenomenon, *Biogeosciences*, *11*(4), 1215-1259, doi: 10.5194/bg-11-1215-2014

Froelich, P. N., M. A. Arthur, W. C. Burnett, M. Deakin, V. Hensley, R. Jahnke, L. Kaul, K. H. Kim, K. Roe, A. Soutar, and C. Vathakanon (1988), Early Diagenesis of organic matter in Peru continental marginal sediments - phosphorite precipitation, *Mar Geol*, *80*(3-4), 309-343, doi: 10.1016/0025-3227(88)90095-3

Fuda, J. L., C. Millot, I. Taupier-Letage, U. Send, and J. M. Bocognano (2000), XBT monitoring of a meridian section across the western Mediterranean Sea, *Deep Sea Res Part I Oceanogr Res Pap*, *47*(11), 2191-2218, doi: 10.1016/s0967-0637(00)00018-2

Gačić, M., G. L. E. Borzelli, G. Civitarese, V. Cardin, and S. Yari (2010), Can internal processes sustain reversals of the ocean upper circulation? The Ionian Sea example, *Geophys Res Lett*, *37*(9), n/a-n/a, doi: 10.1029/2010gl043216

Galloway, J. N., F. J. Dentener, D. G. Capone, E. W. Boyer, R. W. Howarth, S. P. Seitzinger, G. P. Asner, C. C. Cleveland, P. A. Green, E. A. Holland, D. M. Karl, A. F. Michaels, J. H. Porter, A. R. Townsend, and C. J. Vorosmarty (2004), Nitrogen cycles: past, present, and future, *Biogeochemistry*, *70*(2), 153-226, doi: 10.1007/s10533-004-0370-0

Galloway, J. N. (2014), 10.12 - The Global Nitrogen Cycle in *Treatise on Geochemistry (Second Edition)*, edited by K. K. Turekian, pp. 475-498, Elsevier, Oxford.

García Lafuente, J., A. Sánchez Román, G. Díaz del Río, G. Sannino, and J. C. Sánchez Garrido (2007), Recent observations of seasonal variability of the Mediterranean outflow in the Strait of Gibraltar, *Journal of Geophysical Research*, *112*(C10), doi: 10.1029/2006jc003992

Garcia, N., P. Raimbault, E. Gouze, and V. Sandroni (2006), Nitrogen fixation and primary production in western Mediterranean, *C R Biol*, *329*(9), 742-750, doi: 10.1016/j.crvi.2006.06.006

García-Ruiz, J. M., J. I. López-Moreno, S. M. Vicente-Serrano, T. Lasanta–Martínez, and S. Beguería (2011), Mediterranean water resources in a global change scenario, *Earth-Sci Rev*, *105*(3-4), 121-139, doi: 10.1016/j.earscirev.2011.01.006

Garcia-Solsona, E., J. Garcia-Orellana, P. Masque, V. Rodellas, M. Mejias, B. Ballesteros, and J. A. Dominguez (2010), Groundwater and nutrient discharge through karstic coastal springs (Castello, Spain), *Biogeosciences*, *7*(9), 2625-2638, doi: 10.5194/bg-7-2625-2010

Gasparini, G. P., A. Ortona, G. Budillon, M. Astraldi, and E. Sansone (2005), The effect of the Eastern Mediterranean Transient on the hydrographic characteristics in the Strait of Sicily and in the Tyrrhenian Sea, *Deep Sea Res Part I Oceanogr Res Pap*, *52*(6), 915-935, doi: 10.1016/j.dsr.2005.01.001

Gehlen, M., C. Rabouille, U. Ezat, and L. D. GuidiGuilvard (1997), Drastic changes in deep-sea sediment porewater composition induced by episodic input of organic matter, *Limnol Oceanogr*, *42*(5), 980-986

Geider, R. J., and J. La Roche (2002), Redfield revisited: variability of C : N : P in marine microalgae and its biochemical basis, *Eur J Phycol*, *37*(1), 1-17, doi: 10.1017/s0967026201003456

Georgiou, S., A. Mantziafou, S. Sofianos, I. Gertman, E. Ozsoy, S. Somot, and V. Vervatis (2015), Climate variability and deep water mass characteristics in the Aegean Sea (vol 152, pg 146, 2014), *Atmospheric Research*, *153*, 579-579, doi: 10.1016/j.atmosres.2014.10.017

Giorgi, F. (2006), Climate change hot-spots, *Geophys Res Lett*, *33*(8), doi: 10.1029/2006gl025734

Gómez, F., N. González, F. Echevarría, and C. M. García (2000), Distribution and Fluxes of Dissolved Nutrients in the Strait of Gibraltar and its Relationships to Microphytoplankton Biomass, *Estuarine, Coastal and Shelf Science*, *51*(4), 439-449, doi: 10.1006/ecss.2000.0689

Gray, J. S., R. S. S. Wu, and Y. Y. Or (2002), Effects of hypoxia and organic enrichment on the coastal marine environment, *Mar Ecol Prog Ser*, *238*, 249-279, doi: 10.3354/meps238249

Grimm, R., E. Maier-Reimer, U. Mikolajewicz, G. Schmiedl, K. Mueller-Navarra, F. Adloff, K. M. Grant, M. Ziegler, L. J. Lourens, and K.-C. Emeis (2015), Late glacial initiation of Holocene eastern Mediterranean sapropel formation, *Nature Communications*, *6*, doi: 10.1038/ncomms8099

Gu, A. Z., L. Liu, A. Onnis-Hayden, S. Smith, H. Gray, D. Houweling, and I. Takács (2014), Phosphorus Fractionation and Removal in Wastewater Treatment- Implications For Minimizing Effluent Phosphorus, in *White Paper*, edited, p. 136, WERF.

Gualdi, S., S. Somot, L. Li, V. Artale, M. Adani, A. Bellucci, A. Braun, S. Calmanti, A. Carillo, A. Dell'Aquila, M. Déqué, C. Dubois, A. Elizalde, A. Harzallah, D. Jacob, B. L'Hévéder, W. May, P. Oddo, P. Ruti, A. Sanna, G. Sannino, E. Scoccimarro, F. Sevault, and A. Navarra (2013), The CIRCE Simulations: Regional Climate Change Projections with Realistic Representation of the Mediterranean Sea, *Bulletin of the American Meteorological Society*, *94*(1), 65-81, doi: 10.1175/bams-d-11-00136.1

Guerzoni, S., R. Chester, F. Dulac, B. Herut, M. D. Loye-Pilot, C. Measures, C. Migon, E. Molinaroli, C. Moulin, P. Rossini, C. Saydam, A. Soudine, and P. Ziveri (1999), The role of atmospheric deposition in the biogeochemistry of the Mediterranean Sea, *Prog Oceanogr*, *44*(1-3), 147-190

Gustafsson, B. G., F. Schenk, T. Blenckner, K. Eilola, H. E. M. Meier, B. Muller-Karulis, T. Neumann, T. Ruoho-Airola, O. P. Savchuk, and E. Zorita (2012), Reconstructing the Development of Baltic Sea Eutrophication 1850-2006, *Ambio*, *41*(6), 534-548, doi: 10.1007/s13280-012-0318-x

Guyennon, A., M. Baklouti, F. Diaz, J. Palmieri, J. Beuvier, C. Lebaupin-Brossier, T. Arsouze, K. Beranger, J. C. Dutay, and T. Moutin (2015), New insights into the organic carbon export in the Mediterranean Sea from 3-D modeling, *Biogeosciences*, *12*(23), 7025-7046, doi: 10.5194/bg-12-7025-2015

Haddeland, I., J. Heinke, H. Biemans, S. Eisner, M. Florke, N. Hanasaki, M. Konzmann, F. Ludwig, Y. Masaki, J. Schewe, T. Stacke, Z. D. Tessler, Y. Wada, and D. Wisser (2014), Global water resources affected by human interventions and climate change, *Proc Natl Acad Sci U S A*, *111*(9), 3251-3256, doi: 10.1073/pnas.1222475110

Hamoda, M. F. (2004), Water strategies and potential of water reuse in the south Mediterranean countries, *Desalination*, *165*(1-3), 31-41, doi: 10.1016/j.desal.2004.06.004

Heimbürger, L.-E., D. Cossa, B. Thibodeau, A. Khripounoff, V. Mas, J.-F. Chiffoleau, S. Schmidt, and C. Migon (2012), Natural and anthropogenic trace metals in sediments of the Ligurian Sea (Northwestern Mediterranean), *Chemical Geology*, *291*, 141-151, doi: 10.1016/j.chemgeo.2011.10.011

Helcom (2010), Ecosystem Health of the Baltic Sea 2003–2007: HELCOM Initial Holistic Assessment., *Balt. Sea Environ. Proc. No. 122*.

Herrmann, M., C. Estournel, M. Déqué, P. Marsaleix, F. Sevault, and S. Somot (2008a), Dense water formation in the Gulf of Lions shelf: Impact of atmospheric interannual variability and climate change, *Cont Shelf Res*, *28*(15), 2092-2112, doi: 10.1016/j.csr.2008.03.003

Herrmann, M., S. Somot, F. Sevault, C. Estournel, and M. Déqué (2008b), Modeling the deep convection in the northwestern Mediterranean Sea using an eddy-permitting and an eddy-resolving model: Case study of winter 1986–1987, *Journal of Geophysical Research*, *113*(C4), doi: 10.1029/2006jc003991

Herrmann, M., J. Bouffard, and K. Béranger (2009), Monitoring open-ocean deep convection from space, *Geophys Res Lett*, *36*(3), doi: 10.1029/2008gl036422

Herrmann, M., C. Estournel, F. Adloff, and F. Diaz (2014), Impact of climate change on the northwestern Mediterranean Sea pelagic planktonic ecosystem and associated carbon cycle, *J Geophys Res Oceans*, *119*(9), 5815-5836, doi: 10.1002/2014jc010016

Herut, B., M. D. Krom, G. Pan, and R. Mortimer (1999), Atmospheric input of nitrogen and phosphorus to the Southeast Mediterranean: Sources, fluxes, and possible impact, *Limnol Oceanogr*, *44*(7), 1683-1692

Hidalgo, D., and R. Irusta The cost of wastewater reclamation and reuse in agricultural production in Mediterranean countries, paper presented at Proceedings of the IWA International Conference on Water, Economics, Statistics and Finance-Rethymno, Rethymo, Greece, 8–10 July 2005.

Hopkinson, C. S., and J. J. Vallino (2005), Efficient export of carbon to the deep ocean through dissolved organic matter, *Nature*, *433*(7022), 142-145, doi: 10.1038/nature03191

Howarth, R. W., and R. Marino (2006), Nitrogen as the limiting nutrient for eutrophication in coastal marine ecosystems: Evolving views over three decades, *Limnol Oceanogr*, *51*(1), 364-376

Huertas, I. E., A. F. Ríos, J. García-Lafuente, G. Navarro, A. Makaoui, A. Sánchez-Román, S. Rodriguez-Galvez, A. Orbi, J. Ruíz, and F. F. Pérez (2012), Atlantic forcing of the Mediterranean oligotrophy, *Global Biogeochem Cycles*, *26*(2), n/a-n/a, doi: 10.1029/2011gb004167

Ibello, V., C. Cantoni, S. Cozzi, and G. Civitarese (2010a), First basin-wide experimental results on N-2 fixation in the open Mediterranean Sea, *Geophys Res Lett*, *37*, doi: 10.1029/2009gl041635

Ibello, V., C. Cantoni, S. Cozzi, and G. Civitarese (2010b), First basin-wide experimental results on N2fixation in the open Mediterranean Sea, *Geophys Res Lett*, *37*(3), n/a-n/a, doi: 10.1029/2009gl041635

Incarbona, A., B. Martrat, P. G. Mortyn, M. Sprovieri, P. Ziveri, A. Gogou, G. Jordà, E. Xoplaki, J. Luterbacher, L. Langone, G. Marino, L. Rodríguez-Sanz, M. Triantaphyllou, E. Di Stefano, J. O. Grimalt, G. Tranchida, R. Sprovieri, and S. Mazzola (2016), Mediterranean circulation perturbations over the last five centuries: Relevance to past Eastern Mediterranean Transient-type events, *Scientific Reports*, *6*, 29623, doi: 10.1038/srep29623

IPCC (2013), Annex II: Climate System Scenario Tables [Prather, M., G. Flato, P. Friedlingstein, C. Jones, J.-F. Lamarque, H. Liao and P. Rasch (eds.)], in *Climate Change 2013: The Physical Science Basis. Contribution of Working Group I to the Fifth Assessment Report of the Intergovernmental Panel on Climate Change*, edited by T. F. Stocker, D. Qin, G.-K. Plattner, M. Tignor, S.K. Allen, J. Boschung, A. Nauels, Y. Xia, V. Bex and P. M. Midgley, Cambridge University Press, Cambridge, United Kingdom and New York, NY, USA.

Ito, A., and J. E. Penner (2005), Historical emissions of carbonaceous aerosols from biomass and fossil fuel burning for the period 1870-2000, *Global Biogeochem Cycles*, *19*(2), doi: 10.1029/2004gb002374

Jickells, T., A. R. Baker, J. N. Cape, S. E. Cornell, and E. Nemitz (2013), The cycling of organic nitrogen through the atmosphere, *Philosophical Transactions of the Royal Society B-Biological Sciences*, *368*(1621), doi: 10.1098/rstb.2013.0115

Justic, D. (1987), Long term eutrophication of the northern Adriatic Sea *Mar Pollut Bull*, *18*(6), 281-284, doi: 10.1016/0025-326x(87)90505-4

Justic, D., T. Legovic, and L. Rottinisandrini (1987), Trends in oxygen content 1911-1984 and occurence of benthic mortality in the northern Adriatic Sea, *Estuarine Coastal Shelf Sci*, *25*(4), 435-445, doi: 10.1016/0272-7714(87)90035-7

Kanakidou, M., R. A. Duce, J. M. Prospero, A. R. Baker, C. Benitez-Nelson, F. J. Dentener, K. A. Hunter, P. S. Liss, N. Mahowald, G. S. Okin, M. Sarin, K. Tsigaridis, M. Uematsu, L. M. Zamora, and T. Zhu (2012), Atmospheric fluxes of organic N and P to the global ocean, *Global Biogeochem Cycles*, *26*, doi: 10.1029/2011gb004277

Kanakidou, M., S. Myriokefalitakis, N. Daskalakis, G. Fanourgakis, A. Nenes, A. R. Baker, K. Tsigaridis, and N. Mihalopoulos (2016), Past, Present, and Future Atmospheric Nitrogen Deposition, *Journal of the Atmospheric Sciences*, *73*(5), 2039-2047, doi: 10.1175/jas-d-15-0278.1

Karafistan, A., J. M. Martin, M. Rixen, and J. M. Beckers (2002), Space and time distributions of phosphate in the Mediterranean Sea, *Deep Sea Res Part I Oceanogr Res Pap*, *49*(1), 67-82

Karl, D. M., and K. M. Björkman (2015), Dynamics of dissolved organic phosphorus, in *Biogeochemistry of marine dissolved organic matter*, edited by D. A. Hansell and C. A. Carlson, Academic Press, London, Uk.

Karydis, M., and D. Kitsiou (2012), Eutrophication and environmental policy in the Mediterranean Sea: a review, *Environ Monit Assess*, *184*(8), 4931-4984, doi: 10.1007/s10661-011-2313-2

Katsanevakis, S., M. Coll, C. Piroddi, J. Steenbeek, F. Ben Rais Lasram, A. Zenetos, and A. C. Cardoso (2014), Invading the Mediterranean Sea: biodiversity patterns shaped by human activities, *Frontiers in Marine Science*, *1*(32), doi: 10.3389/fmars.2014.00032

Kershaw, F. (2008), Data layers showing mean sea surface productivity in June and December, for the period 2003-2007. Using data from Oregon State University's Ocean productivity database. Cambridge(UK): UNEP World Conservation Monitoring Centre, <data.unep-wcmc.org/datasets/4 >, [Accessed 12/08/2014].

Kim, T.-H., E. Kwon, I. Kim, S.-A. Lee, and G. Kim (2013), Dissolved organic matter in the subterranean estuary of a volcanic island, Jeju: Importance of dissolved organic nitrogen fluxes to the ocean, *J Sea Res*, *78*, 18-24, doi: 10.1016/j.seares.2012.12.009

Kirtman, B., S.B. Power, J.A. Adedoyin, G.J. Boer, R. Bojariu, I. Camilloni, F.J. Doblas-Reyes, A.M. Fiore, M. Kimoto, G.A. Meehl, M. Prather, A. Sarr, C. Schär, R. Sutton, G.J. van Oldenborgh, G. Vecchi, and H. J. Wang (2013), Near-term Climate Change: Projections and Predictability, in *Climate Change 2013: The Physical Science Basis. Contribution of Working Group I to the Fifth Assessment Report of the Intergovernmental Panel on Climate Change*, edited by T. F. Stocker, D. Qin, G.-K. Plattner, M. Tignor, S.K. Allen, J. Boschung, A. Nauels, Y. Xia, V. Bex and P. M. Midgley, Cambridge University Press, Cambridge, United Kingdom and New York, NY, USA.

Klausmeier, C. A., E. Litchman, T. Daufresne, and S. A. Levin (2004), Optimal nitrogen-to-phosphorus stoichiometry of phytoplankton, *Nature*, *429*(6988), 171-174, doi: 10.1038/nature02454

Klein, B., W. Roether, B. B. Manca, D. Bregant, V. Beitzel, V. Kovacevic, and A. Luchetta (1999), The large deep water transient in the Eastern Mediterranean, *Deep Sea Res Part I Oceanogr Res Pap*, *46*(3), 371-414

Klein, B., W. Roether, N. Kress, B. B. Manca, M. R. d'Alcala, E. Souvermezoglou, A. Theocharis, G. Civitarese, and A. Luchetta (2003), Accelerated oxygen consumption in eastern Mediterranean deep waters following the recent changes in thermohaline circulation, *J Geophys Res Oceans*, *108*(C9), doi: 8107 10.1029/2002jc001454

Kouvarakis, G., N. Mihalopoulos, A. Tselepides, and S. Stavrakakis (2001), On the importance of atmospheric inputs of inorganic nitrogen species on the productivity of the Eastern Mediterranean Sea, *Global Biogeochem Cycles*, *15*(4), 805-817, doi: 10.1029/2001gb001399

Krasakopoulou, E., E. Souvermezoglou, A. Pavlidou, and H. Kontoyiannis (1999), Oxygen and nutrient fluxes through the Straits of the Cretan Arc (March 1994-January 1995), *Prog Oceanogr*, *44*(4), 601-624

Kress, N., and B. Herut (2001), Spatial and seasonal evolution of dissolved oxygen and nutrients in the Southern Levantine Basin (Eastern Mediterranean Sea): chemical characterization of the water

masses and inferences on the N : P ratios, *Deep Sea Res Part I Oceanogr Res Pap*, *48*(11), 2347-2372

Kress, N., B. B. Manca, B. Klein, and D. Deponte (2003), Continuing influence of the changed thermohaline circulation in the eastern Mediterranean on the distribution of dissolved oxygen and nutrients: Physical and chemical characterization of the water masses, *J Geophys Res Oceans*, *108*(C9), doi: 8109 10.1029/2002jc001397

Kress, N., H. Herut, and I. Gertman (2012), Nutrient Distribution in the Eastern Mediterranean before and after the Transient Event, in *Life in the Mediterranean Sea: A look at Habitat changes*, edited by N. Stambler, pp. 157-174, Nova Science Publishers.

Kress, N., I. Gertman, and B. Herut (2014), Temporal evolution of physical and chemical characteristics of the water column in the Easternmost Levantine basin (Eastern Mediterranean Sea) from 2002 to 2010, *J Mar Syst*, *135*, 6-13, doi: 10.1016/j.jmarsys.2013.11.016

Kristensen, P., B. Fribourg-Blanc, and S. Nixon (2004), Outlooks on Nutrient Discharges in Europe from Urban Waste Water Treatment Plants. *Rep. Final Draft*, 33 pp.

Kroeger, K. D., P. W. Swarzenski, W. J. Greenwood, and C. Reich (2007), Submarine groundwater discharge to Tampa Bay: Nutrient fluxes and biogeochemistry of the coastal aquifer, *Mar Chem*, *104*(1-2), 85-97, doi: 10.1016/j.marchem.2006.10.012

Krom, M. D., N. Kress, S. Brenner, and L. I. Gordon (1991), Phosphorus limitation of primary productivity in the Eastern Mediterranean, *Limnol Oceanogr*, *36*(3), 424-432

Krom, M. D., S. Brenner, N. Kress, A. Neori, and L. I. Gordon (1992), Nutrient dynamics and new production in a warm-core eddy from the Eastern Mediterranean, *Deep-Sea Res Pt A*, *39*(3-4A), 467-480, doi: 10.1016/0198-0149(92)90083-6

Krom, M. D., S. Groom, and T. Zohary (2003), The Eastern Mediterranean, in *Biogeochemistry of Marine Systems*, edited by K. D. Black and G. S. Shimmield, pp. 91-126, Blackwell Publishing, Oxford, UK.

Krom, M. D., B. Herut, and R. F. C. Mantoura (2004), Nutrient budget for the Eastern Mediterranean: Implications for phosphorus limitation, *Limnol Oceanogr*, *49*(5), 1582-1592

Krom, M. D., E. M. S. Woodward, B. Herut, N. Kress, P. Carbo, R. F. C. Mantoura, G. Spyres, T. F. Thingstad, P. Wassmann, C. Wexels-Riser, V. Kitidis, C. S. Law, and G. Zodiatis (2005), Nutrient cycling in the south east Levantine basin of the eastern Mediterranean: Results from a phosphorus starved system, *Deep-Sea Res Pt II*, *52*(22-23), 2879-2896, doi: 10.1016/j.dsr.2005.08.009

Krom, M. D., K. C. Emeis, and P. Van Cappellen (2010), Why is the Eastern Mediterranean phosphorus limited?, *Prog Oceanogr*, *85*(3-4), 236-244, doi: 10.1016/j.pocean.2010.03.003

Krom, M. D., N. Kress, I. Berman-Frank, and E. Rahav (2014), Past, present and future patterns in the nutrient chemistry of the Eastern Mediterranean., in *The Mediterranean Sea. Its history and present challenges.*, edited by Goffredo S and D. Z, Springer, Dordrecht.

L'Helguen, S., P. Le Corre, C. Madec, and P. Morin (2002), New and regenerated production in the Almeria-Oran front area, eastern Alboran Sea, *Deep Sea Res Part I Oceanogr Res Pap*, *49*(1), 83-99, doi: 10.1016/s0967-0637(01)00044-9

L'Hévéder, B., L. Li, F. Sevault, and S. Somot (2013), Interannual variability of deep convection in the Northwestern Mediterranean simulated with a coupled AORCM, *Clim Dynam*, *41*(3-4), 937-960, doi: 10.1007/s00382-012-1527-5

La Corre, P., P. Morin, and J.-L. Birrien (1984), Repartition de la matiere organique dissoute (N et P dissous), in *Propriétés hydrologiques et chmiques des eaux du bassin occidental de la Méditerranée. Camagne Medripod IV - 15 Octobre - 17 Novembre 1981*, edited by B. Coste, H. J. Minas and M.-C. Bonin, Centre national pour l'exploitation des océans.

Lamarque, J. F., T. C. Bond, V. Eyring, C. Granier, A. Heil, Z. Klimont, D. Lee, C. Liousse, A. Mieville, B. Owen, M. G. Schultz, D. Shindell, S. J. Smith, E. Stehfest, J. Van Aardenne, O. R. Cooper, M. Kainuma, N. Mahowald, J. R. McConnell, V. Naik, K. Riahi, and D. P. van Vuuren (2010), Historical (1850-2000) gridded anthropogenic and biomass burning emissions of reactive gases

and aerosols: methodology and application, *Atmos Chem Phys*, *10*(15), 7017-7039, doi: 10.5194/acp-10-7017-2010

Lamarque, J. F., F. Dentener, J. McConnell, C. U. Ro, M. Shaw, R. Vet, D. Bergmann, P. Cameron-Smith, S. Dalsoren, R. Doherty, G. Faluvegi, S. J. Ghan, B. Josse, Y. H. Lee, I. A. MacKenzie, D. Plummer, D. T. Shindell, R. B. Skeie, D. S. Stevenson, S. Strode, G. Zeng, M. Curran, D. Dahl-Jensen, S. Das, D. Fritzsche, and M. Nolan (2013), Multi-model mean nitrogen and sulfur deposition from the Atmospheric Chemistry and Climate Model Intercomparison Project (ACCMIP): evaluation of historical and projected future changes, *Atmos Chem Phys*, *13*(16), 7997-8018, doi: 10.5194/acp-13-7997-2013

Larsson, U., R. Elmgren, and F. Wulff (1985), Eutrophication and the Baltic Sea - causes and consequences, *Ambio*, *14*(1), 9-14

Laruelle, G. G., H. H. Dürr, R. Lauerwald, J. Hartmann, C. P. Slomp, N. Goossens, and P. A. G. Regnier (2013), Global multi-scale segmentation of continental and coastal waters from the watersheds to the continental margins, *Hydrology and Earth System Sciences*, *17*(5), 2029-2051, doi: 10.5194/hess-17-2029-2013

Lasaga, A. C. (1980), The kinetic treatment of geochemical cycles, *Geochim Cosmochim Acta*, *44*(6), 815-828, doi: 10.1016/0016-7037(80)90263-x

Lascaratos, A. (1993), Estimation of deep and intermediate water mass formation rates in the Mediterranean Sea, *Deep Sea Research Part II: Topical Studies in Oceanography*, *40*(6), 1327-1332, doi: http://dx.doi.org/10.1016/0967-0645(93)90072-U

Lascaratos, A., W. Roether, K. Nittis, and B. Klein (1999), Recent changes in deep water formation and spreading in the eastern Mediterranean Sea: a review, *Prog Oceanogr*, *44*(1-3), 5-36

Lavezza, R., L. Dubroca, F. Conversano, D. Ludicone, N. Kress, B. Herut, G. Civitarese, A. Cruzado, D. Lefevre, K. Souvermezoglou, A. Yilmaz, S. Tugrul, and M. Ribera d'Alcala (2011), Compilation of quality controlled nutrient profiles from the Mediterranean Sea. http://doi.pangaea.de/10.1594/PANGAEA.771907 Supplement to: Lavezza, R; Dubroca, L Conversano, F; Iudicone, D; Kress, N; Herut, B; Civitarese, G; Cruzado, A; Lefèvre, D; Souvermezoglou, K; Yilmaz, A; Tugrul, S; Ribera d'Alcala, M. (2011): MED-Nut, a new Quality Controlled nutrient data base for the Mediterranean Sea. (PDI-828), in prep.

Lazzari, P., C. Solidoro, V. Ibello, S. Salon, A. Teruzzi, K. Béranger, S. Colella, and A. Crise (2012), Seasonal and inter-annual variability of plankton chlorophyll and primary production in the Mediterranean Sea: a modelling approach, *Biogeosciences*, *9*(1), 217-233, doi: 10.5194/bg-9-217-2012

Lazzari, P., G. Mattia, C. Solidoro, S. Salon, A. Crise, M. Zavatarelli, P. Oddo, and M. Vichi (2014), The impacts of climate change and environmental management policies on the trophic regimes in the Mediterranean Sea: Scenario analyses, *J Mar Syst*, *135*, 137-149, doi: 10.1016/j.jmarsys.2013.06.005

Lazzari, P., C. Solidoro, S. Salon, and G. Bolzon (2016), Spatial variability of phosphate and nitrate in the Mediterranean Sea: A modeling approach, *Deep Sea Res Part I Oceanogr Res Pap*, *108*, 39-52, doi: 10.1016/j.dsr.2015.12.006

Le Corre, P., P. Morin, and J.-L. Birrien (1984), Repartition de la matiere organique dissoute (N et P dissous), in *Propriétés hydrologiques et chimiques des eaux du bassin occidental de la Méditerranée: Campagne MEDRIPOD IV 15 octobre-17 Novembre 1981*, edited.

LeBolloch, O., and S. Guerzoni (1995), Acid and alkaline deposition in precipitation on the western coast of Sardinia, Central Mediterranean (40 degrees N, 8 degrees E), *Water Air Soil Pollut*, *85*(4), 2155-2160

Lefèvre, D., M. Denis, C. E. Lambert, and J. C. Miquel (1996), Is DOC the main source of organic matter remineralization in the ocean water column?, *J Mar Syst*, *7*(2-4), 281-291, doi: 10.1016/0924-7963(95)00003-8

Lejeusne, C., P. Chevaldonne, C. Pergent-Martini, C. F. Boudouresque, and T. Perez (2010), Climate change effects on a miniature ocean: the highly diverse, highly impacted Mediterranean Sea, *Trends Ecol Evol*, *25*(4), 250-260

Letscher, R. T., F. Primeau, and J. K. Moore (2016), Nutrient budgets in the subtropical ocean gyres dominated by lateral transport, *Nature Geosci*, *9*(11), 815-819, doi: 10.1038/ngeo2812

Levy, M., L. Memery, and J. M. Andre (1998), Simulation of primary production and export fluxes in the Northwestern Mediterranean Sea, *J Mar Res*, *56*(1), 197-238, doi: 10.1357/002224098321836163

Lohrenz, S. E., G. A. Knauer, V. L. Asper, M. Tuel, A. F. Michaels, and A. H. Knap (1992), Seasonal variability in primary production and particle-flux in the northwestern Sargasso Sea - United-States JGOFS Bermuda Atlantic time-series study, *Deep-Sea Res Pt A*, *39*(7-8A), 1373-1391

Longo, A. F., E. D. Ingall, J. M. Diaz, M. Oakes, L. E. King, A. Nenes, N. Mihalopoulos, K. Violaki, A. Avila, C. R. Benitez-Nelson, J. Brandes, I. McNulty, and D. J. Vine (2014), P-NEXFS analysis of aerosol phosphorus delivered to the Mediterranean Sea, *Geophys Res Lett*, *41*(11), 4043-4049, doi: 10.1002/2014gl060555

Lopez-Vazquez, C. M., C. M. Hooijmans, D. Brdjanovic, H. J. Gijzen, and M. C. M. van Loosdrecht (2008), Factors affecting the microbial populations at full-scale enhanced biological phosphorus removal (EBPR) wastewater treatment plants in the Netherlands, *Water Res*, *42*(10-11), 2349-2360, doi: 10.1016/j.watres.2008.01.001

Loÿe-Pilot, M. D., J. M. Martin, and J. Morelli (1990), Atmospheric input of inorganic nitrogen to the Western Mediterranean, *Biogeochemistry*, *9*(2), 117-134, doi: 10.1007/bf00692168

Lucea, A., C. M. Duarte, S. Agusti, and M. Sondergaard (2003), Nutrient (N, P and Si) and carbon partitioning in the stratified NW Mediterranean, *J Sea Res*, *49*(3), 157-170, doi: 10.1016/s1385-1101(03)00005-4

Ludwig, W., E. Dumont, M. Meybeck, and S. Heussner (2009), River discharges of water and nutrients to the Mediterranean and Black Sea: Major drivers for ecosystem changes during past and future decades?, *Prog Oceanogr*, *80*(3-4), 199-217, doi: 10.1016/j.pocean.2009.02.001

Ludwig, W., A. F. Bouwman, E. Dumont, and F. Lespinas (2010), Water and nutrient fluxes from major Mediterranean and Black Sea rivers: Past and future trends and their implications for the basin-scale budgets, *Global Biogeochem Cycles*, *24*, GB0A13. doi:10.1029/2009gb003594, doi: 10.1029/2009gb003594

Luna, G. M., S. Bianchelli, F. Decembrini, E. De Domenico, R. Danovaro, and A. Dell'Anno (2012), The dark portion of the Mediterranean Sea is a bioreactor of organic matter cycling, *Global Biogeochem Cycles*, *26*, doi: 10.1029/2011gb004168

Macias, D., A. P. Martin, J. Garcia-Lafuente, C. M. Garcia, A. Yool, M. Bruno, A. Vazquez-Escobar, A. Izquierdo, D. V. Sein, and F. Echevarria (2007), Analysis of mixing and biogeochemical tides on the Atlantic-Mediterranean effects induced by flow in the Strait of Gibraltar through a physical-biological coupled model, *Prog Oceanogr*, *74*(2-3), 252-272, doi: 10.1016/j.pocean.2007.04.006

Macias, D., E. Garcia-Gorriz, C. Piroddi, and A. Stips (2014), Biogeochemical control of marine productivity in the Mediterranean Sea during the last 50 years, *Global Biogeochem Cycles*, *28*(8), 897-907, doi: 10.1002/2014gb004846

Macias, D., E. Garcia-Gorriz, and A. Stips (2015), Productivity changes in the Mediterranean Sea for the twenty-first century in response to changes in the regional atmospheric forcing, *Frontiers in Marine Science*, *2*(79), doi: 10.3389/fmars.2015.00079

Macías, D., A. P. Martin, J. García-Lafuente, C. M. García, A. Yool, M. Bruno, A. Vázquez-Escobar, A. Izquierdo, D. V. Sein, and F. Echevarría (2007), Analysis of mixing and biogeochemical effects induced by tides on the Atlantic–Mediterranean flow in the Strait of Gibraltar through a physical–biological coupled model, *Prog Oceanogr*, *74*(2-3), 252-272, doi: 10.1016/j.pocean.2007.04.006

Mackenzie, F. T., L. M. Vera, and A. Lerman (2002), Century-scale nitrogen and phosphorus controls of the carbon cycle, *Chemical Geology*, *190*(1-4), 13-32, doi: 10.1016/s0009-2541(02)00108-0

Mackenzie, F. T., E. H. De Carlo, and A. Lerman (2011), 5.10 - Coupled C, N, P, and O Biogeochemical Cycling at the Land–Ocean Interface, in *Treatise on Estuarine and Coastal Science*, edited, pp. 317-342, Academic Press, Waltham.

Makings, U., I. R. Santos, D. T. Maher, L. Golsby-Smith, and B. D. Eyre (2014), Importance of budgets for estimating the input of groundwater-derived nutrients to an eutrophic tidal river and estuary, *Estuarine Coastal Shelf Sci*, *143*, 65-76, doi: 10.1016/j.ecss.2014.02.003

Malanotte-Rizzoli, P., B. Manca, M. R. d'Alcala, and A. Theocharis (1999), The eastern Mediterranean in the 80's and in the 90's: The big transition emerged from the POEM-BC observational evidence, in *Eastern Mediterranean as a Laboratory Basin for the Assessment of Contrasting Ecosystems*, edited by P. MalanotteRizzoli and V. N. Eremeev, pp. 1-6.

Manzella, G. M. R., G. P. Gasparini, and M. Astraldi (1988), Water exchange between the Eastern and Western Mediterranean through the Straits of Sicily, *Deep-Sea Res Pt A*, *35*(6), 1021-1035

Marbà, N., G. Jorda, S. Agusti, C. Girard, and C. M. Duarte (2015), Footprints of climate change on Mediterranean Sea biota, *Frontiers in Marine Science*, *2*(56), doi: 10.3389/fmars.2015.00056

Markaki, Z., M. D. Loÿe-Pilot, K. Violaki, L. Benyahya, and N. Mihalopoulos (2010), Variability of atmospheric deposition of dissolved nitrogen and phosphorus in the Mediterranean and possible link to the anomalous seawater N/P ratio, *Mar Chem*, *120*(1-4), 187-194, doi: 10.1016/j.marchem.2008.10.005

Marty, J. C., J. Chiaverini, M. D. Pizay, and B. Avril (2002), Seasonal and interannual dynamics of nutrients and phytoplankton pigments in the western Mediterranean Sea at the DYFAMED time-series station (1991-1999), *Deep-Sea Res Pt II*, *49*(11), 1965-1985, doi: 10.1016/s0967-0645(02)00022-x

Marty, J. C., M. Goutx, C. Guigue, N. Leblond, and P. Raimbault (2009), Short-term changes in particulate fluxes measured by drifting sediment traps during end summer oligotrophic regime in the NW Mediterranean Sea, *Biogeosciences*, *6*(5), 887-899

Marty, J. C., and J. Chiaverini (2010), Hydrological changes in the Ligurian Sea (NW Mediterranean, DYFAMED site) during 1995-2007 and biogeochemical consequences, *Biogeosciences*, *7*(7), 2117-2128, doi: 10.5194/bg-7-2117-2010

Masqué, P., J. Fabres, M. Canals, J. A. Sanchez-Cabeza, A. Sanchez-Vidal, I. Cacho, A. M. Calafat, and J. M. Bruach (2003), Accumulation rates of major constituents of hemipelagic sediments in the deep Alboran Sea: a centennial perspective of sedimentary dynamics, *Mar Geol*, *193*(3-4), 207-233, doi: 10.1016/s0025-3227(02)00593-5

Mattia, G., M. Zavatarelli, M. Vichi, and P. Oddo (2013), The Eastern Mediterranean Sea biogeochemical dynamics in the 1990s: A numerical study, *Journal of Geophysical Research: Oceans*, *118*(4), 2231-2248, doi: 10.1002/jgrc.20160

McCarthy, J. J., C. Garside, J. L. Nevins, and R. T. Barber (1996), New production along 140 degrees W in the equatorial Pacific during and following the 1992 El Nino event, *Deep-Sea Res Pt II*, *43*(4-6), 1065-1093, doi: 10.1016/0967-0645(96)00022-7

McDonald, R. I., P. Green, D. Balk, B. M. Fekete, C. Revenga, M. Todd, and M. Montgomery (2011), Urban growth, climate change, and freshwater availability, *Proc Natl Acad Sci U S A*, *108*(15), 6312-6317, doi: 10.1073/pnas.1011615108

McGill, D. A. (1961), A preliminary study of oxygen and phosphate distribution in the Mediterranean Sea, *Deep-Sea Res*, *8*(3-4), 259-269, doi: 10.1016/0146-6313(61)90027-2

MEDAR Group (2002), MEDATLAS/2002 database. Mediterranean and Black Sea database of temperature salinity and bio-chemical parameters. Climatological Atlas. , edited, IFREMER Edition (4 Cdroms).

Medoc Group (1970), Observation of Formation of Deep Water in the Mediterranean Sea, 1969, *Nature*, *227*, 1037-1040

Mercado, J. M., D. Cortes, T. Ramirez, and F. Gomez (2012), Decadal weakening of the wind-induced upwelling reduces the impact of nutrient pollution in the Bay of Malaga (western Mediterranean Sea), *Hydrobiologia*, *680*(1), 91-107, doi: 10.1007/s10750-011-0906-y

Metcalfe & Eddy Inc, T., G., Burton, F., & Stensel, H. D. (2002), *Wastewater engineering treatment and reuse*, 1848 pp., McGraw-Hill Education.

Micheli, F., B. S. Halpern, S. Walbridge, S. Ciriaco, F. Ferretti, S. Fraschetti, R. Lewison, L. Nykjaer, and A. A. Rosenberg (2013), Cumulative Human Impacts on Mediterranean and Black Sea Marine Ecosystems: Assessing Current Pressures and Opportunities, *PLoS ONE*, *8*(12), doi: 10.1371/journal.pone.0079889

Migon, C., G. Copinmontegut, L. Elegant, and J. Morelli (1989), Atmospheirc input of nutrients to the coastal mediterranean area - biogeochemical implications, *Oceanol Acta*, *12*(2), 187-191

Migon, C., and V. Sandroni (1999), Phosphorus in rainwater: Partitioning inputs and impact on the surface coastal ocean, *Limnol Oceanogr*, *44*(4), 1160-1165

Migon, C., V. Sandroni, and J. P. Béthoux (2001), Atmospheric input of anthropogenic phosphorus to the northwest Mediterranean under oligotrophic conditions, *Mar Environ Res*, *52*(5), 413-426, doi: 10.1016/s0141-1136(01)00095-2

Mikaelyan, A. S., A. G. Zatsepin, and V. K. Chasovnikov (2013), Long-term changes in nutrient supply of phytoplankton growth in the Black Sea, *J Mar Syst*, *117*, 53-64, doi: 10.1016/j.jmarsys.2013.02.012

Millero, F. J., D. Means, and C. Miller (1978), Densities of Mediterranean Sea Waters, *Deep-Sea Res*, *25*(6), 563-569, doi: 10.1016/0146-6291(78)90644-6

Millot, C. (1999), Circulation in the Western Mediterranean Sea, *J Mar Syst*, *20*(1-4), 423-442, doi: 10.1016/s0924-7963(98)00078-5

Millot, C. (2009), Another description of the Mediterranean Sea outflow, *Prog Oceanogr*, *82*(2), 101-124, doi: 10.1016/j.pocean.2009.04.016

Millot, C. (2014), Heterogeneities of in- and out-flows in the Mediterranean Sea, *Prog Oceanogr*, *120*, 254-278, doi: 10.1016/j.pocean.2013.09.007

Mills, M. M., C. Ridame, M. Davey, J. La Roche, and R. J. Geider (2004), Iron and phosphorus co-limit nitrogen fixation in the eastern tropical North Atlantic, *Nature*, *429*(6989), 292-294, doi: http://www.nature.com/nature/journal/v429/n6989/suppinfo/nature02550_S1.html

Mongin, M., D. M. Nelson, P. Pondaven, M. A. Brzezinski, and P. Treguer (2003), Simulation of upper-ocean biogeochemistry with a flexible-composition phytoplankton model: C, N and Si cycling in the western Sargasso Sea, *Deep Sea Res Part I Oceanogr Res Pap*, *50*(12), 1445-1480, doi: 10.1016/j.dsr.2003.08.003

Moon, J.-Y., K. Lee, T. Tanhua, N. Kress, and I.-N. Kim (2016), Temporal nutrient dynamics in the Mediterranean Sea in response to anthropogenic inputs, *Geophys Res Lett*, *43*(10), 5243-5251, doi: 10.1002/2016gl068788

Morée, A. L., A. H. W. Beusen, A. F. Bouwman, and W. J. Willems (2013), Exploring global nitrogen and phosphorus flows in urban wastes during the twentieth century, *Global Biogeochem Cycles*, *27*(3), 836-846, doi: 10.1002/gbc.20072

Moutin, T., and P. Raimbault (2002), Primary production, carbon export and nutrients availability in western and eastern Mediterranean Sea in early summer 1996 (MINOS cruise), *J Mar Syst*, *33*, 273-288, doi: 10.1016/s0924-7963(02)00062-3

Myers, P. G., and K. Haines (2000), Seasonal and interannual variability in a model of the Mediterranean under derived flux forcing, *J Phys Oceanogr*, *30*(5), 1069-1082

Nenes, A., M. D. Krom, N. Mihalopoulos, P. Van Cappellen, Z. Shi, A. Bougiatioti, P. Zarmpas, and B. Herut (2011), Atmospheric acidification of mineral aerosols: a source of bioavailable phosphorus for the oceans, *Atmos Chem Phys*, *11*(13), 6265-6272, doi: 10.5194/acp-11-6265-2011

Nixon, S. W. (2003), Replacing the Nile: Are anthropogenic nutrients providing the fertility once brought to the Mediterranean by a great river?, *Ambio*, *32*(1), 30-39

Ozer, T., I. Gertman, N. Kress, J. Silverman, and B. Herut (2016), Interannual thermohaline (1979–2014) and nutrient (2002–2014) dynamics in the Levantine surface and intermediate water masses, SE Mediterranean Sea, *Glob Planet Change*, doi: http://dx.doi.org/10.1016/j.gloplacha.2016.04.001

Palestinian Central Bureau of Statistics (2014), Estimated Population in the Palestine Territory Mid-Year by Governorate 1997-2016, <http://www.pcbs.gov.ps/Portals/_Rainbow/Documents/gover_e.htm>, [Accessed 21/04/2014].

Pantoja, S., D. J. Repeta, J. P. Sachs, and D. M. Sigman (2002), Stable isotope constraints on the nitrogen cycle of the Mediterranean Sea water column, *Deep Sea Res Part I Oceanogr Res Pap*, *49*(9), 1609-1621

Pasqueron de Fommervault, O., C. Migon, F. D'Ortenzio, M. Ribera d'Alcalà, and L. Coppola (2015), Temporal variability of nutrient concentrations in the northwestern Mediterranean sea (DYFAMED time-series station), *Deep Sea Res Part I Oceanogr Res Pap*, *100*, 1-12, doi: http://dx.doi.org/10.1016/j.dsr.2015.02.006

Paytan, A., and K. McLaughlin (2007), The oceanic phosphorus cycle, *Chemical Reviews*, *107*(2), 563-576, doi: 10.1021/cr0503613

Pazi, I. (2008), Water mass properties and chemical characteristics in the Saros Gulf, Northeast Aegean Sea (Eastern Mediterranean), *J Mar Syst*, *74*(1-2), 698-710, doi: 10.1016/j.jmarsys.2008.07.002

Picotti, V., A. Negri, and B. Capaccioni (2014), The Geological Originsand PLeoceanographic History of the Mediterranean Region: Tethys to Present, in *The Mediterranean Sea: Its history and present challenges*, edited by S. Goffredo and Z. Dubinsky, pp. 3-11, Springer, Dodrecht.

Pinardi, N., M. Zavatarelli, M. Adani, G. Coppini, C. Fratianni, P. Oddo, S. Simoncelli, M. Tonani, V. Lyubartsev, S. Dobricic, and A. Bonaduce (2015), Mediterranean Sea large-scale low-frequency ocean variability and water mass formation rates from 1987 to 2007: A retrospective analysis, *Prog Oceanogr*, *132*, 318-332, doi: 10.1016/j.pocean.2013.11.003

Pinhassi, J., L. Gomez-Consarnau, L. Alonso-Saez, M. M. Sala, M. Vidal, C. Pedros-Alio, and J. M. Gasol (2006), Seasonal changes in bacterioplankton nutrient limitation and their effects on bacterial community composition in the NW Mediterranean Sea, *Aquat Microb Ecol*, *44*(3), 241-252, doi: 10.3354/ame044241

Plan-Bleu (2005), A sustainable future for the Mediterranean: The Blue Plan's Environment and Development Outlook*Rep.*, London, Sterling, VA.

Planton, S., P. Lionello, V. Artale, R. Aznar, A. Carrillo, J. Colin, L. Congedi, C. Dubois, A. Elizalde, S. Gualdi, E. Hertig, J. Jocobeit, G. Jorda, L. Li, A. Mariotti, C. Piani, P. Ruti, E. Sanchez-Gomez, G. Sannino, F. Sevault, S. Somot, and M. N. Tsimplis (2012), The Climate of Mediterranean Region in Future Climate Projections, in *The Climate of the Mediterranean Region: From the past to the future*, edited by P. Lionello, Elsevier Insights, Amsterdam.

Polat, S. C., and S. Tugrul (1995), Nutrient and organic-carbon exchanges bteween the Black and Marmara Seas through the Bosphorus Strait, *Cont Shelf Res*, *15*(9), 1115-1132

Powley, H. R., M. D. Krom, K.-C. Emeis, and P. Van Cappellen (2014), A biogeochemical model for phosphorus and nitrogen cycling in the Eastern Mediterranean Sea (EMS) Part 2. Response of nutrient cycles and primary production to anthropogenic forcing: 1950-2000., *J Mar Syst*, *139*, 420-432

Powley, H. R., H. H. Dürr, A. T. Lima, M. D. Krom, and P. Van Cappellen (2016a), Direct Discharges of Domestic Wastewater are a Major Source of Phosphorus and Nitrogen to the Mediterranean Sea, *Environ Sci Technol*, *50*, 8722-8730, doi: 10.1021/acs.est.6b01742

Powley, H. R., M. D. Krom, and P. Van Cappellen (2016b), Circulation and oxygen cycling in the Mediterranean Sea: Sensitivity to future climate change, *Journal of Geophysical Research: Oceans*, *121*, 8230-8247, doi: 10.1002/2016JC012224

Preunkert, S., D. Wagenbach, and M. Legrand (2003), A seasonally resolved alpine ice core record of nitrate: Comparison with anthropogenic inventories and estimation of preindustrial emissions of NO in Europe, *J Geophys Res-Atmos*, *108*(D21), 10, doi: 4681 10.1029/2003jd003475

Pujo-Pay, M., P. Conan, and P. Raimbault (1995), Particulate and dissolved orgainc nitrogen and phosphorus in the north western Mediterranean Sea (EROS Discovery Cruise 1993), in *EROS 2000. (Europrean River Ocean System). Fifth workhop on the north-west Mediterranean Sea. Water pollution Research Report 32.*, edited by J.-M. Martin and H. Barth, Hamburg.

Pujo-Pay, M., P. Conan, L. Oriol, V. Cornet-Barthaux, C. Falco, J. F. Ghiglione, C. Goyet, T. Moutin, and L. Prieur (2011), Integrated survey of elemental stoichiometry (C, N, P) from the western to eastern Mediterranean Sea, *Biogeosciences*, *8*(4), 883-899, doi: 10.5194/bg-8-883-2011

Pusceddu, A., S. Fraschetti, S. Mirto, M. Holmer, and R. Danovaro (2007), Effects of intensive mariculture on sediment biochemistry, *Ecol Appl*, *17*(5), 1366-1378, doi: 10.1890/06-2028.1

Rabalais, N. N., R. J. Diaz, L. A. Levin, R. E. Turner, D. Gilbert, and J. Zhang (2010), Dynamics and distribution of natural and human-caused hypoxia, *Biogeosciences*, *7*(2), 585-619

Rahav, E., B. Herut, N. Stambler, E. Bar-Zeev, M. R. Mulholland, and I. Berman-Frank (2013), Uncoupling between dinitrogen fixation and primary productivity in the eastern Mediterranean Sea, *Journal of Geophysical Research: Biogeosciences*, *118*(1), 195-202, doi: 10.1002/jgrg.20023

Rahav, E., M. J. Giannetto, and E. Bar-Zeev (2016), Contribution of mono and polysaccharides to heterotrophic N-2 fixation at the eastern Mediterranean coastline, *Scientific Reports*, *6*, doi: 10.1038/srep27858

Ramirez, T., D. Cortes, J. M. Mercado, M. Vargas-Yanez, M. Sebastian, and E. Liger (2005), Seasonal dynamics of inorganic nutrients and phytoplankton biomass in the NW Alboran Sea, *Estuarine Coastal Shelf Sci*, *65*(4), 654-670, doi: 10.1016/j.ecss.2005.07.012

Ramirez-Romero, E., D. Macias, C. M. Garcia, and M. Bruno (2014), Biogeochemical patterns in the Atlantic Inflow through the Strait of Gibraltar, *Deep Sea Res Part I Oceanogr Res Pap*, *85*, 88-100, doi: 10.1016/j.dsr.2013.12.004

Rasmussen, E. K., O. S. Petersen, J. R. Thompson, R. J. Flower, and M. H. Ahmed (2009), Hydrodynamic-ecological model analyses of the water quality of Lake Manzala (Nile Delta, Northern Egypt), *Hydrobiologia*, *622*, 195-220, doi: 10.1007/s10750-008-9683-7

Redfield, A. C., B. H. Ketchum, and F. A. Richards (1963), The influence of organisms on the composition of seawater, in *The Sea*, edited by M. N. Hill, pp. 26-77, Interscience, New York.

Regulation (EU) (2012), No 259/2012 of the European Parliament and of the Council of 14 March 2012 amending Regulation EC 648/2004 as regards the use of phosphates amd other phosphorus compounds in consumer laundry detergents and consumer dishwasher detergents, *Official Journal of the European Union*(L94/16)

Rhein, M. (1995), Deep water formation in the western Mediterranean, *Journal of Geophysical Research*, *100*(C4), 6943, doi: 10.1029/94jc03198

Ribera d'Alcala, M., C. Brunet, F. Conversano, F. Corato, and R. Lavezza (2009), Nutrient and pigment distributions in the southern Tyrrhenian Sea during mid-summer and late fall 2005, *Deep-Sea Res Pt II*, *56*(11-12), 676-686, doi: 10.1016/j.dsr2.2008.07.028

Ribera d'Alcalà, M., G. Civitarese, F. Conversano, and R. Lavezza (2003), Nutrient ratios and fluxes hint at overlooked processes in the Mediterranean Sea, *J Geophys Res Oceans*, *108*(C9), 16, doi: 8106 10.1029/2002jc001650

Rixen, M., J. M. Beckers, S. Levitus, J. Antonov, T. Boyer, C. Maillard, M. Fichaut, E. Balopoulos, S. Iona, H. Dooley, M. J. Garcia, B. Manca, A. Giorgetti, G. Manzella, N. Mikhailov, N. Pinardi, and M. Zavatarelli (2005), The Western Mediterranean Deep Water: A proxy for climate change, *Geophys Res Lett*, *32*(12), doi: 10.1029/2005gl022702

Robinson, A. R., J. Sellschopp, and W. G. Leslie (2001), *Mediterranean Sea circulation*, 1689-1706 pp., Academic Press.

Rodellas, V., J. Garcia-Orellana, P. Masque, M. Feldman, and Y. Weinstein (2015), Submarine groundwater discharge as a major source of nutrients to the Mediterranean Sea, *Proc Natl Acad Sci U S A*, *112*(13), 3926-3930, doi: 10.1073/pnas.1419049112

Roether, W., and R. Schlitzer (1991), Eastern Mediterranean deep water renewal on the basis of chlorofluromethane and tritium data, *Dynam Atmos Oceans*, *15*(3-5), 333-354

Roether, W., B. B. Manca, B. Klein, D. Bregant, D. Georgopoulos, V. Beitzel, V. Kovacevic, and A. Luchetta (1996), Recent changes in eastern Mediterranean deep waters, *Science*, *271*(5247), 333-335

Roether, W., B. Klein, V. Beitzel, and B. B. Manca (1998), Property distributions and transient-tracer ages in Levantine Intermediate Water in the Eastern Mediterranean, *J Mar Syst*, *18*(1-3), 71-87

Roether, W., and R. Well (2001), Oxygen consumption in the Eastern Mediterranean, *Deep Sea Res Part I Oceanogr Res Pap*, *48*(6), 1535-1551

Roether, W., B. Klein, B. B. Manca, A. Theocharis, and S. Kioroglou (2007), Transient Eastern Mediterranean deep waters in response to the massive dense-water output of the Aegean Sea in the 1990s, *Prog Oceanogr*, *74*, 540-571, doi: 10.1016/j.pocean.2007.001

Roether, W., and J. E. Lupton (2011), Tracers confirm downward mixing of Tyrrhenian Sea upper waters associated with the Eastern Mediterranean Transient, *Ocean Sci*, *7*(1), 91-99, doi: 10.5194/os-7-91-2011

Rohling, E. J., G. Marino, and K. M. Grant (2015), Mediterranean climate and oceanography, and the periodic development of anoxic events (sapropels), *Earth-Sci Rev*, *143*, 62-97, doi: 10.1016/j.earscirev.2015.01.008

Rössle, W., Pretorius, WA (2001), A review of characterisation requirements for in-line prefermenters. Paper 1: Wastewater characterisation, *Water SA*, *27*(3), 405-412

Ruttenberg, K. C., N. O. Ogawa, F. Tamburini, R. A. Briggs, N. D. Colasacco, and E. Joyce (2009), Improved, high-throughput approach for phosphorus speciation in natural sediments via the SEDEX sequential extraction method, *Limnol. Oceanogr. Meth.*, *7*, 319-333

Ruttenberg, K. C. (2014), 10.13 - The Global Phosphorus Cycle A2 - Holland, Heinrich D, in *Treatise on Geochemistry (Second Edition)*, edited by K. K. Turekian, pp. 499-558, Elsevier, Oxford.

Rydberg, L., G. Ærtebjerg, and L. Edler (2006), Fifty years of primary production measurements in the Baltic entrance region, trends and variability in relation to land-based input of nutrients, *J Sea Res*, *56*(1), 1-16, doi: 10.1016/j.seares.2006.03.009

Ryther, J. H., and W. M. Dunstan (1971), Nitrogen, phosphorus, and eutrophication in coastal marine environment, *Science*, *171*(3975), 1008-&, doi: 10.1126/science.171.3975.1008

Sachs, J. P., and D. J. Repeta (1999), Oligotrophy and nitrogen fixation during eastern Mediterranean sapropel events, *Science*, *286*(5449), 2485-2488

Sanchez-Cabeza, J. A., P. Masque, I. Ani-Ragolta, J. Merino, M. Frignani, F. Alvisi, A. Palanques, and P. Puig (1999), Sediment accumulation rates in the southern Barcelona continental margin (NW Mediterranean Sea) derived from Pb-210 and Cs-137 chronology, *Prog Oceanogr*, *44*(1-3), 313-332, doi: 10.1016/s0079-6611(99)00031-2

Sánchez-Román, A., G. Sannino, J. García-Lafuente, A. Carillo, and F. Criado-Aldeanueva (2009), Transport estimates at the western section of the Strait of Gibraltar: A combined experimental and numerical modeling study, *Journal of Geophysical Research*, *114*(C6), doi: 10.1029/2008jc005023

Sandroni, V., P. Raimbault, C. Migon, N. Garcia, and E. Gouze (2007), Dry atmospheric deposition and diazotrophy as sources of new nitrogen to northwestern Mediterranean oligotrophic surface waters, *Deep Sea Res Part I Oceanogr Res Pap*, *54*(11), 1859-1870, doi: 10.1016/j.dsr.2007.08.004

Santinelli, C., L. Nannicini, and A. Seritti (2010), DOC dynamics in the meso and bathypelagic layers of the Mediterranean Sea, *Deep-Sea Res Pt II*, *57*(16), 1446-1459, doi: 10.1016/j.dsr2.2010.02.014

Santinelli, C., V. Ibello, R. Lavezza, G. Civitarese, and A. Seritti (2012a), New insights into C, N and P stoichiometry in the Mediterranean Sea: The Adriatic Sea case, *Cont Shelf Res*, *44*(0), 83-93, doi: 10.1016/j.csr.2012.02.015

Santinelli, C., R. Sempéré, F. Van Wambeke, B. Charriere, and A. Seritti (2012b), Organic carbon dynamics in the Mediterranean Sea: An integrated study, *Global Biogeochem Cycles*, *26*(4), n/a-n/a, doi: 10.1029/2011gb004151

Santinelli, C. (2015), DOC in the Mediterranean Sea, in *Biogeochemistry of marine dissolved orgainc matter*, edited by D. A. Hansell and C. A. Carlson, pp. 579-608, Academic Press, London, UK.

Santos, I. R., W. C. Burnett, T. Dittmar, I. G. N. A. Suryaputra, and J. Chanton (2009), Tidal pumping drives nutrient and dissolved organic matter dynamics in a Gulf of Mexico subterranean estuary, *Geochim Cosmochim Acta*, *73*(5), 1325-1339, doi: 10.1016/j.gca.2008.11.029

Santos, I. R., J. de Weys, D. R. Tait, and B. D. Eyre (2013), The Contribution of Groundwater Discharge to Nutrient Exports from a Coastal Catchment: Post-Flood Seepage Increases Estuarine N/P Ratios, *Estuar Coasts*, *36*(1), 56-73, doi: 10.1007/s12237-012-9561-4

Sañudo-Wilhelmy, S. A., A. B. Kustka, C. J. Gobler, D. A. Hutchins, M. Yang, K. Lwiza, J. Burns, D. G. Capone, J. A. Raven, and E. J. Carpenter (2001), Phosphorus limitation of nitrogen fixation by Trichodesmium in the central Atlantic Ocean, *Nature*, *411*(6833), 66-69, doi: http://www.nature.com/nature/journal/v411/n6833/suppinfo/411066a0_S1.html

Sarmiento, J. L., T. Herbert, and J. R. Toggweiler (1988), Mediterranean Nutrient Balance and Episodes of Anoxia, *Global Biogeochem Cycles*, *2*(4), 427--444

Sarmiento, J. L., and N. Gruber (2006), *Ocean Biogeochemical Dynamics*, Princeton University Press, Princenton, N.J.

Savenkoff, C., L. Prieur, J. P. Reys, D. Lefevre, S. Dallot, and M. Denis (1993), Deep microbial communitites evidenced in the Liguro-Provencal front by their ETS activity, *Deep Sea Res Part I Oceanogr Res Pap*, *40*(4), 709-725, doi: 10.1016/0967-0637(93)90067-d

Schewe, J., J. Heinke, D. Gerten, I. Haddeland, N. W. Arnell, D. B. Clark, R. Dankers, S. Eisner, B. M. Fekete, F. J. Colon-Gonzalez, S. N. Gosling, H. Kim, X. Liu, Y. Masaki, F. T. Portmann, Y. Satoh, T. Stacke, Q. Tang, Y. Wada, D. Wisser, T. Albrecht, K. Frieler, F. Piontek, L. Warszawski, and P. Kabat (2014), Multimodel assessment of water scarcity under climate change, *Proc Natl Acad Sci U S A*, *111*(9), 3245-3250, doi: 10.1073/pnas.1222460110

Schlitzer, R., W. Roether, H. Oster, H. G. Junghans, M. Hausmann, H. Johannsen, and A. Michelato (1991), Chlorofluromethane and oxygen in the eastern Mediterranean, *Deep-Sea Res Pt A*, *38*(12), 1531-1551, doi: 10.1016/0198-0149(91)90088-w

Schlitzer, R. (2015), Ocean Data View, edited.

Schneider, A., T. Tanhua, W. Roether, and R. Steinfeldt (2014), Changes in ventilation of the Mediterranean Sea during the past 25 year, *Ocean Sci*, *10*(1), 1-16, doi: 10.5194/os-10-1-2014

Schroeder, K., G. P. Gasparini, M. Tangherlini, and M. Astraldi (2006), Deep and intermediate water in the western Mediterranean under the influence of the Eastern Mediterranean Transient, *Geophys Res Lett*, *33*(21), L21607, doi: 10.1029/2006gl027121

Schroeder, K., M. Borghini, G. Cerrati, V. Difesca, R. Delfanti, C. Santinelli, and G. P. Gasparini (2008a), Multiparametric mixing analysis of the deep waters in the Western Mediterranean Sea, *Chem Ecol*, *24*(sup1), 47-56, doi: 10.1080/02757540801970373

Schroeder, K., A. Ribotti, M. Borghini, R. Sorgente, A. Perilli, and G. P. Gasparini (2008b), An extensive western Mediterranean deep water renewal between 2004 and 2006, *Geophys Res Lett*, *35*(18), doi: 10.1029/2008gl035146

Schroeder, K., V. Taillandier, A. Vetrano, and G. P. Gasparini (2008c), The circulation of the western Mediterranean Sea in spring 2005 as inferred from observations and from model outputs, *Deep Sea Res Part I Oceanogr Res Pap*, *55*(8), 947-965, doi: 10.1016/j.dsr.2008.04.003

Schroeder, K., G. P. Gasparini, M. Borghini, G. Cerrati, and R. Delfanti (2010a), Biogeochemical tracers and fluxes in the Western Mediterranean Sea, spring 2005, *J Mar Syst*, *80*(1-2), 8-24, doi: 10.1016/j.jmarsys.2009.08.002

Schroeder, K., S. A. Josey, M. Herrmann, L. Grignon, G. P. Gasparini, and H. L. Bryden (2010b), Abrupt warming and salting of the Western Mediterranean Deep Water after 2005: Atmospheric forcings and lateral advection, *J Geophys Res Oceans*, *115*, doi: 10.1029/2009jc005749

Schroeder, K., J. Garc`ıa-Lafuente, S. A. Josey, V. Artale, Buongiorno, B. Nardelli, A. Carrillo, M. Ga˘ci´c, G. P. Gasparini, M. Herrmann, P. Lionello, W. Ludwig, C. Millot, E. O¨ zsoy, G. Pisacane, J. C. S´anchez-Garrido, G. Sannino, R. Santoleri, S. Somot, M. Struglia, E. Stanev, I. Taupier-Letage, Tsimplis, M. N., M. Vargas-Y´a˜nez, V. Zervakis, and G. Zodiatis (2012),

Circulation of the Mediterranean Sea and its variability, in *The Climate of the Mediterranean Region, from the past to the future*, edited by P. Lionello, Elsevier Insights, Amsterdam.

Schroeder, K., C. Millot, L. Bengara, S. Ben Ismail, M. Bensi, M. Borghini, G. Budillon, V. Cardin, L. Coppola, C. Curtil, A. Drago, B. El Moumni, J. Font, J. L. Fuda, J. García-Lafuente, G. P. Gasparini, H. Kontoyiannis, D. Lefevre, P. Puig, P. Raimbault, G. Rougier, J. Salat, C. Sammari, J. C. Sánchez Garrido, A. Sanchez-Roman, S. Sparnocchia, C. Tamburini, I. Taupier-Letage, A. Theocharis, M. Vargas-Yáñez, and A. Vetrano (2013), Long-term monitoring programme of the hydrological variability in the Mediterranean Sea: a first overview of the HYDROCHANGES network, *Ocean Sci*, *9*(2), 301-324, doi: 10.5194/os-9-301-2013

Schroeder, K., T. Tanhua, H. Bryden, M. Álvarez, J. Chiggiato, and S. Aracri (2015), Mediterranean Sea Ship-based Hydrographic Invesitgations Program (Med-SHIP), *Oceanography*, *28*(3), 12-15, doi: http://dx.doi.org/10.5670/oceanog.2015.71.

Schwarzenbach, R. P., T. Egli, T. B. Hofstetter, U. von Gunten, and B. Wehrli (2010), Global Water Pollution and Human Health, *Annu Rev Environ Resour*, *35*, 109-136, doi: 10.1146/annurev-environ-100809-125342

Seitzinger, S. P., J. A. Harrison, E. Dumont, A. H. W. Beusen, and A. F. Bouwman (2005), Sources and delivery of carbon, nitrogen, and phosphorus to the coastal zone: An overview of Global Nutrient Export from Watersheds (NEWS) models and their application, *Global Biogeochem Cycles*, *19*(4), doi: 10.1029/2005gb002606

Send, U., F. Schott, F. Gaillard, and Y. Desaubies (1995), Observation of a deep convection regime with acoustic tomography, *J Geophys Res Oceans*, *100*(C4), 6927-6941, doi: 10.1029/94jc03311

Servais, P., J. Garnier, N. Demarteau, N. Brion, and G. Billen (1999), Supply of organic matter and bacteria to aquatic ecosystems through waste water effluents, *Water Res*, *33*(16), 3521-3531, doi: 10.1016/s0043-1354(99)00056-1

Sevault, F., S. Somot, A. Alias, C. Dubois, C. Lebeaupin-Brossier, P. Nabat, F. Adloff, M. Deque, and B. Decharme (2014), A fully coupled Mediterranean regional climate system model: design and evaluation of the ocean component for the 1980-2012 period, *Tellus Series a-Dynamic Meteorology and Oceanography*, *66*, doi: 10.3402/tellusa.v66.23967

Severin, T., P. Conan, X. D. de Madron, L. Houpert, M. J. Oliver, L. Oriol, J. Caparros, J. F. Ghiglione, and M. Pujo-Pay (2014), Impact of open-ocean convection on nutrients, phytoplankton biomass and activity, *Deep Sea Res Part I Oceanogr Res Pap*, *94*, 62-71, doi: 10.1016/j.dsr.2014.07.015

Sipler, R. E., and D. A. Bronk (2015), Dynamics of Dissolved Organic Nitrogen, in *Biogeochemistry of Marine Dissolved Organic Matter*, edited by D. A. Hansell and C. A. Carlson, pp. 127-232, Elsevier, London.

Smith, S. J., J. van Aardenne, Z. Klimont, R. J. Andres, A. Volke, and S. D. Arias (2011), Anthropogenic sulfur dioxide emissions: 1850-2005, *Atmos Chem Phys*, *11*(3), 1101-1116, doi: 10.5194/acp-11-1101-2011

Somlyódy, L., and P. Shanahan (1998), Municipal wastewater treatment in central and eastern Europe: Present Situation and Cost-effective development strategies*Rep.*, 164 pp, The International Bank for Reconstruction and Development/World Bank, Washington.

Somot, S., F. Sevault, and M. Déqué (2006), Transient climate change scenario simulation of the Mediterranean Sea for the twenty-first century using a high-resolution ocean circulation model, *Clim Dynam*, *27*(7-8), 851-879, doi: 10.1007/s00382-006-0167-z

Soto-Navarro, J., F. Criado-Aldeanueva, J. García-Lafuente, and A. Sánchez-Román (2010), Estimation of the Atlantic inflow through the Strait of Gibraltar from climatological and in situ data, *Journal of Geophysical Research*, *115*(C10), doi: 10.1029/2010jc006302

Souvermezoglou, E., E. Krasakopoulou, and A. Pavlidou (1999), Temporal variability in oxygen and nutrient concentrations in the southern Aegean Sea and the Straits of the Cretan Arc, *Prog Oceanogr*, *44*(4), 573-600

Stockdale, A., M. D. Krom, R. J. G. Mortimer, L. G. Benning, K. S. Carslaw, R. J. Herbert, Z. B. Shi, S. Myriokefalitakis, M. Kanakidou, and A. Nenes (2016), Understanding the nature of atmospheric

acid processing of mineral dusts in supplying bioavailable phosphorus to the oceans, *Proc Natl Acad Sci U S A*, *113*(51), 14639-14644, doi: 10.1073/pnas.1608136113

Stratford, K., R. G. Williams, and P. G. Drakopoulos (1998), Estimating climatological age from a model-derived oxygen-age relationship in the Mediterranean, *J Mar Syst*, *18*(1-3), 215-226, doi: 10.1016/s0924-7963(98)00013-x

Stratford, K., R. G. Williams, and P. G. Myers (2000), Impact of the circulation on sapropel formation in the eastern Mediterranean, *Global Biogeochem Cycles*, *14*(2), 683-695, doi: 10.1029/1999gb001157

Suari, Y., and S. Brenner (2015), Decadal biogeochemical history of the south east Levantine basin: Simulations of the river Nile regimes, *J Mar Syst*, *148*, 112-121, doi: 10.1016/j.jmarsys.2015.02.004

Taha, A. A., A. S. El-Mahmoudi, and I. M. El-Haddad (2004), Pollution sources and related environmental impacts in the new communities southeast Nile Delta, Egypt, *Emirates Journal for Engineering Research*, *9*(1), 35-49

Tait, D. R., D. V. Erler, I. R. Santos, T. J. Cyronak, U. Morgenstern, and B. D. Eyre (2014), The influence of groundwater inputs and age on nutrient dynamics in a coral reef lagoon, *Mar Chem*, *166*, 36-47, doi: 10.1016/j.marchem.2014.08.004

Takahashi, T., W. S. Broecker, and S. Langer (1985), Redfield ratio based on chemical-data from isopycnal surfaces, *J Geophys Res Oceans*, *90*(NC4), 6907-6924, doi: 10.1029/JC090iC04p06907

Tanaka, T., and F. Rassoulzadegan (2004), Vertical and seasonal variations of bacterial abundance and production in the mesopelagic layer of the NW Mediterranean Sea: bottom-up and top-down controls, *Deep Sea Res Part I Oceanogr Res Pap*, *51*(4), 531-544, doi: 10.1016/j.dsr.2003.12.001

Tanaka, T., T. F. Thingstad, U. Christaki, J. Colombet, V. Cornet-Barthaux, C. Courties, J. D. Grattepanche, A. Lagaria, J. Nedoma, L. Oriol, S. Psarra, M. Pujo-Pay, and F. Van Wambeke (2011), Lack of P-limitation of phytoplankton and heterotrophic prokaryotes in surface waters of three anticyclonic eddies in the stratified Mediterranean Sea, *Biogeosciences*, *8*(2), 525-538, doi: 10.5194/bg-8-525-2011

Tanhua, T., D. Hainbucher, V. Cardin, M. Alvarez, G. Civitarese, A. P. McNichol, and R. M. Key (2013), Repeat hydrography in the Mediterranean Sea, data from the Meteor cruise 84/3 in 2011, *Earth System Science Data*, *5*(2), 289-294, doi: 10.5194/essd-5-289-2013

Testa, J. M., Y. Li, Y. J. Lee, M. Li, D. C. Brady, D. M. Di Toro, W. M. Kemp, and J. J. Fitzpatrick (2014), Quantifying the effects of nutrient loading on dissolved O2 cycling and hypoxia in Chesapeake Bay using a coupled hydrodynamic–biogeochemical model, *J Mar Syst*, *139*, 139-158, doi: 10.1016/j.jmarsys.2014.05.018

Thingstad, T. F., and F. Rassoulzadegan (1995), Nutrient limitations, microbial food webs and biological C-pumps - suggested interactions in a P limited Mediterranean, *Mar Ecol Prog Ser*, *117*(1-3), 299-306, doi: 10.3354/meps117299

Thingstad, T. F., U. L. Zweifel, and F. Rassoulzadegan (1998), P limitation of heterotrophic bacteria and phytoplankton in the northwest Mediterranean, *Limnol Oceanogr*, *43*(1), 88-94

Thingstad, T. F., M. D. Krom, R. F. Mantoura, G. A. Flaten, S. Groom, B. Herut, N. Kress, C. S. Law, A. Pasternak, P. Pitta, S. Psarra, F. Rassoulzadegan, T. Tanaka, A. Tselepides, P. Wassmann, E. M. Woodward, C. W. Riser, G. Zodiatis, and T. Zohary (2005a), Nature of phosphorus limitation in the ultraoligotrophic eastern Mediterranean, *Science*, *309*(5737), 1068-1071, doi: 10.1126/science.1112632

Thingstad, T. F., M. D. Krom, R. F. C. Mantoura, G. A. F. Flaten, S. Groom, B. Herut, N. Kress, C. S. Law, A. Pasternak, P. Pitta, S. Psarra, F. Rassoulzadegan, T. Tanaka, A. Tselepides, P. Wassmann, E. M. S. Woodward, C. W. Riser, G. Zodiatis, and T. Zohary (2005b), Nature of phosphorus limitation in the ultraoligotrophic eastern Mediterranean, *Science*, *309*(5737), 1068-1071, doi: 10.1126/science.1112632

Thingstad, T. F., and R. F. C. Mantoura (2005), Titrating excess nitrogen content of phosphorous-deficient eastern Mediterranean surface water using alkaline phosphatase activity as a bio-indicator, *Limnol. Oceanogr. Meth.*, *3*, 94-100

Thorpe, R. B., and G. R. Bigg (2000), Modelling the sensitivity of Mediterranean Outflow to anthropogenically forced climate change, *Clim Dynam*, *16*(5), 355-368, doi: 10.1007/s003820050333

Touratier, F., and C. Goyet (2011), Impact of the Eastern Mediterranean Transient on the distribution of anthropogenic CO2 and first estimate of acidification for the Mediterranean Sea, *Deep Sea Res Part I Oceanogr Res Pap*, *58*(1), 1-15, doi: 10.1016/j.dsr.2010.10.002

Tovar-Sanchez, A., G. Basterretxea, V. Rodellas, D. Sanchez-Quiles, J. Garcia-Orellana, P. Masque, A. Jordi, J. M. Lopez, and E. Garcia-Solsona (2014), Contribution of Groundwater Discharge to the Coastal Dissolved Nutrients and Trace Metal Concentrations in Majorca Island: Karstic vs Detrital Systems, *Environ Sci Technol*, *48*(20), 11819-11827, doi: 10.1021/es502958t

Toze, S. (1999), PCR and the detection of microbial pathogens in water and wastewater, *Water Res*, *33*(17), 3545-3556, doi: 10.1016/s0043-1354(99)00071-8

Turley, C. M., M. Bianchi, U. Christaki, P. Conan, J. R. W. Harris, S. Psarra, G. Ruddy, E. D. Stutt, A. Tselepides, and F. Van Wambeke (2000), Relationship between primary producers and bacteria in an oligotrophic sea - the Mediterranean and biogeochemical implications, *Mar Ecol Prog Ser*, *193*, 11-18, doi: 10.3354/meps193011

Tyrrell, T. (1999), The relative influences of nitrogen and phosphorus on oceanic primary production, *Nature*, *400*(6744), 525-531, doi: 10.1038/22941

Tziperman, E., and K. Speer (1994), A study of water mass transformation in the Mediterranean Sea - Analysis of climatological data and a simple 3-box model. , *Dynam Atmos Oceans*, *21*(2-3), 53-82, doi: 10.1016/0377-0265(94)90004-3

Ulses, C., C. Estournel, P. Puig, X. D. de Madron, and P. Marsaleix (2008), Dense shelf water cascading in the northwestern Mediterranean during the cold winter 2005: Quantification of the export through the Gulf of Lion and the Catalan margin, *Geophys Res Lett*, *35*(7), doi: 10.1029/2008gl033257

UNEP-MAP-RAC/SPA (2010), The Mediterranean Sea Biodiversity: state of the ecosystems, pressures, impacts and future priorities. By Bazairi, H., Ben Haj, S., Boero, F., Cebrian, D., De Juan, S., Limam, A., Lleonart, J., Torchia, G., and Rais, C., Ed. RAC/SPA, Tunis; 100 pages.*Rep.*

UNEP/MAP (2012), State of Mediterranean Marine and Coastal Environment*Rep.*, Athens.

UNEP/MAP/MED-POL/WHO (2004), Municipal wastewater treatment plants in Mediterranean coastal cities (II)*Rep.*, Athens.

UNEP/MAP/MED-POL/WHO (2008), Municipal wastewater treatment plants in Mediterranean coastal cities: inventory of treatment plants in cities of between 2,000 and 10,000 inhabitants*Rep.*, 98 pp, Athens.

UNEP/WHO (1999), Identification of Priority Pollution Hot Spots and Sensitive Areas in the Mediterranean*Rep.*, 103 pp, Athens.

UNstat (2011), Environmental indicators: Inland water resouces: Wastewater <http://unstats.un.org/unsd/environment/wastewater.htm >, [Accessed 16/01/14].

van Aardenne, J. A., F. J. Dentener, J. G. J. Olivier, C. Goldewijk, and J. Lelieveld (2001), A 1 degrees x 1 degrees resolution data set of historical anthropogenic trace gas emissions for the period 1890-1990, *Global Biogeochem Cycles*, *15*(4), 909-928, doi: 10.1029/2000gb001265

Van Cappellen, P. (2003), Bioremineralization and global biogeochemical cycles, in *Bioreminerlization*, edited by P. Dove, J. DeYoreo and S. Weiner, pp. 357-381, Mineralogical Society of America, Washington, D.C.

Van Cappellen, P., H. R. Powley, K.-C. Emeis, and M. D. Krom (2014), A biogeochemical model for phosphorus and nitrogen cycling in the Eastern Mediterranean Sea (EMS). Part 1. Model development, initial conditions and sensitivity analyses., *J Mar Syst*, *139*, 460-471

Van Den Broeck, N., and T. Moutin (2002), Phosphate in the sediments of the Gulf of Lions (NW Mediterranean Sea), relationship with input by the river Rhone, *Hydrobiologia*, *472*(1-3), 85-94, doi: 10.1023/a:1016308931115

Van Drecht, G., A. F. Bouwman, J. Harrison, and J. M. Knoop (2009), Global nitrogen and phosphate in urban wastewater for the period 1970 to 2050, *Global Biogeochem Cycles*, *23*, GB0A03. doi: 10.1029/2009gb003458 doi: 10.1029/2009gb003458

Van Vuuren, D. P., A. F. Bouwman, and A. H. W. Beusen (2010), Phosphorus demand for the 1970-2100 period: A scenario analysis of resource depletion, *Glob Environ Change*, *20*(3), 428-439, doi: 10.1016/j.gloenvcha.2010.04.004

Van Wambeke, F., U. Christaki, A. Giannokourou, T. Moutin, and K. Souvemerzoglou (2002), Longitudinal and vertical trends of bacterial limitation by phosphorus and carbon in the Mediterranean Sea, *Microb Ecol*, *43*(1), 119-133, doi: 10.1007/s00248-001-0038-4

Vargas-Yanez, M., F. Moya, M. C. Garcia-Martinez, E. Tel, P. Zunino, F. Plaza, J. Salat, J. Pascual, J. L. Lopez-Jurado, and M. Serra (2010), Climate change in the Western Mediterranean Sea 1900-2008, *J Mar Syst*, *82*(3), 171-176, doi: 10.1016/j.jmarsys.2010.04.013

Vargas-Yáñez, M., P. Zunino, K. Schroeder, J. L. López-Jurado, F. Plaza, M. Serra, C. Castro, M. C. García-Martínez, F. Moya, and J. Salat (2012), Extreme Western Intermediate Water formation in winter 2010, *J Mar Syst*, *105-108*, 52-59, doi: 10.1016/j.jmarsys.2012.05.010

Vervatis, V. D., S. S. Sofianos, N. Skliris, S. Somot, A. Lascaratos, and M. Rixen (2013), Mechanisms controlling the thermohaline circulation pattern variability in the Aegean-Levantine region. A hindcast simulation (1960-2000) with an eddy resolving model, *Deep Sea Res Part I Oceanogr Res Pap*, *74*, 82-97, doi: 10.1016/j.dsr.2012.12.011

Vichi, M., T. Lovato, P. Lazzari, G. Cossarini, M. E. Gutierrez, G. Mattia, S. Masina, W. J. McKiver, N. Pinardi, C. Solidoro, L. Tedesco, and M. Zavatarelli (2015), The Biogeochemical Flux model (BFM): Equation Description and USer Manual. BFM version 5.1. BFM Report Series N. 1, Release 1.1, August 2015 Bologna, Italy, http://bfm-community.eu, pp 104*Rep.*

Vilibić, I., and N. Supić (2005), Dense water generation on a shelf: the case of the Adriatic Sea, *Ocean Dynam*, *55*(5-6), 403-415, doi: 10.1007/s10236-005-0030-5

Violaki, K., P. Zarbas, and N. Mihalopoulos (2010), Long-term measurements of dissolved organic nitrogen (DON) in atmospheric deposition in the Eastern Mediterranean: Fluxes, origin and biogeochemical implications, *Mar Chem*, *120*(1-4), 179-186, doi: 10.1016/j.marchem.2009.08.004

Weinstein, Y., Y. Yechieli, Y. Shalem, W. C. Burnett, P. W. Swarzenski, and B. Herut (2011), What Is the Role of Fresh Groundwater and Recirculated Seawater in Conveying Nutrients to the Coastal Ocean?, *Environ Sci Technol*, *45*(12), 5195-5200, doi: 10.1021/es104394r

Weiss, R. F., W. S. Broecker, C. Harmon, and D. Spencer (1983), GEOSECS: Indian Ocean Expedition. Hydrologic data 1977-1978*Rep.*, International Decade of Ocean Exploration, National Science Foundation., Washington D.C., USA.

Wernand, M. R., H. J. van der Woerd, and W. W. C. Gieskes (2013), Trends in Ocean Colour and Chlorophyll Concentration from 1889 to 2000, Worldwide, *PLoS ONE*, *8*(6), doi: 10.1371/journal.pone.0063766

WHO (2005), A regional overview of wastewater management and reuse in the Eastern Mediterranean Region. *Rep. WHO-EM/CEH/139/E*, 66 pp, Cairo.

Williams, P. J. L., P. D. Quay, T. K. Westberry, and M. J. Behrenfeld (2013), The Oligotrophic Ocean Is Autotrophic, in *Annual Review of Marine Science, Vol 5*, edited by C. A. Carlson and S. J. Giovannoni, pp. 535-549.

Williams, P. J. L. (2014), 10.15 - Plankton Respiration, Net Community Production and the Organic Carbon Cycle in the Oceanic Water Column A2 - Holland, Heinrich D, in *Treatise on Geochemistry (Second Edition)*, edited by K. K. Turekian, pp. 593-612, Elsevier, Oxford.

World Bank (2016), World Development INdicators: GDP per capita (constant 2010 US$), <http://databank.worldbank.org/data/reports.aspx?source=2&series=NY.GDP.PCAP.KD&country= >, [Accessed 7th December 2016].

WRC (2002), Phosphates and alternative detergent builders - Final Draft prepared for EU Environment Directorate*Rep.*, 172 pp, Swindon, UK.

Yogev, T., E. Rahav, E. Bar-Zeev, D. Man-Aharonovich, N. Stambler, N. Kress, O. Béjà, M. R. Mulholland, B. Herut, and I. Berman-Frank (2011), Is dinitrogen fixation significant in the Levantine Basin, East Mediterranean Sea?, *Environ Microbiol*, *13*(4), 854-871, doi: 10.1111/j.1462-2920.2010.02402.x

Zaccone, R., A. Boldrin, G. Caruso, R. La Ferla, G. Maimone, C. Santinelli, and M. Turchetto (2012), Enzymatic Activities and Prokaryotic Abundance in Relation to Organic Matter along a West-East Mediterranean Transect (TRANSMED Cruise), *Microb Ecol*, *64*(1), 54-66, doi: 10.1007/s00248-012-0011-4

Zavatarelli, M., F. Raicich, D. Bregant, A. Russo, and A. Artegiani (1998), Climatological biogeochemical characteristics of the Adriatic Sea, *J Mar Syst*, *18*(1-3), 227-263

Zehr, J. P., and B. B. Ward (2002), Nitrogen cycling in the ocean: New perspectives on processes and paradigms, *Appl Environ Microbiol*, *68*(3), 1015-1024, doi: 10.1128/aem.68.3.1015-1024.2002

Zekster, I. S., R. G. Dzhamalov, and L. G. Everett (2007), *Submarine Groundwater*, Taylor and Francis Group, Florida, US.

Zervakis, V., D. Georgopoulos, A. P. Karageorgis, and A. Theocharis (2004), On the response of the Aegean sea to climatic variability: A review, *Int J Climatol*, *24*(14), 1845-1858, doi: 10.1002/joc.1108

Zhai, W. D., H. D. Zhao, N. Zheng, and Y. Xu (2012), Coastal acidification in summer bottom oxygen-depleted waters in northwestern-northern Bohai Sea from June to August in 2011, *Chin Sci Bull*, *57*(9), 1062-1068, doi: 10.1007/s11434-011-4949-2

Zohary, T., and R. D. Robarts (1998), Experimental study of microbial P limitation in the eastern Mediterranean, *Limnol Oceanogr*, *43*(3), 387-395

Zúñiga, D., A. Calafat, A. Sanchez-Vidal, M. Canals, B. Price, S. Heussner, and S. Miserocchi (2007a), Particulate organic carbon budget in the open Algero-Balearic Basin (Western Mediterranean): Assessment from a one-year sediment trap experiment, *Deep Sea Res Part I Oceanogr Res Pap*, *54*(9), 1530-1548, doi: 10.1016/j.dsr.2007.06.001

Zúñiga, D., J. García-Orellana, A. Calafat, N. B. Price, T. Adatte, A. Sanchez-Vidal, M. Canals, J. A. Sanchez-Cabeza, P. Masqué, and J. Fabres (2007b), Late Holocene fine-grained sediments of the Balearic Abyssal Plain, Western Mediterranean Sea, *Mar Geol*, *237*(1-2), 25-36, doi: 10.1016/j.margeo.2006.10.034

Zúñiga, D., A. Calafat, S. Heussner, S. Miserocchi, A. Sanchez-Vidal, J. Garcia-Orellana, M. Canals, J. A. Sánchez-Cabeza, J. Carbonne, N. Delsaut, and G. Saragoni (2008), Compositional and temporal evolution of particle fluxes in the open Algero–Balearic basin (Western Mediterranean), *J Mar Syst*, *70*(1-2), 196-214, doi: 10.1016/j.jmarsys.2007.05.007

Appendix A

A biogeochemical model of phosphorus and nitrogen cycling in the Eastern Mediterranean Sea.

Part 1.

Model development, initialization and sensitivity

Modified from: Philippe Van Cappellen, **Helen R. Powley**, Kay-Christian Emeis and Michael D. Krom (2014) A biogeochemical model of phosphorus and nitrogen cycling in the Eastern Mediterranean Sea. Part 1. Model development, initialization and sensitivity. *Journal of Marine Systems*. **139**: 60-71. doi:10.1016/j.jmarsys.2014.08.016.

A.1 Summary

The Eastern Mediterranean (EMS) is the largest marine basin whose annual primary productivity is limited by phosphorus (P) rather than nitrogen (N). The basin is nearly entirely land-locked and receives substantial external nutrient fluxes, comparable for instance to those of the Baltic Sea. The biological productivity of the EMS, however, is among the lowest observed in the oceans. The water column exhibits very low P and N concentrations with N:P ratios in excess of the Redfield value. These unique biogeochemical features are analysed using a mass balance model of the coupled P and N cycles in the EMS. The present paper describes the conceptual basis, quantitative implementation and sensitivity of the model. The model is initialized for the year 1950, that is, prior to the large increase in anthropogenic nutrient loading experienced by the EMS during the second half of the 20th century. In the companion paper, the model is used to simulate the P and N cycles during the period 1950-2000. The 1950 model set-up and sensitivity analyses support the following conclusions.

(1) Phosphorus-limited primary production in the EMS is most sensitive to the P exchanges with the Western Mediterranean Sea (WMS) associated with the anti-estuarine circulation of the EMS. The supply of P through the Strait of Sicily is mainly under the form of dissolved organic P (DOP), while dissolved inorganic P (PO_4) is primarily exported to the WMS. The efficient export of PO_4 to the WMS maintains the EMS in its ultra-oligotrophic state.

(2) Inorganic molar N:P ratios in excess of the 16:1 Redfield value observed in the water column reflect higher-than-Redfield N:P ratios of the external inputs, combined with negligible denitrification. Model simulations imply that the denitrification flux would have to increase by at least a factor of 14, relative to the 1950 flux, in order for the inorganic N:P ratio of the deep waters to approach the Redfield value.

(3) The higher-than-Redfield N:P ratios of dissolved and particulate organic matter in the EMS further imply the preferential regeneration of P relative to N during organic matter decomposition.

A.2 Introduction

The Eastern Mediterranean Sea (EMS) is a unique part of the global ocean. Although nearly completely surrounded by land, with associated significant nutrient inputs (Krom et al., 2004; Ludwig et al., 2009), the EMS is an ultra-oligotrophic marine basin. Annual primary productivity in the EMS (~60-80 gC m^{-2} yr^{-1}, Béthoux, 1989; Berman-Frank and Rahav, 2012) is even lower than measured in the low productivity areas of the northwestern Sargasso Sea (Lohrenz et al., 1992). The recent geological past of the EMS, however, was punctuated by episodic accumulations of organic-rich sediments (sapropels), which indicate the potential for rapid and dramatic biogeochemical shifts, including the development of eutrophic conditions, changes in phytoplankton community structure and deep-water anoxia (Cita et al., 1977; Sachs and Repeta, 1999; De Lange et al., 2008). The anti-estuarine thermohaline circulation of the EMS (Astraldi et al., 1999) is generally considered to be an important factor maintaining the EMS in its current ultra-oligotrophic state (Krom et al., 2003).

The winter phytoplankton bloom represents the major annual period of carbon fixation in the present-day EMS (Krom et al., 2003). Primary production during the winter bloom is phosphorus (P) rather than nitrogen (N) limited, in contrast to most of the rest of the oceans where N limitation is more commonly observed. In addition, the deep waters of the EMS exhibit anomalously high nitrate to phosphate molar ratios (~28:1; Krom et al., 1991; Kress and Herut, 2001), considerably higher than the Redfield value (16:1, Redfield et al., 1963). Recent work has shown that the very low biological productivity of the EMS, P limitation and the unusual water column nutrient ratios are linked to one another (Krom et al., 2010).

More than 450 million people live in the drainage basin of the Mediterranean, of whom about one-third inhabit coastal regions (FAO, 2003; UNEP/MAP, 2012). Rapid demographic growth and economic development since the 1950s has caused a major increase in nutrient supply to the EMS (Ludwig et al., 2009). Although significant impacts are observed locally in near-shore coastal areas, (e.g., Dell'Anno et al., 2002; Pusceddu et al., 2007), there is little evidence supporting a major evolution in the trophic state of the open waters of the EMS. However, the extent to which the EMS will be able to cope with future anthropogenic nutrient inputs is unknown. Population in the Mediterranean basin is projected to grow an additional 20% during the first quarter of the 21st century (FAO, 2003), while climate change may profoundly modify the thermohaline circulation of the EMS by the end of the century (Somot et al., 2006). A better understanding of basin-scale nutrient cycling will therefore not only help to interpret present and past biogeochemical conditions in the EMS, but also to evaluate the response of the EMS to ongoing and future anthropogenic pressures (de Madron et al., 2011).

Existing biogeochemical models for the Mediterranean Sea range from 1D biogeochemical (e.g. Sarmiento et al., 1988; Béthoux et al., 1992) and foodweb models (e.g., Allen et al., 2002) to fully coupled 3D physical–biogeochemical models (e.g. Lazzari et al., 2012). Most model applications so far have dealt with ecosystem processes, particularly in the euphotic zone, and their seasonal to inter-annual variability. In contrast, our work focuses on basin-wide nutrient cycling in the EMS, and its modification by the large changes in anthropogenic nutrient loading in the recent past (i.e., post-1950). To this end, a mass balance nutrient model has been developed, based on our current conceptual understanding of the key processes controlling the biogeochemical cycling of P and N in the EMS (Krom et al., 2010).

The coupled P and N model uses a simple 3-layer representation of the water column (surface, intermediate and deep waters) and accounts for the exchanges between these three water masses, as well as for the external inputs to and outputs from the basin. The model computes annually averaged reservoir sizes and fluxes, and is initialized for the nominal year 1950, assuming relatively limited anthropogenic impact on the biogeochemical functioning of the EMS prior to the second half of the 20th century (Béthoux et al., 1998). The present paper (Part 1) focuses on the development of the model and the reconstruction of P and N dynamics under 1950 conditions. In the companion paper (Part 2) of the study, the model is used to describe biogeochemical changes in the EMS in response to the historical changes in P and N inputs over the period 1950–2000 (Chapter 2).

A.3 Eastern Mediterranean Sea (EMS): Physical Description

A.3.1 Model domain

The Mediterranean Sea consists of two main basins with distinct hydrodynamic and ecological characteristics: the Western Mediterranean Sea (WMS) and the Eastern Mediterranean Sea (EMS). The EMS is connected to the WMS through the Strait of Sicily. In order to account explicitly for the role of deep-water formation in the cycling of P and N in the EMS, the Adriatic and Aegean Seas are excluded from the EMS. The resulting EMS model domain covers a surface area of 1.33×10^{12} m^2 and is divided in three horizontal layers (Figure A.1): Eastern Mediterranean Surface Water (EMSW: 0-200 m), Eastern Mediterranean Intermediate Water (EMIW: 200-500 m (commonly termed Levantine Intermediate Water in the literature) and Eastern Mediterranean Deep Water (EMDW: >500 m). The corresponding volumes are 2.8×10^{14} m^3 (EMSW), 4×10^{14} m^3 (EMIW) and 17×10^{14} m^3 (EMDW). The depth ranges assigned to the three water masses are average values for the entire EMS basin. In detail, there is considerable temporal and spatial variability in the vertical extent of the water masses caused by mesoscale circulation features.

A.3.2 Circulation

The water cycle imposed in the model calculations is summarized in Figure A.1. Water flow rates are given in Sverdrup units (1 Sv = 10^6 m^3 s^{-1}). The imposed flow rates are based on estimates for the time period prior to the early 1990s, when circulation in the EMS underwent a major disturbance due to a large increase in deep-water formation in the Aegean Sea (Roether et al., 2007). This event is known as the Eastern Mediterranean Transient (EMT), whose effect on nutrient cycling is assessed in Chapter 2.

Relatively low salinity Western Mediterranean Surface Water (WMSW; commonly termed Modified Atlantic Water in the literature) enters the EMS via the Strait of Sicily (Robinson et al., 2001; Krom et al., 2003). This SW becomes progressively more saline as it flows across the EMS from west to east due to intense evaporation and limited precipitation. Ultimately, the EMSW sinks close to the Turkish coast and forms EMIW (Lascaratos, 1993). EMIW then returns westwards while accumulating nutrients and eventually flows out via the Strait of Sicily below the WMSW. Part of the EMIW is diverted into the Aegean and Adriatic seas where it becomes incorporated into the deep waters forming in these basins.

Estimates of EMIW outflow through the Strait of Sicily are between 0.6 and 1.5 Sv (Roether and Schlitzer, 1991), with some higher reported values (up to 3.2 Sv, Manzella et al., 1988). We assign a value of 1.10 Sv based on the work of Astraldi et al. (1999). The inflow of WMSW into the EMS is on the same order of magnitude as the outflow of EMIW. Based on conservation of heat and salt, WMSW inflow is estimated to be 4% higher than outflow of EMIW (Manzella et al., 1988; Astraldi et al., 1999). Hence, WMSW inflow is set at 1.14 Sv. The flow rates of EMIW into the Adriatic Sea and the outflow of Adriatic deep water (ADW) to the EMS through the Strait of Otranto are not statistically different (Astraldi et al., 1999) and are therefore assigned the same value of 0.36 Sv (see below).

Residence times of EMDW based on CFC and tritium distributions as well as oxygen consumption rates fall in the range 100-150 years (average: 126 years; Roether and Schlitzer, 1991; Roether and Well, 2001). However, these estimates only consider the deeper part of the EMDW reservoir (> 1200 m, volume 8.6×10^{14} m^3). To account for the larger EMDW reservoir considered in the present model (volume 17×10^{14} m^3), we use the highest residence time estimate (150 years = 4.7×10^9 s). Under steady state conditions, mass balance then implies a total rate of deep-water formation of 0.36 Sv (= $17 \times 10^{14} / 4.7 \times 10^9$ = 0.36×10^6 m^3 s^{-1}). This is in good agreement with estimates on the order of 0.3 Sv for the formation rate of ADW (Lascaratos et al., 1999), which is generally acknowledged to be the dominant pre-1987 source of EMDW, with only a minor contribution of Aegean Deep Water formation (Roether and Schlitzer, 1991). In the model, we assign 10% of EMDW formation to Aegean-derived Cretan Deep Water, based

on the observations for the central EMS reported by Zervakis et al. (2004). Thus the inflows into the EMDW from the Adriatic and Aegean seas are 0.32 and 0.04 Sv, respectively.

A small surplus of Adriatic water is exported as surface flow to the EMS. The assigned flow rate is on the same order of magnitude as the average yearly flow of the Po river (1500 $m^3 s^{-1}$; Vilibić and Supić, 2005). The general circulation within the Aegean Sea is cyclonic with Levantine Water (probably a mix of surface and intermediate water) travelling north along the western coast of Turkey and exchanging with Black Sea water in the North Aegean. Modified Black Sea Water then moves westward and southward, and ultimately flows into the EMS. The estimate used for the outflow of Aegean surface water to the EMS is 0.01 Sv, based on the lower estimate of the annual contribution of the Dardanelles to the water balance of the Aegean Sea by Pazi (2008).

All remaining water flow rates derive from the water balance condition. As with the Adriatic Sea, deep-water formation in the Aegean Sea balances the inflow of EMIW to the Aegean Sea. Formation of EMIW by upwelling of EMDW balances the total rate of deep-water formation (0.36 Sv). The other source of EMIW, namely sinking of EMSW (mainly in the Rhodes Gyre), is then equal to 1.10 Sv, which agrees closely with independent estimates reported in the literature (~1 Sv, Lascaratos et al., 1999; Myers and Haines, 2000). With the above fluxes, the water residence time in the EMIW reservoir is 8.7 years, consistent with CFC-derived travel times of EMIW to the Strait of Sicily (~ 8 years, Roether et al., 1998). The calculated residence time for EMSW is 7.7 years.

A.4 Phosphorus and nitrogen cycles: 1950

A.4.1 Core assumptions

In addition to the steady state water cycle discussed above, the model for P and N cycling in the EMS rests on the following assumptions.

1. **Prior to 1950, anthropogenic activity had a minimal impact on the biogeochemical functioning and ecology of the EMS.** That is, the pre-1950 EMS is considered to be in a fairly pristine state. Given the long history of human presence in the Mediterranean drainage area, this cannot be strictly true. However, anthropogenic effects on the Mediterranean Sea before 1950 are likely to have been far less pronounced than during the second half of the 20th century (Béthoux et al., 1998).
2. **The cycles of P and N in 1950 are at steady state.** As for the first assumption, the steady state assumption for the pre-1950 EMS cannot be strictly verified. It represents the simplest

assumption to close the elemental budgets (see also Sarmiento et al., 1988; Béthoux et al., 1992; 1998), and initialize the model for the transient simulations in the follow-up paper (Chapter 2).

3. **Phosphorus limits annual primary production in the EMS.** Phosphorus limitation of phytoplankton growth during the major winter bloom is well established (Krom et al., 1991). Primary production becomes N and P co-limited during late spring (Thingstad et al., 2005b), and possibly even N limited during summer (Tanaka et al., 2011). The model, however, does not resolve seasonal variations in nutrient cycling and primary production. Therefore, we assume that the yearly averaged primary production is P limited. As a consequence, N uptake by phytoplankton is directly linked to the availability of P in the surface waters. We further assume that the N:P ratio in newly produced phytoplankton biomass is constant and equal to the standard molar Redfield ratio of 16:1, in agreement with observations (Krom et al., 2010).

A.5 Phosphorus reservoirs

For each of the three water masses, the P reservoirs considered in the model are dissolved inorganic phosphorus (PO_4), dissolved organic P (DOP) and particulate organic P (POP); PO_4 includes all soluble inorganic forms of P that are readily available for biological uptake, POP includes both living and nonliving organic matter. In total, the model includes nine P reservoirs (Figure A.2), whose masses are computed by multiplying the volumes of the corresponding water reservoirs (Figure A.1) by the average P concentrations. Selection of the latter is based on the observational data summarized below.

Concentrations of PO_4 within the 0-200 m depth interval vary from near or below detection at the very surface to values of up to 100 nM around 200 m water depth (McGill, 1961; Kress and Herut, 2001; Krom et al., 2005; Pujo-Pay et al., 2011). The PO_4 concentration increases gradually with depth between EMSW and EMDW. The earliest measurements by McGill (1961) suggest PO_4 concentrations between 100 and 200 nM in the 200-500 m depth interval. Depth profiles in Kress and Herut (2001) for 1999 in the Southern Levantine Basin indicate average values for EMIW closer to 100 nM, while Béthoux (1981) reports an EMIW value of 190 nM for the Ionian Sea, which feeds into the Strait of Sicily. At greater water depths, data collected over the period 1977-2001 in the Ionian Sea yield a range for the PO_4 concentration of 130-230 nM (GEOSECS and MATER-MTP data, Lavezza et al., 2011), while Béthoux et al. (1992) propose a PO_4 concentration on the order of 185 nM for EMDW in 1960.

Compared to PO_4, only limited concentration data are available for the organic P pools; in addition, these data are all of relatively recent date. We primarily rely on the DOP and POP concentration depth profiles presented by Krom et al. (2005). DOP concentrations in the upper 0-200 m fall in the range 10-100 nM, with somewhat lower values at greater depths. POP concentrations are extremely low, with values in the

upper 250 m on the order of 4-20 nM, decreasing to values below 10 nM at depths exceeding 350 m (Krom et al., 2005).

The 1950 values assigned to the concentrations of the different phosphorus pools in the model are educated guesses based on the currently available information. While they should be viewed with caution, we nonetheless believe they yield representative P inventories for the water column of the EMS. When selecting values from the reported ranges derived from measurements made after 1970, we err on the side of the lower values in order to account for the presumably lower pre-1950 nutrient inventories. The model spin up further causes very slight adjustments of the selected concentrations. The final concentration values (i.e., after model spin-up) are summarized in Figure A.2 and the corresponding reservoir sizes are listed in Table A.1.

A.5.1 Nitrogen reservoirs

The N reservoirs represented in the model are dissolved nitrate (NO_3), dissolved ammonium (NH_4), dissolved organic nitrogen (DON), and particulate organic nitrogen (PON). (Note: NO_3 here includes both nitrate and nitrite.) The average concentrations used to obtain the N reservoir sizes in EMSW, EMIW and EMDW are shown on Figure A.3. As for P, we generally select values at the lower ends of the available concentration ranges, assuming that these values are more representative of the EMS in 1950.

Reported concentrations of NO_3 in the 0-200 m depth interval are in the range 0.01-3 μM (Kress and Herut, 2001; Krom et al., 2005). EMDW has a fairly constant NO_3 concentration on the order of 5 μM, with little change observed between 1977 and 2001 (GEOSECS and MATER-MTP data, Lavezza et al., 2011). Measured NO_3 concentrations of EMIW are intermediate between those of EMSW and EMDW. The limited reliable data on NH_4 show a small drop in concentration with depth, with values always well below 1 μM (Krom et al., 2005). DON is the largest pool of N in the upper water column (Krom et al., 2005), while NO_3 overtakes DON as the major form of dissolved N in the deeper waters of the EMS. Values of PON in EMSW range between 0.1 and 0.5 μM, and exhibit distinctly lower values in the EMDW (Krom et al., 2005).

The relative differences among the concentrations assigned to the various P and N species in the three water layers are in general agreement with the recent data on P and N distributions of Pujo-Pay et al. (2011). The 1950 EMS nutrient concentrations imposed in the model yield molar NO_3:PO_4 ratios in the range 21-28, with the highest value in the EMDW. Krom et al. (2005) report that, albeit variable, NO_3:PO_4 ratios of nutrient depleted surface waters of the EMS are predominantly >16, with values up to and higher than 50 observed during the winter season (Kress and Herut, 2001). The DON:DOP and

PON:POP ratios imposed in the model are in line with observed values, which are on the order of 50-75 for DON:DOP and 30 for PON:POP (Moutin and Raimbault, 2002; Krom et al., 2005).

A.5.2 Phosphorus input and output fluxes

A.5.2.1 Surface flow inputs

The riverine supply of total P to the EMS (excluding the rivers flowing into the Adriatic and Aegean) is estimated by Ludwig et al. (2009) to be $8x10^3$ t P yr^{-1} in the year 1963. According to the same authors, on average 48% of total riverine P is dissolved PO_4, 8% is DOP, and the rest is particulate P, part of which may be solubilized upon entering the sea (Froelich et al., 1988). Given the P-starved nature of the EMS, we assume somewhat arbitrarily that 75% of the riverine supply of particulate P ultimately dissolves in seawater, generating PO_4. The estimated 1950 riverine input of soluble P to the surface waters of the EMS is then $0.23x10^9$ mol P yr^{-1}, with $0.21x10^9$ mol P yr^{-1} and $0.02x10^9$ mol P yr^{-1} delivered in the form of dissolved PO_4 and DOP, respectively.

Surface flows from the Adriatic and Aegean seas into the EMS are estimated to be 0.005 and 0.01 Sv, respectively (Figure A.1, section A.3.2). Assigning average winter concentrations of 60 nM PO_4 to Southern Adriatic surface water (Zavatarelli et al., 1998) and 25 nM to Cretan Sea surface water (Krasakopoulou et al., 1999), we obtain the following dissolved PO_4 input fluxes: $0.011x10^9$ mol P yr^{-1} (Adriatic surface flow) and $0.008x10^9$ mol P yr^{-1} (Cretan surface flow), or a combined flux of $0.02x10^9$ mol P yr^{-1}. Concentrations of DOP have only recently been measured in the Southern Adriatic by Santinelli et al. (2012a). The data indicate DOP concentrations in the surface waters very similar to those observed in the EMS. In the absence of any further information, we assume that the 1950 DOP to PO_4 ratios of the surface waters of the Adriatic and Aegean are similar to that of EMSW in the EMS ($DOP:PO_4 \approx 2$). The combined surface flow input of DOP from the Adriatic and Aegean seas to the EMS is then $0.04x10^9$ mol P yr^{-1}. As surface inflow from the Adriatic and Aegean seas represents less than 1% of the total external inputs of P to the EMS, the uncertainties associated with the corresponding PO_4 and DOP fluxes have little influence on the model outcomes. Far more important is the input of phosphorus to EMSW via the inflow of WMSW through the Strait of Sicily.

A.5.2.2 Inflow from Western Mediterranean Sea

According to Krom et al. (2004), the flux of dissolved PO_4 from WMS to EMS equals $2.2x10^9$ mol P yr^{-1}. This flux estimate, however, is representative of conditions at the end of the 20^{th} century. Mass balance calculations by Béthoux et al. (1992) for the year 1960 yield a lower PO_4 flux of $1.9x10^9$ mol P yr^{-1}. The latter value is adjusted slightly downward to $1.60x10^9$ mol P yr^{-1} to balance the inputs and outputs of P in

1950. Measurements obtained in 1996 indicate relatively high DOP concentrations in WMSW (>60nM, Moutin and Raimbault, 2002). We therefore use a DOP:PO_4 ratio of ~2 for WMSW, similar to EMSW, to estimate the input flux of DOP from the WMS at 3.30×10^9 mol P yr^{-1}.

A.5.2.3 Atmospheric deposition

Krom et al. (2004) estimate leachable PO_4 deposition to the Eastern Mediterranean, including the Adriatic and Aegean seas, to be around 0.95×10^9 mol P yr^{-1}. Markaki et al. (2010) report that 38% of leachable P in atmospheric deposition is in the form of DOP, yielding an additional flux of 0.58×10^9 mol P yr^{-1}. These estimates, however, are representative for the latter part of the 20th century. Atmospheric deposition of PO_4 in 1990 may have exceeded that in 1950 by a factor of three (Chapter 2), while DOP deposition probably also increased during the same period due to enhanced biomass burning. According to Ito and Penner (2005) biomass burning in the northern hemisphere has increased by a factor of 1.4 since 1950. Using these factors, and pro-rating to the surface area of the model domain (i.e., excluding the Adriatic and Aegean seas), yields 1950 atmospheric inputs of PO_4 and DOP of 0.38×10^9 mol P yr^{-1} and 0.33×10^9 mol P yr^{-1}, respectively.

A.5.2.4 Outflow fluxes

The output fluxes of dissolved P from EMS to WMS are computed from the water outflow through the Strait of Sicily (1.1 Sv, Figure A.1) and the corresponding EMIW concentrations in 1950 (Figure A.2). The calculations yield PO_4 and DOP fluxes to the WMS of 3.73×10^9 mol P yr^{-1} and 1.48×10^9 mol P yr^{-1}, respectively. Combining the PO_4 outflow flux via the Strait of Sicily with the surface inflow flux of PO_4 from the WMS (1.60×10^9 mol P yr^{-1}, section A.5.2.1) results in a net export of PO_4 to the WMS of 2.13×10^9 mol P yr^{-1}, which is about half the net export of PO_4 through the Strait of Sicily estimated by Krom et al. (2004). A lower flux in 1950, however, is consistent with the significant rise in anthropogenic P inputs to the EMS during the second part of the 20th century (Chapter 2). The output fluxes of dissolved P due to upwelling of EMIW into the Adriatic and Aegean seas are similarly computed from the corresponding water flows (0.32 and 0.04 Sv, Figure A.1) and the PO_4 and DOP concentrations of EMIW (Figure A.2).

A.5.2.5 Deep-water formation

The EMIW flowing into the Adriatic Sea and the Aegean Sea returns to the EMS as EMDW (Figure A.1; section A.3.2). In the model, we assume that the deep-water flowing into the EMS carries with it the PO_4 and DOP originally present in EMIW, plus additional PO_4 and DOP acquired in the Adriatic and Aegean basins. The fluxes of additional PO_4 and DOP are estimated by correcting the combined riverine and

atmospheric inputs to the Adriatic Sea and Aegean Sea for P burial in sediments accumulating in the two basins and P export via surface flow to the EMS (section A.5.2.1). In other words, the dissolved P fluxes in and out of the Adriatic and Aegean seas are assumed to be at steady state.

Estimates of the riverine inputs of PO_4 and DOP to the Adriatic Sea and Aegean Sea are derived from the 1963 river inputs of total P given by Ludwig et al. (2009), following the same procedure as used to estimate the riverine inputs of dissolved P to the EMS (section A.5.2.1). For the Aegean Sea, net PO_4 and DOP inputs from the Black Sea are assumed to be the same as those reported by Krom et al. (2004). The atmospheric inputs of soluble PO_4 to the Adriatic Sea and Aegean Sea in 1950 are estimated following the approach outlined in section A.5.2.2, using the deposition fluxes of leachable and non-leachable P to the entire Eastern Mediterranean Sea of Krom et al. (2004), pro-rated for the surface areas of the Adriatic Sea and Aegean Sea. The P burial flux for the entire Eastern Mediterranean Sea of Krom et al. (2004) is similarly pro-rated to the surface areas of the Adriatic Sea and Aegean Sea in order to obtain the POP burial fluxes. The resulting excess inputs of PO_4 and DOP to the EMDW associated with deep-water formation in the Adriatic plus Aegean seas are then 0.06×10^9 mol P yr^{-1} (PO_4) and 0.03×10^9 mol P yr^{-1} (DOP). Thus, 95% of the input of total dissolved P (PO_4 plus DOP) to the EMDW associated with Adriatic and Aegean deep-water formation originates from EMIW. That is, in the model, the primary function of Adriatic and Aegean deep-water formation is to transfer nutrient P and N from the EMIW to the EMDW reservoir.

A.5.2.6 Sediment burial

The pre-anthropogenic burial flux of POP for the EMS including the Adriatic and Aegean Seas has been estimated to be on the order of 1×10^9 mol P yr^{-1} (Krom et al., 2004). Prorating this flux to the surface area of the EMS model domain yields a 1950 burial flux of 0.80×10^9 mol P yr^{-1}. This value is slightly adjusted to 0.78×10^9 mol P yr^{-1}, in order to insure steady state.

A.5.3 Nitrogen input and output fluxes

A.5.3.1 Surface flow inputs

Ludwig et al. (2009) estimate the riverine supply of total N to the EMS (excluding rivers flowing into the Adriatic and Aegean seas) in 1963 to be 41×10^3 t N yr^{-1} or 2.9×10^9 mol N yr^{-1}. A lower riverine flux (2.6×10^9 mol N yr^{-1}) is assigned to 1950, to account for the rising use of nitrogen fertilizer use in Europe during the 1950s (Federico, 2005). Ludwig and coworkers further propose that 75% of total riverine N is in the form of NO_3, the rest being mainly DON, while NH_4 represents only about 5%. Surface flow fluxes from the Adriatic and Aegean add minor amounts of N to the total surface inflow into the EMS.

Using representative surface water NO_3 concentrations for the southern Adriatic Sea (1.2 μM, Zavatarelli et al., 1998) and Cretan Sea (0.6 μM, Krasakopoulou et al., 1999), and keeping the same proportions of NO_3, DON and NH_4 as for the rivers, the combined surface flow input fluxes to the EMS are then $2.4x10^9$ mol N yr^{-1} (NO_3), $0.6x10^9$ mol N yr^{-1} (DON) and $0.2x10^9$ mol N yr^{-1} (NH_4).

A.5.3.2 Inflow from Western Mediterranean

The 1950 NO_3 flux associated with WMSW flowing into the EMS is derived from the estimated 1950 PO_4 flux from WMS to EMS ($1.60x10^9$ mol P yr^{-1}, section A.5.2.1) multiplied by an estimate of the NO_3:PO_4 ratio of surface waters near the Strait of Sicily (10-30, Moutin and Raimbault, 2002; Ribera d'Alcalà et al., 2003; Pujo-Pay et al., 2011). This approach yields NO_3 fluxes ranging between 16 and $48x10^9$ mol N yr^{-1}. We assign the mid-range value of $32x10^9$ mol N yr^{-1}. Assuming that the 1950 DON:NO_3 ratio of WMSW reaching the Strait of Sicily is similar to values reported for the surface waters of the WMS in more recent times (~3, Pujo-Pay et al., 2011), the DON flux is then of the order of $100x10^9$ mol N yr^{-1}.

A.5.4 Atmospheric deposition

Budget calculations by Krom et al. (2004) yield an atmospheric deposition flux of inorganic N to the EMS, including the Adriatic and Aegean, of $111x10^9$ mol N yr^{-1}, while measurements indicate that DON may additionally contribute 32% of leachable N deposition (Markaki et al., 2010; Violaki et al., 2010). As with P (section A.5.2.2), N deposition flux estimates for the latter part of the 20^{th} century must be revised downward. From the ice core data of Preunkert et al. (2003) and Fagerli et al. (2007), we estimate that NO_3 and NH_4 deposition between 1950 and 1990 increased by factors of 3 and 2.1, respectively. We further assume that DON deposition increased by 40% during the same time period. Pro-rating to the surface area of the model domain and making small adjustments to balance N inputs and outputs for the EMS results in the fluxes shown in Figure A.3.

A.5.4.1 Outflow fluxes

Outflow fluxes of dissolved N to the WMS are calculated using the EMIW concentrations of NO_3, DON and NH_4 (Figure A.3) and the water flow through the Strait of Sicily (Figure A.1). Similarly, the upwelling fluxes of NO_3, DON and NH_4 into the Adriatic and Aegean seas are derived from the corresponding water fluxes and EMIW concentrations. As with PO_4, the resulting net export of NO_3 from the EMS to the WMS in 1950 is lower than that estimated by Krom et al. (2004) for the 1990s.

A.5.4.2 Deep-water formation

Nutrient distributions in the Southern Adriatic Basin were recently reported by Santinelli et al. (2012a). In the deep waters, the average molar NO_3:PO_4 ratio is around 23. In combination with the estimated 1950 PO_4 flux (Figure A.2) this yields a NO_3 flux to the EMDW via Adriatic deep-water formation on the order of $30x10^9$ mol N yr^{-1}. Adriatic Deep Water further exhibits comparable molar NO_3 and DON concentrations, implying a DON flux to the EMDW of similar magnitude as that of NO_3. Assuming that NH_4 represents ≤1% of total dissolved N in Adriatic Deep Water, and after minor adjustments to balance input and output fluxes for the EMS, we obtain the fluxes shown on Figure A.3. As for Adriatic Deep Water formation, the NO_3 input to EMDW associated with Aegean Deep Water formation is estimated using observed NO_3:PO_4 ratios in Cretan Deep Water (Krasakopoulou et al., 1999) together with the 1950 PO_4 flux from the Aegean to the EMDW estimated in section A.5.2.4. Because no DON and NH_4 concentrations are available for Cretan Deep Water, we estimate the corresponding fluxes assuming the same NO_3:DON:NH_4 ratios as in EMDW (Krom et al., 2005).

A.5.4.3 Sediment processes

Krom et al. (2004) estimate a denitrification flux of $10x10^9$ mol N yr^{-1} for the entire EMS, including the Adriatic and Aegean Seas. Denitrification, however, is largely confined to the sediments accumulating below the productive waters of the Northern Adriatic Sea (7.1×10^9 mol yr^{-1}; Krom et al., 2004). Pro-rating the remainder to the surface area of the model domain gives a denitrification flux of $2.3x10^9$ mol N yr^{-1}. Similarly, pro-rating the burial rate for the entire EMS basin estimated by Krom et al. (2004) yields a burial flux of $22x10^9$ mol N yr^{-1}. Slight adjustments to insure steady state then yield the removal fluxes shown in Figure A.3

A.5.5 Internal phosphorus and nitrogen cycling

Average gross primary production in the EMS falls in the range 60-80 gC m^{-2} yr^{-1} (Béthoux, 1989). The lower value of 60 gC m^{-2} yr^{-1} is used as the 1950 estimate. Together with the standard Redfield ratio (106:16:1) and the surface area of the EMS, this yields P and N photosynthetic assimilation fluxes in the EMSW of $63x10^9$ mol P yr^{-1} and $1000x10^9$ mol N yr^{-1}. Béthoux (1989) further estimates the export production to be on the order of 12 gC m^{-2} y^{-1}. Combining this with a C:N ratio of 106:12.6 for sinking organic detritus (Krom et al., 1991), we obtain a sinking flux of PON of $159x10^9$ mol N y^{-1}. Similarly, given basin-wide integrated N:P ratios of decomposed organic matter in the range 23-30 (Krom et al., 2005), the corresponding export of POP should be on the order of $6x10^9$ mol P y^{-1}. The model spin-up yields the slightly modified flux values shown in Figures A.2 and A.3.

Once values are assigned to the concentrations of dissolved P and N species in the EMSW, EMIW and EMDW reservoirs, the up- and downwelling fluxes are fixed by the corresponding water fluxes. In addition, all the turbulent mixing fluxes of dissolved P and N species are assumed to be proportional to the concentration differences between the source and receptor reservoirs (i.e., the same turbulent diffusion coefficient applies to all dissolved species). All other remaining internal fluxes then derive from the condition of steady state.

The reasonableness of the resulting fluxes can be verified for the vertical eddy diffusion fluxes of PO_4 and NO_3. The concentration gradients driving the diffusion fluxes can be estimated from the concentration differences of PO_4 (110 – 25 = 85 nM) and NO_3 (2.5 – 0.5 = 2.0 μM) between EMIW and EMSW and the midpoint distance between the two reservoirs (350 – 100 = 250 m). Combined with representative values for the vertical turbulent diffusion coefficient near the nutricline (1-1.5 $cm^2\ s^{-1}$, Krom et al., 1992; Crispi et al., 2002) and the surface area of the EMS, the fluxes are computed to be on the order of 1-2x10^9 mol P yr^{-1} and 30-50x10^9 mol N yr^{-1}. These fluxes are in order-of-magnitude agreement with those shown on Figures A.2 and A.3. The latter are higher, however, which is not unexpected as the actual concentration gradients controlling the upward diffusive fluxes are likely to be steeper than estimated here.

A further independent check on the internal fluxes can be obtained from the observed west to east change in PO_4 concentration of the EMDW. Adriatic deep water enters the EMS via the western Ionian Basin and then travels eastwards to the East Levantine Basin. During the eastward transit the EMDW PO_4 concentration increases by about 0.05 μM (Krom et al., 2014). This increase can be attributed to the mineralization of organic P in the EMDW reservoir. Together with an EMDW residence time of 150 years and an EMDW volume of 17x10^{14} m^3 (Figure A.1), the observed increase in PO_4 concentration translates into a rate of EMDW PO_4 accumulation of 0.57x10^9 mol P yr^{-1}. The latter is in good agreement with the model-predicted DOP mineralization flux in the EMDW (0.71 x10^9 mol P yr^{-1}, Figure A.2).

In the model, recycling of organic P and N is treated as a two step process, with POP and PON first producing DOP and DON, followed by mineralization into dissolved inorganic P and N. In this simple model representation, the net fluxes associated with these two steps integrate the effects of multiple biogeochemical and food web processes, such as, exudation, grazing, cell lysis, heterotrophy and bacterial assimilation of DOP and DON (Zehr and Ward, 2002). In addition, the model assumes that all NH_4 produced during the mineralization of organic N is transformed into NO_3 via nitrification, although NH_4 may be assimilated directly by algae (Dugdale and Goering, 1967). For the EMS, isotopic data suggest that ammonia assimilation by phytoplankton is a relatively unimportant process, implying that nitrate is the principal N source for phytoplankton (Emeis et al., 2010). This is consistent with the observations of

Krom et al. (1992), who report that the main winter phytoplankton bloom coincides with the upward mixing of nitrate into the euphotic zone.

A.6 Numerical model and sensitivity analyses

A.6.1 Numerical model

The ordinary differential equations expressing the mass balances for the 21 P plus N reservoirs are presented in Appendix A.10. The equations are solved in MATLAB® using solver ode15s. For most internal fluxes, a simple linear dependence on the mass of the source reservoir is assumed (Lasaga, 1980). The first-order rate constants are then calculated from the initial (i.e., 1950) estimates of the corresponding reservoir masses and fluxes. For the turbulent mixing of P and N, the fluxes are assumed to depend linearly on the difference in concentration between EMIW and EMSW. The turbulent mixing fluxes can therefore switch direction during model simulations.

For NH_4, first-order flux equations cause unacceptably large variations in the reservoir masses, because of the small size of the NH_4 reservoirs. To dampen these variations, the flux equations for DON mineralization and nitrification are therefore assumed to be inversely proportional to the mass of the receiving reservoir. Thus, high NO_3 concentrations slow down the conversion of NH_4 to NO_3 while high NH_4 concentrations slow down the mineralization of DON. As an example, the nitrification flux at a given time t is related to the corresponding EMSW reservoir masses of NH_4 and NO_3 by

$$F_{\text{nit}}(t) = k_{\text{nit}} \cdot \frac{NH_4(t)}{NO_3(t)} \qquad \text{(A.1)}$$

where the rate constant k is obtained from the initial 1950 flux and reservoir masses:

$$k_{\text{nit}} = F_{\text{nit}}(0) \cdot \frac{NO_3(0)}{NH_4(0)} \qquad (2)$$

The same approach applies to the mineralization fluxes of DON to NH_4. With these formulations, and the imposed input and output fluxes, the model is spun up till steady state.

A.6.2 Sensitivity analyses

The model's sensitivity to the imposed water cycle, the external nutrient inputs and the internal transformation and transport processes is analyzed using factorial design (Box et al., 1978; Dale et al., 2006). The responses of the following two model outcomes are considered: primary production, expressed as the assimilatory uptake of PO_4 in the EMSW, and the EMDW NO_3:PO_4 ratio. These

outcomes are directly related to two of the most prominent biogeochemical features of the EMS, the pronounced oligotrophy and the unusual water column nutrient ratios.

The sensitivity of primary production to the water cycle, external nutrient inputs and internal processes are based on 2^9, 2^{10} and 2^{12} full factorial designs, respectively. Only the effects of the P cycle are investigated, as the model assumes P-limited primary production. The imposed 1950 water and nutrient fluxes are varied by ±10%. When analysing the sensitivity to internal fluxes, the external inputs remain constant, and vice versa. Yate´s algorithm (Box et al., 1978) is used to calculate the effects on the model response. The estimates of effect are ranked in ascending order to calculate cumulative frequency. The resulting probability-effect plots are shown in Figure A.4. On such a plot, when the response is not sensitive to a flux or combination of fluxes, the corresponding point aligns along the vertical centered on the origin (i.e., zero effect). Any sensitive flux or combination of fluxes produces an effect that deviates from this vertical line.

Primary production in the EMS is most sensitive to the P exchanges associated with the water flows between the EMS and WMS, the imposed PO_4 assimilation flux, the biogeochemical processes that recycle POP to PO_4 within EMSW and EMIW, and the transport processes that move P between these two water masses. Processes within the EMDW play a much smaller role in controlling primary production, although the inflow of Adriatic deep water into the EMDW has a noticeable effect. The latter is related to the associated input of PO_4, some of which may ultimately reach the EMSW and be utilized by primary producers. The sensitivity analysis highlights the key role of nutrient P inflow from the WMS, not only in the inorganic form but also as DOP. In addition, primary production appears to be more sensitive to the input of PO_4 to the EMS associated with Adriatic Deep Water formation than to the combined P inputs via rivers, surface flow from the Adriatic plus Aegean seas, and atmospheric deposition.

The results in Figure A.4 also imply that primary production is sensitive to single fluxes rather than combinations of fluxes. This is generally true for other model responses (not shown). In other words, higher order interactions have a negligible effect on the model dynamics, and they are therefore not included in the sensitivity analyses of the EMDW NO_3:PO_4 ratio shown in Figure A.4. The latter are based on a 2^9 full factorial design, and $2_V^{25-15}$and 2_V^{28-18} fractional factorial designs for the water cycle, external nutrient inputs and internal processes, respectively, following the same approach as described above, but now applied to both the P and N cycles.

The EMDW NO_3:PO_4 ratio is most sensitive to the supply of dissolved P and N via deep-water formation in the Adriatic Sea, upwelling from the EMDW to the EMIW, surface inflow from the WMS, as well as to

biogeochemical processes taking place in the EMDW plus sediment burial. The main role of Adriatic deep-water formation is to remove P and N from the EMIW and transfer them to the EMDW. Comparison of the effects associated with the internal and external fluxes implies that the nutrient inflow from the Adriatic Sea and WMS exert a larger influence on the EMDW NO_3:PO_4 ratio than the breakdown, mineralization and burial of POP and PON in the EMDW itself. Note that the effects of inorganic PO_4 and NO_3 are larger than those of DOP and DON for the deep-water inflow from the Adriatic Sea, but that the opposite is true for the surface inflow from the WMS.

A.7 Discussion

The coupled mass balance model for P and N provides a quantitative framework for describing and analyzing the unique nutrient dynamics in the Eastern Mediterranean Sea (EMS). In the present paper, the model is initialized for nominal year 1950, that is, prior to the large increases in nutrient inputs experienced by the Mediterranean Sea during the second half of the 20th century (Chapter 2). Water flows, nutrient reservoir masses and nutrient fluxes into, from and within the EMS are estimated based on an exhaustive review and interpretation of the available literature. The model spin-up to steady state then yields the values of concentrations, reservoir masses and fluxes shown in Figures A.1 and A.2 and Table A.1, with the corresponding molar N:P ratios summarized in Table A.2. These values should be viewed as order of magnitude estimates, in particular for the organic forms of P and N for which only limited data are available. However, as shown in the companion paper, the predicted changes in nutrient distributions over the period 1950-2000 are consistent with independent observations not used when initializing the model (Chapter 2). Here, we discuss the principal outcomes of the 1950 model as they relate to the characteristic nutrient-based features of the EMS, namely ultra-oligotrophy, low nutrient water column concentrations, and non-Redfieldian organic and inorganic N:P ratios.

The very low productivity of the EMS cannot be ascribed to abnormally low nutrient inputs. The 1950 estimates of the total external supply fluxes of soluble P and N (inorganic plus organic species) to the surface waters of the EMS by rivers, atmospheric deposition and surface inflow from the WMS, Adriatic Sea and Aegean Sea, normalized to the surface area of the EMS, are 0.004 mol P m^{-2} yr^{-1} and 0.15 mol N m^{-2} yr^{-1}. These values are comparable to those reported, for example, for the Baltic Sea (0.006 moles P m^{-2} yr^{-1} and 0.38 moles N m^{-2} yr^{-1}; Artioli et al., 2008). The latter is similarly land-locked, but exhibits markedly higher primary productivity than the EMS (Rydberg et al., 2006).

Note that the budgets in Figures A.2 and A.3 do not include P and N inputs to the EMS from coastal runoff or submarine groundwater inflow. Nutrient inputs by diffuse coastal runoff from Turkey and Middle Eastern plus North African countries are likely to be negligible because of the (semi-)arid climate

conditions. (Note: while coastal runoff may be a significant source of reactive P and N in the Adriatic and Aegean Seas, the latter are not included in the EMS model domain.) According to Zekster et al. (2007), submarine groundwater inflow to the entire Mediterranean Sea may amount up to 25% of the riverine discharge. The karstic coast of Turkey in particular could be an important conduit for submarine groundwater flow to the EMS. As the concentrations of nutrients in discharging groundwater can be quite high (Weinstein et al., 2011), submarine groundwater inputs could therefore be a non-negligible source of nutrient P and N to the EMS. Further work will be needed to fill this knowledge gap in the biogeochemistry of the EMS.

New production in the EMS is supported by nutrients supplied to the surface waters from external sources and by turbulent mixing from the intermediate water (EMIW). Of these, the largest nutrient supply is from the WMS, primarily in the form of DOP and DON. A substantial fraction (~50%) of the DOP imported from the WMS is remineralized in the EMSW and, hence, represents a significant contribution to the new production in the EMS. According to the 1950 budgets shown in Figures A.2 and A.3, the net supplies of dissolved P and N to the EMSW account for 10 and 17% of the annual gross primary productions of POP and PON, respectively. Conversely, this implies that the recycling of P in the EMSW fuels 90% of the annual production of POP. Such high recycling efficiency of the limiting nutrient, and the corresponding high fraction of regenerated production, are typical for oligotrophic marine systems (e.g., Sarmiento and Gruber, 2006).

At steady state, new production and export production balance each other. Hence, 10 and 17% of the POP and PON produced annually in the EMSW sink into the EMIW reservoir. Further organic matter decomposition in EMIW and EMDW ultimately results in the burial in the sediments of the EMS of 1 and 2 % of the annual gross production of POP and PON, respectively. Organic matter burial rates of a few % or less are common for open ocean waters (e.g., Van Cappellen, 2003). What sets the EMS apart from other areas of the global ocean is the large lateral export of regenerated nutrients, which permanently removes dissolved P and N from the EMIW reservoir to the WMS. Note, however, that for the estimated 1950 P budget the inflow and outflow fluxes of total dissolved P (i.e., PO_4 plus DOP) through the Strait of Sicily are nearly identical. The major difference is the speciation of P in the inflow and outflow. Whereas DOP dominates dissolved P supplied from the WMS, PO_4 is the main form exported to the WMS. The latter limits the build-up of PO_4 in EMIW and, hence, the upward transfer of PO_4 back to the euphotic zone by turbulent mixing. Supply of N to the EMSW is similarly limited by the outflow of NO_3 to the WMS. The efficient export to the WMS also translates into short residence times of P and N in the EMIW reservoir, on the order of 9 years, in contrast to the EMDW where residence times are on the order of 200 years.

While the anti-estuarine circulation helps explain the low water column PO_4 and NO_3 concentrations and the resulting low productivity of the EMS, it does not in itself explain why the molar N:P ratios of all the dissolved and particulate reservoirs in the EMS exceed the 16:1 Redfield ratio (Table A.2). In the proposed model, these ratios result from the combination of higher-than-Redfield inputs of reactive N relative to reactive P, the absence of significant denitrification, and the preferential regeneration of PO_4 relative to NO_3 during the decomposition of organic matter (Krom et al., 2010).

According to the 1950 flux estimates, molar N:P ratios supplied by atmospheric deposition, surface inflow (rivers plus surface inflow from WMS, Adriatic and Aegean) and deep water input (from Adriatic and Aegean) equal 91, 26 and 36, respectively. The combined external delivery of soluble P (PO_4 plus DOP) and N (NO_3, NH_4 plus DON) to the EMS has an N:P ratio of 34. Many other marine basins have external N:P supply ratios greater than 16, even after subtracting the anthropogenic contributions. For instance, the external N:P supply ratio for the Baltic Sea may have exceeded 50 prior to the 20th century (Larsson et al., 1985). At the global scale, estimates of the supply by rivers of dissolved P and N from natural sources to the ocean yield an overall N:P ratio of 45 (Seitzinger et al., 2005). In most oceanic basins, however, higher-than-Redfield inputs of N are compensated by the net loss of fixed nitrogen due to denitrification (Tyrrell, 1999). In contrast, in the EMS denitrification is restricted by the ultra-oligotrophic conditions, which results in a low deposition flux of organic matter at the seafloor and, hence, the absence of anaerobic conditions in surficial sediments. The estimated 1950's denitrification flux of 2.5×10^9 moles N yr^{-1} represents approximately 1% of the total reactive N input to the EMS and, therefore, has only a minimal effect on basin-wide N:P ratios.

Although N:P ratios have been determined for the various organic and inorganic reservoirs of the EMS, the NO_3:PO_4 ratio of the EMDW has received most attention. Measurements of NO_3:PO_4 ratios in the deeper parts of the basin were the first to demonstrate the unusual nutrient composition of the EMS and, consequently, the EMDW NO_3:PO_4 ratio has been measured most often (Krom et al., 1991; Kress and Herut, 2001; Kress et al., 2003; Pujo-Pay et al., 2011). Model calculations show that the 1950 denitrification flux would have to increase 14-fold for the EMDW NO_3:PO_4 ratio to approach the Redfield value of 16:1, all else unchanged (Figure A.5). With a 14-fold increase, the denitrification flux would equal 34.6×10^9 moles N yr^{-1}. The latter represents on the order of 3.5% of the assimilatory uptake of N by primary production, which falls within the range estimated for the global ocean (2-6%), based on a global marine productivity of 50 Pg C yr^{-1} (Carr et al., 2006) and a range of denitrification of 175-450 Tg N yr^{-1} (Codispoti, 2007). The model calculations, however, do not take into account the feedback between denitrification and nitrogen fixation: as denitrification lowers the N:P ratio of the EMS, nitrogen fixation is likely to increase. Thus, the denitrification flux would have to increase by more than a factor of 14 for

the EMDW NO_3:PO_4 ratio to reach 16. As a corollary, the mass balance model implies that the lack of significant denitrification in the EMS requires that nitrogen fixation must play a minor role in the N cycle of the EMS, as corroborated by existing field measurements (Ibello et al., 2010a; Bonnet et al., 2011; Yogev et al., 2011).

Most of the organic P and organic N in the EMS derive from primary production in the EMSW. Primary producers are assumed to synthesize new biomass with Redfield composition, which is in agreement with field and experimental data for the EMS (Krom et al., 2010). The higher-than-Redfield PON:POP and DON:DOP ratios that are systematically observed in the EMS (Moutin and Raimbault, 2002; Krom et al., 2005; Pujo-Pay et al., 2011) therefore imply a more efficient recycling of P relative to N during organic matter decomposition. In the model, 90% and 83% of the gross production of POP and PON, respectively, are regenerated back to inorganic nutrients within the EMSW. Hence, settling of particulate matter and downwelling of surface waters transfer N-enriched organic matter to the EMIW. Preferential recycling of P continues below the EMSW, hence sustaining higher-than-Redfield N:P ratios of particulate and dissolved organic matter throughout the EMS. The difference in recycling efficiency between P and N is also reflected in the relative abundances of organic and inorganic forms of the two elements in the EMS. Integrated over the entire water column, inorganic dissolved PO_4 and N (NO_3 + NH_4) account for 76% and 59% of total reactive P (PO_4 + POP + DOP) and N (NO_3 + NH_4 + PON + DON), respectively. The preferential regeneration of organic P relative to organic N may reflect the P-limited nature of biological productivity in the EMS, as also proposed for other oligotrophic marine systems (Clark et al., 1998).

A.8 Conclusions

The EMS is a P-limited, ultra-oligotrophic marine basin with unusually high water column N:P ratios. The proposed biogeochemical nutrient model is consistent with the hypothesis that the anti-estuarine circulation of the EMS is primarily responsible for the low dissolved NO_3 and PO_4 concentrations throughout the water column, as well as the low primary productivity of the EMS, which is among the lowest of the world's oceans. In addition, the nutrient model highlights aspects of the P and N cycles that have previously received less or no attention, in particular the roles of the organic pools of P and N.

According to the reconstructed 1950 nutrient budgets, the principal external source of P and N to the EMS is the WMS. The surface inflow from the WMS, however, mainly delivers DOP and DON to the surface waters of the EMS. Furthermore, while Adriatic and Aegean deep-water formation represents an important nutrient input to the EMDW, it mostly carries dissolved P and N from the EMIW. Both the lateral export of inorganic nutrients to the WMS, and the transfer of P and N from EMIW to EMDW

through Adriatic and Aegean deep-water formation, severely limit the upward flux of PO_4 from intermediate water depths to the euphotic zone, where it would otherwise fuel primary production.

All the external nutrient inputs to the EMS are characterized by higher-than-Redfield N:P ratios, which in itself is not unusual. However, in contrast to other marine basins or the global ocean, the water column nutrient inventories in the EMS maintain these higher-than-Redfield N:P ratios, because minimal amounts of fixed N are removed by denitrification. The very high molar N:P ratios of the particulate and dissolved organic pools (≥ 31) further imply a preferential regeneration of P relative to N during organic matter decomposition. This may be generally true for P-starved oligotrophic marine systems.

The proposed biogeochemical model for the EMS is based on well-established oceanographic processes. The initialization of the model for the year 1950 offers, we believe, a reasonable representation of the conditions prevailing in the EMS prior to the large increases in anthropogenic nutrient inputs. Because of the absence of relevant measurements going back to the 1950s, direct model validation is not possible, however. In the companion paper, we evaluate to what extent the model is capable of reproducing more recent observations, starting from the initial conditions presented here.

A.9 Tables and figures

Table A.1: Concentration ranges of the P and N pools considered in the EMS biogeochemical model (in units of nM and μM, respectively), plus the reservoir masses after model spin-up (masses are given in units of 10^9 moles). The corresponding concentrations of the P and N pools are shown in Figures A.2 and A.3.

	PO_4	**DOP**	**POP**	**NO_3**	**NH_4**	**DON**	**PON**
Range		nM			μM		
EMSW	0-100	10-100	4-20	0.01-3	0.04-0.08	2-11	0.1-0.5
EMIW	30-200	30-80	3-10	0.5-6	0.05-0.06	2-5	0.1-0.3
EMDW	130-230	0-70	2.5-8	3-6	<0.1	0-5	0.05-0.15
Mass		10^9 mol			10^9 mol		
EMSW	7.0	14.1	2.0	148	23	737	80
EMIW	43.1	17.1	2.1	1021	19	1056	65
EMDW	299.1	71.4	5.8	8234	89	4312	185

Table A.2: Molar N:P ratios of the various nutrient reservoirs after model spin-up. See text for detailed discussion.

	NO_3:PO_4	DON:DOP	PON:POP
EMSW	21	52	40
EMIW	24	62	31
EMDW	28	60	32

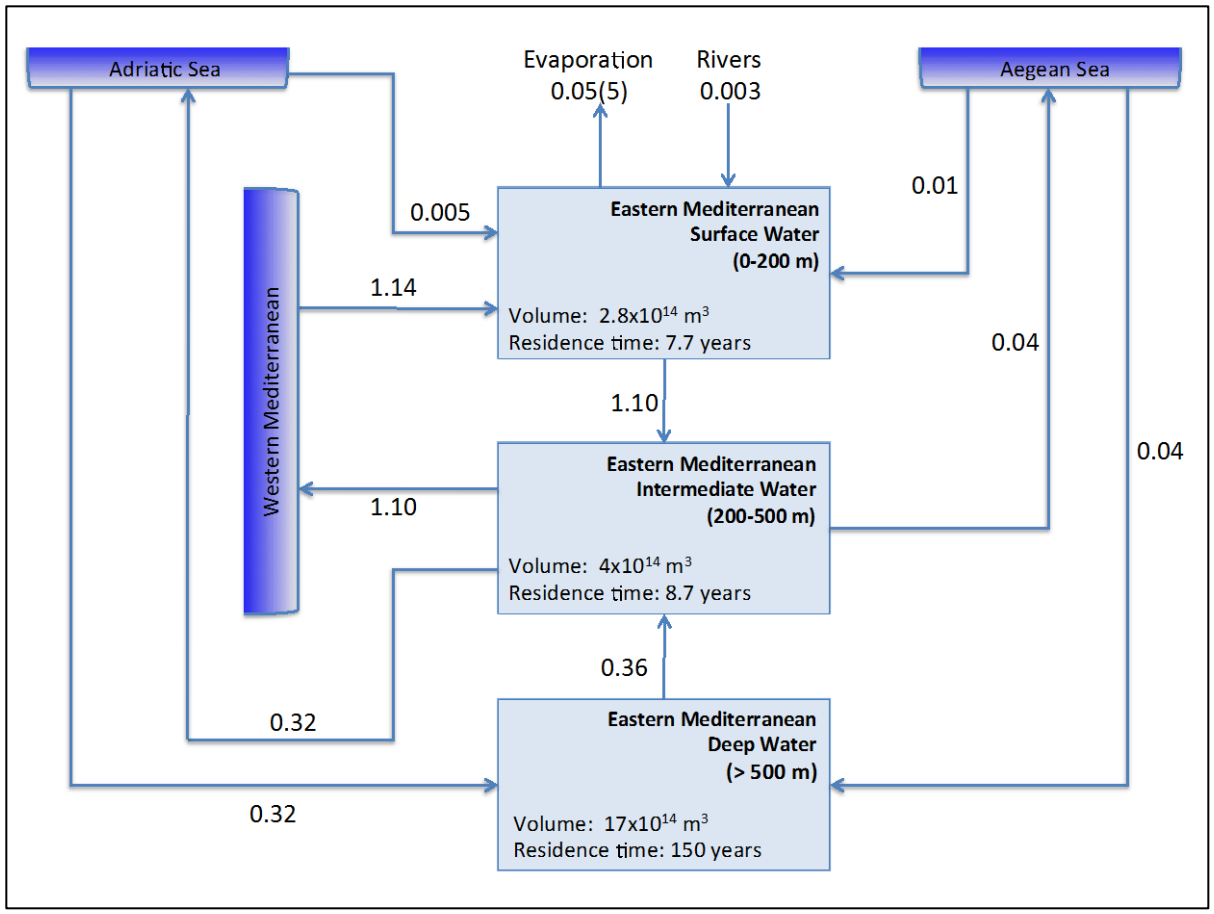

Figure A.1: Water cycle of the EMS. Water fluxes are given in Sverdrup units (1 Sv = 10^6 m^3 s^{-1}).

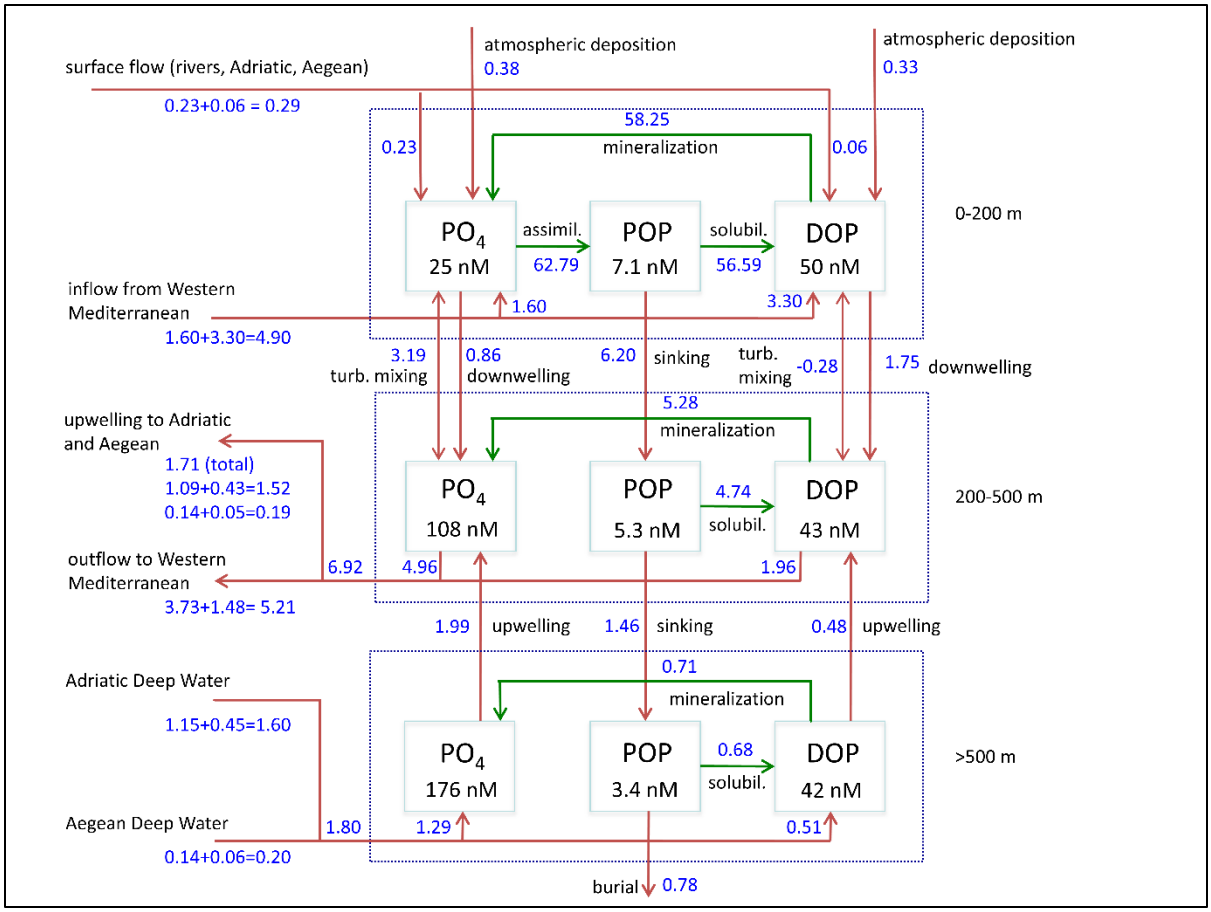

Figure A.2: Steady state phosphorus model for the EMS in 1950. For each P reservoir, the concentration is indicated in units of nM. (Note: The corresponding reservoir masses are listed in Table A.1.) Fluxes are expressed in 10^9 mol P yr^{-1}. Upward (downward) turbulent mixing fluxes are assigned positive (negative) values.

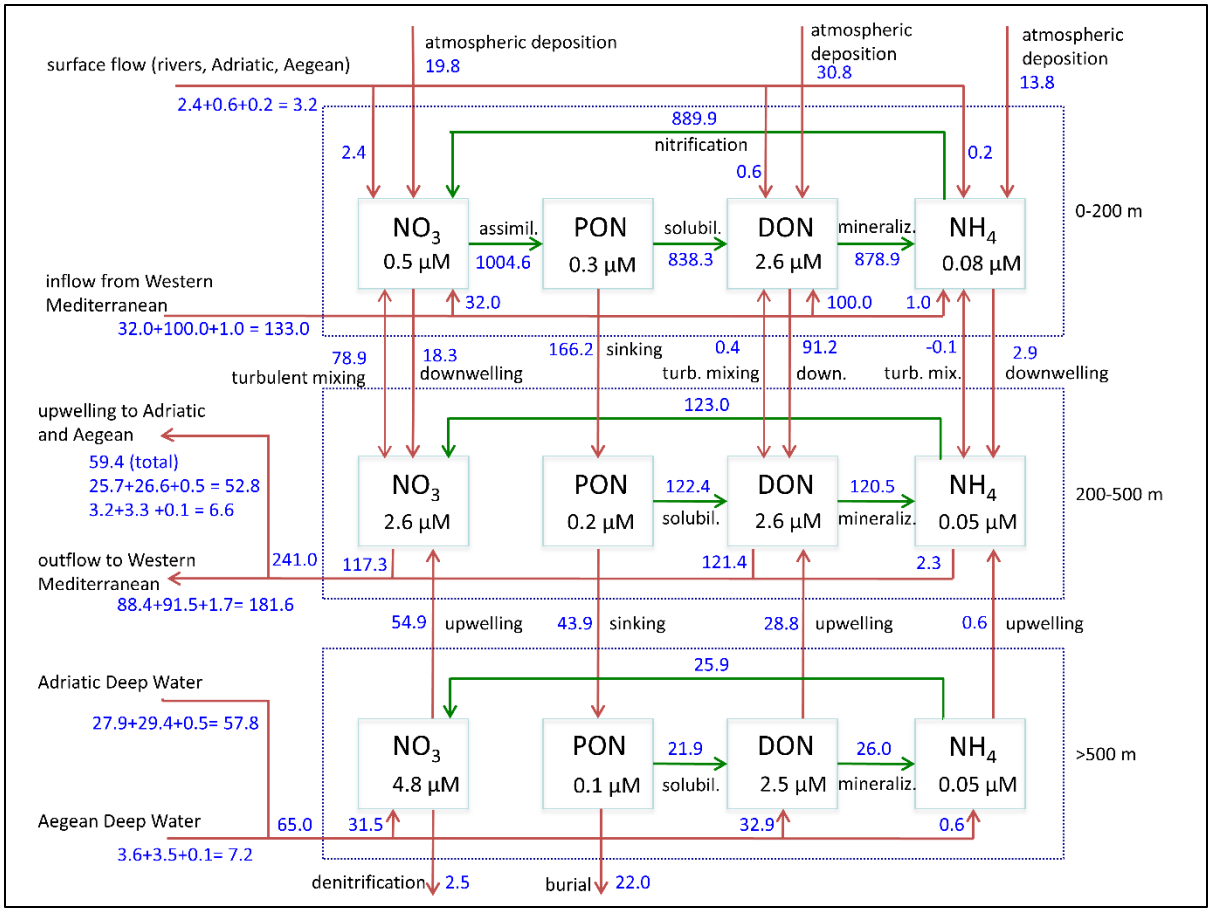

Figure A.3: Steady state nitrogen model for the EMS in 1950. For each N reservoir, the imposed concentration is indicated, in units of µM. The corresponding reservoir masses are listed in Table A.1. Fluxes are expressed in 10^9 mol N yr^{-1}. Upward (downward) turbulent mixing fluxes are assigned positive (negative) values.

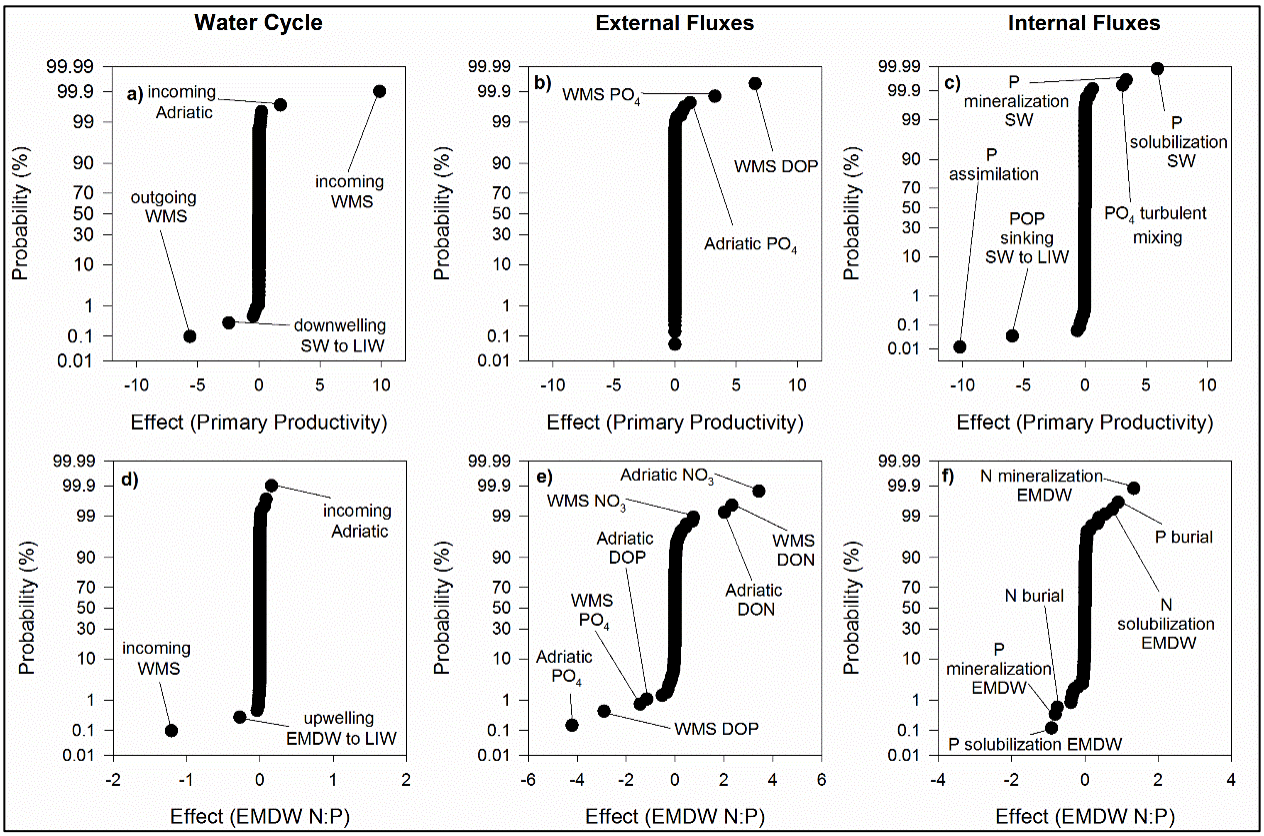

Figure A.4: Factorial design analyses: effects of water cycle, external nutrient inputs and internal fluxes on primary production (panels a-c) and the EMDW NO_3:PO_4 ratio (panels d-f). Only those effects that are significant are identified. See text for complete discussion.

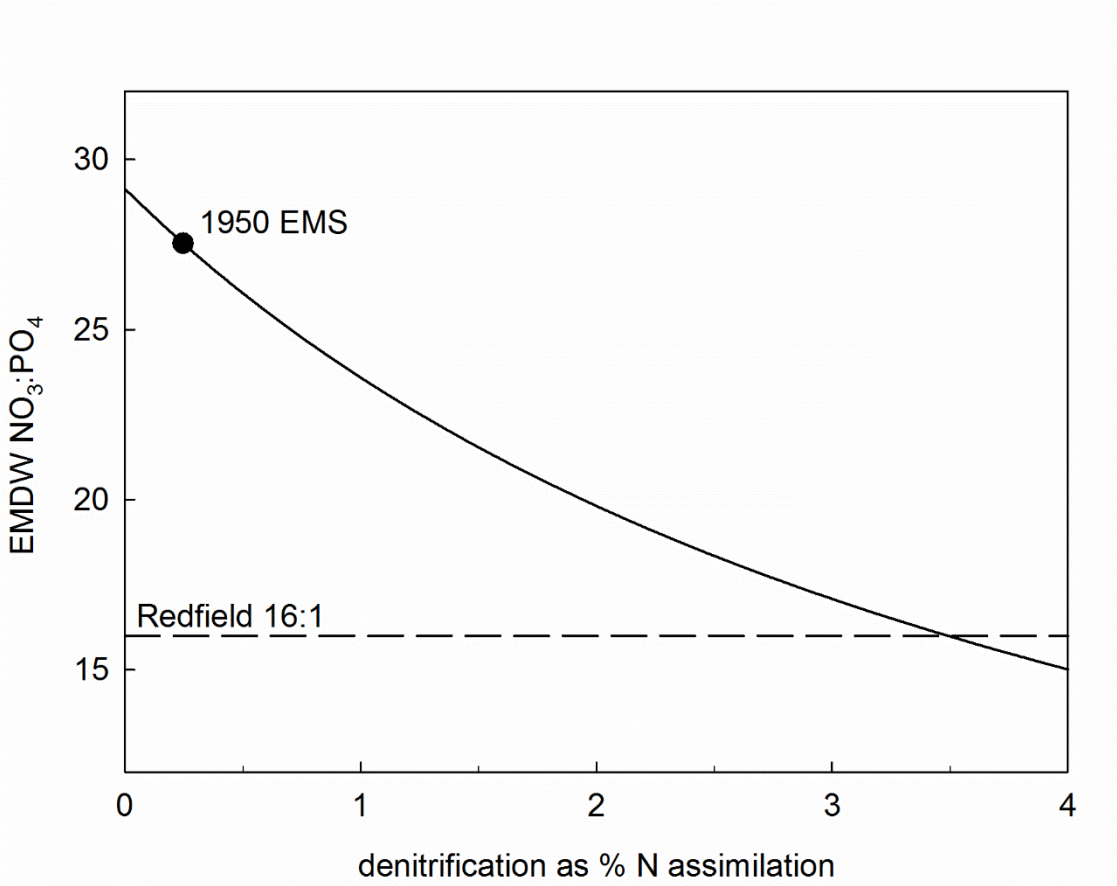

Figure A.5: Model-predicted NO_3:PO_4 ratio in the EMDW as a function of the denitrification flux, expressed relative to the assimilative NO_3 uptake flux by primary producers. The symbol corresponds to the best estimate of the denitrification flux in 1950 (see Figure A.3). Results plotted are obtained by varying the denitrification flux and running the model to steady state, with all other conditions unchanged. The EMDW NO_3:PO_4 ratio reaches the Redfield value (16:1) when denitrification equals 3.5% of the photosynthetic NO_3 uptake in the EMSW. See text for complete discussion.

A.10 Supporting Information: Mass equations

$$\frac{dPO_{4_{SW}}}{dt} = A_{PO_4} + S_{PO_4} + WMS_{PO_4} + t_{PO_4} + Pmin_{EMSW} - assim_P - down_{PO_4}$$

$$\frac{dPO_{4_{EMIW}}}{dt} = down_{PO_4} + up_{PO_4} + Pmin_{EMIW} - t_{PO_4} - WMS\_out_{PO_4} - Aeg\_out_{PO_4} - Adr\_out_{PO_4}$$

$$\frac{dPO_{4_{EMDW}}}{dt} = Pmin_{EMDW} + Aeg_{PO_4} + Adr_{PO_4} - up_{PO_4}$$

$$\frac{dPOP_{SW}}{dt} = assim_P - Psol_{SW} - Pexp_{SW-EMIW}$$

$$\frac{dPOP_{EMIW}}{dt} = Pexp_{SW-LIW} - Pexp_{LIW-EMDW} - Psol_{EMIW}$$

$$\frac{dPOP_{EMDW}}{dt} = Pexp_{LIW-EMDW} - B_{POP} - Psol_{EMDW}$$

$$\frac{dDOP_{SW}}{dt} = A_{DOP} + S_{DOP} + WMS_{DOP} + t_{DOP} + Psol_{SW} - Pmin_{SW} - down_{DOP}$$

$$\frac{dDOP_{EMIW}}{dt} = down_{DOP} + up_{DOP} + Psol_{EMIW} - t_{DOP} - WMS\_out_{DOP} - Pmin_{LIW} - Aeg\_out_{DOP} - Adr\_out_{DOP}$$

$$\frac{dDOP_{EMDW}}{dt} = Psol_{EMDW} + Aeg_{DOP} + Adr_{DOP} - up_{DOP} - Pmin_{EMDW}$$

$$\frac{dNO_{3_{EMSW}}}{dt} = A_{NO_3} + S_{NO_3} + WMS_{NO_3} + t_{NO_3} + Nnit_{SW} - assim_N - down_{NO_3}$$

$$\frac{dNO_{3_{EMIW}}}{dt} = down_{NO_3} + up_{NO_3} + Nnit_{EMIW} - t_{NO_3} - WMS\_out_{NO_3} - Aeg\_out_{NO_3} - Adr\_out_{NO_3}$$

$$\frac{dNO_{3_{EMDW}}}{dt} = Nmin_{EMDW} + Aeg_{NO_3} + Adr_{NO_3} - up_{NO_3} - denit$$

$$\frac{dPON_{EMSW}}{dt} = assim_N - Nsol_{SW} - Nexp_{SW-EMIW}$$

$$\frac{dPON_{EMIW}}{dt} = Nexp_{EMSW-EMIW} - Nexp_{EMIW-EMDW} - Nsol_{EMIW}$$

$$\frac{dPON_{EMDW}}{dt} = Nexp_{EMIW-EMDW} - B_{PON} - Psol_{EMDW}$$

$$\frac{dDON_{EMSW}}{dt} = A_{DON} + S_{DON} + WMS_{DON} + t_{DON} + Nsol_{EMSW} - Nmin_{EMSW} - down_{DON}$$

$$\frac{dDON_{EMIW}}{dt} = down_{DON} + up_{DON} + Nsol_{EMIW} - t_{DON} - WMS\_out_{DON} - Nmin_{EMIW} - Aeg\_out_{DON} - Adr\_out_{DON}$$

$$\frac{dDON_{EMDW}}{dt} = Nsol_{EMDW} + Aeg_{DON} + Adr_{DON} - up_{DON} - Nmin_{EMDW}$$

$$\frac{dNH_{4_{EMSW}}}{dt} = A_{NH_4} + S_{NH4} + WMS_{NH_4} + t_{NH_4} + Nmin_{EMSW} - Nnit_{EMSW} - down_{NH_4}$$

$$\frac{dNH_{4_{EMIW}}}{dt} = down_{NH_4} + up_{NH_4} + Nmin_{EMIW} - t_{NH_4} - WMS\_out_{NH_4} - Nnit_{EMIW} - Aeg\_out_{NH_4} - Adr\_out_{NH_4}$$

$$\frac{dNH_{4_{EMDW}}}{dt} = Nmin_{EMDW} + Aeg_{NH_4} + Adr_{NH_4} - up_{NH_4} - Nnit_{EMDW}$$

Input fluxes

A_x	Atmospheric deposition	$x=PO_4,DOP,NO_3,NH_4,DON$
S_x	Surface flow inputs	
WMS_x	Inflow from Western Mediterranean Sea	
Aeg_x	Deep water formation from Aegean Sea	
Adr_x	Deep water formation from Adriatic Sea	

Output fluxes

WMS_out_x	Export to Western Mediterranean Sea	$x=PO_4,DOP,NO_3,NH_4,DON$
Aeg_out_x	Upwelling of EMIW to Aegean Sea	
Adr_out_x	Upwelling of EMIW to Adriatic Sea	
B_x	Burial of organic matter	$x= POP,PON$
denit	Denitrification	

Internal Processes

$assim_x$	Assimilation by phytoplankton	$x=P,N$
$Psol_x$	Solubilization of POP to DOP	$x = EMSW, EMIW, EMDW$
$Pmin_x$	Mineralization of DOP to PO_4	
$Nsol_x$	Solubilization of PON to DON	
$Nmin_x$	Mineralization of DON to NH_4	
$Nnit_x$	Nitrification of NH_4 to NO_3	
$Pexp_x$	POP export from water layer	$x = EMSW\text{-}IW, EMIW\text{-}EMDW$
$Nexp_x$	PON export from water layer	
t_x	Turbulent mixing from EMIW to EMSW	$x=PO_4,DOP,NO_3,NH_4,DON$

Circulation

$down_x$	Downwelling from EMSW to EMIW	$x=PO_4,DOP,NO_3,NH_4,DON$
up_x	Upwelling from EMDW to EMIW	

Units

All fluxes are expressed in mol (P or N) per year

Appendix B

Supporting Information: Chapter 2

A biogeochemical model of phosphorus and nitrogen cycling in the Eastern Mediterranean Sea. Part 2. Response of nutrient cycles and primary production to anthropogenic forcing: 1950-2000

Table B.1: Decadal values of the anthropogenic forcing functions for external reactive P and N inputs to the EMS imposed in the model simulations. For each external source the forcing functions gives the change in input flux relative to the input flux in 1950 (Equation 2.1 in text). Minimum and maximum values of the forcing function during the 1950-2000 period are also reported. Abbreviations: WMS = Western Mediterranean Sea, Atm = atmospheric deposition, Adr = Adriatic deep water formation, Aeg = Aegean deep water formation, add = additional nutrient acquired by EMIW during Adriatic and Aegean deep water formation.

	1950	**1960**	**1970**	**1980**	**1990**	**2000**	**Min (Year)**	**Max (Year)**
Phosphorus								
Riverine	1.00	1.10	0.66	2.07	1.98	1.39	0.46 (1967)	2.23 (1984)
WMS	1.00	1.00	1.01	1.04	1.08	1.13	1.00 (1950)	1.13 (2000)
Atm PO_4	1.00	1.55	2.25	2.47	2.09	1.46	1.00 (1950)	2.48 (1979)
Atm DOP	1.00	1.17	1.30	1.37	1.41	1.41	1.00 (1950)	1.41 (1995)
Adr add PO_4	1.00	1.55	3.32	7.82	6.20	3.58	1.00 (1950)	8.07 (1982)
Adr add DOP	1.00	1.18	1.83	3.03	2.73	1.92	1.00 (1950)	3.12 (1983)
Aeg add PO_4	1.00	1.47	2.48	3.11	2.78	1.31	1.00 (1950)	3.13 (1982)
Aeg add DOP	1.00	1.22	1.68	2.11	2.18	1.60	1.00 (1950)	2.21 (1987)
Nitrogen								
Riverine	1.00	1.16	1.84	3.14	4.41	5.16	1.00 (1950)	5.16 (2000)
WMS	1.00	1.03	1.11	1.21	1.30	1.38	1.00 (1950)	1.38 (2000)
Atm NO_3	1.00	1.30	1.97	2.60	2.94	2.90	1.00 (1950)	2.97 (1994)
Atm NH_4	1.00	1.18	1.55	1.94	2.18	2.13	1.00 (1950)	2.21 (1994)
Atm DON	1.00	1.17	1.30	1.37	1.41	1.41	1.00 (1950)	1.41 (1995)
Adr add NO_3	1.00	1.18	2.27	3.86	4.72	4.71	1.00 (1950)	4.79 (1994)
Adr add NH_4	1.00	1.14	1.68	2.30	2.67	2.64	1.00 (1950)	2.71 (1994)
Adr add DON	1.00	1.13	1.58	2.12	2.44	2.44	1.00 (1950)	2.48 (1995)
Aeg add NO_3	1.00	1.35	2.32	3.53	4.32	4.32	1.00 (1950)	4.41 (1995)
Aeg add NH_4	1.00	1.17	1.61	2.08	2.38	2.35	1.00 (1950)	2.42 (1994)
Aeg add DON	1.00	1.21	1.65	1.95	1.98	1.81	1.00 (1950)	2.00 (1986)

Table B.2: Responses of P and N concentrations in the year 2000 to changes in the WMS input of reactive P and N. The ±10% WMS simulations impose forcing functions that yield inputs in 2000 that are respectively 10% higher and 10% lower than in the baseline scenario, for all reactive P and N species. The baseline and ±10% WMS scenarios all start with the same 1950 inputs.

		1950	**2000 Concentrations**		
		Concentrations	**Baseline**	**-10% WMS**	**+ 10% WMS**
PO_4 (nM)	EMSW	24.9	28.7	27.2	30.4
	EMIW	107.6	121.0	117.3	125.7
	EMDW	175.9	183.3	183.1	183.9
DOP (nM)	EMSW	50.4	58.1	54.9	61.6
	EMIW	42.7	49.1	46.8	51.7
	EMDW	42.0	44.5	44.2	45.2
POP (nM)	EMSW	7.1	8.1	7.7	8.6
	EMIW	5.3	6.1	5.8	6.5
	EMDW	5.4	3.9	3.8	4.1
NO_3 (µM)	EMSW	0.53	0.77	0.81	0.72
	EMIW	2.55	3.38	3.31	3.43
	EMDW	4.84	5.08	5.07	5.09
NH_4 (µM)	EMSW	0.08	0.13	0.13	0.13
	EMIW	0.05	0.07	0.07	0.07
	EMDW	0.05	0.06	0.06	0.06
DON (µM)	EMSW	2.63	4.52	4.26	4.76
	EMIW	2.64	3.90	3.71	4.10
	EMDW	2.54	2.78	2.75	2.81
PON (µM)	EMSW	0.28	0.33	0.31	0.35
	EMIW	0.16	0.19	0.18	0.20
	EMDW	0.11	0.13	0.12	0.13

Figure B.1: Evolution of the concentrations of reactive P (PO4, DOP and DOP) from 1950 to 2000, in the surface waters (EMSW), Eastern Mediterranean Intermediate Water (EMIW) and Eastern Mediterranean Deep Water (EMDW). The solid lines represent the baseline model; dashed lines correspond to the ±10% WMS input scenarios. See the caption of Table B.2 for details on the scenarios.

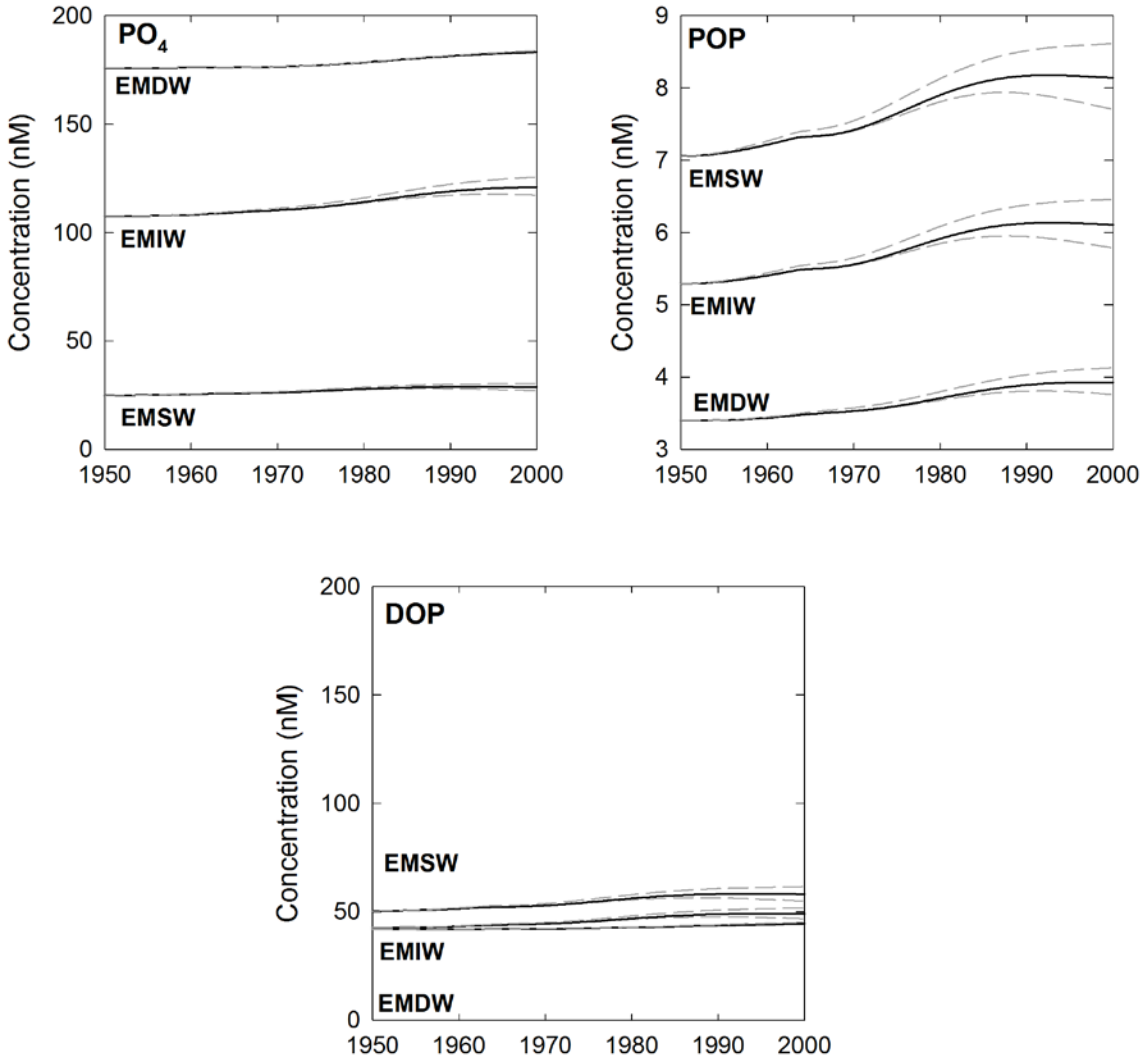

Figure B.2: Evolution of the concentrations of reactive N (NO_3, NH_4, DON and PON) from 1950 to 2000, in the surface waters (EMSW), Levantine Intermediate Water (EMIW) and Eastern Mediterranean Deep Water (EMDW). The solid lines represent the baseline model; dashed lines correspond to the ±10% WMS input scenarios. See the caption of Table B.2 for details on the scenarios.

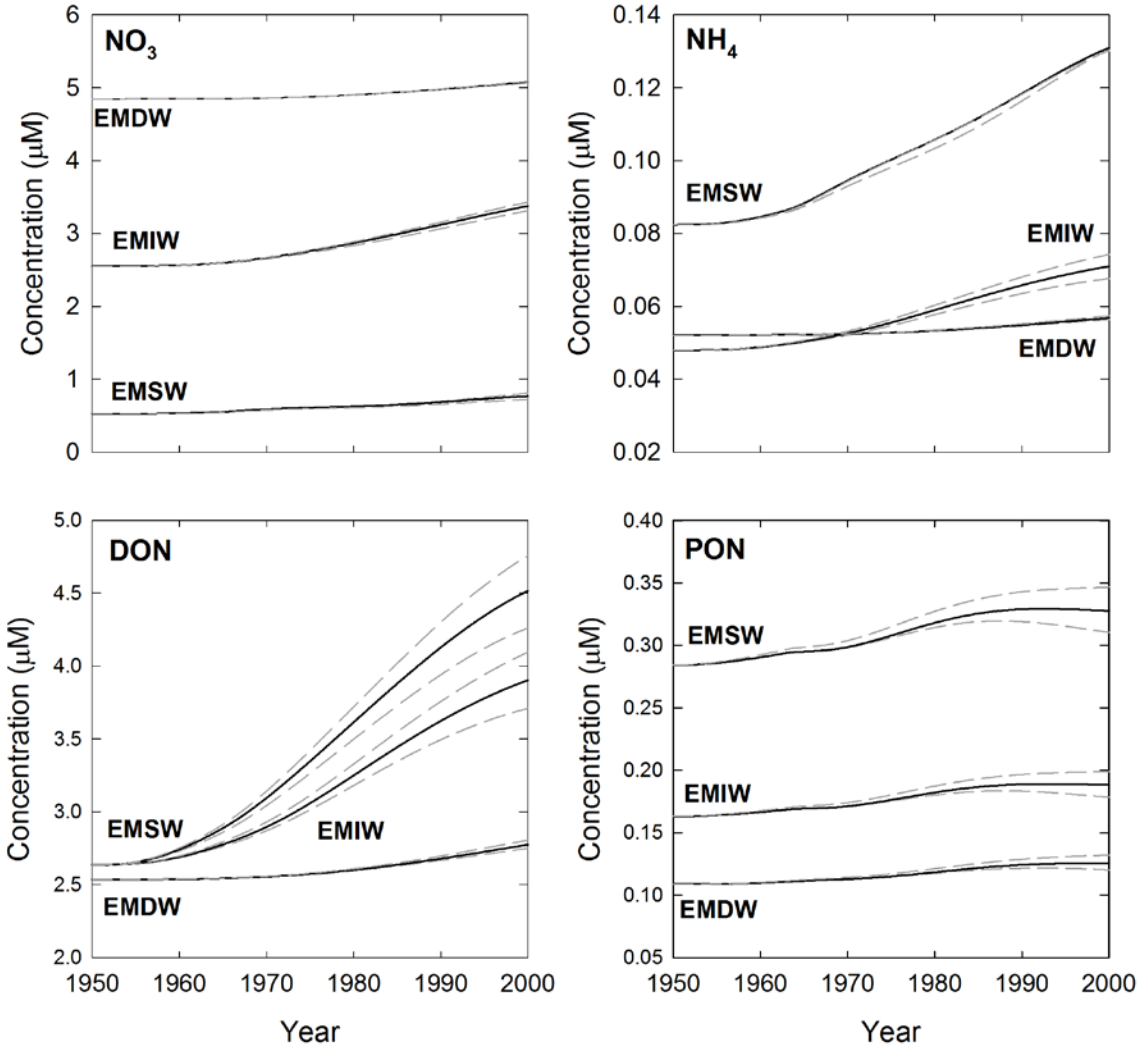

Figure B.3: Evolution of the NO_3:PO_4, DON:DOP and PON:POP molar ratios of the surface waters (EMSW), Levantine Intermediate Water (EMIW) and Eastern Mediterranean Deep Water (EMDW) from 1950 to 2000. The solid lines represent the baseline model; dashed lines correspond to the ±10% WMS input scenarios. See the caption of Table B.2 for details on the scenarios.

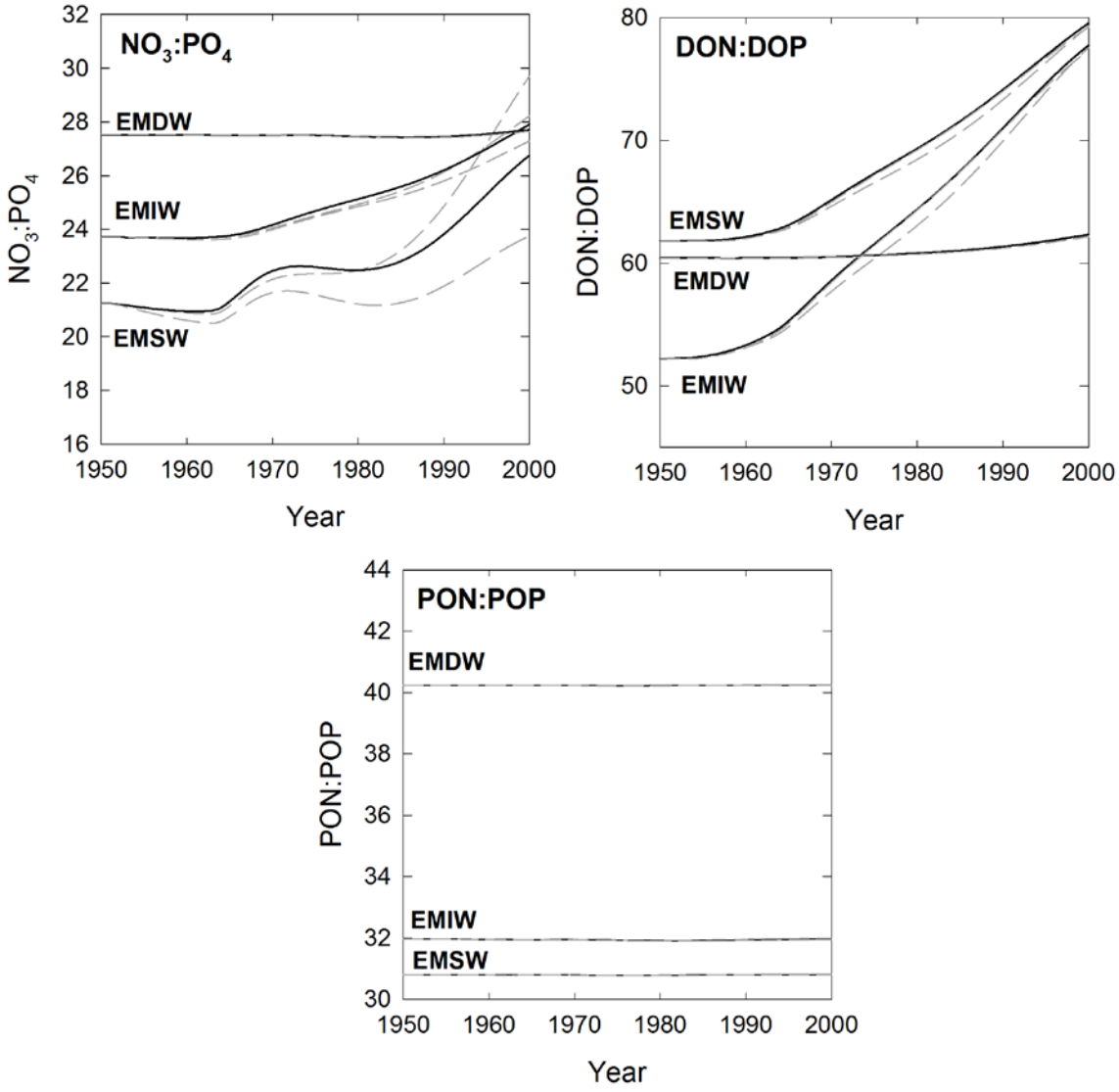

Figure B.4: Sensitivity of EMS primary productivity to inflow from the Western Mediterranean Sea (WMS). The predicted primary production in year 2000 is plotted for model simulations in which the baseline anthropogenic forcing functions for P and N inputs from the WMS are scaled by factors of 0.5, 1, 2, 3, 4, 5 and 20. All other forcing functions remain identical to those in the baseline simulation discussed in the main text

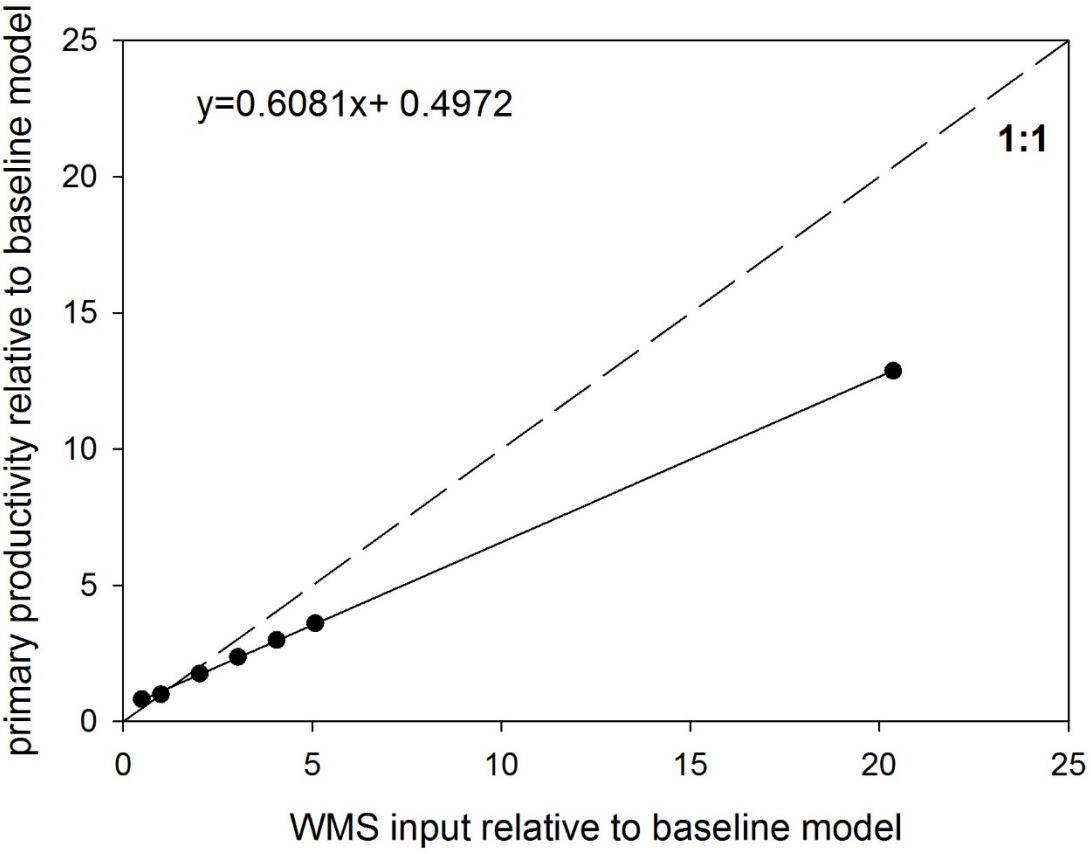

Appendix C

Supporting Information: Chapter 3

Direct discharges of domestic wastewater are an important source of phosphorus and nitrogen to the Mediterranean Sea

C.1 Estimations of terms in Equation 3.1 (Section 3.3, main text)

P,N_{capita} – Annual per capita phosphorus and nitrogen loads in domestic wastewater

The annual per capita loads of P and N in domestic wastewater, P_{capita} and N_{capita} , are computed by considering the P and N contents of human excreta (Equation 3.2 in main text). For P, we also add the contributions of laundry and dishwasher detergents (Equation 3.3 in main text). The P_{capita} and N_{capita} values are estimated individually for each country along the Mediterranean; the resulting loads for year 2003 are given in Table C.7.

The P and N loads associated with human excreta are related to the annual per capita protein supply to a country, as compiled by the Statistics Division of the Food and Agriculture Organization (FAO) of the United Nations (Faostat, 2013). Dietary protein contains 1.6 and 16% P and N, respectively (Morée et al., 2013). The protein supply rates are corrected for the losses by retail businesses and households, along with human losses through sweat, blood and hair loss. Retail and household losses account for 17% of gross protein supply in Europe and 13% in North African and West and Central Asia, while 3% of P and N intake is lost on average through hair sweat and blood (Morée et al., 2013).

Domestic release of P from dishwashers (P_D) is estimated from the country's market exchange rate based gross national domestic product (GDP) expressed in 1995 U.S. dollars capita^{-1} yr^{-1}, using the equations presented by Van Drecht et al. (2009). For countries with a GDP below US$10,000 capita^{-1} yr^{-1} households with dishwashers are rare, and we therefore assume that they contribute negligibly to the P loads in wastewater. For the other countries, we impose a maximum fraction of 80% of the population with access to dishwashers.

Inputs of P from laundry detergents (P_L) are also calculated with the equations of Van Drecht et al. (2009), which relate laundry detergent usage and the fraction of P-free laundry detergent to a country's GDP. However, for a number of countries the actual P-free laundry detergent usage is known, in which case we use the reported fractions (WRC, 2002). In addition, for countries with GDP >US$33,000 capita^{-1} yr^{-1} laundry detergents are assumed to be P-free (Van Drecht et al., 2009).

pop – Population

Populations of coastal cities were obtained directly from the UNEP-MAP surveys (UNEP/MAP/MED-POL/WHO, 2004; 2008). Individual countries report permanent populations, population equivalents, or both. Population equivalent includes the increase in seasonal population due to tourism. When both permanent population and population equivalent are reported, permanent population is used in the analysis as this results in better fits between observed and modeled P and N inputs (see section 3.3). Details of the population distribution per country and per region/basin are summarized in Table C.2a.

f_c – Fraction of population connected to sewerage system

For each city, f_c is obtained directly from the available United Nations surveys (UNEP/MAP/MED-POL/WHO, 2004; 2008), or, if unavailable, the average f_c of the host country for the year closest to 2003 is imposed (Table C.8). In case the permanent population is less than the population connected to the sewage network, the permanent population is used in the calculations, assuming f_c= 1.

$f_{P,N}$ – Fraction of P or N removed from wastewater stream in WWTP

We use the average retentions of P and N for the different types of wastewater treatment reported in Kristensen et al. (2004) (Table C.9). These values are representative for Nordic countries. WWTPs in developing countries may have less efficient retentions (Van Drecht et al., 2009). Untreated wastewater and wastewater that has undergone pretreatment are assigned a retention of zero.

C.2 Gaza and Egypt

In addition to the coastal cities included in the two UNEP-MAP surveys (UNEP/MAP/MED-POL/WHO, 2004; 2008), we also estimate P and N sewage inputs to the MS from Northern Egypt and the Gaza Strip. According to Rasmussen et al. (2009), the El-Baqar drain releases 42.5×10^6 mol P yr^{-1} and 988.6×10^6 mol N yr^{-1} into Lake Manzella in the Nile Delta. Channels connect this coastal lake to the MS. The wastewater flowing through the El-Baqar drain mainly originates in East Cairo and is mostly untreated although some primary treatment may occur (Taha et al., 2004). Around 40% of the water discharge from the drain is of commercial and domestic origin (Taha et al., 2004). As a first approximation we therefore assume that domestic sewage inputs to the MS from Northern Egypt equal 40% of the total P and N inputs from the El-Baqar drain to Lake Manzella, that is, 17×10^6 mol P yr^{-1} and 395×10^6 mol N yr^{-1}.

The Gaza Strip, with a population of 1.221 million in 2003 (Palestinian Central Bureau of Statistics, 2014), has three WWTPs (WHO, 2005). Applying the network connectivity of the Palestinian Territory (54%) (WHO, 2005) yields 653,235 people connected to the sewage network. Two of the WWTPs operate reasonably well, serving 420,000 inhabitants and providing secondary treatment (WHO, 2005). This implies that sewage effluent from an additional 233,235 people is probably discharged into the Mediterranean untreated. In total, we estimate that the Gaza strip discharges 7.1×10^6 and 104×10^6 mol yr^{-1} of P and N into the MS, respectively.

C.3 Model check

As a check on the empirical modeling approach we use to calculate direct wastewater P and N discharges into the MS, we compare our model-predicted input and output fluxes of P and N for individual WWTPs to available measured values for WWTPs in Italy, Spain and Cyprus (EEA, 2012). As can be seen in

Figure C.1, the predicted N and P inputs to WWTPs are in general agreement with reported values, with a Nash Sutcliffe efficiency, *E*, of 0.734 and 0.789 for P and N, respectively. Note that the uncertainties on the model-calculated input fluxes reflect to a large degree missing data on population size and connectivity to the sewerage system for WWTPs in Spain and Italy. The error bars on Figure C.1 correspond to the high and low estimates obtained as outlined in Table C.10.

The P and N discharge fluxes from WWTPs are calculated using the reported (not modeled) input fluxes to the WWTPs, and the average P and N retention efficiencies for the different types of wastewater treatment (Table C.9). Note, however, that for many WWTPs in Spain and Italy the treatment type is not reported. In those cases, secondary treatment is assumed, as it is the most common treatment type in countries surrounding the MS. In addition, uncertainty still surrounds the proportion of treated to untreated wastewater for a given WWTP when connectivity to the sewage network is not reported. Despite the uncertainties associated with the missing data, good agreement between modeled and measured output fluxes is observed, with *E* of 0.328 and 0.862 for P and N, respectively.

C.4 Speciation of P and N in wastewater

Relatively little data exist on the chemical speciation of P and N discharged from WWTPs; here we use all available information although, at this stage, we cannot assess how representative our estimations are for WWTPs in the Mediterranean coastal region (Table C.12). Average P speciation after primary, secondary and tertiary treatment are derived from detailed studies on 12 WWTPs across the United States (Gu et al., 2014). Speciation of P in untreated sewage is calculated from measurements at WWTPs in South Africa and the Netherlands (Rössle, 2001; Lopez-Vazquez et al., 2008). For N, raw and primary treated N speciation are based on observations at South African WWTPs (Rössle, 2001). The predicted raw sewage N speciation is within the range reported for 3 WWTPs in France (Servais et al., 1999). Secondary and tertiary N speciation are estimated from N discharges at the same WWTPs in France. The resulting, model-derived fluxes of individual P and N species in direct domestic wastewater discharges to the Mediterranean Sea are presented in Table C.3.

C.5 Projections (2050)

Wastewater discharges for the year 2050 are projected using estimated changes in population growth, dietary habits and connectivity to the sewage system as described in the main text. A protein intake of 115 g capita^{-1} day^{-1} is assigned to all Mediterranean countries in 2050, which corresponds to the combined 2003 average value of France, Greece, Italy and Spain, that is, the 2003 EU countries bordering the MS (Faostat, 2013). According to Faostat, protein intake in these 4 countries increased steadily between 1960 and 1990, then stabilized at an average value of 115 g capita^{-1} day^{-1} by the turn of the century (Faostat,

2013). In comparison, per capita protein intake in SMCs increased at an approximate constant rate from 1960 to 2010, and will likely approach that of NMCs in the next few decades. Thus it is not unreasonable to assume that SMCs will exhibit a protein intake in 2050 similar to that reached in 2003 by the EU countries.

The mitigation strategies considered are summarized in Table 2 of the main text. The 50% minimum wastewater recycling in scenarios B and H is a reasonable future, mid-century recycling rate for treated wastewater in Mediterranean countries: in the early 2000s, Cyprus, Israel, Libya, Syria and Lebanon already recycled over 88% of their treated wastewater, with other Mediterranean countries recycling up to 50% of treated wastewater (FAO, 2014). An unknown fraction of the reused wastewater might enter the sea through agricultural runoff or submarine groundwater discharge. We have currently no basis to estimate what these fractions are for Mediterranean countries and therefore assume that re-used wastewater does not contribute P or N to the MS.

The legislation limiting P use in detergents (scenarios D, E and G) is based upon the 2012 EU amendment (Regulation (EU) 259/2012) to Regulation (EC) No 648/2004 (Regulation (EU) 2012), which states that all EU member countries should have no more than 0.5 g P per load in laundry detergent after July 2013 and no more than 0.3 g per load in dishwasher detergents by January 1, 2017. This results in an estimated reduction of P inputs in EU countries by 92% for laundry detergents and 82% for dishwasher detergents compared to pre-regulation inputs (BIO by Deloitte, 2014). In scenarios D, E and G, these percent reductions are applied to the 2003 (baseline) laundry and dishwasher detergents in all Mediterranean countries (the baseline values are given in Table C.7).

In scenarios C, E, F, G, H, and I (WWTP upgrades) we use the average P and N retentions given in Table C.9. The WWTPs projected to be constructed are taken into account in the 2050 scenarios and are assigned the planned treatment level. If no treatment level is reported for a projected WWTP, secondary treatment is assumed.

C.6 Figures and tables

Figure C.1: Observed total P (TP) and total N (TN) input fluxes to WWTPs (Panels A and B) and discharge fluxes from WWTPs (Panels C and D) (EEA, 2012) plotted against the modeled values using the approach followed in our study. Solid lines represent the 1:1 relationships. Error bars indicate maximum and minimum model estimated fluxes.

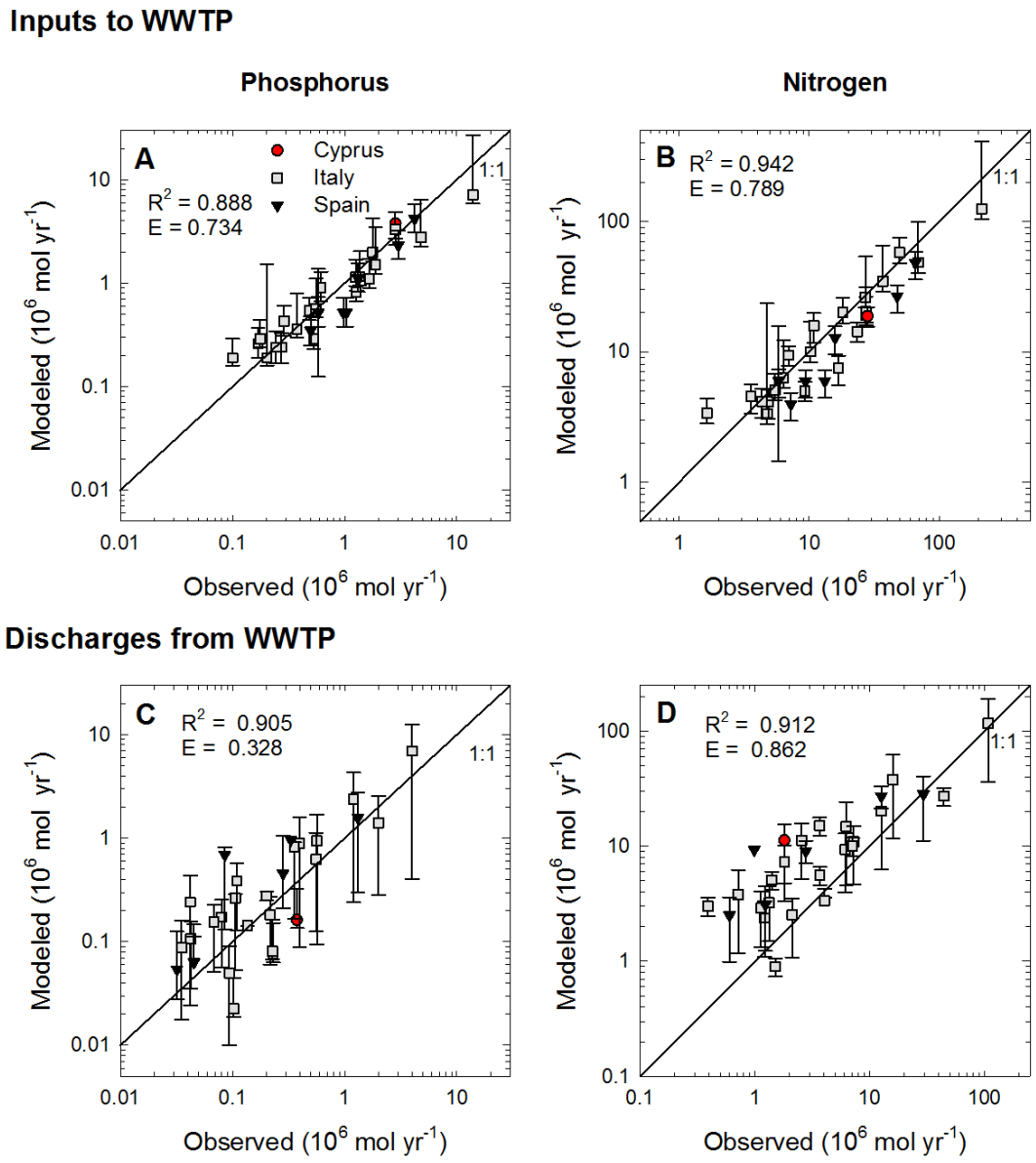

Figure C.2: Estimated 2003 (baseline) direct TP discharges to the Mediterranean Sea associated with untreated and variably treated domestic wastewater. NMC = North Mediterranean Countries, EMC = East Mediterranean Countries, SMC = South Mediterranean Countries.

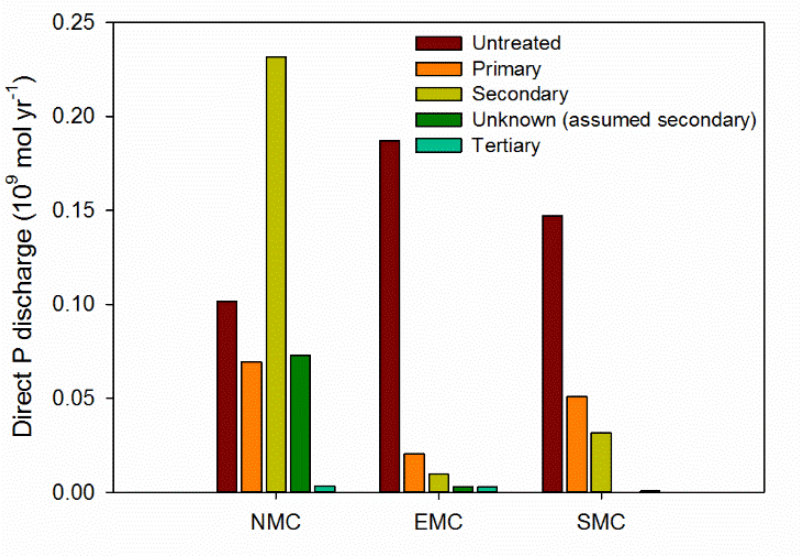

Figure C.3: Predicted impacts of imposing EU P legislation for laundry and dishwasher detergents on the 2003 (baseline) direct domestic wastewater discharges of TP to North Mediterranean Countries (NMC), East Mediterranean Countries (EMC), South Mediterranean Countries (SMC), and all Mediterranean Countries (Total).

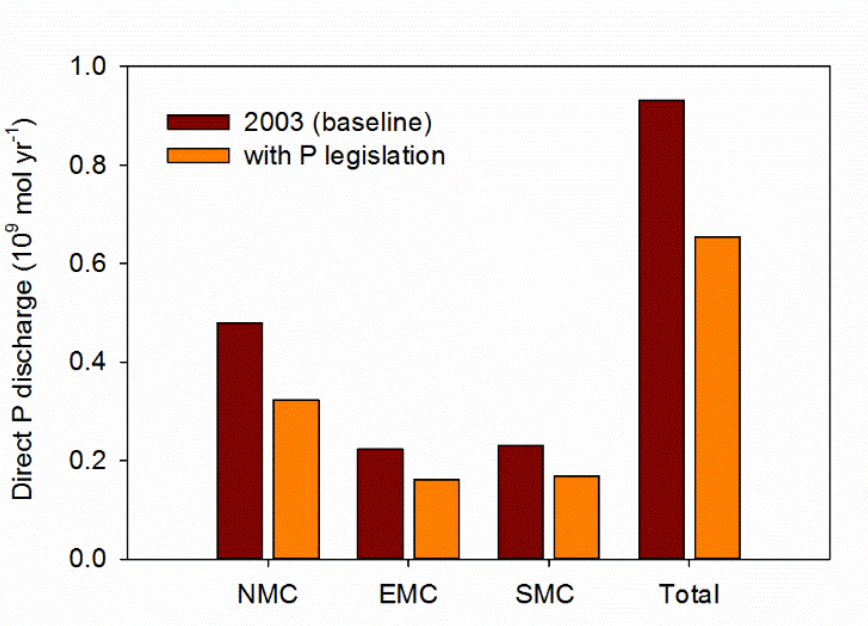

Table C.1: Model-estimated direct domestic wastewater discharges of a) TP and b) TN for Mediterranean regions, basins and individual countries in 2003 (baseline). Inputs from coastal cities with >10,000 inhabitants and 2000-10,000 inhabitants are given separately. Values in brackets are minimum and maximum estimations. Data availability assessments for cities with >10,000 inhabitants are provided. Units: 10^6 mol yr^{-1}. WMS = Western Mediterranean Sea, EMS = Eastern Mediterranean Sea.

Table C1a

Region/basin /country	Cities with population>10000			Cities with population 2000-10000	Total P	Data availability for cities with population>10000
	Treated	Untreated	Total			
WMS	214	87	301 (124-689)	51 (14-101)	353 (138-789)	
EMS	215	169	384 (209-658)	195 (89-291)	579 (298-949)	
NMC	316	56	372 (120-866)	107 (33-202)	479 (153-1068)	
EMC	35	53	89 (63-145)	134 (69-178)	222 (132-323)	
SMC	78	147	225 (150-366)	5 (1-11)	230 (150-347)	
Adriatic	26.3	11.2	37 (20-110)	38.0 (10.8-70.8)	75 (30-181)	
Aegean	85.7	12.0	98 (25-147)	6.7 (3.7-9.5)	104 (29-156)	
Alboran	17.2	33.7	51 (27-123)	3.7 (0.8-8.5)	55 (27-131)	
NW Med	140.8	13.7	154 (55-373)	19.3 (5.3-35.1)	174 (60-408)	
SW Med	17.9	24.6	42 (24-88)	1.3 (0.5-2.4)	44 (24-90)	
Tyrrhenian	38.0	15.3	53 (18-105)	27.1 (7.3-54.6)	80 (26-160)	
Ionian	16.3	5.1	21 (6-44)	13.3 (3.7-27.5)	35 (9-72)	
Central	6.9	42.2	49 (35-69)	8.4 (5.1-11.3)	58 (40-80)	
N Levantine	23.6	48.4	72 (54-116)	127.6 (65.3-169.7)	200 (119-285)	
S Levantine	56.3	50.3	107 (70-172)	0.7 (0.0-1.9)	107 (70-174)	
Albania	0.0	2.3	2.3 (1.8-3.0)	0.4 (0-0.5)	2.6 (1.8-3.5)	Medium: No data on connection to sewage network in 25% of cases
Algeria	10.3	37.0	47.3 (30.9-66.0)	nd	47.3 (30.9-66.0)	Medium: No information on connection to sewage network in approximately 20% of cases
Cyprus	0.0	0.0	0.0	0	0	Good: All wastewater is recycled
Croatia	6.5	5.5	12.0 (9.8-18.3)	7.5 (2.7-10.0)	19.5 (12.5-28.3)	Good
Egypt	48.7	45.6*	94.3* (62.9-152.4)	0.7 (0.0-1.8)	95.0 (62.9-154.2)	Medium: No discharge location stated for untreated wastewater
France	74.9	0.0	74.9 (40.1-119.4)	4.9 (0.7-6.5)	79.8 (40.8-125.8)	Good: Population equivalent rather than permanent population reported
Gaza	3.4	3.7	7.1 (3.6-11.6)	nd	7.1 (3.6-11.6)	n/a
Greece	88.5	14.6	103.1 (25.5-151.3)	0.4 (0.2-1.5)	103.5 (25.7-152.8)	Medium: Population equivalent rather than permanent population reported. Treatment type missing in 4% of cases. No data on where wastewater discharged in 30% of cities
Israel	4.1	0.0	4.1 (2.1-6.4)	0 (0-0.1)	4.1 (2.1-6.5)	Good: Wastewater mostly reused
Italy	63.3	17.8	81.1 (24.5-226.1)	79.2** (21.8-162.1)	160.3 (46.2-388.2)	Poor: Connection to sewage network is not reported in ~27% of cases. No treatment type stated when WWTP is present in ~47% of cases. No information on where wastewater is discharged
Lebanon	7.5	33.6	41.1 (33.6-67.2)	111 (56.5-147.6)	152.1 (90.1-214.8)	Good
Libya	0.8	28.6	29.3 (23.1-38.9)	0.2 (0.1-0.4)	29.6 (23.2-39.4)	Medium: Some wastewater recycled. No data on where wastewater discharged in 70% of cities
Malta	0.0	3.7	3.7 (3.1-5.0)	7.0 (4.9-9.3)	10.7 (7.9-14.3)	Good
Morocco	0.2	18.0	18.2 (14.9-24.4)	2.3 (0.2-6.1)	20.5 (15.0-30.5)	Good

Monaco	0.5	0.0	0.5 (0.1-1.3)	nd	0.5 (0.1-1.3)	Good
Montenegro	nd	nd	nd	1.7 (0.2-2.3)	1.7 (0.2-2.3)	n/a
Slovenia	0.6	0.7	1.3 (1.1-2.0)	0.3 (0.1-0.5)	1.6 (1.2-2.4)	Good
Spain	81.5	11.5	93.1 (14.1-339.4)	5.8 (2.5-9.8)	98.8 (16.7-349.1)	Poor: No data given on connection of population to sewage system or where water is discharged. Permanent population and population equivalent given
Syria	0	11.0	11.0 (9.0-14.6)	3.9 (1.7-5.1)	14.8 (10.8-19.7)	Medium/Good: Location of discharge of treated water not given in 43% of cases
Tunisia	18.0	18.0	35.9 (17.7-54.2)	1.8 (0.2-2.4)	37.8 (18.0-56.6)	Medium: No data on f_c in approximately one third of cases Large portions of wastewater recycled as well as discharged to sea
Turkey	20.4	4.9	25.3 (15.0-45.0)	19.1 (10.7-25.4)	44.4 (25.7-70.4)	Medium: Population missing for 5 cities. Treatment type missing for 17% of cites with a WWTP
Total	**429**	**256**	**685 (333-1347)**	**246 (103-391)**	**932 (435-1738)**	

nd= no data; *Includes additional 17.0 x 10^6 mol yr^{-1} not calculated from UNEP/MAP/MED-POL/WHO (2004) data;** includes data from cities > 10,000 inhabitants; n/a = not applicable . Good quality indicates that the data is complete for the purposes of this study.

Table C1b:

Region/basin /country	Cities with population >10000			Cities with population 2000-10000	Total N	N:P effluent
	Treated	Untreated	Total			
WMS	3219	1340	4559 (2964-9100)	889 (348-1506)	5448 (3312-10606)	15.5
EMS	3804	2683	6487 (4365-10122)	3108 (1513-4093)	9595 (5877-14215)	16.6
NMC	4823	787	5610 (3479-11823)	1846 (722-3031)	7455 (4201-14854)	15.6
EMC	831	811	1642 (1095-2358)	2063 (1116-2415)	3705 (2212-4773)	16.7
SMC	1370	2425	3795 (2755-5041)	87 (22-153)	3882 (2777-5194)	16.9
Adriatic	554	163	717 (433-1934)	649 (232-1037)	1366 (665-2972)	18.1
Aegean	1483	161	1645 (951-2330)	130 (69-177)	1775 (1021-2506)	17.0
Alboran	261	516	777 (516-1604)	58 (22-111)	835 (538-1715)	15.3
NW Med	1982	190	2172 (1440-4711)	315 (130-524)	2487 (1570-5234)	14.3
SW Med	268	378	646 (460-1127)	19 (12-30)	665 (472-1157)	15.2
Tyrrhenian	708	256	964 (548-1659)	497 (184-840)	1461 (732-2500)	18.2
Ionian	281	72	352 (168-645)	254 (93-438)	607 (261-1082)	17.5
Central	138	631	769 (605-971)	103 (64-121)	872 (669-1092)	15.1
N Levantine	416	737	1153 (908-1611)	1959 (1053-2292)	3111 (1961-3903)	15.6
S Levantine	933	918	1851 (1300-2631)	13 (1-28)	1864 (1301-2659)	17.4
Albania	0.0	35.7	36 (30-42)	5.6 (0.1-6.6)	41 (30-49)	15.9
Algeria	169.4	574.2	744 (526-905)	nd	744 (526-905)	15.7
Cyprus	0.0	0.0	0.0	0	0	nd
Croatia	85.6	67.7	153 (127-200)	93.1 (34.2-109.0)	246 (161-308)	12.6
Egypt	824.7	851.1*	1676* (1166-2382)	11.9 (0.6-25.3)	1688 (1167-2408)	17.8
France	1014.9	0.4	1015 (776-1418)	67.5 (18.5-109.4)	1083 (794-1527)	13.6
Gaza	51.8	52.3	104 (79-153)	nd	104 (79-153)	14.7
Greece	1276.4	186.7	1463 (990-2012)	37.1 (8.9-78.8)	1500 (999-2091)	14.5
Israel	53.8	0.0	54 (41-75)	0 (0-0.9)	54 (41-76)	13.3
Italy	1304.1	310.9	1615 (811-3884)	1462.1** (542.7-2490.2)	3077 (1354-6374)	19.2
Lebanon	120.6	510.8	631 (524-900)	1689.4 (889.3-1976.6)	2321 (1423-2877)	15.3
Libya	19.5	430.1	450 (360-529)	3.9 (2.0-5.5)	454 (362-534)	15.3
Malta	0.0	41.6	42 (34-49)	77.6 (54.6-90.7)	119 (89-139)	11.1
Morocco	19.5	282.1	302 (241-361)	39.6 (8.1-84.2)	341 (249-446)	16.7
Monaco	7.6	0.0	8 (5-21)	nd	8 (5-21)	16.5
Montenegro	nd	nd	nd	25.5 (2.9-29.9)	26 (3-30)	14.8
Slovenia	10.0	11.7	22 (18-28)	4.5 (2.0-6.3)	26 (20-34)	16.4
Spain	1124.5	131.9	1256 (687-4170)	72.7 (58.3-110.1)	1329 (746-4280)	13.4
Syria	0	166.8	167 (138-195)	58.4 (26.7-68.4)	225 (165-263)	15.2
Tunisia	336.7	287.4	624 (462-864)	32.0 (11.3-37.4)	656 (473-902)	17.4
Turkey	604.4	81.4	686 (313-1035)	315.5 (190.5-369.2)	1001 (504-1404)	22.6
Total	**7023**	**4023**	**11046 (7329-19222)**	**3997 (1860-5599)**	**15043 (9190-24821)**	**16.1**

nd = no data; *Includes additional 395.4 x 10^6 mol yr^{-1} not calculated from UNEP/MAP/MED-POL/WHO (2004) data;** includes data from cities > 10,000 inhabitants

Table C.2: Model-estimated direct domestic wastewater discharges in 2003 (baseline) for a) TP and b) TN normalized to the corresponding sea surface area, coastal urban population, continental shelf volume and coastal administrative area. Results are shown for the entire Mediterranean Sea (MS), the Western (WMS) and Eastern Mediterranean Sea (EMS), regions (NMC, EMC, SMC), basins and individual countries.

Table C2a:

Region/ basin/ country	*Wastewater discharge of P to MS (10^6 mol yr^{-1})*	*% treated*	*Normalized to sea area (10^{-3} mol m^{-2} yr^{-1})*	*Population in database (10^3 inhabitants)[a]*	*Normalized to population (mol capita^{-1} yr^{-1})*	*Coastline length (km)[b]*	*Normalized to coastline length (10^3 mol km^{-1})*	*Continental Shelf Volume (km^3)[c]*	*Normalized to continental shelf volume (10^3 mol km^{-3} yr^{-1})*	*Coastal region administrative area (10^3 km^2)[b]*	*Normalized to coastal region administrative area (10^3 mol km^{-2} yr^{-1})*
MS	***932 (435-1738)***	***53***	***0.37***	***76003***	***12.3***	***45807***	***20***	***42.2***	***22***	***1136***	***0.8***
WMS	353 (138-789)	71	0.42	28006	12.6	n/a	n/a	12.5	28	n/a	n/a
EMS	579 (298-949)	42	0.35	47997	12.1	n/a	n/a	29.7	19	n/a	n/a
NMC	479 (153-1068)	79	n/a	37221	12.9	34239	14	29.1	16	460	1.0
EMC	222 (132-323)	16	n/a	19313	11.5	5833	38	1.4	154	152	1.5
SMC	230 (150-347)	36	n/a	19468	11.8	5735	40	11.7	20	524	0.4
Alboran	55 (27-131)	38	0.72	4822	11.3	n/a	n/a	n/a	n/a	n/a	n/a
NW Med.	174 (60-408)	90	0.69	12474	13.9	n/a	n/a	6.2*	33 **	n/a	n/a
SW Med.	44 (24-90)	44	0.16	3324	13.2	n/a	n/a	2.5*	29 **	n/a	n/a
Tyrrhenian	80 (26-160)	69	0.33	7386	10.9	n/a	n/a	3.8	21	n/a	n/a
Adriatic	75 (30-181)	59	0.58	6382	11.8	n/a	n/a	10.1	7	n/a	n/a
Ionian	35 (9-72)	71	0.19	3251	10.7	n/a	n/a	3.9	9	n/a	n/a
Central	58 (40-80)	15	0.09	6007	9.6	n/a	n/a	6.3	9	n/a	n/a
Aegean	104 (29-156)	82	0.52	9732	10.7	n/a	n/a	5.1	20	n/a	n/a
N Levantine	200 (119-285)	12	1.80	12139	16.4	n/a	n/a	4.3***	71***	n/a	n/a
S Levantine	107 (70-174)	53	0.25	10485	10.2	n/a	n/a	4.3***	71***	n/a	n/a
Albania	2.6 (1.8-3.5)	0	n/a	307	8.5	418	6.2	n/a	n/a	7.8	0.3
Algeria	47.3 (30.9-66.0)	22	n/a	4290	11.0	1200	39.4	n/a	n/a	47.0	1.0
Cyprus	0	100	n/a	474	0	782	0	n/a	n/a	9.3	0
Croatia	19.5 (12.5-28.3)	33	n/a	1165	16.7	5835	3.3	n/a	n/a	26.2	0.7
Egypt	95.0 (62.9-154.2)	52	n/a	5226	18.2	955	99.5	n/a	n/a	114.8	0.8
France	79.8 (40.8-125.8)	100	n/a	5860	13.6	1703	46.8	n/a	n/a	46.2	1.7
Gaza	7.1 (3.6-11.6)	47	n/a	1221	5.7	55	129.1	n/a	n/a	0.4	19.6
Greece	103.5 (25.7-152.8)	86	n/a	7972	13.0	15021	6.9	n/a	n/a	101.0	1.0
Israel	4.1 (2.1-6.5)	100	n/a	3685	1.1	179	22.7	n/a	n/a	19.9	0.2
Italy	160.3 (46.2-388.2)	71	n/a	14048	11.4	7375	21.7	n/a	n/a	165.8	1.0
Lebanon	152.1 (90.1-214.8)	5	n/a	7931	19.2	225	675.8	n/a	n/a	4.9	31.1
Libya	29.6 (23.2-39.4)	3	n/a	4081	7.2	1770	16.7	n/a	n/a	274.9	0.1
Malta	10.7 (7.9-14.3)	0	n/a	418	25.7	180	59.6	n/a	n/a	0.3	34.0
Morocco	20.5 (15.0-30.5)	12	n/a	1706	12.0	512	40.0	n/a	n/a	42.0	0.5

Monaco	0.5 (0.1-1.3)	100	n/a	35	13.1	4	114.6	n/a	n/a	0.002	229.3
Montenegro	1.7 (0.2-2.3)	0	n/a	84	20.7	294	5.9	n/a	n/a	6.5	0.3
Slovenia	1.6 (1.2-2.4)	54	n/a	94	17.0	47	34.0	n/a	n/a	1.0	1.5
Spain	98.8 (16.7-349.1)	88	n/a	6764	14.6	2580	38.3	n/a	n/a	95.5	1.0
Syria	14.8 (10.8-19.7)	0	n/a	813	18.3	183	81.1	n/a	n/a	4.2	3.5
Tunisia	37.8 (18.0-56.6)	52	n/a	4164	9.1	1298	29.1	n/a	n/a	45.7	0.8
Turkey	44.4 (25.7-70.4)	46	n/a	5663	7.8	5191	8.6	n/a	n/a	122.6	0.4

[a]This study [b]Plan-Bleu (2005); [c]Laruelle et al. (2013); n/a = not applicable;*Includes Alboran Sea; **Total discharges to Alboran Sea split equally between NW and SW Med.; ***Calculated for N Levantine and S Levantine together

Table C2b:

Region/ basin/ country	*Wastewater discharge of N to MS (10^6 mol yr^{-1})*	*% treated*	*Normalized to population (mol $capita^{-1}$ yr^{-1})*	*Normalized to sea area (10^{-3} mol m^{-2} yr^{-1})*	*Normalized to coastline (10^3 mol km^{-1} yr^{-1})*	*Normalized to continental shelf volume (10^3 mol $km^{-3}yr^{-1}$)*	*Normalized to coastal region administrative area (10^3 mol km^{-2} yr^{-1})*
MS	15043 (9190-24821)	55	198	6	328	356	6.0
WMS	5448 (3312-10606)	71	195	6	n/a	436	n/a
EMS	9595 (5877-14215)	46	200	6	n/a	323	n/a
NMC	7455 (4201-14854)	80	200	n/a	218	256	7.3
EMC	3705 (2212-4773)	22	192	n/a	635	2573	11.0
SMC	3882 (2777-5194)	38	199	n/a	677	332	3.3
Alboran	835 (538-1715)	38	173	11	n/a	n/a	n/a
NW Med.	2487 (1570-5234)	89	199	10	n/a	470 *	n/a
SW Med.	665 (472-1157)	43	200	2	n/a	435 *	n/a
Tyrrhenian	1461 (732-2500)	71	198	6	n/a	380	n/a
Adriatic	1366 (665-2972)	66	214	10	n/a	136	n/a
Ionian	607 (261-1082)	74	187	3	n/a	156	n/a
Central	872 (669-1092)	19	145	1	n/a	138	n/a
Aegean	1775 (1021-2506)	85	182	9	n/a	347	n/a
N Levantine	3111 (1961-3903)	13	256	28	n/a	1152**	n/a
S Levantine	1864 (1301-2659)	51	178	4	n/a	1152**	n/a
Albania	41 (30-49)	0	135	n/a	99	n/a	2.4
Algeria	744 (526-905)	23	173	n/a	620	n/a	7.1
Cyprus	0	100	0	n/a	0	n/a	0
Croatia	246 (161-308)	35	212	n/a	42	n/a	4.3
Egypt	1688 (1167-2408)	50	323	n/a	1767	n/a	6.6
France	1083 (794-1527)	100	185	n/a	636	n/a	10.6
Gaza	104 (79-153)	50	84	n/a	1892	n/a	129.5
Greece	1500 (999-2091)	88	188	n/a	100	n/a	6.7
Israel	54 (41-76)	100	15	n/a	301	n/a	1.2
Italy	3077 (1354-6374)	73	219	n/a	417	n/a	8.4
Lebanon	2321 (1423-2877)	5	293	n/a	10315	n/a	214.3
Libya	454 (362-534)	5	111	n/a	256	n/a	0.7
Malta	119 (89-139)	0	285	n/a	662	n/a	170.2
Morocco	341 (249-446)	17	200	n/a	666	n/a	3.7
Monaco	8 (5-21)	100	216	n/a	1891	n/a	1707.6
Montenegro	26(3-30)	0	305	n/a	87	n/a	1.8
Slovenia	26 (20-34)	55	279	n/a	558	n/a	11.3
Spain	1329 (746-4280)	90	196	n/a	515	n/a	6.3
Syria	225 (165-263)	0	277	n/a	1231	n/a	24.3
Tunisia	656 (473-902)	56	158	n/a	505	n/a	6.5
Turkey	1001 (504-1404)	60	177	n/a	193	n/a	3.7

n/a = not applicable; *Total discharges to Alboran Sea split equally between NW and SW Med.; **calculated for N Levantine and S Levantine together

Table C.3: Estimated emissions of individual P and N species associated with direct discharges of domestic wastewater into the WMS, EMS, Adriatic Sea and Aegean Sea in 2003 (baseline), based on the total TP and TN loads estimated in this study and the average speciation percentages given in Table C.12. DIP = Dissolved inorganic phosphorus, PIP = particulate inorganic phosphorus; DOP = Dissolved organic phosphorus; NO_3 = nitrate plus nitrite; PON = particulate organic nitrogen, DON = dissolved organic nitrogen; NH_4 = ammonium.

	Phosphorus				Nitrogen			
	DIP	PIP	POP	DOP	NO_3	PON	DON	NH_4
	10^6 mol yr^{-1} (%TP or TN)							
WMS	150.2	70.2	94.0	38.2	1123.4	319.1	582.2	3423.4
	(42.6)	(19.9)	(26.7)	(10.8)	(20.6)	(5.9)	(10.7)	(62.8)
EMS*	176.5	99.1	91.8	31.6	353.5	507.9	899.5	4691.4
	(44.2)	(24.8)	(23.0)	(7.9)	(5.5)	(7.9)	(13.9)	(72.7)
Adriatic	32.4	16.2	19.3	7.6	288.5	83.0	150.0	844.7
	(42.9)	(21.5)	(25.5)	(10.0)	(21.1)	(6.1)	(11.0)	(61.9)
Aegean	41.6	18.2	30.7	13.8	666.5	83.3	157.2	867.9
	(39.9)	(17.4)	(29.5)	(13.2)	(37.6)	(4.7)	(8.9)	(48.9)
Total	400.7	203.7	235.8	91.2	2431.9	993.1	1788.9	9827.4
	(43.0)	(21.9)	(25.3)	(9.8)	(16.2)	(6.6)	(11.9)	(65.3)

*excluding Adriatic and Aegean Seas

Table C.4: Regional TP and TN discharges into the Mediterranean Sea estimated in this study for 2003 (baseline) compared to values reported in the literature.

Area	Population (million)	P emitted (10^6 mol yr^{-1})	N emitted (10^6 mol yr^{-1})	Reference
Gulf of Lions	2.07	TP:38.8 (22.2-62.3)	TN:525(406-733)	This study
	1.5	TP:22.1 (17.7-26.5)	TN:606 (485-727)	(de Madron et al., 2003b)
Aegean	9.7	DIP: 41.6	NO_3: 667	This study
	10	DIP: 96	NO_3:398	(de Madron et al., 2010)
West Istrian coast of former Yugoslavia	0.370	TP: 6.30 (5.1-9.5)	TN: 85.1(71-110)	This study
	0.275	TP: 12	TN: 94	(Degobbis and Gilmartin, 1990)
Malaga	0.562-0.978	DIP: 3.8 (0.52-10.8)	NO_3:38.1 (24.4-85.6)	This study
	nd	DIP: 1.5-5.6	NO_3:0.3-2.1	(Mercado et al., 2012)

nd = no data; *Note: only Malaga reports direct effluent data.

Table C.5: Projected TP inputs to the Mediterranean Sea from direct domestic wastewater effluents in 2050 due to population growth, without (no mitigation) and with implementation of different mitigation measures. Units: 10^6 mol yr^{-1}.

				2050 P treatment options													
	Baseline (2003) population	2050 population (% increase)	Baseline P discharge (2003)	No mitigation	All WWTPs operational: no treat upgrades	50% treated waste-water re-used	Min tertiary treatment in eutrophic areas	Detergent legislation in all countries	Min tertiary treatment in eutrophic areas + detergent legislation	No treatment to primary + all WWTPs operational	Upgrade primary to secondary + all WWTPs operational	Upgrade secondary to tertiary+ all WWTPs operational	No treatment to secondary + all WWTPs operational	Upgrade primary to tertiary+ all WWTPs operational	Min secondary treatment + all WWTPs operational	Min secondary treatment +WWTPs operational + detergent legislation	Min secondary treatment +WWTPs operational + wastewater re-used	Min tertiary treatment + all WWTPs operational
Regional	*10^3 inhabitants*			*10^6 mol yr^{-1}*														
WMS	28006	41564 (48%)	353	506	478	380	466	346	321	442	452	246	416	398	390	262	229	49
EMS	47997	88861 (85%)	579	1091	1046	955	732	787	531	873	991	823	747	876	692	498	398	91
NMC	37221	42576 (14%)	479	549	539	366	423	364	284	511	514	230	490	461	465	307	263	59
EMC	19313	39472 (104%)	222	452	452	428	392	330	288	341	440	431	261	414	249	182	133	36
SMC	19468	48378 (148%)	230	597	533	541	383	438	280	463	490	407	412	399	369	271	231	45
Country																		
Albania	307	816 (166%)	2.6	6.9	6.9	6.9	6.9	5.1	5.1	4.9	6.9	6.9	3.5	6.9	3.5	2.6	1.7	0.4
Algeria	4290	9047 (111%)	47.3	99.7	91.7	89.5	99.7	72.3	72.3	73.7	85.9	82.9	60.7	73.6	54.8	39.8	27.9	6.6
Cyprus	474	870 (84%)	0.0	0.0	0.0	0.0	0.0	0.0	0.0	0.0	0.0	0.0	0.0	0.0	0.0	0.0	0.0	0.0
Croatia	1165	1543 (32%)	19.5	25.8	25.8	21.5	24.4	15.4	14.5	20.9	23.3	25.8	17.2	17.9	14.7	8.7	7.3	1.8
Egypt	5226	15933 (205%)	95.0	289.6	282.5	257.3	78.7	214.8	58.4	246.3	245.3	254.4	220.1	167.4	182.9	135.6	123.9	21.9
France	5860	7763 (32%)	79.8	105.6	105.6	64.4	69.9	65.2	43.1	105.6	88.7	63.0	105.6	53.3	88.7	54.8	54.0	10.6
Greece	7972	9177 (15%)	103.5	119.2	117.1	72.9	41.6	74.1	25.8	113.4	117.1	26.1	110.8	117.1	110.8	68.8	60.3	14.2
Israel	3685	6162 (67%)	4.1	6.8	6.8	6.8	3.3	4.0	1.9	6.8	5.7	4.2	6.8	3.3	5.7	3.3	5.7	0.7
Italy	14048	13403 (-5%)	160.3	153.0	147.6	101.2	144.1	125.5	118.3	137.4	142.5	64.6	130.1	131.7	125.0	102.5	64.8	15.9
Lebanon	7931	13894 (75%)	152.1	266.4	266.4	266.4	210.4	189.8	149.9	192.9	262.5	266.4	139.7	254.3	135.9	96.8	72.6	16.3
Libya	4081	9440 (131%)	29.6	68.4	36.6	68.4	68.4	48.3	48.3	35.9	36.5	7.3	35.4	36.1	35.2	24.8	18.7	4.4
Malta	418	528 (26%)	10.7	13.6	11.2	13.6	13.6	7.4	7.4	8.6	11.2	9.1	6.8	11.2	6.8	3.7	3.4	0.8
Morocco	1706	4327 (154%)	20.5	51.9	34.9	50.7	51.9	38.0	38.0	31.5	34.9	14.8	29.1	34.9	29.1	21.3	16.4	3.9
Monaco	35	51 (45%)	0.5	0.7	0.7	0.3	0.7	0.5	0.5	0.7	0.7	0.1	0.7	0.7	0.7	0.5	0.3	0.1
Slovenia	94	125 (32%)	1.6	2.1	2.1	1.5	0.5	1.6	0.4	1.8	1.8	2.1	1.6	1.1	1.3	1.0	0.6	0.2
Spain	6764	8160 (21%)	98.8	119.2	119.2	80.8	118.0	67.3	66.6	115.2	118.8	29.5	112.3	117.9	111.9	63.1	70.1	15.1
Tunisia	4164	9631 (131%)	37.8	87.3	87.3	74.9	84.4	65.1	62.9	75.3	87.3	47.5	66.6	87.3	66.6	49.6	43.8	8.4
Turkey	5663	13097 (131%)	44.4	102.7	102.7	80.5	102.7	78.8	78.8	86.7	95.5	88.0	75.2	80.3	68.0	52.2	35.0	14.0
Syria	813	2596 (219%)	14.8	47.4	47.4	47.4	47.4	33.7	33.7	33.6	47.4	47.4	23.7	47.4	23.7	16.8	11.8	2.8
Gaza	1221	3723 (205%)	7.1	28.5	28.5	26.9	28.5	23.7	23.7	21.2	28.5	25.6	16.0	28.5	16.0	13.2	8.0	1.9
Montenegro	84	140 (67%)	1.7	2.9	2.9	2.9	2.9	2.0	2.0	2.1	2.9	2.9	1.4	2.9	1.4	1.0	0.7	0.2
Total	***76003***	***130425 (72%)***	***932***	***1598***	***1524***	***1335***	***1198***	***1132***	***852***	***1315***	***1443***	***1069***	***1163***	***1274***	***1082***	***760***	***627***	***140***

Table C.6: Projected TP inputs to the Mediterranean Sea from domestic wastewater effluents in 2050 due to the combined effects of population growth, dietary changes and increased connectivity of population to the sewage network, without (no mitigation) and with implementation of different mitigation measures. Bold headings identify scenarios included in Figure 3.3 in the main text. Units: 10^6 mol yr^{-1}.

			2050 P treatment options													
	Baseline P discharge (2003)	**No mitigation (Scenario A)**	All WWTPs operational : no treatment upgrades	**50% treated waste-water re-used (Scenario B)**	**Min tertiary treatment in eutrophic areas (Scenario C)**	**Detergent legislation in all countries (Scenario D)**	**Min tertiary treatment in eutrophic areas + detergent legislation (Scenario E)**	No treatment to primary + all WWTPs operational	Upgrade primary to secondary + all WWTPs operational	Upgrade secondary to tertiary+ all WWTPs operational	No treatment to secondary + all WWTPs operational	Upgrade primary to tertiary + all WWTPs operational	**Min secondary treatment + all WWTPs operational (Scenario F)**	**Min secondary treatment+ WWTPs operational + detergent legislation (Scenario G)**	**Min secondary treatment+ WWTPs operational +50% treated wastewater re-used (Scenario H)**	**Min tertiary treatment + all WWTPs operational (Scenario I)**
Regional									*10^6 mol yr^{-1}*							
WMS	353	636	586	498	597	462	437	533	560	313	495	504	468	334	271	59
EMS	579	1395	1318	1238	1088	1064	836	1093	1255	1039	931	1122	867	658	494	114
NMC	479	633	608	435	512	440	361	573	582	261	547	529	521	360	292	67
EMC	222	586	586	555	540	453	417	442	572	555	337	543	323	250	172	45
SMC	230	813	710	746	634	634	495	613	660	535	542	553	491	383	301	61
Country																
Albania	2.6	14.5	14.5	14.5	14.5	11.1	11.1	10.3	14.5	14.5	7.2	14.5	7.2	5.6	3.6	0.9
Algeria	47.3	151.1	141.1	138.3	151.1	117.9	117.9	111.0	133.8	129.8	89.3	118.5	82.0	63.9	41.6	9.8
Cyprus	0.0	0.0	0.0	0.0	0.0	0.0	0.0	0.0	0.0	0.0	0.0	0.0	0.0	0.0	0.0	0.0
Croatia	19.5	34.8	34.8	29.2	33.3	23.9	22.9	27.9	31.5	34.8	23.0	24.5	19.7	13.5	9.8	2.4
Egypt	95.0	336.1	327.9	298.7	160.4	261.3	124.7	285.9	284.7	295.3	255.4	194.3	212.3	165.0	143.8	25.5
France	79.8	102.3	102.3	62.8	68.1	64.9	43.2	101.9	86.1	61.6	101.6	52.2	85.4	54.2	51.9	10.3
Greece	103.5	116.5	114.5	71.4	46.5	73.6	29.4	110.8	114.5	26.4	108.1	114.5	108.1	68.3	58.9	14.5
Israel	4.1	6.4	6.4	6.4	3.1	3.8	1.8	6.4	5.4	3.9	6.4	3.1	5.4	3.1	5.4	0.6
Italy	160.3	218.6	198.4	150.5	206.2	182.2	171.9	187.7	193.1	73.9	180.0	181.9	174.6	145.6	90.3	22.7
Lebanon	152.1	331.9	331.9	331.9	288.7	255.3	222.1	240.4	327.0	331.9	174.1	316.9	169.3	130.2	90.4	20.3
Libya	29.6	146.6	84.2	146.6	146.6	114.4	114.4	78.9	84.0	27.6	75.0	83.5	74.8	58.4	39.0	9.5
Malta	10.7	13.6	11.2	13.6	13.6	7.5	7.5	8.7	11.2	9.2	6.8	11.2	6.8	3.8	3.4	0.8
Morocco	20.5	67.8	45.6	66.2	67.8	52.8	52.8	41.1	45.6	19.8	37.8	45.6	37.8	29.5	21.3	5.2
Monaco	0.5	0.7	0.7	0.3	0.7	0.5	0.5	0.7	0.7	0.1	0.7	0.7	0.7	0.5	0.3	0.1
Slovenia	1.6	2.3	2.3	1.7	1.2	1.8	0.9	2.0	2.0	2.3	1.8	1.2	1.4	1.1	0.7	0.2
Spain	98.8	125.9	125.9	87.1	124.6	71.7	70.9	120.3	125.5	35.2	116.2	124.6	115.8	65.9	72.2	15.6
Tunisia	37.8	111.6	111.6	96.3	107.8	87.7	84.7	95.7	111.6	62.4	84.1	111.6	84.1	66.1	55.1	10.7
Turkey	44.4	124.2	124.2	95.9	124.2	97.7	97.7	105.6	116.3	100.6	92.1	99.8	84.2	66.3	43.7	15.9
Syria	14.8	61.2	61.2	61.2	61.2	47.4	47.4	43.4	61.2	61.2	30.6	61.2	30.6	23.7	15.3	3.7
Gaza	7.1	62.4	62.4	59.8	62.4	48.4	48.4	45.7	62.4	57.9	33.7	62.4	33.7	26.1	16.9	4.0
Montenegro	1.7	3.4	3.4	3.4	3.4	2.5	2.5	2.4	3.4	3.4	1.7	3.4	1.7	1.3	0.8	0.2
Total	***932***	***2032***	***1904***	***1736***	***1685***	***1526***	***1273***	***1627***	***1814***	***1351***	***1426***	***1625***	***1336***	***992***	***764***	***173***

Table C.7: Gross per capita protein supply, and per capita P and N inputs to WWTPs (for P, see Equation 3.3 of the main text), in individual countries in 2003 (baseline).

Country	Gross 2003 Protein Supply (kg capita^{-1} yr^{-1})	P_{diet} (kg capita^{-1} yr^{-1})	P_L (kg capita^{-1} yr^{-1})	P_D (kg capita^{-1} yr^{-1})	P_{capita} (kg capita^{-1} yr^{-1})	N_{diet}=N_{capita} (kg capita^{-1} yr^{-1})
Albania	35.7	0.46	0.18	0	0.64	4.58
Algeria	31.0	0.42	0.18	0	0.60	4.18
Croatia	27.6	0.35	0.28	0	0.63	3.54
Egypt	34.3	0.46	0.18	0	0.64	4.63
France	42.9	0.55	0.23	0.18	0.97	5.50
Gaza	63.7	0.31	0.18***	0***	0.50	3.14
Greece	42.7	0.55	0.26	0.14	0.95	5.47
Israel	45.6	0.62	0.36	0.13	1.10	6.15
Italy	41.1	0.53	0	0.14	0.67	5.27
Lebanon	30.9	0.42	0.19	0	0.61	4.17
Libya	27.9	0.38	0.18**	0**	0.55	3.76
Malta	41.5	0.53	0.42	0.11	1.06	5.32
Monaco	nd	0.55*	0	0.26	0.81	5.50*
Montenegro	nd	nd	nd	nd	0.64****	4.27****
Morocco	32.1	0.43	0.18	0	0.61	4.33
Slovenia	36.5	0.47	0	0.18	0.65	4.68
Spain	41.1	0.53	0.36	0.13	1.02	5.27
Syria	29.5	0.40	0.18	0	0.58	3.98
Tunisia	33.3	0.45	0.17	0	0.62	4.49
Turkey	37.3	0.50	0.17	0	0.67	5.03

nd= no data; *Used estimate for France as protein supply not reported; ** Calculated using average of North African countries; ***Calculated using Syrian values; ****average of Albania, Croatia and Slovenia.

Table C.8: Average, country-specific fractions of the population connected to the sewage network (f_c), with treatment (f_t) and without treatment (f_u), in 2003. The values listed are applied in Equation 3.1 in the main text when, for a given coastal city, connectivity was not provided in the database. Wastewater discharges from inhabitants not connected to the sewage network (f_n) are assumed not to drain into the Mediterranean Sea.

Country	Year	Connected (f_c)	Connected with treatment (f_t)	Connected without treatment (f_u)	Not connected (f_n)
Algeria[a]	2008/2009	0.86	0.53	0.33	0.14
Albania[b]	2002	0.597	0.573	0.024	0.403
Croatia[a]	2008	0.442	0.273	0.169	0.558
Cyprus[c]	2003	0.23	0.23	0	0.77
Egypt[d]	nd	0.538	nd	nd	0.538
France[c]	2004	0.82	0.80	0.02	0
Greece[c]	2007	0.85	0.85	0	0.18
Italy[a]	1999/2005	0.94	0.69	0.25	0.06
Israel[a]	2007	0.938	0.910	0.028	0.062
Libya[e]	nd	0.743	0.598	0.145	0.257
Malta[c]	2003	1.0	0.36	0.64	0
Monaco[a]	2009	1.0	1.00	0	0
Morocco[a]	2000/2005	0.872	0.80	0.072	0.128
Slovenia[c]	2003	0.47	0.26	0.21	0.53
Spain[c]	2006	0.96	0.91	0.05	0.04
Syria[d]	nd	0.71	0.16	0.55	0.29
Tunisia[a]	2008	0.559	0.525	0.034	0.441
Turkey[c]	2003	0.67	0.30	0.37	0.33

nd = no data; [a] UNstat (2011); [b] average of Eastern countries (EEA, 2013); [c]Eurostat (2014); [d] WHO (2005); [e]Average of North African countries.

Table C.9: Relative retentions of P and N for each wastewater treatment type. Values in parentheses are minimum and maximum estimates.

	% P retained	% N retained
Untreated	0	0
Pre-treatment	0	0
Primary	29 [a] (10-30) [a b]	25 [a] (10-25) [a b]
Secondary	50 [a] (45-90) [a b]	45 [a] (35-55) [a b]
Tertiary	94 [a] (88-95) [a b]	60 [a] (45-83) [a b]

[a] Kristensen et al. (2004); [b]Van Drecht et al. (2009)

Table C.10: Upper and lower estimates for P and N emissions to the Mediterranean Sea associated with direct domestic wastewater discharges.

	High estimate	**Low estimate**
Pop^t	Population equivalent (if stated)**	Permanent population (if stated)
f_c *	• Increase f_c by 10%*** • Increase untreated fraction of f_c by 10%***	• Decrease f_c by 10%**** • Decrease untreated fraction of f_c by 10%****
f_R	Minimum in range for each treatment type (Table C.9)	Maximum in range for each treatment type (Table C.9)
Treatment type*	Primary	Tertiary

*when none stated in UNEP/MAP/MED-POL/WHO (2004; 2008); **Population equivalent includes population connected to sewage system when greater than population; *** to a maximum of 100%; ****to a minimum of 0%.

Table C.11: Uncertainties assigned to parameters in Equations 3.2 and 3.3 of the main text to calculate average upper and lower uncertainty on the P and N input per capita to the sewerage network. The uncertainties are used to calculate average uncertainties on P,N_{capita} in Equation 3.1 of the main text.

Parameter	Uncertainty (+/-)%
Protein supplied	10*
Retail losses	10
N fraction of protein	5*
N:P protein	5
f_H	5
P_L	15**
P_D	15**

*Morée et al. (2013); **If no P in detergent in original calculation assume 0.17 and 0.1 kg P capita^{-1} yr^{-1} for upper uncertainty of P_L and P_D (lowest non-zero value reported)

Table C.12: Input and ancillary information used in calculating the direct domestic wastewater P and N emissions from settlements with 2000-10,000 inhabitants in 2003, based on data from UNEP/MAP/MED-POL/WHO (2008).

Country	No. of settlements	Population	Treatment Facilities	Predominant treatment type	Discharge outlet	Calculation	P estimate (10^6 mol yr^{-1})	N estimate (10^6 mol yr^{-1})
Albania	3	17,200	None	None	Direct (surface)/cesspools	P,N_{capita}* pop*100% connectivity	0.4	5.6
Croatia	83	368,042	51% settlements served by WWTP	Pretreatment	Submarine outfalls	P,N_{capita} *pop*100% connectivity	7.5	93.1
Cyprus	24	106,958	33% settlements served by WWTP	Tertiary	Treated: re-used Untreated: septic tanks	n/a	0	0
Egypt	12	65,458	17% settlements served by WWTP	Secondary	Treated: sea by canals Untreated: soil	P,N_{capita} * pop*100% connectivity*(1-secondary f_R	0.7	11.9
France	77	762,100	Almost all settlements have WWTP, only 41% of settlements discharge to sea	Secondary	Submarine outfalls/direct (surface)	P,N_{capita} * pop*100% connectivity*(1-secondary f_R)*0.41	4.9	67.5
Greece	178	764,580	31% settlements served by WWTP, 42% no treatment, 23% WWTP under construction	Tertiary	Treated: Direct (surface)/submarine outfall. Untreated: septic tanks	P,N_{capita} * pop*100% connectivity*(1-tertiary f_R)*0.31	0.4	37.1
Israel	8	44982	100% settlements served by WWTP	Secondary	Water mainly reused	n/a	0	0
Italy	117	652,231	79% of settlements served by WWTP, 3% WWTP under construction.	Primary	nd	P,N_{capita} * pop*100% connectivity*(1-primary f_R)	10.0	184.2
Italy > 10,000 pop	123	5,392,791		Secondary	nd	(P,N_{capita} * pop*av. country connectivity to treatment*(1-secondary f_R) + (P,N_{capita} *pop*av. country connectivity to no treatment)	69.2	1278.0
Lebanon	13	5,675,000	3 settlements have WWTP, remainder: projected to have WWTP.	None	nd	P,N_{capita} *pop*100% connectivity	111.0	1689.4
Libya	15	19497	27% settlements served by WWTP	Primary	Submarine outfalls	P,N_{capita} *pop*100% connectivity*(1-primary f_R)	0.2	3.9
Malta	42	204221	14% settlements served by WWTP, 86% WWTP under construction	None	Untreated: submarine outfalls/direct (surface)	P,N_{capita} * pop*100% connectivity	7.0	77.6
Montenegro	9	83808	None	None	Submarine outfalls	P,N_{capita} (average of Albania, Croatia and Slovenia)* pop*100% connectivity	1.7	25.5
Morocco	38	232748	74% settlements served by WWTP, 5% WWTP under construction	Secondary	nd	P,N_{capita} * pop*100% connectivity*(1-secondary f_R)	2.3	39.6
Slovenia	5	18045	100% settlements served by WWTP	Primary	Submarine outfalls/ estuaries	P,N_{capita} * pop*100% connectivity*(1-primary f_R)	0.3	4.5
Spain	76	351654	95% settlements served by WWTP.	Secondary	Submarine outfall/ re-used	P,N_{capita} * pop*100% connectivity*(1-secondary f_R)	5.8	72.7
Syria	53	205776	None	None	Submarine outfalls/direct (surface)	P,N_{capita} * pop*100% connectivity	3.9	58.4
Tunisia	26	181229	92% settlements served by WWTP	Secondary	Direct (surface)	P,N_{capita} * pop*100% connectivity*(1-secondary f_R)	1.8	32.0
Turkey	192	878242	81% settlements not served by WWTP	None	Submarine outfalls	P,N_{capita} * pop*100% connectivity	19.1	315.5

nd= no data; n/a = not applicable

Table C.13: Speciation of P and N in WWTP effluent after different treatment types, given as percentages of TP and TN, respectively. Numbers in brackets represent the observed range. DIP: dissolved inorganic phosphorus, PIP: particulate inorganic phosphorus, POP: particulate organic phosphorus, DOP: dissolved organic phosphorus, NO_3: nitrate plus nitrite, PON: particulate organic nitrogen, DON: dissolved organic nitrogen, NH_4: ammonium.

	Untreated [a.b.]	Primary [c.]*	Secondary [c.]	Tertiary[c.]
Phosphorus				
DIP	44	49 (21-64)	40 (1.3-90)	10 (1.3-73)
PIP	27	23 (8-57)	15 (0.6-70)	22 (3-70)
POP	22	21 (3-39)	31 (0.2-81)	37 (7-79)
DOP[†]	7	7 (1-15)	14 (1.3-52)	31 (3-86)
	Untreated	Primary[d.]	Secondary[b.]	Tertiary[b.]
Nitrogen				
NO_3	0[d.] (0-1)[b.]	0	36 (0.7-91)	75.5 (75-76)
PON	16[d.] (13-18)[b.]	6.5	4 (2-7)	3.5(3.5-4.0)
DON	9[d.] (6-26)[b.]	10.5	8 (5-11)	6 (3-8)
NH_4	75[d.] (60-75)[b.]	83	52 (0.3-81)	15 (13-17)

[a.] Lopez-Vazquez et al. (2008); [b.] Servais et al. (1999); [c.]Gu et al. (2014); [d.]Rössle (2001) *Calculated from raw sewerage P values in Metcalfe & Eddy Inc (2002) [†] Acid hydrolysable P is considered as DOP

Table C.14: Concentration of TP and annualized cost for each wastewater treatment type. TP concentrations are calculated using an untreated effluent TP concentration of 12 mg L^{-1} (Somlyódy and Shanahan, 1998) and the P retention estimates for each treatment type in Table C.9.

	mg TP L^{-1}	**Cost € m^{-3}**
Primary	8.52	0.23[ab]
Secondary	6	0.35[a]
Tertiary	0.72	0.50[a]

[a] Hidalgo and Irusta () [b] Somlyódy and Shanahan (1998)

Table C.15: Reported percentage of treated wastewater recycled in Mediterranean countries for the year closest to 2003 (FAO, 2014). Values are used to calculate the additional recycling needed to have a minimum 50% recycling of treated wastewater in scenarios B and E of the main text.

Country	% of treated wastewater recycled	Year
Albania	ns	n/a
Algeria	3.1	2012
Croatia	ns	n/a
Cyprus	95	2005, 2007
Egypt	28.6	1993, 1996
France	10.9	2008
Greece	4.8	2003, 2007
Israel	87.8	2004, 2007
Italy	2.2	2004, 2006, 2007
Lebanon	50	1991
Libya	100	2008
Malta	100	1993
Monaco	ns	n/a
Morocco	0.3	2008, 2010
Slovenia	ns	n/a
Spain	11.2-15.7	2002, 2004, 2006
Syria	100	2009, 2012
Turkey	3	2004
Tunisia	23	2003

ns = not stated; n/a = not applicable

Appendix D

Supporting Information: Chapter 4

Circulation and oxygen cycling in the Mediterranean Sea:

Sensitivity to future climate change

Figure D.1: Average oxygen concentrations (in µM) along a west to east transect across the Mediterranean Sea based on data collected between 1906 and 1987 (pre-EMT) (MEDAR Group, 2002). Figure generated in Ocean Data View (Schlitzer, 2015).

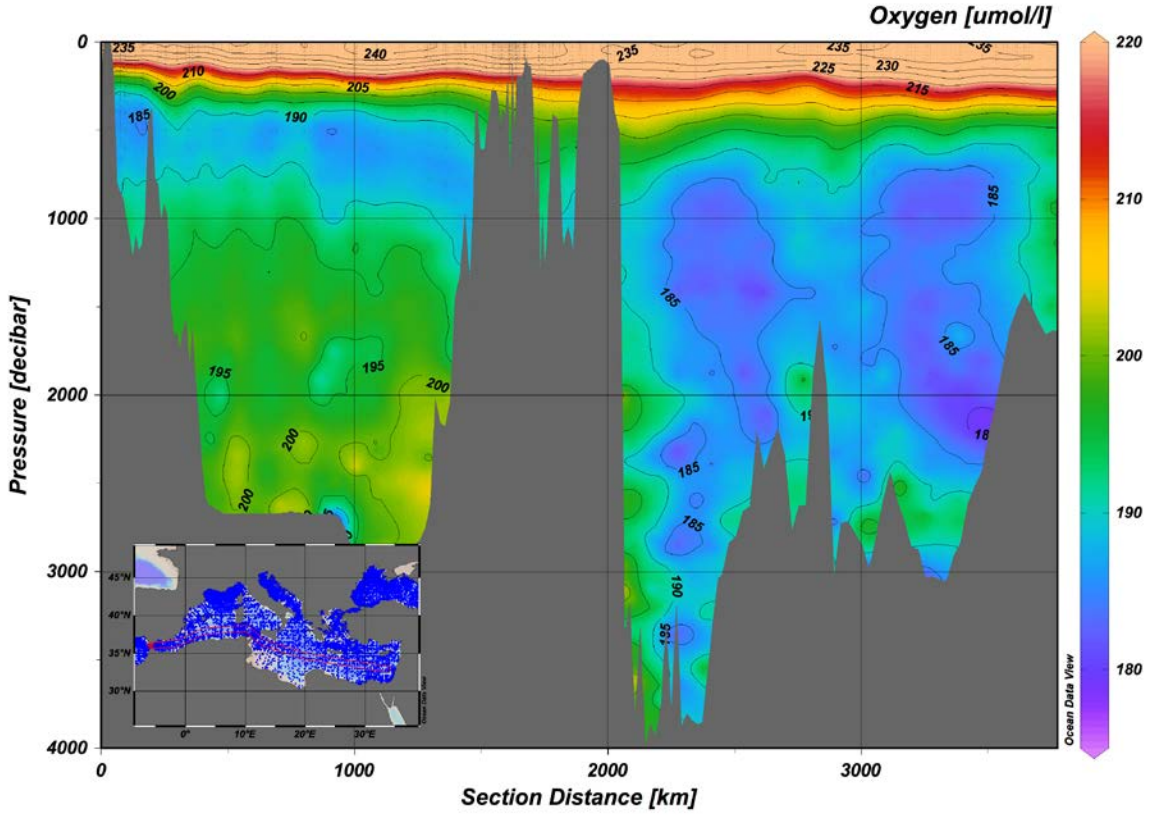

Figure D.2: Assumed linear relationship between O_2 consumption in the EMDW and O_2 supply to the EMDW. The line is anchored by the O_2 consumption rates before (this study) and during the EMT (literature estimates). The y intercept represents the oxygen consumption rate associated with the degradation of sinking POC, from which $\boldsymbol{F_{max}^{POC}}$ is computed using the DW O_2 concentration in the Michaelis-Menten kinetic term $\left(\frac{[\boldsymbol{O_2}]_{\boldsymbol{EMDW}}}{[\boldsymbol{O_2}]_{\boldsymbol{EMDW}}+\ \boldsymbol{K_s}}\right)$ in Equation 4.2 of the main text.

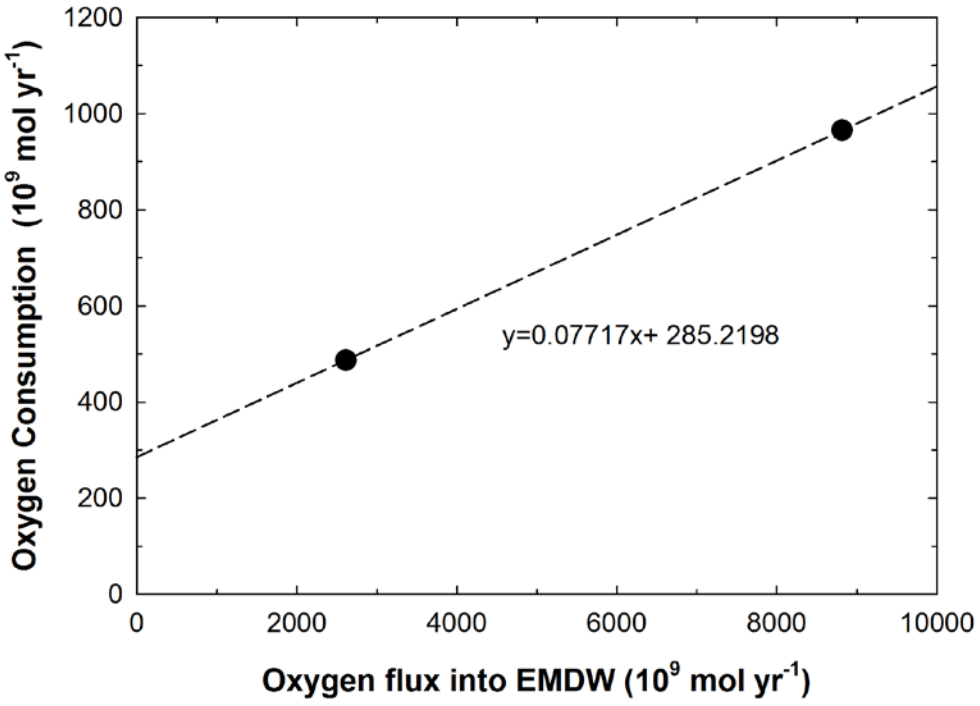

Figure D.3: Factorial design analysis showing the sensitivity of the baseline (pre-EMT) intermediate water (IW) and deep water (DW) oxygen concentrations in the WMS and EMS to model parameters, using Equation (4.1) for IW and DW oxygen consumption. SW = surface water, NWM = North-West Mediterranean; Atl = Atlantic; Adr = Adriatic; Aeg= Aegean; SoS= Strait of Sicily. See text for details.

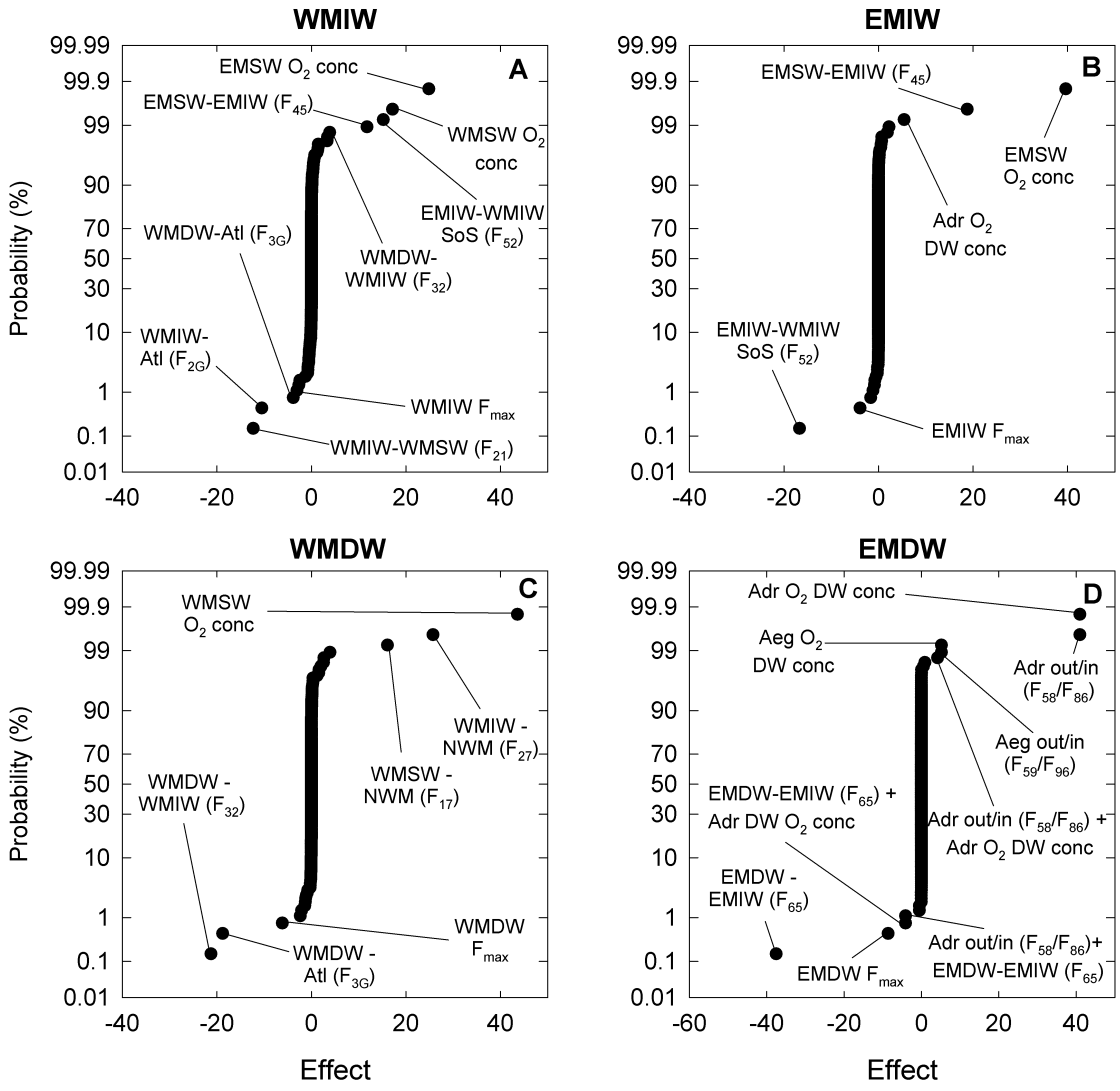

Table D.1: Existing estimates of the range and long term average of annual deep-water formation rates in the North-West Mediterranean Sea.

Reference	Model/ observations	Year	Range of annual deep water formation rates	Long term average
Lascaratos (1993)	Model			0.3 Sv
Tziperman and Speer (1994)	Model			~1 Sv
Send et al. (1995)	Observations	1991		0.3 Sv
Rhein (1995)	Tracer distribution/ Model	1991-1992		1.22 Sv
Castellari et al. (2000)	Model	1980-1988	0-3.4Sv	0.2-1.6 Sv
Somot et al. (2006)	Model			0.93 Sv
Herrmann et al. (2008b)	Model	1986-1987	1.3-2.1 Sv	
Schroeder et al. (2008b)	Observations	2004-2006		2.4 Sv
Herrmann et al. (2009)	Model	1999-2007	0-1.3 Sv	
de Madron et al. (2013)	Observations	2012		1.1 Sv
L'Hévéder et al. (2013)	Model	1958-2001	0-3.2 Sv	1.08 Sv (mean of formation events)*
				0.60 Sv (all years)**

*DW formation only occurs in 53% of years; **includes years when DW formation did not occur

Table D.2: Oxygen concentrations (μM) used to initialize the oxygen model. Depth intervals of observed values match model water layer depths (WMSW: 0-150m; WMIW: 150-600m; WMDW >600m; EMSW: 0-200m EMIW 200-500m; EMDW: >500m). Numbers in brackets represent ranges in concentration reported in the literature. Initial concentrations assigned in the model are given in Figure 4.2 of the main text.

Year	WMS			EMS			Adr DW	Aeg DW	Reference
	SW	IW	DW	SW	IW	DW			
1906-1987	233 (222-236)	195 (186-215)	199 (190-202)	229 (222-234)	204 (195-220)	187 (175-195)	228 (220-235)	232* (230-235)*	MEDAR Group (2002)
1948-1958	223 (212-234)	192 (174-201)	197 (179-201)	219 (212-234)	197 (190-212)	179 (165-201)			McGill (1961)
Aug/Sept 1987	218[d] (202-223)	190[e] (190-193)	195[f] (192-197)	243[d] (226-274)	215[e] (195-226)	188[f] (181-199)	229[g] (228-231)	233[h] (230-236)	Schlitzer et al. (1991)
July 1969	240 (222-272)	195 (189-213)	204 (189-212)						Banoub and Williams (1972)
Oct/Nov 1981	235 (205-260)	190 (180-210)	203 (195-210)						MEDRIPOD IV Coste et al. (1984)
Dec 1977				240[a] (219-254)	214[b] (209-214)	198[c] (192-203)			GEOSECS Weiss et al. (1983)
Winter 1994							(200-210)		Civitarese et al. (1998)
Sept 2007, Jan 2008							230 (222-236)		Santinelli et al. (2012a)
October 1987, April 1992								(219-237)	Souvermezoglou et al. (1999)
1994								(200-230)	Krasakopoulou et al. (1999)

[a] ρ=1028.557 kg/m^3; [b] ρ=1023.936kg/m^3; [c]ρ=1029.204 kg/m^3;[d]1028 kg/m^3; [e] ρ=1028.98 kg/m^3; [f] ρ=1029.125 kg/m^3 [g] ρ=1029.317 kg/m^3; [h] ρ=1029.223 kg/m^3 *Average concentration during EMT.

Table D.3: F_{max} values used in Equation (4.1).

	F_{max} (10^9 mol yr^{-1})
EMIW	1699
WMIW	749
EMDW	503
EMDW	665

Table D.4: Parameters in Equation (4.2) for deep water O_2 consumption. See main text for details.

	F_{max} (10^9 mol yr^{-1})		**Initial O_2 Concentration (μM)**	
	DOC	POC	DOC	POC
EMDW	3259	295	0.40	187
WMDW	1988	144	2.09	197

Table D.5: Model predicted oxygen consumption fluxes (μM yr^{-1}) in the Western and Eastern Mediterranean deep-water using either Equation (4.1) or Equation (4.2) for deep-water oxygen consumption.

Location	Year	Depth	Consumption flux (μM yr^{-1})	Equation
Western Mediterranean				
WMDW	Pre-EMT	>600m	0.71	(4.1) and (4.2)
WMDW	2006-2011	>600m	0.71	(4.1)
WMDW	2006-2011	>600m	1.07	(4.2)
			(Max: 1.36 in 2006)	
Eastern Mediterranean				
EMDW	Pre-EMT	>500m	0.29	(4.1) and (4.2)
EMDW	1995-1998	>500m	0.29	(4.1)
EMDW	1995-1998	>500m	0.57	(4.2)
			(Max: 0.64 in 1995)	

Appendix E

Supporting Information: Chapter 5

Understanding the unique biogeochemistry in the Mediterranean Sea: Insights from a coupled phosphorus and nitrogen model

E.1 Mass balance model

Justification of the mass balance model setup is presented in section 5.3 of the main text. The following provides additional information on selected input and output fluxes for the WMS.

E.1.1 External inputs of P and N

E.1.1.1 Atlantic Surface Water

According to Huertas et al. (2012), the mean NO_3 concentration of Atlantic surface water (ASW) entering the WMS through the Strait of Gibraltar during the period 2005-2008 is 3.2 μM. However, these authors use the 37 isohaline to separate the incoming ASW from Mediterranean outflow water. Atlantic surface water has a salinity of 36.2±0.2 (Schroeder et al., 2012), hence implying some admixing of Mediterranean water in order to reach salinity of 37. Macías et al. (2007) estimate that the inclusion of mixing of Mediterranean outflow water increases the incoming NO_3 concentration within the Strait of Gibraltar to 130% of the true ASW concentration or, alternatively, that approximately 16% of outflowing NO_3 is re-circulated with the incoming ASW. Assigning an outgoing NO_3 concentration on the east side of the Strait of Gibraltar of 9.1 μM (Huertas et al., 2012) thus implies that 1.5 μM of NO_3 in the incoming water comes from recirculation of outflowing water. Therefore the NO_3 concentration of end-member ASW west of the Strait of Gibraltar is assigned a value of 1.6 μM (3.1 μM-1.5 μM). (Note: in the latter calculation we adjust the inflow NO_3 concentration from 3.2 to 3.1 μM, which is more representative of the NO_3 concentration west of the Strait of Gibraltar after mixing with Mediterranean outflow water has occurred.)

The NO_3:PO_4 ratios of incoming ASW fall mostly in the range 9-17:1 (Coste et al., 1984; Coste et al., 1988; Gómez et al., 2000; Dafner et al., 2003; Huertas et al., 2012), although values as high as 93:1 have been reported (Ramirez-Romero et al., 2014). We use a ratio of 10:1 to account for the predominantly less than Redfield NO_3:PO_4 ratio of ASW (Gómez et al., 2000; Huertas et al., 2012). Concentrations of incoming DOP and DON are assigned values of 0.14 μM and 4.5 μM, respectively, based upon average concentrations observed in the top 150 m of the water column at station 7 during the MEDRIPOD IV cruise (Le Corre et al., 1984). It is possible that mixing of ASW with Mediterranean outflow water decreases the incoming DOP and DON concentration through the Strait of Gibraltar, however. Doval et al. (2001) report a surface water DON concentration of 5.2 μM for the east Atlantic Ocean indicating that our estimated concentrations of DOP and DON may be slightly underestimated.

E.1.1.2 Atmospheric deposition: PO_4 and NO_3

Reported dry, wet and bulk deposition fluxes of leachable P and N in the WMS for the period 1984-2005 are compiled in Table E.1. We assume that these fluxes are representative of the mid 1990s. The leachable fractions of particulate P vary between 8% for soil derived dust to 100% for anthropogenic particulates (Bergametti et al., 1992; Migon and Sandroni, 1999; Migon et al., 2001). Because of the different methods and analytical techniques used to determine atmospheric P deposition fluxes, the values in Table E.1 represent variable combinations of dissolved, complexed and total particulate P. We use the following average WMS deposition rates of leachable inorganic P and inorganic N: 0.45 mmol P m^{-2} yr^{-1} and 45 mmol N m^{-2} yr^{-1} (Table E.1). These values are consistent with the estimates of atmospheric deposition rates in the WMS compiled by Guerzoni et al. (1999): 0.55 mmol m^{-2} yr^{-1} leachable inorganic P and 38-44 mmol m^{-2} yr^{-1} leachable inorganic N. The average deposition rates are then combined with the surface area of the WMS of $815x10^3$ km^2 to obtain leachable inorganic P and N deposition fluxes for the mid 1990s of 0.37 $x10^9$ mol P yr^{-1} and 36.7 x 10^9 mol N yr^{-1}.

E.1.2 Sinks of P and N

E.1.2.1 Burial flux of phosphorus

Samples from sediment cores were obtained to estimate the POP burial flux in the WMS (see Table E.6 for details). Total P and PIP in the samples were determined following the method of Aspila et al. (1976) modified to be comparable to results obtained with the sequential extraction (SEDEX) method (Ruttenberg et al., 2009). All equipment used was acid washed for at least 24 hours and milli-Q rinsed. Sediment was wet sieved through a 125 μM mesh size sieve before freeze-drying (except for Alb 2). 10 ml 1M HCl was added to 0.1g freeze-dried sediment and shaken for 16 hours to determine PIP. For TP, 0.4 ml of 1M $Mg(NO_3)_2$ was added to 0.1g freeze-dried sediment and ashed in a muffle furnace for 2 hours at 500°C, followed by digestion with 10 ml 1M HCl for 16 hours. All digested samples were filtered through 0.45 μm pore size polycarbonate filters. Each sample was done in duplicate. Filtrate solutions were analyzed in triplicate by ICP-OES (Thermo Scientific iCAP 6000). The calibration curve had a minimum detection limit of 0.0025 mg l^{-1} and standard error of 0.000001 mg l^{-1}. An error of <8% was recorded on sample and matrix spikes and QCs. Standard deviation of triplicates was <4%. Particulate organic P was calculated as the difference between TP and PIP concentrations.

The sediment POP burial rate for the Gulf of Lions reported in the main text is further verified using the TP burial rates in the Gulf of Lions of (Van Den Broeck and Moutin, 2002). In core CN36, 29% of TP is POP. Using this POP:TP ratio along with the reported TP burial flux in the Gulf of Lions gives a flux of

0.07-0.12x10^9 mol P yr^{-1} (Table E.8). This is similar to our estimate of the POP burial in the Gulf of Lions (Table E.5).

E.1.2.2 Denitrification

Gehlen et al. (1997) determined denitrification rates on sediment cores collected between 1994 and 1995 at the DYFAMED site in the north-west Mediterranean Sea. This site is representative of deep basin conditions within the WMS: the coring site is located at approximately 2300 m water depth and is separated from the coast by the Ligurian current. Gehlen et al. (1997) estimate that 0.04-0.17 mmol m^{-2} d^{-1} of N is lost through denitrification. Taking a low-end average value of 0.07 mmol m^{-2} d^{-1} gives a denitrification flux for the WMS, excluding the Gulf of Lions, of 19.7x10^9 mol N yr^{-1} (Table E.9). In addition to the flux from the open ocean, Denis and Grenz (2003) estimate that 0.032-0.074 mmol m^{-2} d^{-1}, or approximately 0.4x10^9 mol N yr^{-1}, is denitrified in the Gulf of Lions. Thus the total denitrification flux for the open WMS plus the Gulf of Lions is estimated as 20.1x10^9 mol N yr^{-1} (Table E.9).

E.1.3 Deep-water formation

The WMSW and WMIW flowing into the NWM return to the WMS as WMDW (Figure 5.1). We assume that the deep water flowing into the WMDW therefore contains the P and N present in the WMSW and WMIW flowing into the NWM plus additional P and N acquired in the NWM. The additional net reactive P and N inputs are obtained by summing atmospheric deposition and N_2 fixation within the NWM, minus losses from burial and denitrification. Atmospheric deposition, N_2 fixation, burial and denitrification are all pro-rated for the surface area of the model NWM (25,000 km^2) from the corresponding fluxes applied to the entire WMS. The speciation of the excess inputs of reactive P and N entering the WMDW from atmospheric deposition and N_2 fixation are divided into the same proportions as the speciation of dissolved reactive P and N observed in the WMDW.

TABLES:

Table E.1: Atmospheric deposition fluxes rates of leachable inorganic P and inorganic N (NO_3+NH_4) in the WMS. Fluxes are given in units of mmol m^{-2} yr^{-1}.

Location	Year	N	P	Reference
Wet Deposition				
Cap Ferrat	1997-1998		0.12	Migon and Sandroni (1999)
Sardinia	1992-1994	17.6		LeBolloch and Guerzoni (1995)
Cap Ferrat	1986-1987	43.6-51.9	0.44-0.52	Migon et al. (1989)
Corsica	1984-1986	29.2		Loÿe-Pilot et al. (1990)
Average		*31.5*	*0.30*	
Dry Deposition				
Cap Ferrat,	1998		0.02-0.12	Migon et al. (2001)
Cap Ferrat	2004-2005	25.8	0.03	Sandroni et al. (2007)
Average		*25.8*	*0.05*	
Bulk Deposition (Wet and Dry)				
Capo Carallo, Corsica	1985-1987		0.42-0.82	Bergametti et al. (1992)
Ostriconi	2001-2002	25.4	0.46	Markaki et al. (2010)
Cap Spartel	2001-2002	28.2	0.61	Markaki et al. (2010)
Cape Bear	2001-2002	45.9	0.57	Markaki et al. (2010)
Mahdia	2001-2002	18.1	0.37	Markaki et al. (2010)
Gozo	2001-2003	46.1	0.36	Markaki et al. (2010)
Average		*32.7*	*0.47*	
Total Average (wet+dry;bulk)		***45.0***	***0.45***	

Table E.2: NO_3 and NH_4 concentrations and NO_3:(NO_3+NH_4) ratio in SGD at coastal locations of the MS.

Site	NO_3 (μM)	NH_4 (μM)	NO_3/(NO_3+NH_4)	Reference
Balearic Islands, Spain	1031	2.2	0.998	Garcia-Solsona et al. (2010)
Dol Bay, Israel	330	5.4	0.98	Weinstein et al. (2011)
Sa Nau, Majorca	80	0.9	0.99	Tovar-Sanchez et al. (2014)

Table E.3: Proportions of dissolved organic P (DON) and dissolved organic N (DON) in total P and N, respectively, in fresh or low salinity SGD globally. Brackets give range of values reported.

Site	Salinity	DON/TN	DOP/TP	Reference
Upper gulf of Thailand	'fresh'	0.40 (0.06-0.83)	0.43 (0.01-0.83)	Burnett et al. (2007)
Tampa Bay, Florida	'fresh'	0.50		Kroeger et al. (2007)
Hudson Bay, Jeju Islands, Sea of Korea	0-5	(0.02-0.08)		Kim et al. (2013)
Queensland Australia	<5	0.47 (0-0.64)	0.03 (0-0.13)	Makings et al. (2014)
New South Wales, Australia		0.39	0.57	Santos et al. (2013)
Tropical reef lagoon, Cook Islands	<7	0.38 (0.09-0.74)	0.34 (0-0.67)	Tait et al. (2014)
Gulf of Mexico	Freshwater endmember	0.26 (0.24-0.28)		Santos et al. (2009)
Marina Lagoon, Mediterranean Coast, Egypt	<5	0.44* (0-0.97)	0.78* (0-0.99)	El-Gamal et al. (2012)

*Assume TN = TDN and TP = TDP

Table E.4: Reported SGD ages in coastal zones.

Location	SGD age (years)	Reference
Mediterranean Region		
Sicily	2-30	Burnett et al. (2006)
Syrian Coast	~60	Charideh and Rahman (2007)
Turkish Coast	Several 10s – several 100s	Bayari et al. (2011)
Worldwide		
Bay of Bengal	10 to >80	Dowling et al. (2003)
Coral reef lagoon, Australia	10-93	Tait et al. (2014)
Submarine freshwater spring, Japan	30-40	Asai et al. (2013)

Table E.5: Burial fluxes of N and P based on sediment core data.

	Area (10^3 km^2)	PON burial rate (mol N m^{-2} yr^{-1})	PON burial flux (10^9 mol N yr^{-1})	POP burial rate (mol P m^{-2} yr^{-1})	POP burial flux (10^9 mol P yr^{-1})
WMS	717.4	0.0037[a] – 0.005[b]	2.7-3.6	0.0002-0.0009	0.16-0.65
Alboran Sea	76	0.068[c]	5.2	0.004	0.30
Gulf of Lions	21.6	0.14[d,e]	3.0		0.01-0.17
Total	**815**		**10.9-11.8**		**0.56-1.13**

[a] Zúñiga et al. (2007a), [b] Heimbürger et al. (2012) [c] Masqué et al. (2003), [d] de Madron et al. (2003a) [e] Denis and Grenz (2003).

Table E.6: Sediment cores analyzed for POP concentrations in this study.

Sediment core	Location	Water depth (m)	Position	Sediment accumulation rate (g cm^{-2} yr^{-1})	Reference
T6	Alboran Sea	1993	35º55.74'N 1 º 32.59'W	0.063±0.006	Masqué et al. (2003)
Alb 1		962	36 º 14.31N 4 º 15.52'W	0.079±0.005	Masqué et al. (2003)
Alb 2		1300	36 º 00.31N 4 º 17.04' W	0.058±0.002	Masqué et al. (2003)
Alb E		1011	36 º 13.17N 4 º 02.48'W	0.043±0.002	Masqué et al. (2003)
Alb D		946	36 º 14.67N 4 º 28.15'W	0.101±0.010	Masqué et al. (2003)
T3		1076	35 º 48.18N 3 º 02.56'W	0.075±0.007	Masqué et al. (2003)
EB2	Catalan slope	1300	40º59.2'N 1 º 57.6'W	0.261±0.010	Sanchez-Cabeza et al. (1999)
CN36		500	41º04.5'N 1 º 55.6'W	0.51±0.02	Sanchez-Cabeza et al. (1999)

Table E.7: Particulate organic P (POP) concentrations and corresponding burial fluxes for the sediment cores analyzed. Uncertainties represent differences between duplicates.

Sediment Core	Depth interval (cm)	POP concentration (μmol/gdw)	POP flux (10^3 mol m^{-2} yr^{-1})
T6	0-0.5	6.4*	4.0*
	3-3.5	5.4±0.2	3.4±0.4
Alb 1	1.0-2.0	5.7±1.5	4.5±1.4
Alb 2	0-0.5	6.4±0.7	3.7±0.6
	5-5.5	5.7±0.6	3.3±0.5
Alb E	0-0.5	6.4±0.2	2.8±0.2
Alb D	0-0.5	7.1±0.2	7.1±0.9
T3	0-1.0	6.7±0.2	5.0±0.6
EB2	0-0.5	3.1±0.1	8.8±0.6
	5-5.5	2.9±0.3	7.6±1.1
CN36	1.0-2.0	4.7±0.3	23.9 ±4.2

* No duplicate run due to limited sample size.

Table E.8: Estimated organic P burial in the Gulf of Lions using mass accumulation rates for the Gulf of Lions and POP contents of core CN36 on the Catalan margin (Table E.7). See text for details.

Sedimentary Unit	Area (km^2)[a]	Mass accumulation rate (g cm^{-2} yr^{-1})[a]	POP burial (10^9 mol yr^{-1})
Proximal Rhone Pro-delta	10	30-50	0.01-0.02
Distal Rhone prodelta	600	0.2-0.6	0.01-0.02
Mid shelf mud belt	4500	0.15	0.03
Outer shelf	6500	0.14	0.04
Slope	10000	0.01-0.12	0.01-0.06
Total	**21610**		**0.10-0.17**

[a] Van Den Broeck and Moutin (2002)

Table E.9: Denitrification fluxes reported for the WMS.

	Area (10^3 km^{-2})	Rate (mol N m^{-2} yr^{-1})	Flux (10^9 mol N yr^{-1})
WMS	768.4	0.03 (0.02-0.06)[a]	19.7 (11.5-47.6)
Gulf of Lions	21.6	0.01-0.03[b]	0.2-0.6
Total	**815**		**20.1 (11.7-48.2)**

[a] Gehlen et al. (1997); [b]Denis and Grenz (2003)

Table E.10: Steady state internal model fluxes for the WMS and EMS in 1950. Units: 10^9 mol yr^{-1}.

		P		N	
		WMS	EMS	WMS	EMS
Assimilation	SW	94.7	59.0	1515	944
Solubilization		84.2	53.2	1254	788
Mineralization		85.4	54.4	1315	825
Nitrification				1324	837
Solubilization	IW	6.9	4.5	185	115
Mineralization		6.8	5.0	180	118
Nitrification				182	121
Solubilization	DW	3.2	0.7	78	21
Mineralization		3.7	0.7	84	25
Nitrification				84	25
Sinking POM	SW-IW	10.6	5.8	274	156
	IW-DW	3.7	1.4	89	41
Turbulent mixing*	IW-SW	2.2;-0.3	3.0;-0.3	57;-0.4; -0.2	77;-2.0;-1.7

*reported for PO_4 and DOP for P, and NO_3, DON and NH_4 for N. POM = particulate organic matter

Table E.11: Residence times (years) of reactive P and N species in 1950. P = total reactive phosphorus; N=total reactive nitrogen.

		P	PO_4	DOP	POP	N	NO_3	NH_4	DON	PON
SW	WMS	1.4	0.08	0.13	0.03	1.5	0.09	0.004	0.32	0.04
	EMS	2.5	0.11	0.24	0.03	3.7	0.18	0.03	0.83	0.08
IW	WMS	5.1	6.0	3.3	0.26	5.3	1.4	0.02	2.9	0.14
	EMS	5.4	5.3	2.5	0.34	6.0	5.3	0.16	4.5	0.39
DW	WMS	40	42	5.7	0.74	38	38	0.10	16	0.54
	EMS	117	150	57	3.8	119	143	3.5	81	4.2

Table E.12: Sensitivity (percent change) of primary productivity and DW NO_3:PO_4 ratio to a ±10% perturbation. Only the most sensitive model parameters identified by the fractional factorial design analyses (Figure 5.2) are included. Responses of more than 5% are highlighted in bold.

Perturbation	WMS primary productivity		EMS primary productivity		WMDW NO_3:PO_4		EMDW NO_3:PO_4	
	+	-	+	-	+	-	+	-
Atlantic SW-WMSW	**8.5**	**-8.5**	**6.6**	**-6.6**	-2.5	3.0	-4.4	**5.0**
WMIW-Atlantic	-2.7	3.0	-2.1	2.3	-0.3	0.3	0.3	-0.3
WMDW-Atlantic	-1.2	1.4	-0.9	1.1	0.2	-0.3	0.5	-0.6
WMIW-WMSW	2.6	-2.7	2.0	-2.0	-0.4	0.4	-0.1	0.1
WMDW-WMIW	1.3	-1.4	1.0	-1.0	-0.1	0.1	-0.2	0.2
WMSW–EMSW	-2.3	2.4	**5.7**	**-6.0**	0.2	-0.2	-1.8	2.1
EMIW-WMIW	0.2	-0.2	-4.2	**5.0**	0.1	-0.1	0.0	0.0
WMIW-NWM	-0.7	0.7	-0.5	0.5	0.0	0.0	0.0	0.0
EMDW-EMIW	0.0	0.0	0.0	0.0	0.1	-0.1	-0.4	0.4
Atlantic PO_4 conc	4.5	-4.5	3.4	-3.4	-4.5	4.9	**-7.2**	**7.7**
Atlantic DOP conc	4.0	-4.0	3.2	-3.2	-4.0	4.4	**-6.5**	**7.0**
EMS PO_4 atm dep	0.2	-0.2	0.8	-0.8	-0.4	0.4	-1.0	1.1
EMS P burial	-0.2	0.2	-0.5	0.5	0.3	-0.4	1.9	-2.1
WMS P burial	-0.2	0.2	-0.1	0.1	0.8	-0.8	0.3	-0.3
WMSW P sol	0.2	-0.2	4.9	**-5.3**	-0.7	0.7	-0.3	0.4
EMSW P sol	-0.1	0.1	**-7.9**	**9.4**	0.0	0.0	0.0	0.0
WMSW P min	2.0	-2.3	-2.6	3.0	-0.1	0.2	1.1	-1.2
EMSW P min	-0.1	0.1	2.6	-2.9	0.0	0.0	-0.4	0.4
WMS P assim	**-7.9**	**9.3**	-1.9	2.2	0.0	0.1	0.7	-0.8
EMS P assim	**5.3**	**-5.7**	4.4	-4.7	0.0	0.1	**-8.8**	**10.4**
WMSW-WMIW POP sink	**-5.1**	**5.9**	-4.3	4.9	0.1	0.0	**9.4**	**-9.7**
EMSW-EMIW POP sink	-0.2	0.2	-4.8	**5.4**	0.7	-0.7	0.4	-0.3
Atlantic NO_3 conc	0.0	0.0	0.0	0.0	1.6	-1.6	2.5	-2.5
Atlantic DON conc	0.0	0.0	0.0	0.0	4.5	-4.5	**6.9**	**-6.9**
EMS DON atm dep	0.0	0.0	0.0	0.0	0.5	-0.5	0.7	-0.7
EMS NO_3 atm dep	0.0	0.0	0.0	0.0	0.7	-0.7	1.5	-1.5
EMS NH_4 atm dep	0.0	0.0	0.0	0.0	0.5	-0.5	1.0	-1.0
EMS N burial	0.0	0.0	0.0	0.0	-0.3	0.4	-1.5	1.7
WMS N burial	0.0	0.0	0.0	0.0	-0.5	0.5	-0.2	0.2
WMS denit	0.0	0.0	0.0	0.0	-1.3	1.3	-0.3	0.3
WMSW N sol	0.0	0.0	0.0	0.0	0.0	0.0	**6.6**	**-7.8**
EMSW N sol	0.0	0.0	0.0	0.0	0.6	-0.7	0.1	-0.1
WMSW-WMIW PON sink	0.0	0.0	0.0	0.0	0.0	0.0	**-7.1**	**7.3**
EMSW-EMIW PON sink	0.0	0.0	0.0	0.0	-0.6	0.6	-0.1	0.1
WMDW N sol	0.0	0.0	0.0	0.0	0.4	-0.5	0.1	-0.2
EMDW N sol	0.0	0.0	0.0	0.0	0.3	-0.4	1.5	-1.7
WMDW N min	0.0	0.0	0.0	0.0	1.6	-1.9	-0.1	0.1
EMDW N min	0.0	0.0	0.0	0.0	0.0	0.0	2.3	-2.5

Appendix F

Supporting Information: Chapter 6

Phosphorus and Nitrogen Trajectories in the Mediterranean Sea (1950-2030): Diagnosing basin wide anthropogenic enrichment

F.1 Model forcing functions

The change in reactive P and N inputs into the MS with time are modeled by applying anthropogenic forcing functions to 1950 model inputs (Chapter 5) following the method in Chapter 2. The following sections justify the applied anthropogenic forcing functions for the WMS over 1950-2030 and those for the EMS over 2000-2030 in addition to SGD and wastewater discharges into the EMS over 1950-2030. The remaining anthropogenic forcing functions for the EMS for 1950 to 2000 are justified in Chapter 2.

F.1.1 Atmospheric Deposition

The same forcing function for atmospheric deposition in the WMS is applied to each P and N species (PO_4, DOP, NO_3, NH_4, and DON) for 1950 to 2000 as that used for the EMS (Chapter 2), for lack of any detailed estimates on how the temporal evolution of these inputs may vary between the two seas. In the EMS, PO_4 deposition was modeled to change in proportion to acid processing in the atmosphere (Chapter 2) as this increases the P solubility in dust (Nenes et al., 2011; Stockdale et al., 2016). Thus the 2000 to 2030 forcing function for both seas is calculated from the linear interpolation of regional emissions of NO_x and SO_x for the years 2000 and 2030 (Lamarque et al., 2013) to represent the amount of acid within the atmosphere. The resulting forcing function for the WMS and EMS for 1950 to 2030 increases by a maximum of 2.5 in 1979 before decreasing thereafter to 1.3 in 2030. Model predicted deposition of NO_X and NH_x in Europe, Africa and former USSR, and Middle East for the years 2000 and 2030 are used to create the forcing function for NO_3 and NH_4 deposition (Lamarque et al., 2013). A maximum increase in NO_3 and NH_4 deposition of 3.0 and 2.0 occurs in 1994. Thereafter NO_3 deposition to decreases to 2.8 in 2030 whilst NH_4 deposition initially decreases to 2.1 in 2000 before increasing to 2.2 by 2030.

DON and DOP deposition in the EMS between 1950 and 2000 are assumed to change due to biomass burning (Chapter 2). We use global estimates of anthropogenic organic carbon emissions to calculate the forcing function for DON and DOP deposition between 2000 and 2030 (IPCC, 2013). A maximum increase of 1.4 with respect to 1950 occurs in 1995 and deposition thereafter remains approximately constant. Forcing functions of atmospheric deposition for all P and N species between 2000 and 2030 use the mean value of all reported model runs and assumes a linear relationship in emissions/deposition over that time period. Maximum and minimum estimates of the forcing function for 2000 to 2030 were calculated from the maximum and minimum range of model estimates reported. The resulting range in estimates are greatest for DOP and DON deposition with the maximum estimate predicting an increase in organic matter deposition between 2000 and 2030 and the minimum estimate predicting a decrease.

F.1.2 Rivers

The riverine forcing function between 1950 and 2000 for the WMS is calculated from Ludwig et al. (2009), assuming that the speciation of riverine input does not vary with time. The relative change in riverine inputs from 2000-2030 for both WMS and EMS are calculated from estimates of 2000 and 2030 inputs by Ludwig et al. (2010) using the Millennium Ecosystem Assessment scenarios. The mean of all four scenario was taken for the best estimate, and maximum and minimum trends used for the range in inputs. The resulting forcing function for P inputs between 1950 and 2030 results in a peak value of 7.8 in 1984 in the WMS compared to a peak of 2.4 in the EMS. The differences between the two seas over this time period are in a large part to the construction of the Aswan Dam, which significantly reduced P inputs to the EMS immediately after its closure. Riverine P fluxes in both basins thereafter declined to a minimum in 2000 of 3.0 and 1.5 in the WMS and EMS respectively before increasing between 2000 and 2030, especially within the EMS. Contrasting trends are observed in the forcing function between the WMS and EMS for N however due to differences in population growth estimates between these two basins (Ludwig et al., 2010). In the WMS, the forcing function for riverine N reaches a maximum of 6.6 in 2000 before decreasing to 5.6 in 2030 whereas in the EMS the riverine N forcing function continues to increase throughout 1950 to 2030, to a value of 5.9 by 2030.

F.1.3 Direct domestic wastewater discharges

Changes in direct wastewater discharges of N are assumed to follow population trends within Mediterranean countries between 1950 and 2030 (FAOSTAT, 2016). Population trends for each individual country are weighted to their wastewater input (Chapter 3) to calculate the overall change in wastewater inputs for the WMS and EMS. Note that although we are using country population trends rather than coastal trends, predicted population increase between 2000 and 2025 is similar to that of coastal areas predicted over the same time period by Plan-Bleu (2005) (results not shown). The resulting forcing function of N inputs from wastewater continually increases throughout 1950-2030 to a maximum of 1.9 in the WMS and 3.2 in the EMS. For P, population together with laundry and dishwasher P-detergent use influences wastewater P discharges with time. We apply same N:P ratio trend as in rivers to wastewater, thus accounting for the temporal change of P in detergents as well as P derived from protein consumption from population. For the EMS however, we exclude the Levantine basin from riverine inputs to calculate the N:P trends due to the difference in responses of P and N to the closure of the Aswan Dam in 1963 (Ludwig et al., 2009). The resulting forcing function for P increased throughout 1950 to 2030 reaching a maximum of 1.6 in the WMS and 3.2 in the EMS. For N we assume maximum and minimum bounds in population estimates of 5% by 2030 with the error increasing linearly between

2015 and 2030. The maximum and minimum range in wastewater discharges of P are taken from the resulting maximum and minimum range in N:P ratios of applied riverine inputs.

F.1.4 Submarine groundwater discharges

SGD of P and N has only recently been quantified into the MS (Rodellas et al., 2015) and little is known about how it might change with time (Moon et al., 2016). Nitrogen input through SGD is assumed to change in relation to fertilizer input on land. We further assume a 30 year time lag between fertilizer input and discharge at the coastal zone based upon GW ages discharging into the MS and worldwide (Chapter 2). Fertilizer consumption of inorganic N from 1920-2000 (to represent 1950-2030 inputs from SGD) for each individual Mediterranean country (Erisman et al., 2011; FAOSTAT, 2015a) is weighted to regional GW discharges (Zekster et al., 2007) and used to calculate the overall changes in the WMS and EMS respectively. The forcing function for NO_3 and NH_4 SGD in the WMS increases to 2.3 between 1950 and 1970 before remaining stable to 1985. Thereafter it increases sharply to a maximum of 22.7 in 2030. In the EMS a linear increase between 1950 and 1991 to 5.1 occurs from NO_3 and NH_4 from SGD before increasing dramatically to reach a maximum of 55.9 in 2030. By 2030 the forcing functions in both the WMS and EMS are starting to stabilize. Similarly, changes in European manure input and worldwide manure input for 1920-1960 (Erisman et al., 2011) and individual countries for 1960-2000 (FAOSTAT, 2015b) are used to estimate changes in DON for the WMS and EMS respectively, resulting in a maximum forcing function of 1.9 and 2.1 by 2030.

It is assumed that P in SGD does not change with time as the 2000 freshwater flux is extremely small suggesting that P from fertilizer input is potentially adsorbed within the aquifer. Due to the time lag between N inputs and resulting changes in SGD, maximum and minimum estimates for 2000 to 2030 are not undertaken for this forcing function.

F.1.5 Nitrogen fixation

It is likely that changing reactive P and N concentrations within surface waters of the WMS between 1950 and 2000 would alter N_2 fixation rates. However, no evidence exists of a correlation between N_2 fixation and nutrient availability (Sandroni et al., 2007; Berman-Frank and Rahav, 2012). Therefore, due to the limited nature of our understanding of N_2 fixation within the MS, and how it relates to N and P concentrations, the flux is not modeled to change with time.

F.2 Climate change circulation scenarios

To investigate the impact of climatic changes in circulation on water column reactive P and N concentrations and primary productivity, the two extreme climate change circulation scenarios presented in Chapter 4, WC1 and WC3, were applied to the model for the years 2000 to 2030 and are termed climate change scenario S1 and climate change scenario S2 in this paper, respectively. From 1950-2000, the random circulation described in section 6.3.3.1 of the main text is used to calculate IW/DW formation fluxes. From 2000 onwards, the IW/DW formation fluxes are still randomly assigned on a year by year basis but the mean IW/DW formation rates used within the random circulation calculations change with time. For a substantial weakening of the THC (Scenario S1), the same values for IW/DW formation are used as in Chapter 4 for WC1 for the year 2100 but we do not account for the shallowing of the THC i.e. there is no flow out of the NWM to WMIW, or from the Adriatic to EMIW. A strengthening of the THC across the whole of the MS (Scenario S2) is applied to the model using the formation rates described in scenario WC3 for 2100 in Chapter 4. We assume that the switch from the mean baseline circulation to the mean climate change circulations occur at a linear rate between 2000 and 2100 due to the linearity of modeled changes in temperature and salinity between 2000 and 2100 (Adloff et al., 2015). It is also assumed that standard deviation of DW formation rates and probability of IW/DW formation do not change with time, that is, they are the same from 2000 to 2030 as prior to 2000 in random circulation scenario where the mean is also constant with time.

F.3 Figures and Tables

Figure F.1: Anthropogenic forcing functions of reactive P and N between 1950 and 2030 imposed in the model. Note the forcing function calculates the change relative to 1950 for each individual input. Dashed lines represent maximum and minimum estimates for the period 2000 to 2030. See main text and section F.1 for details.

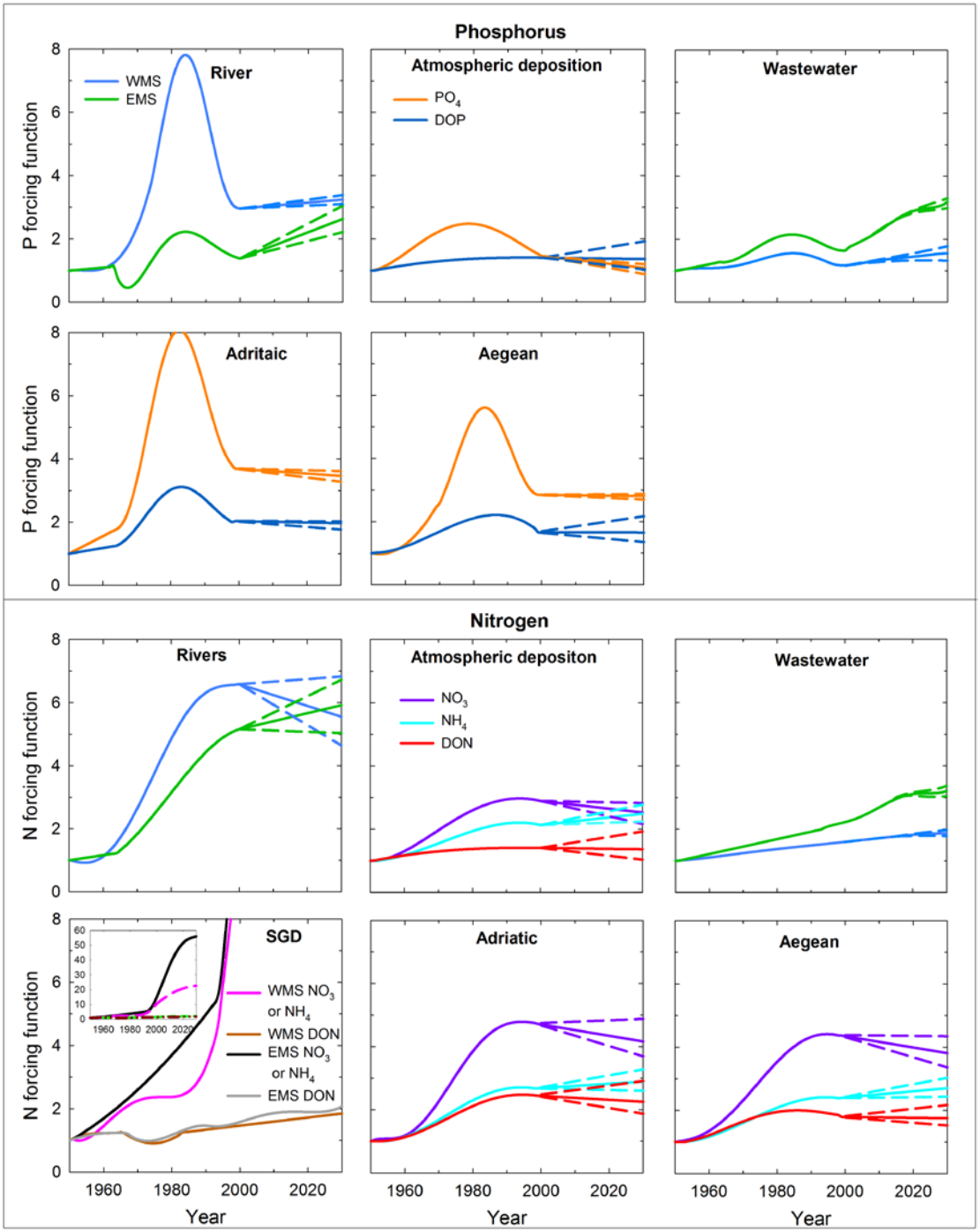

Figure F.2: Sin wave of temporal evolution of the Adriatic Deep Water input into the EMDW (see Equation 6.1) in the historical circulation scenarios (Simulations 4 and 5).

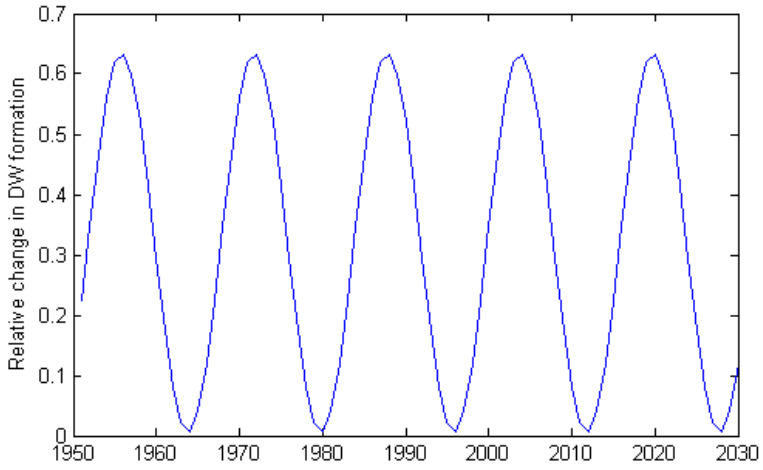

Figure F.3: Trajectories of land derived phosphorus (black continuous line) and nitrogen (red dashed line) inputs into the WMS and EMS relative to 1950 values. Land derived inputs refer to those inputs from: atmospheric deposition, rivers, direct wastewater discharges, submarine groundwater discharges and additional nutrients added to the Adriatic Sea, Aegean Sea and NWM.

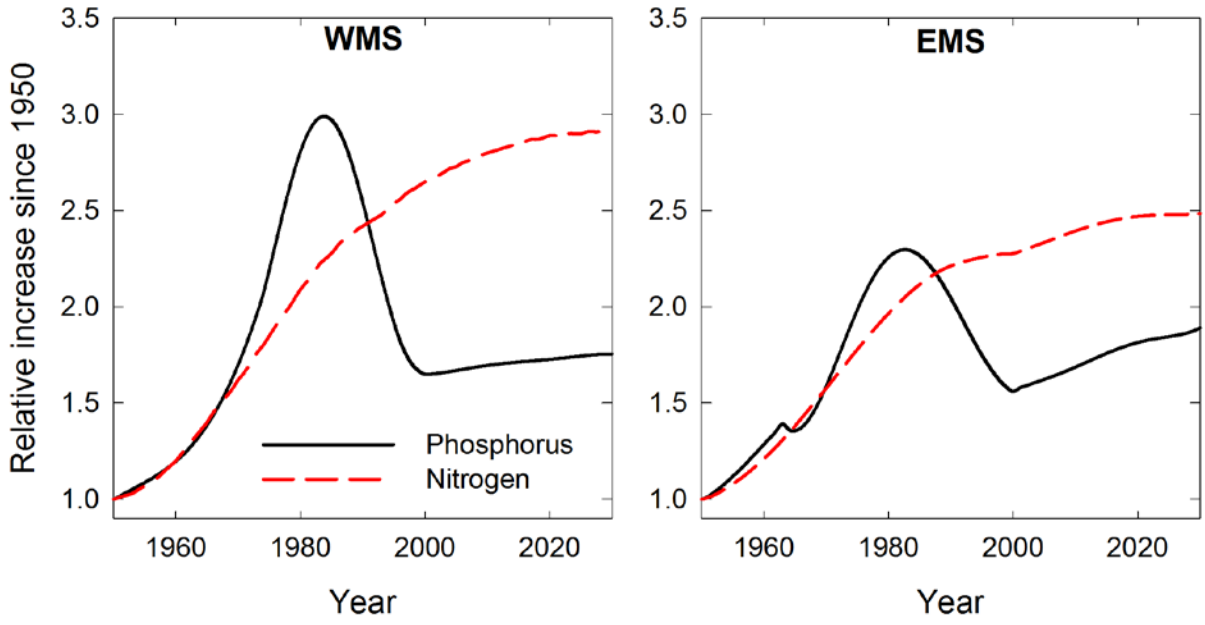

Figure F.4: Dissolved reactive P and N surface water concentrations in the WMS and EMS from changes in circulation alone (Simulation 1; red shading and red lines) against changes due to nutrient enrichment and circulation changes (Simulation 2; blue shading and blue lines). The model was run 500 times randomly changing the circulation. Mean, 10^{th} and 90^{th} percentiles are shown. Dashed line between 2000 and 2030 represents uncertainty in input estimates for this time period. Note changes in units of scale on y axis for P and N. See section 6.3.3 of the main text and Table 6.2 for details of model simulations.

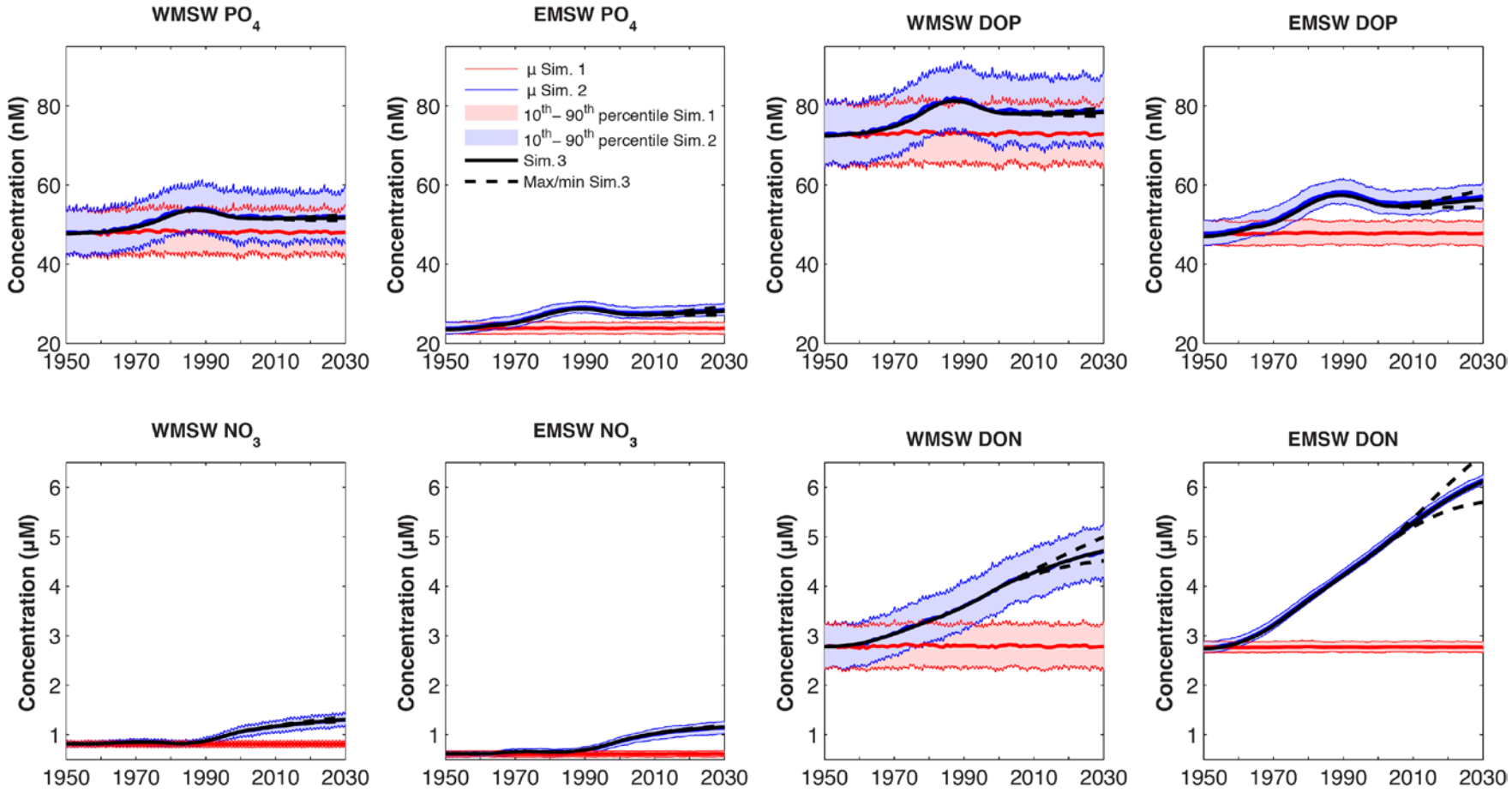

Figure F.5: Relative change in reactive P (A-C) and N (D-G) concentrations since 1950 in the WMS (green lines) and EMS (black lines) for surface water (SW; solid line), intermediate water (IW; dashed line) and deep water (DW; dash-dot line). Note difference in scales between Figures A-C and D-G.

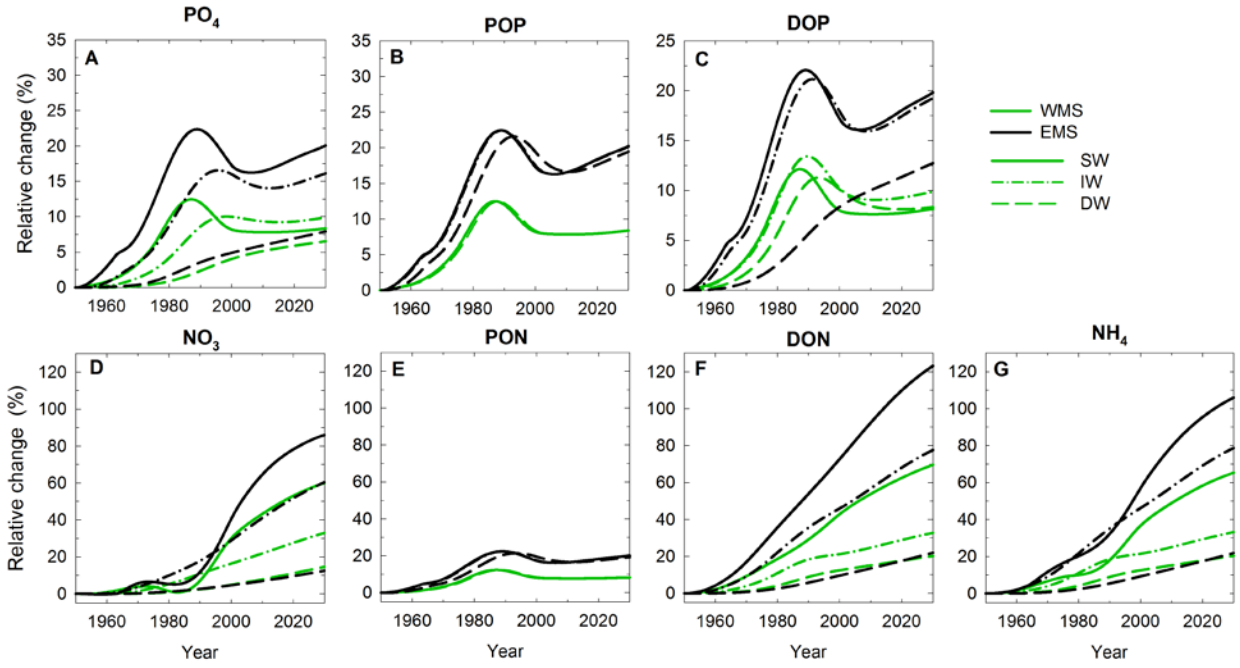

Figure F.6: Changes in deep water PO_4 and NO_3 concentrations due to historical changes in the THC and nutrient enrichment (Simulation 5 and 7) in comparison to constant circulation with anthropogenic nutrient enrichment (Simulation 3; red line). See section 6.3.3.2 for details on how historical circulation were made and Table 6.2 the explanation of the different model runs.

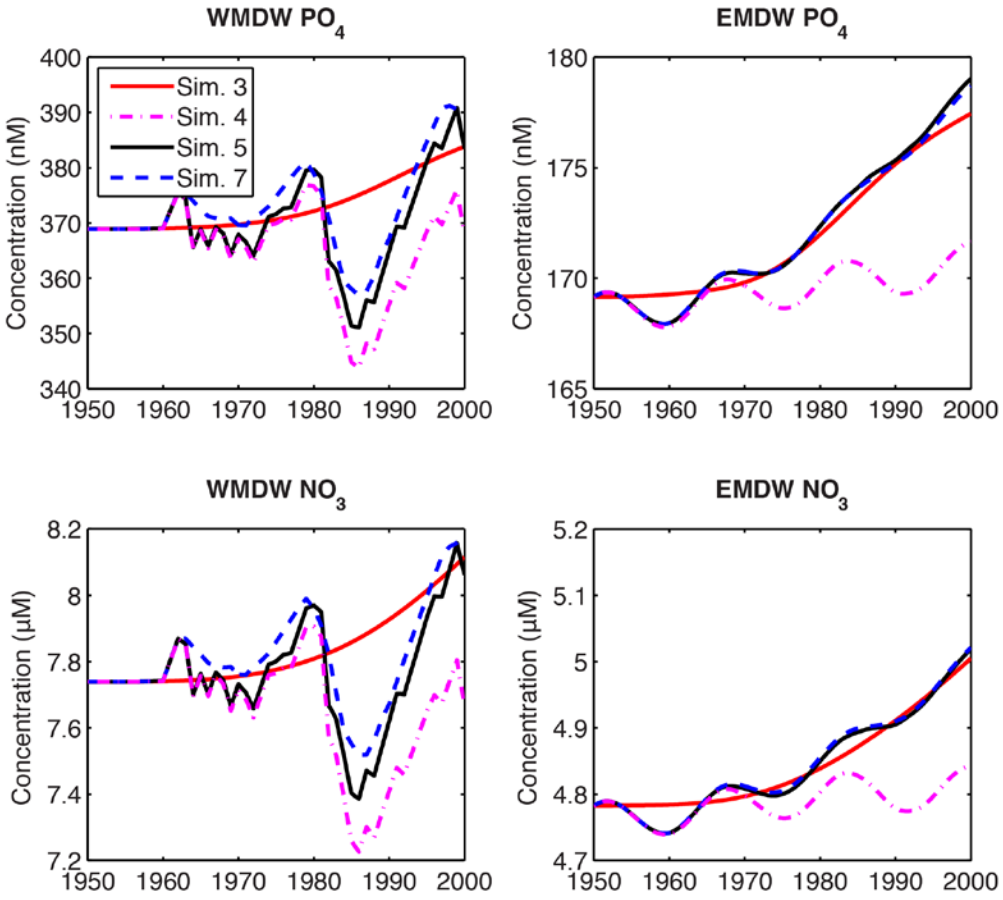

Figure F.7: Same as Figure F.3 but for NO_3:PO_4 DW ratios of the WMS and EMS.

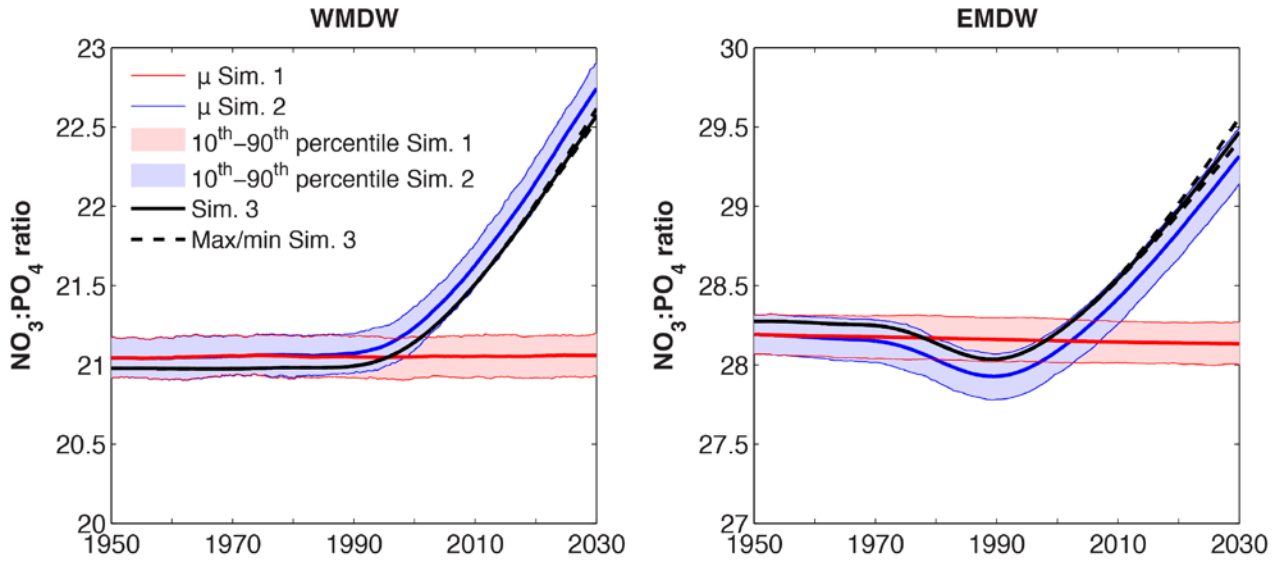

Figure F.8: Changes in intermediate water NO_3:PO_4 IW and DW ratios in the EMS and WMS from historical inter-annual variability in the thermohaline circulation between 1960 and 2000 with: constant reactive P and reactive N inputs (Simulation 4); 1950-2000 reactive P and reactive N inputs (Simulation 5); and using a 5 year running average with 1950-2000 reactive P and reactive N inputs (Simulation 7), compared to 1950-2000 reactive P and N inputs with constant circulation (Simulation 3; red line). See main text for details of how the historical circulation predictions were made.

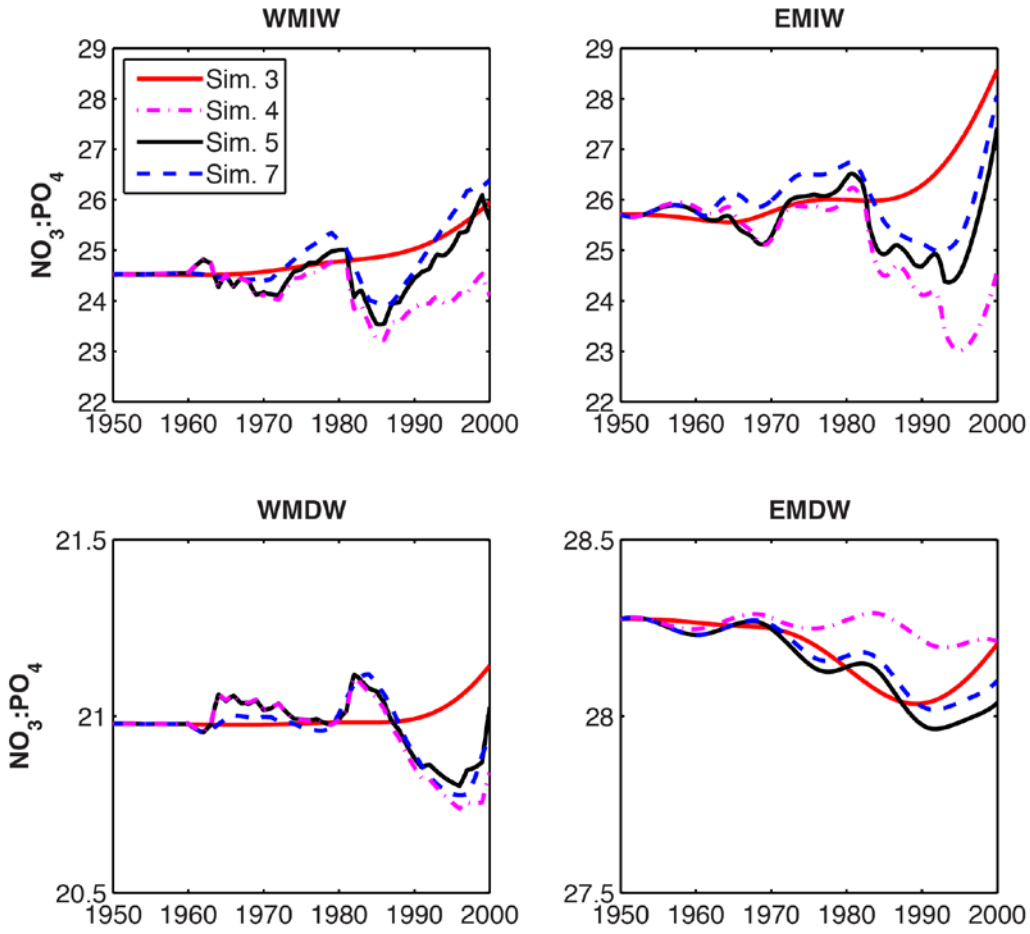

Figure F.9: Primary productivity in the WMS (A and C) and EMS (B and D) between 1950 and 2000 in the historical circulation scenario with constant reactive P and N inputs (Simulation 4; A and B) and 1950 to 2030 P and N inputs (Simulation 5; C and D). Relative change since 1950 (black line, left axis) and absolute primary productivity (brown line, right axis) are shown.

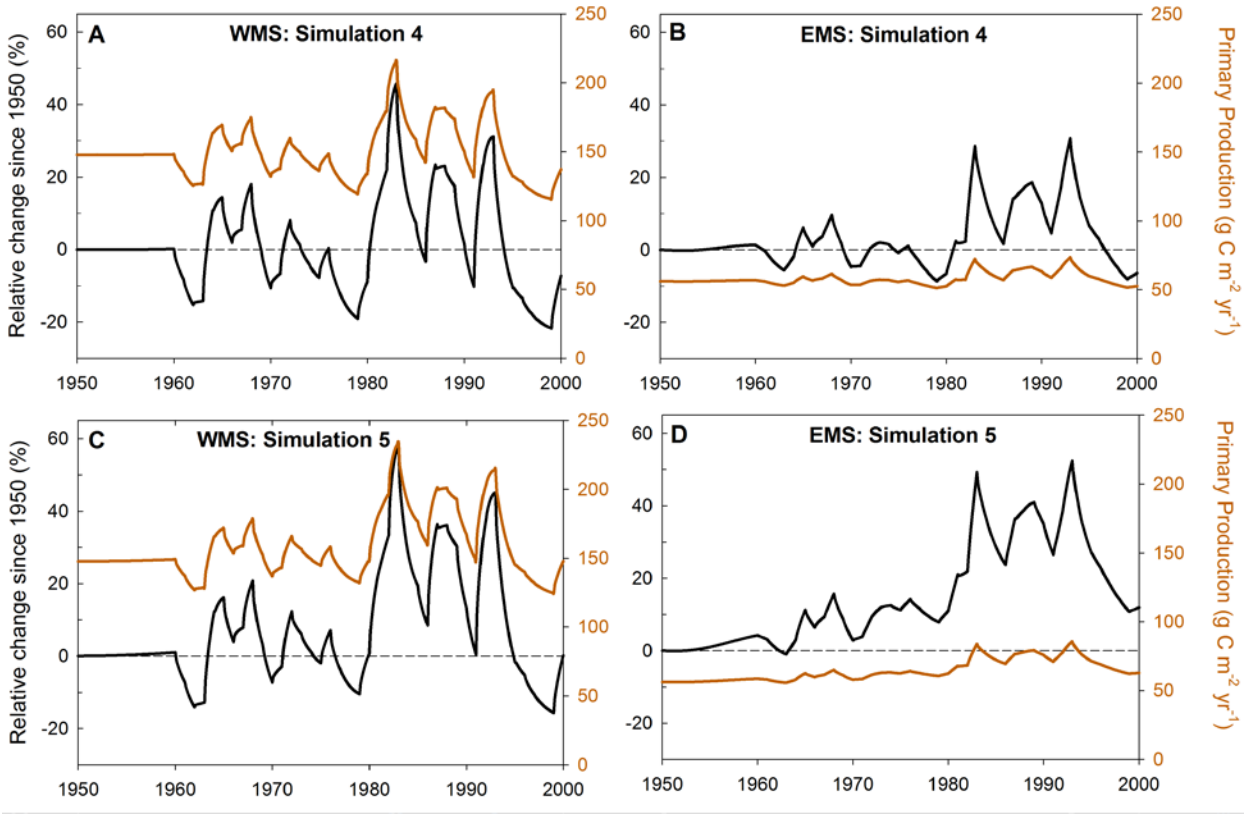

Figure F.10: Fate of anthropogenic P and N added to the WMS (A and C) and EMS (B and D) in Simulation 3, expressed as the percentage of additional reactive P and N supplied to the WMS and EMS over the period 1950 to 2030. Burial, denitrification (Denit) and outflow to Atlantic (Atl), EMS and WMS are expressed as the percentage of additional reactive P and N supplied, while accumulation in the water column differentiates between the different nutrient species.

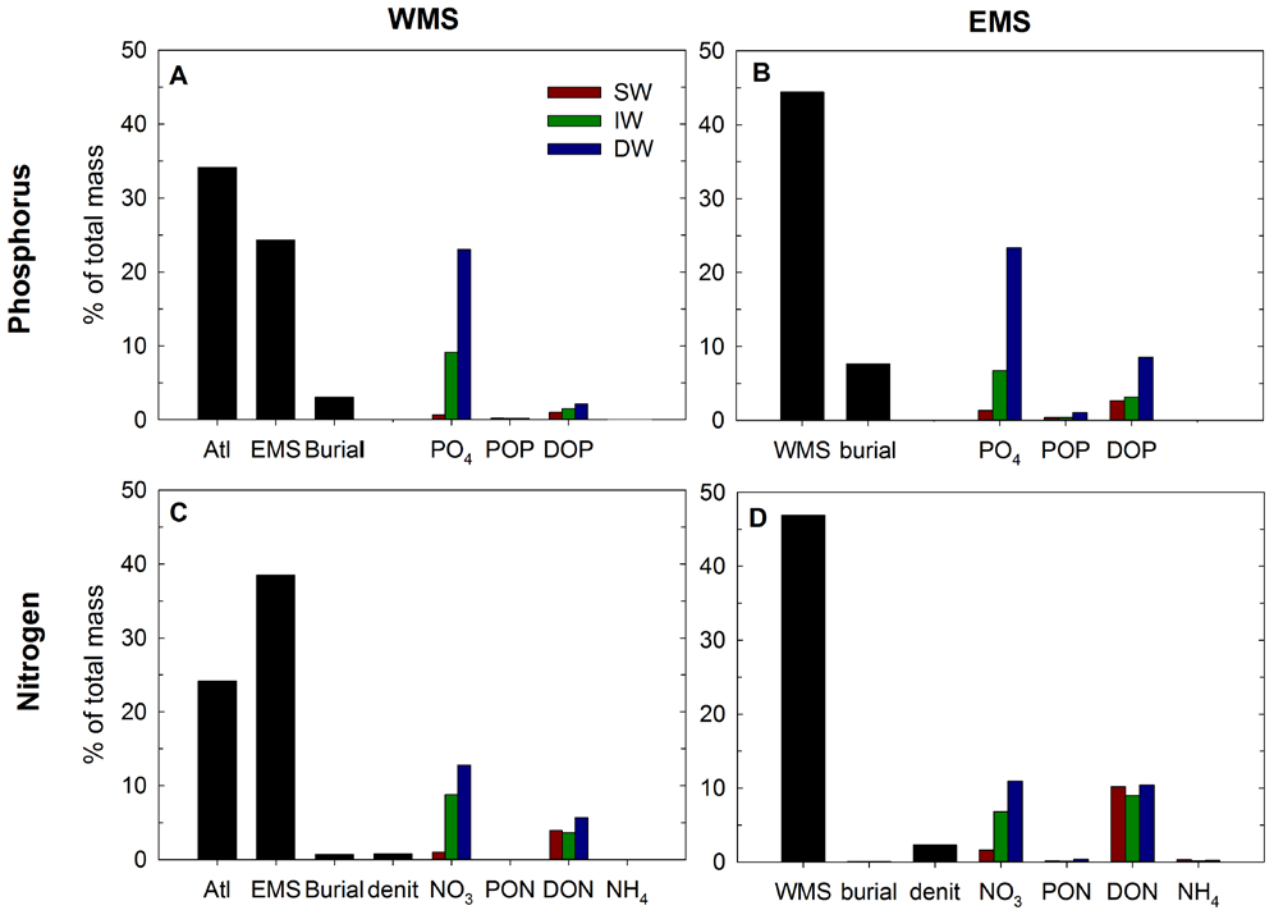

Figure F.11: Reactive N:P ratios of input (solid lines) and output (dashed lines) fluxes into the WMS (green lines) and EMS (black lines) between 1950 and 2030 for Simulation 3.

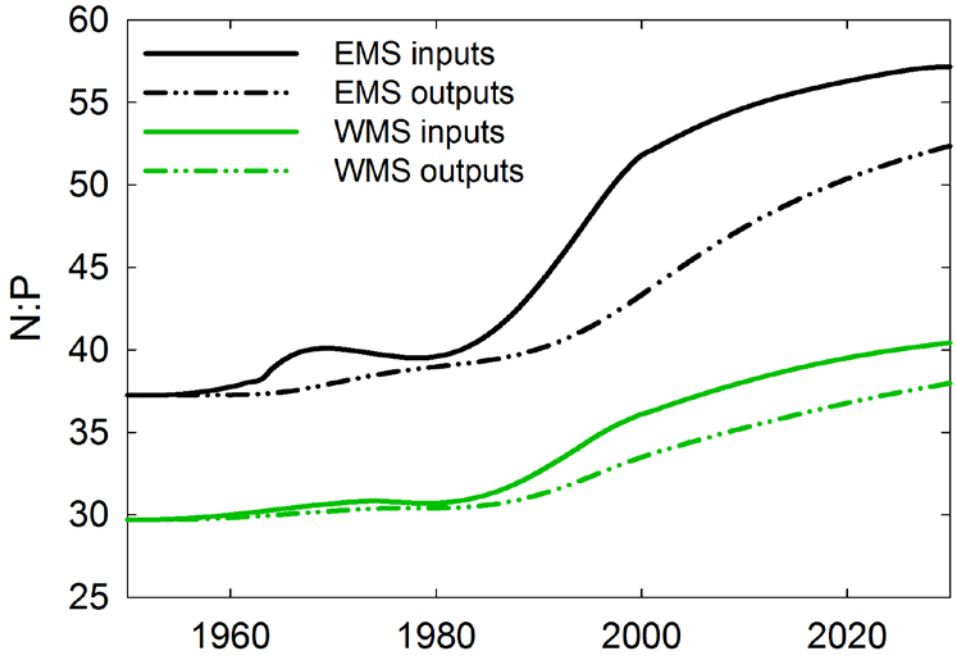

Figure F.12: Changes in primary productivity in the WMS (A-B) and EMS (C-D) due to climatic induced changes in circulation and constant (A and C) and changing (B and D) P and N inputs over the period 1950 to 2030. Error bars for random circulation and climate change scenarios represent 10^{th}-90^{th} percentiles of ensemble of 500 runs; those for constant circulation represent range in model inputs over 2000 to 2030.

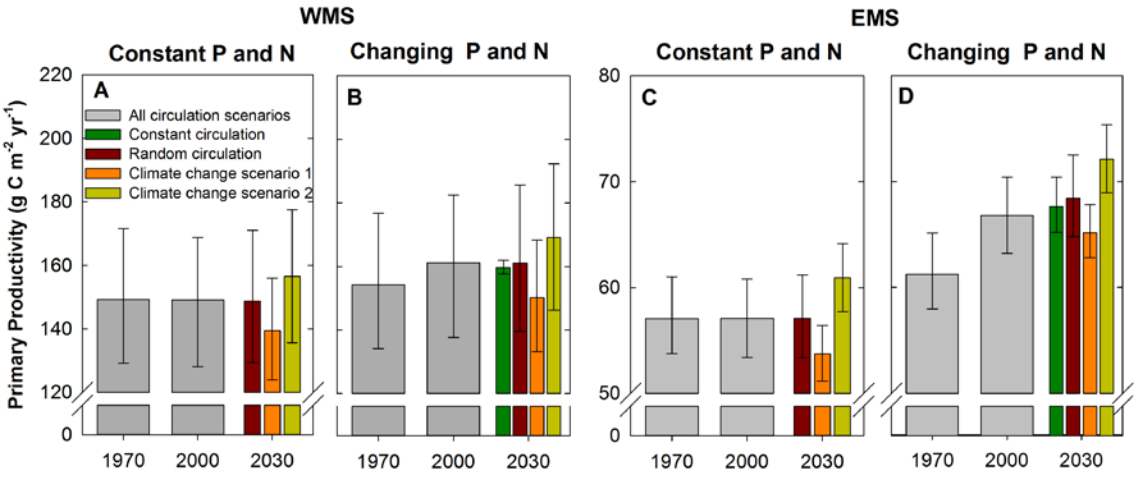

Table F.1: Decadal values of anthropogenic forcing functions for a) phosphorus and b) nitrogen, applied to the model, representing the change in each flux relative to 1950. Numbers in brackets from 2010-2030 represent the maximum and minimum predicted forcing function. Minimum and maximum values of the forcing function over 1950-2030 and year they occurred (brackets) are also reported.

	Species	**Sea**	**1950**	**1960**	**1970**	**1980**	**1990**	**2000**	**2010**	**2020**	**2030**	**Min**	**Max**
Phosphorus													
River	PO_4 and DOP	WMS	1.0	1.1	2.4	7.0	6.1	3.0	3.1 (3.0-3.1)	3.2 (3.1-3.2)	3.2 (3.1-3.4)	1.0 (1950)	7.8 (1984)
	PO_4 and DOP	EMS	1.0	1.1	0.7	2.1	2.0	1.4	1.8 (1.7-1.9)	2.2 (1.9-2.5)	2.6 (2.2-3.1)	0.5 (1967)	2.6 (2030)
Atmospheric Deposition	PO_4	WMS and EMS	1.0	1.5	2.2	2.5	2.1	1.5	1.3 (1.3-1.4)	1.2 (1.1-1.3)	1.1 (0.9-1.2)	1.0 (1950)	2.5 (1979)
	DOP	WMS and EMS	1.0	1.2	1.3	1.4	1.4	1.4	1.4 (1.3-1.6)	1.4 (1.2-1.8)	1.4 (1.0-1.9)	1.0 (1950)	1.4 (1995)
Wastewater	PO_4 and DOP	WMS	1.0	1.1	1.2	1.5	1.5	1.2	1.3 (1.3-1.4)	1.4 (1.3-1.6)	1.6 (1.3-1.8)	1.0 (1950)	1.6 (1985)
	PO_4 and DOP	EMS	1.0	1.2	1.5	2.1	2.0	1.6	2.3 (2.3-2.3)	2.9 (2.8-2.9)	3.2 (3.0-3.3)	1.0 (1950)	3.2 (2030)
Adriatic	PO_4	EMS	1.0	1.6	3.3	7.8	6.2	3.7	3.6 (3.5-3.7)	3.5 (3.4-3.6)	3.5 (3.3-3.6)	1.0 (1950)	8.1 (1982)
	DOP	EMS	1.0	1.2	1.8	3.0	2.7	2.0	2.0 (1.9-2.0)	2.0 (1.8-2.0)	2.0 (1.8-2.0)	1.0 (1950)	3.1 (1983)
Aegean	PO_4	EMS	1.0	1.3	2.6	5.3	4.6	2.9	2.8 (2.8-2.9)	2.8 (2.7-2.9)	2.8 (2.7-2.9)	1.0 (1950)	5.6 (1983)
	DOP	EMS	1.0	1.2	1.7	2.1	2.2	1.7	1.7 (1.5-1.9)	1.7 (1.5-2.0)	1.7 (1.4-2.2)	1.0 (1950)	2.2 (1987)

Table F.1b:

	Species	Sea	1950	1960	1970	1980	1990	2000	2010	2020	2030	Min	Max
Nitrogen													
River	NO_3, DON and NH_4	WMS	1.0	1.1	2.6	4.8	6.3	6.6	6.2 (5.9-6.7)	5.9 (5.3-6.7)	5.6 (4.6-6.8)	0.9 (1955)	6.6 (2000)
	NO_3, DON and NH_4	EMS	1.0	1.2	1.8	3.1	4.4	5.2	5.4 (5.1-5.7)	5.7 (5.1-6.2)	5.9 (5.0-6.7)	1.0 (1950)	5.9 (2030)
Atmospheric Deposition	NO_3	WMS and EMS	1.0	1.3	2.0	2.6	2.9	2.9	2.8 (2.7-2.9)	2.6 (2.4-2.9)	2.5 (2.2-2.8)	1 (1950)	3.0 (1994)
	DON	WMS and EMS	1.0	1.2	1.3	1.4	1.4	1.4	1.4 (1.3-1.6)	1.4 (1.2-1.8)	1.4 (1.0-1.9)	1.0 (1950)	1.4 (1995)
	NH_4	WMS and EMS	1.0	1.2	1.5	1.9	2.2	2.1	2.2 (2.2-2.3)	2.4 (2.2-2.6)	2.5 (2.2-2.8)	1.0 (1950)	2.5 (2030)
Wastewater	NO_3, DON and NH_4	WMS	1.0	1.1	1.2	1.4	1.5	1.6	1.7 (1.7-1.7)	1.8 (1.8-1.8)	1.9 (1.8-2.0)	1.0 (1950)	1.9 (2029)
	NO_3, DON and NH_4	EMS	1.0	1.2	1.4	1.7	1.9	2.2	2.7 (2.7-2.7)	3.1 (3.1-3.2)	3.2 (3.0-3.4)	1.0 (1950)	3.2 (2030)
SGD	NO_3 and NH_4	WMS	1.0	1.5	2.3	2.4	3.3	10.2	16.8	20.8	22.7	1.0 (1950)	22.7 (2030)
	DON	WMS	1.0	1.2	1.0	1.0	1.3	1.5	1.6	1.7	1.9	0.9 (1975)	1.9 (2030)
	NO_3 and NH_4	EMS	1.0	1.7	2.6	3.7	5.0	14.6	36.5	51.4	55.9	1.0 (1950)	55.9 (2030)
	DON	EMS	1.0	1.2	1.0	1.2	1.5	1.6	1.9	1.9	2.1	1.0 (1950)	2.1. (2030)
NWM	NO_3, DON and NH_4	WMS	1.0	1.3	1.8	2.3	2.6	2.6	2.5 (2.4-2.7)	2.5 (2.3-2.8)	2.5 (2.1-2.9)	1.0 (1950)	2.6 (1994)
Adriatic	NO_3	EMS	1.0	1.2	2.3	3.9	4.7	4.7	4.5 (4.3-4.8)	4.3 (4.0-4.8)	4.2 (3.7-4.9)	1.0 (1950)	4.8 (1994)
	DON	EMS	1.0	1.1	1.6	2.1	2.4	2.4	2.4 (2.2-2.6)	2.3 (2.1-2.8)	2.3 (1.9-2.9)	1.0 (1950)	2.5 (1995)
	NH_4	EMS	1.0	1.1	1.7	2.3	2.7	2.7	2.8 (2.6-2.9)	2.8 (2.6-3.1)	2.9 (2.6-3.3)	1.0 (1950)	2.9 (2030)
Aegean	NO_3	EMS	1.0	1.3	2.3	3.5	4.3	4.3	4.2 (4.0-4.4)	4.0 (3.7-4.4)	3.8 (3.4-4.3)	1.0 (1950)	4.4 (1995)
	DON	EMS	1.0	1.2	1.6	1.9	2.0	1.8	1.8 (1.7-1.9)	1.8 (1.6-2.1)	1.8 (1.5-2.2)	1.0 (1950)	2.0 (1986)
	NH_4	EMS	1.0	1.2	1.6	2.1	2.4	2.4	2.5 (2.4-2.6)	2.6 (2.4-2.8)	2.7 (2.4-3.0)	1.0 (1950)	2.7 (2030)

Table F.2: Model predicted reactive P and N concentrations and N:P ratios for all reservoirs for Simulation 3 in a) the WMS and b) the EMS. See Table 6.2 of main text for description of model simulations.

Table F.2a:

	Water Mass	1950	1960	1970	1980	1990	2000	2010	2020	2030	Max	Min
PO_4 (nM)	WMSW	48	48	49	52	53	52	51	52	52	54	48
	WMIW	269	269	272	280	292	296	294	294	295	296	269
	WMDW	369	369	370	372	378	384	388	391	393	393	369
DOP (nM)	WMSW	72	73	75	79	81	78	78	78	78	81	72
	WMIW	44	44	45	48	50	49	48	48	48	50	44
	WMDW	27	27	27	29	30	30	29	29	29	30	27
POP (nM)	WMSW	17	17	18	19	19	19	19	19	19	19	17
	WMIW	8.4	8.4	8.6	9.1	9.4	9.0	9.0	9.0	9.1	9.4	8.4
	WMDW	3.0	3.0	3.1	3.3	3.4	3.3	3.3	3.3	3.3	3.4	3.0
NO_3 (µM)	WMSW	0.8	0.8	0.8	0.8	0.9	1.1	1.2	1.3	1.3	1.3	0.8
	WMIW	6.6	6.6	6.7	6.9	7.3	7.7	8.0	8.4	8.8	8.8	6.6
	WMDW	7.7	7.7	7.8	7.8	7.9	8.1	8.3	8.6	8.9	8.9	7.7
NH_4 (µM)	WMSW	0.03	0.03	0.03	0.03	0.03	0.04	0.04	0.05	0.05	0.05	0.03
	WMIW	0.01	0.01	0.01	0.01	0.01	0.01	0.01	0.01	0.01	0.01	0.01
	WMDW	0.01	0.01	0.01	0.01	0.01	0.01	0.01	0.01	0.01	0.01	0.01
DON (µM)	WMSW	2.8	2.8	3.0	3.3	3.6	4.0	4.3	4.5	4.7	4.7	2.8
	WMIW	2.7	2.8	2.8	3.0	3.2	3.3	3.4	3.5	3.6	3.6	2.7
	WMDW	2.5	2.5	2.5	2.6	2.7	2.8	2.9	2.9	3.0	3.0	2.5
PON (µM)	WMSW	0.38	0.38	0.39	0.42	0.43	0.41	0.41	0.41	0.41	0.43	0.38
	WMIW	0.12	0.12	0.12	0.13	0.13	0.13	0.13	0.13	0.13	0.14	0.12
	WMDW	0.05	0.05	0.05	0.06	0.06	0.06	0.06	0.06	0.06	0.06	0.05
NO_3: PO_4	WMSW	17	17	17	16	16	21	23	24	25	25	15
	WMIW	25	25	25	25	25	26	27	29	30	30	25
	WMDW	21	21	21	21	21	21	22	22	23	23	21
DON: DOP	WMSW	38	39	41	42	44	51	55	58	60	60	38
	WMIW	62	62	63	63	65	69	71	73	75	75	62
	WMDW	92	92	91	91	90	94	98	100	102	102	90
PON: POP	WMSW	22	22	22	22	22	22	22	22	22	22	22
	WMIW	14	14	14	14	14	14	14	14	14	14	14
	WMDW	18	18	18	18	18	18	18	18	18	18	18

Table F.2b:

EMS	Water Mass	1950	1960	1970	1980	1990	2000	2010	2020	2030	Max	Min
PO_4 (nM)	EMSW	23	24	25	28	29	27	27	28	28	29	23
	EMIW	102	102	105	110	117	118	116	116	118	118	102
	EMDW	169	169	170	172	175	177	179	181	183	182	169
DOP (nM)	EMSW	47	48	50	55	57	55	55	56	56	57	47
	EMIW	40	41	42	46	48	47	46	47	48	49	40
	EMDW	38	39	39	39	41	42	42	43	43	43	38
POP (nM)	EMSW	6.6	6.8	7.1	7.8	8.1	7.8	7.7	7.9	8.0	8.1	6.6
	EMIW	5.0	5.1	5.3	5.8	6.1	5.9	5.8	5.9	6.0	6.1	5.0
	EMDW	3.1	3.1	3.3	3.5	3.7	3.7	3.6	3.6	3.7	3.8	3.1
NO_3 (µM)	EMSW	0.6	0.6	0.7	0.7	0.7	0.9	1.0	1.1	1.2	1.2	0.6
	EMIW	2.6	2.6	2.7	2.9	3.1	3.4	3.7	4.0	4.2	4.2	2.6
	EMDW	4.8	4.8	4.8	4.8	4.9	5.0	5.1	5.2	5.4	5.4	4.8
NH_4 (µM)	EMSW	0.09	0.09	0.10	0.11	0.12	0.14	0.16	0.18	0.19	0.19	0.09
	EMIW	0.05	0.05	0.05	0.06	0.06	0.07	0.07	0.08	0.08	0.08	0.05
	EMDW	0.05	0.05	0.05	0.05	0.05	0.06	0.06	0.06	0.06	0.06	0.05
DON (µM)	EMSW	2.7	2.9	3.2	3.7	4.2	4.7	5.3	5.8	6.1	6.1	2.7
	EMIW	2.7	2.7	2.9	3.3	3.6	3.9	4.2	4.5	4.8	4.8	2.7
	EMDW	2.6	2.6	2.6	2.7	2.7	2.8	2.9	3.0	3.2	3.2	2.6
PON (µM)	EMSW	0.27	0.27	0.29	0.31	0.33	0.31	0.31	0.32	0.32	0.33	0.27
	EMIW	0.15	0.16	0.16	0.18	0.19	0.18	0.18	0.18	0.18	0.19	0.15
	EMDW	0.10	0.10	0.11	0.12	0.12	0.12	0.12	0.12	0.12	0.12	0.10
NO_3: PO_4	EMSW	27	26	26	24	24	32	38	40	41	41	23
	EMIW	26	26	26	26	26	29	32	34	36	36	26
	EMDW	28	28	28	28	28	28	29	29	29	29	28
DON: DOP	EMSW	58	59	64	68	73	86	96	104	109	109	58
	EMIW	67	67	69	72	75	83	91	96	100	100	67
	EMDW	67	67	67	67	67	68	69	71	73	73	67
PON: POP	EMSW	40	40	40	40	40	40	40	40	40	40	40
	EMIW	31	31	31	31	31	31	31	31	31	31	31
	EMDW	33	33	33	33	33	33	33	33	33	33	33

Table F.3: Literature values for water column phosphorus (PO_4; POP; DOP) concentrations (nM), for surface water (SW), intermediate water (IW) and deep water (DW) within the WMS.

Cruise	Year	PO_4			POP			DOP			Ref
		SW	IW	DW	SW	IW	DW	SW	IW	DW	
Atlantis 151	1948	75 (0-200)	250 (100-350)	350 (200-400)							1
Atlantic 242	1958	100 (0-200)	325 (200-400)	400 (300->500)							1
R.V John Murray	1969	60 (10-110)	280 (190-330)	370 (140-470)				75 (0-160)	50 (20-60)	60 (0-140)	2
BORHA II	1972/1975				25 (5-100)	3 (2-5)	2 <2				3
	<1976	60 (0-150)	260 (0-380)	370 (350-400)							4
MEDRIPOD IV	1981	200 (50-350)*	400 (330-470)*	385 (350-320*)	30 (1-80)	2 (0.3-5.2)	1 (0.3-2.9)	80 (0-170)	50 (0-140)	50 (0-130)	5
INTERSITE	1984	40 (0-170)	340	340 (340-350)				70 (60-75)	40 (40-45)	40 (25-40)	6
Medatlante	1988-1989		380 (300-420)	390 (370-420)							7
EROS	1993	90 (0-280)			30 (10-80)			20 (0-90)	<13	0	8
SEMAPHORE	1994	60 (0-130)	330 (130-400)	370 (360-400)							9
FRONTS	1996	70 (0-225)	320 (260-370)	350 (340-370)	20 (15-25)	20 (0-55)	10 (0-15)	180 (10-400)	20 (0-80)		10
MINOS*	1996	50 (0-100)	350 (280-420)	400 (360-440)	20 (10-30)	0	0	80 (60-100)	60 (50-70)	30 (10-50)	11
MEDOCC 05	2005	200 (90-300)	350 (250-450)	420 (350-480)							12
BOUM	2008	50 (0-250)	330 (250-450)	390 (350-460)	20 (12-25)	9** (1-20)	4*** (1-10)	40 (30-60)	10** (0-60)	10*** (0-30)	13
METEOR	2011	120 (0-250)*	370 (270-460)*	380 (340-420)*							14

[1]. McGill (1961) [2.]Banoub and Williams (1972), [3] Copin-Montegut and Copin-Montegut (1983),[4.]Millero et al. (1978), [5].Coste et al. (1984) , [6.]Aminot and Kérouel (2004)[7.]Béthoux et al. (1992), [8.]Pujo-Pay et al. (1995); [9.]Béthoux et al. (1998), [10] Lucea et al. (2003); [11] Moutin and Raimbault (2002)[12] Schroeder et al. (2010a), [13] Pujo-Pay et al. (2011); [14.]Tanhua et al. (2013); *error:+/- 1sd; Depth interval **75-1250m; ***1000-3000m;

Table F.4: Reported WMS nitrogen (NO_3, PON, DON, NH_4) concentrations (μM) for surface water (SW), intermediate water (IW) and deep water (DW).

Cruise	Year	NO_3			PON			DON			NH_4			Ref.
		SW	IW	DW	SW	IW	DW	SW	IW	DW	SW	IW	DW	
R.V John Murray	1969	1.8 (0.6-3.4)	6.1 (3.3-6.8)	6.4 (5.4-8.1)	0.2 (0.1-0.35)	0.07 (0.02-0.08)	0.05 (0.02-0.09)	4.5 (4.0-6.1)	3.4 (2.0-4.6)	4.5 (1.4-6.7)				1
BORHA II	1972/1975				0.73 (0.1-2.2)	0.05 (0.03-0.11)	0.03 (0.015-0.03)							2
	<1978	0.55 (0-2.1)	6.6 (3.9-7.9)	8.4 (8.0-9.0)										3
Medripod IV	1981	3.5 (0.5-6.5)*	8.3 (7.2-9.4)*	8.3 (8.0-8.6)*	0.17 (0.14-0.74)	0.03 (0.01-0.06)	0.01 (<0.01-0.02)	4.0 (2.6-6.4)	3.4 (2.6-4.4)	3.3 (2.4-4.3)				4
INTERSITE	1984	1.1 (0-4.3)	7.6 (4-8.0)	7.8 (7.8-8.0)				3.7 (3.6-4.1)	3.0	2.7 (2.7-3.0)				5
MedAtlante	1988-1989		8.7 (7.9-9.3)	8.4 (7.5-8.7)										6
EROS	1993	2.9 (0-7.3)	>6.9		0.5 0.1-1.5	<0.2	<0.05	6.0 (5.2-7.5)	3.9 (3.8-3.9)	4.1 (3.9-4.7)				7
SEMAPHOR	1994	2.5 (0.1-4.5)	8.3 (6.8-9.1)	8. 6 (8.3-9.0)										8
VERIMED	1995				0.6 (0.3-1.8)			4.1 (3.3-5.3)		3.0 (2.9-3.0)				9
FRONTS	1996	0.4 (0-1.4)	3.0 (1.4-4.0)	2.0 (1.6-2.2)	0.45 (0.3-0.66)	0.30 (0.23-0.3)	0.34 (0.2-0.4)	3.9 (2.0-4.5)	1.4 (0.1-2.7)					10
MINOS*	1996	1.2 (0-2.6)	8.0 (6.7-9.3)	8.5 (7.9-9.1)	0.40 (0.2-0.6)	0.10	0.00	4.6 (4.0-5.2)	3.1 (2.8-3.4)	2.8 (2.7-2.9)				11
MEDOCC 05	2005	5.0 (0.5-6.0)	7 (5-9)	8 (7-9.5)										12
BOUM	2008	1.6 (0-6.0)	8.0 (6-9.5)	9.1 (8-9.5)	0.40 (0.15-0.55)	0.12** (0.03-0.22)	0.06*** (0.01-0.13)	4.7 (3.9-5.0)	4.0 (3.5-4.5)	3.3 (3.0-3.5)	0.007 (0-0.055)	0.001** (0-0.007)		13
METEOR	2011	2.9 (0-5.9)*	7.9 (6.0-9.9)*	8.0 (7.3-8.8)*										14

[1.] Banoub and Williams (1972), [2.] Copin-Montegut and Copin-Montegut (1983),[3] Millero et al. (1978), [4] Coste et al. (1984), [5.] Aminot and Kérouel (2004) [6.]Béthoux et al. (1992), [7.] Pujo-Pay et al. (1995) [8.]Béthoux et al. (1998), [9.] Doval et al. (1999); [10.] Lucea et al. (2003) [11.] Moutin and Raimbault (2002), [12] Schroeder et al. (2010a), [13]Pujo-Pay et al. (2011); [14]Tanhua et al. (2013) *error:+/- 1sd; Depth interval **75-1250m; ***1000-3000m.

Table F.5: Model predicted dissolved reactive P and N concentrations for 1950, 1970, 2000 and 2030 in the random circulation scenarios with constant (Simulation 1) and changing nutrient (Simulation 2) inputs and two climate change scenarios (see section F.2 for details on climate change scenarios). Numbers in brackets represent 10^{th}-90^{th} percentile range of ensemble of 500 runs; arrow indicates direction of concentration change in the climate change scenario relative to 1950 for constant nutrient inputs and 2030 for 1950 to 2030 nutrient inputs.

		Constant nutrients (Simulation 1)			1950-2030 nutrients (Simulation 2)				
		1950	2030 S1	2030 S2	1970	2000	2030	2030 S1	2030 S2
PO_4 IW	WMS	270 (256-284)	269↓ (255-283)	282↑ (268-295)	272 (254-289)	295 (277-311)	295 (277-312)	293↓ (279-307)	308↑ (294-321)
	EMS	103 (98-107)	101↓ (97-105)	115↑ (110-121)	107 (101-112)	120 (114-126)	120 (114-125)	118↓ (113-123)	131↑ (126-137)
PO_4 DW	WMS	365 (351-378)	370↑ (360-381)	358↓ (346-369)	367 (353-380)	380 (368-394)	390 (377-404)	398↑ (387-408)	382↓ (370-393)
	EMS	170 (169-172)	173↑ (171-174)	164↓ (162-165)	171 (169-173)	179 (178-180)	184 (183-186)	186↑ (184-187)	179↓ (178-180)
DOP IW	WMS	44 (41-47)	42↓ (40-44)	46↑ (43-49)	46 (42-49)	49 (45-52)	49 (45-52)	46↓ (44-49)	50↑ (47-54)
	EMS	41 (39-43)	38↓ (37-40)	43↑ (41-45)	43 (41-45)	48 (46-50)	48 (46-51)	46↓ (45-48)	50↑ (49-52)
DOP DW	WMS	27 (25-30)	26↓ (24-27)	29↑ (27-32)	28 (25-30)	30 (28-33)	30 (27-32)	27↓ (26-29)	32↑ (29-34)
	EMS	39 (38-39)	38↓ (38-39)	40↑ (39-41)	39 (39-40)	42 (42-43)	44 (43-45)	43↓ (43-44)	45↑ (45-46)
NO_3 IW	WMS	6.6 (6.3-6.9)	6.6 (6.3-6.9)	6.8↑ (6.5-7.1)	6.6 (6.3-7.0)	7.6 (7.3-7.9)	8.7 (8.3-9.0)	8.8↑ (8.6-9.1)	8.7 (8.4-9.0)
	EMS	2.6 (2.5-2.8)	2.6 (2.5-2.8)	2.9↑ (2.8-3.1)	2.7 (2.5-2.9)	3.4 (3.2-3.6)	4.2 (4.0-4.5)	4.3↑ (4.1-4.5)	4.3↑ (4.1-4.5)
NO_3 DW	WMS	7.7 (7.4-8.0)	7.8↑ (7.6-8.0)	7.5↓ (7.3-7.8)	7.7 (7.4-8.0)	8.1 (7.8-8.4)	8.9 (8.6-9.1)	9.0↑ (8.8-9.2)	8.7↓ (8.5-8.9)
	EMS	4.8 (4.8-4.9)	4.9↑ (4.8-4.9)	4.6↓ (4.5-4.6)	4.8 (4.8-4.9)	5.0 (5.0-5.1)	5.4 (5.4-5.4)	5.4 (5.4-5.5)	5.4 (5.4-5.5)
DON IW	WMS	2.8 (2.6-2.9)	2.6↓ (2.5-2.7)	2.9↑ (2.7-3.0)	2.9 (2.7-3.0)	3.3 (3.1-3.5)	3.7 (3.4-3.9)	3.5↓ (3.3-3.7)	3.7 (3.5-3.9)
	EMS	2.7 (2.6-2.8)	2.6↓ (2.5-2.7)	2.8↑ (2.8-2.9)	3.0 (2.9-3.1)	4.0 (3.9-4.1)	4.8 (4.7-4.9)	4.7↓ (4.6-4.8)	4.7↓ (4.6-4.8)
DON DW	WMS	2.5 (2.4-2.6)	2.4↓ (2.3-2.5)	2.6↑ (2.5-2.7)	2.5 (2.4-2.7)	2.8 (2.7-3.0)	3.0 (2.9-3.2)	2.9↓ (2.8-3.0)	3.1↑ (3.0-3.3)
	EMS	2.6 (2.6-2.6)	2.6 (2.6-2.6)	2.7↑ (2.6-2.7)	2.6 (2.6-2.7)	2.9 (2.8-2.9)	3.2 (3.1-3.2)	3.1↓ (3.1-3.1)	3.4↑ (3.4-3.5)